frontiers | Research Topics

Specialized metabolites from medicinal plants: The structural identification, biological activity and biosynthesis pathways

Edited by
Zhixing Qing, Chun-Tao Che, Hongjie Zhang, Chunpeng Wan and Zhou Yuan

Published in
Frontiers in Plant Science
Frontiers in Pharmacology

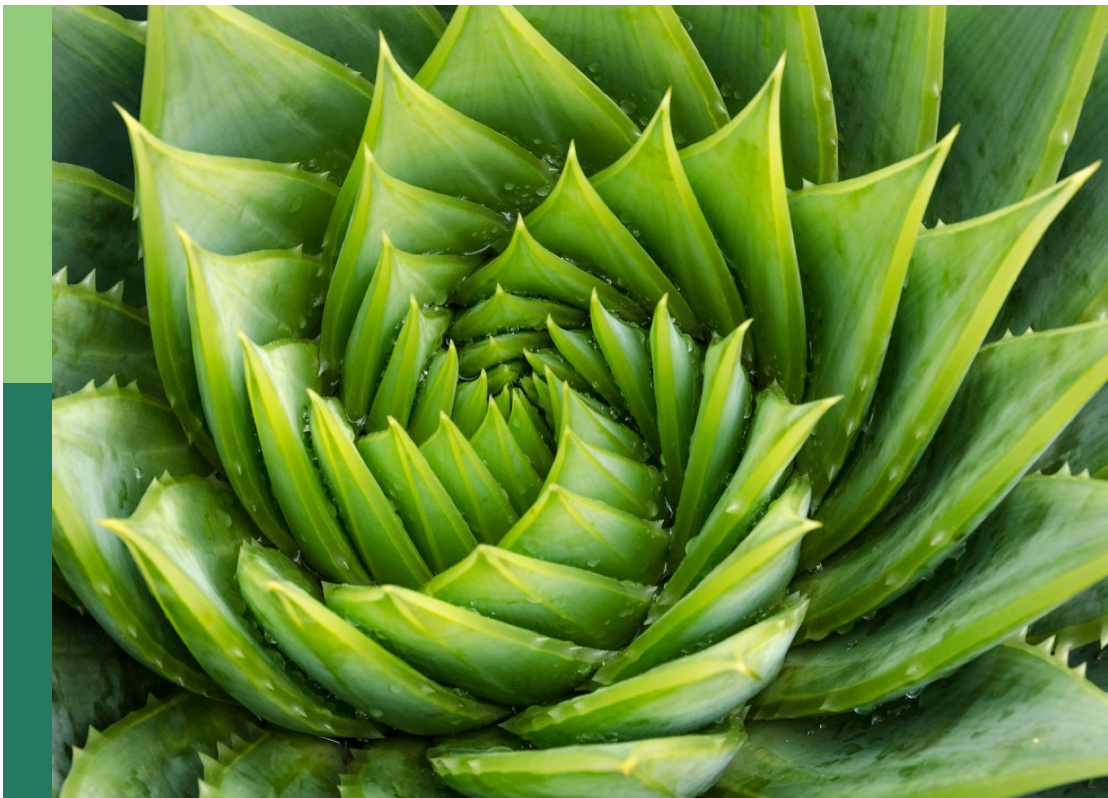

ISSN 1664-8714
ISBN 978-2-8325-5022-9
DOI 10.3389/978-2-8325-5022-9

About Frontiers

Frontiers is more than just an open access publisher of scholarly articles: it is a pioneering approach to the world of academia, radically improving the way scholarly research is managed. The grand vision of Frontiers is a world where all people have an equal opportunity to seek, share and generate knowledge. Frontiers provides immediate and permanent online open access to all its publications, but this alone is not enough to realize our grand goals.

Frontiers journal series

The Frontiers journal series is a multi-tier and interdisciplinary set of open-access, online journals, promising a paradigm shift from the current review, selection and dissemination processes in academic publishing. All Frontiers journals are driven by researchers for researchers; therefore, they constitute a service to the scholarly community. At the same time, the *Frontiers journal series* operates on a revolutionary invention, the tiered publishing system, initially addressing specific communities of scholars, and gradually climbing up to broader public understanding, thus serving the interests of the lay society, too.

Dedication to quality

Each Frontiers article is a landmark of the highest quality, thanks to genuinely collaborative interactions between authors and review editors, who include some of the world's best academicians. Research must be certified by peers before entering a stream of knowledge that may eventually reach the public - and shape society; therefore, Frontiers only applies the most rigorous and unbiased reviews. Frontiers revolutionizes research publishing by freely delivering the most outstanding research, evaluated with no bias from both the academic and social point of view. By applying the most advanced information technologies, Frontiers is catapulting scholarly publishing into a new generation.

What are Frontiers Research Topics?

Frontiers Research Topics are very popular trademarks of the *Frontiers journals series*: they are collections of at least ten articles, all centered on a particular subject. With their unique mix of varied contributions from Original Research to Review Articles, Frontiers Research Topics unify the most influential researchers, the latest key findings and historical advances in a hot research area.

Find out more on how to host your own Frontiers Research Topic or contribute to one as an author by contacting the Frontiers editorial office: frontiersin.org/about/contact

Specialized metabolites from medicinal plants: The structural identification, biological activity and biosynthesis pathways

Topic editors

Zhixing Qing — Hunan Agricultural University, China
Chun-Tao Che — University of Illinois Chicago, United States
Hongjie Zhang — Hong Kong Baptist University, Hong Kong, SAR China
Chunpeng Wan — Jiangxi Agricultural University, China
Zhou Yuan — Huazhong University of Science and Technology, China

Citation

Qing, Z., Che, C.-T., Zhang, H., Wan, C., Yuan, Z., eds. (2024). *Specialized metabolites from medicinal plants: The structural identification, biological activity and biosynthesis pathways*. Lausanne: Frontiers Media SA.
doi: 10.3389/978-2-8325-5022-9

Table of contents

frontiers | Frontiers in Plant Science

TYPE Original Research
PUBLISHED 07 June 2023
DOI 10.3389/fpls.2023.1196609

OPEN ACCESS

EDITED BY
Chunpeng (Craig) Wan,
Jiangxi Agricultural University, China

REVIEWED BY
Yanjie Zhang,
Zhengzhou University, China
Feng Xiong,
Chinese Academy of Sciences (CAS), China

*CORRESPONDENCE
Hailin Liu
liuhailin@caas.cn
Peng Cui
hb_njfu@163.com

RECEIVED 30 March 2023
ACCEPTED 10 May 2023
PUBLISHED 07 June 2023

CITATION
He B, Qian K, Han X, Li J, Zhou Q, Xu L-a, Liu H and Cui P (2023) Novel mechanisms for the synthesis of important secondary metabolites in *Ginkgo biloba* seed revealed by multi-omics data.
Front. Plant Sci. 14:1196609.
doi: 10.3389/fpls.2023.1196609

Novel mechanisms for the synthesis of important secondary metabolites in *Ginkgo biloba* seed revealed by multi-omics data

Bing He[1], Kun Qian[1], Xin Han[2], Jianyang Li[1], Qi Zhou[3], Li-an Xu[2], Hailin Liu[1]* and Peng Cui[1]*

[1]Agricultural Genomics Institute at Shenzhen, Chinese Academy of Agricultural Sciences, Shenzhen, China, [2]Co-Innovation Center for Sustainable Forestry in Southern China, Nanjing Forestry University, Nanjing, China, [3]Institute of Forestry Breeding, Zhejiang Academy of Forestry, Hangzhou, China

Although the detailed biosynthetic mechanism is still unclear, the unique secondary metabolites of *Ginkgo biloba*, including ginkgolic acids (GAs) and terpene trilactones, have attracted increasing attention for their potent medicinal, physiological and biochemical properties. In particular, GAs have shown great potential in the fields of antibacterial and insecticidal activities, making it urgent to elucidate their biosynthetic mechanism. In this study, we systematically revealed the landscape of metabolic-transcriptional regulation across continuous growth stages of *G. biloba* seeds (GBS) based on multi-omics mining and experimental verification, and successfully identified all major types of GAs and terpene trilactones along with more than a thousand kinds of other metabolites. The phenological changes and the essential gene families associated with these unique metabolites were analyzed in detail, and several potential regulatory factors were successfully identified based on co-expression association analysis. In addition, we unexpectedly found the close relationship between large introns and the biosynthesis of these secondary metabolites. These genes with large introns related to the synthesis of secondary metabolites showed higher gene expression and expression stability in different tissues or growth stages. Our results may provide a new perspective for the study of the regulatory mechanism of these unique secondary metabolites in GBS.

KEYWORDS

ginkgolic acids, secondary metabolites, large intron, gene expression, Ginkgo biloba

1 Introduction

As the only surviving member of the Ginkgo family, *Ginkgo biloba* is a relict plant from the Quaternary Ice Age and is widely known as the "living fossil" (Zhou and Zheng, 2003). In addition to its special evolutionary status, as a typical economic gymnosperm, *G. biloba* also possesses a variety of values, including edible, medicinal and ornamental uses. For

example, a standardized preparation of *G. biloba* extract (EGB761) is among the best-selling herbal remedies in America and many European countries (Gulec et al., 2006; Nabavi and Silva, 2019). The dietary supplements sales of *G. biloba* exceed US$ 1.26 billion annually in the global market (Mei et al., 2017), and are utilized to treat thrombosis, inflammation, cardiovascular condition and Alzheimer's disease (Sasaki et al., 2002; Rodriguez et al., 2007). In addition, *G. biloba* seed (GBS) has a very long history of consumption around the world for its important secondary metabolites, which mainly contains the medicinal substances flavonoids and terpenoids, together with the unique ginkgo phenolic acids (van Beek, 2005; Mahadevan and Park, 2008). Unlike flavonoids, which are ubiquitous in plants and have a relatively clear synthetic pathway, the research into the unique metabolites of Ginkgo has lagged behind (Ye et al., 2020; He et al., 2021).

The terpenoids in *G. biloba* are a unique class of terpene trilactones, which are composed of sesquiterpene (bilobalide) and diterpenes (ginkgolide). Ginkgolide is a potent platelet activating factor (PAF) antagonist, which can selectively inhibit platelet aggregation and prevent thrombosis, and is widely used in the treatment of cardiovascular and cerebrovascular diseases (Yang et al., 2017). Bilobalide, on the other hand, does not appear to have PAF antagonistic activity and has been shown to exert central neuroprotective effects (Atzori et al., 1993). In terms of industrial applications, currently these terpene trilactones could only be extracted directly from *G. biloba* tissues due to the unclear biosynthesis mechanism and cost limitations. Meanwhile, it should be mentioned that the terpenoid content of Ginkgo tissues is not satisfactory and could easily be affected by seasonal changes or other environmental factors, causing problems for downstream industrial preparation (Cartayrade et al., 1997).

Ginkgo phenolic acids are another group of important secondary metabolites in GBS, which are mainly concentrated in mature sarcotesta. Ginkgo phenolic acids belong to the urushiolic acids, which include three major groups of ginkgolic acids (GAs), ginkgols, and bilobols (van Beek, 2002). The GAs are referred to various n-alkyl phenolic acids with side chain length of 13-17 and side chain double bond number of 0-2, which are the main substance of ginkgo phenolic acids, accounting for 90% (Yang et al., 2014). Ginkgo phenolic acids have long been considered a typical hazardous substance due to their strong sensitization and cytotoxicity, and their proportion has been strictly limited in the preparation of ginkgo medicinal remedies. On the other hand, due to their unique hydrophobicity and hydrophilicity, ginkgo phenolic acids have been gradually applied in many fields, including antimicrobial (Lee et al., 1998), chemical (Jiang et al., 2017) and pest control (Pan et al., 2006b). Among them, GA (15:1) has been shown to prevent the acylation of small ubiquitin-related modifier proteins (SUMO) to regulate cell functions, which has been utilized as a potential treatment for cancer and neurological diseases (Fukuda et al., 2009; Baek et al., 2017).

Although some progress has been made in recent years on the anabolic regulation of important secondary metabolites in *G. biloba* (He et al., 2015; Li et al., 2018; Ye et al., 2020), most of the current research is still focused on leaves, and there is still a lack of research on the regulation of secondary metabolite synthesis in GBS considering its rich editable values. In addition, the results of systematic analysis of GAs are obviously insufficient compared to those of flavonoids and other substances. With the flourishing development of multi-omics analysis technology, new insights could be provided for the study of the *in vivo* synthesis mechanism. In this study, we aim to construct a metabolite map of GBS during the whole development period supported by these multi-omics data, and mainly focus on these unique secondary metabolites including GAs and terpene trilactones based on their detailed systematic characterization, in an attempt to better explain the specific mechanisms of their anabolism.

2 Materials and methods

2.1 Sample collection and preparation

Due to the relatively long developmental process of GBS, which takes about half a year from pollination to seed maturity, including the physiological post-ripening phenomenon. The plump seeds of a healthy female *G. biloba* tree aged about 20 years were selected and sampled every month from June to October on the campus of Nanjing Forestry University (32°4'N, 118°48'E). Samples from three representative periods (June 1, August 1, and October 1, respectively) with three replicates were selected for subsequent analysis based on the morphological observation. After sampling, these tissues were immediately frozen in liquid nitrogen and stored at -80°C until further treatment.

2.2 Metabolomic analysis

Biological samples were first lyophilized in a lyophilizer (SCIENTZ-100F/A) and subsequently ground (30 Hz, 1.5 min) to powder using a grinding machine. The 100 mg of powder was then weighed and dissolved in 1.0 mL of extract. The dissolved samples were refrigerated overnight at 4 °C overnight and swirled three times during this time to improve the extraction rate. After centrifugation (rotation speed: 12000 rpm, 10 min), the supernatant was extracted with the samples filtered through a microporous membrane (0.22 μm pore size) and stored in injection bottles for UPLC-MS/MS analysis.

The data acquisition system consisted mainly of an UPLC-ESI-MS/MS system (SHIMADZU Nexera X2 Series, www.shimadzu.com) and a tandem mass spectrometer (Applied Biosystems 6500 Q TRAP, www.appliedbiosystems.com). Both positive and negative ion modes were controlled by Analyst 1.6.3 software (AB Sciex). Instrument tuning and quality calibration were performed with 10 and 100 μmol/L polypropylene glycol solution in QQQ and LIT modes, respectively. QQQ scanning adopts MRM mode and sets collision gas (nitrogen) as the medium. DP and CE of each MRM ion pair were completed by further optimization, and a specific set of MRM ion pairs would be monitored at each period based on the eluted metabolites.

2.3 Identification and quantification of metabolites

The metabolites were characterized according to the secondary spectral information. The isotopic signals and the repetitive signals containing K^+ ions, Na^+ ions or NH_4^+ ions, and the repetitive signal of other substances of high molecular weight were removed. Metabolites were quantified by multiple reaction monitoring (MRM) using triple quadrupole mass spectrometry. In the MRM mode, the precursor ions (parent ions) of the target substance were first screened by the quadrupole, and the corresponding ions of other molecular weight substances were excluded to first eliminate the interference. After ionization induced by the collision chamber, the precursor ions would break and form many fragments. Then, a characteristic fragment ion was selected by triple quadrupole filtration to eliminate the interference of non-target ions in order to make the quantification results more accurate. After obtaining the metabolite spectrum of different samples, the mass spectrum peaks of all substances were integrated with the peak area, and these peaks identified as the same metabolite in different samples were integrated with correction.

Due to the typically high-dimensional nature of metabolomic data, the traditional principal component analysis (PCA) may not be able to cluster these data well, resulting in the poor interpretation of the analysis results. Therefore, the identification of differential metabolites was conducted with orthogonal partial least squares discriminant analysis (OPLS-DA), which combines both orthogonal signal correction (OSC) and the partial least squares discriminant analysis (PLS-DA) (Thevenot et al., 2015). In contrast to PCA, which is an unsupervised classification method, PLS-DA is a multivariate statistical analysis method with supervised pattern recognition. It could extract the components of the independent variable X and the dependent variable Y, and then calculate the correlation between each component. Based on the analysis results of the variable importance in projection (VIP) values in the OPLS-DA model, differential metabolites were screened by combining fold changes, p-values of t-test and VIP values, and the filtering standard was set as fold change > 1 and VIP > 1 with p-value should be less than 0.05.

2.4 Transcriptome sequencing and analysis

RNA concentration and purity were measured using NanoDrop 2000 (Thermo Fisher Scientific, Wilmington, USA, www.thermofisher.com). RNA integrity was assessed using the RNA Nano 6000 Assay Kit of the Agilent Bioanalyzer 2100 system (Agilent Technologies, CA, USA, www.agilent.com). A total amount of 1 μg RNA per sample was used as input for the RNA sample preparation. Clustering of the indexed samples was performed on a cBot Cluster Generation System using the TruSeq PE Cluster Kit v4-cBot-HS according to the manufacturer's instructions. After clustering, library preparations were sequenced on an Illumina Hiseq X Ten platform to generate paired-end reads. Raw reads were first trimmed with fastp to remove reads containing adapter, poly-N, or low quality (Chen et al., 2018). Only reads with a unique match were further analyzed and annotated based on the reference genome (Liu et al., 2021). HISAT2 (Kim et al., 2019) was utilized to align the reads to the reference genome, and quantification of gene expression levels was estimated by fragments per kilobase of transcript per million fragments mapped (FPKM) using StringTie (Pertea et al., 2015). Differential expression analysis was performed with DESeq2 based on the negative binomial distribution (Love et al., 2014). The resulting p-values were adjusted using the Benjamini and Hochberg's approach to control for false discovery rate (FDR) (Thissen et al., 2002).

2.5 Gene family analysis and functional validation

The identification of gene families related to secondary metabolite biosynthesis was performed using BLAST with e-values of $1e^{-10}$, and the potential members were further filtered based on the evidence of full-length transcript according to our previous data (Han et al., 2021). The Ka/Ks rate of these gene families was calculated using KaKs_calculator 2.0 (Wang et al., 2010). Weighted Gene Correlation Network Analysis (WGCNA) was utilized to infer the gene co-expression pattern (Langfelder and Horvath, 2008), and the transposable elements were identified with EDTA (Ou et al., 2019).

The same batch of collected seeds was used for the qRT-PCR experiment with three biological replicates. An RNAprep Pure Plant Kit (Polysaccharides&Polyphenolics-rich) (Tiangen Biotech, Beijing, China, www.tiangen.com) was applied to extract total RNA from each sample. PrimeScript™ RT Master Mix (Takara, Tokyo, Japan, www.takarabiomed.com) was used for reverse transcription, and the reverse transcribed product was diluted 3-fold for real-time quantitative experiments. The according primers were designed (Supplementary File 1) and the qRT-PCR analysis was performed using SYBR Premix Ex Taq (Takara, Tokyo, Japan, www.takarabiomed.com) and ViiA 7 Real-Time PCR System (Thermo Fisher, USA, www.thermofisher.com), and each reaction was subjected to 3 technical replicates. PCR amplification was performed under the following conditions: 95 °C for 10 min; 95 °C for 15 s, and 60 °C for 60 s with 45 cycles; 95 °C for 15 s, 60 °C for 60 s, and 95 °C for 15 s. EIF3D was set as the endogenous control, and the relative expression level was calculated using the $2^{-\Delta\Delta Ct}$ method.

3 Results

3.1 The landscape of GBS metabolites across continuous developmental stages

Ginkgo seeds were sampled at three developmental stages: June, August, and October, along with the quality assessment of these samples (Figure 1). The correlation results of the metabolome showed that the sample results within the same batch were satisfactory, and the results of the principal component analysis (PCA) were able to fully reveal the significant differences between

FIGURE 1
Morphological observations of the complete developmental stages of GBS.

samples from different batches. The transcriptome results were also in line with our expectations. These results demonstrated the robustness of the data quality, which could strongly support our subsequent analysis.

A total of 1,043 kinds of metabolites were detected, and the number was far more than 780 kinds obtained from *G. biloba* leaves during the same sampling periods, showing vigorous metabolic activity (He et al., 2021). The substances detected were mainly primary metabolites, including carboxylic acids and derivatives, fatty acids, and related oxidation compounds. All metabolites were then clustered into nine groups according to their expression (Figure 2). The results showed that most of the metabolites in ginkgo seeds were more active in June and August, and 208 of them (Group 1) significantly increased from June to August and maintained until October, while the expression levels of other 389 metabolites (Group 2), on the contrary, decreased from June to October. The number of metabolites between these two groups with opposite expression trends accounted for more than half of all

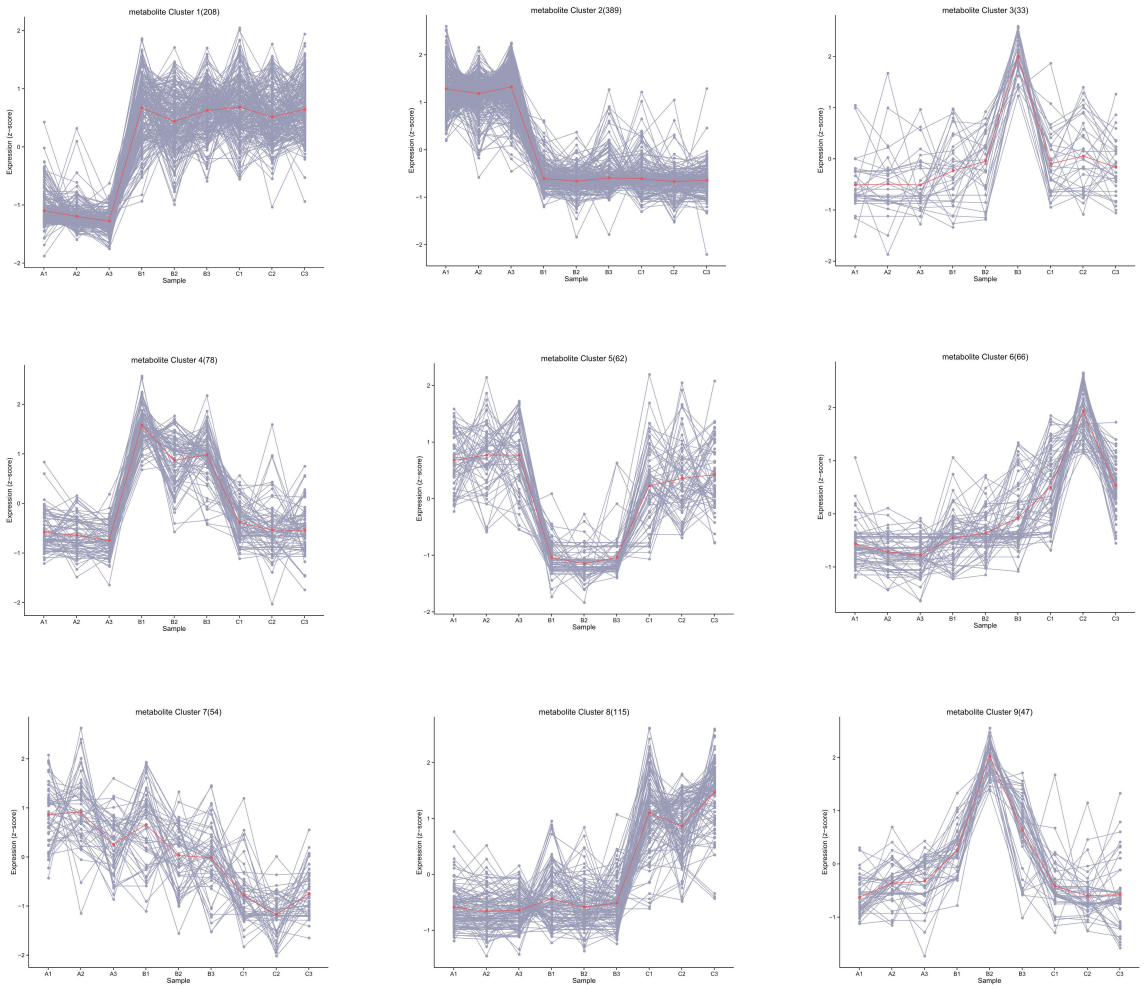

FIGURE 2
Classification of the trend changes in the content of all metabolites over different time periods.

metabolites, and their functional enrichment results also showed differences. Metabolites of Group 1 with obvious up-regulated expression trend were mainly enriched in amino acid and lipid metabolism, including biosynthesis of unsaturated fatty acid biosynthesis and linoleic acid metabolism together with glycine, serine and threonine metabolism, showing an active tendency in energy metabolism and storage (Figure 3A). On the other hand, metabolites of Group 2 with a downward tendency were mainly enriched with flavonoid biosynthesis, which was another class of important secondary metabolites in *G. biloba*.

Subsequently, the differential metabolites were screened by combining the fold changes and VIP values generated by the OPLS-DA model to further observe the content change of metabolites in different developmental stages (Figure 3B). From June to August, the number of down-regulated metabolites was much higher than that of up-regulated metabolites, and the levels of other 386 metabolites were relatively stable. One of the most significantly up-regulated substances during this period was turanose (log2 (fold change) > 18), which is an isomer of sucrose, and the most representative down-regulated metabolites were myricetin-3-O-glucoside and tricin-7-O-glucoside (Figure 3C). Tricin is biosynthesized as a component of plant secondary metabolites through a combination of phenylpropanoid and polyketide pathways, and it has been extensively studied due to its biological significance in plant growth as well as its potential for pharmaceutical importance (Zhou and Ibrahim, 2010). Both this metabolite and myricetin-3-O-glucoside belong to the flavonoid group, and their content changes were consistent with other typical flavonoids within these two periods, reaching the peak in June and dramatically decreasing in August.

According to our results, there seemed to be a significant decrease in metabolite activity and a steady state between August and October compared to the previous two months. Among them, most metabolites showed no significant change, and other 167 and 126 metabolites were up- and down-regulated, respectively (Figure 3D). This statistic was slightly different from the previous clustering results based on simple trend analysis, which mainly involved distinguishing the significance of the difference. The most representative metabolite, methyl cinnamate, which is an ester within the cinnamate family (Bhatia et al., 2007), was up-

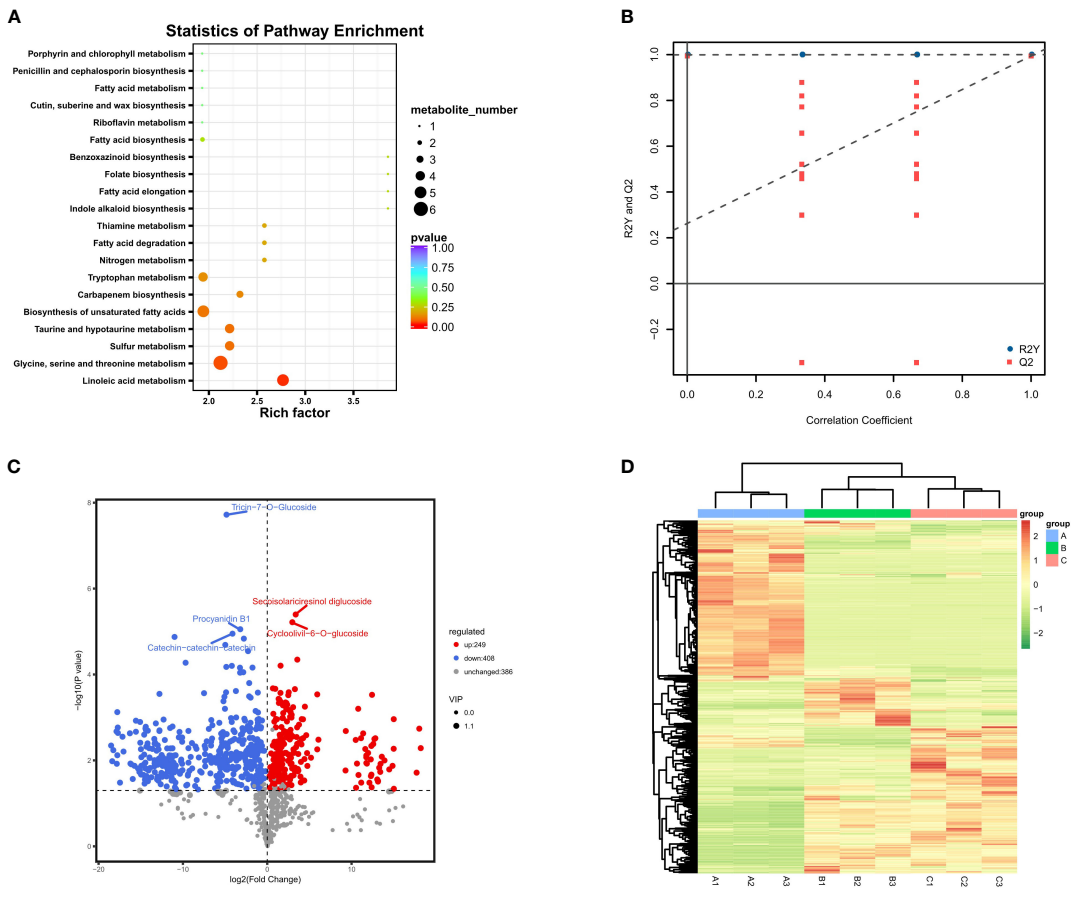

FIGURE 3
Differential metabolite results; **(A)** Annotated bubble diagram of metabolites for Group 1; **(B)** Permutation plot of the OPLS-DA model. The horizontal axis indicates the similarity to the original model, and the vertical axis indicates the value of R2Y or Q2. The blue and red dots represent R2Y and Q2 of the model after Y replacement, respectively, and the dashed line is the fitted regression line. If R2Y and Q2 are smaller than R2Y and Q2 of the original model, then the model could be screened for differential metabolites according to VIP values; **(C)** Volcanic map of differential metabolites between June and August. The horizontal coordinate represents the fold change of each substance compared in this group, and the size of the scatter point represents the VIP value generated from the OPLS-DA model; **(D)** Heatmap of all metabolites based on VIP values. **(A–C)** represent June, August and October, respectively.

regulated throughout August and October with the highest fold change value. It is worth mentioning that the most significantly up-regulated metabolites during this period were also highly enriched in the phenylpropanoid biosynthetic pathway, which is involved in the synthesis of various terpenoids, including trans-cinnamaldehyde and p-coumaric acid. In particular, there seemed to be significant differences in metabolic activity at different developmental stages in GBS. The primary metabolic activity was more vigorous from June to August, while the metabolic activity tended to be stable after August and gradually accumulated secondary metabolites including terpene trilactones.

3.2 Identification of the unique secondary metabolites in *G. biloba*

From a continuous developmental perspective, June to August produced many more differential metabolites compared to August to October, and these content differences appeared to persist over a long period of time, culminating in 165 differential metabolites being present in the comparative results for any two time points (Figure 4A). As the unique secondary metabolites identified in *G. biloba* with potential sensitization, mutagenicity and strong cytotoxicity, all major ginkgo phenolic acids were successfully mined in our research based on their differences in side chain length and double bond number, including GA (13:0), GA (15:0), GA (15:1), GA (17:1) and GA (17:2). The chemical structures of these metabolites are similar to urushic acid in *Pelargonium hortorum*, and it is inferred that the more double chains on the hydrocarbon group, the more susceptible to sensitization (Narnoliya et al., 2017). Among them, GA (15:1) accounted for more than 60% of the total, and the content of GA (17:2) was the lowest (Figure 4B). According to the previous clustering results of ginkgo metabolites, the expression trends of all GAs were similar. The levels of GAs peaked in June and then decreased rapidly without any obvious fluctuation since then, which was also consistent with the results of other Group 2 metabolites.

In contrast to the hazardous properties of GAs, the unique terpene trilactones are widely used in the treatment of human cardiovascular diseases. Our results were also fruitful for the identification of terpene trilactones in GBS. A total of seven types of terpene trilactones were identified, including six typical diterpenes (Ginkgolide A/B/J/K/M/Q, respectively) and one sesquiterpene (bilobalide). Interestingly, the content variation of terpene trilactones showed a clear difference when compared to GAs (Figure 4C). According to the previous clustering results, all GAs shared a consistent tendency to be classified in Group 2, while different groups were confirmed among these terpene trilactones. Specifically, Ginkgolide A and bilobalide were in Group 5 with other 60 metabolites, and the typical characteristic of this group was the double peak phenomenon, which had a much higher content in June and October and decreased dramatically in August. On the other hand, Ginkgolide B、J and K were in Group 8, and the change trend of this group was completely opposite to that of Group 2. The contents of these terpenoids didn't change much in the early

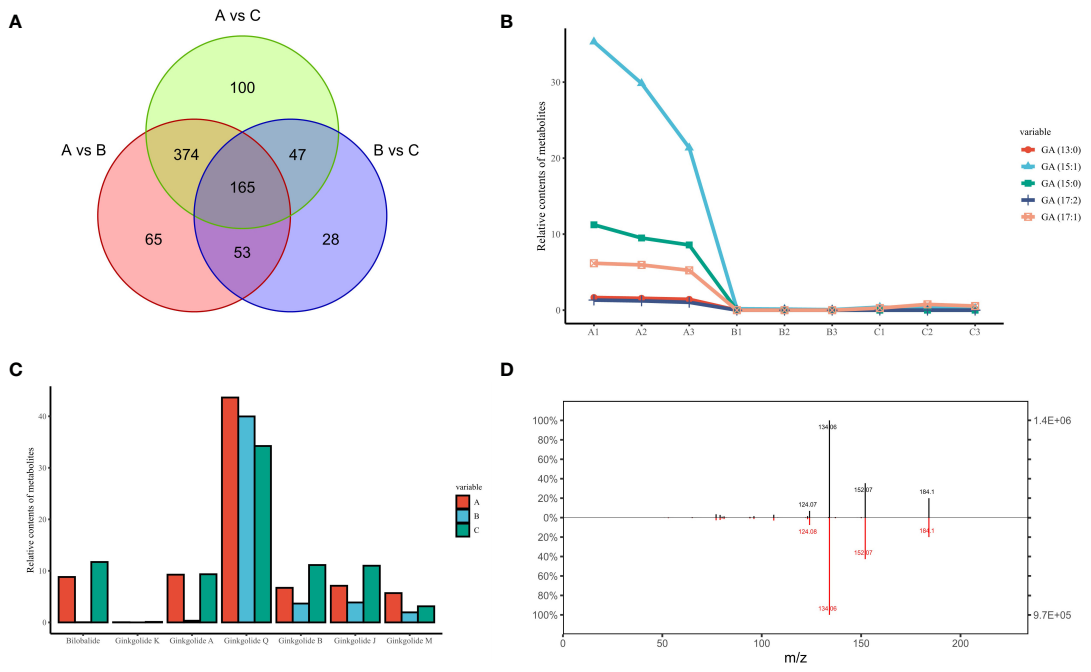

FIGURE 4
The unique secondary metabolites identified in GBS; **(A)** Venn diagram of all differential metabolites in three time periods; **(B)** Content variation of five representative GAs in three time periods; **(C)** Content variation of all types of terpenoids unique to GBS in three time periods; **(D)** Secondary spectrum of ginkgotoxin and its mirror image of the standard. The upper and lower plots represent the secondary spectrum extracted from the standard and the sample, respectively. The vertical axis represents the mass charge ratio (m/z).

months and gradually reached the peak around October. These results indicated the complexity of the terpene trilactone biosynthesis in GBS, and there seems to be a potential antagonistic relationship in their synthesis processes, although these terpenoids share common precursors.

In addition to the various GAs and terpene trilactones, the unique neurotoxin in GBS, ginkgotoxin (4′-O-methylpyridoxine, MPN), was also observed (Figure 4D). Ginkgotoxin is an antivitamin which is structurally related to vitamin B6 (pyridoxine), and excessive consumption of GBS could easily lead to poisoning, causing drowsiness, convulsions and seizures, loss of consciousness and even death (Leistner and Drewke, 2010). It is an inhibitor of pyridoxal kinase and glutamic acid decarboxylase in mouse brain, and its toxic effect could be alleviated by pyridoxine (Kobayashi et al., 2015). In our study, the variation trend of ginkgotoxin content was consistent with that of GAs, which reached the highest content in June and then decreased rapidly without any significant fluctuation.

3.3 Multi-omics analysis of GA synthesis revealed active involvement of large introns

Although metabolome analysis could intuitively obtain the atlas and content trends of all metabolites in GBS, the combination analysis of transcriptome and other multi-omics data is necessary to reveal the detailed synthesis and regulation mechanisms. Co-expression analysis was first performed based on the relative content of values with WGCNA method, and nearly 400 metabolites were grouped together with all GAs into the same module, which was very similar to the previous clustering results in Group 2 (Figure 5A). Then, all metabolites in this module were further annotated and a correlation network was constructed according to their correlation weight in order to identify the essential metabolites related to GA synthesis. According to our results, palmitoleic acid and erucic acid, which are considered as the primary precursors of GAs, were found to be closely related

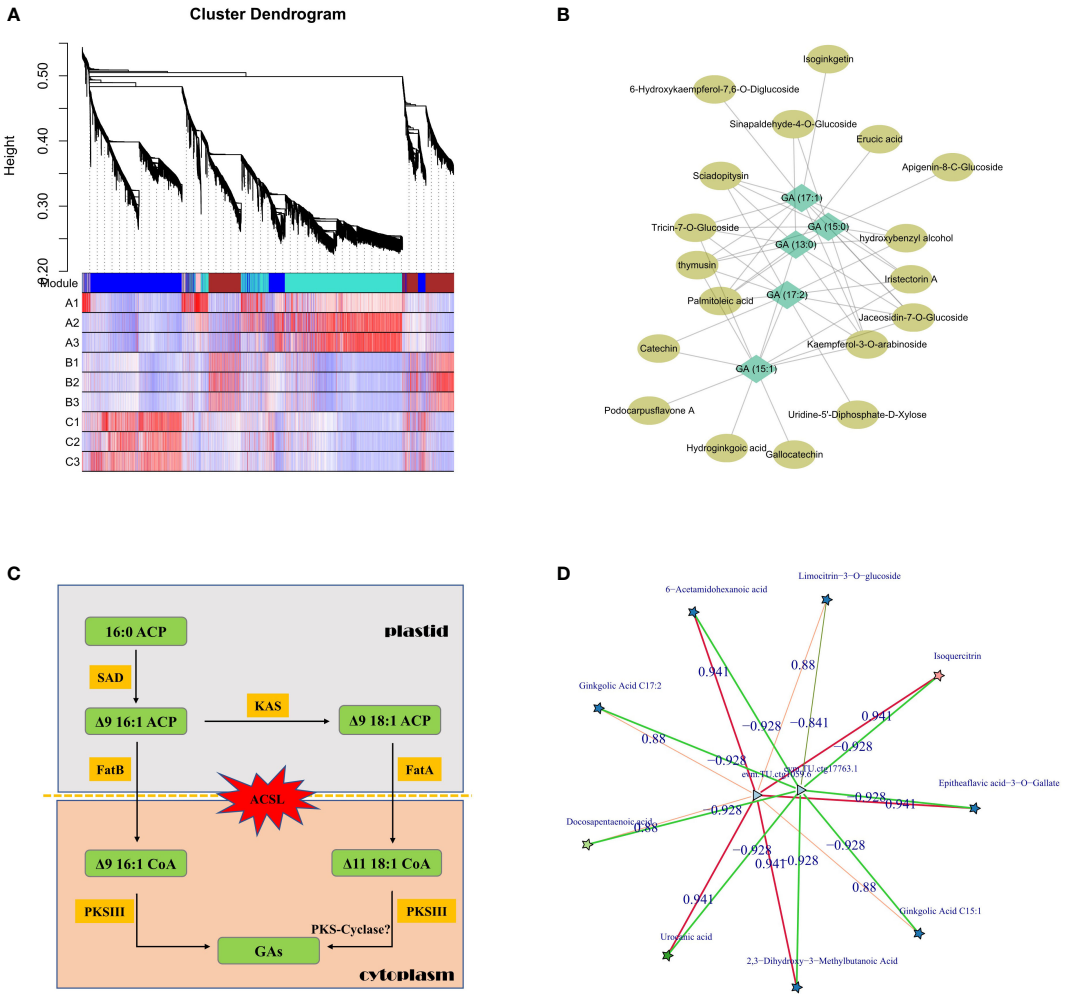

FIGURE 5
Regulation of GA synthesis in GBS; **(A)** Clustering and co-expression results of all metabolites based on WGCNA method; **(B)** Correlation network diagram of GAs and other representative metabolites; **(C)** Inferred pathway and related genes involved in GAs synthesis in plastid and cytoplasm. Genes of the ACSL family, which are responsible for transmembrane transport, underwent a significant intron length expansion; **(D)** Co-expression network of candidate essential genes involved in the regulation of GA synthesis based on transcriptome and metabolome. Stars represent metabolites and triangles represent genes. The red and green lines represent positive and negative correlations, respectively.

metabolites along with several flavonoid derivatives (Figure 5B). Subsequently, we mainly focused on metabolic pathways for further analysis using homologous comparison and literature mining. According to previous studies, the aromatic ring and long-chain alkyl/alkenyl group of GAs are thought to be synthesized by steps that could be divided into two parts: 1. the synthesis of free palmoleyl CoA and oleyl CoA generated from malonyl CoA/acetyl CoA based on fatty acid synthesis; 2. the synthesis of GAs from long-chain oleyl CoA using polyketides (Gellerman et al., 1976).

The synthesis of GAs is based on palmitoleic acid and oleic acid, which initially contain the necessary alkyl side chains, and the levels of both metabolites were significantly altered in our study. In this process, acyl carrier protein (ACP) is the center of fatty acid synthesis as an intermediate conserved carrier, and stearoyl-ACP desaturase (SAD) protein is a key rate-limiting enzyme in this process. It is a homodimer composed of conserved domains belonging to the ferritin family, and is the only known soluble desaturase group in plants which could regulate the ratio of saturated fatty acids (Knutzon et al., 1992). According to our results, six genes encoding SAD protein were identified in GBS, and analysis of their expression patterns showed that four of them had significantly higher expression in June than in August, while the other two genes remained relatively stable. Association analysis with the metabolome further revealed that one of them was highly positively correlated with GA (15:1) and GA (17:2) content changes. Beta-ketoacyl-ACP synthase (KAS) is another important enzyme in this process, and it is the core element of the fatty acid synthase (FAS) complex, which could catalyze the condensation of malonyl-ACP and palmitic acid to long-chain fatty acids (Mindrebo et al., 2020). A total of nine genes encoding for KAS were identified in GBS, and two of them showed a significant correlation with the variation in GA content. Chromosomal mapping of these genes revealed that four of them were distributed in obvious clusters on chromosome 6, and one of them was not only an important regulator of GA synthesis, but also highly correlated with the synthesis of other metabolites, such as isoquercitrin, which is a typical compound of flavonoids.

The next key step in the synthesis of GAs is the formation of the phenol-lipid benzene ring. After obtaining the main long-chain fatty acid precursor, several condensation reactions would occur to generate different types of GAs, and type III polyketide synthase protein (PKS III) is the key rate-limiting enzyme. PKS III is characterized by its ability to reuse homologous proteins and to react directly with acyl-CoA substrates independently of ACP activation (Yu et al., 2012). Many members have been identified in this family, of which chalcone synthase (CHS), stilbene synthase (STS), and FAE1-type keto-acyl CoA synthase (KCS) are their typical representatives. Chalcone is an important precursor of flavonoid synthesis and the CHS family is widely distributed in plants, while STS is highly homologous to CHS with amino acid sequence similarity of nearly 70% and could form resveratrol from coumaryl CoA (Schroder and Schroder, 1990). KCS is a rate-limiting enzyme that catalyzes the first step condensation reaction in the synthesis of very long chain fatty acids (VLCFAs), and the studies on the KCS family have been mainly in model plants with few studies in other species (Sagar et al., 2015). According to our results, a total of 31 genes encoding PKS III were identified in GBS, including 15 genes encoding KCS, and several of them had the consistent expression pattern with GAs. Surprisingly, although previous studies on the synthesis of phenolic acids in other species showed that PKS-Cyclase might play a key role in the formation of phenyl rings, and then catalyze the reaction between hydrogen ions and ketone groups similar to the aldol condensation in order to form double bonds (Nakano et al., 2009), not even one gene encoding PKS-Cyclase was found in GBS according to the homology comparison in this study (Figure 5C).

In addition to analyzing the key genes and enzymes of GA synthesis based on metabolic pathways, other associated regulatory factors were also investigated based on the co-expression network. Through rigorous screening, two differentially expressed genes (DEGs) were identified that were most highly correlated with GAs (Figure 5D). Functional annotation of these two genes showed one putative annotation for GDSL esterase, and the other one had an unknown annotation. The encoded protein of this unannotated gene showed very low conservation with other species, indicating that it should be a Ginkgo-specific gene involved in GA synthesis. Lipase is one of the key enzymes in seed oil degradation, which includes GDSL esterase because of its highly conserved glycine (G)-aspartic acid (D)-serine (S)-leucine (L) motif at the N-terminus of the protein. GDSL esterases are widely distributed in plants with diverse members, but only a few of them have been identified with clear molecular functions (Lai et al., 2017). A study in *Arabidopsis* has confirmed that several GDSL esterases could alter the fatty acid composition of seeds by acting downstream of the gibberellin signaling pathway, which is also consistent with our results (Chen et al., 2012).

Fatty acids from exogenous or endogenous sources must first be activated to form acyl-CoA before entering most metabolic pathways. This activation step is catalyzed by acyl-CoA synthase (ACS) through a two-step reaction involving the formation of the intermediate fatty acyl-AMP with the release of pyrophosphate, and the formation of fatty acyl-CoA to release AMP (Mashek et al., 2004). In *G. biloba*, nearly 30 members have been identified encoding ACSs distributed on different chromosomes, including the long-chain ACSs (ACSL) that preferentially activate the most abundant fatty acids including GAs (12-20 carbons) (Figure 6A). Surprisingly, more than 50% of the *GbACSL* genes in GBS were extremely long, with the average length of all ACSL genes reaching 73 Kbp and the longest even reaching 418 Kbp. The length of these genes was much longer than other genes related to GA synthesis, whose average length was less than 3 Kbp (Figure 5B). Further analysis showed that introns instead of exons were surprisingly elongated among these genes, and transposable elements might play an important role in their intron elongation. Meanwhile, it should be mentioned that these non-TE regions also accounted for a large proportion, which might be composed of some other decayed elements (Figure 6C). Interestingly, the integration analysis results showed that these large introns did not seem to impose a burden on the transcription of these *GbACSL* genes, and on the contrary, the expression of these genes was significantly increased (Figure 6D). In addition, the expression patterns of these large genes appeared to be more stable, maintaining a conserved expression pattern and largely unaffected by period changes, as further confirmed by subsequent

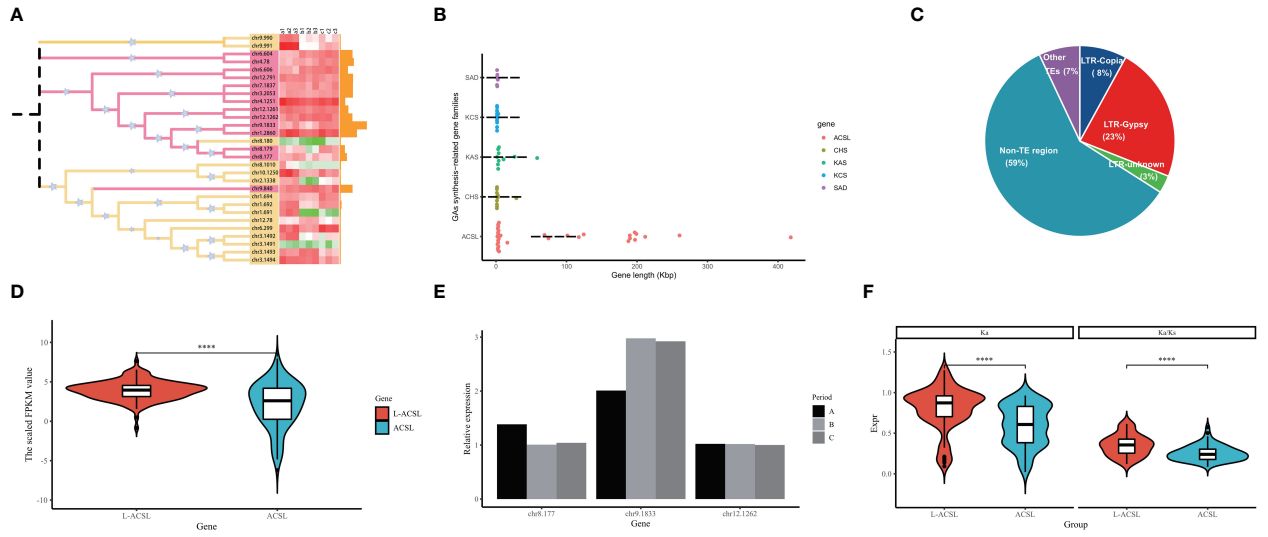

FIGURE 6
Analysis results of the ACSL gene family in GBS; **(A)** Phylogenetic tree and expression pattern of all ACSL gene family members in GBS. The heatmap represents the FPKM values of all samples in three time periods, and the bar chart represents the length of each gene; **(B)** Length distribution of *GbACSL* and other GA synthesis-related gene family members; **(C)** Detailed composition of the intron regions of *GbACSL* gene members; **(D)** Violin plot of the expression of *GbACSL* genes with and without large introns; **(E)** Expression results of *GbACSL* genes with large introns validated by RT-PCR experiments; **(F)** Ka/Ks results for *GbACSL* genes with and without large introns. **** p value < 0.0001.

qRT-PCR experimental validation of our RNA-seq results (Figure 6E).The selection pressure analysis results of these *GbACSL* genes were consistent with the expression patterns, and genes with large introns tended to have higher Ka/Ks values for positive selection (Figure 6F).

3.4 Co-expression analysis for precursors of terpene trilactone synthesis in GBS

According to the co-expression results based on metabolome and transcriptome, all types of unique terpene trilactones identified in GBS were successfully correlated with the gene expression profile, except for Ginkgolide K due to its extremely low content (Figure 7A). Two major biosynthetic pathways of terpene trilactones in *G. biloba* could be identified, including the mevalonate pathway (MVA) in the cytoplasm and the 2-C-methyl-D-erythritol-4-phosphate pathway (MEP) in the plastid. It is generally concluded that the biosynthesis of various ginkgolides is mainly through the MEP pathway, while the biosynthesis of the sesquiterpene (bilobalide) is achieved through the MVA pathway, or it may be the degradation product of ginkgolides (Penuelas and Munne-Bosch, 2005). HMGR (3-hydroxy-3-methylglutaryl coenzyme A reductase) is the first rate-limiting enzyme in the MVA pathway of terpenoid synthesis. It could catalyze 3-hydroxy-3-methylglutaryl-CoA to obtain mevalonate, which is an important precursor of terpenoid synthesis. Previous studies showed that the gene family encoding HMGR in other plants was generally small (Kim et al., 2014). Meanwhile, more than 10 members of the HMGR family were identified in GBS based on homology comparison, which was also the largest number of gene families related to terpenoid synthesis in GBS. Most of these genes were distributed in a typical cluster arrangement on chromosome 9 and chromosome 4. On the other hand, despite the large number of members, only a few HMGR genes were significantly positively correlated with terpene trilactone levels in both periods based on the results of co-expression analysis (Figure 7B). DXS (1-deoxy-D-xylulose-5-phosphate synthase) is the first enzyme in the MEP synthesis pathway. It catalyzes pyruvate and glyceraldehyde-3-phosphate to synthesize 1-deoxy-D-xylulose-5-phosphate, and also plays a critical role in terpenoid metabolism as a major rate-limiting enzyme (Estevez et al., 2001). In GBS, four genes encoding DXS were identified, one of which showed a high and stable expression level. Similar to the results of *GbACSL*, this highly expressed gene also had a very long length of 122 Kbp as well, including two large introns with the length of 48 Kbp and 70 Kbp respectively, which was the longest one among all rate-limiting genes involved in the synthesis of ginkgo terpenoids. Then, these highly associated genes obtained from previous co-expression predictions were further annotated, and the results showed that these genes seemed to be closely associated with seed and embryo development in addition to their active involvement in terpene biosynthesis (Figure 7C).

Farnesyl diphosphate synthase (FPS) is another key enzyme in this pathway with two aspartic acid-rich regions. It catalyzes the condensation reaction of two molecules of isopentenyl pyrophosphate (IPP) and one molecule of dimethylallyl pyrophosphate (DMAPP) to (2Z, 6E)-farnesyl diphosphate, which could provide the C15 scaffold for sesquiterpenoid formation (Estevez et al., 2001). Although only one gene encoding FPS was identified, this large gene length of more than 109 Kbp still maintained high expression. The corresponding enzyme of FPS is geranylgeranyl diphosphate synthase (GGPPS) in the MEP pathway, which could catalyze three molecules of IPP and one

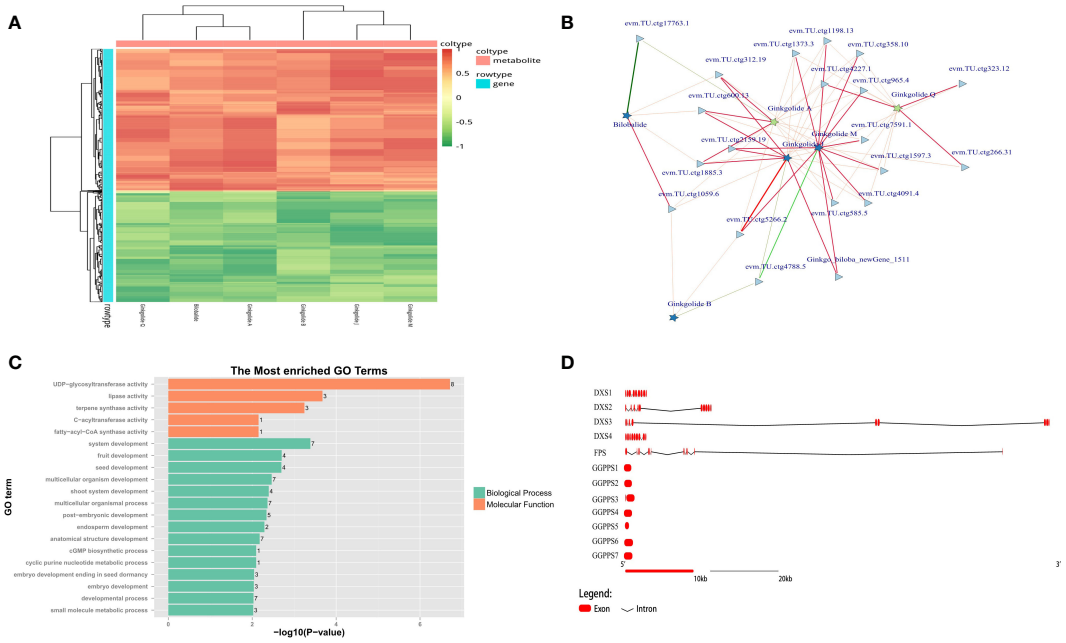

FIGURE 7
Mining results of terpene trilactone co-expression data in GBS; **(A)** Co-expression heatmap of the terpene trilactones identified in GBS and all genes; **(B)** Association network of ginkgo terpene trilactones and the essential genes based on Spearman's correlation coefficient. The red and green lines represent positive and negative correlation, respectively, and the width of the lines indicates the strength of the correlation; **(C)** Functional annotation results of the extracted essential genes closely related to terpenoid synthesis in GBS; **(D)** Gene structure diagram of the genes involved in terpene trilactone synthesis in GBS.

molecule of DMAPP to form geranylgeranyl diphosphate (GGPP), providing the C20 backbone for diterpenoid formation (Schmidt and Gershenzon, 2007). GGPPS is not only involved in the synthesis of ginkgolides, but also closely related to the synthesis of chlorophyll, carotenoids and gibberellins. Seven members encoding GGPPS were identified, and none of them was a large gene with an average length of less than 2 Kbp and an intronless structure (Figure 7D). According to our results, there seemed to be a delicate balance between the number and the length of genes in GGPPS and FPS that shared similar functions.

4 Discussion

As a unique secondary metabolite of *G. biloba*, the rich content of ginkgo phenolic acids in GBS is difficult to ignore for their strong sensitizing toxicity and cytotoxicity. Due to the significant antibacterial properties of GAs, including the inhibition of a variety of gram-negative and positive bacteria, rice blast fungus and other fungi, as well as the inhibition of aphids, cabbage caterpillars and other insects, GAs have the potential to be developed as biological pesticides (Muroi and Kubo, 1996; Pan et al., 2006a). Meanwhile, compared with flavonoids in *G. biloba* with clear pharmacological activities, the biosynthesis and regulatory mechanism together with the derivative efficacy of GAs have not been thoroughly studied, which severely limits their effective utilization. More than 30,000 tons of the GBS testa would be discarded each year during the production process of Ginkgo-related remedies, which not only pollutes the environment but also causes a great waste of resources (Boateng, 2022). The unique terpenoids of *G. biloba* also had the same doubts about the detailed biosynthesis and regulation mechanisms. The synthesis of terpene trilactones in GBS involves oxidation, cyclization, and rearrangement reactions, resulting in their complex structures, making their analysis lag behind that of other metabolites (Ding et al., 2008).

In this study, based on multi-omics analysis and functional validation, we systematically analyzed the phonological changes and synthetic pathways related to GAs and terpenoids in GBS, focusing on their major rate-limiting enzyme families. Analysis of the expression patterns and chromosome mapping of these genes further revealed that most of them were arranged in clusters, and the role of large introns in their expression should be paid more attention. Recent studies have shown that cytochrome P450 (CYP450) enzymes may play an important role in the downstream synthesis of terpene trilactones (Zheng et al., 2019). According to the homologous alignment results, a very large and complex group of CYP450 family and the complete loss of PKS-Cyclase in GBS suggested that there might be a unique aldol condensation reaction in the downstream synthesis process of GAs.

The heterogeneous distribution of large genes was observed during the analysis of genes related to secondary metabolite synthesis in GBS, and the enrichment was most significant in the *GbACSL* gene family. The length of these large genes exceeded the range of most plant genes, and further analysis revealed that intron elongation played an essential role. Combined with the existing features of the Ginkgo genome, a considerable number of LTR-RTs insertion events were identified in *G. biloba* and other gymnosperm genomes, which may provide some explanation for the dramatic

increase in the length of Ginkgo introns (Liu et al., 2021). On the other hand, it is worth considering whether these intron-lengthening genes were simply randomly generated by violent transposable element insertions. From the point of view of energy consumption, the retention of large introns means the additional loss of energy during replication and transcription. For a large 100 Kb intron, it would be a million times harder to bring its ends together than for a 1 Kb intron in length, and a stretched 100 Kb RNA could even expand to a size larger than that of the mammalian nucleus (Shepard et al., 2009). It could be easily deduced that introns should have several advantages to compensate for these costly disadvantages, and the current results clearly showed that the significant increase in intron size is not meaningless and would lead to a stable high expression during transcription in GBS. Moreover, compared with Arabidopsis and other angiosperms, no whole genome duplication (WGD) event could be identified in Ginkgo or other gymnosperms, although this event should be a cornerstone of genome evolution in angiosperms (Clark and Donoghue, 2018), and genes with large introns in GBS showed functional enrichment along with higher positive selection pressure. These results suggest that large genes in *G. biloba* may tend to acquire their own introns independently, and the proportion of large introns in these families may be an effective indicator of their preference for environmental adaptation.

Combined with our current results, we believe it's very possible that these large genes may further promote the growth or environmental adaptation of *G. biloba*. As for the typical large *GbACSL* gene family in this study, due to the key role of lipids in cell growth and energy metabolism, higher expression of this family, which is responsible for the acetylation of all C12-20 members of lipids, may not only be involved in the precursor synthesis of GAs, but also plays an essential role in the formation of plant signal transducers and other lipid-related molecules. Another typical example is the GGPPS and FPS gene families in terpenoid synthesis. These two families have similar functions and both use IPP and DMAPP as substrates, and the emergence of large genes seems to lead these two families to different paths in the selection of gene length and gene number. On the other hand, how to explain the significant positive correlation between these large introns and gene expression remains an unresolved doubt. We speculated that one possibility is the high-frequency occurrence of intron-mediated enhancement (IME), which has also been observed in Arabidopsis and several other plants (Gallegos and Rose, 2015). Meanwhile, it should be mentioned that these enlarged introns had no particular positional preference in the ginkgo genes, whereas IME usually occurs at the first intron, suggesting that a novel mechanism may regulate gene expression in *G. biloba*, and more multi-omics data would be obtained in our subsequent work to unravel this mystery.

Conclusion

In this study, the global metabolite landscape of GBS throughout the almost complete growth cycle was revealed by UPLC-MS/MS platform, and the anabolic regulation mechanism of the unique GAs and terpene trilactones in GBS was systematically analyzed by integrating metabolomics, transcriptomics and other multi-omics data. Most members of the key rate-limiting enzymes within the synthetic pathways of these secondary metabolites were successfully identified along with several important regulatory factors. In addition, large introns seemed to play a very important role in the expression of genes related to secondary synthesis and metabolism in GBS.

Data availability statement

The original contributions presented in the study are publicly available. This data can be found here: NCBI Bioproject, accession PRJNA973135.

Author contributions

PC and HL conceived and designed the experiments. BH and XH analyzed the data and wrote the paper. KQ and JL performed the experimental validation and data calibration. L-AX modified the manuscript and QZ curated the experimental validation data. All authors contributed to the article and approved the submitted version.

Funding

This research was funded by Fundamental Research Funds for Central Non-profit Scientific Institution (Y2020PT25), National Natural Science Foundation of China (31902064), and Guangdong Basic and Applied Basic Research Foundation (2019A1515111150).

Conflict of interest

The authors declare that the research was conducted in the absence of any commercial or financial relationships that could be construed as a potential conflict of interest.

Publisher's note

Supplementary material

The Supplementary Material for this article can be found online at: https://www.frontiersin.org/articles/10.3389/fpls.2023.1196609/full#supplementary-material

SUPPLEMENTARY FILE 1
The primer information of related genes for qRT-PCR.

References

Atzori, C., Bruno, A., Chichino, G., Bombardelli, E., Scaglia, M., and Ghione, M. (1993). Activity of bilobalide, a sesquiterpene from ginkgo biloba, on pneumocystis carinii. *Antimicrob. Agents Chemother.* 37, 1492–1496. doi: 10.1128/AAC.37.7.1492

Baek, S. H., Lee, J. H., Kim, C., Ko, J. H., Ryu, S. H., Lee, S. G., et al. (2017). Ginkgolic acid c 17:1, derived from ginkgo biloba leaves, suppresses constitutive and inducible STAT3 activation through induction of PTEN and SHP-1 tyrosine phosphatase. *Molecules* 22 (2), 276. doi: 10.3390/molecules22020276

Bhatia, S. P., Wellington, G. A., Cocchiara, J., Lalko, J., Letizia, C. S., and Api, A. M. (2007). Fragrance material review on methyl cinnamate. *Food Chem. Toxicol.* 45, S113–S119. doi: 10.1016/j.fct.2007.09.077

Boateng, I. D. (2022). A critical review of current technologies used to reduce ginkgotoxin, ginkgotoxin-5'-glucoside, ginkgolic acid, allergic glycoprotein, and cyanide in ginkgo biloba l. *seed. Food Chem.* 382, 132408. doi: 10.1016/j.foodchem.2022.132408

Cartayrade, A., Neau, E., Sohier, C., Balz, J. P., Carde, J. P., and Walter, J. (1997). Ginkgolide and bilobalide biosynthesis in ginkgo biloba .1. sites of synthesis, translocation and accumulation of ginkgolides and bilobalide. *Plant Physiol. Bioch* 35, 859–868.

Chen, M., Du, X., Zhu, Y., Wang, Z., Hua, S., Li, Z., et al. (2012). Seed fatty acid reducer acts downstream of gibberellin signalling pathway to lower seed fatty acid storage in arabidopsis. *Plant Cell Environ.* 35, 2155–2169. doi: 10.1111/j.1365-3040.2012.02546.x

Chen, S. F., Zhou, Y. Q., Chen, Y. R., and Gu, J. (2018). Fastp: an ultra-fast all-in-one FASTQ preprocessor. *Bioinformatics* 34, 884–890. doi: 10.1093/bioinformatics/bty560

Clark, J. W., and Donoghue, P. C. J. (2018). Whole-genome duplication and plant macroevolution. *Trends Plant Sci.* 23, 933–945. doi: 10.1016/j.tplants.2018.07.006

Ding, S., Dudley, E., Song, Q., Plummer, S., Tang, J., Newton, R. P., et al. (2008). Mass spectrometry analysis of terpene lactones in ginkgo biloba. *Rapid Commun. Mass Spectrom* 22, 766–772. doi: 10.1002/rcm.3424

Estevez, J. M., Cantero, A., Reindl, A., Reichler, S., and Leon, P. (2001). 1-Deoxy-D-xylulose-5-phosphate synthase, a limiting enzyme for plastidic isoprenoid biosynthesis in plants. *J. Biol. Chem.* 276, 22901–22909. doi: 10.1074/jbc.M100854200

Fukuda, I., Ito, A., Hirai, G., Nishimura, S., Kawasaki, H., Saitoh, H., et al. (2009). Ginkgolic acid inhibits protein SUMOylation by blocking formation of the E1-SUMO intermediate. *Chem. Biol.* 16, 133–140. doi: 10.1016/j.chembiol.2009.01.009

Gallegos, J. E., and Rose, A. B. (2015). The enduring mystery of intron-mediated enhancement. *Plant Sci.* 237, 8–15. doi: 10.1016/j.plantsci.2015.04.017

Gellerman, J. L., Anderson, W. H., and Schlenk, H. (1976). Synthesis of anacardic acids in seeds of ginkgo biloba. *Biochim. Biophys. Acta* 431, 16–21. doi: 10.1016/0005-2760(76)90255-1

Gulec, M., Iraz, M., Yilmaz, H. R., Ozyurt, H., and Temel, I. (2006). The effects of ginkgo biloba extract on tissue adenosine deaminase, xanthine oxidase, myeloperoxidase, malondialdehyde, and nitric oxide in cisplatin-induced nephrotoxicity. *Toxicol. Ind. Health* 22, 125–130. doi: 10.1191/0748233705th255oa

Han, X., He, B., Xin, Y., Xu, M., and Xu, L. A. (2021). Full-length sequencing of ginkgo biloba l. reveals the synthesis of terpenoids during seed development. *Ind. Crop Prod.* 170, 113714. doi: 10.1016/j.indcrop.2021.113714

He, B., Gu, Y. C., Xu, M., Wang, J. W., Cao, F. L., and Xu, L. A. (2015). Transcriptome analysis of ginkgo biloba kernels. *Front. Plant Sci.* 6, 113434. doi: 10.3389/fpls.2015.00819

He, B., Liu, H. L., Han, X., Cui, P., and Xu, L. A. (2021). Multi-omics analysis of ginkgo biloba preliminarily reveals the co-regulatory mechanism between stilbenes and flavonoids. *Ind. Crop Prod* 167. doi: 10.1016/j.indcrop.2021.113434

Jiang, L., Si, Z. H., Li, M. H., Zhao, H., Fu, Y. H., Xing, Y. X., et al. (2017). H-1 NMR-based metabolomics study of liver damage induced by ginkgolic acid (15:1) in mice. *J. Pharmaceut. BioMed.* 136, 44–54. doi: 10.1016/j.jpba.2016.12.033

Kim, Y. J., Lee, O. R., Oh, J. Y., Jang, M. G., and Yang, D. C. (2014). Functional analysis of 3-hydroxy-3-methylglutaryl coenzyme a reductase encoding genes in triterpene saponin-producing ginseng. *Plant Physiol.* 165, 373–387. doi: 10.1104/pp.113.222596

Kim, D., Paggi, J. M., Park, C., Bennett, C., and Salzberg, S. L. (2019). Graph-based genome alignment and genotyping with HISAT2 and HISAT-genotype. *Nat. Biotechnol.* 37, 907. doi: 10.1038/s41587-019-0201-4

Knutzon, D. S., Thompson, G. A., Radke, S. E., Johnson, W. B., Knauf, V. C., and Kridl, J. C. (1992). Modification of brassica seed oil by antisense expression of a stearoyl-acyl carrier protein desaturase gene. *Proc. Natl. Acad. Sci. U.S.A.* 89, 2624–2628. doi: 10.1073/pnas.89.7.2624

Kobayashi, D., Yoshimura, T., Johno, A., Ishikawa, M., Sasaki, K., and Wada, K. (2015). Decrease in pyridoxal-5 '-phosphate concentration and increase in pyridoxal concentration in rat plasma by 4 '-o-methylpyridoxine administration. *Nutr. Res.* 35, 637–642. doi: 10.1016/j.nutres.2015.05.015

Lai, C. P., Huang, L. M., Chen, L. O., Chan, M. T., and Shaw, J. F. (2017). Genome-wide analysis of GDSL-type esterases/lipases in arabidopsis. *Plant Mol. Biol.* 95, 181–197. doi: 10.1007/s11103-017-0648-y

Langfelder, P., and Horvath, S. (2008). WGCNA: an r package for weighted correlation network analysis. *BMC Bioinf.* 9, 559. doi: 10.1186/1471-2105-9-559

Lee, J. S., Cho, Y. S., Park, F. J., Kim, J., Oh, W. K., Lee, H. S., et al. (1998). Phospholipase c gamma 1 inhibitory principles from the sarcotestas of ginkgo biloba. *J. Nat. Prod* 61, 867–871. doi: 10.1021/np970367q

Leistner, E., and Drewke, C. (2010). Ginkgo biloba and ginkgotoxin. *J. Nat. Prod* 73, 86–92. doi: 10.1021/np9005019

Li, B., Neumann, E. K., Ge, J. Y., Gao, W., Yang, H., Li, P., et al. (2018). Interrogation of spatial metabolome of ginkgo biloba with high-resolution matrix-assisted laser desorption/ionization and laser desorption/ionization mass spectrometry imaging. *Plant Cell Environ.* 41, 2693–2703. doi: 10.1111/pce.13395

Liu, H. L., Wang, X. B., Wang, G. B., Cui, P., Wu, S. G., Ai, C., et al. (2021). The nearly complete genome of ginkgo biloba illuminates gymnosperm evolution. *Nat. Plants* 7, 748. doi: 10.1038/s41477-021-00933-x

Love, M. I., Huber, W., and Anders, S. (2014). Moderated estimation of fold change and dispersion for RNA-seq data with DESeq2. *Genome Biol.* 15, 550. doi: 10.1186/s13059-014-0550-8

Mahadevan, S., and Park, Y. (2008). Multifaceted therapeutic benefits of ginkgo biloba l.: chemistry, efficacy, safety, and uses. *J. Food Sci.* 73, R14–R19. doi: 10.1111/j.1750-3841.2007.00597.x

Mashek, D. G., Bornfeldt, K. E., Coleman, R. A., Berger, J., Bernlohr, D. A., Black, P., et al. (2004). Revised nomenclature for the mammalian long-chain acyl-CoA synthetase gene family. *J. Lipid Res.* 45, 1958–1961. doi: 10.1194/jlr.E400002-JLR200

Mei, N., Guo, X., Ren, Z., Kobayashi, D., Wada, K., and Guo, L. (2017). Review of ginkgo biloba-induced toxicity, from experimental studies to human case reports. *J. Environ. Sci. Health C Environ. Carcinog Ecotoxicol Rev.* 35, 1–28. doi: 10.1080/10590501.2016.1278298

Mindrebo, J. T., Patel, A., Kim, W. E., Dayis, T. D., Chen, A. C., Bartholow, T. G., et al. (2020). Gating mechanism of elongating beta-ketoacyl-ACP synthases. *Nat. Commun.* 11, 1727. doi: 10.1038/s41467-020-15455-x

Muroi, H., and Kubo, I. (1996). Antibacterial activity of anacardic acid and totarol, alone and in combination with methicillin, against methicillin-resistant staphylococcus aureus. *J. Appl. Bacteriol* 80, 387–394. doi: 10.1111/j.1365-2672.1996.tb03233.x

Nabavi, S. M., and Silva, A. S. (2019). *Nonvitamin and nonmineral nutritional supplements* (San Diego, CA, United States: Academic Press, London, United Kingdom).

Nakano, C., Ozawa, H., Akanuma, G., Funa, N., and Horinouchi, S. (2009). Biosynthesis of aliphatic polyketides by type III polyketide synthase and methyltransferase in bacillus subtilis. *J. Bacteriol* 191, 4916–4923. doi: 10.1128/JB.00407-09

Narnoliya, L. K., Kaushal, G., Singh, S. P., and Sangwan, R. S. (2017). *De novo* transcriptome analysis of rose-scented geranium provides insights into the metabolic specificity of terpene and tartaric acid biosynthesis. *BMC Genomics* 18, 74. doi: 10.1186/s12864-016-3437-0

Ou, S., Su, W., Liao, Y., Chougule, K., Agda, J. R. A., Hellinga, A. J., et al. (2019). Benchmarking transposable element annotation methods for creation of a streamlined, comprehensive pipeline. *Genome Biol.* 20, 275. doi: 10.1186/s13059-019-1905-y

Pan, W., Luo, P., Fu, R., Gao, P., Long, Z., Xu, F., et al. (2006). Acaricidal activity against panonychus citri of a ginkgolic acid from the external seed coat of ginkgo biloba. *Pest Manag Sci.* 62, 283–287. doi: 10.1002/ps.1152

Penuelas, J., and Munne-Bosch, S. (2005). Isoprenoids: an evolutionary pool for photoprotection. *Trends Plant Sci.* 10, 166–169. doi: 10.1016/j.tplants.2005.02.005

Pertea, M., Pertea, G. M., Antonescu, C. M., Chang, T. C., Mendell, J. T., and Salzberg, S. L. (2015). StringTie enables improved reconstruction of a transcriptome from RNA-seq reads. *Nat. Biotechnol.* 33, 290. doi: 10.1038/nbt.3122

Rodriguez, M., Ringstad, L., Schafer, P., Just, S., Hofer, H. W., Malmsten, M., et al. (2007). Reduction of atherosclerotic nanoplaque formation and size by ginkgo biloba (EGb 761) in cardiovascular high-risk patients. *Atherosclerosis* 192, 438–444. doi: 10.1016/j.atherosclerosis.2007.02.021

Sagar, M., Pandey, N., Qamar, N., Singh, B., and Shukla, A. (2015). Domain analysis of 3 keto acyl-CoA synthase for structural variations in vitis vinifera and oryza brachyantha using comparative modelling. *Interdiscip Sci.* 7, 7–20. doi: 10.1007/s12539-013-0017-8

Sasaki, Y., Noguchi, T., Yamamoto, E., Giddings, J. C., Ikeda, K., Yamori, Y., et al. (2002). Effects of ginkgo biloba extract (EGb 761) on cerebral thrombosis and blood pressure in stroke-prone spontaneously hypertensive rats. *Clin. Exp. Pharmacol.* 29, 963–967. doi: 10.1046/j.1440-1681.2002.03761.x

Schmidt, A., and Gershenzon, J. (2007). Cloning and characterization of isoprenyl diphosphate synthases with farnesyl diphosphate and geranylgeranyl diphosphate synthase activity from Norway spruce (Picea abies) and their relation to induced oleoresin formation. *Phytochemistry* 68, 2649–2659. doi: 10.1016/j.phytochem.2007.05.037

Schroder, J., and Schroder, G. (1990). Stilbene and chalcone synthases: related enzymes with key functions in plant-specific pathways. *Z Naturforsch. C J. Biosci.* 45, 1–8. doi: 10.1515/znc-1990-1-202

Shepard, S., McCreary, M., and Fedorov, A. (2009). The peculiarities of large intron splicing in animals. *PloS One* 4, e7853. doi: 10.1371/journal.pone.0007853

Thevenot, E. A., Roux, A., Xu, Y., Ezan, E., and Junot, C. (2015). Analysis of the human adult urinary metabolome variations with age, body mass index, and gender by implementing a comprehensive workflow for univariate and OPLS statistical analyses. *J. Proteome Res.* 14, 3322–3335. doi: 10.1021/acs.jproteome.5b00354

Thissen, D., Steinberg, L., and Kuang, D. (2002). Quick and easy implementation of the benjamini-hochberg procedure for controlling the false positive rate in multiple comparisons. *J. Educ. Behav. Stat.* 27, 77–83. doi: 10.3102/10769986027001077

van Beek, T. A. (2002). Chemical analysis of ginkgo biloba leaves and extracts. *J. Chromatogr A* 967, 21–55. doi: 10.1016/S0021-9673(02)00172-3

van Beek, T. A. (2005). Ginkgolides and bilobalide: their physical, chromatographic and spectroscopic properties. *Bioorgan Med. Chem.* 13, 5001–5012. doi: 10.1016/j.bmc.2005.05.056

Wang, D., Zhang, Y., Zhang, Z., Zhu, J., and Yu, J. (2010). KaKs_Calculator 2.0: a toolkit incorporating gamma-series methods and sliding window strategies. *Genomics Proteomics Bioinf.* 8, 77–80. doi: 10.1016/S1672-0229(10)60008-3

Yang, Y. F., Li, Y., Wang, J. H., Sun, K., Tao, W. Y., Wang, Z. Z., et al. (2017). Systematic investigation of ginkgo biloba leaves for treating cardio-cerebrovascular diseases in an animal model. *ACS Chem. Biol.* 12, 1363–1372. doi: 10.1021/acschembio.6b00762

Yang, X. M., Wang, Y. F., Li, Y. Y., and Ma, H. L. (2014). Thermal stability of ginkgolic acids from ginkgo biloba and the effects of ginkgol C17:1 on the apoptosis and migration of SMMC7721 cells. *Fitoterapia* 98, 66–76. doi: 10.1016/j.fitote.2014.07.003

Ye, J. B., Mao, D., Cheng, S. Y., Zhang, X., Tan, J. P., Zheng, J. R., et al. (2020). Comparative transcriptome analysis reveals the potential stimulatory mechanism of terpene trilactone biosynthesis by exogenous salicylic acid in ginkgo biloba. *Ind. Crop Prod* 145, 112104. doi: 10.1016/j.indcrop.2020.112104

Yu, D. Y., Xu, F. C., Zeng, J., and Zhan, J. X. (2012). Type III polyketide synthases in natural product biosynthesis. *IUBMB Life* 64, 285–295. doi: 10.1002/iub.1005

Zheng, X., Li, P., and Lu, X. (2019). Research advances in cytochrome P450-catalysed pharmaceutical terpenoid biosynthesis in plants. *J. Exp. Bot.* 70, 4619–4630. doi: 10.1093/jxb/erz203

Zhou, J. M., and Ibrahim, R. K. (2010). Tricin-a potential multifunctional nutraceutical. *Phytochem. Rev.* 9, 413–424. doi: 10.1007/s11101-009-9161-5

Zhou, Z., and Zheng, S. (2003). The missing link in ginkgo evolution. *Nature* 423, 821–822. doi: 10.1038/423821a

frontiers | Frontiers in Pharmacology

TYPE Original Research
PUBLISHED 29 June 2023
DOI 10.3389/fphar.2023.1224906

OPEN ACCESS

EDITED BY
Zhou Yuan,
Huazhong University of Science and Technology, China

REVIEWED BY
Jun Lu,
Chengdu University of Traditional Chinese Medicine, China
Vikram Kumar,
Amity University Jaipur, India
Weiguang Sun,
Huazhong University of Science and Technology, China

*CORRESPONDENCE
Zhengzhi Wu,
szwzz001@163.com

†These authors have contributed equally to this work and share first authorship

RECEIVED 18 May 2023
ACCEPTED 19 June 2023
PUBLISHED 29 June 2023

CITATION
Li Z, Yan X, Wei J, Pu L, Zhu G, Cao Y, Liu Z, Liu Y, Li Y, Li L, Li X and Wu Z (2023), A novel colchicine-myricetin heterozygous molecule: design, synthesis, and effective evaluations on the pathological models of acute lung injury *in vitro* and *in vivo*. *Front. Pharmacol.* 14:1224906. doi: 10.3389/fphar.2023.1224906

A novel colchicine-myricetin heterozygous molecule: design, synthesis, and effective evaluations on the pathological models of acute lung injury *in vitro* and *in vivo*

Zhiyue Li[1,2,3†], Xueqin Yan[1,2†], Jiangchun Wei[1,2†], Liuyang Pu[1], Guanbao Zhu[1,4], Yongkai Cao[1], Zhanyan Liu[1], Yaqian Liu[1], Yan Li[1], Limin Li[1], Xinping Li[1] and Zhengzhi Wu[1,2*]

[1]Shenzhen Institute of Translational Medicine, The First Affiliated Hospital of Shenzhen University, Shenzhen, China, [2]Wu Zhengzhi Academician Workstation, Ningbo College of Health Sciences, Ningbo, China, [3]Shenzhen Institute of Advanced Technology, Chinese Academy of Sciences, Shenzhen, China, [4]Graduate School, Guangxi University of Chinese Medicine, Nanning, China

Acute lung injury (ALI) is an inflammatory condition and there are no effective treatments. A novel new compound----colchicine-myricetin hybrid (CMyrH) was herein designed and synthesized. To evaluate the activity of CMyrH in ALI, we used a bleomycin (BLM) induced BEAS-2B injury model *in vitro* and established a well-recognized rat model of BLM-induced lung injury *in vivo*. The results demonstrated that colchicine-myricetin hybrid protected BEAS-2B cells against BLM-induced cell injury in an increased dose manner, and reduced wet/dry weight ratio, histological scoring, and inflammation cytokines IL-1β, IL-6, IL-18, and TNF-α levels of lung tissue of the rats. Furthermore, we found colchicine-myricetin hybrid inhibited caspase-1, ASC, GSDMD, and NLRP-3 expression *in vivo*. Meanwhile, we used molecular docking to analyze the binding mode of colchicine-myricetin hybrid and human neutrophil elastase (HNE), it revealed that colchicine-myricetin hybrid showed strong binding affinity toward human neutrophil elastase when compared to its parent molecules. In conclusion, It is suggested that colchicine-myricetin hybrid antagonized acute lung injury by focusing on multi-targets via multi-mechanisms, and might be served as a potential therapeutic agent for acute lung injury.

KEYWORDS

colchicine-myricetin hybrid, colchicine, bleomycin, inflammation, acute lung injury, neutrophil elastase

1 Introduction

Acute lung injury (ALI) is a life-threatening clinical inflammatory condition characterized by lung vascular permeability, pulmonary edema, massive alveolar damage, and recruitment of numerous inflammatory cells to the lungs. Loss of control over the migration of inflammatory cell infiltrations toward the inflamed lung tissue shares in the pathology of ALI and its more severe form, acute respiratory distress syndrome (ARDS)

(Zhan et al., 2022; Hafez et al., 2023). Despite improvements in general supportive treatment and ventilatory care strategies designed to limit lung injury, no specific pharmacological therapy has yet proven to be efficacious in the management of acute lung injury (ALI) or ARDS. The most common causes of ALI are pneumonia and sepsis, despite recent progress, there is still a lack of knowledge on revealing pathological mechanisms of this condition (Bandela et al., 2022). Multiple studies have been performed to better elucidate the underlying pathogenic mechanisms of ALI. Examples of mechanisms explored in preclinical models of ALI include NOD-like receptor family pyrin domain-containing 3 (NLRP3) inflammasome and neutrophil elastase (NE) signaling. NLRP3, a key component of the inflammasome, plays a critical role in the secretion of IL-1β and in pyroptosis, which is an inherently inflammatory caspase-1-dependent mechanism of cell death triggered by various pathological stimuli that have been critically implicated in the pathogenesis of acute lung injury (Peiró et al., 2017; Hsu et al., 2022). NE is an active protease released from neutrophils involved in tissue damage by inducing direct cytotoxicity and proinflammatory mediator release (Ishida et al., 2023). Numerous evidence suggests that NE acts as a key target in ALI, and inhibitors of this protease are able to inhibit ALI in patients with cardiopulmonary bypass as well as other animal models associated with ALI (Pan et al., 2023). Bleomycin (BLM), originally designed as an anti-cancer drug, has now been demonstrated to cause ALI in multiple *in vitro* and *in vivo* experiment paradigms (Albanawany et al., 2022; Li et al., 2023; Lv et al., 2023). As such, BLM is widely accepted as an ALI inducer for identifying lung-protective compounds (Su et al., 2019; Chen et al., 2022). Intratracheal bleomycin administration induces acute lung inflammation and epithelial cell injury, followed by epithelial cell repair and fibrotic reactions (Chung et al., 2019). Herein, we used the bleomycin model of ALI to assess the effectiveness of CMyrH in the pathology.

Herb medicine is a great source from which a lot of drugs have been developed. (−)-Colchicine 1) is an iso-quinoline alkaloid isolated from medicinal plants including *Colchicum autumnale L.* and *Gloriosa superba L.* (Misra et al., 2023). Originally, colchicine was characterized as a mitotic inhibitor and universally applied in the treatment of cancer. In 2009, colchicine was approved by US FDA to treat gout and other related disorders. More encouragingly, colchicine has been proposed as a beneficial drug in the treatment of coronavirus disease 2019 (COVID-19) due to its excellent anti-inflammatory actions (Kacar et al., 2020; Pascual-Figal et al., 2021; Kasiri et al., 2023; Perricone et al., 2023). Whereas colchicine turned out to be an effective anti-inflammatory and anti-cancer agent, colchicine is still in the preclinical stages of development due to its high toxicity and severe side effects, including severe diarrhea, neuropathy, rhabdomyolysis, and bone marrow suppression (Spasevska et al., 2017; Kacar et al., 2020). Myricetin 2) is a flavonol compound existing in fruits and berries and has been reported to exert numerous pharmacological activities including antiviral, antioxidation and anti-tumor (Chaves et al., 2022; Sedbare et al., 2022). Myricetin is also well-recognized for its anti-inflammatory properties that act by inhibiting the formation of the NLRP3 inflammasome, which plays a key role in the innate immune response and the pathogenesis of many inflammatory diseases (Skrajnowska et al., 2021). At present, myricetin is listed as a natural health product and dietary supplement in Europe and has been approved by the FDA for pharmaceuticals, foods, and health products in the United States (Liu et al., 2020).

Since that, both colchicine and myricetin are able to counteract inflammatory response simultaneously, and myricetin possesses excellent safety, the hybridization of colchicine and myricetin may produce additive effects and reduce adverse and even toxic effects to treat complicated inflammatory diseases where ALI is involved. We have recently conducted a series of works exploring new drug candidates based on the concise synthesis and modification of (−)-colchicine 1) (Li et al., 2022; Pu et al., 2022). Herein we put forward our conception that the synthesis of a new hybrid of colchicine and myricetin to find a new bioactive molecule applied in anti-acute lung injury (Figure 1).

2 Materials and methods

2.1 Chemistry

General Information. Reaction mixtures at temperatures higher than ambient temperature were heated in an oil bath. All general chemicals were used directly without further purification. Petroleum ether (PE) refers to the fraction boiling in the 60°C–90°C range. Melting points were detected with an RY-I apparatus and uncorrected. NMR spectra of new compounds were recorded on a Bruker AV 400 spectrometer at 400 MHz (1H NMR), and 101 MHz (13C NMR). Chemical shifts were reported in ppm relative to internal TMS for 1H NMR data, and deuterated solvent for 13C NMR data, respectively. Data are recorded in the following format: chemical shift, multiplicity, coupling constant in hertz (Hz), and signal area integration in natural numbers. High-resolution mass spectra (HRMS) were obtained on Bruker Maxis impact instrument with ESI ion source and TOF mass analyzer.

2.2 Synthesis of CMyrH

To the solution of myricitrin (0.8 g, 1.72 mmol) in MeCN (40 mL), was added K_2CO_3 (1.8 g, 12.9 mmol) and dimethyl sulfate (1.2 mL, 12.9 mmol). The reaction mixture was refluxed for 24 h, then filtrated and concentrated in a vacuum. The obtained residue was dissolved in EtOH (40 mL), then was added conc. HCl (1.4 mL). The solution was stirred at 70°C for 12 h, then concentrated in a vacuum to remove EtOH. The residue was dissolved in DCM (40 mL) and washed with a saturated NaCl solution. The organic phase was dried over Na_2SO_4 and then concentrated *in vacuo* to yield crude product 4.

Compound 5 was synthesized according to the reported procedure (lit.). To the solution of compound 4 (620 mg, 1.6 mmol) and 5 (767 mg, 1.68 mmol) in DCM, was added EDCI (460 mg, 2.4 mmol) and DMAP (20 mg, 0.16 mmol). The solution was stirred at 25°C for 12 h. The contents were adsorbed on silica gel. The product was purified by column chromatography with EA to give the product CMyrH (595 mg, 45% yield) as a light yellow solid. MP 182°C–184°C. ^{1}H NMR (400 MHz, $CDCl_3$) δ 7.53–7.43 (m, 3H), 7.41 (d, J = 11.1 Hz, 1H), 7.05 (s, 2H), 6.63 (d, J = 11.3 Hz, 1H), 6.55

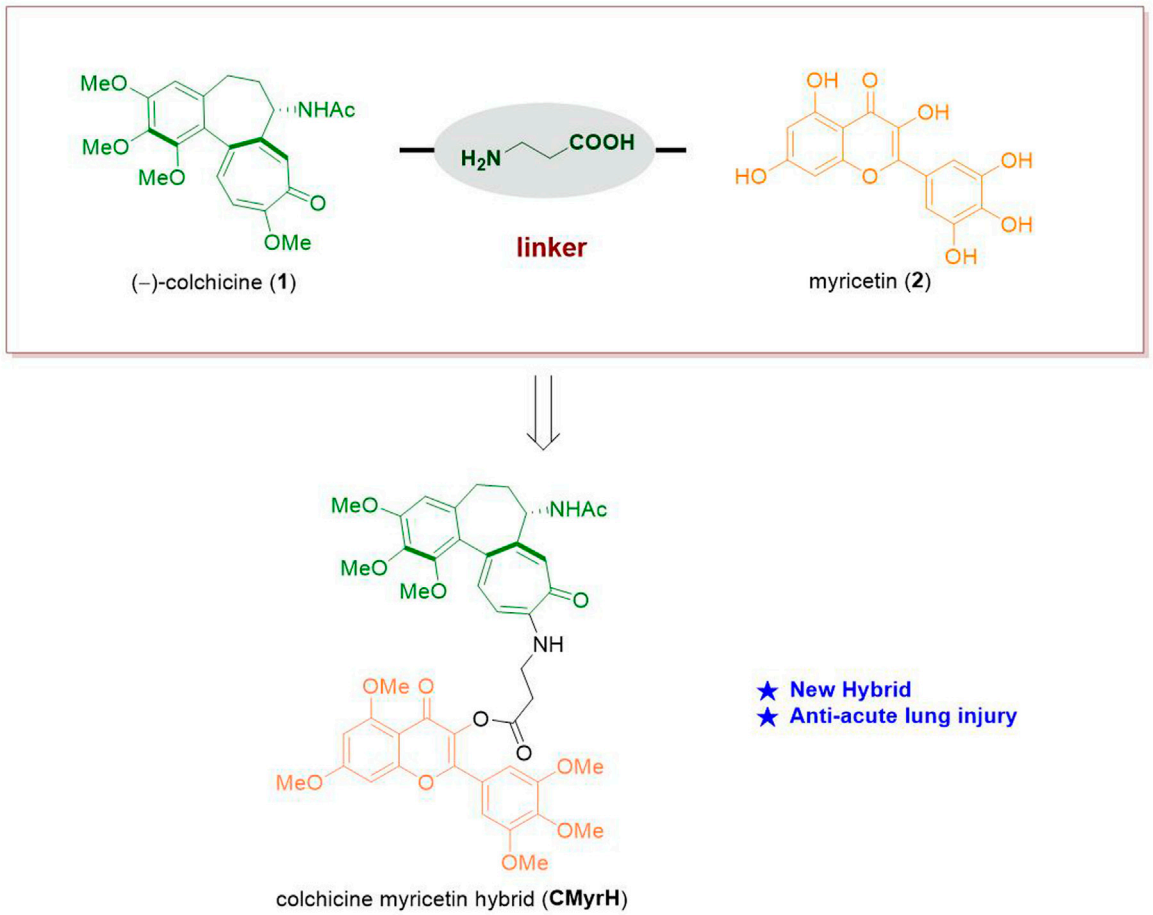

FIGURE 1
The design of a new hybrid of colchicine (1) and myricetin (2).

(d, J = 2.2 Hz, 1H), 6.51 (s, 1H), 6.40 (d, J = 2.2 Hz, 1H), 4.71–4.64 (m, 1H), 3.95 (s, 3H), 3.94 (s, 3H), 3.92 (s, 3H), 3.91 (s, 3H), 3.89 (s, 3H), 3.88 (s, 6H), 3.62 (s, 3H), 3.08 (t, J = 7.4 Hz, 2H), 2.46 (dd, J = 13.3, 6.5 Hz, 1H), 2.36 (td, J = 12.9, 6.7 Hz, 1H), 2.28–2.18 (m, 1H), 1.98 (s, 3H), 1.94–1.80 (m, 3H). ^{13}C NMR (101 MHz, $CDCl_3$) δ 175.47, 170.48, 170.07, 168.84, 164.74, 161.30, 159.34, 153.84, 153.40, 153.04, 151.45, 151.42, 151.24, 141.66, 140.70, 139.11, 134.68, 134.08, 130.99, 126.95, 124.81, 123.68, 108.75, 108.33, 107.32, 105.77, 104.98, 96.41, 92.88, 61.56, 61.45, 61.15, 60.56, 56.55, 56.48, 56.26, 56.04, 52.68, 38.51, 37.25, 33.31, 30.21, 23.01, 14.34. HRMS (m/z): calculated for $C_{44}H_{46}N_2NaO_{14}$ $[M + Na]^+$) 849.2841, found 849.2859.

2.3 Drugs and chemicals

Colchicine (Q107209-15g) was purchased from Chemxyz Biotechnology Co., Ltd. (Shanghai, China), and myricetin (MED80097-25g) was from MedBio Pharmaceutical Technology Inc., (Shanghai, China). Bleomycin (B5507-15un) was from Sigma (St. Louis, MO, USA). Dulbecco's modified Eagle's medium (DMEM), fetal bovine serum (FBS), and other cell culture supplements were from Gibco (Grand Island, NY, USA).

2.4 Cell culture and treatment

Human bronchial epithelial cells (BEAS-2B cells, purchased from Procell, Wuhan, China) were incubated in DMEM with 10% FBS under the conditions of 5% CO2 at 37°C. BEAS-2B cells were passaged (dilution, 1:3) when attaining 90% confluency. For the establishment of models, BEAS-2B cells were disposed of diverse concentrations (0.01, 0.1, 0.3, 1, 3, 10, and 30 μg/mL) of BLM for 24 h. For the evaluation of protection of CmyrH, myricetin and colchicine, cells were pre-treated with CMyrH (0.01 μM, 0.1 μM, 0.3 μM, 1 μM, 3 μM, 10 μM), myricetin (0.01 μM, 0.1 μM, 1 μM, 3 μM, 10 μM, 30 μM, 100 μM) or colchicine (0.01 nM, 0.1 nM, 1 nM, 0.01 μM, 0.1 μM, 0.3 μM) for 2 h, and then exposed to BLM for 24 h.

2.5 Cell viability analysis

CCK-8 assay was applied to evaluate the cell viability of BEAS-2B cells. Briefly, BEAS-2B cells (2500 cells/well) were seeded into 96-well plates. The next day, cells were pre-treated with CMyrH, myricetin or colchicine for 2 h, and therewith undergo BLM for 24 h. At the end of treatment, CCK-8 solution (Fluorescence,

Beijing, China) was directly pipetted into the culture medium (100 μL per well) and cells were further incubated at 37°C for 1 h. The absorbance was measured at 562 nm using a microplate reader.

2.6 Animals and care

Adult male-specific pathogen-free Sprague-Dawley rats (200 ± 20 g, 6–8 weeks) were purchased from the Guangdong VRLAT Co., Ltd. (Certificate: SYXK (Guangdong) 2022–0063). All rats were housed in standard cages in a climate-controlled room (24°C) under 12/12 h of light/dark cycles for 5 days. The experimental protocol was approved by the Animal Experimentation Ethics Committee of the Shenzhen Second People's Hospital, protocol number 202300110. All the experimental procedures were carried out in accordance with the international guidelines for the care and use of laboratory animals.

2.7 Rat BLM-induced acute lung injury model

Acute lung injury was induced by airway delivery of bleomycin (BLM, 5 mg/kg) in rats, applying a previously described method (Albert et al., 2020; Zhou et al., 2020). Briefly, the trachea was exposed by making a small midline incision on the neck following anesthesia with isoflurane, and inoculated with 5 mg/kg bleomycin solution in 0.1 mL of PBS using a sterile syringe with a 28-gauge needle. Survival of rats were then checked three times daily for a period of 3 days.

2.8 Rat groups and drug treatment

Rats were weighed and randomly divided into six groups (9 rats per group). Rats from Col-treated groups were treated with different doses of colchicine (1.0 and 1.5 mg/kg, i.p.) and the CMyrH-treated groups with CMyrH (1.0 and 3.0 mg/kg, i.p.). Control and ALI-model rats were treated with saline only. Rats were euthanized with an overdose of 5% isofluorane inhalation 3 days after treatment, followed by cervical dislocation after lung tissues and blood samples harvesting.

2.9 Lung wet/dry weight ratio

At the endpoint, rats were sacrificed, the right upper lungs were removed, weighed (wet weight), and dried at 55°C for 72 h. The resulting dry lungs were weighed (dry weight), and the ratio between the two values was determined, without correction for blood content.

2.10 Lung pathology

The extracted lungs were histopathologically examined and assessed for inflammatory changes. For each group of rats, the left lobe of the lung of 4/8 rats was fixed in 4% of paraformaldehyde, and fixed sections of paraffin-embedded lungs were stained with hematoxylin and eosin (H&E). Lung lesions were scored at four levels (from 0 (normal), 1 (mild), 2 (moderate) to 3 (severe)) by the % of the affected tissue, as previously published (Glineur et al., 2014; Abdel-Daim et al., 2018; Qin et al., 2020).

2.11 Immunohistochemical staining

Immunohistochemical staining was performed on 4 mum paraffin sections prepared from the abovementioned resected specimens. Sections were incubated at 4°C overnight with a rabbit anti-caspase-1 polyclonal antibody (1:200, 22915-1-AP; Proteintech, Chicago, USA), a rabbit anti-ASC polyclonal antibody (1:100, GTX55818; Genetex, USA), a rabbit anti-NLRP-3 polyclonal antibody (1:200, bs10021R; Biosis, Beijing, China), a rabbit anti-GSDMD polyclonal antibody (1:200, 20770-1-AP; Proteintech, Chicago, USA) and a rabbit anti-NE polyclonal antibody (1:100, A13015; Abclonal, Wuhan, China) according to the manufacturer's protocol. The IHC images were analyzed using a TEKsqray Digital Slide Scanner (SQS-40P, Shenzhen, China) and ImageJ software.

2.12 Inflammatory cytokines assay

Lung tissue lysates were prepared by homogenizing tissue in ice-cold lysis buffer containing 1 mM phenylmethane sulfonyl fluoride (PMSF), protease and phosphatase inhibitor cocktails (Servicebio, Wuhan, China), using a high-speed low-temperature tissue grinding machine (Servicebio, Wuhan, China), and then centrifuged at 13,000 rpm for 15 min at 4°C. The supernatant was collected and used to measure total protein concentration with the BCA assay (Solarbio, Beijing, China). The levels of inflammatory cytokines IL-1β, IL-6, IL-18 and TNF-α were measured by ELISA, using a Quantikine ELISA Kit (Spbio, Wuhan, China) and a microplate reader (Molecular devic, Guangzhou, China) at 450 nm, according to the manufacturer's protocol, specific for each investigated cytokine.

2.13 Molecular docking and data processing

The crystal structure of neutrophil elastase (PDB ID: 6SMA) was obtained from the RSCB PDB database (http://www.rcsb.org/) and saved as a PDB format file. The structures of the proposed ligands were drawn through ChemDraw 15.0 and then converted to a 3D structure following energy minimization by Chem3D 16.0. The molecular docking was performed by Autodock 4.2, and binding energy was predicted to evaluate the affinity of the target proteins and active components. The best binding conformations were selected from 50 lowest energy docked structures based on a criterion combining the lowest binding energy and root-mean-square deviation values (RMSD <1) (Bahuguna et al., 2022), and were displayed by PyMOL. Here, if the binding energy of the ligand <0, the receptors bind spontaneously, and if the binding

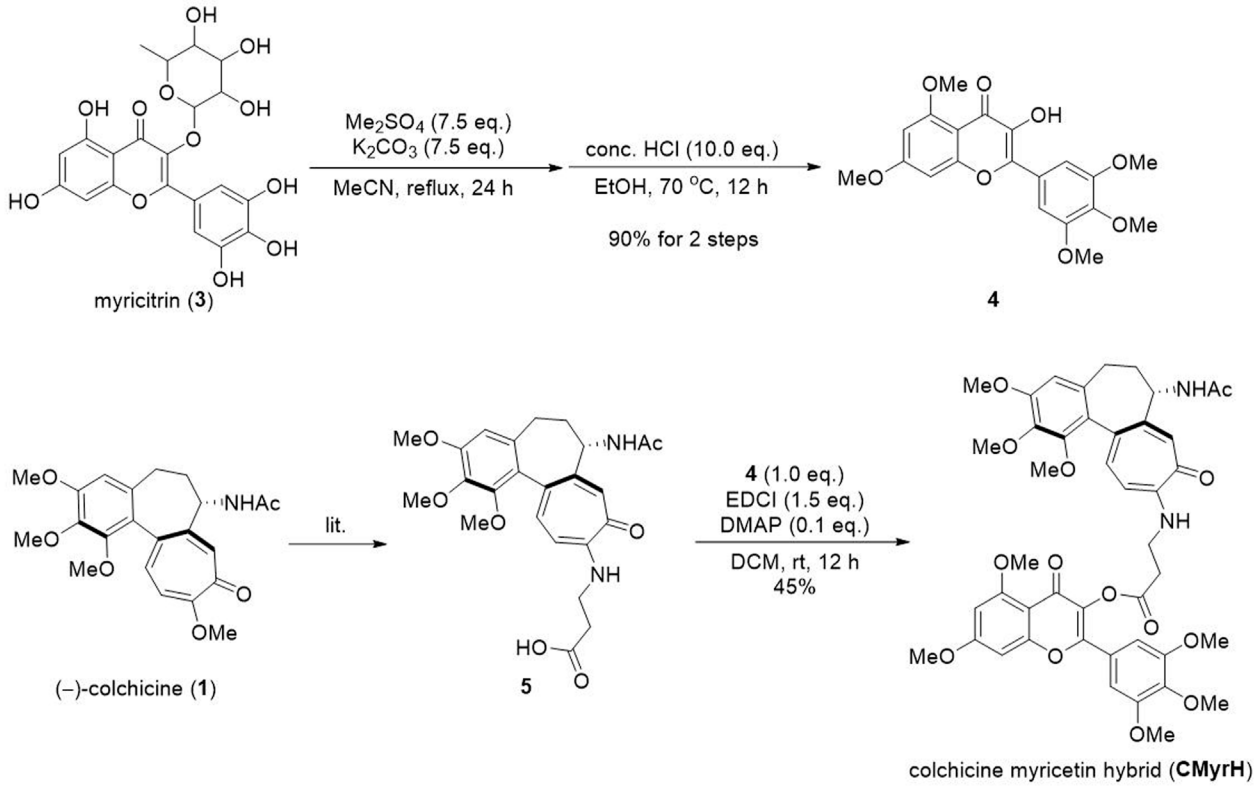

FIGURE 2
The synthesis route of CMyrH.

energy is ≤ −5.0 kcal/mol, they form a stable docking (Guo et al., 2022).

2.14 Statistical analysis

Statistical analyses were performed using GraphPad Prism Software (version 7.0 and 8.0). One-way ANOVA followed by posthoc tests, incorporating a Bonferroni correction for multiple comparisons, was employed, where $p < 0.05$ was considered significant. The cell viability and inflammatory cytokines were presented as mean ± SEM, and the lung W/D ratio was expressed as means ± SD. Cumulative survival rates were compared using the log-rank statistical analysis. Histological scores were expressed as median (interquartile range) and analyzed by the Kruskal–Wallis test followed by the Mann-Whitney U test.

3 Results

3.1 Chemical synthesis of CMyrH

The synthetic method was shown in Figure 2. The myricitrin 3) was firstly methylated with excess dimethyl sulfate and Potassium carbonate. After being refluxed in MeCN for 24 h, the crude product was directly treated with HCl to afford the intermediate 4. Then compound 5 was synthesized from (−)-colchicine 1) in one step according to our reported procedure (Pu et al., 2022). Compounds 4 and 5 underwent an esterification reaction with EDCI and DMAP to provide the new hybrid CMyrH in moderate yield.

3.2 CMyrH alleviated BLM-induced BEAS-2B cell injury

Since BLM at the dose of 10 μM resulted in approximately 50% cell death (Figure 3A), then 10 μM inducer was chosen for the subsequent experiments. To evaluate the protective effects of CMyrH, colchicine or myricetin against BLM-induced ALI, BEAS-2B cells were pretreated for 2 h with different concentrations of these compounds, then exposed to 10 μM BLM. It was found that CMyrH at 3 μM, colchicine at 0.01 nM, and myricetin at 30–100 μM protected BEAS-2B cells from BLM-induced injury (Figures 3C–E).

3.3 CMyrH decreased the toxicity of colchicine and improved the survival

After an intratracheal BLM challenge, the survival rates of the model and CMyrH (1.0 mg/kg and 3.0 mg/kg, i.p.) groups remained at 100% within 72 h. However, we found that 6 out of 9 rats at colchicine doses of 1.5 mg/kg (vs. CMyrH 3.0 mg/kg i.p. group, log-rank test, $p = 0.004$) and 2 out of 9 rats at colchicine doses of

10.3389/fphar.2023.1224906

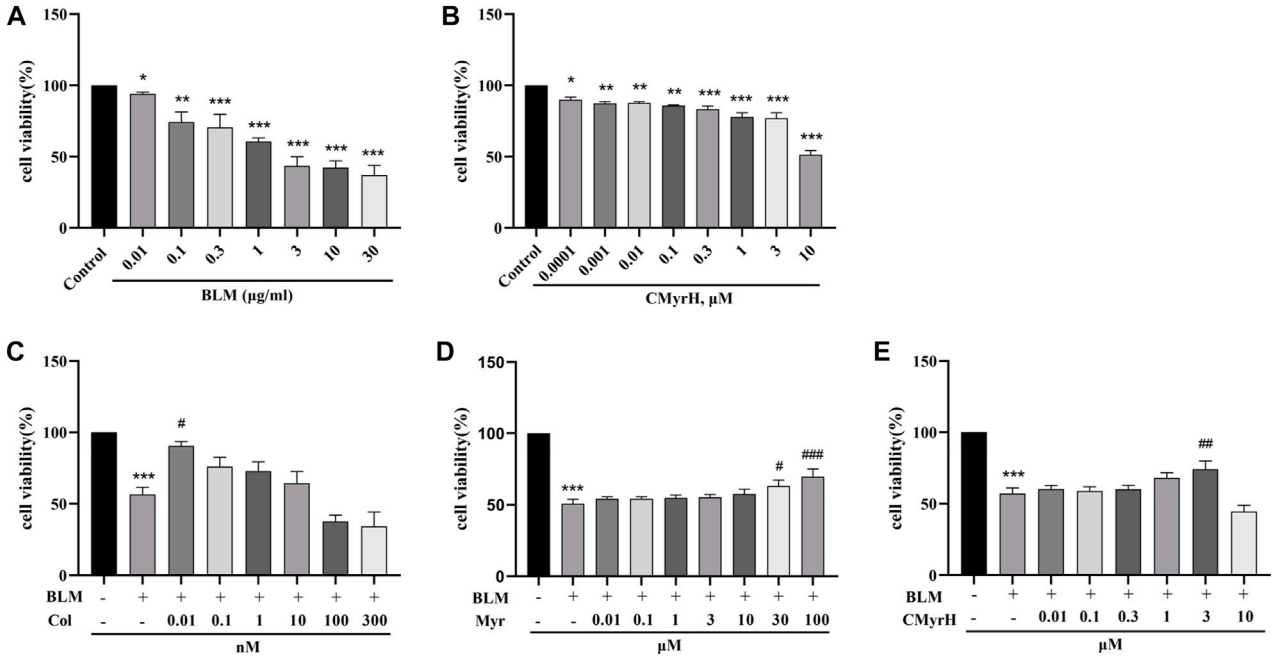

FIGURE 3
CMyrH protected against BLM-induced BEAS-2B injury. Effect of BLM **(A)** and CMyrH **(B)** treatment on BEAS-2B cell viability. Colchicine **(C)**, myricetin **(D)** and CMyrH **(E)** reversed the decrease in cell survival induced by BLM. All data are presented as mean ± SEM (n = 6 per group). $^{*}p < 0.05$, $^{**}p < 0.01$, $^{***}p < 0.001$, *versus* control group; $^{\#}p < 0.05$, $^{\#\#}p < 0.01$, $^{\#\#\#}p < 0.001$, *versus* BLM group.

1.0 mg/kg (vs. CMyrH 1.0 mg/kg i.p. group, log-rank test, $p = 0.145$) were dead during 3 days of drug treatment (Figure 4A).

3.4 CMyrH decreased acute pulmonary edema in the ALI model

The lung wet/dry weight ratio (W/D) was elucidated to estimate pulmonary edema. Lung edema formation was significantly enhanced in the model group, as shown by an increased lung W/D ($p < 0.001$). All CMyrH and colchicine treatments led to a reduced lung W/D as compared to the model ($p < 0.001$), but no differences in the lung W/D were detected between COL- (1.0 mg/kg) and CMyrH- (3.0 mg/kg) treatment groups (Figure 4B).

3.5 CMyrH improved BLM-induced pathological alterations in lung tissue

Histologically, the lungs of BLM-induced rats showed moderate-to-severe pneumonia. CMyrH- (1.0 mg/kg) treated rats showed less severe (moderate) histopathological changes in the lungs. CMyrH- (3.0 mg/kg) and COL- (1.0 mg/kg) showed multifocal bronchiolitis and bronchitis to mild to moderate bronchointerstitial pneumonia (Figure 5). As shown in Figure 4C, median scoring of the severity of lung tissue damage at the end of the study demonstrated substantially reduced pathological scores in rats treated with 3.0 mg/kg CMyrH ($p < 0.01$) and 1.0 mg/kg colchicine ($p < 0.05$). The CMyrH- (1.0 mg/kg) treated rats also had reduced pathological median scores in lung tissues compared to the ALI-model rats, but this difference was not statistically significant ($p < 0.05$).

3.6 CMyrH attenuated BLM-induced lung inflammation via suppression of inflammatory cytokine expression

As shown in Figures 4D–G, the lung cytokine productions of IL-1β, IL-6, IL-18 and TNF–α in ALI-model rats were significantly increased postoperative administration of BLM. However, Treatments with both drugs (CMyrH and colchicine) mitigated the cytokine overproductions of IL-1β, IL-6, IL-18 and TNF-α, as compared to the ALI-model rats. The higher dose of CMyrH more effectively alleviated the inflammatory cytokines levels than the low dose.

3.7 CMyrH suppressed pyroptosis via inhibition of NLRP3, ASC, caspase-1, GSDMD expression

According to our research, the ALI-model group, when compared with the control group, showed elevated expression of NLRP3, ASC, caspase-1 and GSDMD, with an increase in the levels of IL-1β and IL-18. However, the groups which received CMyrH (1.0 and 3.0 mg/kg) exhibited a weak expression of caspase-1, ASC, GSDMD and NLRP3 accompanied by a reduction in IL-1β and IL-18 secretion in a dose-dependent manner than ALI-model rats. The present IHC analysis results suggested the ability of CMyrH to suppress pyroptosis caused by BLM in the rats' lung tissues.

10.3389/fphar.2023.1224906

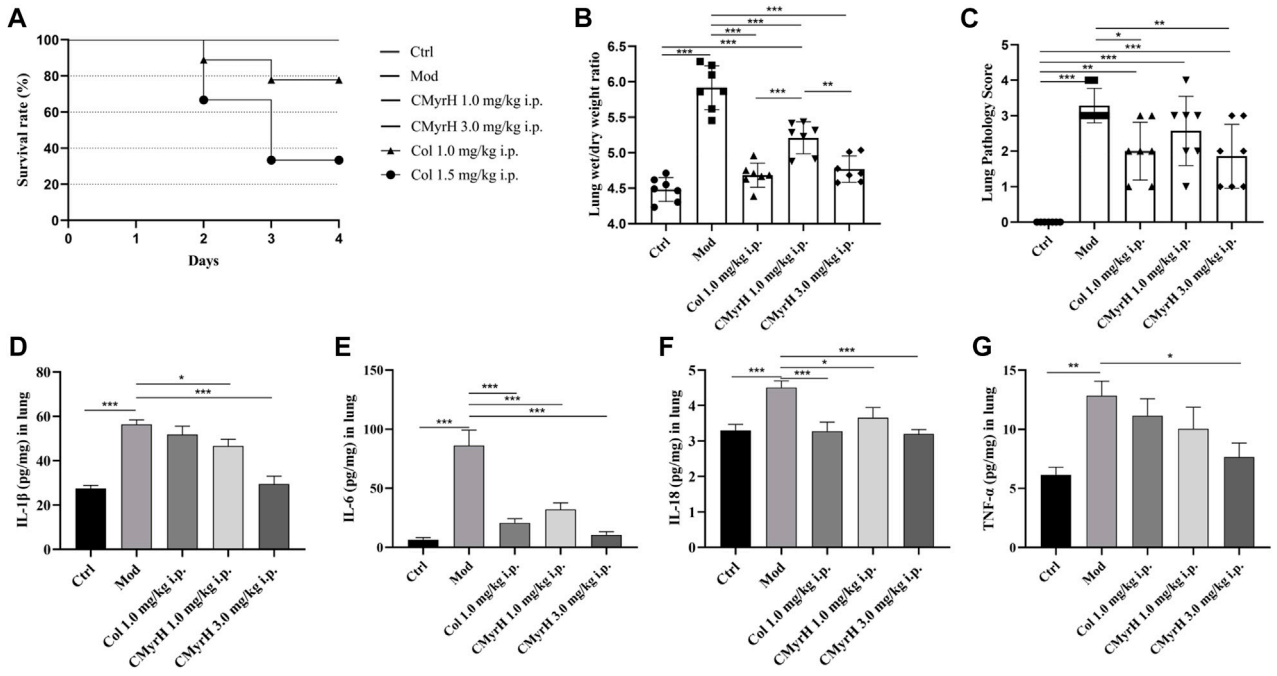

FIGURE 4
CMyrH improved survival, reduced pulmonary edema, restored pulmonary histology, repressed the production of proinflammatory cytokines, and was less toxic than colchicine. Panel 4**(A)**, the survival curve showed a significant difference in survival rate between BLM-challenged rats treated with colchicine or CMyrH. Panel 4 **(B)**, CMyrH reduced wet to dry lung weight ratio of lung tissues of rats at 72 h. Lung water content was determined in the right upper lobe (n = 7 per group) and measured via determination of lung wet-to dry-weight ratios, without correction for blood content. Panel 4 **(C)**, CMyrH downregulated histological scoring of lung tissues from BLM-induced rats following treatment. Lung lesions were scored from 0 to 3 based on a histopathologic scheme (n = 7). Panels 4 **(D–G)**, CMyrH alleviated the levels of IL-1β **(D)**, IL-6 **(E)**, IL-18 **(F)** and TNF-α **(G)** in the lung tissue of rats.

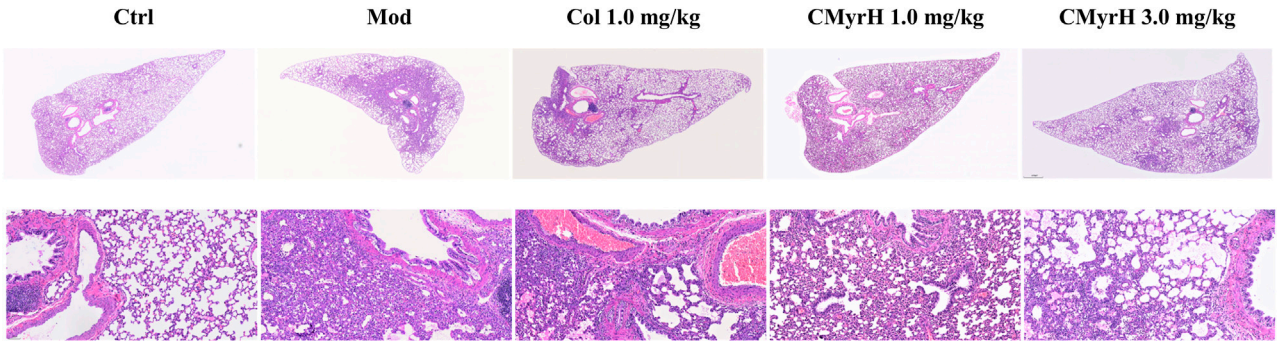

FIGURE 5
Microscopic pathological changes in the lung from treated rats. Lung sections (4 mum) were H&E stained with representative images shown from each group above (magnification ×40 and 200×).

3.8 CMyrH inhibited neutrophil elastase activity by blocking the enzyme's active site

The docking results provided the first evaluation as to which CMyrH exhibited a stronger binding affinity (higher docking score value) to NE, namely, CMyrH-b, which exhibited a higher affinity to NE than CMyrH-a, -c, and -d. Furthermore, silico studies showed that CMyrH inhibited NE protein by forming both a covalent bond between α-/β-unsaturated carbonyl groups in the colchicine fragment of CMyrH-b and Ser195, a hydrogen bond between the amino groups outside the 7-membered ring in colchicine fragment of CMyrH-b and Ser214, and a hydrogen bond between the ketone carbonyl groups in myricetin fragment of CMyrH-b and Gly216. Results showed that CMyrH has the highest binding energy values, −13.54 kcal/mol for NE protein (Ki value was 118.49 pM), followed by colchicine and myricetin with docking scores

10.3389/fphar.2023.1224906

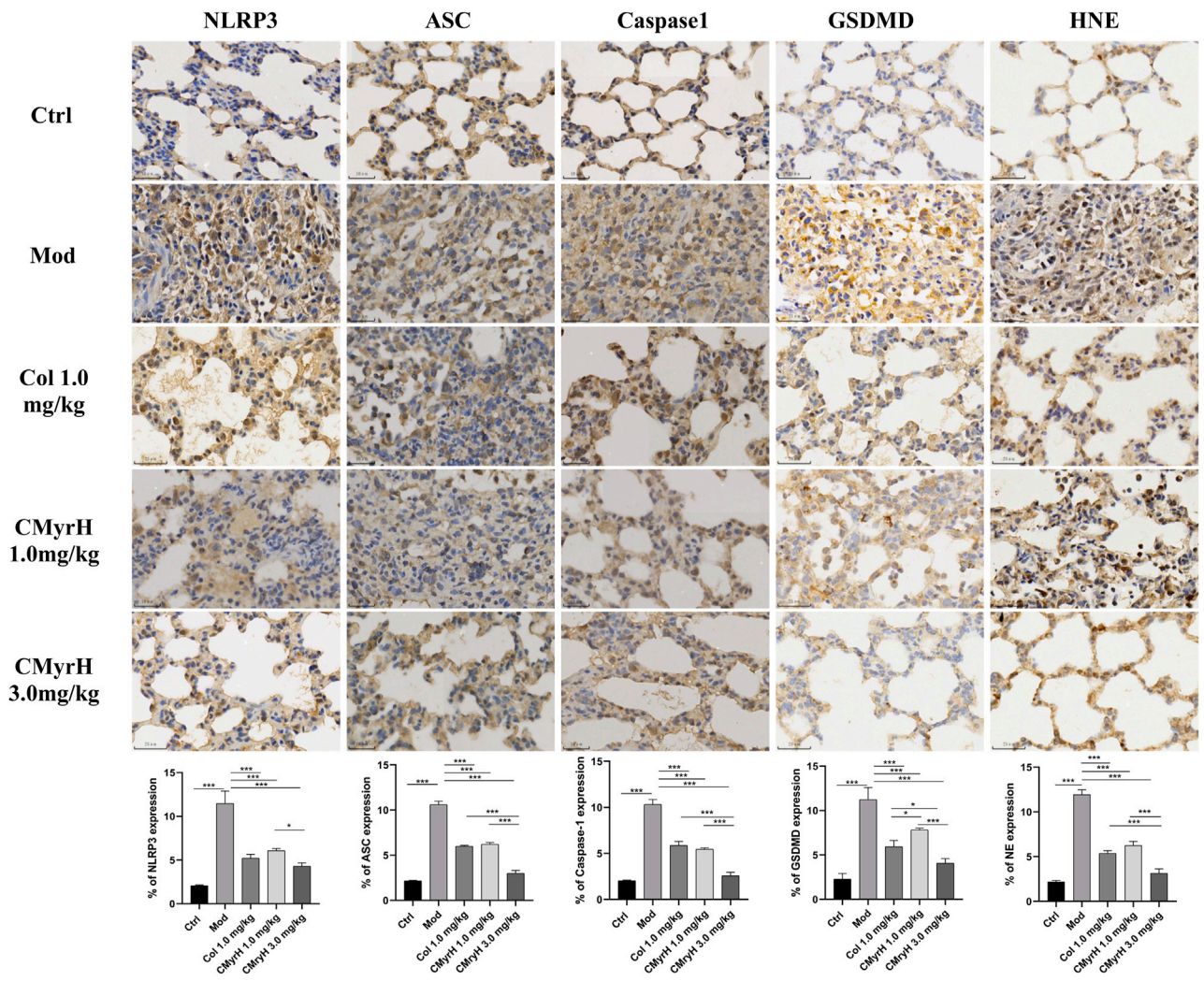

FIGURE 6
Effects of CMyrH on NLRP3, ASC, Caspase-1, GSDMD and HNE immunoreactivities in lung sections. The five upper lines, immunohistochemical detection of NLRP3, ASC, Caspase-1, GSDMD and HNE expression in lung tissues, x400. The bottom line, corresponding NLRP3, ASC, Caspase-1, GSDMD and HNE labeling index values. Values were presented as mean ± SD of 4 rats per group. *$p < 0.05$, **$p < 0.01$, ***$p < 0.001$.

of −5.86 kcal/mol and −1.89 kcal/mol (Ki values were 51.03 μM and 40.93 mM), respectively.

4 Discussion

4.1 Efficient synthesis of a novel hybrid CMyrH

As for some adverse reactions, we altered the chemical structure of Colchicine to enhance its clinical application. Colchicine-CD44-Targeted Peptide conjugate decreased the cytotoxic effect of colchicine while maintaining anti-inflammatory against gout (Zoghebi et al., 2019). However, there were few studies about the hybridization of Colchicine with bioactive natural molecules to exert its efficient biological effects with low toxicity in ALI. In this current study, we designed a new kind of C-10-modified Colchicinoid which was a heterozygous molecule of Colchicine and Myricetin with a simple amino acid as the linker (Figure 2).

4.2 CMyrH caused lower toxicity and decreased BLM-induced BEAS-2B cells injury than colchicine

Subsequently, we used human lung epithelial BEAS-2B cells to estimate the effects of CMyrH and its parent molecules on BLM-induced cell injury. As shown in Figure 3, CMyrH antagonized significantly BLM-induced BEAS-2B cells injury, in a dose-dependent manner, especially in the 3 μM group; myricetin revised BLM-induced injury in increased dose-manner at 30 μM; colchicine reversed BLM-induced injury at 0.01 nM, but the safety range between the upper and lower limits was extremely narrow and

10.3389/fphar.2023.1224906

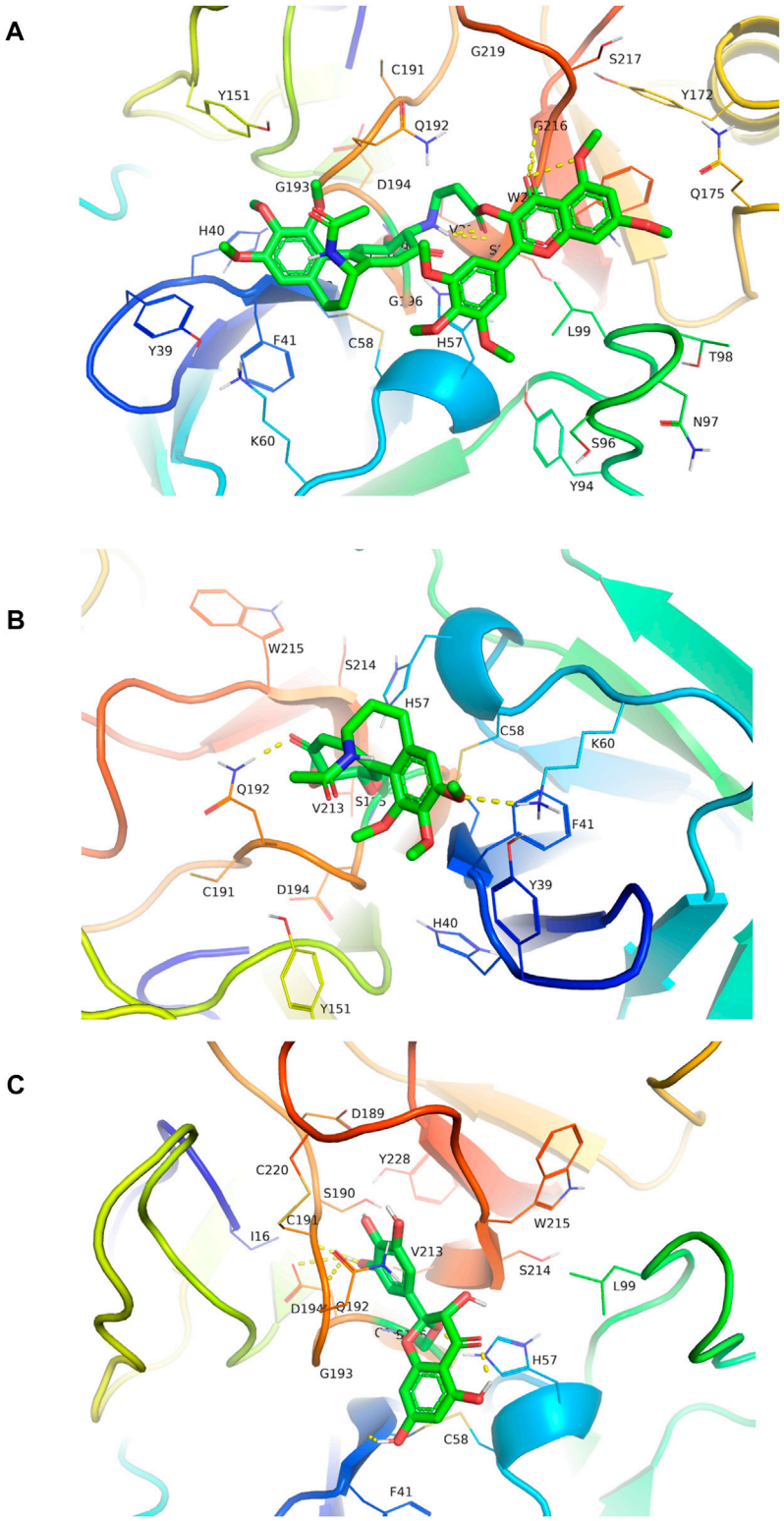

FIGURE 7
Molecular docked CMyrH panel **(A)**, colchicine panel **(B)**, and myricetin panel **(C)** into neutrophil elastase crystal structure (6SMA) using AutoDock 4.2. CMyrH bounded to amino acid residue Ser195 via a covalent bond and to Ser214 and Gly216 via two hydrogen bonds in the active site of NE protein. Among the three docking complexes, CMyrH has the highest binding energy values of −13.54 kcal/mol for NE protein (Ki value was 118.49 pM) as compared to others.

even overlap, which creates difficulties when setting therapeutic margins. Thus, these results suggested that a novel hybrid CMyrH exhibited a better and safer anti-inflammatory effect on BLM-induced BEAS-2B cell injury compared with colchicine.

4.3 CMyrH ameliorated BLM-mediated inflammation in a ALI rat model

In the end, the CMyrH's ability to improve ALI was further verified by using a rat BLM-induced acute lung injury model. As shown in Figures 4B–C and Figures 5H, E staining of lung tissue sections revealed less lung injury in rats administered CMyrH (at 1.0 mg/kg and 3.0 mg/kg) for 3 days post-challenge, with significantly lower lung injury score and W/D, indicating mild lung inflammation and pulmonary edema. CMyrH 1.0 mg/kg i.p. was relatively safe in rats up to 72 h, in addition, an acute toxicity study of CMyrH showed no signs of toxicity or cause mortality in rats even at doses = 3.0 mg/kg (Figure 4A). For reference, colchicine at 1.0 mg/kg reduced histopathological end scores and W/D in their lung tissues compared to the model rats (Figures 4B,C), however, colchicine administration for 72 h showed severe toxic effects with a 22.2%, 66.7% mortality rate at the doses of 1.0 mg/kg and 1.5 mg/kg i.p. (Figure 4A). Furthermore, multiple cytokines in lung tissue dramatically declined after treatment with the diverse concentration of CMyrH (1.0 mg/kg and 3.0 mg/kg), importantly, a high dose of CMyrH remarkably reversed proinflammatory cytokines including IL-1β, IL-6, IL-18 and TNF-α more than that of a low dose (Figures 4D–G). These findings indicated that threefold doses of CMyrH had already achieved anti-inflammation efficacy comparable or even superior to colchicine, without severe toxicity or treatment-related deaths.

4.4 CMyrH suppressed NLRP3 inflammasome-mediated pyroptosis caused by BLM in the rats' lung tissues

Pyroptosis is a form of cell death triggered by the innate immune system that has been implicated in the pathogenesis of acute lung injury (Hsu et al., 2022; Liang et al., 2022). Activated NLRP3 recruits ASC and caspase-1 to form the NLRP3 inflammasome, resulting in the cleavage of gasdermin D (GSDMD) and membrane pores formation (pyroptosis) accompanied by the proinflammatory cytokines IL-1β and IL-18 release (Faria et al., 2021; Tummers and Green, 2022). In the current study, the immunohistochemical expression of caspase-1, ASC, GSDMD and NLRP3 was investigated in lung sections to reflect on the anti-pyroptosis potential of CMyrH. Our findings showed a decrease in caspase-1, ASC, GSDMD and NLRP3 immunoreactivity in lung sections accompanied by a reduction in cytokine production of IL-1β and IL-18 affiliated to both CMyrH-treated (1.0 mg/kg and 3.0 mg/kg) groups. These evidences suggested that CMyrH might protect rats against ALI caused by BLM by alleviating lung inflammation through the inhibition of pyroptosis.

4.5 CMyrH antagonized ALI by binding to the active site of the neutrophil elastase enzyme

Human neutrophil elastase (HNE) is a potent serine protease secreted by activated polymorphonuclear neutrophils (PMNs), whose uncontrolled production can result in inflammatory-derived disease conditions. (González-Fernández et al., 2018.). Besides its crucial role in powerful host defense, HNE is well known as one of the most destructive enzymes in the human body (Thierry, 2020). It is reported that excessive HNE activity is involved in the pathogenesis of ALI, thereby administering anti-NE might prevent lung tissue damage caused by inflammation (Conrad and Eltzschig, 2020). Analyzing the resultant *in silico* interactions of the CMyrH-b molecule with the residues of host HNE protein showed that CMyrH-b molecule significantly hit most of the active site residues of the HNE protein with strong interactions, such as covalent bond and hydrogen bonding. The docking score with NE indicated that CMyrH was the highest affinity binding with the lowest energy value −13.54 kcal/mol (Ki value was 118.49 pM) as compared to other docking complexes. Immunohistochemical studies confirmed this result, with lung tissues from CMyrH-treated rats analyzed showing a decrease in immunoreactivity for antibodies specific to HNE (Figure 6 Figure 7). It is suggested that CMyrH-b had a strong inhibitory effect on neutrophil elastase, which might also be an important mechanism for CMyrH-b to antagonize ALI.

5 Conclusion

In conclusion, we herein designed and synthesized a novel hybrid CMyrH by splicing colchicine and myricetin. CMyrH exerted strong anti-inflammatory abilities to alleviate bleomycin-induced BEAS-2B cell injury, and to protect the lung from inflammatory injury and pulmonary edema in a rat model of ALI, even conferring a survival benefit. The present findings insinuated a superior potential of CMyrH over colchicine in inhibiting NLRP3 inflammasome-mediated pyroptosis. And the key to CMyrH's pharmacological properties also included its stable binding to the active site in the NE enzyme. These findings obtained *in vitro* and *in vivo* models of bleomycin-induced ALI were confirming the promising therapeutic potential for ALI of novel hybrid CMyrH supporting their future employment as a novel inflammation strategy.

Data availability statement

The original contributions presented in the study are included in the article/Supplementary Material, further inquiries can be directed to the corresponding author.

Ethics statement

The animal study was reviewed and approved by the Animal Experimentation Ethics Committee of the Shenzhen Second People's Hospital.

Author contributions

ZL animal study, design and drafting of the manuscript. XY and JW cell experiments and acquisition of data. LP synthetic work. YC molecular docking analysis work. YL, GZ, ZL, and XL animal experiments. YL and LL cell biology studies. ZW supervision, project research design, revision and editing. All authors contributed to the article and approved the submitted version.

Funding

This work was supported by the major new drug innovation project of the Ministry of Science and Technology of China (No. 2017ZX09301001), the China Central Finance Improvement Project for the National Key Laboratory of Traditional Chinese Medicine (China Central Finance. CS [2021] No. 151), the special key project of science, Shenzhen Basic Discipline Layout Project (JCYJ20220818101806014) and technology of Guangdong Province with strong traditional Chinese medicine (No. 20215002).

Conflict of interest

The authors declare that the research was conducted in the absence of any commercial or financial relationships that could be construed as a potential conflict of interest.

Publisher's note

Supplementary material

The Supplementary Material for this article can be found online at: https://www.frontiersin.org/articles/10.3389/fphar.2023.1224906/full#supplementary-material

References

Abdel-Daim, M. M., Eltaysh, R., Hassan, A., and Mousa, S. A. (2018). Lycopene attenuates tulathromycin and diclofenac sodium-induced cardiotoxicity in mice. *Int. J. Mol. Sci.* 19 (2), 344. doi:10.3390/ijms19020344

Albanawany, N. M., Samy, D. M., Zahran, N., El-Moslemany, R. M., Elsawy, S. M., and Abou Nazel, M. W. (2022). Histopathological, physiological and biochemical assessment of resveratrol nanocapsules efficacy in bleomycin-induced acute and chronic lung injury in rats. *Drug Deliv.* 29 (1), 2592–2608. doi:10.1080/10717544.2022.2105445

Albert, K., Krischer, J. M., Pfaffenroth, A., Wilde, S., Lopez-Rodriguez, E., Braun, A., et al. (2020). Hidden microatelectases increase vulnerability to ventilation-induced lung injury. *Front. Physiol.* 11, 530485. doi:10.3389/fphys.2020.530485

Bahuguna, A., Khaket, T. P., Bajpai, V. K., Shukla, S., Park, I., Na, M., et al. (2022). N-Acetyldopamine dimers from Oxya chinensis sinuosa attenuates lipopolysaccharides induced inflammation and inhibits cathepsin C activity. *Compu.t Struct. Biotechno.l J.* 20, 1177–1188. doi:10.1016/j.csbj.2022.02.011

Bandela, M., Belvitch, P., Garcia, J. G. N., and Dudek, S. M. (2022). Cortactin in lung cell function and disease. *Int. J. Mol. Sci.* 23 (9), 4606. doi:10.3390/ijms23094606

Chaves, O. A., Lima, C. R., Fintelman-Rodrigues, N., Sacramento, C. Q., de Freitas, C. S., Vazquez, L., et al. (2022). Agathisflavone, a natural biflavonoid that inhibits SARS-CoV-2 replication by targeting its proteases. *Int. J. Biol. Macromol.* 222 (Pt A), 1015–1026. doi:10.1016/j.ijbiomac.2022.09.204

Chen, L., Ma, Q., Zhang, G., Lei, Y., Wang, W., Zhang, Y., et al. (2022). Protective effect and mechanism of loganin and morroniside on acute lung injury and pulmonary fibrosis. *Phytomedicine* 99, 154030. doi:10.1016/j.phymed.2022.154030

Chung, K. P., Hsu, C. L., Fan, L. C., Huang, Z., Bhatia, D., Chen, Y. J., et al. (2019). Mitofusins regulate lipid metabolism to mediate the development of lung fibrosis. *Nat. Commun.* 10 (1), 3390. doi:10.1038/s41467-019-11327-1

Conrad, C., and Eltzschig, H. K. (2020). Disease mechanisms of perioperative organ injury. *Anesth. Analg.* 131 (6), 1730–1750. doi:10.1213/ANE.0000000000005191

Faria, S. S., Costantini, S., de Lima, V. C. C., de Andrade, V. P., Rialland, M., Cedric, R., et al. (2021). NLRP3 inflammasome-mediated cytokine production and pyroptosis cell death in breast cancer. *J. Biomed. Sci.* 28 (1), 26. doi:10.1186/s12929-021-00724-8

Glineur, S. F., Bowen, A. B., Percopo, C. M., Garcia-Crespo, K. E., Dyer, K. D., Ochkur, S. I., et al. (2014). Sustained inflammation and differential expression of interferons type I and III in PVM-infected interferon-gamma (IFNγ) gene-deleted mice. *Virology* 468-470, 140–149. doi:10.1016/j.virol.2014.07.039

González-Fernández, E., Staderini, M., Yussof, A., Scholefield, E., Murray, A. F., Mount, A. R., et al. (2018). Electrochemical sensing of human neutrophil elastase and polymorphonuclear neutrophil activity. *Biosens. Bioelectron.* 119, 209–214. doi:10.1016/j.bios.2018.08.013

Guo, Y., Luo, N., and Kang, X. (2022). Potential mechanism of the Shunaoxin pill for preventing cognitive impairment in type 2 diabetes mellitus. *Front. Neurol.* 13, 977953. doi:10.3389/fneur.2022.977953

Hafez, S. M. N. A., Saber, E. A., Aziz, N. M., Kamel, M. Y., Aly, A. A., Abdelhafez, E. M. N., et al. (2023). Potential protective effect of 3,3'-methylenebis(1-ethyl-4-hydroxyquinolin-2(1H)-one) against bleomycin-induced lung injury in male albino rat via modulation of Nrf2 pathway: Biochemical, histological, and immunohistochemical study. *Naunyn Schmiedeb. Arch. Pharmacol.* 396 (4), 771–788. doi:10.1007/s00210-022-02324-1

Hsu, C. G., Chávez, C. L., Zhang, C., Sowden, M., Yan, C., and Berk, B. C. (2022). The lipid peroxidation product 4-hydroxynonenal inhibits NLRP3 inflammasome activation and macrophage pyroptosis. *Cell Death Differ.* 29 (9), 1790–1803. doi:10.1038/s41418-022-00966-5

Ishida, Y., Zhang, S., Kuninaka, Y., Ishigami, A., Nosaka, M., Harie, I., et al. (2023). Essential involvement of neutrophil elastase in acute acetaminophen hepatotoxicity using BALB/c mice. *Int. J. Mol. Sci.* 24 (9), 7845. doi:10.3390/ijms24097845

Kacar, M., Savic, S., and van der Hilst, J. C. H. (2020). The efficacy, safety and tolerability of canakinumab in the treatment of familial mediterranean fever: A systematic review of the literature. *J. Inflamm. Res.* 13, 141–149. doi:10.2147/JIR.S206204

Kasiri, H., Ghazaiean, M., Rouhani, N., Naderi-Behdani, F., Ghazaeian, M., and Ghodssi-Ghassemabadi, R. (2023). The effects of colchicine on hospitalized COVID-19 patients: A randomized, double-blind, placebo-controlled clinical trial. *J. Investig. Med.* 71 (2), 124–131. doi:10.1177/10815589221141815

Li, L. F., Yu, C. C., Huang, C. Y., Wu, H. P., Chu, C. M., Liu, P. C., et al. (2023). Attenuation of ventilation-enhanced epithelial-mesenchymal transition through the phosphoinositide 3-Kinase-γ in a murine bleomycin-induced acute lung injury model. *Int. J. Mol. Sci.* 24 (6), 5538. doi:10.3390/ijms24065538

Li, Z., Hu, S., Pu, L. Y., Li, Z., Zhu, G., Cao, Y., et al. (2022). Design, synthesis and biological evaluation of a novel colchicine-magnolol hybrid for inhibiting the growth of Lewis lung carcinoma *in vitro* and *in vivo*. *Front. Chem.* 10, 1094019. doi:10.3389/fchem.2022.1094019

Liang, S., Xing, M., Chen, X., Peng, J., Song, Z., and Zou, W. (2022). Predicting the prognosis in patients with sepsis by a pyroptosis-related gene signature. *Front. Immunol.* 13, 1110602. doi:10.3389/fimmu.2022.1110602

Liu, M., Guo, H., Li, Z., Zhang, C., Zhang, X., Cui, Q., et al. (2020). Molecular level insight into the benefit of myricetin and dihydromyricetin uptake in patients with alzheimer's diseases. *Front. Aging Neurosci.* 12, 601603. doi:10.3389/fnagi.2020.601603

Lv, K., Li, M., Sun, C., Miao, Y., Zhang, Y., Liu, Y., et al. (2023). Jingfang Granule alleviates bleomycin-induced acute lung injury via CD200-CD200R immunoregulatory pathway. *J. Ethnopharmacol.* 311, 116423. doi:10.1016/j.jep.2023.116423

Misra, A., Chaudhary, M. K., Singh, S. P., Tripathi, D., Barik, S. K., and Srivastava, S. (2023). Docking experiments suggest that gloriosine has microtubule-targeting properties similar to colchicine. *Sci. Rep.* 13 (1), 4854. doi:10.1038/s41598-023-31187-6

Pan, T., Tuoerxun, T., Chen, X., Yang, C. J., Jiang, C. Y., Zhu, Y. F., et al. (2023). Corrigendum: The neutrophil elastase inhibitor, Sivelestat, attenuates acute lung injury in patients with cardiopulmonary bypass. *Front. Immunol.* 14, 1165081. doi:10.3389/fimmu.2023.1165081

Pascual-Figal, D. A., Roura-Piloto, A. E., Moral-Escudero, E., Bernal, E., Albendín-Iglesias, H., Pérez-Martínez, M. T., et al. (2021). Colchicine in recently hospitalized patients with COVID-19: A randomized controlled trial (col-COVID). *Int. J. Gen. Med.* 14, 5517–5526. doi:10.2147/IJGM.S329810

Peiró, C., Lorenzo, Ó., Carraro, R., and Sánchez-Ferrer, C. F. (2017). IL-1β inhibition in cardiovascular complications associated to diabetes mellitus. *Front. Pharmacol.* 8, 363. doi:10.3389/fphar.2017.00363

Perricone, C., Scarsi, M., Brucato, A., Pisano, P., Pigatto, E., Becattini, C., et al. (2023). Treatment with COLchicine in hospitalized patients affected by COVID-19: The COLVID-19 trial. *Eur. J. Intern Med.* 107, 30–36. doi:10.1016/j.ejim.2022.10.016

Pu, L. Y., Li, Z., Huang, F., Li, L., Ma, Y., Ma, M., et al. (2022). Efficient synthesis of novel colchicine-magnolol hybrids and evaluation of their inhibitory activity on key proteases of 2019-nCoV replication and acute lung injury. *Nat. Prod. Res.* 1-10, 1–10. doi:10.1080/14786419.2022.2138870

Qin, H., Zhang, J., Yang, H., Yao, S., He, L., Liang, H., et al. (2020). Safety assessment of water-extract sericin from silkworm (*Bombyx mori*) cocoons using different model approaches. *Biomed. Res. Int.* 2020, 9689386. doi:10.1155/2020/9689386

Sedbare, R., Raudone, L., Zvikas, V., Viskelis, J., Liaudanskas, M., and Janulis, V. (2022). Development and validation of the UPLC-DAD methodology for the detection of triterpenoids and phytosterols in fruit samples of vaccinium macrocarpon aiton and vaccinium oxycoccos L. *Molecules* 27 (14), 4403. doi:10.3390/molecules27144403

Skrajnowska, D., Brumer, M., Kankowska, S., Matysek, M., Miazio, N., and Bobrowska-Korczak, B. (2021). Covid 19: Diet composition and health. *Nutrients* 13 (9), 2980. doi:10.3390/nu13092980

Spasevska, I., Ayoub, A. T., Winter, P., Preto, J., Wong, G. K., Dumontet, C., et al. (2017). Modeling the Colchicum autumnale tubulin and a comparison of its interaction with colchicine to human tubulin. *Int. J. Mol. Sci.* 18 (8), 1676. doi:10.3390/ijms18081676

Su, X., Liu, K., Xie, Y., Zhang, M., Wang, Y., Zhao, M., et al. (2019). Protective effect of a polyphenols-rich extract from Inonotus Sanghuang on bleomycin-induced acute lung injury in mice. *Life Sci.* 230, 208–217. doi:10.1016/j.lfs.2019.05.074

Thierry, A. R. (2020). Anti-protease treatments targeting plasmin(ogen) and neutrophil elastase may Be beneficial in fighting COVID-19. *Physiol. Rev.* 100 (4), 1597–1598. doi:10.1152/physrev.00019.2020

Tummers, B., and Green, D. R. (2022). The evolution of regulated cell death pathways in animals and their evasion by pathogens. *Physiol. Rev.* 102 (1), 411–454. doi:10.1152/physrev.00002.2021

Zhan, P., Lu, X., Li, Z., Wang, W. J., Peng, K., Liang, N. N., et al. (2022). Mitoquinone alleviates bleomycin-induced acute lung injury via inhibiting mitochondrial ROS-dependent pulmonary epithelial ferroptosis. *Int. Immunopharmacol.* 113 (Pt A), 109359. doi:10.1016/j.intimp.2022.109359

Zhou, B., Magana, L., Hong, Z., Huang, L. S., Chakraborty, S., Tsukasaki, Y., et al. (2020). The angiocrine Rspondin3 instructs interstitial macrophage transition via metabolic-epigenetic reprogramming and resolves inflammatory injury. *Nat. Immunol.* 21 (11), 1430–1443. doi:10.1038/s41590-020-0764-8

Zoghebi, K. A., Bousoik, E., Parang, K., and Elsaid, K. A. (2019). Design and biological evaluation of colchicine-CD44-targeted Peptide conjugate in an *in vitro* model of crystal induced inflammation. *Molecules* 25 (1), 46. doi:10.3390/molecules25010046

frontiers | Frontiers in Pharmacology

TYPE Original Research
PUBLISHED 03 July 2023
DOI 10.3389/fphar.2023.1166022

OPEN ACCESS

EDITED BY
Zhixing Qing,
Hunan Agricultural University, China

REVIEWED BY
Chao Ai,
Guangdong Ocean University, China
JingHong Liu,
Changsha University, China

*CORRESPONDENCE
Jun Zhou,
15304690053@163.com
Binsheng He,
hbscsmu@163.com
Qian Lin,
linqian@caas.cn

†These authors have contributed equally to this work and share first authorship

RECEIVED 14 February 2023
ACCEPTED 13 June 2023
PUBLISHED 03 July 2023

CITATION
Chen F, Wang Y, Wang K, Chen J, Jin K, Peng K, Chen X, Liu Z, Ouyang J, Wang Y, Zhang X, Zou H, Zhou J, He B and Lin Q (2023), Effects of *Litsea cubeba* essential oil on growth performance, blood antioxidation, immune function, apparent digestibility of nutrients, and fecal microflora of pigs.
Front. Pharmacol. 14:1166022.
doi: 10.3389/fphar.2023.1166022

Effects of *Litsea cubeba* essential oil on growth performance, blood antioxidation, immune function, apparent digestibility of nutrients, and fecal microflora of pigs

Fengming Chen[1†], Yushi Wang[2†], Kaijun Wang[3†], Jiayi Chen[1], Ke Jin[2], Kaiqiang Peng[4], Xu Chen[4], Zhimou Liu[4], Jiang Ouyang[1], Yong Wang[2], Xiaoya Zhang[2], Haowei Zou[5], Jun Zhou[1]*, Binsheng He[1]* and Qian Lin[1,2]*

[1]Hunan Provincial Key Laboratory of the TCM Agricultural Biogenomics, Changsha Medical University, Changsha, Hunan, China, [2]Institute of Bast Fiber Crops, Chinese Academy of Agricultural Sciences, Changsha, China, [3]State Key Laboratory for Conservation and Utilization of Subtropical Agro-bioresources, College of Animal Science and Technology, Guangxi University, Nanning, Guangxi, China, [4]Hunan Nuoz Biological Technology Co., Ltd., Yiyang, Hunan, China, [5]College of Animal Science and Technology, Hunan Agricultural University, Changsha, Hunan, China

The purpose of this experiment was to investigate the effects of *Litsea cubeba* essential oil (LCO) on the growth performance, blood antioxidation, immune function, apparent digestibility of nutrients, and fecal microflora in fattening pigs. A total of 120 pigs were randomly assigned to five groups, with six replicate pens per treatment and four pigs per pen, and they were fed basal diet, chlortetracycline (CTC), and low-, medium-, and high-concentration LCO. The results of the study showed that compared with the control treatment and CTC addition treatment of the basic diet, the catalase level in the serum of the pigs treated with 500 mg/kg LCO in the diet of finishing pigs was significantly increased ($p < 0.05$). The apparent digestibility of crude protein, crude ash, and calcium in pigs with different levels of LCO was significantly increased compared with the control treatments fed the basal diet ($p < 0.05$). In addition, compared with the control treatment fed the basal diet and the treatment with *CTC*, the apparent digestibility of ether extract in pigs treated with medium-dose LCO was significantly increased ($p < 0.05$), and the apparent digestibility of pigs was significantly increased after the addition of low-dose LCO ($p < 0.05$). Among the genera, the percentage abundance of *SMB53* ($p < 0.05$) was decreased in the feces of the *CTC* group when compared to that in the medium-LCO group. At the same time, the relative abundance of *L7A_E11* was markedly decreased in the feces of the control and medium- and high-concentration LCO group than that in the *CTC* group ($p < 0.05$). In conclusion, adding the level of 250 mg/kg LCO in the diet of pig could improve the growth performance and blood physiological and biochemical indicators of pigs, improve the antioxidant level of body and the efficiency of digestion and absorption of nutrients, and show the potential to replace *CTC*.

KEYWORDS

essential oil, antioxidant, microbiota, gut, pig

1 Introduction

Aromatic and volatile oils are obtained from plant tissues by steam distillation. They consist of aliphatic, aromatic, and terpene compounds (Hyldgaard et al., 2012). Essential oils have numerous applications, including spices, food, the chemical industry, and cosmetics. They have certain inhibitory effects on microorganisms (Burt, 2004), making them widely used in these industries. Through research, scholars found that probiotics, plant essential oil, organic acids, etc., as functional additives, can improve animal growth performance, improve animal intestinal health, and have effects similar to that of antibiotics, which is of great significance to the livestock and poultry breeding industry (Suiryanrayna and Ramana, 2015; Liu et al., 2018). At present, the substitutes for antibiotics in feed mainly include organic acids (He RX. et al., 2020), enzyme preparations (Zhang et al., 2020; Vangroenweghe et al., 2021), probiotics (Pan et al., 2017; Csernus and Czeglédi, 2020), antimicrobial peptides (Wang et al., 2016), medium-chain fatty acids (Ren et al., 2020), and essential oils (Li P. et al., 2012; Cheng et al., 2018; Yi et al., 2018). As one of the main antibiotic substitutes, essential oil promotes the growth of weaned piglets and regulates intestinal microorganisms. Plant essential oils are considered potential substitutes for antibiotics and play an active role in improving animal growth performance and preventing diarrhea (Tian and Piao, 2019).

Plant essential oils have antibacterial, anti-inflammatory and antioxidant functions, which can improve the immunity and antioxidation of animals, regulate the structure of intestinal flora, improve intestinal health, and promote animal growth (Zeng et al., 2015a; Zhai et al., 2018). Under normal circumstances, the free radicals produced by the body in the process of oxidative metabolism can be removed by the antioxidant system in time to maintain the balance between oxidation and antioxidation in the body. When the animal body is subjected to stress (such as weaning and bacterial or viral infection), a large number of free radicals are produced in the body, which leads to the imbalance of redox state and oxidative damage (Jiang et al., 2017). A large number of studies have found that essential oils derived from plants (such as oregano essential oil, thyme essential oil, and clove essential oil) have strong antioxidant activity (Bozin et al., 2006; Bounatirou et al., 2007; Wei and Shibamoto, 2010; Teixeira et al., 2013). In addition, phenols, aldehydes, and their derivatives in the main components of essential oil have antioxidant function (Amorati et al., 2013). Essential oils can exert their antioxidant function in two ways: 1) essential oils can directly react with oxygen free radicals, thus reducing the number of oxygen free radicals in the body (Foti, 2007); 2) essential oils can regulate the activities of antioxidant enzymes in the body and indirectly participate in antioxidant function (Choi et al., 2020).

Essential oil also has the function of promoting the growth of intestinal probiotics and protecting against pathogenic bacteria and inhibiting their proliferation, thus improving the structure of intestinal flora (Ouwehand et al., 2010). The mechanism of essential oil inhibiting pathogenic bacteria may be that its active components have strong surface activity and fat solubility, can quickly penetrate the cell membrane of pathogenic microorganisms, make their contents flow out, and effectively prevent the process of respiratory oxidation in mitochondria. Microorganisms lose their energy source and die (Di Pasqua et al., 2007). *L. cubeba* is a deciduous shrub or small tree with high appreciation value and application value in China. *L. cubeba* essential oil (LCO) is composed of *trans-citral*, *cis-citral*, *d-limonene*, and other chemicals derived from the fruit of *L. cubeba* (Thielmann and Muranyi, 2019). LCO is active against *V. parahaemolyticus*, *L. monocytogenes*, *H. anomala* (Liu and Yang, 2012), and *Botrytis cinerea*, a fungus causing the putrefaction of fruits and vegetables (Wang L. et al., 2019). The purpose of this experiment is to explore the effects of LCO on growth performance, apparent digestibility of nutrients, serum immunity, and antioxidant indexes of Taoyuan black pigs, so as to provide data support for the rational application of LCO in pigs.

TABLE 1 Experimental design and grouping.

Group	Diet
Con	Basal diet
CTC	Basal diet +75 g/t chlortetracycline (15%) premix
LCO1	Basal diet +250 g/t LCO
LCO2	Basal diet +500 g/t LCO
LCO3	Basal diet +1000 g/t LCO

2 Materials and methods

2.1 Ethical approval

All the experiment procedures were reviewed and approved by the animal care committee of Changsha Medical University (No. 2021-08), Changsha, China.

2.2 Animals, diets, and treatments

The experiment adopted a single-factor randomized trial design. The 120 fattening pigs of the same breed with good health status and similar body weight were selected and randomly divided into five treatments (six replicates per treatment and four pigs per replicate). In addition, the animals used in the experiment were prefed for 7 days, and the formal test was conducted for 35 days. The test groupings are shown in Table 1.

The basal diet used in the experiment was formulated with reference to the nutritional requirements of fattening pigs in NRC (2012) and Chinese pig breeding standards (NY-T65-2004). The diet was composed of corn, soybean meal, and rice bran meal. The nutrition level is shown in Table 2, and the test pigs were fed pelleted feed for the whole period.

2.3 Sampling and collection

At the beginning and end of the experiment, the test pigs were weighed on an empty stomach in repeated units. During the test period, the daily feed intake of each repeated test pig was recorded, and the average daily feed intake (ADFI), average daily gain (ADG) and feed-to-weight ratio (F/G) of the test pigs were calculated.

TABLE 2 Composition and nutrition levels of the basal diet (air-dry basis, %).

Item	Content
Ingredients	
Corn	27.50
Rice bran	10.00
Rice bran meal	16.00
Broken rice	30.00
Soybean meal	12.50
Premix1)	4.00
Total	100.00
Nutrient level2	
DE (Mcal/kg)	3.20
CP	15.02
Ca	0.55
TP	0.76
AP	0.20
Lys	1.15
Thr	0.60
Met	0.25
Met + Cys	0.50

1) Premix contained per kg VA, 325IU; VD, 37.5IU; VE, 2.75IU; VK_3, 0.013 mg; VB_2, 0.63 mg; VB_6, 0.25 mg; VB_{12}, 2.5 mg; biotin, 0.013 mg; folic acid, 0.08 mg; D-pantothenic acid, 2.00 mg; hydrochloric acid, 2.5 mg; choline chloride, 0.08 mg; antioxidants, 12.50 mg; $FeSO_4{\cdot}H_2O$, 12.50 mg; $CuSO_4{\cdot}H_2O$, 0.88 mg; ZnO, 15.00 mg; $MnSO_4{\cdot}H_2O$, 0.50 mg; Na_2SeO_3 0.04 mg; KI, 0.04 mg. 2) Digestible energy was a calculated value.

(ADG) and feed-to-weight ratio (F/G). We used disposable sterile gloves to collect 500 g of feed samples for each treatment, and at the same time, we randomly collected fresh and clean fecal samples in each replicate, approximately 1 kg for each replicate. Then, we stored them in separate packages for testing.

For each repetition, 20 mL of blood was collected from the anterior vena cava from a pig close to the average body weight of the treatment, placed in an ordinary centrifuge tube, kept at room temperature for 30 min, centrifuged at 3500 r/min for 10 min, and separated. Serum was divided into 1.5 mL centrifuge tubes and stored at −80 C for routine physiological, biochemical, antioxidant, and immune indicators of the serum to be tested.

2.4 Serum index detection

The serum levels of aspartate aminotransferase (AST), alanine aminotransferase (ALT), alkaline phosphatase (ALP), urea, glucose (GLU), total cholesterol (TC), triglyceride (TG), low-density lipoprotein (LDL), high-density lipoprotein (HDL), total protein (TP), and albumin (ALB) in the pigs were measured by using an automatic biochemical analyzer, and the level of globulin (GLB) was calculated (Wang et al., 2022a). A spectrophotometer or microplate reader was used to test total antioxidant capacity (T-AOC), superoxide dismutase (SOD), glutathione (GSH), glutathione peroxidase in pig serum (GPX), catalase (CAT), and malondialdehyde (MDA) levels, including the determination of six antioxidant indicators. The levels of IgA, IgG, and IgM and the levels of complements C3 and C4 in the serum of the test pigs were determined by the enzyme-linked immunosorbent assay.

2.5 Nutrient digestibility determination

The digestibility of dietary dry matter, energy, crude protein, crude fat, crude fiber, crude ash, calcium, and phosphorus was analyzed by the endogenous indicator (acid-insoluble ash) method.

2.6 DNA extraction and PCR amplification

As previously reported, DNA extraction of fecal samples and 16S ribosomal RNA amplification were carried out (Wang et al., 2022b). Fecal samples were extracted for DNA using an E.Z.N.A. ® Soil DNA Kit (Omega Biotek, Norcross, GA, United States) on the basis of the standard protocol. Using universal primers targeting the V3–V4 region 338F/806R, 16S rRNA from bacteria was amplified and sample sequenced using an Illumina Miseq PE300 platform (Illumina, SD, United States) (Wang H. et al., 2019). Sequence reads from the original sequence were uploaded to NCBI's Sequence Read Archive under accession number PRJNA953808.

2.7 Statistical analysis

After preliminary processing of the experimental data with Excel 2007 software, one-way ANOVA was performed with SPSS 19.0 statistical software. If the difference between groups was significant ($p < 0.05$), Duncan's method was used for multiple comparisons. Furthermore, $0.05 < p < 0.1$ was considered a trend. Test results are presented in the form of mean ± standard deviation. In addition, orthogonal polynomial contrasts were used to analyze the linear and quadratic effects of different dietary levels of LCO on various indicators of pigs.

3 Results

3.1 Effect of dietary LCO levels on growth performance in Taoyuan black pigs

The effects of different dietary levels of LCO on the growth performance of finishing pigs are shown in Table 3. Compared with the control treatment of the basal diet and the addition of chlortetracycline, the addition of different levels of LCO in the finishing pig diet had no effect on the average final weight, ADG, and ADFI of the test pigs ($p > 0.05$). However, from the numerical point of view, the average final weight and ADG of the pigs in the experimental treatment with 250 mg/kg of LCO in the diet were the highest, and the diets supplemented with different levels of LCO improved the ADFI compared with the control group of the basal diet. At the same time, dietary supplementation with different levels

TABLE 3 Effect of dietary LCO levels on growth performance in *Taoyuan* black pigs (kg).

Item	CTC level, mg/kg	LCO levels, mg/kg				SEM	*p*-value	*p*-value	
	75	0	250	500	1000			Linear	Quadratic
Average initial weight (kg)	82.03 ± 2.46	82.69 ± 2.84	80.83 ± 4.68	80.97 ± 3.26	81.67 ± 4.30	0.624	0.894	0.578	0.463
Average final weight (kg)	107.63 ± 2.91	107.36 ± 3.32	109.47 ± 4.39	108.58 ± 3.86	107.36 ± 5.30	0.704	0.866	0.941	0.327
ADG (kg)	0.74 ± 0.06	0.72 ± 0.06	0.83 ± 0.10	0.80 ± 0.10	0.75 ± 0.07	0.015	0.118	0.404	0.023
ADFI (kg)	2.62 ± 0.09	2.50 ± 0.16	2.59 ± 0.10	2.63 ± 0.08	2.63 ± 0.07	0.032	0.191	0.033	0.477
F/G	3.55 ± 0.25	3.50 ± 0.09	3.15 ± 0.28	3.32 ± 0.36	3.55 ± 0.33	0.059	0.078	0.897	0.014

In the same row, values with different small letter superscripts mean a significant difference ($p < 0.05$), the same as in the following.

of LCO had a tendency to reduce the feed-to-weight ratio of pigs ($p = 0.078$), and the treatment group supplemented with 250 mg/kg LCO in the diet obtained the best feed-to-weight ratio.

3.2 Effect of dietary LCO levels on serum biochemical indices in Taoyuan black pigs

The effects of different LCO levels in diet on serum physiological and biochemical indexes of finishing pigs are shown in Table 4. Compared with the control treatment and *CTC* addition treatment in the basal diet, adding different levels of LCO to the diet of finishing pigs had no significant effect on the serum GLU, TG, TCHO, ALB, H-DLC, ALP, AST, and ALT levels of pigs ($p > 0.05$). At the same time, the addition of high-level LCO to the diet had a tendency to increase the serum TP and GLB levels of pigs ($0.05 < p < 0.10$), and there was a significant linear positive correlation between this trend and the addition of different levels of LCO to the diet ($p < 0.05$). In addition, compared with *CTC* treatment, the serum L-DLC levels of pigs in the treatment group supplemented with 250 and 500 mg/kg LCO were significantly decreased ($p < 0.05$).

3.3 Effect of dietary LCO levels on serum antioxidant indices in Taoyuan black pigs

As shown in Table 5, compared with the control treatment and *CTC* addition treatment of the basic diet, the catalase level in the serum of the pigs treated with 500 mg/kg LCO in the diet of finishing pigs was significantly increased ($p < 0.05$), and there was a significant secondary correlation between the catalase level in the serum of the pigs treated with different LCO levels in the diet ($p < 0.05$). In addition, T-AOC and the levels of SOD, GSH-Px, GSH, and MDA in serum of pigs were not significantly affected ($p > 0.05$).

3.4 Effect of dietary LCO levels on serum immune indices in Taoyuan black pigs

The effects of different dietary levels of LCO on the serum immune-related indicators of pigs are shown in Table 6. There was no significant difference in the serum IgA, IgG, IgM, C3, and C4 levels of the test pigs between the treatments ($p > 0.05$), but

TABLE 4 Effect of dietary LCO levels on serum biochemical indices in *Taoyuan* black pigs.

Item	CTC level, mg/kg	LCO levels, mg/kg				SEM	*p*-value	*p*-value	
	75	0	250	500	1000			Linear	Quadratic
GLU/(mmol/L)	2.68 ± 0.67	2.46 ± 0.88	3.62 ± 2.89	2.61 ± 0.22	2.85 ± 0.92	0.178	0.296	0.922	0.273
TG/(mmol/L)	0.50 ± 0.20	0.50 ± 0.15	0.61 ± 0.10	0.57 ± 0.14	0.60 ± 0.14	0.031	0.741	0.420	0.576
TCHO/(mmol/L)	2.54 ± 0.17	2.16 ± 0.71	1.96 ± 0.45	1.88 ± 0.63	2.73 ± 0.25	0.123	0.117	0.201	0.081
UREA/(mmol/L)	4.93 ± 1.32	3.50 ± 0.97	4.74 ± 0.81	5.00 ± 0.35	5.23 ± 0.86	0.269	0.119	0.006	0.454
TP/(g/L)	65.11 ± 7.53	58.63 ± 10.37	60.27 ± 8.47	60.93 ± 7.95	75.10 ± 2.25	2.064	0.058	0.015	0.137
ALB/(g/L)	24.19 ± 1.88	22.19 ± 5.99	20.62 ± 1.90	20.58 ± 3.27	25.80 ± 2.50	0.833	0.195	0.224	0.096
GLB/(g/L)	40.93 ± 5.93	36.43 ± 6.44	39.65 ± 8.04	40.34 ± 4.75	49.30 ± 3.78	1.539	0.081	0.012	0.356
H-DLC/(mmol/L)	0.88 ± 0.07	0.84 ± 0.10	0.88 ± 0.09	0.86 ± 0.09	1.02 ± 0.17	0.050	0.209	0.093	0.256
L-DLC/(mmol/L)	1.11 ± 0.16^{a}	0.93 ± 0.22^{ab}	0.74 ± 0.16^{b}	0.70 ± 0.18^{b}	0.88 ± 0.17^{ab}	0.048	0.040	0.438	0.095
ALP/(U/L)	74.53 ± 5.75	79.14 ± 14.86	70.22 ± 9.62	72.10 ± 4.76	84.96 ± 9.37	2.255	0.242	0.417	0.056
AST/(U/L)	20.75 ± 3.75	18.93 ± 3.64	17.52 ± 1.79	18.02 ± 1.65	21.15 ± 5.28	0.770	0.514	0.368	0.212
ALT/(U/L)	55.65 ± 10.51	42.75 ± 11.37	41.02 ± 7.58	41.87 ± 6.49	53.10 ± 8.87	2.307	0.107	0.130	0.166

TABLE 5 Effect of dietary LCO levels on serum antioxidant indices in *Taoyuan* black pigs.

Item	CTC level, mg/kg	LCO levels, mg/kg				SEM	*p*-value	*p*-value	
	75	0	250	500	1000			Linear	Quadratic
SOD/(U/mL)	35.19 ± 16.77	41.69 ± 10.11	39.07 ± 8.81	37.96 ± 10.35	39.72 ± 8.35	2.298	0.945	0.745	0.651
GSH-Px/(U/mL)	1751 ± 343	1553 ± 239	1737 ± 291	1656 ± 147	1626 ± 263	56.18	0.820	0.665	0.379
CAT/(U/mL)	4.19 ± 1.07^{b}	4.65 ± 1.35^{b}	5.61 ± 0.59^{ab}	6.79 ± 1.08^{a}	4.70 ± 0.34^{b}	0.286	0.012	0.534	0.006
GSH/(μmol/L)	43.37 ± 11.71	37.70 ± 9.95	49.59 ± 3.65	53.23 ± 2.73	45.39 ± 5.10	2.440	0.087	0.029	0.017
T-AOC/(mmol/L)	1.17 ± 0.13	1.31 ± 0.05	1.13 ± 0.16	1.23 ± 0.22	1.29 ± 0.20	0.040	0.519	0.835	0.160
MDA/(nmol/mL)	2.55 ± 0.86	2.58 ± 0.58	2.44 ± 0.84	2.48 ± 0.61	2.23 ± 0.48	0.171	0.955	0.505	0.831

TABLE 6 Effect of dietary LCO levels on serum immune indices in *Taoyuan* black pigs.

Item	CTC level, mg/kg	LCO levels, mg/kg				SEM	*p*-value	*p*-value	
	75	0	250	500	1000			Linear	Quadratic
IgA (μg/mL)	641.90 ± 36.78	634.34 ± 17.11	643.09 ± 39.82	647.85 ± 48.28	651.09 ± 54.70	8.923	0.982	0.564	0.980
IgG (mg/mL)	19.60 ± 1.73	17.24 ± 1.63	19.71 ± 2.14	18.77 ± 1.26	18.57 ± 1.73	0.405	0.304	0.284	0.146
IgM (mg/mL)	19.70 ± 0.72	19.93 ± 1.39	20.15 ± 1.02	19.62 ± 0.79	20.55 ± 1.66	0.310	0.799	0.681	0.631
C3 (μg/mL)	107.26 ± 12.24	103.37 ± 7.09	101.94 ± 7.74	104.78 ± 4.04	100.02 ± 9.07	1.965	0.789	0.685	0.700
C4 (μg/mL)	7.62 ± 0.85	7.62 ± 0.70	7.16 ± 0.45	6.94 ± 0.66	7.47 ± 0.85	0.194	0.605	0.529	0.234

from the numerical point of view, the diets added different levels of LCO increased serum immunoglobulin levels in experimental pigs.

3.5 Effect of dietary LCO levels on nutrient apparent digestibility in Taoyuan black pigs

Table 7 shows the effects of different dietary levels of LCO on the apparent digestibility of nutrients in pigs. Compared with the control treatment fed the basal diet and the *CTC* treatment, the experimental treatments with different levels of LCO increased the apparent digestibility of DM and GE and decreased the apparent digestibility of CF ($0.05 < p < 0.10$). Moreover, the apparent digestibility of CP, Ash, and Ca in pigs with different levels of LCO was significantly increased compared with the control treatments fed the basal diet ($p < 0.05$). In addition, compared with the control treatment fed the basal diet and the treatment with *CTC*, the apparent digestibility of EE in pigs treated with medium-dose LCO was significantly increased ($p < 0.05$), and the apparent digestibility of pigs was significantly increased after the addition of low-dose LCO ($p < 0.05$). At the same time, the apparent digestibility of CP, Ash, and Ca, as well as the changing trend of the ADE, had noticeable linear positive correlations with different dietary levels of LCO ($p < 0.05$). These indicated that the addition of different levels of LCO in the diet could significantly improve the efficiency of nutrient digestion and absorption in pigs.

3.6 Effect of dietary LCO levels on bacterial diversity in the feces of Taoyuan black pigs

The rarefaction curves reached a plateau and fully measured most of the bacterial diversity (Figure 1A). In addition, the PCoA showed that the *CTC* group stayed away from the LCO1 group, and the other group sets of samples were not completely separated (Figure 1B).

Based on the five treatments, Figure 2 shows the differences in fecal bacterial diversity among *Taoyuan* black pigs. The bacterial composition of the LCO2 group had a higher Chao1 estimator and lower Simpson index than the other four groups, and the *CTC* group showed the lowest observed_species and Chao1 in the feces. However, the difference between the four indicators in the five groups was not statistically significant ($p > 0.05$).

Firmicutes, *Bacteroidetes*, and *Spirochetes* were the dominant phyla in the feces of *Taoyuan black* pigs, accounting for more than 90% of the total fecal bacterial community (Figure 3). When the diet of LCO proportion increased from 0% to 0.1%, the abundance of cyanobacteria in Con, LCO2, and LCO3 was significantly decreased than that in the *CTC* group ($p < 0.05$). Within the bacterial population, the top 30 genera were identified across all samples (Figure 4A), and the genus *Streptococcus* was the most abundant genera, followed by *Lactobacillus*, *Treponema*, *SMB53*, and *Clostridium*, which were predominant genera of feces in the *Taoyuan black* pigs. Among the genera, the percentage

TABLE 7 Effect of dietary LCO levels on nutrient apparent digestibility in *Taoyuan* black pigs.

Item	CTC level, mg/kg	LCO levels, mg/kg				SEM	*p*-value	*p*-value	
	75	0	250	500	1000			Linear	Quadratic
DM	84.09 ± 0.57	82.18 ± 1.14	84.91 ± 2.76	85.58 ± 3.20	85.66 ± 2.20	0.464	0.065	0.017	0.439
CP	82.03 ± 1.08 ab	80.49 ± 1.22b	82.84 ± 1.09a	83.25 ± 2.05a	83.16 ± 1.36a	0.336	0.021	0.004	0.218
EE	87.29 ± 1.02b	87.84 ± 1.34b	88.48 ± 0.79 ab	89.83 ± 0.53a	88.63 ± 0.92 ab	0.258	0.013	0.051	0.242
Ash	34.95 ± 2.05a	30.51 ± 1.88b	36.10 ± 2.82a	37.28 ± 3.93a	36.64 ± 3.37a	0.739	0.012	0.004	0.141
CF	44.95 ± 5.51	38.20 ± 6.48	35.45 ± 3.79	39.11 ± 3.33	36.23 ± 2.84	1.187	0.056	0.724	0.862
Ca	39.99 ± 2.76 ab	34.33 ± 3.47b	41.63 ± 6.39a	43.10 ± 4.28a	43.98 ± 4.36a	1.082	0.020	0.005	0.379
P	48.41 ± 3.81	46.89 ± 2.84	44.16 ± 3.13	44.90 ± 3.19	49.17 ± 4.87	0.766	0.224	0.665	0.048
GE	86.38 ± 0.68	85.46 ± 1.23	88.62 ± 1.99	88.03 ± 2.66	87.49 ± 2.25	0.404	0.067	0.066	0.098
ADE (Mcal/kg)	3.27 ± 0.03b	3.17 ± 0.06c	3.38 ± 0.11a	3.25 ± 0.04bc	3.27 ± 0.03b	0.018	0.001	0.023	0.005

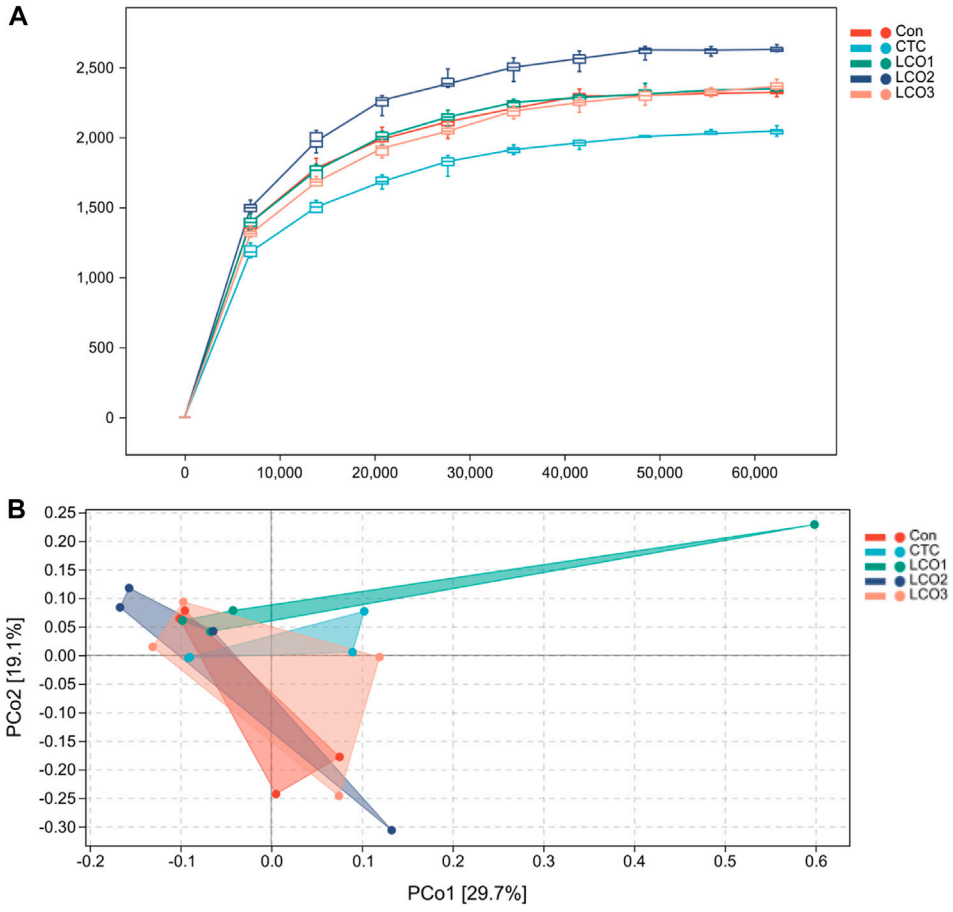

FIGURE 1
(A) Rarefaction curves of observed bacterial sequences in the fecal contents of pigs. **(B)** Principal coordinates analysis (PCoA) of fecal contents bacterial community of pigs. Con represents the group fed a basal diet, and CTC represents the group fed a basal diet with antibiotics, LCO1, LCO2, and LCO3 combined with 250 mg/kg, 500 mg/kg, and 1000 mg/kg, respectively.

abundance of *SMB53* (3.50 ± 2.17 vs. 1.56 ± 0.19; $p < 0.05$) was decreased in the feces of the *CTC* group when compared to that in the LCO2 group (Figure 4B). At the same time, the relative abundance of *L7A_E11* was markedly decreased in the feces of the Con, LCO2, and LCO3 group than that in the *CTC* group ($p < 0.05$).

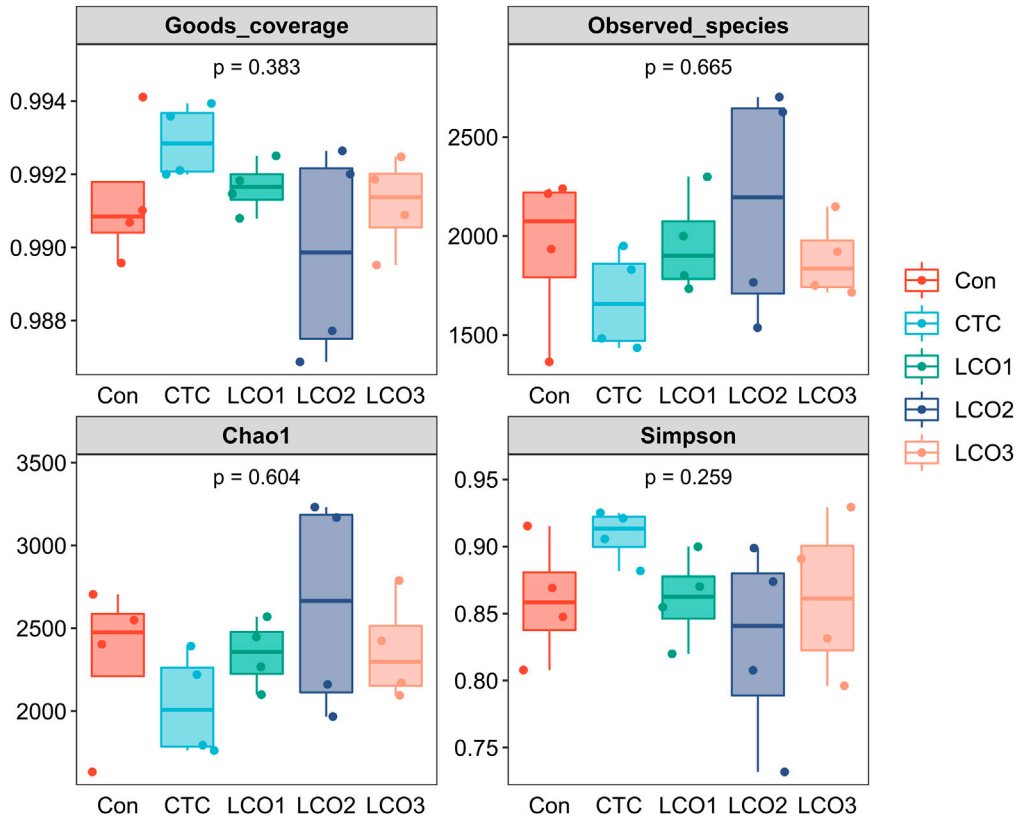

FIGURE 2
Alpha diversity indices of the fecal bacterial communities in pigs. Con represents the group fed a basal diet, and CTC represents the group fed a basal diet with antibiotics, LCO1, LCO2, and LCO3 combined with 250 mg/kg, 500 mg/kg, and 1000 mg/kg, respectively.

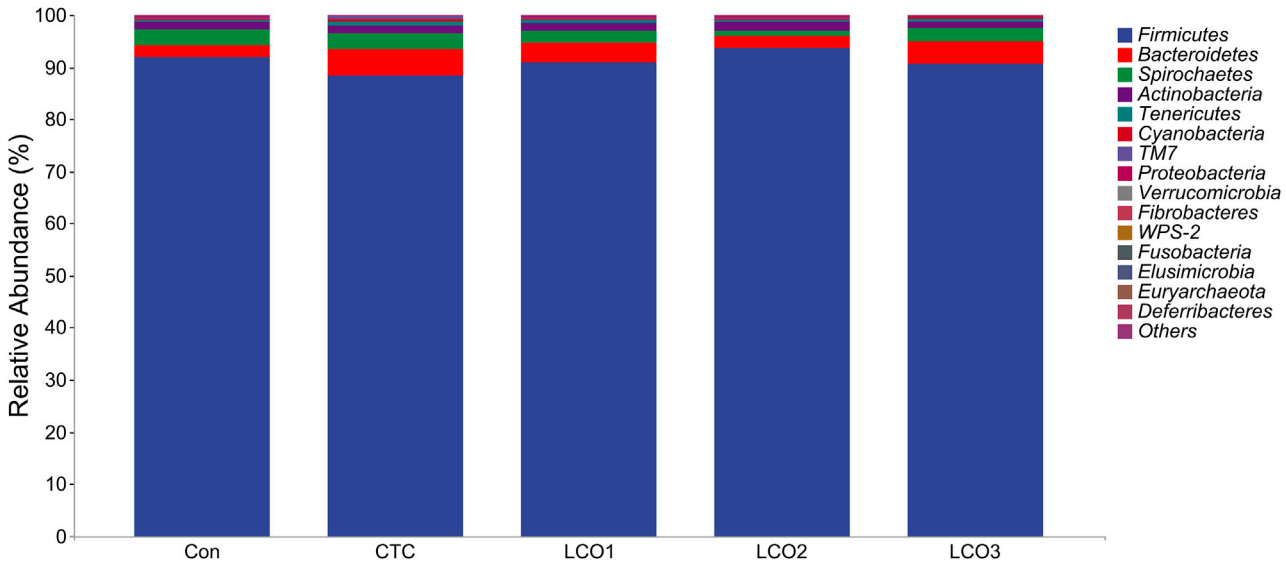

FIGURE 3
Distribution of fecal bacteria at the phylum level in pigs. Con represents the group fed a basal diet, and CTC represents the group fed a basal diet with antibiotics, LCO1, LCO2, and LCO3 combined with 250 mg/kg, 500 mg/kg, and 1000 mg/kg, respectively.

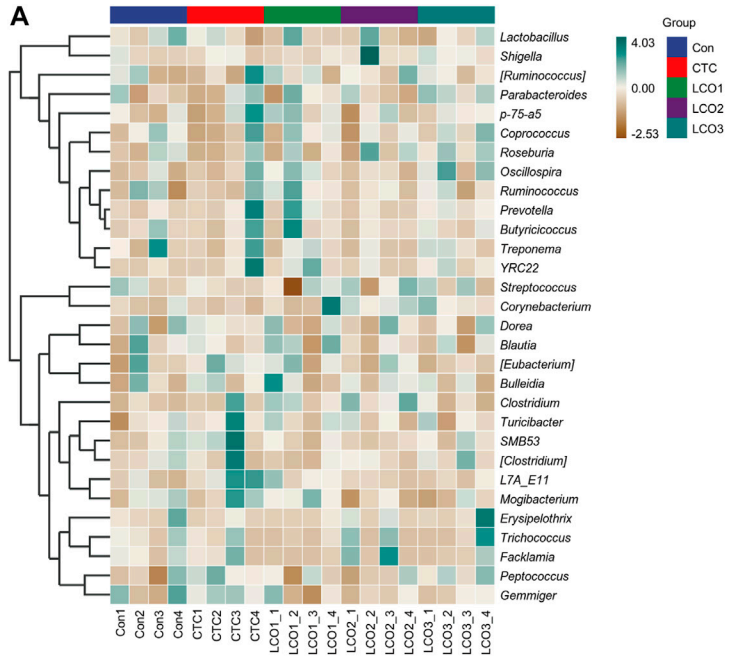

FIGURE 4
Effects of different concentrations LCO on fecal bacteria at the genus level in pigs. **(A)** Distribution of fecal top 30 bacteria at the genus level in pigs. **(B)** Distribution of different bacteria at the genus level in pigs. Con represents the group fed a basal diet, and CTC represents the group fed a basal diet with antibiotics, LCO1, LCO2, and LCO3 combined with 250 mg/kg, 500 mg/kg, and 1000 mg/kg, respectively.

4 Discussion

Currently, traditional Chinese medicine (TCM) research mainly focuses on polysaccharides and flavonoids (Zhong et al., 2016; Ma et al., 2021). There have been many studies on the application effect of plant essential oil in piglet production, but the results vary. The study of Li SY. et al. (2012) showed that the addition of 100 or 150 mg/kg plant essential oils containing thymol and cinnamaldehyde to the diet of weaned piglets could significantly improve the average daily gain and feed conversion efficiency. The study of Gois et al. (2016) showed that the growth performance of piglets was unaffected by pepper essential oil, but it increased the density of intestinal villi. Charal et al. (2016) added 50 mg/kg star anise essential oil to the diets of lactating sows and weaned piglets. There was no significant difference between star anise essential oil and other essential oils in terms of affecting sow performance, but weaned piglets consumed significantly more feed after being fed star anise essential oil. The results of this experiment showed that adding different levels of LCO to the diets of finishing pigs did not significantly affect their growth rates, but the treatment group adding 250 mg/kg LCO in the diet obtained the best feed weight ratio. This indicated that adding an appropriate amount of LCO to the diet for fattening pigs can create economic benefits by saving feed.

In addition to providing information about the body's health and immune function, blood biochemical indexes reveal its biological characteristics (Hussain et al., 2016). Animal growth performance is affected by oxidative stress (Mruk et al., 2002), and due to excess production and accumulation of reactive oxygen species (ROS), this imbalance occurs in the oxidative system (Hussain et al., 2016). MDA is a metabolite produced by peroxidation between free radicals and biofilm lipids. MDA reflects the extent of tissue peroxidation and indirectly indicates cell damage caused by oxygen free radicals. SOD is a common antioxidant enzyme in the animal body, which can catalyze the disproportionation of superoxide anion (O^{-}_{2}) into oxygen (O_2) and hydrogen peroxide (H_2O_2) and remove O^{-}_{2} from the mitochondrial membrane and mitochondrial matrix, which is usually an indicator of the body's ability to respond to oxidative stress. GSH-Px is involved in the reduction of glutathione. T-AOC is used to reflect the scavenging ability of the antioxidant system to oxygen free radicals, and it is often used as a reference index of total antioxidant capacity (Moine et al., 2018; Li et al., 2019). Previous studies have shown that the addition of oregano essential oil (Zhang et al., 2015), cinnamaldehyde (Luo et al., 2020), and the mixture of cinnamaldehyde and thymol (Tian and Piao, 2019) can increase the activity of antioxidant enzymes and reduce the content of MDA in serum. This experiment proved that LCO can improve the level of CAT in the body to improve the ability of pigs to cope with stress. IgA, IgG, and IgM are the main substances of animal humoral immunity, and they can specifically combine with corresponding antigens to play a role. Serum IL-1 β, IL-10, and IFN-γ are involved in the immune response of many kinds of cells, and their contents can judge the inflammation of the body. The content of immunoglobulin can be used as an index to evaluate the immune function of weaned piglets (Grivennikov et al., 2010). Although LCO has no significant effect on the content of IgA, IgG, and IgM in pig serum, from the numerical point of view, the addition of different

levels of LCO to the diet has increased the level of pig serum immunoglobulin to a certain extent.

Studies have shown that plant essential oils can increase the secretion and activity of endogenous digestive enzymes by increasing the secretion of animal saliva and bile and finally improve the digestibility of nutrients in the diet (Lee et al., 2003). The study of Zeng et al. (Yan et al., 2010) also showed that the addition of plant essential oils to the diet could significantly improve the apparent digestibility of crude protein in piglets. Amad et al. (2011) demonstrated that the addition of mixed essential oils of star anise and thyme could significantly improve the apparent digestibility of crude protein and crude fat in broilers. This experiment was conducted to explore the effect of LCO on nutrient digestibility of *Taoyuan black* pigs in order to clarify the effect of LCO on nutrient digestion of pigs. Based on the results, the addition of LCO could effectively improve the apparent digestibility of EE in weaned pigs. This may be due to the fact that the fat in the diet breaks down into free fatty acids and glycerol under the action of intestinal lipase and enters the bloodstream in the form of chylous particles (Qing-Hui et al., 2016). An imbalance in the interaction between gut microbiota and other factors can disrupt intestinal mucosal homeostasis (Luo et al., 2022). Studies have shown that the addition of plant essential oils to animal diets is beneficial to the balance of intestinal microorganisms and the secretion of digestive enzymes (Helander et al., 1998; Jang et al., 2004). Zeng et al. (2015b) significantly increased the digestibility of dry matter, crude protein, and energy after adding cinnamaldehyde and thymol to the diet of piglets. The experiment of Yan et al. (2010) in growing and finishing pigs demonstrated that the addition of menthol-based plant essential oil significantly improved the digestibility of crude protein and main amino acids, while the addition of cinnamaldehyde-based plant essential oil did not significantly affect the apparent digestibility of dietary nutrients. Li P. et al. (2012) found that the addition of 18 mg/kg thymol and cinnamaldehyde to the diet of weaned piglets could increase the digestibility of nutrients, reduce the content of IL-6 in blood and the number of *Escherichia coli* in feces, and increase the total antioxidant capacity in blood, but it did not significantly affect the growth performance of piglets. Van Noten et al. (2020) added 500 mg/kg thymol to the diet of weaned piglets and found that it decreased intestinal permeability and diarrhea rate, but had no significant effect on the growth performance of pigs. Thus, it can be seen that there is a significant difference in the addition level of essential oil in the diet of weaned piglets, and the adding effect is different, which needs to be further studied. Finally, the diet supplemented with different levels of LCO could significantly improve the nutrient digestion and absorption efficiency of finishing pigs.

It is very important to study fecal microbiota for the growth and health of animals (Wu et al., 2017; Wang H. et al., 2019; Wang et al., 2022c). Microbiota in the gut play an important role in digestion, metabolism, immunity, and pathogen defense in animals (Cani and Delzenne, 2009; Wang et al., 2021). To study the complex relationship between the host and microbiota, it was essential to better understand how host and microbes interact. The development of gene sequencing technology allows us to study how changes in the animal diet affect the structure and function of intestinal microorganisms (He B. et al., 2020; Wang et al., 2022d). Several studies have demonstrated the antibacterial activity of various essential oils (Si et al., 2006; Tu et al., 2018). The study on the antibacterial model of plant essential oil by Helander et al. (1998) showed that plant essential oil decomposes the bacterial cell membrane and releases the substances in the membrane from the cell to the external medium. Animal experiments demonstrated that added plant essential oil could increase the number of lactic acid bacteria in piglet feces and reduce the number of *E. coli* (Wei and Shibamoto, 2007). In this study, lactic acid bacteria and *E. coli* in pig feces were not affected by the level of LCO. To maintain digestive function and absorption of nutrients, the intestinal structures and microbiota must remain intact. It was believed that the intestinal bacterial community played a significant role in preserving intestinal function (Sczesnak et al., 2011; Chen J. et al., 2015). The ecosystem contained more than 100 trillion microorganisms, mostly bacteria (Collins et al., 2012). Several factors affect the composition and activity of the microbiota in the intestine, including age, environment, and diet. Diet was the most important factor (Fan et al., 2015; Sonnenburg et al., 2016; Ma et al., 2017). Dietary patterns could affect not only weight but also bone density (Chen Y. et al., 2015). In addition to colonization, gut microbiota-mediated immunity was also influenced by the diet (Saresella et al., 2017). In this study, the bacteria at the major phyla and genus levels of pig feces were not significantly changed. Species-based definitions of a healthy gut microbiome were difficult due to the high variability between and within species (Nguyen et al., 2015; Sender et al., 2016). Even so, gut microbiota and metabolites seem to remain relatively stable (Sender et al., 2016; McCoy et al., 2017). The results of the study of Wei et al. (2017) showed that supplementation of the mixture of thymol and carvol could reduce the relative abundance of *Enterococcus* and *E. coli* and increase the *Lactobacillus* abundance in the jejunum of weaned piglets. Manzanilla et al. (2004) added 15 and 30 mg/kg carvanol, cinnamaldehyde, and pepper essential oil to the diet could significantly increase the ratio of lactic acid bacteria to enterobacteria in the jejunal chyme of piglets. In this experiment, the cyanobacteria abundance had a downward trend in LCO compared to *CTC* treatment. According to the study of Ley et al. (2005), the cyanobacteria group has a logical intestine-associated branch. It is possible that this group is the descendant of ancestral non-photosynthetic cyanobacteria that have adapted to live in animal gastrointestinal tracts.

5 Conclusion

To sum up, adding a certain level of LCO to the diet of pigs could improve the growth performance and blood physiological and biochemical conditions of pigs, improve the antioxidant level of the pig body and the efficiency of digestion and absorption of nutrients, and show the potential to replace antibiotics (CTC). In general, it was considered that 250 mg/kg of LCO should be added to the diet under the experimental conditions.

Data availability statement

The data presented in the study are deposited in the NCBI repository, accession number PRJNA953808.

Ethics statement

The animal study was reviewed and approved by the animal care committee of Changsha Medical University, Changsha, China. Written informed consent was obtained from the owners for the participation of their animals in this study.

Author contributions

Conceptualization: QL and BH; methodology: FC; software: YuW and KW; validation: JC and KP; formal analysis: KW; investigation: YuW; resources: JZ and data curation: KJ, XC, ZL, JO, YoW, XZ, and HZ; writing—original draft preparation: FC; writing—review and editing: KW; supervision: JC; project administration: BH and QL; and funding acquisition: QL. All authors contributed to the article and approved the submitted version.

Funding

This research was funded by the Science and Technology Innovation Program of Hunan Province (2022RC1160), Key R&D Program of Hunan Province (2020NK 2061), Science Research Project of Hunan Provincial Department of Education (22B0894), and ESI Discipline Special Project of Changsha Medical University (2022CYY023 and 2022CYY018).

Conflict of interest

Authors KP, XC, and ZL were employed by the company Hunan Nuoz Biological Technology Co., Ltd.

The remaining authors declare that the research was conducted in the absence of any commercial or financial relationships that could be construed as a potential conflict of interest.

Publisher's note

References

Amad, A. A., Männer, K., Wendler, K. R., Neumann, K., and Zentek, J. (2011). Effects of a phytogenic feed additive on growth performance and ileal nutrient digestibility in broiler chickens. *Poult. Sci.* 90 (12), 2811–2816. doi:10.3382/ps.2011-01515

Amorati, R., Foti, M. C., and Valgimigli, L. (2013). Antioxidant activity of essential oils. *J. Agric. Food Chem.* 61 (46), 10835–10847. Epub 2013/10/26. doi:10.1021/jf403496k

Bounatirou, S., Smiti, S., Miguel, M. G., Faleiro, L., Rejeb, M. N., Neffati, M., et al. (2007). Chemical composition, antioxidant and antibacterial activities of the essential oils isolated from Tunisian Thymus capitatus Hoff. et Link. *Food Chem.* 105 (1), 146–155. doi:10.1016/j.foodchem.2007.03.059

Bozin, B., Mimica-Dukic, N., Simin, N., and Anackov, G. (2006). Characterization of the volatile composition of essential oils of some lamiaceae spices and the antimicrobial and antioxidant activities of the entire oils. *J. Agric. Food Chem.* 54 (5), 1822–1828. Epub 2006/03/02. doi:10.1021/jf051922u

Burt, S. (2004). Essential oils: Their antibacterial properties and potential applications in foods-a review. *Int. J. Food Microbiol.* 94 (3), 223–253. Epub 2004/07/13. doi:10.1016/j.ijfoodmicro.2004.03.022

Cani, P. D., and Delzenne, N. M. (2009). The role of the gut microbiota in energy metabolism and metabolic disease. *Curr. Pharm. Des.* 15 (13), 1546–1558. Epub 2009/05/16. doi:10.2174/138161209788168164

Charal, J. W., Bidner, T. D., Southern, L. L., and Lavergne, T. A. (2016). Effect of anise oil fed to lactating sows and nursery pigs on sow feed intake, piglet performance, and weanling pig feed intake and growth performance11Approved for publication by the director of the Louisiana Agricultural Experiment Station as Publ. No. 2015-230-22599. *Prof. Animal Sci.* 32 (1), 99–105. doi:10.15232/pas.2015-01433

Chen, J., Li, Y., Tian, Y., Huang, C., Li, D., Zhong, Q., et al. (2015a). Interaction between microbes and host intestinal health: Modulation by dietary nutrients and gut-brain-endocrine-immune Axis. *Curr. Protein Pept. Sci.* 16 (7), 592–603. Epub 2015/07/01. doi:10.2174/1389203716666150630135720

Chen, Y., Xiang, J., Wang, Z., Xiao, Y., Zhang, D., Chen, X., et al. (2015b). Associations of bone mineral density with lean mass, fat mass, and dietary patterns in postmenopausal Chinese women: A 2-year prospective study. *PLoS One* 10 (9), e0137097. Epub 2015/09/04. doi:10.1371/journal.pone.0137097

Cheng, C., Xia, M., Zhang, X., Wang, C., Jiang, S., and Peng, J. (2018). Supplementing oregano essential oil in a reduced-protein diet improves growth performance and nutrient digestibility by modulating intestinal bacteria, intestinal morphology, and antioxidative capacity of growing-finishing pigs. *Anim. (Basel)* 8 (9), 159. Epub 2018/09/22. doi:10.3390/ani8090159

Choi, J., Wang, L., Liu, S., Lu, P., Zhao, X., Liu, H., et al. (2020). Effects of a microencapsulated formula of organic acids and essential oils on nutrient absorption, immunity, gut barrier function, and abundance of enterotoxigenic *Escherichia coli* F4 in weaned piglets challenged with *E. coli* F4. *J. Anim. Sci.* 98 (9), skaa259. Epub 2020/08/12. doi:10.1093/jas/skaa259

Collins, S. M., Surette, M., and Bercik, P. (2012). The interplay between the intestinal microbiota and the brain. *Nat. Rev. Microbiol.* 10 (11), 735–742. doi:10.1038/nrmicro2876

Csernus, B., and Czeglédi, L. (2020). Physiological, antimicrobial, intestine morphological, and immunological effects of fructooligosaccharides in pigs. *Arch. Anim. Breed.* 63 (2), 325–335. Epub 2020/09/24. doi:10.5194/aab-63-325-2020

Di Pasqua, R., Betts, G., Hoskins, N., Edwards, M., Ercolini, D., and Mauriello, G. (2007). Membrane toxicity of antimicrobial compounds from essential oils. *J. Agric. Food Chem.* 55 (12), 4863–4870. Epub 2007/05/15. doi:10.1021/jf0636465

Fan, P., Li, L., Rezaei, A., Eslamfam, S., Che, D., and Ma, X. (2015). Metabolites of dietary protein and peptides by intestinal microbes and their impacts on gut. *Curr. Protein Pept. Sci.* 16 (7), 646–654. Epub 2015/07/01. doi:10.2174/1389203716666150630133657

Foti, M. C. (2007). Antioxidant properties of phenols. *J. Pharm. Pharmacol.* 59 (12), 1673–1685. Epub 2007/12/07. doi:10.1211/jpp.59.12.0010

Gois, F. D., Cairo, P. L. G., de Souza Cantarelli, V., Costa, L. C., Fontana, R., Allaman, I. B., et al. (2016). Effect of Brazilian red pepper (Schinus terebinthifolius Raddi) essential oil on performance, diarrhea and gut health of weanling pigs. *Livest. Sci.* 183, 24–27. doi:10.1016/j.livsci.2015.11.009

Grivennikov, S. I., Greten, F. R., and Karin, M. (2010). Immunity, inflammation, and cancer. *Cell* 140 (6), 883–899. Epub 2010/03/23. doi:10.1016/j.cell.2010.01.025

He, B., Zhu, R., Yang, H., Lu, Q., Wang, W., Song, L., et al. (2020b). Assessing the impact of data preprocessing on analyzing next generation sequencing data. *Front. Bioeng. Biotechnol.* 8, 817. Epub 2020/08/28. doi:10.3389/fbioe.2020.00817

He, R. X., Wu, Y. Y., Han, Y. M., et al. (2020a). Effects of compond organic acids on growth performance, serum biochemical indicators and nutrient apparent digestibility of weaning piglets [J]. *Chin. J. Animal Nutr.* 32 (7), 3118–3126. (in Chinese). doi:10.3969/j.issn.1006-267x.2020.07.021

Helander, I. M., Alakomi, H. L., Latva-Kala, K., Mattila-Sandholm, T., Pol, I., Smid, E. J., et al. (1998). Characterization of the action of selected essential oil components on gram-negative bacteria. *J. Agric. Food Chem.* 46 (9), 3590–3595. doi:10.1021/jf980154m

Hussain, T., Tan, B., Yin, Y., Blachier, F., Tossou, M. C., and Rahu, N. (2016). Oxidative stress and inflammation: What polyphenols can do for us? *Oxid. Med. Cell Longev.* 2016, 7432797. Epub 2016/10/16. doi:10.1155/2016/7432797

Hyldgaard, M., Mygind, T., and Meyer, R. L. (2012). Essential oils in food preservation: Mode of action, synergies, and interactions with food matrix components. *Front. Microbiol.* 3, 12. Epub 2012/02/01. doi:10.3389/fmicb.2012.00012

Jang, I. S., Ko, Y. H., Yang, H. Y., Ha, J., Kim, J. Y., Kang, S-Y., et al. (2004). Influence of essential oil components on growth performance and the functional activity of the pancreas and small intestine in broiler chickens. *Asian-Australas. J. Anim. Sci.* 17, 394–400. doi:10.5713/ajas.2004.394

Jiang, X. R., Li, X. L., Awati, A., Bento, H. B. S., Zhang, H. J., VjjoA, B., et al. Effect of an essential oils blend on growth performance, and selected parameters of oxidative stress and antioxidant defence of *Escherichia coli* challenged piglets. (2017) 26:38–43.

Lee, K. W., Everts, H., Kappert, H. J., Frehner, M., Losa, R., and Beynen, A. C. (2003). Effects of dietary essential oil components on growth performance, digestive enzymes and lipid metabolism in female broiler chickens. *Br. Poult. Sci.* 44 (3), 450–457. Epub 2003/09/11. doi:10.1080/0007166031000085508

Ley, R. E., Bäckhed, F., Turnbaugh, P., Lozupone, C. A., Knight, R. D., and Gordon, J. I. (2005). Obesity alters gut microbial ecology. *Proc. Natl. Acad. Sci. U. S. A.* 102 (31), 11070–11075. Epub 2005/07/22. doi:10.1073/pnas.0504978102

Li, P., Piao, X., Ru, Y., Han, X., Xue, L., and Zhang, H. (2012a). Effects of adding essential oil to the diet of weaned pigs on performance, nutrient utilization, immune response and intestinal health. *Asian-Australas J. Anim. Sci.* 25 (11), 1617–1626. Epub 2012/11/01. doi:10.5713/ajas.2012.12292

Li, S., Wu, B., Fu, W., and Reddivari, L. (2019). The anti-inflammatory effects of dietary anthocyanins against ulcerative colitis. *Int. J. Mol. Sci.* 20 (10), 2588. Epub 2019/05/30. doi:10.3390/ijms20102588

Li, S. Y., Ru, Y. J., Liu, M., Xu, B., Péron, A., and Shi, X. G. (2012b). The effect of essential oils on performance, immunity and gut microbial population in weaner pigs. *Livest. Sci.* 145 (1), 119–123. doi:10.1016/j.livsci.2012.01.005

Liu, T. T., and Yang, T. S. (2012). Antimicrobial impact of the components of essential oil of Litsea cubeba from Taiwan and antimicrobial activity of the oil in food systems. *Int. J. Food Microbiol.* 156 (1), 68–75. Epub 2012/03/31. doi:10.1016/j.ijfoodmicro.2012.03.005

Liu, Y., Espinosa, C. D., Abelilla, J. J., Casas, G. A., Lagos, L. V., Lee, S. A., et al. (2018). Non-antibiotic feed additives in diets for pigs: A review. *Anim. Nutr.* 4 (2), 113–125. doi:10.1016/j.aninu.2018.01.007

Luo, Q., Li, N., Zheng, Z., Chen, L., Mu, S., Chen, L., et al. (2020). Dietary cinnamaldehyde supplementation improves the growth performance, oxidative stability, immune function, and meat quality in finishing pigs. *Livest. Sci.* 240, 104221. doi:10.1016/j.livsci.2020.104221

Luo, W., Tian, L., Tan, B., Shen, Z., Xiao, M., Wu, S., et al. (2022). Update: Innate lymphoid cells in inflammatory bowel disease. *Dig. Dis. Sci.* 67 (1), 56–66. Epub 2021/02/21. doi:10.1007/s10620-021-06831-8

Ma, N., Tian, Y., Wu, Y., and Ma, X. (2017). Contributions of the interaction between dietary protein and gut microbiota to intestinal health. *Curr. Protein Pept. Sci.* 18 (8), 795–808. Epub 2017/02/22. doi:10.2174/1389203718666170216153505

Ma, W., Wei, S., Peng, W., Sun, T., Huang, J., Yu, R., et al. (2021). Antioxidant effect of polygonatum sibiricum polysaccharides in D-galactose-induced heart aging mice. *Biomed. Res. Int.* 2021, 6688855. Epub 2021/04/17. doi:10.1155/2021/6688855

Manzanilla, E. G., Perez, J. F., Martin, M., Kamel, C., Baucells, F., and Gasa, J. (2004). Effect of plant extracts and formic acid on the intestinal equilibrium of early-weaned pigs. *J. Anim. Sci.* 82 (11), 3210–3218. Epub 2004/11/16. doi:10.2527/2004.82113210x

McCoy, K. D., Geuking, M. B., and Ronchi, F. (2017). Gut microbiome standardization in control and experimental mice. *Curr. Protoc. Immunol.* 117 (13), 23 1 1–23. Epub 2017/04/04. doi:10.1002/cpim.25

Moine, L., Rivoira, M., Díaz de Barboza, G., Pérez, A., and Tolosa de Talamoni, N. (2018). Glutathione depleting drugs, antioxidants and intestinal calcium absorption. *World J. Gastroenterol.* 24 (44), 4979–4988. Epub 2018/12/05. doi:10.3748/wjg.v24.i44.4979

Mruk, D. D., Silvestrini, B., Mo, M. Y., and Cheng, C. Y. (2002). Antioxidant superoxide dismutase - a review: Its function, regulation in the testis, and role in male fertility. *Contraception* 65 (4), 305–311. Epub 2002/05/22. doi:10.1016/s0010-7824(01)00320-1

Nguyen, T. L., Vieira-Silva, S., Liston, A., and Raes, J. (2015). How informative is the mouse for human gut microbiota research? *Dis. Model Mech.* 8 (1), 1–16. Epub 2015/01/07. doi:10.1242/dmm.017400

Ouwehand, A., Tiihonen, K., Kettunen, H., Peuranen, S., Schulze, H., and Rautonen, N. (2010). *In vitro* effects of essential oils on potential pathogens and beneficial members of the normal microbiota. *Veterinarni Med.* 55, 71–78. doi:10.17221/152/2009-vetmed

Pan, L., Zhao, P. F., Ma, X. K., Shang, Q. H., Xu, Y. T., Long, S. F., et al. (2017). Probiotic supplementation protects weaned pigs against enterotoxigenic *Escherichia coli* K88 challenge and improves performance similar to antibiotics. *J. Anim. Sci.* 95 (6), 2627–2639. Epub 2017/07/21. doi:10.2527/jas.2016.1243

Qing-Hui, A. I., Yan, J., and Kang-Sen, M. (2016). Research progresses of lipids and fatty acids transport IN FISH. *ACTA HYDROBIOL. SIN.* 40. 859–868. doi:10.7541/2016.111

Ren, C., Wang, Y., Lin, X., Song, H., Zhou, Q., Xu, W., et al. (2020). A combination of formic acid and monolaurin attenuates enterotoxigenic *Escherichia coli* induced intestinal inflammation in piglets by inhibiting the NF-κB/MAPK pathways with modulation of gut microbiota. *J. Agric. Food Chem.* 68 (14), 4155–4165. Epub 2020/03/24. doi:10.1021/acs.jafc.0c01414

Saresella, M., Mendozzi, L., Rossi, V., Mazzali, F., Piancone, F., LaRosa, F., et al. (2017). Immunological and clinical effect of diet modulation of the gut microbiome in multiple sclerosis patients: A pilot study. *A Pilot Study* 8, 1391. doi:10.3389/fimmu.2017.01391

Sczesnak, A., Segata, N., Qin, X., Gevers, D., Petrosino Joseph, F., Huttenhower, C., et al. (2011). The genome of Th17 cell-inducing segmented filamentous bacteria reveals extensive auxotrophy and adaptations to the intestinal environment. *Cell Host Microbe* 10 (3), 260–272. doi:10.1016/j.chom.2011.08.005

Sender, R., Fuchs, S., and Milo, R. (2016). Revised estimates for the number of human and bacteria cells in the body. *PLoS Biol.* 14 (8), e1002533. Epub 2016/08/20. doi:10.1371/journal.pbio.1002533

Si, W., Gong, J., Tsao, R., Zhou, T., Yu, H., Poppe, C., et al. (2006). Antimicrobial activity of essential oils and structurally related synthetic food additives towards selected pathogenic and beneficial gut bacteria. *J. Appl. Microbiol.* 100 (2), 296–305. doi:10.1111/j.1365-2672.2005.02789.x

Sonnenburg, E. D., Smits, S. A., Tikhonov, M., Higginbottom, S. K., Wingreen, N. S., and Sonnenburg, J. L. (2016). Diet-induced extinctions in the gut microbiota compound over generations. *Nature* 529 (7585), 212–215. doi:10.1038/nature16504

Suiryanrayna, M. V., and Ramana, J. V. (2015). A review of the effects of dietary organic acids fed to swine. *J. Anim. Sci. Biotechnol.* 6, 45. Epub 2015/10/27. doi:10.1186/s40104-015-0042-z

Teixeira, B., Marques, A., Ramos, C., Neng, N. R., Nogueira, J. M. F., Saraiva, J. A., et al. (2013). Chemical composition and antibacterial and antioxidant properties of commercial essential oils. *Ind. Crops Prod.* 43, 587–595. doi:10.1016/j.indcrop.2012.07.069

Thielmann, J., and Muranyi, P. (2019). Review on the chemical composition of Litsea cubeba essential oils and the bioactivity of its major constituents citral and limonene. *J. Essent. Oil Res.* 31 (5), 361–378. doi:10.1080/10412905.2019.1611671

Tian, Q. Y., and Piao, X. S. (2019). Essential oil blend could decrease diarrhea prevalence by improving antioxidative capability for weaned pigs. *Anim. (Basel)* 9 (10), 847. Epub 2019/10/24. doi:10.3390/ani9100847

Tu, X-F., Hu, F., Thakur, K., Li, X-L., Zhang, Y-S., and Wei, Z-J. (2018). Comparison of antibacterial effects and fumigant toxicity of essential oils extracted from different plants. *Ind. Crops Prod.* 124, 192–200. doi:10.1016/j.indcrop.2018.07.065

Van Noten, N., Degroote, J., Van Liefferinge, E., Taminiau, B., De Smet, S., Desmet, T., et al. (2020). Effects of thymol and thymol α-D-glucopyranoside on intestinal function and microbiota of weaned pigs. *Anim. (Basel)* 10 (2), 329. Epub 2020/02/26. doi:10.3390/ani10020329

Vangroenweghe, F., Poulsen, K., and Thas, O. (2021). Supplementation of a β-mannanase enzyme reduces post-weaning diarrhea and antibiotic use in piglets on an alternative diet with additional soybean meal. *Porc. Health Manag.* 7 (1), 8. Epub 2021/01/13. doi:10.1186/s40813-021-00191-5

Wang, H., Hu, C., Cheng, C., Cui, J., Ji, Y., Hao, X., et al. (2019b). Unraveling the association of fecal microbiota and oxidative stress with stillbirth rate of sows. *Theriogenology* 136, 131–137. Epub 2019/07/01. doi:10.1016/j.theriogenology.2019.06.028

Wang, K., Ma, J., Li, Y., Han, Q., Yin, Z., Zhou, M., et al. (2022b). Effects of essential oil extracted from Artemisia argyi leaf on lipid metabolism and gut microbiota in high-fat diet-fed mice. *Sec. Nutr. Microbes* 9. doi:10.3389/fnut.2022.1024722

Wang, K., Peng, X., Lv, F., Zheng, M., Long, D., Mao, H., et al. (2021). Microbiome-metabolites analysis reveals unhealthy alterations in the gut microbiota but improved meat quality with a high-rice diet challenge in a small ruminant model. *Anim. (Basel)* 11 (8), 2306. Epub 2021/08/28. doi:10.3390/ani11082306

Wang, K., Peng, X., Yang, A., Huang, Y., Tan, Y., Qian, Y., et al. (2022c). Effects of diets with different protein levels on lipid metabolism and gut microbes in the host of different genders. *Front. Nutr.* 9, 940217. Epub 2022/07/06. doi:10.3389/fnut.2022.940217

Wang, K., Yan, Q., Ren, A., Zheng, M., Zhang, P., Tan, Z., et al. (2022d). Novel linkages between bacterial composition of hindgut and host metabolic responses to SARA induced by high-paddy diet in young goats. *Sec. Animal Nutr. Metabolism* 8. doi:10.3389/fvets.2021.791482

Wang, K., Zhou, M., Gong, X., Zhou, Y., Chen, J., Ma, J., et al. (2022a). Starch–protein interaction effects on lipid metabolism and gut microbes in host. *Front. Nutr.* 9, 1018026. doi:10.3389/fnut.2022.1018026

Wang, L., Hu, W., Deng, J., Liu, X., Zhou, J., and Li, X. (2019a). Antibacterial activity of Litsea cubeba essential oil and its mechanism against Botrytis cinerea. *Rsc Adv.* 9 (50), 28987–28995. doi:10.1039/C9RA05338G

Wang, S., Zeng, X., Yang, Q., and Qiao, S. (2016). Antimicrobial peptides as potential alternatives to antibiotics in food animal industry. *Int. J. Mol. Sci.* 17 (5), 603. Epub 2016/05/07. doi:10.3390/ijms17050603

Wei, A., and Shibamoto, T. (2007). Antioxidant activities and volatile constituents of various essential oils. *J. Agric. Food Chem.* 55 (5), 1737–1742. Epub 2007/02/14. doi:10.1021/jf062959x

Wei, A., and Shibamoto, T. (2010). Antioxidant/lipoxygenase inhibitory activities and chemical compositions of selected essential oils. *J. Agric. Food Chem.* 58 (12), 7218–7225. Epub 2010/05/27. doi:10.1021/jf101077s

Wei, H. K., Xue, H. X., Zhou, Z. X., and Peng, J. (2017). A carvacrol-thymol blend decreased intestinal oxidative stress and influenced selected microbes without changing the messenger RNA levels of tight junction proteins in jejunal mucosa of weaning piglets. *Animal* 11 (2), 193–201. Epub 2016/07/16. doi:10.1017/s1751731116001397

Wu, F., Guo, X., Zhang, J., Zhang, M., Ou, Z., and Peng, Y. (2017). Phascolarctobacterium faecium abundant colonization in human gastrointestinal tract. *Exp. Ther. Med.* 14 (4), 3122–3126. Epub 2017/09/16. doi:10.3892/etm.2017.4878

Yan, L., Wang, J. P., Kim, H. J., Meng, Q. W., Ao, X., Hong, S. M., et al. (2010). Influence of essential oil supplementation and diets with different nutrient densities on growth performance, nutrient digestibility, blood characteristics, meat quality and fecal noxious gas content in grower–finisher pigs. *Livest. Sci.* 128 (1), 115–122. doi:10.1016/j.livsci.2009.11.008

Yi, D., Fang, Q., Hou, Y., Wang, L., Xu, H., Wu, T., et al. (2018). Dietary supplementation with oleum cinnamomi improves intestinal functions in piglets. *Int. J. Mol. Sci.* 19 (5), 1284. Epub 2018/04/26. doi:10.3390/ijms19051284

Zeng, Z., Xu, X., Zhang, Q., Li, P., Zhao, P., Li, Q., et al. (2015b). Effects of essential oil supplementation of a low-energy diet on performance, intestinal morphology and microflora, immune properties and antioxidant activities in weaned pigs. *Anim. Sci. J.* 86 (3), 279–285. doi:10.1111/asj.12277

Zeng, Z., Zhang, S., Wang, H., and Piao, X. (2015a). Essential oil and aromatic plants as feed additives in non-ruminant nutrition: A review. *J. Anim. Sci. Biotechnol.* 6 (1), 7. Epub 2015/03/17. doi:10.1186/s40104-015-0004-5

Zhai, H., Liu, H., Wang, S., Wu, J., and Kluenter, A-M. (2018). Potential of essential oils for poultry and pigs. *Anim. Nutr.* 4 (2), 179–186. doi:10.1016/j.aninu.2018.01.005

Zhang, J., Liu, Y., Yang, Z., Yang, W., Huang, L., Xu, C., et al. (2020). Illicium verum extracts and probiotics with added glucose oxidase promote antioxidant capacity through upregulating hepatic and jejunal Nrf2/Keap1 of weaned piglets. *J. Anim. Sci.* 98 (3), skaa077. Epub 2020/03/13. doi:10.1093/jas/skaa077

Zhang, T., Zhou, Y. F., Zou, Y., Hu, X. M., Zheng, L. F., Wei, H. K., et al. (2015). Effects of dietary oregano essential oil supplementation on the stress response, antioxidative capacity, and HSPs mRNA expression of transported pigs. *Livest. Sci.* 180, 143–149. doi:10.1016/j.livsci.2015.05.037

Zhong, W. J., Luo, Y. J., Li, J., Wu, Y. P., Gao, Y. J., Luo, H. J., et al. (2016). Polymethoxylated flavonoids from citrus reticulata blanco. *Biochem. Syst. Ecol.* 68, 11–14. doi:10.1016/j.bse.2016.02.031

frontiers | Frontiers in Plant Science

TYPE Original Research
PUBLISHED 28 July 2023
DOI 10.3389/fpls.2023.1199215

OPEN ACCESS

EDITED BY
Chunpeng (Craig) Wan,
Jiangxi Agricultural University, China

REVIEWED BY
Shuiming Xiao,
China Academy of Chinese Medical Sciences, China
Li Yang,
NingboTech University, China

*CORRESPONDENCE
Tao Zhou
364462907@qq.com
Jin Pei
peixjin@163.com

†These authors have contributed equally to this work

RECEIVED 03 April 2023
ACCEPTED 10 July 2023
PUBLISHED 28 July 2023

CITATION
Wen F, Chen S, Wang Y, Wu Q, Yan J, Pei J and Zhou T (2023) The synthesis of *Paris* saponin VII mainly occurs in leaves and is promoted by light intensity.
Front. Plant Sci. 14:1199215.
doi: 10.3389/fpls.2023.1199215

The synthesis of *Paris* saponin VII mainly occurs in leaves and is promoted by light intensity

Feiyan Wen[1,2†], Siyu Chen[1,2†], Yue Wang[1,2], Qinghua Wu[1,2], Jie Yan[1,2], Jin Pei[1,2*] and Tao Zhou[1,2*]

[1]State Key Laboratory of Southwestern Chinese Medicine Resources, Chengdu University of Traditional Chinese Medicine, Chengdu, Sichuan, China, [2]College of Pharmacy, Chengdu University of Traditional Chinese Medicine, Chengdu, Sichuan, China

Unraveling the specific organs and tissues involved in saponin synthesis, as well as the light regulatory mechanisms, is crucial for improving the quality of artificially cultivated medicinal materials of *Paris* plants. *Paris* saponin VII (PS VII), a high-value active ingredient, is found in almost all organs of *Paris* plant species. In this study, we focused on *Paris polyphylla* var. *yunnanensis* (Franch.) Hand. - Mzt. (PPY) and found that PS VII synthesis predominantly occurs in leaves and is increased by high light intensity. This intriguing discovery has unveiled the potential for manipulating non-traditional medicinal organ leaves to improve the quality of medicinal organ rhizomes. The analysis of the impact of organ differences on saponin concentration in *P. polyphylla* var. *chinensis* (Franch.) Hara (PPC), *P. fargesii* Franch. (PF), and PPY revealed consistency among the three *Paris* species and was mainly dominated by PS VII. Notably, the leaves and stems exhibited much higher proportions of PS VII than other organs, accounting for 80–90% of the four main saponins. Among the three *Paris* species, PPY had the highest concentration of PS VII and was selected for subsequent experiments. Further investigations on saponin subcellular localization, temporal variation, and stem wound fluid composition demonstrated that PS VII is synthesized in mesophyll cells, released into the intercellular space through exocytosis, and then transported to the rhizome via vascular tissue. These findings confirm the significant role of leaves in PS VII synthesis. Additionally, a ^{13}C-glucose feeding to trace PS VII biosynthesis revealed that only PS VII in the leaves exhibited incorporation of the labeled carbon, despite conducting ^{13}C-glucose feeding in leaves, stems, rhizomes, and roots. Thus, the leaves are indeed the primary organ for PS VII synthesis in PPY. Furthermore, compared with plants under 100 μmol m^{-2} s^{-1}, plants under 400 μmol m^{-2} s^{-1} exhibited a higher PS VII concentration, particularly in the upper epidermal cells of the leaves. We propose that high light intensity promotes PS VII synthesis in leaves through three mechanisms: (1) increased availability of substrates for saponin synthesis; (2) protection of leaves from high light damage through enhanced saponin synthesis; and (3) enhanced compartmentalization of saponins within the leaves, which in turn feedback regulates saponin synthesis.

KEYWORDS

***Paris* saponin VII, synthesis organ, leaf, light intensity, PPY**

Introduction

Paris, a genus belonging to the Melanthiaceae family, is predominantly distributed in Asia with a partial presence in Europe. Throughout Asia, the wild resources of *Paris* are in a critically endangered state due to overexploitation and habitat degradation. Recognizing this threat, the International Union for Conservation of Nature (IUCN) has designated *Paris* as 'vulnerable' on its Red List, highlighting the decline in wild populations. In China, the entire genus *Paris*, with the exception of *Paris verticillata* M.-Bieb., is listed under special state key protection for wild plants. At present, the artificial cultivation industry of *Paris* species has achieved a certain scale. The main cultivated species are *Paris polyphylla* var. *yunnanensis* (Franch.) Hand. - Mzt. (PPY) and *Paris polyphylla* var. *chinensis* (Franch.) Hara (PPC), which are listed in the Chinese Pharmacopoeia. *Paris* species all contain Paris saponins (PS), which are isoprene compounds that exhibit a diverse range of pharmacological activities, including antioxidant, anticancer, anti-inflammatory, antifungal, and hypolipidemic functions (Qin et al., 2018; Ding et al., 2021). However, despite cultivation periods lasting nearly 8 years, the saponin concentration in most cultivated medicinal materials of *Paris* fails to meet the minimum standards required for medicinal use (Wu et al., 2017). This discrepancy raises concerns about the environmental adaptability of *Paris* plant growth and the synthetic biology of saponin, particularly the lack of clarity regarding the synthesis organelle. These factors serve as key limitations in achieving high-quality medicinal materials of *Paris*.

The principal saponins identified in *Paris* species comprise *Paris* saponin VII, H, VI, II, I, Dioscin, and Gracillin (Zhou et al., 2021). In the current version of National Pharmacopoeia Commission, (2020), PS VII, PS II, and PS I are designated as quality control components for medicinal materials of *Paris* (*Paridis Rhizoma*). In addition, PS H is recognized as an important hemostatic active ingredient (Bi et al., 2021). Typically, the *Paris* rhizome with the highest saponin concentration and biomass accumulation is used as medicinal material. However, studies have revealed the presence of PSs in various organs of PPY, including the root, stem, leaf, flower, fruit, and seeds. Analysis of saponin types in different organs has shown a consistent composition of PS VII in leaves and stems, which differs from that found in the rhizome. Moreover, the concentration of PS VII in the rhizome increases gradually during the initial years of growth (usually within the first 4 years) but remains lower than that in the leaves (Wen, unpublished data). Notably, young *Paris* plant leaves have the highest concentration of PS VII (Wen unpublished data). These findings provide evidence supporting the significant role of leaves in the synthesis of PS VII.

Leaves have been speculated to be a major organ for the synthesis of steroidal saponins in medicinal plants. For instance, the subcellular localization of ginsenoside Rb_1 in *Panax ginseng* has been identified in chloroplasts, the cytoplasm of parenchymal cells, and the vascular phloem cells of leaves (Yokota et al., 2011). In *Dioscorea* species, including *Paris* species, Diosgenin saponins play a pivotal role. In *Dioscorea zingiberensis*, the distribution of diosgenin saponins is predominantly observed in multiple plant tissues. These include the epidermis of the leaves, the palisade tissue, spongy tissue, phloem in the vascular tissues of the stem, and the ground tissue within the rhizomes. (Li et al., 2022). By analyzing spatial and temporal variations, immunohistochemical localization, and transcriptome data, it has been revealed that diosgenin is first synthesized in the leaves of *Dioscorea zingiberensis*, converted into dioscin, and subsequently transported to the rhizome for storage (Li et al., 2022). Similarly, in PPY, transcriptome analysis has indicated that genes responsible for regulating PS synthesis are specifically expressed in the leaves where they are significantly more highly expressed than in the rhizome (Gao et al., 2020). Based on these findings, we hypothesize that in PPY, the leaves, rather than the rhizome, serve as the primary organ for the synthesis of PS.

Despite extensive research on the pharmacological activities of saponins in disease treatment, our understanding of their biological functions, particularly their synthesis, distribution, and accumulation in response to biotic and abiotic stress, remains limited. Unlike mobile organisms, plants growing in soil have developed mechanisms to protect themselves from external damage, often utilizing specialized metabolites (Liu et al., 2019a; Hunziker et al., 2021). Optimization of chemical defenses is one strategy employed by plants to defend against herbivores (Gershenzon and Ullah, 2022), and saponins have been identified as a class of defense compounds that exhibit toxicity or deterrent effects on insects, molluscs, fungi, and microorganisms (Faizal and Geelen, 2013; Hussain et al., 2019; Ninkuu et al., 2021). The unique chemical structure of saponins, characterized by a hydrophobic terpenoid backbone with attached hydrophilic saccharide groups, contributes to those functions by altering cell membrane permeability, ultimately leading to cell damage (Stewart et al., 2018).

In addition to their role in response to biotic stress, saponin biosynthesis can be induced to mitigate abiotic stressors, such as light, temperature, and drought (Szakiel et al., 2011; de Costa et al., 2013; Rogowska and Szakiel, 2020). The natural habitat and cultivation areas of PPY primarily encompass Yunnan and the plateau of western Sichuan in China, with total solar radiation ranging from 5,000 to 5,850 MJ m^{-2} per year, which is approximately the annual average for China as a whole (5,900 MJ m^{-2}). Interestingly, PPY grown in areas with lower light intensity, such as Sichuan and Guizhou in China, where total solar radiation ranges from 3,350 to 4,190 MJ m^{-2} per year, exhibits significantly lower saponin concentrations than PPY grown in Yunnan. Previous studies have shown that optimizing light quality and intensity can increase the total saponin concentration and rhizome biomass of PPY (Zhang et al., 2018). Additionally, LED light exposure has been found to increase the accumulation of triterpenoid saponin glycosides in *in vitro* culture of *Bacopa monnieri* when combined with precursor feeding (Watcharatanon et al., 2019), while saponins in *Centella asiatica* have been shown to increase resistance to UV oxidation damage (Müller et al., 2013).

Traditional Chinese medicine and crops have played a significant role in promoting human health and survival. However, our understanding of the growth habits and survival strategies of medicinal plants lags behind that of crops. This knowledge gap has resulted in outdated cultivation techniques, small-scale production, and an inconsistent quality of medicinal herbs. Although advancements in sequencing technologies and

molecular biology have led to the identification of whole-genome sequences of over 100 medicinal plant species and the elucidation of synthetic pathways for important medicinal components, their impact on high-quality herbal medicine production has been limited. To address this issue, it is essential to gain insights into the tissue-specific and environmentally regulated mechanisms underlying the synthesis of medicinal components. Such understanding is a prerequisite for developing cultivation practices that achieve both high quality and high yield in medicinal plants. To bridge this knowledge gap, a series of experiments were conducted using plant physiological and biochemical analysis methods. These included variability analysis at the tissue level, spatial and temporal specificity analysis, isotopic ^{13}C labeling, and transmission electron microscopy observation. The aim was to clarify the main organs responsible for the synthesis of PS and how their synthesis is regulated by light intensity. Specifically, two hypotheses were tested: (1) the leaf is the main organ for the synthesis of PS, and (2), high light intensity increases the synthesis of PS in leaves.

Materials and methods

Plant materials

The study employed 5-year-old plants of three *Paris* species: *P. polyphylla* var. *chinensis* (PPC), *P. fargesii* (PF), and *P. polyphylla* var. *yunnanensis* (PPY). These plants were collected from different locations in China: PPC from Sichuan Pengzhou (103°44′E, 31°13′ N), PF from Sichuan Dujiangyan (103°33′E, 30°55′N), and PPY from Yunnan Wenshan (104°11′E, 23°04′N). Analysis of saponins in the leaves, stems, rhizomes, and roots of these plants was conducted to evaluate their similarities and differences. Additional 5-year old *P. polyphylla* var. *yunnanensis*(PPY) plants were collected for a leaf saponin transport experiment and the sampling of stem wound fluid. To avoid interference from saponin accumulation in perennial rhizomes, 2-year-old seedlings were used for the ^{13}C-glucose ($^{13}C_6H_{12}O_6$) feeding and light intensity experiments. The weight of the seminal root of the seedlings was controlled at approximately 2 ± 0.2 g. The seedlings were initially harvested from Wenshan, Yunnan during winter and then cultivated in a climate chamber. The following year, seedlings of the same height were selected for the experiments after the plants had achieved stable growth in height.

Experimental design and plant management

The experiment was conducted using a randomized block design with three replicates in a greenhouse environment. The greenhouse maintained a relative humidity of 75% and a day/night temperature of 20°C/10°C, and a photoperiod of 12 h day/12 h night during the plant growth period. PPY has the characteristics of a typical heliophyte herb; according to the daily sunshine hours during the growing period in Yunnan, a photoperiod of 12 h day/ 12 h night was employed. The irradiance was provided by light-emitting diode (LED) lamps. Our previous study found that 2-year-old PPY seedlings can tolerate a light intensity of up to 400 μmol m^{-2} s^{-1} for cultivation in the laboratory (data not shown), with higher photosynthesis and only slight photoinhibition. Thus, light intensities of 100 and 400 μmol m^{-2} s^{-1} were chosen as the low and high light intensity treatments, respectively. All seedlings were placed under 100 μmol m^{-2} s^{-1} before treatment. During the plant growth period, the distance gap between LED lamps and the plant canopy was 30 cm. Irradiance was measured routinely using a quantum sensor (Highpoint, Taiwan).

The 5-year-old PPY were individually placed in pots measuring 10×10×10 cm. Six PPY were used for the leaf saponin transport experiment and three for the stem wound fluid sampling. The 2-year-old seedlings were placed in seedling disc of 25 holes; 100 seedlings were used under each light intensity (100 and 400 μmol m^{-2} s^{-1}) in follow-up experiments. All seedlings received regular watering and nutrient supply according to their respective treatments.

The experiment involving ^{13}C-glucose ($^{13}C_6H_{12}O_6$) feeding track PS VII biosynthesis via plant organs was set to four groups as follows (Figure 1A). In group 1, the leaves were sprayed with 0.2%^{13}C-glucose solution at a volume of 1 ml per leaf, administered once every 2 days (Yuan et al., 2020). In groups 2 and 3, the roots of the seedlings were fed with 0.2%^{13}C-glucose solution. Additionally, in Group 3, the stem of the seedlings was partially severed near the rhizome end to facilitate feeding through the stem's vascular bundle. Group 4 served as the control group without any ^{13}C-glucose treatment. The experimental treatment time lasted for 10 days. In each group, three 2-year-old seedlings were subjected to a light intensity of 100 μmol m^{-2} s^{-1}. All groups were cultivated hydroponically using Hoagland's nutrient solution; the culture medium was changed every 2 days and the solution was ventilated with an air pump (Zhou et al., 2016).

Plant sampling

Four organ samples of the three *Paris* species were collected from origin for PS analysis. To investigate the PS flowing in the leaves, a specific procedure was followed for leaf sampling. Each seedling's three leaves were individually wrapped in aluminum foil to avoid exposure to light (Figure 2A). Sampling was conducted daily at 5 pm, with a 24-h interval time series (0, 24, 48, and 72 h) followed. For the collection of stem wound fluid, the stem of the seedlings was severed near the rhizome end to obtain the fluid. A negative pressure pump with a pressure of 0.05 MPa was used to facilitate the outflow of the stem wound fluid within a few minutes. The fluid was then concentrated on 2 cm^2 filter paper and immediately subjected to 75% ethanol extraction for the analysis of saponins (Figure 3A). Fresh PPY leaves were sampled and fixed for PS subcellular chemical localization using a transmission electron microscope (TEM).

At the conclusion of the ^{13}C-glucose experiment, which lasted 10 days, the leaves, stems, rhizomes, and roots of each group were collected individually. These collected plant organs were thoroughly washed to remove any surface impurities. Subsequently, quantitative analysis of PS VII and the ratio of $^{13}C/^{12}C$ in different plant organs was

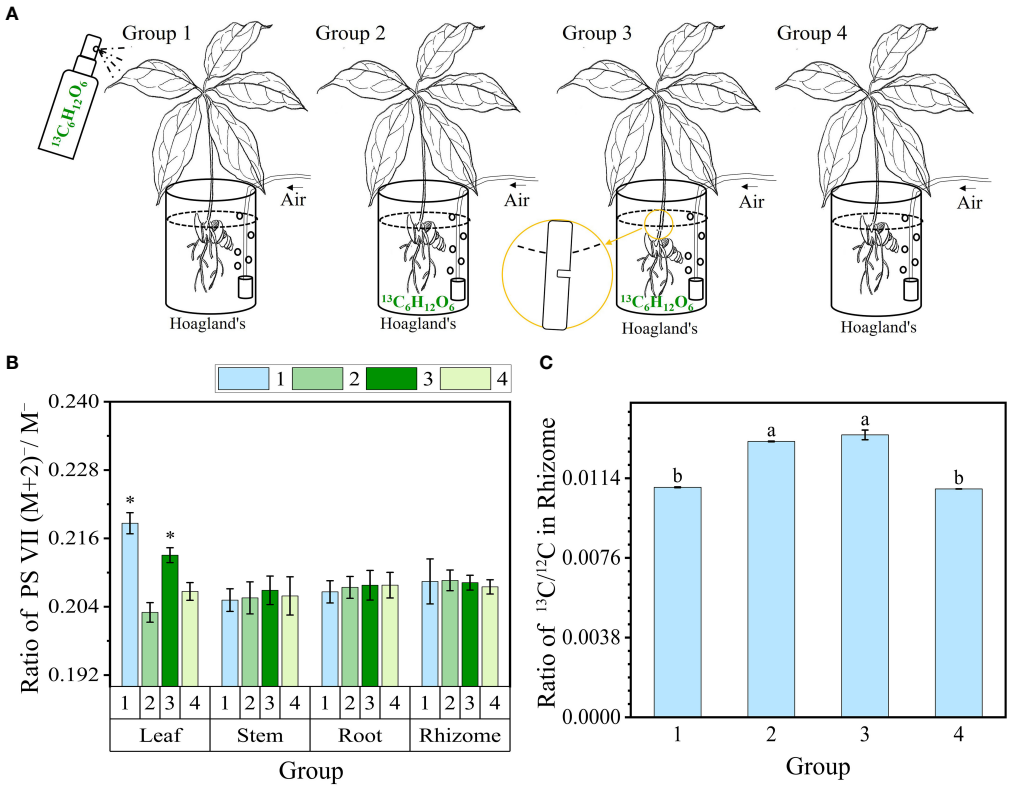

FIGURE 1
^{13}C-glucose ($^{13}C_6H_{12}O_6$) feeding track PS VII biosynthesis via plant organs. **(A)** Schematic diagram illustrating glucose feeding in different organs. Groups 1–3 were fed in the leaf, rhizome, and stem vascular bundle, and group 4 was not fed. **(B)** The ratio of PS VII $(M+2)^-/M^-$ in organs. **(C)** The ratio of $^{13}C/^{12}C$ isotopes in rhizomes of four groups. PS, *Paris* saponins. Each column represents the mean (± SE) of three replicates. * indicates a significant difference (t-test at $p \leq 0.01$). Data with different letters are significantly different between four groups ($p \leq 0.05$).

performed. In the following light intensity processing experiment, the light intensities of two groups were set as 100 µmol m^{-2} s^{-1} and 400 µmol m^{-2} s^{-1}. Throughout the 1-week treatment period, various photosynthetic parameters and chlorophyll fluorescence were measured. Then, the seedlings from the two groups were sampled to determine chlorophyll concentration. To examine cell morphology and chloroplast arrangement, the leaves were fixed with formalin-aceto-alcohol (FAA) solution, stained with red and solid green, and then sliced for observation under a general microscope. The distribution of saponins in the upper and lower epidermis was observed using chemical chromogenic techniques via TEM. At the same time, the upper and lower epidermis of the leaves were manually separated using pointed tweezers (approximately 2 mg of dried weight). Sections of leaves of considerable weight without major vascular tissue were removed by scissors. Subsequently, whole leaves without petioles, stems, rhizomes, and roots were collected separately. All samples for quantification were first incubated at 105°C for 30 mins and then dried at 60°C until a constant weight was reached.

Measurement of *Paris* saponin VII, H, II, and I

The dried samples were ground to a fine powder using a steel ball mill (Tissuelyser-48, Jingxin, China). Approximately 30 mg of powder of each sample was subjected to ultrasonic and extracted in 2 ml of 75% v/v ethyl alcohol water at 25°C for 20 min twice, and three parallel samples were prepared. The extract solution was filtered, merged and dried with nitrogen, and then dissolved to a volume of 1 ml with chromatographic methanol. The extraction and preparation process for the filter-paper-adsorbed stem wound fluid was the same as with other organs. The preparation method for the upper and lower epidermis tissue was the same as above, except the dose was approximately 2 mg and the final volume was 200 µl. Before injection, a 0.22-µm organic phase filter (Jinteng, China) was used for filtration. Saponins were identified through comparison with retention times and coelution of authentic standard solutions. The main saponins were identified through qualitative analysis of the filter-paper-adsorbed stem wound fluid and other organs. The proportions of PS VII, PS H, PS II, and PS I in the sum of the four main saponins were calculated to compare the similarity of the saponin types and the proportion difference. In other experiments, quantitative concentrations of PS VII, PS H, PS II, and PS I were determined.

The determination of four saponins was carried out using a UFLC-MS/MS system, equipped with two LC-30D pumps, an SIL-30AC autosampler, a CTO-20AC column oven (Simadzu, Japan), and Qtrap 5500 mass spectrometry coupled with an electrospray ionization (ESI) interface, controlled by Analyst 1.6.2 software for operation, data acquisition, and analysis (AB SCIEX, USA).

10.3389/fpls.2023.1199215

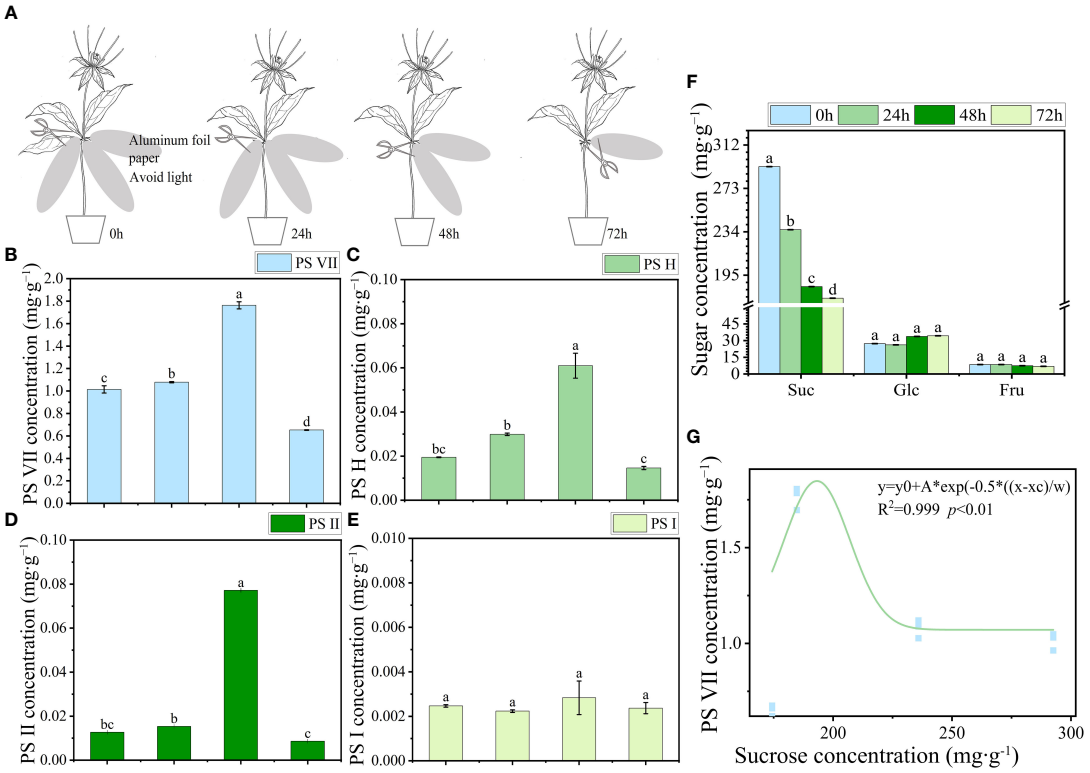

FIGURE 2
The transport characteristics of saponins and soluble sugar in PPY leaves. **(A)** Schematic diagram illustrating the use of aluminum foil for covering and sampling leaves. **(B–E)** Concentration of PS VII, PS H, PS II, and PS I, respectively. **(F)** Soluble sugar concentration in leaves. **(G)** Correlation between saponins and sucrose concentration. Each column represents the mean (± SE) of three replicates. PS, *Paris* saponins. Data with different letters are significantly different ($p \leq 0.05$).

Chromatographic separations were performed on a Waters Acquity UPLC BEH C_{18} column (100 mm × 2.1 mm, 1.7 µm) at 35°C. The mobile phase was composed of 0.01% ammonia water in water (solvent A) and acetonitrile (solvent B) with a gradient elution: 0–1.0 min, 10–90% B; 1–2.5 min, 90% B (Yang et al., 2017). The flow rate was 0.5 ml min^{-1}. The volume of the injection was 0.1 µl.

The mass spectrometer was operated in negative mode. The operating parameters of the ion source were designed as follows: ion spray voltage, −4.50 kV; source temperature, 500°C; curtain gas, 20 psi; ion source gas1, 60 psi; ion source gas2, 60 psi; and declustering potential, 100V. The multiple reaction monitoring (MRM) transitions were employed for quantification. Ion pairs of 1029.5–737.3, 869.4–721.3, 1013.5–721.3, and 853.4–721.4 were selected for the quantification of VII, H, II, and I, with collision energies of −60, −42, −59, and −44, respectively.

Determination of sucrose, glucose and fructose concentration

Sucrose, glucose, and fructose concentration were determined in leaves. Dried leaves were extracted in 80% v/v ethanol at 80°C for 10 min. Before loading to an HPLC system, the extracts were filtered through 0.22 µm water phase filters (Jinteng, China). The HPLC assays of sucrose, glucose, and fructose were run on a Waters Binary HPLC System (Waters 1525–2707, Milford, USA) equipped with a refractive index detector (2414, Waters, Milford, USA). The analytical conditions were as follows: column Agilent Hi-Plea Ca (8% crosslinked) 300 mm × 7.7 mm, 8 µm in diameter (Agilent Technologies, Inc., USA); column temperature of 85°C; mobile phase Milli-Q water; and a flow rate of 0.6 ml min^{-1} (Zhou et al., 2022). Data were collected and processed by the Waters chromatography station Data Apex. Sugars were identified through comparison with retention times and the coelution of authentic standard solutions.

^{13}C-glucose ($^{13}C_6H_{12}O_6$) feeding track PS VII biosynthesis via plant organs

High-resolution liquid chromatography-mass spectrometry was applied to track ^{13}C-PS VII biosynthesis via plant organs. LC-MS can analyze a variety of substances in complex samples, and high-resolution mass spectrometry has the advantage of resolving isotope peaks. The exoisotope-labeled compounds have the same molecular structure and similar molecular weights, physicochemical properties, and retention times as the unlabeled compounds. Therefore, in the detection of PS VII labeled with different amounts of ^{13}C molecules, extraction of the target molecule ion by high-resolution mass spectrometry can be used to resolve isotope

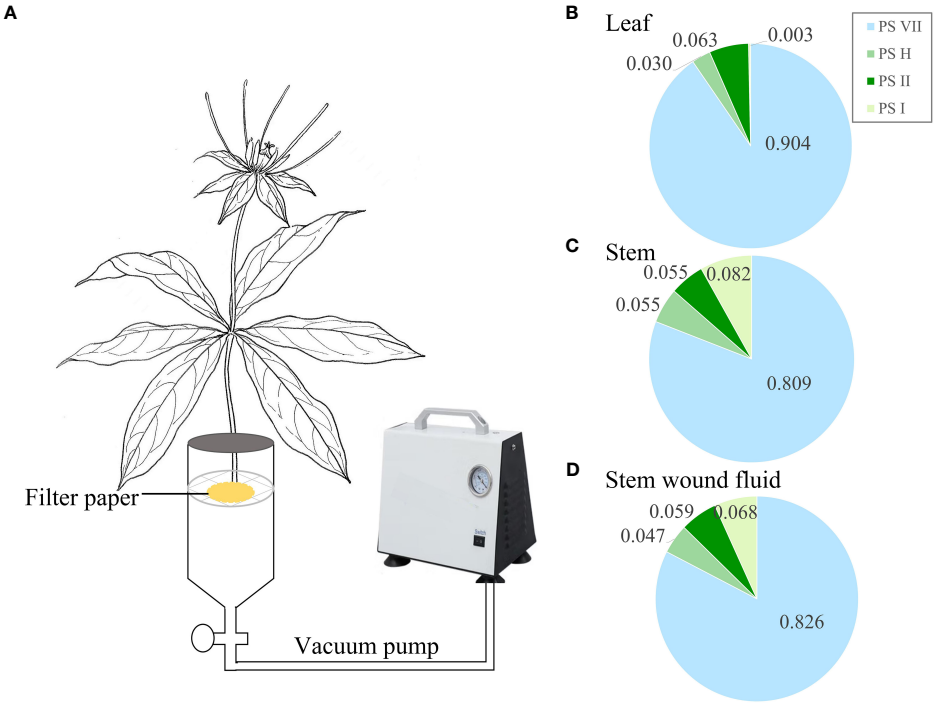

FIGURE 3
Saponin composition in stem wound fluid. **(A)** Schematic diagram illustrating the collection of stem wound fluid from wounded stem. **(B–D)** Proportion of the concentrations of the four main saponins in leaf, stem, and stem wound fluid, respectively. PS, *Paris* saponins. Each column represents the mean (± SE) of three replicates.

peaks and calculate the ratio of PS VII labeled with different amounts of ^{13}C. Owing to the natural abundance of ^{13}C, there will be a series of small peaks exiting in the position of the PS VII molecular ion peak (M^-), mainly $(M+1)^-$, $(M+2)^-$, $(M+3)^-$, $(M+4)^-$, etc. These are the isotope ion peaks of PS VII, which are mainly caused by the presence of ^{13}C. Owing to the constant ratio of ^{13}C isotope in the natural state, the ratios of $(M+1)^-/M^-$, $(M+2)^-/M^-$, $(M+3)^-/M^-$, and $(M+4)^-/M^-$ are generally fixed. When compounds labeled with exogenous ^{13}C were entered into the mass spectrum and detected, the abundance of total ^{13}C increased and the ratio of series isotope ion peaks changed. Therefore, in this study, the plants were fed with ^{13}C-glucose ($^{13}C_6H_{12}O_6$) and PS VII was synthesized with an exogenous ^{13}C label; the ratio of the series isotope ion peak changes were used to track and infer the biosynthesis of saponins. Owing to its advantages of high sensitivity, simplicity, and stability, this isotope tracking method has been widely used in drug chemical synthesis and absorption, distribution, metabolism, and elimination *in vivo* (Lozac'h et al., 2018; Martin et al., 2020).

The liquid chromatographic separation conditions were as follows: samples were eluted with the mobile phases of 0.1% formic acid water (A) and acetonitrile (B) with a BEH C18 column (1.7 µm, 2.1 × 100 mm, Waters, Milford, MA, USA) maintained at 40°C. The optimized gradient elution had a flow rate of 0.3 ml min^{-1}, and the optimized gradient procedure was designed as follows: started with 10% B and linearly increased to 30% B for 8 min, then linearly increased to 45% B from 8 min to 16 min, linearly increased to 50% B from 16 min to 24 min, and linearly increased to 70% B from 24 min to 30 min. Finally, the gradient was rapidly decreased to its initial condition for 0.1 min then maintained at 10% B for the next 2.9 min. Samples of a 5 µl volume were injected for analysis (Wang et al., 2021).

Mass spectrometry conditions were as follows: All MS and MS/MS data were acquired from a Thermo QExactive Plus (Thermo Fisher Scientific, San Jose, CA, USA), which is equipped with a heated electrospray ionization source (HESI) via negative ion mode. The parameters of the HESI source were set as follows: capillary voltage, 3.0 kV; capillary temperature, 350°C; sheath gas (N_2), 35 arbitrary units; and auxiliary gas (N_2), 15 arbitrary units. Through full scanning (operated from *m/z* 100–1500), saponins were identified, and the appropriate collision energy was given to obtain the clear fragmentation pattern of the plausible saponins. According to the fracture rule, the structures of saponins were predicted. Xcalibur 4.2 software (Thermo Fisher Scientific, USA) was used for data acquisition and processing. The raw data files of the control and sample groups and blanks were imported into Compound Discoverer™ 3.0 software (Thermo Scientific, Fremont, CA, USA) to identify saponins by accurately calculating the mass and fragments of saponins, and the maximum tolerance of mass error was set at 5 ppm.

A negative ion mass spectrum of PS VII ($C_{51}H_{82}O_{21}$, 1030.5349) was detected and mainly ionized with $COOH^-$ ions in formic acid water (Figure S1). To rule out the effect of ^{13}C natural abundance, the ratio of both marked and unmarked ion currents was calculated in each organ of the four groups. The calculation method of the ratio is the abundance of the series isotope ion peaks

with ^{13}C and the PS VII molecular ion peak (M^-), i.e., $(M+1)^-/M^-$, $(M+2)^-/M^-$, $(M+3)^-/M^-$, and $(M+4)^-/M^-$. M^- means the sum of the peak areas of ion current $(M+COOH)^-$ and M^-, which were mainly ionized with $COOH^-$ ions in formic acid water. The calculation formula is illustrated as follows:

$$\text{Ratio} = (M+2)^-/M^- PS : (M+2)^- \text{include}(M+2 + COOH)^- \text{and}(M+2)^-; M^- \text{include}(M+COOH)^- \text{and } M^-.$$

The $^{13}C/^{12}C$ ratio in rhizomes of four groups were analyzed by gas chromatography combustion isotope ratio mass spectrometry (GC/IRMS, Delta V Advantage, Thermo Fisher, Germany). Dried rhizome was grinded through a 200-mesh sieve, and 0.2 mg of powder sample was wrapped in a tin cup. Solid samples were placed into the combustion tube and converted into CO_2, which was separated by GC and detected by IRMS. Isodat software (Thermo Fisher Scientific, Germany) was used for data acquisition and processing.

Leaf tissue distribution of saponins by transmission electron microscopy

Leaf saponins for cytochemical localization were treated as following (Chen et al., 2019): leaf samples were cut into 1-mm^3 fragments and fixed with 3% glutaraldehyde (prepared with 3% lead acetate in 0.1 M sodium cacodylate buffer at a pH of 7.4) at 4°C. Samples were then washed four times for 30 min each time with 3% lead acetate, following which, the cuts were incubated with 1% osmic acid (prepared with 3% lead acetate in 0.1 M sodium cacodylate buffer at a pH of 7.4) overnight at 4°C, then washed twice (each for 30 min) with 0.1 M sodium cacodylate buffer at a pH of 7.4. The fragments were then gradually dehydrated with a grade series of ethanol of 30%, 50%, 70%, 80%, 90%, 95%, and 100%. The 100% ethanol step was repeated three times. Next, samples were incubated with epoxy propane transition and embedded with Epon812. The fragments were sliced into semi-lamellar sections to enable the positioning of the leaf cross-sections under a light microscope. Then, the semi-lamellar of the leaves was cut into 60–90-nm long sections using an ultramicrotome UC7rt (LEICA, Germany). After samples were stained with uranyl acetate, the sections were subsequently examined and photographed using a transmission electron microscope JEM-1400-FLASH (JEOL, Japan). The control sample was subjected to the same procedures as described above, but the fixing step with lead acetate was excluded.

Determination of chlorophyll concentration, fluorescence, and photosynthetic rate

The fresh leaf samples were ground in liquid nitrogen, and 0.1 g of powder was extracted in 10 ml of 80% v/v aqueous acetone at 25° C in the dark for 48 h. Chlorophyll a+b (Chl a+b) and Chlorophyll a/b (Chl a/b) were measured directly in the extract at 663, 645, and 470 nm using an enzyme-labeled instrument (SpectraMax iD3, Molecular Devices, USA) (Arnon, 1949; Porra et al., 1989; HK and Buschmann, 2001). The chlorophyll fluorescence parameters maximal photochemical efficiency (*Fv/Fm*) and non-photochemical quenching coefficient NPQ(Fm/Fm'-1) were measured using a MINI-PAM-II portable fluorometer (Walz, Effeltrich, Germany). Before the measurement, the leaves required dark adaptation for 30 min, and the photochemical light was set to 178 μmol $m^{-2}s^{-1}$. Maximum photochemical efficiency (*Fv/Fm*), apparent electron transfer rate (ETR), and other chlorophyll fluorescence parameters of PS II were determined according to the instructions. Three plants were measured for each treatment and the average value was obtained. The photosynthesis rate (Pn) and stomatal conductance (Cs) were measured using a Li-6400 photosynthesis system (Li-COR, Lincoln, NE, USA). The measurements were taken on a sunny day in a greenhouse between 10:00 h and 12:00 h. The photosynthetic photon flux density was set as 500 μ mol m^{-2} s^{-1}, and CO_2 was set at 400 μ mol mol^{-1}. The chamber temperature was 20°C and the vapor pressure deficit was 0.5–1.0 kPa.

Statistical analysis

The data, including PS VII, PS H, PS II, and PS I levels and sugar quantification results, were analyzed using one-way ANOVA (SPSS 19.0), and t tests were used to assess the significant differences between the 100- and 400-μmol m^{-2} s^{-1} treatments ($p \leq 0.05$). Empirical polynomial (inverse third order) equations were used in Origin 2021 (Origin Pro Learning Edition) to analyze the relationship between PS VII and sucrose concentration in leaves (Zhou et al., 2020). Histograms representing chlorophyll concentration, fluorescence, and photosynthetic rate were generated using Origin 2021 (Origin Pro Learning Edition).

Results

PS VII has the highest concentration in leaves of medicinal *Paris* species

PS VII, H, II, and I concentrations were analyzed in various organs, including leaves, stems, rhizomes, and roots (Figure 4). Four saponins were found in the leaves, stems, rhizomes, and roots of PPC, PF, and PPY. However, the concentrations (Figures 4A–C) and proportions (Figures 4D–G) of these saponins in the four organs varied among the different plant species. The main saponin in the leaves, stems, and roots of the three *Paris* species was PS VII (Figures 4D, E, G), especially in leaves and stem, where the proportion of PS VII was up to 80–90% (Figures 4D, E). In the rhizome, PS VII was also the main saponin in PPC and PF, but not in PPY (Figure 4F). In the rhizome of PPY, PS I had highest concentration, followed by PS VII. These findings suggest that PS VII is present in all organs of the three *Paris* species and its concentration is dominant compared with the other detected saponins. As a result, PS VII was chosen as the focus of further research in this study.

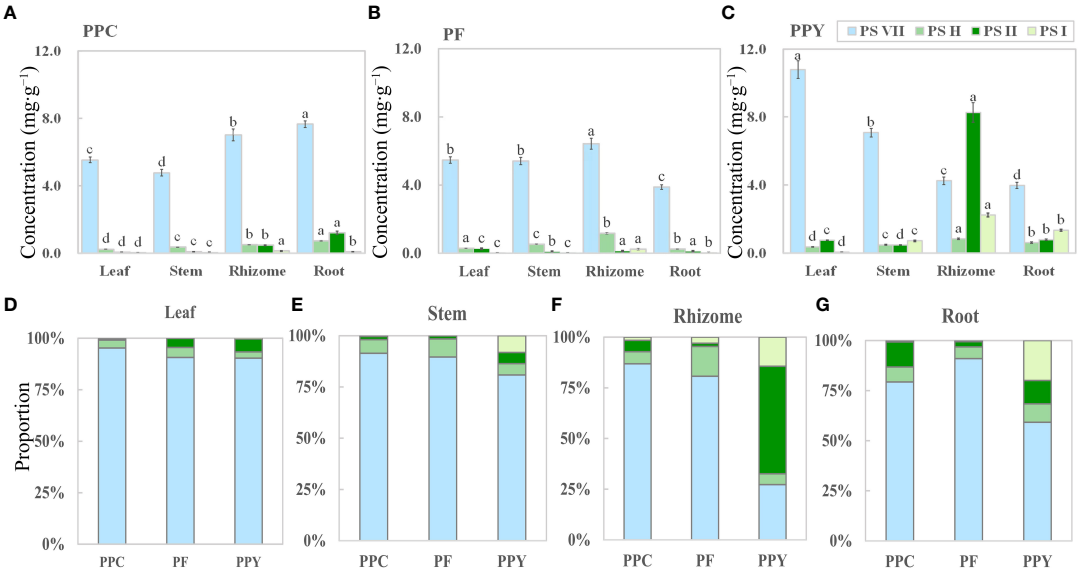

FIGURE 4
The organ-specific distribution of saponins in medicinal *Paris* species. **(A–C)** The concentration of PS VII, PS H, PS II, and PS I in four organs of PPC, PF, and PPY (mg g^{-1}), respectively. **(D–G)** Proportion of PSs in the leaves, stems, rhizomes, and roots of PPC, PF, and PPY (%), respectively. PS, *Paris* saponins; PPC, *Paris polyphylla* var. *chinensis*; PF, *Paris fargesii*; PPY, *Paris polyphylla* var. *yunnanensis*. Each column represents the mean (± SE) of three replicates. The letters on the columns mean significantly different in the same saponin type between organs ($p \leq 0.05$).

PS VII flow from leaf to rhizome through vascular tissues

To investigate the potential movement of PSs out of the leaves, an experiment was conducted by covering the leaves with aluminum foil to block incoming light. The concentrations of PSs and soluble sugars, such as sucrose, glucose, and fructose, were monitored at specific time intervals: 0, 24, 48, and 72 h after the covering was applied. The concentrations of PS VII, H, and II in leaves increased from 0 h to 48 h, but then decreased sharply from 48 h to 72 h (Figures 2B–D). By contrast, the sucrose concentration in leaves showed a decreasing trend as the covering time increased. Between 0 h and 48 h, there was a sharp decline in sucrose levels (from 292.55 to 184.70 mg g^{-1}), followed by a stable period from 48 h to 72 h (184.70 to 174.34 mg g^{-1}) (Figure 2F). The rate of reduction in sucrose concentration in leaves was notably faster than that of saponins. These suggest that the transport of sucrose from the leaves (source) to the rhizomes (sink) was more rapid, resulting in an increase in the concentration of PSs in the leaves during the initial 0 to 48 h. Although the sucrose concentration in the leaves remained stable between 48 h and 72 h, there was a continued reduction in PS concentration in the leaves, leading to a sharp decrease. The trend in PS VII concentration showed a significant correlation with the sucrose concentration in the leaves (Figure 2G). However, no significant changes were observed in the concentrations of PS I, glucose, and fructose throughout the 72-h period.

The decreased concentration of PS in leaves does not automatically prove that saponins are being transported out of the leaves, as they might be being broken down or synthesized into other substances. Therefore, the stem wound fluid, leaves, and stems of PPY were obtained to analyze the similarity of PS (Figure 3). In stem wound fluid, the saponin type and proportions of the four saponins were almost the same as that of stem and leaves, and PS VII was the main saponin (Figures 3B–D). This proved that saponins in PPY can be transported to other organs via the fibrovascular tissue of leaves and stem.

^{13}C-glucose feeding traces specificity in PS VII biosynthetic organs

The above results have proved that the leaves were an important organ for the synthesis of PS VII in PPY. However, from these results, we cannot conclude that the leaf is the major organ in the synthesis of PS VII, as the rhizome also contains high concentrations of PS VII. To further prove hypothesis 1, we conducted ^{13}C-glucose labeling experiments to trace the synthesis sites and pathways of PS VII in PPY. PS VII concentrations in four organs of PPY in four groups (Figure 1A) were detected by high resolution liquid chromatography-mass spectrometry. The results showed that only the ratio of PS VII molecules (M+2) $^{-}$/M^{-} increased significantly in the leaves of group 1 and group 3 (Figure 1B). In group 1, PS VII marked with two ^{13}C was synthesized in leaves of PPY after spraying with ^{13}C-glucose. In group 3, ^{13}C-glucose was feeding at the stem incision, and PS VII marked with two ^{13}C could also be synthesized in leaves. However, the ratio of PS VII molecules (M+2)$^{-}$/M^{-} in stems, rhizomes, and roots was obviated, with no differences among groups 1, 2, and 3. All the results suggested that leaves are the main synthesis organ of PS VII in PPY.

At the same time, the ratios of (M+1) $^{-}$/M^{-}, (M+3) $^{-}$/M^{-}, and (M+4) $^{-}$/M^{-}, i.e., marked with one, three, or four ^{13}Cs in each

organ, were not significantly different between all the groups (Figures S2A–C). The results are consistent with the saponin biosynthetic pathway. Acetyl-coenzyme A can be produced from glycolysis. And PSs, which are isoprenoid compounds, are biosynthesized *de novo* from acetyl-coenzyme A via the mevalonate (MVA) pathway in the cytoplasm or the 2-C-methyl-D-erythritol 4-phosphate (MEP) pathway in the plastids (Vranová et al., 2013). After plants have been fed exogenous ^{13}C-glucose, acetyl-coenzyme A with two ^{13}Cs is produced from ^{13}C-glucose glycolysis and is then used to biosynthesize PS VII with a maximum probability of two ^{13}C. Therefore, there are higher levels of PS VII marked with two ^{13}C than other molecules in the leaves.

To certify the success of root ^{13}C-glucose feeding, further analysis of the ^{13}C/^{12}C isotope ratio in rhizomes was carried out. The ^{13}C/^{12}C isotope ratios of groups 2 and 3 were much higher than those of groups 1 and 4 (Figure 1C). The results showed that ^{13}C-glucose had significantly entered the rhizomes through feeding in groups 2 and 3.

TEM subcellular chemical localization of PSs in leaves

To visualize the specific sites of PS synthesis in leaves, subcellular chemical localization was carried out using TEM. The TEM images revealed the presence of saponin precipitations localized in various cellular components, including the membrane, chloroplasts, mitochondria, and cell wall (Figure 5A). These saponin precipitations appeared as needle crystals bundled along the membrane (Figure 5B). The exocytosis of saponins occurred from both the chloroplast and cell, leading to their release into the intercellular space via transmembrane transport. Subsequently, the saponins dispersed peripherally along the intercellular space, exhibiting a gradual reduction in abundance (Figure 5C). Additionally, the observations revealed instances in which saponin precipitations detached from the cellular membrane and entered small vesicles within the intercellular space or inside the cells (Figure 5D).

Physiological response of PPY leaves under light intensity treatments

Based on the aforementioned findings, it is evidenced that the synthesis of PS VII primarily occurs in the leaves rather than the rhizome. To investigate the potential regulation of PS synthesis in leaves by light intensity, we initiated an examination of the photosynthetic and fluorescence properties of the leaves under two different light intensity treatments, 100 μmol m^{-2} s^{-1} and 400 μmol m^{-2} s^{-1}. This initial assessment was conducted to ensure the appropriateness of the selected light intensity treatments for further investigations.

Total chlorophyll (Chl a+b), chlorophyll a/b, photosynthetic rate, and Cs showed no difference between the two light intensity treatments (Figures 6A, B). However, chlorophyll fluorescence identified a slight inhibition of the photosynthetic system under 400 μmol m^{-2} s^{-1} (Figure 6C). The level of *Fv/Fm* under 400 μmol m^{-2} s^{-1} was lower than that of leaves under 100 μmol m^{-2} s^{-1}. By contrast, the NPQ of leaves under 400 μmol m^{-2} s^{-1} was significantly higher than that under 100 μmol m^{-2} s^{-1}. In addition, we examined the anatomical characteristics of the leaves to further visualize the effect of light intensity on leaf morphology (Figure 6D). Plants exhibit adaptive responses to different light intensities through morphological changes, including alterations in cell morphology and chloroplast arrangement. Under 100 μmol m^{-2} s^{-1}, there was a reduced number of mesophyll cells, with

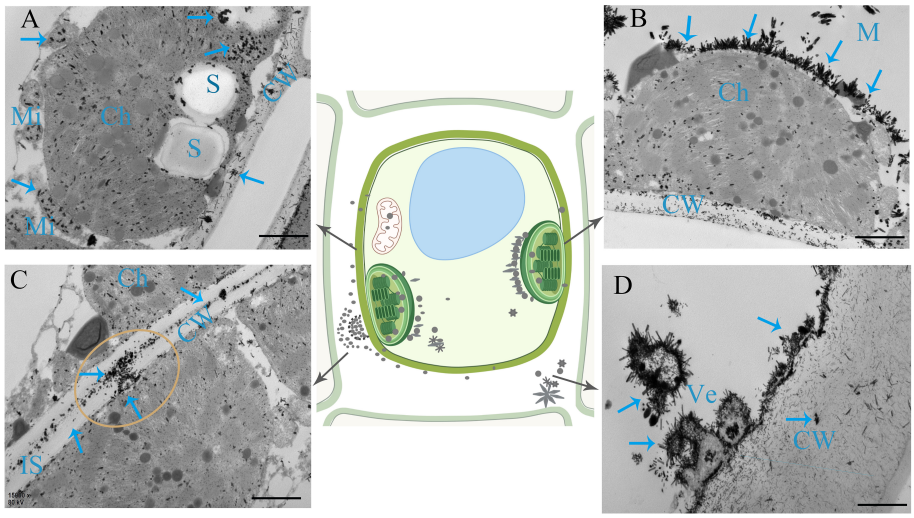

FIGURE 5
Subcellular chemical localization of PS in leaves. **(A)** Saponin precipitations can be observed as black masses positioned on the membrane. Chloroplasts (Ch), mitochondria (Mi), and cell walls (CW) are indicated by blue arrows. **(B)** Saponin precipitations in the form of needle crystals bundle positioned along the membrane. **(C)** Saponins are exocytosed into the intercellular space (IS) through transmembrane transport from the chloroplast and cell. **(D)** Saponin precipitations shed from the membrane into a small vesicle (Ve). S, starch grains. Bars=1 μm.

chloroplasts arranged laterally along the cells. This arrangement provided a larger chloroplast surface area exposed to light, facilitating photosynthesis. By contrast, leaves subjected to 400 μmol m^{-2} s^{-1} exhibited an increased number of mesophyll cells, and chloroplasts were arranged more closely together longitudinally. Taken together, these results indicate that 400 μmol m^{-2} s^{-1} in the greenhouse should be an appropriate light intensity for investigating whether the synthesis of PSs in leaves is regulated by high light intensity, as this had a slight photoinhibitory effect on PPY leaves but did not affect their photosynthetic capacity.

PS VII concentration in different organs and tissues of leaves in response to light intensities

The concentration of PS VII in leaves under 400 μmol m^{-2} s^{-1} was significantly higher than that under 100 μmol m^{-2} s^{-1} (Figure 7A). Similarly, in the stem, the concentration of PS VII was also higher under 400 μmol m^{-2} s^{-1} than under 100 μmol m^{-2} s^{-1} (Figure 7B). However, no significant difference in PS VII concentration was observed between the two light intensity treatments in the rhizome and root (Figure S3).

To further understand how high light intensity increases PS synthesis, we quantified the level of PS VII in tissues (including leaf tissue without vein, upper epidermal cells, and lower epidermal cells) of the leaf under two light intensity treatments. Under both light intensity treatments, the level of PS VII in the upper epidermal cells, low epidermal cells, and leaf tissue sequentially declined (Figure 7C). High light intensity (400 μmol m^{-2} s^{-1}) increased PS VII concentration in all three leaf tissues, particularly the upper epidermal cells. The ratio of PS VII concentration in the upper epidermal cells to that in the entire leaf tissue was 2.5 under 400 μmol m^{-2} s^{-1}, which was 31.6% higher than the ratio observed under 100 μmol m^{-2} s^{-1} (Figure 7D).

The differential distribution of PSs in leaf tissue under the two light intensity treatments was further confirmed through the cytochemical localization of saponins using TEM (Figure 8). In comparison to the 100 μmol m^{-2} s^{-1} treatment (Figures 8D–F), a greater number of saponin precipitations were observed in the upper and lower epidermis leaves exposed to a light intensity of 400 μmol m^{-2} s^{-1} (Figures 8G–I). Conversely, the control group (CK) showed no saponin precipitations (Figures 8A–C). These findings suggest that the increase in PS synthesis in leaves under high light intensity is accompanied by enhanced translocation and accumulation of saponins in the upper epidermal cells. This phenomenon may contribute to improved resistance against photodamage.

Discussion

The purpose of this study was to investigate the role of the leaf in PS VII synthesis and to explore the influence of light intensity on this process.

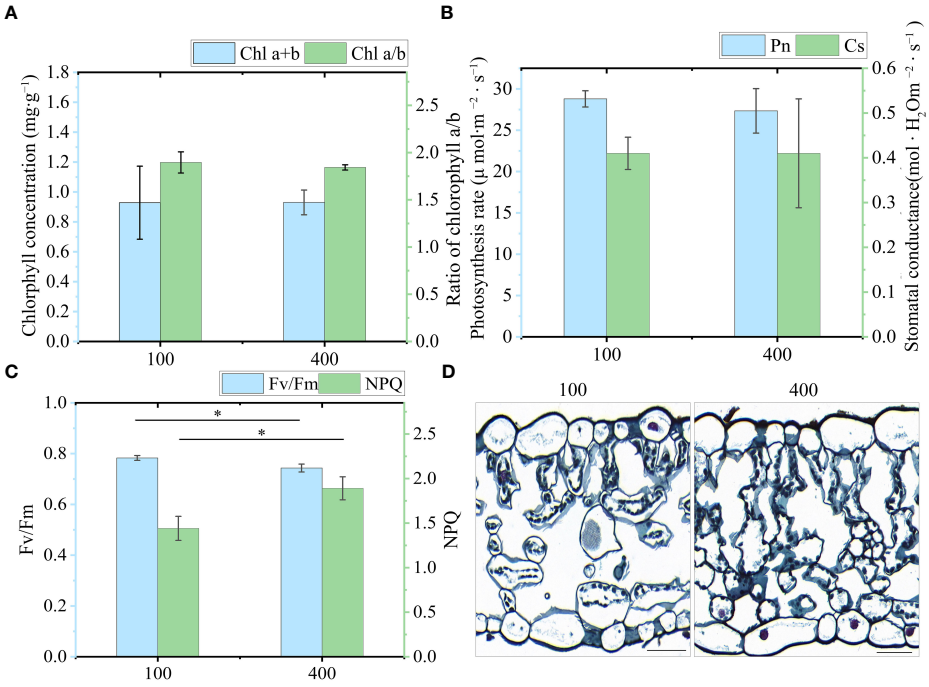

FIGURE 6
Physiological response of leaves under two light intensities. **(A)** Chlorophyll a+b (Chl a+b) and Chlorophyll a/b (Chl a/b). **(B)** Photosynthesis rate (Pn) and stomatal conductance (Cs). **(C)** *Fv/Fm* and NPQ (Fm/Fm'-1). **(D)** Characteristics of a transverse leaf section under 100 μmol m^{-2} s^{-1} and 400 μmol m^{-2} s^{-1} light intensity. Bar=50 μm. Each column represents the mean (± SE) of three replicates. * indicates a significant difference between the given light treatments (t-test at $p \leq 0.01$).

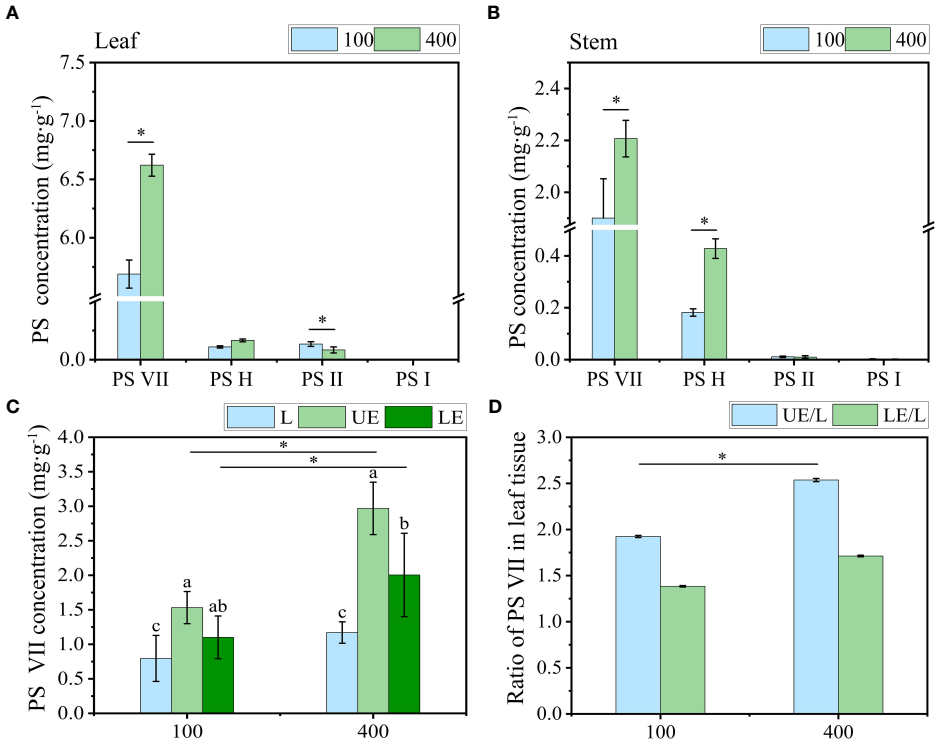

FIGURE 7
The effect of light intensity on PS concentration in **(A)** leaf and **(B)** stem. **(C)** Concentration of PS VII in leaf tissue without vein (L), upper epidermal cells (UE) and lower epidermal cells (LE). **(D)** Ratio of PS VII in leaf tissue of PPY. PS, *Paris* saponins. Each column represents the mean (± SE) of three replicates. * indicates s significant difference between the two given light intensity treatments (t-test at $p \leq 0.01$). Data with different letters are significantly different between the partial leaf tissue ($p \leq 0.05$).

The leaf is a major organ in the synthesis of PS VII

Studies on various plant species have shown that the synthesis and accumulation of saponins can occur in different organs, emphasizing the important role of leaves in saponin synthesis. For example, studies on *Achyranthes bidentata*, *Polygala tenuifolia*, and *Cyclocarya paliurus* have found high saponin concentrations in leaves, particularly in the palisade tissue (Li and Hu, 2009; Teng et al., 2009; Chen et al., 2019). The presence of saponins in the stem vascular bundles of plants such as *Achyranthes bidentata*, *Panax notoginseng*, and *Panax ginseng* suggests that stems can also act as transport organs for saponins (Li and Hu, 2009; Yokota et al., 2011; Mu et al., 2016). In the case of *Dioscorea zingiberensis*, comprehensive research has revealed that diosgenin saponins are synthesized in the leaves and then transported through the stem to the rhizome for storage, supported by the specific expression of diosgenin biosynthetic genes in the leaves (Li et al., 2022). These findings align with the observation that the accumulation of rhizome saponins in perennial plants gradually increases with age during the initial years (Wang and Li, 2018). Additionally, in the present study, we observed high concentrations of saponins, particularly PS VII, in the leaves of PPC, PF, and PPY, and identified the transport of saponins from leaves to the rhizome through the stem (Figure 3). However, it is important to note that these results alone do not conclusively establish that leaves are the main organ for the synthesis of PS VII.

Although the genome of PPY has been sequenced, the specific genes and enzymes responsible for regulating the synthesis of PS VII remain unknown (Li et al., 2020). In light of this, rather than adopting genetic approaches, we opted for physiological methods to explore the specific organ responsible for PS VII synthesis. We used ^{13}C labeling in our study, which is a well-established method for tracing the synthesis sites and pathways of substances (Wang et al., 2018; Wu et al., 2022). To expedite the experiment and ensure the reliability of our results, the plants were fed with ^{13}C-glucose, which is rapidly metabolized to acetyl-CoA, a precursor for saponin synthesis (Vranová et al., 2013). In both the leaf and stem vascular bundle feeding treatments, the ratio of ^{13}C-labeled PS VII to unlabeled PS VII in the leaves was higher than the ratio in the control group (Figure 1B). Conversely, in the rhizome and stem vascular bundle feeding treatments, there was no significant difference in the ratio of ^{13}C-labeled PS VII to unlabeled PS VII in the rhizome between the labeling and non-labeling treatments (Figure 1B). The concentration of ^{13}C in the rhizome was quantified and found to be significantly higher in the two labeling treatments than in the no feeding treatment (Figure 1C), confirming the successful labeling of the rhizome with ^{13}C-glucose. Additionally, the process of saponin release from the cells into the intercellular space in the leaves, followed by diffusion along the intercellular space, was observed (Figure 5C). Interestingly, PS VII labeled with ^{13}C was not detected in the rhizome when the leaves were fed with ^{13}C-glucose, which challenges the notion that PS VII is transported from the leaves through the stem to the rhizome. One possible explanation for this

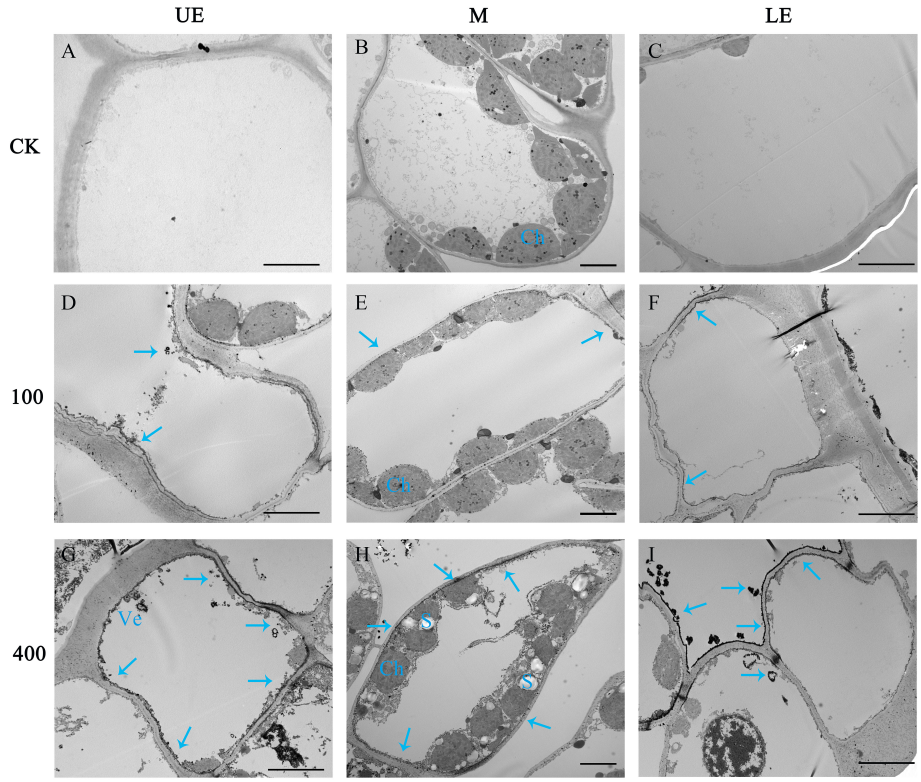

FIGURE 8
The effect of light intensity on the distribution of saponins in leaf cells. Saponin precipitations can be observed as black masses indicated with blue arrows. **(A–C)** Group CK with no saponin precipitation. **(D–F)** PPY leaves under LED 100 μmol m^{-2} s^{-1}. **(G–I)** PPY leaves under LED 400 μmol m^{-2} s^{-1}. UE, upper epidermal cell; M, mesophyll cell; LE, lower epidermal cell; Ch, chloroplast (Ch); Ve, vesicle. Bars=5 μm **(B, E, H)**; 10 μm **(A, C, D, F, G, I)**.

discrepancy is that the transit speed of saponins from leaves to rhizome is slow, as indicated by the lack of decrease in PS VII concentration after the leaves were covered with foil for 48 h (Figure 2B).

Although the synthesis of saponins is typically attributed to the leaves in the majority of reported plant species, it cannot be regarded as an absolute rule. In our current study, intriguingly, the rhizome of PPY exhibited the highest proportion of PS II, albeit at a significantly lower concentration than PS VII in the leaves (Figure 4C). Additionally, there was no difference in the ratios of ^{13}C-labeled PS II to unlabeled PS II in the leaves of plants under leaf-feeding and non-feeding treatments (Figures S2D–G), indicating that the leaves may not be the main site of PS II synthesis in PPY. This conclusion may contradict previous findings reported in the literature. One possible explanation might be that most of the studies conducted focused only on total saponin levels and tissue localization, without detailing the saponin types, ignoring the tissue specificity of different types of saponin synthesis. Therefore, the question is why the leaves specifically synthesize PS VII. The reason for this can mainly be attributed to the chemical structural and functional properties of PS VII, whereby: (1) unlike most of the saponins in PPY, including PS H, I, dioscin, and gracillin, which are linked with a trisaccharide chain (Li, 1998), PS VII has a tetrasaccharide chain linked at the C-3 position, providing greater resistance to biotic and abiotic stresses in field conditions, including predation, pathogenic microorganisms, and high light intensity. Additionally, pharmacological studies have shown that PS VII exhibits stronger cytotoxic and anti-inflammatory properties than saponins with a trisaccharide chain (Fan et al., 2015; Zhang et al., 2019; Ahmad et al., 2021); (2) the synthesis of PS VII in leaves aligns with the concept of phyto-economics, as it is more convenient and requires less energy (Züst and Agrawal, 2017; He et al., 2022). Owing to the glycosidic linkage of PS VII, it can be enzymatically modified, leading to the formation of other saponins through the relinking of sugar chains or changes in the linkage position (Hua et al., 2022; Song et al., 2022). However, we still lack more direct and convincing evidence of the variability of the synthetic organization of the saponin types in *Paris* species and other plant species with saponins, and further work is needed to unravel their mystery so that a contribution can be made to the production of high-quality *Paris* herbs and human health. Nevertheless, these results certify that the leaf of PPY is a major organ in the synthesis of PS VII.

PS VII synthesis in leaves regulated by light intensity

The synthesis, transport, and distribution of plant metabolites play a crucial role in plant defense against biotic stresses. For instance, plants protect themselves from attackers by using specialized metabolites and from herbivores by optimizing the distribution of chemical defenses (Hunziker et al., 2021). Mature

leaves often allocate defense compounds to vulnerable or reproductive parts of the plant to enhance defense mechanisms against herbivory (Hunziker et al., 2021; Gershenzon and Ullah, 2022). Additionally, saponins in plants such as *Centella asiatica* have been found to increase resistance against UV oxidation damage (Müller et al., 2013). Additionally, the level of leaf saponin concentration can influence the response to high light stress, with variations observed between young and old leaves (Chen et al., 2019). Nevertheless, the specific mechanisms underlying saponin synthesis, distribution, and accumulation in leaves in response to abiotic stresses, particularly light intensity, are poorly understood.

The present study revealed that plants grown under a light intensity of 400 μmol m^{-2} s^{-1}, which slightly inhibited the growth of PPY in the controlled environment, exhibited higher PS VII concentration in leaves than those grown under 100 μmol m^{-2} s^{-1}. Additionally, the distribution of saponins in leaf cell types was also regulated, with a higher proportion of saponins found in the leaf epidermal cells of plants grown under 400 μmol m^{-2} s^{-1}. The explanations for the light-induced regulation of saponin synthesis and distribution may be based on the following aspects: (1) high light intensity increases the availability of substrates for saponin synthesis, thus driving the reaction in a positive direction. This is supported by the higher number of starch granules observed under 400 μmol m^{-2} s^{-1} than under 100 μmol m^{-2} s^{-1} (Figure 8H). (2) Similar to the role of saponins in resistance to UV oxidative damage (Müller et al., 2013), the increased synthesis and distribution of saponins in epidermal cells under high light intensity may help protect against high light damage. (3) High light intensity promotes the transport of saponins to epidermal cells, and this feedback regulation may further modulate saponin synthesis. Compartmentalization of secondary metabolism, such as saponin synthesis, can effectively control the rate and direction of metabolic flow, reduce the cytotoxicity of intermediates, and minimize the metabolic burden on cells (Sun et al., 2023). The slow rate of PS VII translocation between organs (Figure 2), suggests that compartmentalization of PS VII in leaves is an effective strategy for maintaining its synthesis rate. However, how light intensity regulates saponin synthesis and distribution in leaves is still unclear, and further work is needed to elucidate the underlying mechanisms.

Indeed, understanding the relationship between light and the expression and signaling pathways of key genes involved in saponin synthesis, such as *PgMYB2*, *PgMYC2*, *PgWRKY1*, and *PgWRKY22*, and genes including *PgDELLA*, *PnDS*, and *PnSE* (Rahimi et al., 2016; Deng et al., 2017; Liu et al., 2019b; Zheng et al., 2023), is crucial in unraveling the light-mediated regulation of saponin synthesis in *Paris* plants. These transcription factors and genes have been shown to play important roles in the light-mediated regulation of saponin synthesis in *Panax*. Further investigation into the expression patterns and signaling pathways of these genes in *Paris* plants during saponin synthesis will provide valuable insights into the molecular mechanisms underlying the light regulation of saponin metabolism. By gaining a higher-order understanding of these regulatory processes, it will be possible to increase the production of high-quality medicinal materials from *Paris* plants through environmentally friendly and resource-efficient cultivation practices.

Conclusion

In the present study, chemical phenotypic analysis, subcellular localization, and ^{13}C tracing have demonstrated at the physiological level that the leaf rather than the rhizome of PPY is the main organ for the synthesis of PS VII. However, PS VII is not stored in the leaves but is instead transported through the vascular tissue to the rhizome for storage. The synthesis of PS VII in leaves is regulated not only by genetics but also by environmental cues, such as light intensity. The proposed physiological mechanisms underlying the positive effects of high light intensity on PS VII synthesis are as follows: (1) high light intensity increases the availability of substrates required for saponin synthesis; (2) promoting saponin synthesis protects leaves from potential damage caused by high light; and (3) high light intensity enhances the compartmentalization of saponins within the leaves, including transfer to the upper epidermal cells, which in turn feedback regulates saponin synthesis. These studies partially unveil the tissue-specific and light-regulated properties of PS VII synthesis in PPY and lays the theoretical foundation for the development of double high (high yield and high quality) cultivation practices. The tissue specificity of the synthesis of saponin types and the genetic and ecological mechanisms of light-regulated saponin synthesis should be the focus of future studies.

Data availability statement

The original contributions presented in the study are included in the article/Supplementary Material. Further inquiries can be directed to the corresponding authors.

Author contributions

FW, TZ, and JP planned and designed the study and wrote the manuscript. FW, SC, and YW cultivated the plants and carried out the chemical analysis experiments and statistical analysis. QW and JY conducted the fieldwork. FW and TZ analyzed the data. FW and SC contributed equally. All authors contributed to the article and approved the submitted version.

Funding

This work was supported by the Innovation Team and Talents Cultivation Program of the National Administration of Traditional Chinese Medicine (ZYYCXTD-D-202209).

Acknowledgments

We also thank the experimentalist Minghai Tang, West China Hospital, Sichuan University, for help with the saponin analysis and Yifan Li for drawing the sketch of the plant.

Conflict of interest

The authors declare that the research was conducted in the absence of any commercial or financial relationships that could be construed as a potential conflict of interest.

Publisher's note

All claims expressed in this article are solely those of the authors and do not necessarily represent those of their affiliated organizations, or those of the publisher, the editors and the reviewers. Any product that may be evaluated in this article, or claim that may be made by its manufacturer, is not guaranteed or endorsed by the publisher.

Supplementary material

The Supplementary Material for this article can be found online at: https://www.frontiersin.org/articles/10.3389/fpls.2023.1199215/full#supplementary-material

References

Ahmad, B., Gamallat, Y., Khan, M. F., Din, S. R., Israr, M., Ahmad, M., et al. (2021). Natural polyphyllins (I, II, D, VI, VII) reverses cancer through apoptosis, autophagy, mitophagy, inflammation, and necroptosis. *OncoTargets Ther.* 14, 1821–1841. doi: 10.2147/OTT.S287354

Arnon, D. I. (1949). Copper enzymes in isolated chloroplasts. Polyphenoloxidase in beta vulgaris. *Plant Physiol.* 24 (1), 1–15. doi: 10.1104/pp.24.1.1

Bi, L., Liu, Y., Yang, Q., Zhou, X., Li, H., Liu, Y., et al. (2021). Paris saponin H inhibits the proliferation of glioma cells through the A1 and A3 adenosine receptor–mediated pathway. *Int. J. Mol. Med.* 47 (4), 30. doi: 10.3892/ijmm.2021.4863

Chen, X., Wang, Y., Zhao, H., Fu, X., and Fang, S. (2019). Localization and dynamic change of saponins in Cyclocarya paliurus (Batal.) Iljinskaja. *PloS One* 14 (10), e0223421. doi: 10.1371/journal.pone.0223421

de Costa, F., Yendo, A. C. A., Fleck, J. D., Gosmann, G., and Fett-Neto, A. G. (2013). Accumulation of a bioactive triterpene saponin fraction of Quillaja brasiliensis leaves is associated with abiotic and biotic stresses. *Plant Physiol. Biochem. PPB* 66, 56–62. doi: 10.1016/j.plaphy.2013.02.003

Deng, B., Huang, Z. J., Ge, F., Liu, D. Q., Lu, R. J., and Chen, C. Y. (2017). An AP2/ERF family transcription factor PnERF1 raised the biosynthesis of saponins in panax notoginseng. *J. Plant Growth Regul.* 36 (3), 691–701. doi: 10.1007/s00344-017-9672-z

Ding, Y.-G., Zhao, Y.-L., Zhang, J., Zuo, Z.-T., Zhang, Q.-Z. , Wang, Y.-Z., et al. (2021). The traditional uses, phytochemistry, and pharmacological properties of Paris L. (Liliaceae): A review. *J. Ethnopharmacol.* 278, 114293. doi: 10.1016/j.jep.2021.114293

Faizal, A., and Geelen, D. (2013). Saponins and their role in biological processes in plants. *Phytochem. Rev.* 12 (4), 877–893. doi: 10.1007/s11101-013-9322-4

Fan, L., Li, Y., Sun, Y., Han, J., Yue, Z., Meng, J., et al. (2015). Paris saponin VII inhibits the migration and invasion in human A549 lung cancer cells. *Phytother. Res. PTR* 29 (9), 1366–1372. doi: 10.1002/ptr.5389

Gao, X., Zhang, X., Chen, W., Li, J., Yang, W., Zhang, X., et al. (2020). Transcriptome analysis of Paris polyphylla var. yunnanensis illuminates the biosynthesis and accumulation of steroidal saponins in rhizomes and leaves. *Phytochemistry* 178, 112460. doi: 10.1016/j.phytochem.2020.112460

Gershenzon, J., and Ullah, C. (2022). Plants protect themselves from herbivores by optimizing the distribution of chemical defenses. *Proc. Natl. Acad. Sci. USA* 119 (4), e2120277119. doi: 10.1073/pnas.2120277119

He, Z., Webster, S., and He, S. Y. (2022). Growth-defense trade-offs in plants. *Curr. Biol. CB* 32 (12), R634–R639. doi: 10.1016/j.cub.2022.04.070

HK, L., and Buschmann, C. (2001). Chlorophylls and carotenoids: measurementand characterization by UV–vis spectroscopy. *Curr. Protoc. Food Anal. Chem.* 1 (1), F4–F3. doi: 10.1002/0471142913.faf0403s01

Hua, X., Song, W., Wang, K., Yin, X., Hao, C., Duan, B., et al. (2022). Effective prediction of biosynthetic pathway genes involved in bioactive polyphyllins in Paris polyphylla. *Commun. Biol.* 5 (1), 50. doi: 10.1038/s42003-022-03000-z

Hunziker, P., Lambertz, S. K., Weber, K., Crocoll, C., Halkier, B. A., and Schulz, A. (2021). Herbivore feeding preference corroborates optimal defense theory for specialized metabolites within plants. *Proc. Natl. Acad. Sci. USA* 118 (47), e2111977118. doi: 10.1073/pnas.2111977118

Hussain, M., Debnath, B., Qasim, M., Bamisile, B. S., Islam, W., Hameed, M. S., et al. (2019). Role of saponins in plant defense against specialist herbivores. *Molecules (Basel Switzerland)* 24 (11), 2067. doi: 10.3390/molecules24112067

Li, H. (1998). *The Genus Paris (Trilliaceae)* (Beijing: S. Press).

Li, J., and Hu, Z. (2009). Accumulation and dynamic trends of triterpenoid saponin in vegetative organs of Achyranthus bidentata. *J. Integr. Plant Biol.* 51 (2), 122–129. doi: 10.1111/j.1744-7909.2008.00764.x

Li, J., Lv, M., Du, L., Yunga, A., Hao, S., Zhang, Y., et al. (2020). An enormous Paris polyphylla genome sheds light on genome size evolution and polyphyllin biogenesis. *Cold Spring Harbor Lab.* doi: 10.1101/2020.06.01.126920

Li, Y., Tan, C., Li, Z., Guo, J., Li, S., Chen, X., et al. (2022). The genome of Dioscorea zingiberensis sheds light on the biosynthesis, origin and evolution of the medicinally important diosgenin saponins. *Horticul. Res.* 9, uhac165. doi: 10.1093/hr/uhac165

Liu, Q., Khakimov, B., Cárdenas, P. D., Cozzi, F., Olsen, C. E., Jensen, K. R., et al. (2019a). The cytochrome P450 CYP72A552 is key to production of hederagenin-based saponins that mediate plant defense against herbivores. *New Phytol.* 222 (3), 1599–1609. doi: 10.1111/nph.15689

Liu, T., Luo, T., Guo, X., Zou, X., Zhou, D., Afrin, S., et al. (2019b). PgMYB2, a MeJA-responsive transcription factor, positively regulates the dammarenediol synthase gene expression in panax ginseng. *Int. J. Mol. Sci.* 20 (9), 2219. doi: 10.3390/ijms20092219

Lozac'h, F., Fahrni, S., Maria, D. D., Welte, C., Bourquin, J., Synal, H.-A., et al. (2018). Evaluation of cAMS for 14C microtracer ADME studies: opportunities to change the current drug development paradigm. *Bioanalysis* 10 (5), 321–339. doi: 10.4155/bio-2017-0216

Martin, J., Cassidy, K., Czeskis, B., Alberts, J., Lao, Y. B., Gluff, J., et al. (2020). 14C-tirzepatide ADME studies in rat and monkey. *Diabetes* 69, 940-P. doi: 10.2337/db20-940-P

Mu, T., Zhao, C., Chen, Z., Wen, G., Yang, S., Wei, F., et al. (2016). Histological locations and contents of anthocyanins and saponins of green-purple transitional aerial stems of panax notoginseng. *Acta Bot. Boreal* 36 (03), 1772–1780. doi: 10.7606/j.issn.1000-4025.2016.09.1772

Müller, V., Albert, A., Barbro Winkler, J., Lankes, C., Noga, G., and Hunsche, M. (2013). Ecologically relevant UV-B dose combined with high PAR intensity distinctly affect plant growth and accumulation of secondary metabolites in leaves of Centella asiatica L. Urban. *J. Photochem. Photobiol. B Biol.* 127, 161–169. doi: 10.1016/j.jphotobiol.2013.08.014

National Pharmacopoeia Commission. (2020). *"Pharmacopoeia of the People's Republic of China. Part I"* (Beijing: China Pharmaceutical Science and Technology Press), 271.

Ninkuu, V., Zhang, L., Yan, J., Fu, Z., Yang, T., and Zeng, H. (2021). Biochemistry of terpenes and recent advances in plant protection. *Int. J. Mol. Sci.* 22 (11), 5710. doi: 10.3390/ijms22115710

Porra, R. J., Thompson, W. A., and Kriedemann, P. E. (1989). Determination of accurate extinction coefficients and simultaneous equations for assaying chlorophylls a and b extracted with four different solvents: verification of the concentration of chlorophyll standards by atomic absorption spectroscopy. *Biochim. Biophys. Acta (BBA) - Bioenergetics* 975 (3), 384–394. doi: 10.1016/S0005-2728(89)80347-0

Qin, X.-J., Ni, W., Chen, C.-X., and Liu, H.-Y. (2018). Seeing the light: Shifting from wild rhizomes to extraction of active ingredients from above-ground parts of Paris polyphylla var. yunnanensis. *J. Ethnopharmacol.* 224, 134–139. doi: 10.1016/j.jep.2018.05.028

Rahimi, S., Kim, Y.-J., Sukweenadhi, J., Zhang, D., and Yang, D.-C. (2016). PgLOX6 encoding a lipoxygenase contributes to jasmonic acid biosynthesis and ginsenoside production in Panax ginseng. *J. Exp. Bot.* 67 (21), 6007–6019. doi: 10.1093/jxb/erw358

Rogowska, A., and Szakiel, A. (2020). The role of sterols in plant response to abiotic stress. *Phytochem. Rev.* 19 (6), 1525–1538. doi: 10.1007/s11101-020-09708-2

Song, W., Zhang, C., Wu, J., Qi, J., Hua, X., Kang, L., et al. (2022). Characterization of three paris polyphylla glycosyltransferases from different UGT families for steroid functionalization. *ACS Synthetic Biol.* 11 (4), 1669–1680. doi: 10.1021/acssynbio.2c00103

Stewart, M. P., Langer, R., and Jensen, K. F. (2018). Intracellular delivery by membrane disruption: mechanisms, strategies, and concepts. *Chem. Rev.* 118 (16), 7409–7531. doi: 10.1021/acs.chemrev.7b00678

Sun, S., Shen, X., Li, Y., Li, Y., Wang, S., Li, R., et al. (2023). Single-cell RNA sequencing provides a high-resolution roadmap for understanding the multicellular compartmentation of specialized metabolism. *Nat. Plants* 9 (1), 179–190. doi: 10.1038/s41477-022-01291-y

Szakiel, A., Paczkowski, C., and Henry, M. (2011). Influence of environmental abiotic factors on the content of saponins in plants. *Phytochem. Rev.* 10 (4), 471–491. doi: 10.1007/s11101-010-9177-x

Teng, H.-M., Fang, M.-F., Cai, X., and Hu, Z.-H. (2009). Localization and dynamic change of saponin in vegetative organs of Polygala tenuifolia. *J. Integr. Plant Biol.* 51 (6), 529–536. doi: 10.1111/j.1744-7909.2009.00830.x

Vranová, E., Coman, D., and Gruissem, W. (2013). Network analysis of the MVA and MEP pathways for isoprenoid synthesis. *Annu. Rev. Plant Biol.* 64, 665–700. doi: 10.1146/annurev-arplant-050312-120116

Wang, P., Guo, L., Jaini, R., Klempien, A., McCoy, R. M., Morgan, J. A., et al. (2018). A 13C isotope labeling method for the measurement of lignin metabolic flux in Arabidopsis stems. *Plant Methods* 14, 51. doi: 10.1186/s13007-018-0318-3

Wang, G., Hao, R., Liu, Y., Wang, Y., Man, S., and Gao, W. (2021). Tissue distribution, metabolism and absorption of Rhizoma Paridis Saponins in the rats. *J. Ethnopharmacol.* 273, 114038. doi: 10.1016/j.jep.2021.114038

Wang, Y. Z., and Li, P. (2018). Effect of cultivation years on saponins in Paris Polyphylla var. yunnanensis using ultra-high liquid chromatography-tandem mass spectrometry and Fourier transform infrared spectroscopy. *Plant Growth Regul.* 84 (2), 373–381. doi: 10.1007/s10725-017-0348-2

Watcharatanon, K., Ingkaninan, K., and Putalun, W. (2019). Improved triterpenoid saponin glycosides accumulation in *in vitro* culture of Bacopa monnieri (L.) Wettst with precursor feeding and LED light exposure. *Ind. Crops Products* 134, 303–308. doi: 10.1016/j.indcrop.2019.04.011

Wu, Z., Zhang, J., Xu, F., Wang, Y., and Zhang, J. (2017). Rapid and simple determination of polyphyllin I, II, VI, and VII in different harvest times of cultivated Paris polyphylla Smith var. yunnanensis (Franch.) Hand.-Mazz by UPLC-MS/MS and FT-IR. *J. Natural Medicines* 71 (1), 139–147. doi: 10.1007/s11418-016-1043-8

Wu, J., Zhu, W., Shan, X., Liu, J., Zhao, L., and Zhao, Q. (2022). Glycoside-specific metabolomics combined with precursor isotopic labeling for characterizing plant glycosyltransferases. *Mol. Plant* 15 (10), 1517–1532. doi: 10.1016/j.molp.2022.08.003

Yang, G., Lu, W., Pan, M., Zhang, C., Zhou, Y., Hu, P., et al. (2017). An LC-MS/MS method for simultaneous determination of nine steroidal saponins from Paris polyphylla var. in rat plasma and its application to pharmacokinetic study. *J. Pharm. Biomed. Anal.* 145, 675–681. doi: 10.1016/j.jpba.2017.07.052

Yokota, S., Onohara, Y., and Shoyama, Y. (2011). Immunofluorescence and immunoelectron microscopic localization of medicinal substance, Rb1, in several plant parts of Panax ginseng. *Curr. Drug Discovery Technol.* 8 (1), 51–59. doi: 10.2174/157016311794519938

Yuan, X., Xu, P., Yu, Y., and Xiong, Y. (2020). Glucose-TOR signaling regulates PIN2 stability to orchestrate auxin gradient and cell expansion in Arabidopsis root. *Proc. Natl. Acad. Sci. United States America* 117 (51), 32223–32225. doi: 10.1073/pnas.2015400117

Zhang, C., Li, C., Jia, X., Wang, K., Tu, Y., Wang, R., et al. (2019). *In vitro* and *in vivo* anti-inflammatory effects of polyphyllin VII through downregulating MAPK and NF-κB pathways. *Molecules (Basel Switzerland)* 24 (5), 875. doi: 10.3390/molecules24050875

Zhang, Q., Liang, S., Cao, J., and He, Z. (2018). Effects of different intensity of LED yellow light on the growth, photosynthetic characteristics and saponins content of P. Polyphylla var. Yunnanensis. *Modern Food Sci. Technol.* 34 (03), 178–183. doi: 10.13982/j.mfst.1673-9078.2018.03.026

Zheng, H., Fu, X., Shao, J., Tang, Y., Yu, M., Li, L., et al. (2023). Transcriptional regulatory network of high-value active ingredients in medicinal plants. *Trends In Plant Sci.* 28 (4), 429–446. doi: 10.1016/j.tplants.2022.12.007

Zhou, T., Du, Y., Ahmed, S., Liu, T., Ren, M., Liu, W., et al. (2016). Genotypic differences in phosphorus efficiency and the performance of physiological characteristics in response to low phosphorus stress of soybean in Southwest of China. *Front. Plant Sci.* 7. doi: 10.3389/fpls.2016.01776

Zhou, T., Qiu, X., Zhao, L., Yang, W. J., Wen, F. Y., Wu, Q. H., et al. (2022). Optimal light intensity and quality increased the saffron daughter corm yield by inhibiting the degradation of reserves in mother corms during the reproductive stage. *Ind. Crops Products* 176, 114396. doi: 10.1016/j.indcrop.2021.114396

Zhou, T., Wang, L., Sun, X., Wang, X. C., Chen, Y. L., Rengel, Z., et al. (2020). Light intensity influence maize adaptation to low P stress by altering root morphology. *Plant Soil* 447 (1-2), 183–197. doi: 10.1007/s11104-019-04259-8

Zhou, N., Xu, L., Park, S.-M., Ma, M.-G., Choi, S.-E., and Si, C. (2021). Genetic Diversity, Chemical Components, and Property of Biomass Paris polyphylla var. yunnanensis. *Front. In Bioeng. Biotechnol.* 9. doi: 10.3389/fbioe.2021.713860

Züst, T., and Agrawal, A. A. (2017). Trade-offs between plant growth and defense against insect herbivory: an emerging mechanistic synthesis. *Annu. Rev. Plant Biol.* 68, 513–534. doi: 10.1146/annurev-arplant-042916-040856

frontiers | Frontiers in Plant Science

TYPE Original Research
PUBLISHED 22 August 2023
DOI 10.3389/fpls.2023.1217956

OPEN ACCESS

EDITED BY
Zhixing Qing,
Hunan Agricultural University, China

REVIEWED BY
Zhou Yuan,
Huazhong University of Science and Technology, China
Keyu Chen,
Hunan University of Technology and Business, China

*CORRESPONDENCE
Siyuan Zhu
zhusiyuan@caas.cn
Qian Lin
linqian@caas.cn

RECEIVED 06 May 2023
ACCEPTED 05 June 2023
PUBLISHED 22 August 2023

CITATION
Fu Y, Liu T, Wang X, Wang Y, Gong Q, Li G, Lin Q and Zhu S (2023) Untargeted metabolomics reveal rhizosphere metabolites mechanisms on continuous ramie cropping.
Front. Plant Sci. 14:1217956.
doi: 10.3389/fpls.2023.1217956

Untargeted metabolomics reveal rhizosphere metabolites mechanisms on continuous ramie cropping

Yafen Fu[1], Tongying Liu[1], Xin Wang[1], Yanzhou Wang[1], Qiulin Gong[2], Guang Li[1], Qian Lin[1]* and Siyuan Zhu[1]*

[1]Institute of Bast Fiber Crops, Chinese Academy of Agricultural Sciences, Changsha, China, [2]Selenium Resources Development and Utilization Center, Yichun Agricultural and Rural Bureau, Jiangxi, China

Ramie is an important fiber feed dual-purpose crop in China and plays an important role in the national economy. However, ramie yield and quality can be reduced after many years of continuous cultivation. Currently, relatively little research has been conducted on rhizosphere metabolites and their pathways in continuous ramie cropping. Therefore, a healthy group (CK) and obstacle groups (XZQG, JZ, DJY, and GXD) with 8 years of continuous cultivation were selected for the study. LC-MS and GC-MS untargeted metabolomics were used to explore and analyze ramie rhizosphere metabolites and pathways. The results revealed that significant differences in the agronomic traits of ramie occurred after 8 years of continuous cultivation, with dwarfed plants and decreased yields in the obstacle groups. Metabolomic analysis identified 49 and 19 rhizosphere metabolites, including lipids, organic acids, phenols, and amino acids. In addition, four differential metabolic pathways (phenylpropanoid biosynthesis, fatty acid metabolism, amino acid metabolism, and ascorbate and aldarate metabolism) were elucidated. It was also clarified that sinapic acid, jasmonic acid, glutamine, and inositol might be the main metabolites affecting ramie continuous-cropping obstacle groups, and they were significantly correlated with ramie agronomic traits and physiological indicators. This provided important insights into the mechanisms affecting continuous ramie cropping. Accordingly, it is expected that the increase or decrease of sinapic acid, jasmonic acid, glutamine, and inositol in the soil will alleviate obstacles to continuous ramie cropping and promote the healthy development of the ramie industry in the future.

KEYWORDS

ramie, untargeted metabolomics, rhizosphere metabolites, metabolic pathways, continuous cropping

1 Introduction

Ramie (*Boehmeria nivea* L. Gaud) belongs to the genus Boehmeria, family Urticaceae, and is a perennial herbaceous fiber plant with persistent roots, commonly known as "Chinese grass." China accounts for more than 90% of the world's ramie production in terms of the area under cultivation and total production, is rich in germplasm resources, and dominates the international market. Ramie fiber is an excellent raw material for the textile industry, and its root system has a high medicinal value (Rehman et al., 2020). Under normal conditions, ramie roots can self-renew and grow for 10–20 years or even longer. However, after 3–5 years of continuous long-term cultivation, ramie renewal, root damage and root rot are inevitable. This is a major crop disorder that commonly occurs after heavy ramie cropping. Pathogenic microorganisms intensify, cell structure changes, and in severe cases, the life span shortens, and whole plant death can occur (Wang Y. et al., 2020; Zhu et al., 2018). These phenomena were typical of persistent ramie diseases. Therefore, it is important to understand the complex mechanisms of the obstacles to continuous ramie cropping.

Continuous cropping is the practice of planting the same crop or family on the same plot of land for many years. This can result in poor plant growth and development, smaller yellow leaves, increased disease, reduced crop quality, and lower yield (Lyu et al., 2022). In recent decades, experts worldwide have begun to use crop science and ecology to study the barriers to continuous cropping at greater depths. For example, continuous cropping of soybean leads to the frequent occurrence of soil-borne fungal diseases (Song et al., 2022); long-term continuous cropping of strawberry leads to unfavorable inter-root soil conditions and reduces soil physicochemical properties and enzyme activities (Li et al., 2018); and continuous cropping of oil flax reduces the diversity of soil bacteria and affects the structure of the bacterial community (Wang L. G. et al., 2022). Wang Y. et al. (2020) found that continuous ramie cropping negatively affected ramie itself, affecting the physiological, biochemical, and root microbial community diversity. According to the results of Bai (2017), potential chemosensitive substances in ramie have a negative impact on ramie itself, affecting its physiology, biochemistry, and root microbial community diversity.

The effects of continuous cropping are significant, while two categories of factors are reported in the literature regarding the formation of disorders in crops: abiotic and biotic. Abiotic factors are mainly considered as altered physical and chemical properties of the soil, improper application of fertilizers and herbicides, soil nutrient imbalance, poor soil structure, and irrigation practices (Subhashini and Kumar, 2019; Wang S. et al., 2020). Biotic factors include mainly many biotic and abiotic factors, such as changes in microbial communities (Dong et al., 2017), enrichment of soil-borne plant pathogens (Liu et al., 2014), decreased soil enzyme activity (Fu et al., 2017), changes in soil physicochemical properties (Kaur and Singh, 2014; Perez-Brandan et al., 2014; Li et al., 2018), and plant self-toxicity (Van Wyk et al., 2017). In recent years, research on cropping barriers has focused on the chemosensitization of plant autotoxic substances, which is defined as a biological phenomenon in which an organism affects the germination, growth, survival, and reproduction of other organisms in the same community by producing one or more biochemical substances (Xu et al., 2012; Huang et al., 2021). The long-term continuous cropping of soybean leads to the accumulation of harmful secondary metabolites (phenolic acids, benzene, and esters) in root secretions, resulting in soybean autotoxicity and reduced yield and quality (Cui et al., 2018). Previous studies in our laboratory (Wang Y. et al., 2020) found that metabolites such as cysteine, glycine, uracil, and malonic acid were disturbed after continuous ramie cropping and were used as risk markers. The present study builds on these findings by selecting a healthy control group and four species that developed continuous crop disorder to further explore the changes in ramie rhizosphere metabolites and their mechanisms in various continuous cropping groups.

Metabolomics is an important component of systems biology that identifies the full spectrum of detectable metabolites present in biological systems (Wang R. et al., 2022). It is a powerful bioanalytical tool widely used for qualitative and quantitative studies of metabolites in various test samples. Although untargeted gas chromatography-mass spectrometry (GC-MS) and liquid chromatography-mass spectrometry (LC-MS) have been widely used to detect many plant metabolites (Dhawi et al., 2016; Son et al., 2016), few studies have reported the application of metabolomics to explore crop-linked disorders in ramie. Therefore, in this study, we used an untargeted metabolomics approach that combines LC-MS and GC-MS. We selected a healthy group after 8 years of cultivation (CK) and ramie varieties (XZQG, JZ, DJY, and GXD) that developed continuous crop disorder as experimental materials to investigate the effects of continuous and non-continuous group treatments on ramie biomass, rhizosphere soil physicochemical properties and rhizosphere Metabolites and metabolic pathways. These results provide a comprehensive understanding of the stress state of ramie after continuous cropping. It may provide important insights into the mechanisms of the obstacles to continuous ramie cropping and may help to alleviate the effects of continuous ramie cropping by regulating related metabolites and metabolic pathways to promote the healthy development of the ramie industry.

2 Materials and methods

2.1 Plant materials collection

Ramie cultivars were planted in a test field at the Institute of Bast Fiber Crops, Chinese Academy of Agricultural Sciences, Changsha, China. Five ramie germplasm resources, comprising a healthy (CK) and four damaged varieties (XZQG, JZ, DJY, and GXD), that had been cultivated for 8 years and provided the names, collection sites, categories, and resequencing data summary in Table S1. The experiment began in March 2015 and lasted until June 2022, during which the plot was cultivated using a continuous cropping system (3 seasons per year for 5 consecutive years). All the plots were cultivated under the same cropping system and

conditions, including annual sowing time, harvest time, fertilization, and irrigation methods. The rhizosphere soil samples were collected on August 3, 2022, from successive crops and then mixed thoroughly. The mixed soil samples from each group were divided into two parts for GC-MS and LC-MS analyses (6 samples were randomly selected for both, n = 6), and 30 ramie rhizosphere soil samples were prepared for each of these two analyses. All collected samples were stored at −80°C immediately after preparation.

2.2 Plant agronomic traits and physiological measurements

The measured agronomic traits included stem length (SL, cm), stem diameter (SD, mm), bark thickness (BT, mm), bark weight (BW, kg), Fiber yield (FY, g) and fiber yield (FOR, %). Following simultaneous sampling, enzyme activity was measured in the collected rhizosphere soil samples. The activities of the soil enzymes acid phosphatase (S-ACP), neutral phosphatase (S-NP), urease (S-UE), and sucrase (S-SC) were measured using ELISA kits (MLBIO, Shanghai, China) as describe by Zhao et al. (2022). Soil pH was measured using a pH after the samples were dried at 105°C for 24 hours to determine soil moisture content. Soil pH was determined using a calibrated pH meter (soil: solution ratio of 1:2.5).

2.3 Sample preparation

For untargeted metabolite analysis, each sample of approximately 0.5 g was sonicated for 2 min by adding 1 mL of pre-cooled solvent (methanol/water 1:1 (v/v), containing L-2-chlorophenylalanine, 2 μg/mL), followed by centrifugation (10 min at 4°C and 12000 rpm) and 1 mL was transferred to a sample vial. Next, 200 μL of methanol-water (1:4 (v:v)) was redissolved for 3 min, and the reaction was carried out at −40°C for 30 min. The sample was then centrifuged (10 min at 4°C and 12000 rpm), and 150 μL of the supernatant was aspirated, filtered through a 0.22 μm organic phase pinhole filter, and transferred to a vial for LC-MS analysis. In parallel, a 100 μL aliquot of the supernatant was transferred to a glass sampling vial, and then 80 μL of methoxypyridine hydrochloride solution (15 mg/mL) was added, vortexed for 2 min, and then incubated at 37°C for 60 min. Subsequently, 50 μL of BSTFA derivatization reagent and 20 μL of hexane were added, vortexed for 2 min, and then incubated at 70°C for 60 min. Samples were incubated at 25°C for 30 min and subjected to GC-MS metabolomic analysis.

2.4 LC-MS-based untargeted metabolomics analysis

LC-MS setup: The injection volume was 10 μL. The separation was performed on an HSS T3 C18 column (100 mm × 2.1 mm × 1.8 μm, Waters) with the column temperature maintained at 50 °C. The gradient elution program was set as follows: 0-2 min, 100% A; 2-11 min, 0%-100% B; 11-13 min, 100% B; 13-15 min, 0%-100% A. The Q-TOF mass spectrometer was operated in positive and negative ion modes. ESI source temperature: 120°C; desorption temperature: 450°C; desorption gas: 800 L/h; cone gas: 50 L/h; TOF mass range: 50-1200 Da; scan time: 0.2s. The LC-MS metabolic profiles were acquired using an ACQUITY UHPLC system (Waters Corporation Milford, USA) with an AB SCIEX Triple TOF 5600 system (AB SCIEX, Framingham, MA, USA) in the ESI positive and negative ion modes. The QC samples were injected at regular intervals (every 6 samples) throughout the analysis to provide a data set to assess reproducibility. The raw LC-MS data were provided by Luminous (Shanghai, China), and metabolites were identified primarily based on RT m/z pairs and tandem mass spectrometry (MS/MS) spectra, HMDB (https://hmdb.ca/), LIPID MAPS (https://lipidmaps.org/), and a self-constructed database. The data matrix, including 3D datasets of m/z, RT peaks, and intensities, was exported as an Excel file for further analysis.

2.5 GC-MS-based untargeted metabolomics analysis

GC-MS setup: GC-MS analysis was performed using a hybrid quadrupole-Orbitrap GC-MS/MS system (Q Exactive GC, ThermoFisher). The sample volume injected was 1 μL at a carrier gas flow rate of 1 mL/min of helium. The oven temperature was initially set to 50°C and held for 1 min, ramped up to 100°C at 10°C/min, and immediately ramped up to 200°C at 10°C/min and held for 1 min, then ramped up to 320°C at 10°C/min. The ion source temperature was set to 230°C. The scan range was 50.0 to 650.0 m/z, and the mass spectrum was acquired in electron ionization mode (70 eV).

The raw data from the GC-MS analysis were converted to ABF (Analysis Base File) format using analysis base file converter software, and peak detection, deconvolution, alignment, and filtering were performed to identify the metabolites based on the LUG database ((Untargeted database of GC–MS from Lumingbio)), removing all internal standards and false positive peaks. The raw data matrix of the sample information, retention times, and peak intensities was then exported to an Excel file for further analysis.

2.6 Multivariate and univariate analysis and biological pathway analysis

Partial least squares discriminant analysis (PLS-DA) is a supervised clustering method that uses multiple linear regression techniques to maximize separation between groups and to help understand which variables carry class separation information (Yang et al., 2018). PLS-DA was performed on the LC-MS and GC-MS results using online resources (http://www.metaboanalyst.ca/). The variable importance (VIP) in the projection is the weighted sum of squares from the PLS-DA analysis, which indicates the importance of a variable to the overall model. Metabolites with a VIP > 1 and $P < 0.05$were

considered significant. Univariate (one-way ANOVA) analysis of LC-MS/MS results was performed using an online resource (http://www.metaboanalyst.ca/) (Miska et al., 2021). Biological pathway analysis was performed on all metabolites data using MetaboAnalyst 5.0. The calculated impact value threshold for pathway identification was set to 0.1 (Li et al., 2022).

3 Results

3.1 Effects of continuous soil cropping on ramie

After 8 years of continuous cropping of ramie plants, the ramie grown in the 1-year rhizosphere soil was very robust (defined as the CK group), whereas the ramie grown in the four varieties in the continuous cropping had weak growth and low yield (defined as the obstacle groups). The values of plant height, stem diameter, bark thickness, weight, and weight of fresh and dry fibers were lower in the impaired group than in the healthy group (P<0.001; Figure 1). These findings confirm that there is a great difference between growing the CK and obstacle groups in the same field.

Most of the pH values tested in the 8-year rhizosphere soil were bellow pH 7, indicating an acidic soil. At the same time, there were significant differences in the rhizosphere soil enzyme activities among the different planting years. The activities of polyphenol oxidase, neutral phosphatase, and urease were lower than the CK group, whereas the urease activity increased (Table 1). Meanwhile, it was found that there were significant differences in soil enzyme activities among different cropping years ($P < 0.001$, Figure 1). The activities of soil acid phosphatase (S-ACP) and soil neutral phosphatase(S-NP) decreased with increasing years of continuous cropping and were all lower than those of the CK group, whereas soil urease (S-UE) activity increased after 8 years of continuous cropping (Table 1).

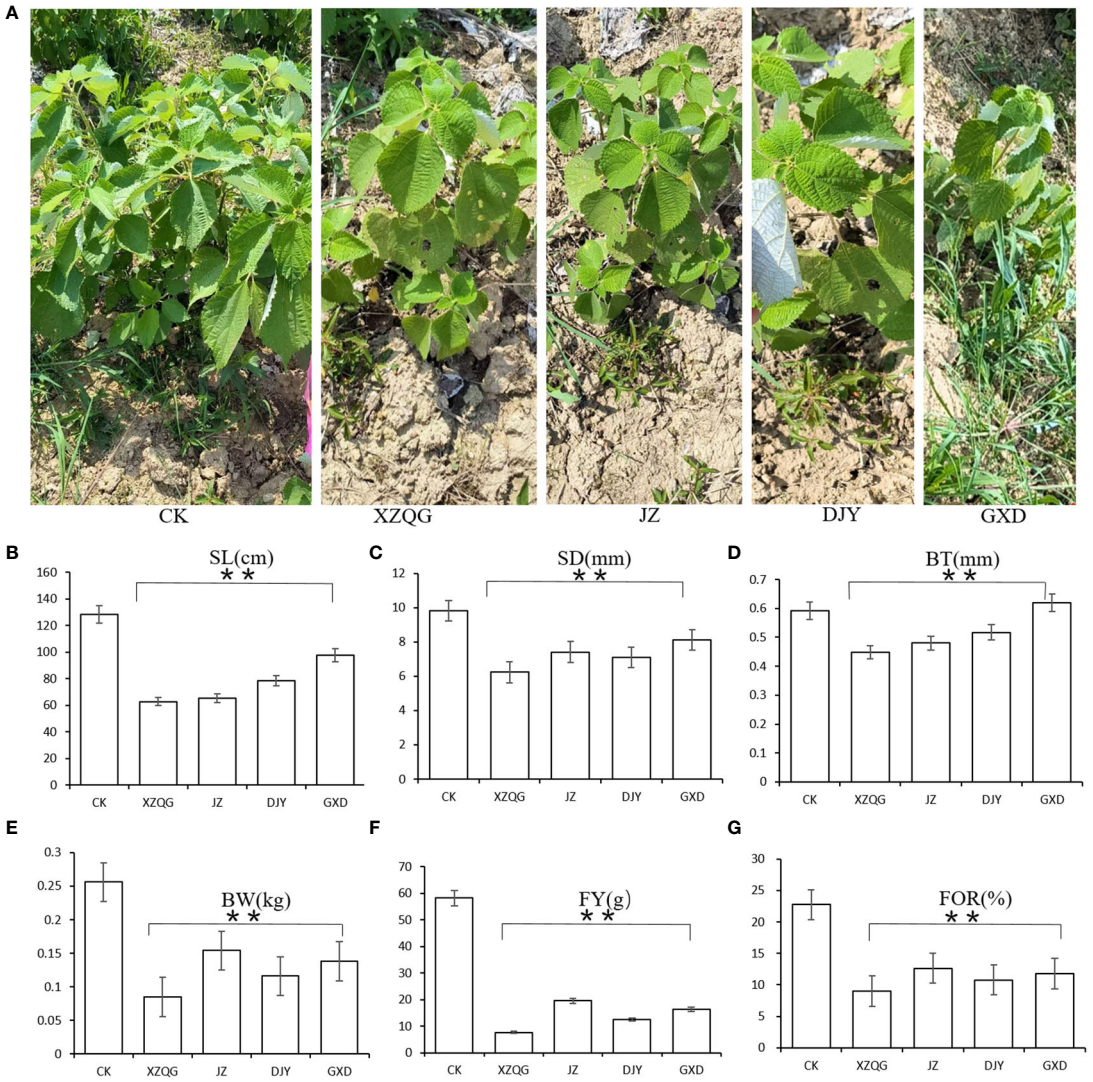

FIGURE 1
(A) Diagram of ramie after five years of continuous cropping. From left to right: CK; XZQG; JZ; DJY; GXD. **(B)** SL. **(C)** SD. **(D)** BT. **(E)** BW. **(F)** FY. **(G)** FOR. **indicates a significant difference at the p <0.001 level.

10.3389/fpls.2023.1217956

TABLE 1 Differences in soil chemical parameters between the CK and Obstacle group.

	CK	XZQG	JZ	DJY	GXD	*P*-value
PH	7.03 ± 0.10	5.42 ± 0.02	5.24 ± 0.02	4.79 ± 0.03	5.82 ± 0.02	<0.001
S-ACP (nmol/h/g)	1155.40 ± 7.64	2096.21 ± 4.58	2482.29 ± 3.51	3067.51 ± 6.54	1697.94 ± 2.64	<0.001
S-NP (nmol/h/g)	842.09 ± .00	158.99 ± 2.65	547.69 ± 2.00	283.19 ± 2.52	628.19 ± 1.00	<0.001
S-UE (μg/d/g)	52.72 ± 1.15	67.76 ± 1.00	70.16 ± 4.16	57.68 ± 1.00	87.68 ± 1.53	<0.001
S-SC (mg/d/g)	8.00 ± 0.15	6.14 ± 0.15	5.93 ± 0.10	6.54 ± 0.01	5.97 ± 0.06	<0.001

Values followed by different letters were significantly different according to Duncan's multiple range tests (P <0.001).

3.2 Metabolic profiles analyzed by GC–MS and LC–MS

Metabolite profiling was performed on the rhizosphere soil samples of the CK and four obstacle groups (XZQG, JZ, DJY, and GXD) using LC-MS and GC-MS. In the LC-MS analysis, PLS-DA was used to identify the metabolites that led to the separation between the CK and obstacle groups. The results showed that the different groups underwent relatively clear clustering, and there was no significant sample overlap, suggesting that the metabolites detected using LC-MS differed significantly between species (Figure 2A). Furthermore, when the CK group was compared with each obstacle group, the CK group and the other groups were located within a 95% Hotelling's T^2 ellipse in the PLS-DA models, showing a clear separation (Figures 2B-E). A further 7-fold internal cross-validation and 200 permutation tests were performed to assess these models' predictive accuracy and statistical significance. The slopes of the R2Y and Q2Y straight lines were found to be very close to the horizontal straight line for each group compared to the CK group (Figure S1). In the GC-MS analysis, the CK group in the PLS-DA models showed the same significant separation from the other total obstacle groups (Figure 2G), as well as when compared individually (Figures 2H-K). The blue regression line at the Q2 point was below zero with the vertical axis in the 200 permutations 1 component test, and these PLS-DA models showed a low overfitting risk. These results suggest that the PLS-DA models can identify enriched metabolites that differ between the CK and obstacle groups (Figure S2).

3.3 Changed metabolites in ramie soil between the CK and obstacle groups

A comprehensive LC-MS and GC-MS untargeted metabolomics approach was used to analyze the overall metabolic profiles of continuous ramie crop soil samples. We selected metabolite peaks with a coefficient of variation (CV) <15% in 30 quality control samples and selected metabolites with large differences based on the VIP value of the PLS-DA model (VIP>1) and the corrected *p*-value of the Student's t-test (p-value < 0.05). As shown in Figure 2, the differentially expressed metabolites produced under different explosive exposures in the LC-MS analysis were mainly lipids and lipid-like molecules (47–69), organic acids and their derivatives (27–53), and organic oxygen compounds (25–46), whose abnormal differences in metabolites may be responsible for cytotoxicity. Simultaneously, when the CK group and the obstacle groups were analyzed using LC-MS untargeted metabolomics, 49 metabolites were identified and quantified (Figure 2F), of which 27 were upregulated, and 22 were downregulated (VIP>1; Table S2). In GC-MS analysis, the differential metabolites mainly included organic oxygen compounds (5–23), organic acids and their derivatives (2–20), lipids and lipid-like molecules (8–10), organic heterocyclic compounds (2–7), phenylpropanoids and their derivatives (1–5), among others (Figure 3), while the CK group combined with obstacle group analysis revealed that 19 metabolites were quantified (Figure 2L); 12 metabolites showed an increasing trend and 7 metabolites showed a decreasing trend (VIP>1, Table S3).

3.4 Metabolic pathways of differential abundant metabolites

The above significantly altered metabolites are involved in several important metabolic pathways. Subsequently, we searched 49 metabolites from the LC-MS (Figure 2F) and 19 metabolites from the GC -MS (Figure 2L), determined using the Venn diagrams in the KEGG database, which revealed 10 metabolic pathways Tables S2, S3) that were altered in continuous ramie soil crops. Simultaneously, we performed enrichment analysis using MetaboAnalyst 5.0 to characterize the affected biological pathways and constructed as chematic diagram showing that there were 20 differential metabolites of interest in these differentially enriched metabolic pathways (Figure 4). These differentially enriched metabolic pathways were classiedas phenolic, lipid, aminoacid, nucleoside, ascorbate, and aldarate metabolic pathways.

Among these differentially enriched metabolic pathways, seven had impact values >0.1, which is the correlation threshold following pathway enrichment and topological analysis. Based on negative log (*P*) and impact values, we identified ramie as a significantly correlated pathway in soil secretion for phenylalanine, tyrosine and tryptophan biosynthesis; phenylalanine metabolism; pyrimidine metabolism; fatty acid metabolism; histidine biosynthesis; arginine biosynthesis; and ascorbate and aldarate

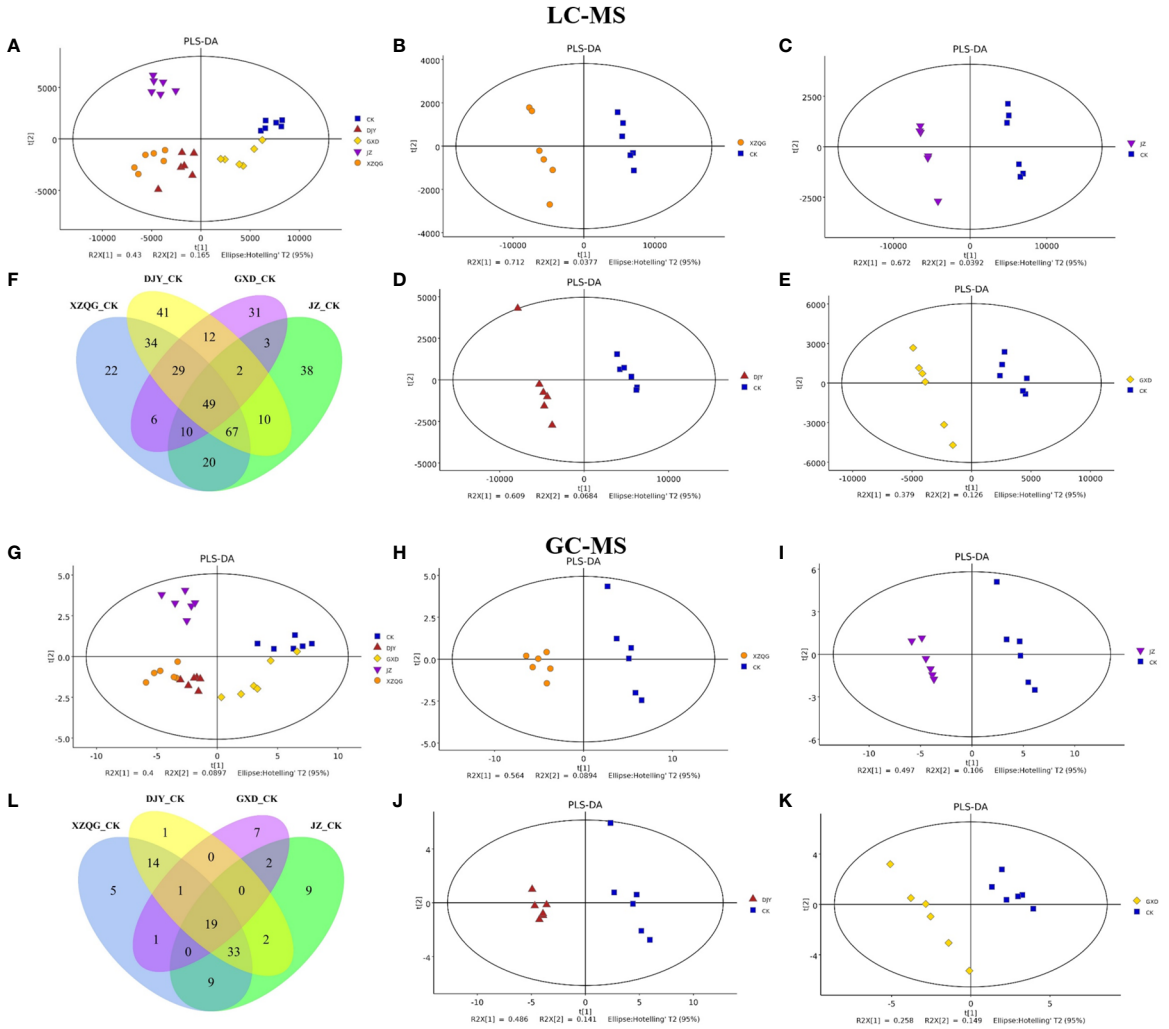

FIGURE 2
Metabolomic analysis of ramie continuous crop obstacle groups. **(A)** PLS-DA score plots of LC-MS between CK group and all obstacle groups **(B-E)** PLS-DA score plots of LC-MS between CK group and each obstacle group, **(F)** LC-MS metabolite Venn diagram; **(G)** PLS-DA score plots of GC-MS between CK group and all obstacle groups **(H-K)** PLS-DA score plots of GC-MS between CK group and each obstacle group, **(L)** GC-MS metabolite Venn diagram.

metabolism. Their impact values were 0.5, 0.36, 0.23, 0.23, 0.16, 0.14, 0.13, respectively (Figure 5).

3.5 Associations between metabolic changes and physiological parameters

A Spearman correlation analysis was performed to evaluate the relationship between the 20 annotated metabolites and 11 physiological parameters in continuous ramie cropping soils. Only the correlations with $P < 0.05$ were highlighted in the heat map (Figure 6). In phenylpropanoid biosynthesis following continuous ramie cropping, caffeic acid, sinapinic acid, trans-ferulic acid, and phenylalanine were positively correlated with SL, BT, SD, BW, FOR, FY, PH, S-NP, and S-SC, and negatively correlated with S-ACP and S-UE, suggesting that phenolic acids could be used in ramie metabolic pathways. Regarding fatty acid metabolism, tetracosanoic acid, jasmonic acid, and 4-hydroxycrotonic acid were positively correlated with agronomic traits (SL, BT, SD, BW, FY, and FOR) and negatively correlated with S-UE, indicating that highly expressed lipid metabolites may disrupt normal plant growth homeostasis and adversely affect plants. In amino acid and derivative metabolism, L-histidine, L-lysine, and citrulline were positively correlated with S-UE and S-ACP and negatively correlated with other physiological indicators, which demonstrated that soil urease activity and soil acid phosphatase activity were enhanced after years of continuous ramie cultivation. Plant antioxidant capacity was also enhanced. Myo-inositol, which is derived from ascorbate and aldarate metabolism, has important antioxidant effects and can scavenge reactive oxygen species and free radicals. Accordingly, myo-Inositol was positively correlated with S-ACP, S-SC, and S-UE and negatively correlated with other physiological indicators, implying that this metabolite may also be an effective metabolite for improving the environment during continuous cropping.

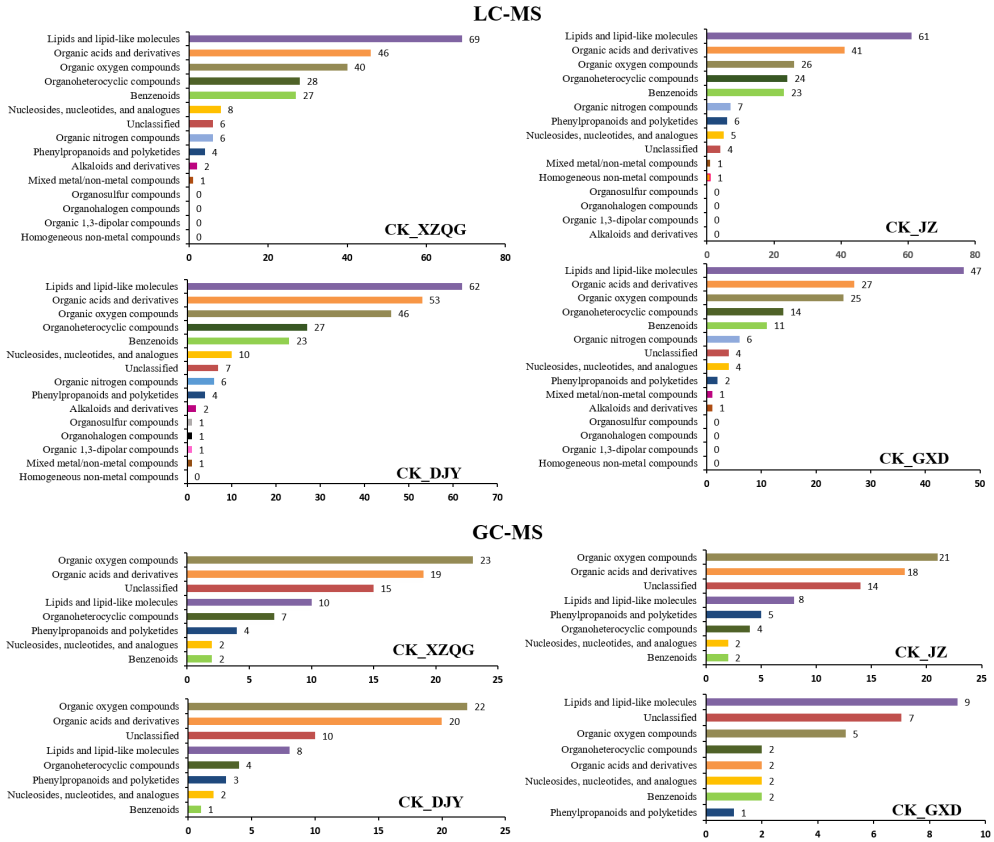

FIGURE 3
Analysis of differentially expressed metabolites classification statistics using LC-MS and GC-MS.

4 Discussion

The current data suggest that ramie may have undergone strong metabolic changes following 8 years of continuous cropping. Identifying these metabolites could be useful in developing potential chemical markers for monitoring or even predicting whether ramie plants are affected by continuous cropping. In the present study, a combination of metabolomic analyses focusing on 49 metabolites in LC-MS and 19 differential metabolites in GC-MS and their significantly related metabolic pathways, revealed significant differences with ramie agronomic properties, enzyme activity, and other indicators, which provided new insights into the barrier response of soil metabolites after continuous ramie cropping.

4.1 Phenylpropanoid pathway

The phenylpropanoid pathway, a classical metabolic pathway associated with the induction of resistance, can inhibit or scavenge ROS in cells under biotic or abiotic stress, thereby protecting proteins, membrane lipids, DNA, enzymes, and other organellar components from severe damage (Chen et al., 2006; Xu et al., 2019; Oliva et al., 2021; Wang et al., 2021). Notably, in the present study, some compounds associated with phenylpropanoid biosynthesis, such as cinnamic acid and cis-p-coumaric acid, increased the relative abundance of ramie growth in the obstacle group by 1–3-fold compared to the CK group ($P<0.05$), which may be due to an overreaction of stress to ROS, producing secondary metabolites that protect themselves from oxidative damage by reactive oxygen species generated by adversity stress. This is similar to the findings of Zhao et al. (2018), who found that phenylalanine and 4-hydroxycinnamic acid levels were enhanced in maize under adverse stress. Interestingly, phenylalanine, as well as derivatives of hydroxycinnamic acid (caffeic acid, trans-ferulic acid, and mustardic acid), showed a significant downward trend relative to the CK group, especially the downstream phenylpropanoid pathway compound (mustardic acid), which showed a 5–10-fold decrease in relative abundance (Table S4). It is well known that aromatic acids are important metabolites for the study of phenylpropanoid metabolism involved in the regulation of plant growth and development and response to adversity. They are widely present in the plant kingdom, where they possess antioxidant, antibacterial, anti-inflammatory, anticancer, and anxiolytic activities (Nićiforović and Abramovič, 2014). This suggested that the metabolism of the phenylpropanoid biosynthetic pathway was disrupted after ramie crop succession. Meanwhile, correlation analysis of physiological indicators of ramie showed that phenylalanine, caffeic acid, sinapinic acid, and trans-ferulic acid in the phenol propane pathway were positively correlated with SL, BT, SD, and S-NP and significantly correlated with SL with correlation coefficients of

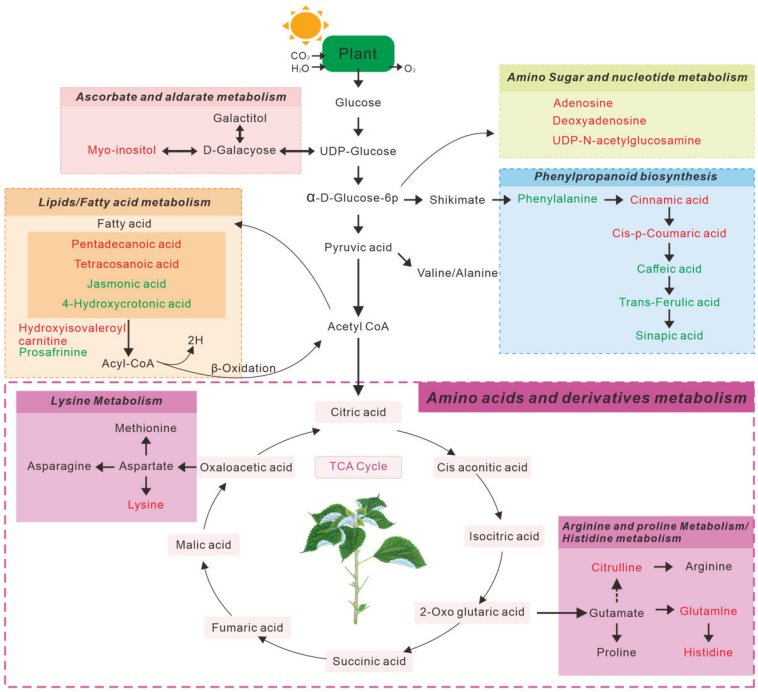

FIGURE 4
Schematic diagram of the main metabolic pathways affected by ramie rhizosphere soil metabolites. The red text represents metabolites with increased concentrations, and green text represents metabolites with decreased concentrations.

0.814, 0.982, 0.961, and 0.972, respectively (Table S4). In addition, the metabolomic analysis results showed that these metabolites were downregulated, indicating that these phenolic acid products in ramie inter-root metabolites seriously affected the normal growth of ramie plants and led to poor plant growth. This indicates that these metabolites can promote plant growth at certain concentrations. Interestingly, cinnamic acid and cis-p-coumaric acid in the phenolpropane pathway were negatively correlated with SL, BT, PH, SD,

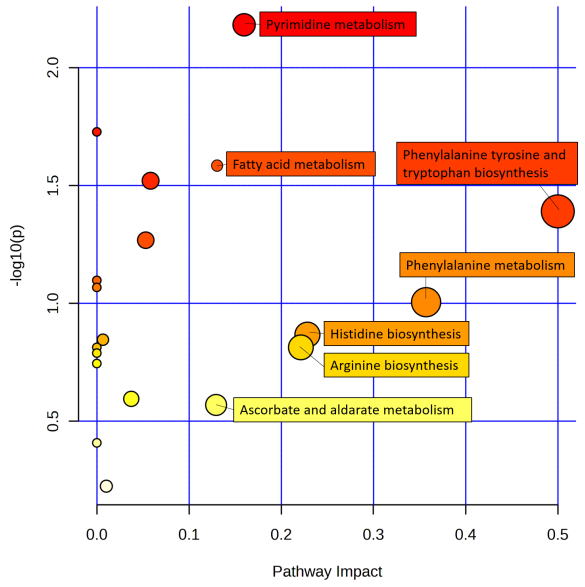

FIGURE 5
Schematic metabolome profiles of the significant metabolic pathways in ramie after continuous cropping. Each bubble in the figure is a metabolic pathway, with the x-axis indicating pathway enrichment and the y-axis indicating pathway impact. The size and color represent the enrichment and impact values of the major pathway, respectively.

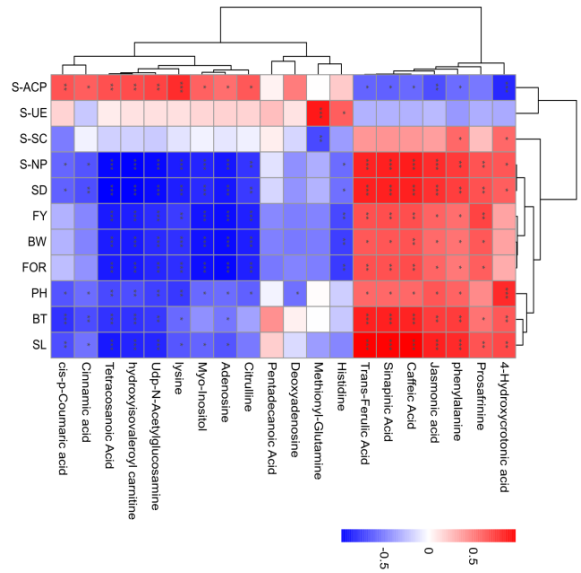

FIGURE 6
Association network analysis between metabolite changes and physiological parameters in continuous ramie cropping soil. The absolute values of Pearson correlation coefficients above the threshold are shown ($P<0.01$), and the correlation levels are indicated as red (positive correlation) or blue (negative correlation), with darker colors indicating stronger correlations. Symbols provided on bars: *: $P < 0.05$; **: $P < 0.01$; ***: $P < 0.001$.

and S-NP; in particular, cinnamic acid and cis-p-coumaric acid were correlated with BT with the highest correlation coefficients of -0.683 and -0.781, respectively (Table S4). These two metabolites were upregulated in the metabolomic analysis, indicating that high concentrations of phenolic acids can inhibit ramie growth and lead to the development of succession disorders. This result was mirrored in a similar study by Li et al. (2017), in which cinnamic acid had an inhibitory regulatory effect on cucumber morphogenesis and development. In conclusion, while some metabolites (phenylalanine, caffeic acid, sinapinic acid, trans-ferulic acid) were depleted to protect the plants from adverse stress, the intermediates of phenylalanine metabolism (cinnamic acid, cis-p-coumaric acid) appeared to accumulate, indicating that the accumulation and depletion of secondary metabolites in ramie are both manifestations of ramie's response to continuous ramie cropping and subsequently ensure the normal growth of ramie.

4.2 Fatty acid metabolism

Fatty acids, which are components of cell membranes, are essential for maintaining cell fluidity and integrity under various stress levels (Raval et al., 2017). Interestingly, the fatty acids that were upregulated in the CK group compared with those in the obstacle groups were mainly saturated fatty acids, including pentadecanoic acid and tetracosanoic acid, some of which are metabolites derived from the malonyl-CoA precursor of flavonoid biosynthesis (Lyu et al., 2018). Raval et al. (2017) also found a higher accumulation of palmitic and stearic acids in an adversity study. This could indicate that adversity induces changes in fatty acid composition. However, unsaturated fatty acids make membranes more susceptible to ROS attack (Paupière et al., 2014). In the current study, unsaturated fatty acids (jasmonic acid and 4-hydroxycrotonic acid) were significantly down-regulated by 1–3 fold relative to the CK group, demonstrating that the saturated level of fatty acids seems to have a critical effect on membrane stability and normal growth of ramie plants. Simultaneously, jasmonic acid and 4-hydroxycrotonic acid were positively correlated with agronomic traits, such as SL, BT, PH, SD, and S-NP, especially in the jasmonic acid variable with SL, BT, SD, and S-NP, with significant correlations of 0.857, 0.749, 0.739, and 0.811, respectively (Table S4). These results are similar to the view that jasmonic acid initiates the plant immune defense response and activates related genes and metabolites (Zhang et al., 2017). Notably, jasmonic acid is an endogenous growth regulator present in higher plants with physiological effects, such as inhibition of plant growth, promotion of leaf senescence, and enhancement of resistance. More strikingly, jasmonic acid-like JA-mediated signaling pathways are closely related to plant resistance and can induce the expression of resistance genes, effectively mediating plant defense responses to pathogenic bacteria, herbivores, and abiotic stresses, inducing the expression of a series of defense genes, synthesis of defense response chemicals, and modulation of plant immune and stress responses (Han, 2017). Preliminarily, jasmonic acid may be one of the factors affecting ramie succession.

4.3 Amino acid and derivatives metabolism

The accumulation of amino acids and other nitrogenous compounds has been observed in many studies on plants exposed to adversity (Sanchez et al., 2008). The current study showed that the altered amino acids were mainly involved in the metabolism of arginine, proline, histidine, and lysine. Specifically, lysine, citrulline, histidine, and methionyl glutamine were upregulated, especially methionyl glutamine was upregulated by a factor of 10–40 (Figure S3). Glutamine is an important form of nitrogen present in plants and is a precursor for the intracellular biosynthesis of many important substances, such as nucleic acids, nucleotides, amino sugars, and proteins, as well as a carrier of nitrogen during ammonia and urea synthesis *in vivo*. Glutamine is also an important component of the nitrogen cycle; in rapidly multiplying and differentiating cells and tissues, it is preferentially selected as the main energy source and plays a key role in nitrogen assimilation, recycling, transport, and storage. (Zhao et al., 2018). The increase in glutamine and glutamate levels was also consistent with previous reports showing that glutamine is significantly upregulated and elevated in response to adverse stress (Rizhsky et al., 2004). In addition, the correlation between glutamine and S-UE was significant, with a correlation coefficient of 0.889 (Table S4), indicating that glutamine affected urease activity in ramie soil and was closely related to soil nutrient regulation. In conclusion, the increase in glutamine may imply that ramie was under adverse stress after continuous cropping and needed to continuously enhance nitrogen assimilation, cycling, transport, and storage.

4.4 Ascorbate and aldarate metabolism

The ascorbic acid pathway is critical for regulating plant growth, inducing flowering, delaying senescence, scavenging self-reactive oxygen species and free radicals, reducing damage caused by stress, and ensuring normal metabolic function (Gallie, 2013). A study conducted on two wheat species showed that endogenous ascorbic acid content increased because of cold stress (Kader et al., 2011). An explanation for the elevated ascorbic acid levels could be an expression of plant stress resistance (Sivaci et al., 2014). While inositol is considered an essential vitamin-like ascorbic acid pathway substance that is converted to the TCA cycle through galactose metabolism, the plant body can synthesize inositol autonomously; if inositol metabolism is insufficient or impaired in plants, plant stress tolerance, growth, and development will be limited (Sang et al., 2017). In contrast, in the current study, vitamin and cofactor metabolism (inositol) after ramie crop succession played critical roles as intermediates of sugar, fatty acid, and amino acid metabolism. As shown in Figures 5, S3, one inositol metabolite was significantly upregulated in severe tillage soil damage stress, suggesting that ramie plants may reduce the concentration of reactive oxygen species through the ascorbic acid metabolic pathway, thereby mitigating free radical damage to plants. The antioxidant process involved in ascorbic acid is also an important defensive response of ramie in response to inheritance

disorders. In contrast, in the present study, the metabolism of vitamins and cofactors (inositol) after ramie crop succession played a critical role as intermediates of sugar, fatty acid, and amino acid metabolisms. As shown in Figure 5; Supplementary Tables S3, one inositol metabolite was significantly upregulated in severe tillage soil damage stress, suggesting that ramie plants may reduce the concentration of reactive oxygen species through the ascorbic acid metabolic pathway, thereby mitigating free radical damage to plants. The antioxidant process involved in ascorbic acid is also an important defensive response of ramie in response to inheritance disorders. According to the correlation analysis with physiological indicators of ramie, inositol metabolites were negatively correlated with SD, BW, FOR, FY, and S-NP, with correlation coefficients of -0.811 -0.904 -0.917 -0.895 -0.836, respectively (Table S4). This indicated that traits such as SD, BW, FY, and S-NP of ramie reflected adverse effects when more inositol metabolites were secreted into the soil and that inositol metabolites can be used as a marker of disease.

As mentioned above, this study simultaneously elucidated that sinapic acid, jasmonic acid, glutamine, and myo-inositolmay be the main metabolites affecting ramie continuous cropping obstacles, and provided important insights into the mechanisms of the obstacles to continuous ramie cropping.

5 Conclusion

In summary, in the present study, metabolomics based on LC-MS and GC-MS was used to systematically investigate the metabolite composition, abundance, and metabolic pathways in ramie following continuous ramie cropping, revealing significant changes in the levels of phenylpropane compounds, fatty acids, amino acids, and other important metabolites. Furthermore, we demonstrated the enhanced resistance of ramie plants to the ramie continuous cropping barrier, predicted that these metabolites may function in concert to establish a complex metabolic network for mitigating ramie continuous cropping barriers, and provided important insights into the mechanism of the obstacles to continuous ramie cropping.

Data availability statement

The original contributions presented in the study are included in the article/Supplementary Material. Further inquiries can be directed to the corresponding authors.

Author contributions

SZ designed the experiments. QL and YW and provided experimental methods. QG and GL performed the research, YF, TL and XW analyzed the data and wrote the manuscript and reviewed the manuscript. All authors contributed to the article and approved the submitted version.

Funding

This work was supported by grants from the National Natural Science Foundation of China (31571618 and 31771734), the Agricultural Science and Technology Innovation Program (ASTIP-IBFC), Supported by China Agriculture Research System of MOF and MARA (CARS-16-E12), and the science and technology innovation Program of Hunan Province(2022RC1160).

Acknowledgments

We thank the Shanghai Luming Biological Technology Co., Ltd (Shanghai, China) for providing metabonomics services.

Conflict of interest

The authors declare that the research was conducted in the absence of any commercial or financial relationships that could be construed as a potential conflict of interest.

Publisher's note

Supplementary material

The Supplementary Material for this article can be found online at: https://www.frontiersin.org/articles/10.3389/fpls.2023.1217956/full#supplementary-material

References

Bai, Y. (2017). Effect of potential allelochemicals from ramieon rhizosphere microbial diversity andphysiology and biochemistry of ramie [D]. Hunan Agricultural University.

Chen, J. Y., Wen, P. F., Kong, W. F., Pan, Q. H., Wan, S. B., and Huang, W. D. (2006). Changes and subcellular localizations of the enzymes involved in phenylpropanoid metabolism during grape berry development. *J. Plant Physiol.* 163 (2), 115–127. doi: 10.1016/j.jplph.2005.07.006

Cui, J. Q., Sun, H. B., Sun, M. B., Liang, R. T., Jie, W. G., and Cai, B. Y. (2018). Effects of funneliformis mosseae on root metabolites and rhizosphere soil properties to continuously-cropped soybean in the potted-experiments. *Int. J. Mol. Sci.* 24, 19 (8):2160. doi: 10.3390/ijms19082160

Dhawi, F., Datta, R., and Ramakrishna, W. (2016). Mycorrhiza and heavy metal resistant bacteria enhance growth, nutrient uptake and alter metabolic profile of

sorghum grown in marginal soil. *Chemosphere* 157, 33–41. doi: 10.1016/j.chemosphere.2016.04.112

Dong, L., Xu, J., Zhang, L., Yang, J., Liao, B., Li, X., et al. (2017). High-throughput sequencing technology reveals that continuous cropping of American ginseng results in changes in the microbial community in arable soil. *Chin. Med.* 12, 18. doi: 10.1186/s13020-017-0139-8

Fu, H. D., Zhang, G. X., Zhang, F., Sun, Z. P., Geng, G. M., and Li, T. L. (2017). Effects of continuous tomato monoculture on soil microbial properties and enzyme activities in a solar greenhouse. *Sustainability* 9, 317. doi: 10.3390/su9020317

Gallie, D. R. (2013). The role of l-ascorbic acid recycling in responding to environmental stress and in promoting plant growth. *J. Exp. Bot.* 64 (2), 433–443. doi: 10.1093/jxb/ers330

Han, G. Z. (2017). Evolution of jasmonate biosynthesis and signaling mechanisms. *J. Exp. Bot.* 68 (6), 1323–1331. doi: 10.1093/jxb/erw470

Huang, W., Sun, D., Wang, R., and An, Y. (2021). Integration of transcriptomics and metabolomics reveals the responses of sugar beet to continuous cropping obstacle. *Front. Plant Sci.* 12. doi: 10.3389/fpls.2021.711333

Kader, D. Z. A., Saleh, A. A. H., Elmeleigy, S. A., and Dosoky, N. S. (2011). Chilling-induced oxidative stress and polyamines regulatory role in two wheat varieties. *J. Taibah Univ. Sci.* 5, 14–24. doi: 10.1016/S1658-3655(12)60034-X

Kaur, J., and Singh, J. P. (2014). Long-term effects of continuous cropping and different nutrient management practices on the distribution of organic nitrogen in soil under rice-wheat system. *Plant Soil Environ. doi* 60, 63–68. doi: 10.17221/440/2013-Pse

Li, W., Liu, Q., and Chen, P. (2018). Effect of long-term continuous cropping of strawberry on soil bacterial community structure and diversity. *J. Integr. Agric.* 17 (11), 2570–2582. doi: 10.1016/S2095-3119(18)61944-6

Li, J., Li, Y., Tian, Y., Qu, M., Zhang, W., and Gao, L. (2017). Melatonin Has the Potential to Alleviate Cinnamic Acid Stress in Cucumber Seedlings. *Frontiers in plant science*, 8, 1193. doi: 10.3389/fpls.2017.01193

Li, J., Shu, X., Xu, J., Su, S. M., Chan, U. I., Mo, L., et al. (2022). S100A9-CXCL12 activation in BRCA1-mutant breast cancer promotes an immunosuppressive microenvironment associated with resistance to immunotherapy. *Nat. Commun.* 13 (1), 1481. doi: 10.1038/s41467-022-29151-5

Liu, X., Zhang, J. L., Gu, T. Y., Zhang, W. M., Shen, Q. R., Yin, S. X., et al. (2014). Microbial community diversities and taxa abundances in soils along a seven-year gradient of potato monoculture using high throughput pyrosequencing approach. *PloS One* 9, 86610. doi: 10.1371/journal.pone.0086610

Lyu, J., Jin, N., Meng, X., Jin, L., Wang, S., Xiao, X., et al. (2022). Exogenous silicon alleviates the adverse effects of cinnamic acid-induced autotoxicity stress on cucumber seedling growth. *Front. Plant Sci.* 13. doi: 10.3389/fpls.2022.968514

Lyu, X., Ng, K. R., Mark, R., Lee, J. L., and Chen, W. (2018). Comparative metabolic profiling of engineered saccharomyces cerevisiae with enhanced flavonoids production. *J. Funct. Foods* 44, 274–282. doi: 10.1016/j.jff.2018.03.012

Miska, J., Rashidi, A., Lee-Chang, C., Gao, P., Lopez-Rosas, A., Zhang, P., et al. (2021). Polyamines drive myeloid cell survival by buffering intracellular pH to promote immunosuppression in glioblastoma. *Sci. Adv.* 7 (8):eabc8929. doi: 10.1126/sciadv.abc8929

Nićiforović, N., and Abramovič, H. (2014). Sinapic acid and its derivatives: natural sources and bioactivity. *Compr. Rev. Food Sci. Food Saf.* 13 (1), 34–51. doi: 10.1111/1541-4337.12041

Oliva, M., Guy, A., Galili, G., Dor, E., Schweitzer, R., Amir, R., et al. (2021). Enhanced production of aromatic amino acids in tobacco plants leads to increased phenylpropanoid metabolites and tolerance to stresses. *Front. Plant Sci.* 11. doi: 10.3389/fpls.2020.604349

Paupière, M. J., van Heusden, A. W., and Bovy, A. G. (2014). Themetabolic basis of pollen thermo-tolerance:perspectives for breeding. *Metabolites* 4, 889–920. doi: 10.3390/metabo4040889

Perez-Brandan, C., Huidobro, J., Grumberg, B., Scandiani, M. M., Luque, A. G., Meriles, J. M., et al. (2014). Soybean fungal soil-borne diseases: a parameter for measuring the effect of agricultural intensification on soil health. *Can. J. Microbiol.* 60 (2), 73–84. doi: 10.1139/cjm-2013-0792

Raval, S. S., Mahatma, M. K., Chakraborty, K., Bishi, S. K., Singh, A. L., Rathod, K. J., et al. (2017). Metabolomics of groundnut (Arachis hypogaea l.) genotypes under varying temperature regimes. *Plant Growth Regul.* 84 (3), 493–505. doi: 10.1007/s10725-017-0356-2

Rehman, M., Fahad, S., Saleem, M., Hafeez, M., Rahman, M., Liu, F., et al. (2020). Red light optimized physiological traits and enhanced the growth of ramie (Boehmeria nivea l.). *Photosynthetica* 58 (4), 922–931. doi: 10.32615/ps.2020.040

Rizhsky, L., Liang, H., Shuman, J., Shulaev, V., Davletova, S., and Mittler, R. (2004). When defense pathways Collide.The response of arabidopsis to a combination of drought and heat stress. *Plant Physiol.* 134, 1683–1696. doi: 10.1104/pp.103.033431

Sanchez, D. H., Lippold, F., Redestig, H., Hannah, M. A., Erban, A., Kra¨mer, U., et al. (2008). Integrative functional genomics of salt acclimatization in the model legume lotus japonicas. *Plant J.* 53 (6), 973–987. doi: 10.1111/j.1365-313X.2007.03381.x

Sang, S., Chen, Y., Yang, Q., and Wang, P. (2017). Arabidopsis inositol polyphosphate multikinase delays flowering time through mediating transcriptional activation of FLOWERING LOCUS c. *J. Exp. Bot.* 68 (21-22), 5787–5800. doi: 10.1093/jxb/erx397

Sivaci, A., Kaya, A., and Duman, S. (2014). Effects of ascorbic acid on some physiological changes of pepino (Solanum muricatum ait.) under chilling stress. *Acta Biol Hungarica* 65 (3), 305–318. doi: 10.1556/ABiol.65.2014.3.7

Son, S. Y., Kim, N. K., and Lee, S. M. (2016). Metabolite fingerprinting, pathway analyses, and bioactivity correlations for plant species belonging to the cornaceae, fabaceae, and *Rosaceae* families. *Plant Cell Rep* 35 (9), 1917–1931. doi: 10.1007/s00299-016-2006-y

Song, X., Huang, L., Li, Y., Zhao, C., Tao, B., and Zhang, W. (2022). Characteristics of soil fungal communities in soybean rotations. *Front. Plant Sci.* 13. doi: 10.3389/fpls.2022.926731

Subhashini, D. V., and Kumar, H. (2019). Effect of long-term application of mineral fertilizers and FYM on microbial dynamics, yield and quality of FCV tobacco (*Nicotiana tabacum*) grown in vertisols. *Indian J. Agric. Sci.* 89, 1328–1333. doi: 10.56093/ijas.v89i8.92867

Van Wyk, D. A. B., Adeleke, R., Rhode, O. H. J., Bezuidenhout, C. C., and Mienie, C. (2017). Ecological guild and enzyme activities of rhizosphere soil microbial communities associated with bt-maize cultivation under field conditions in north West province of south Africa. *J. Basic Microbiol.* 57, 781–792. doi: 10.1002/jobm.201700043

Wang, S., Cheng, J., Li, T., and Liao, Y. (2020). Response of soil fungal communities to continuous cropping of flue-cured tobacco. *Sci. Rep.* 10, 19911. doi: 10.1038/s41598-020-77044-77048

Wang, R., Liu, J., Jiang, W., Ji, P., and Li, Y. (2022). Metabolomics and microbiomics reveal impacts of rhizosphere metabolites on alfalfa continuous cropping. *Front. Microbiol.* 13. doi: 10.3389/fmicb.2022.833968

Wang, F., Xiao, J., Zhang, Y., Li, R., Liu, L., and Deng, J. (2021). Biocontrol ability and action mechanism of bacillus halotolerans against botrytis cinerea causing grey mould in postharvest strawberry fruit. *Postharvest Biol. Technol.* 174, 111456. doi: 10.1016/j.postharvbio.2020.111456

Wang, L. G., Ye, C. L., Chen, J., Li, J. J., and Luo, J. J. (2022). Effects of continuous cropping on bacteria community in oil flax soil. *Agr. Res. Arid Areas* 40, 70–75. doi: 10.7606/j.issn.1000-7601.2022.01.08

Wang, Y., Zhu, S., Liu, T., Guo, B., Li, F., and Bai, X. (2020). Identification of the rhizospheric microbe and metabolites that led by the continuous cropping of ramie (Boehmeria nivea l. gaud). *Sci. Rep.* 10 (1), 20408. doi: 10.1038/s41598-020-77475-3

Xu, M., Galhano, R., Wiemann, P., Bueno, E., Tiernan, M., Wu, W., et al. (2012). Genetic evidence for natural product-mediated plant-plant allelopathy in rice (Oryza sativa). *New Phytol.* 193 (3), 570–575. doi: 10.1111/j.1469-8137.2011.04005.x

Xu, J., Zhang, Z., Li, X., Wei, J., and Wu, B. (2019). Effect of nitrous oxide against botrytis cinerea and phenylpropanoid pathway metabolism in table grapes. *Sci. Hortic.* 254, 99–105. doi: 10.1016/j.scienta.2019.04.061

Yang, C., Hao, R. J., Du, X. D., Wang, Q. H., Deng, Y. W., Sun, R. J., et al. (2018). GC–TOF/MS-based metabolomics studies on the effect of protein sources in formulated diet for pearl oyster pinctada fucata martensii. *Aquaculture* 486, 139–147. doi: 10.1016/j.aquaculture.2017.12.020

Zhang, T., Gao, C., Yue, Y., Liu, Z., Ma, C., Zhou, G., et al. (2017). Time-course transcriptome analysis of compatible and incompatible pollen-stigma interactions in brassica napus l. *Front. Plant Sci.* 8. doi: 10.3389/fpls.2017.00682

Zhao, X., Dong, Q., Han, Y., Zhang, K., Shi, X., Yang, X., et al. (2022). Maize/peanut intercropping improves nutrient uptake of side-row maize and system microbial community diversity. *BMC Microbiol.* 22, 14. doi: 10.1186/s12866-021-02425-6

Zhao, L., Huang, Y., and Keller, A. A. (2018). Comparative metabolic response between cucumber (Cucumis sativus) and corn (Zea mays) to a $Cu(OH)_2$ nanopesticide. *J. Agric. Food Chem.* 66 (26), 6628–6636. doi: 10.1021/acs.jafc.7b01306

Zhu, S., Wang, Y., Xu, X., Liu, T., Wu, D., Zheng, X., et al. (2018). Potential use of high-throughput sequencing of soil microbial communities for estimating the adverse effects of continuous cropping on ramie (Boehmeria nivea l. gaud). *PloS One* 13 (5), e0197095. doi: 10.1371/journal.pone.0197095

frontiers | Frontiers in Plant Science

TYPE Original Research
PUBLISHED 30 August 2023
DOI 10.3389/fpls.2023.1231809

OPEN ACCESS

EDITED BY
Chun-Tao Che,
University of Illinois Chicago, United States

REVIEWED BY
Jun Murata,
Suntory Foundation for Life Sciences, Japan
Trinh-Don Nguyen,
University of British Columbia, Canada

*CORRESPONDENCE
Isabel Desgagné-Penix
Isabel.Desgagne-Penix@uqtr.edu

RECEIVED 30 May 2023
ACCEPTED 14 August 2023
PUBLISHED 30 August 2023

CITATION
Majhi BB, Gélinas S-E, Mérindol N, Ricard S and Desgagné-Penix I (2023) Characterization of norbelladine synthase and noroxomaritidine/norcraugsodine reductase reveals a novel catalytic route for the biosynthesis of Amaryllidaceae alkaloids including the Alzheimer's drug galanthamine. *Front. Plant Sci.* 14:1231809. doi: 10.3389/fpls.2023.1231809

Characterization of norbelladine synthase and noroxomaritidine/norcraugsodine reductase reveals a novel catalytic route for the biosynthesis of Amaryllidaceae alkaloids including the Alzheimer's drug galanthamine

Bharat Bhusan Majhi[1], Sarah-Eve Gélinas[1], Natacha Mérindol[1], Simon Ricard[1] and Isabel Desgagné-Penix[1,2]*

[1]Department of Chemistry, Biochemistry and Physics, Université du Québec à Trois-Rivières, Trois-Rivières, Québec, QC, Canada, [2]Plant Biology Research Group, Université du Québec à Trois-Rivières, Trois-Rivières, Québec, QC, Canada

Amaryllidaceae alkaloids (AAs) are a large group of plant specialized metabolites with diverse pharmacological properties. Norbelladine is the entry compound in AAs biosynthesis and is produced from the condensation of tyramine and 3,4-dihydroxybenzaldehyde (3,4-DHBA). There are two reported enzymes capable of catalyzing this reaction *in-vitro*, both with low yield. The first one, norbelladine synthase (NBS), was shown to condense tyramine and 3,4-DHBA, while noroxomaritidine/norcraugsodine reductase (NR), catalyzes a reduction reaction to produce norbelladine. To clarify the mechanisms involved in this controversial step, both *NBS* and *NR* homologs were identified from the transcriptome of *Narcissus papyraceus* and *Leucojum aestivum*, cloned and expressed in *Escherichia coli*. Enzymatic assays performed with tyramine and 3,4-DHBA with each enzyme separately or combined, suggested that NBS and NR function together for the condensation of tyramine and 3,4-DHBA into norcraugsodine and further reduction into norbelladine. Using molecular homology modeling and docking studies, we predicted models for the binding of tyramine and 3,4-DHBA to NBS, and of the intermediate norcraugsodine to NR. Moreover, we show that NBS and NR physically interact in yeast and *in-planta*, that both localize to the cytoplasm and nucleus and are expressed at high levels in bulbs, confirming their colocalization and co-expression thus their ability to work together in the same catalytic route. Finally, their co-expression in yeast led to the production of norbelladine. In all, our study establishes that both NBS and NR participate in the biosynthesis of norbelladine by catalyzing the first key steps associated in the biosynthesis of the Alzheimer's drug galanthamine.

KEYWORDS

Amaryllidaceae alkaloids, Leucojum aestivum, Narcissus papyraceus, norbelladine synthase, noroxomaritidine/norcraugsodine reductase, enzyme activity

1 Introduction

Amaryllidaceae alkaloids (AAs) are a large group of plant specialized metabolites with large therapeutical potential. The greatest commercial success among AAs is galanthamine, produced by many *Narcissus, Galanthus* and *Leucojum* species, and presently used as an acetylcholinesterase inhibitor to fight Alzheimer's disease symptoms (Heinrich and Lee Teoh, 2004). Other AAs with strong antiviral activity, such as lycorine and cherylline, are intensively studied to fight emerging infectious diseases (Wang et al., 2014; Zhang et al., 2020; Ka et al., 2021). AAs have complex carbon skeletons and are challenging to chemically synthesize. Hence, they are often extracted directly from plants, limiting their broad usage due to the often low and variable quantity produced *in vivo*. Their massive extraction could lead to a loss in the biodiversity of the endogenous flora of some countries. One interesting alternative would be to heterologously biosynthesize them in host microorganisms, developing a sustainable platform of production, but this requires prior knowledge of the metabolic pathway. Unfortunately, much more is known about the pharmacology of AAs than about their biosynthesis. Few genes encoding biosynthetic enzymes are known and scarcely any of the accepted enzymatic reactions have been thoroughly characterized (Desgagné-Penix, 2021).

Despite their diverse chemical structures, AAs share norbelladine as a common biosynthetic origin (Figure 1).

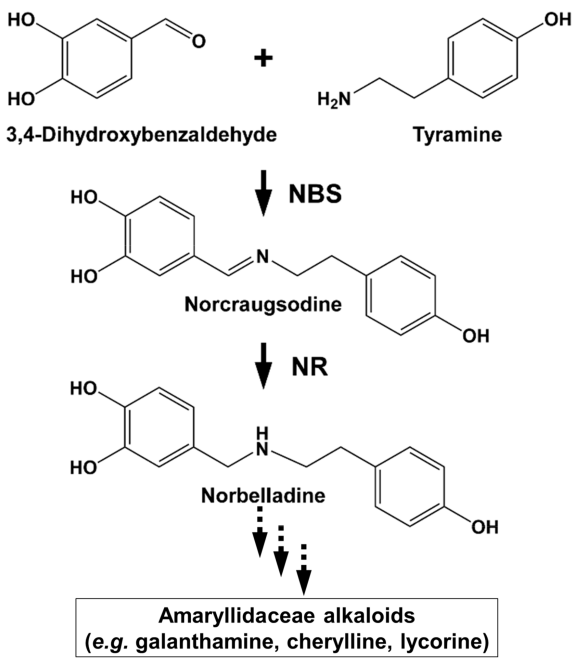

FIGURE 1
Norbelladine synthase (NBS) and noroxomaritidine/norcraugsodine reductase (NR) are involved in the proposed biosynthetic pathway for galanthamine, lycorine and haemanthamine. NBS catalyzes the condensation of tyramine and 3,4-dihydroxybenzaldehyde (3,4-DHBA) to form norcraugsodine while noroxomaritidine/norcraugsodine reductase (NR) reduces the latter to form norbelladine, the common precursor to all Amaryllidaceae alkaloids produced in plants including galanthamine, cherylline, and lycorine.

Following its synthesis, norbelladine undergoes several chemical modifications performed by a myriad of enzymes catalyzing various reactions, such as *O*- and *N*-methylations (OMTs, NMTs), C–C and C–O bond formation, oxidations and reductions, demethylations, and hydroxylations resulting in a array of different structural types of AAs (Eichhorn et al., 1998; El Tahchy et al., 2010; El Tahchy et al., 2011; Kilgore et al., 2014; Saliba et al., 2015; Kilgore et al., 2016a).

Previous studies have tried to unravel norbelladine biosynthesis because of its pivotal role in AAs biosynthesis. We and others identified several AA biosynthetic genes encoding enzymes involved in these early steps (Kilgore et al., 2014; Kilgore et al., 2016b; Singh and Desgagné-Penix, 2017; Singh et al., 2018; Hotchandani et al., 2019; Tousignant et al., 2022). Norbelladine originates from the condensation of tyramine and 3,4-dihydroxybenzaldehyde (3,4-DHBA), respectively derived from L-tyrosine and L-phenylalanine. The enzymes responsible for tyramine and 3,4-DHBA biosynthesis are well known and often found in most plant species (*e.g.*, tyrosine decarboxylase (TYDC), phenylalanine ammonia-lyase (PAL), cinnamate 4-hydroxylase (C4H), *etc.*). Nevertheless, it is uncertain which enzymes and intermediates specific to Amaryllidaceae are responsible for norbelladine synthesis. The currently accepted model states that the condensation of tyramine and 3,4-DHBA leads to the formation of the imine norcraugsodine, which is further reduced into norbelladine (Battersby et al., 1961). To date, there are two reported enzymes able to catalyze these reactions *in vitro*, but both perform poorly (Kilgore et al., 2016b; Singh et al., 2018). The first one is norbelladine synthase (NBS), recently characterized from two plant species *N. pseudonarcissus* (*Np*KANBS) and *L. aestivum* (*La*NBS). NBS was shown to condense tyramine and 3,4-DHBA to form low levels of norbelladine (Singh et al., 2018; Tousignant et al., 2022). The second one, noroxomaritidine/norcraugsodine reductase (NR) from *N. pseudonarcissus* (*Np*KANR) mainly catalyzes noroxomaritidine reduction, but also produces above background levels of norbelladine following incubation with tyramine, 3,4-DHBA and NADPH (Kilgore et al., 2016b). Therefore, the contribution of these two enzymes to norbelladine synthesis *in vivo* is still not clear.

We hypothesized that norbelladine is formed through two separate reactions (*i.e.*, condensation and reduction) catalyzed by two distinctive enzymes (Figure 1). In this study, we characterized the NBS and NR enzymes from two Amaryllidaceae plants species *N. papyraceus* and *L. aestivum* to try and elucidate the crucial reactions involved in norbelladine synthesis. We propose that for NBS or NR to induce norbelladine synthesis efficiently, the two-step mechanism requires the catalytic activity of both enzymes interacting together in a metabolon.

2 Materials and methods

2.1 Plant materials and growth condition

Paperwhite narcissus (*Narcissus papyraceus*) and summer snowflake (*Leucojum aestivum*) bulbs were purchased from

Vesey's (York, PE, Canada). Bulbs were planted in plastic pots using autoclaved AGRO MIX G6 potting soil (Fafard, Saint-Bonaventure, QC, Canada). The plants were kept at room temperature with exposure to tube lighting in long day (16 h of light/8 h of dark) conditions until flowering. The plants were watered when necessary to keep the soil moist. Different tissues such as bulbs, roots, stems, leaves, and flowers were collected, flash frozen in liquid nitrogen, and stored at −80°C until further used. *Nicotiana benthamiana* (Goodin et al., 2008) plants were grown in a growth chamber in long day (16 h of light/8 h of dark) conditions at 22°C.

2.2 Bacterial and yeast strains and growth conditions

The bacteria used in this study were *Escherichia coli* DH5α (Invitrogen), *E. coli* Rosetta (DE3) pLysS (Novagen), and *Agrobacterium tumefaciens* GV3101 (Holsters et al., 1980). The yeast strain (*Saccharomyces cerevisiae*) used is Y2HGold (Clontech Laboratories). The bacteria were grown in Luria-Bertani (LB) medium supplemented with the appropriate antibiotics at the following temperatures: *E. coli* at 37°C; and *A. tumefaciens* at 28°C. Antibiotics were used at the following concentrations (μg/mL): ampicillin, 100; chloramphenicol, 34; kanamycin, 50; rifampicin, 50; gentamicin, 30. Yeasts were grown at 30°C in selective synthetic complete medium.

2.3 PCR amplification, cloning, and construction of vectors

RNA was extracted from *N. papyraceus* (*Np*) and *L. aestivum* (*La*) bulbs using CTAB (cetrimonium bromide) method as described by Singh and Desgagné-Penix (2017). cDNA was synthesized from 1 μg RNA samples using SensiFAST cDNA synthesis kit (Bioline) according to manufacturer's protocol. The open reading frame (ORF) of full length *NpNBS*, *NpNR*, *NpTR*, *LaNBS*, *LaNR*, and *LaTR* were amplified from bulbs cDNA using PrimeStar GXL premix (TaKaRa Bio) in 50 μL reaction with 0.2 μM forward and reverse primers (Supplementary Table S2). PCR program parameters: 2 min 98°C 1 cycle, 10 s 98°C, 20 s 55°C, 1 min 72°C for 35 cycles, 5 min 72°C 1 cycle, and final infinite hold at 4°C. A classical restriction digestion based cloning approach was used to clone and create all the desired vectors.

For protein expression in *E. coli*, *NpNBS*, *NpNR*, *NpTR (tropinone reductase)*, *LaNBS*, *LaNR*, and *LaTR* were fused to the C-terminus of the maltose binding protein (MBP) in the pMAL-c2x vector (New England Biolabs). Precisely, the full-length ORFs were amplified from cDNA by PCR using primers reported (respective restriction enzyme sites are underlined, Supplementary Table S2). PCR products were cleaned using GenepHlow Gel/PCR kit (Geneaid). Purified PCR products of *NpNBS*, *NpNR*, *LaNBS*, and *LaNR* were digested with *Bam*HI and *Hin*dIII, while *NpTR* and *LaTR* were digested with *Bam*HI and *Sal*I and ligated into pMAL-c2x vector digested with *Bam*HI/*Hin*dIII and *Bam*HI/*Sal*I respectively, using T_4 DNA ligase (New England Biolabs). The recombinant plasmids were transformed into chemically competent *E. coli* DH5α cells by heat shock transformation and colonies were selected on ampicillin LB agar plates. The positive clones were identified by colony PCR in a 20 μL reaction using Taq DNA polymerase with ThermoPol buffer (New England Biolabs) with PCR parameters: 5 min 95°C 1 cycle, 30 s 95°C, 40 s 55°C, 1 min 68°C for 30 cycles, 5 min 68°C 1 cycle, and final infinite hold at 4°C. The resulting plasmids were verified by DNA sequencing to ensure the correct sequence and exclude undesired mutations.

For split luciferase complementation assays (SLCA) in *N. benthamiana* leaves, the *NpNBS*, *NpNR*, *NpTR*, *LaNBS*, *LaNR*, and *LaTR* genes were cloned into pCAMBIA1300:CLuc fused to the C-terminal (398-550 amino acids) of firefly luciferase (Cluc), and *NpNBS*, *NpNR*, *LaNBS*, and *LaNR* into pCAMBIA1300:Nluc fused to the N-terminal (2-416 amino acids) of firefly luciferase (Nluc) and driven by the CaMV 35S promoter (Chen et al., 2008). The full-length ORFs were amplified by PCR using reported primers from cDNA (respective restriction enzyme sites are underlined, Supplemental Table S2). After cleaning up using GenepHlow Gel/PCR kit (Geneaid), PCR products were digested with the mentioned restriction enzyme pair and ligated into the corresponding sites of pCAMBIA1300:Cluc or pCAMBIA1300:Nluc vectors using T_4 DNA ligase. The recombinant plasmids were transformed into chemically competent *E. coli* DH5α cells and colonies were selected on kanamycin LB agar plates. The positive clones were identified by colony PCR. The resulting binary vectors were verified by DNA sequencing.

For yeast two-hybrid assays, genes encoding full-length *NpNBS*, *NpNR*, *NpTR*, *LaNBS*, *LaNR*, and *LaTR* were amplified from *N. papyraceus* and *L. aestivum* bulbs cDNA and cloned into the pGBKT7 (bait) or pGADT7 (prey) vectors (Clontech Laboratories) in frame with the GAL4 DNA binding domain (DNA-BD) or GAL4 activation domain (AD). The full-length genes were amplified by PCR using primers reported (respective restriction enzyme sites are underlined, Supplemental Table S2). After cleaning up using GenepHlow Gel/PCR kit (Geneaid), PCR products were digested with the mentioned restriction enzyme pair and ligated into the corresponding sites of pGBKT7 (bait) or pGADT7 (prey) vectors using T_4 DNA ligase. The recombinant plasmids were transformed into chemically competent *E. coli* DH5α cells. Colonies with bait plasmids were selected on kanamycin while colonies with prey plasmids were selected with ampicillin LB agar plates. The positive clones were identified by colony PCR. The resulting plasmids were verified by DNA sequencing.

For subcellular localization, *NpNBS*, *NpNR*, *LaNBS*, and *LaNR* coding sequences were fused upstream to the gene encoding the yellow fluorescence protein (YFP) in the pBTEX binary vector under the control of the CaMV 35S promoter (Frederick et al., 1998). The full-length ORFs were amplified (respective restriction enzyme sites are underlined, Supplemental Table S2). The PCR products were cleaned up using GenepHlow Gel/PCR kit (Geneaid), digested with *Kpn*I/*Xba*I, and ligated into pBTEX-YFP vector digested with *Kpn*I/*Xba*I using T_4 DNA ligase. The recombinant plasmids were transformed into chemically competent *E. coli* DH5α cells and colonies were selected on kanamycin LB agar plates. The positive clones were identified by colony PCR. The resulting plasmids/binary vectors were verified by DNA sequencing.

2.4 Expression and purification of MBP fusion proteins in *E. coli*

NpNBS, *NpNR*, *NpTR*, *LaNBS*, *LaNR*, and *LaTR* were cloned into the pMAL-c2x vector. The purified plasmids were transformed using heat shock transformation into chemically competent *E. coli* Rosetta (DE3) pLysS strain for protein expression. Transformed cells were selected on LB plates with ampicillin, and chloramphenicol overnight at 37°C. The positive colonies were screened by colony PCR. A PCR positive single colony was picked and grown overnight at 37°C at 220 rpm in 12.5 mL LB broth containing ampicillin and chloramphenicol. The overnight grown pre-culture was added into fresh 250 mL LB broth containing ampicillin and chloramphenicol and grown at 220 rpm at 37°C to an OD_{600} = 0.5 to 0.6. The cultures were brought to room temperature and Isopropyl-β-D-thiogalactopyranoside (IPTG) was added to a final concentration of 0.25 mM to induce protein expression. The cultures were further incubated for 20 h at 18°C at 150 rpm. Bacterial cultures were pelleted at 10,000 rpm for 15 min at 4°C, resuspended in 25 mL column binding buffer (25 mM Tris-HCl [pH 7.5], 150 mM NaCl, and 1 mM EDTA) and frozen at −80°C overnight. The cultures were thawed on ice water and 1 mM phenylmethylsulfonyl fluoride [PMSF] with 0.1x protease inhibitor cocktail (Cell Signaling Technology) was added. Cultures were then lysed using a sonicator at 41% amplitude for a total of 8 min with 15 s run and 35 s cooling time in ice. The lysates were centrifuged twice at 14,000 rpm for 20 min at 4°C to pellet the cell debris and the clear supernatants were collected. Supernatants were mixed with 500 µL of amylose resin beads (New England Biolabs) (prewashed with column binding buffer and resuspended to 50% slurry) and incubated for 1 h at 4°C with constant rocking. The mixture was passed twice through the filter columns (Thermo Scientific) with gravitational flow to retain the beads with bound proteins in the column matrix. The beads were washed with gravitational flow in the columns three times with 30 mL column binding buffer. The bead slurry was transferred to microcentrifuge tubes and centrifuged at 1000 rpm for 1 min and the supernatant was removed. Finally, the bound proteins from the bead pellet were eluted twice (elution 1 and 2) each time in 500 µL elution buffer (15 mM maltose in column binding buffer) by centrifugation at 1000 rpm for 1 min and supernatant/elute was collected. The protein samples were flash frozen in liquid nitrogen and stored at −80°C. Protein quantification was done using DC protein assay kit (Bio-Rad) according to the manufacturer's instructions with bovine serum albumin (BSA) as standard, and protein samples were fractionated by 10% (v/v) SDS-PAGE and stained with Coomassie Blue.

2.5 Protein analysis and alignment

The *in-silico* protein analysis was done by DNAMAN analysis software (Lynnon BioSoft). Protein sequences of *Np*NBS, and *La*NBS were aligned with *Narcissus pseudonarcissus* 'King Alfred' norbelladine synthase (*NpKA*NBS; GenBank: AYV96792.1), and *Thalictrum flavum* norcoclaurine synthase (*Tf*NCS; GenBank: ACO90248.1). Similarly, *Np*NR, *La*NR, *Np*TR and *La*TR were aligned with *N. pseudonarcissus* noroxomaritidine/norcraugsodine reductase (*NpKA*NR; KU295569) using CLUSTAL W algorithm in T-Coffee software (Notredame et al., 2000) with default parameters. Sequence alignments were formatted using Boxshade program (https://embnet.vital-it.ch/software/BOX_form.html).

2.6 Molecular homology modelling and docking

Amino acid sequences corresponding to *Np*NBS, *La*NBS, *Np*NR, *La*NR, *Np*TR, *La*TR candidates were uploaded on Protein Homology/analogY Recognition Engine V 2.0 (Phyre2) (Kelley et al., 2015) website, I-Tasser from Zhang lab (Yang and Zhang, 2015) and MOE 2020.09 software (Chemical Computing Group) to model NBS and NR proteins. Following close analysis of predicted structures and comparison by superimposition with orthologs and homologs, the most consistent models were selected. *La*NR from I-Tasser, *Np*NR and *La* and *Np*TR models from Phyre2 were used, while NBS were best modeled by MOE. MOE was further used to analyze the resulting homology model conformation and prepare receptors for docking. First, modeled structures were compared to their template crystal structures in complex with their ligands downloaded from the Protein Data Bank (for NBS: norcoclaurine synthase from *Thalictrum flavum* in complex with dopamine and hydroxybenzaldehyde 2VQ5 (Ilari et al., 2009), NR: noroxomaritidine/norcraugsodine reductase in complex with NADP+ and tyramine 5FF9 *NpKA*NR (Kilgore et al., 2016b), TR: Tropinone reductase-II complexed with NADP+ and pseudotropine 2AE2 and 5FF9 (Yamashita et al., 1999), aligning amino-acid sequences and then superimposing the structures.

Structure preparation consisted of correcting issues, capping, charging termini, selecting appropriate alternate, and calculate optimal hydrogen position and charges using Protonate 3D. Fixed receptor and tethered active site energy minimization was performed for each modeled protein in presence of template ligands prior to docking. Ready to dock ligands were uploaded from ZINC15 (Sterling and Irwin, 2015) when available, or manually drawn (from SMILES), washed, prepared, and minimized with MOE. The MMFF94× force field was used. Receptors active site was predicted using MOE Site Finder and used as docking site to place ligand using Triangle Matcher as placement method for 200 poses and tethered induced fit as refinement to perform flexible docking. Ten resulting poses were analyzed. The most probable poses based on literature description of templates active site, on comparison with crystalized templates interactions and on scores are presented. For NBS, 3,4-DHBA was docked first, the most consistent pose was further included in the active site used for tyramine docking. Similarly for NR, NADPH was docked first, and the most consistent pose compared to template crystals was further included in the active site used to dock norcraugsodine. PLIP was used to analyze interactions between ligands and receptors (Adasme et al., 2021), and were further processed using PyMOL (Shrödinger).

2.7 Substrates and standards preparation

Norbelladine and norcraugsodine were synthesized as previously described (Singh et al., 2018). Standard solutions of 3,4-DHBA (Fisher Scientific), tyramine (Sigma-Aldrich), and papaverine (Sigma-Aldrich) were prepared at 1000 mg/L in LC-MS grade methanol (Sigma-Aldrich). Standard solutions of norbelladine and norcraugsodine were prepared as previously described (Singh et al., 2018). From these standard solutions, dilutions were performed to obtain working solutions of 100 mg/L in methanol, and 1 mg/L in the mobile phase (ammonium acetate 10 mM (Sigma-Aldrich) (pH 5.0), and acetonitrile (Sigma-Aldrich) [60:40]). Standards and solutions were stored in the dark at −20°C.

2.8 Enzymatic assays

Single enzyme assays were performed at 35°C for 2 h. All the enzymatic reactions were terminated by the addition of 10 µL of 20% trichloroacetic acid (TCA). Negative controls were purified MBP-tag protein from *E. coli*, and reactions without substrate or cofactor. The catalytic activity of purified NBS enzymes were analyzed following the method of Singh et al., 2018 with minor modifications. Reactions were conducted using 80 µg of purified proteins in 100 mM HEPES buffer (pH 6.0), with 10 µM tyramine and 300 µM 3,4-DHBA, in a total volume of 100 µL. Reaction components were equilibrated at 35°C and the reaction was started by the addition of enzyme to the substrate and buffer mixture. NR and TR single enzyme assays were performed as previously reported by Kilgore et al., (2016b) with minor modifications. The assay mix contained 60 µg of purified proteins, 10 µM tyramine, 300 µM 3,4-DHBA, and 1 mM NADPH in 100mM sodium citrate buffer (pH 6.0), in a total volume of 100 µL. The assays with NBS and NR or TR together in a single-step reaction contained 80 µg of purified NBS enzyme, 60 µg of purified NR/TR enzyme, 10 µM tyramine, 300 µM 3,4-DHBA, and 1 mM NADPH in 100mM HEPES buffer (pH 6.0), in a total volume of 100 µL. The assays with NBS and NR/TR in two-step reactions were conducted as follows: 80 µg of purified NBS enzyme in 100 mM HEPES buffer (pH 6.0), with 10 µM tyramine and 300 µM 3,4-DHBA, in a total volume of 100 µL was incubated at 35°C for 2 h. The NBS enzyme was inactivated by boiling at 95°C for 10 min, sample was centrifuged, and the supernatant (100 µL) was used as norcraugsodine solution, and 60 µg of purified NR/TR enzyme and 1 mM NADPH were added and incubated for additional 2 h. Following the reaction termination, papaverine (1000 mg/L) was added to all the reaction serving as an internal standard for the relative quantification of detected compounds. All reactions were performed in triplicates. The reaction samples were diluted 100 fold with mobile phase (ammonium acetate 10 mM [pH 5.0], and acetonitrile [60:40]) and analysis of the enzymatic product (norbelladine) using a high-performance liquid chromatography (HPLC) system coupled with a tandem mass spectrometer (MS/MS) was carried out as described by (Tousignant et al., 2022).

2.9 Derivatization of norcraugsodine and GC-MS analysis

Norcraugsodine (257 m/z) could not be detected by GC-MS without derivatization. For the derivatization, dry enzymatic assay samples were reconstituted in 300 µL HPLC grade acetonitrile and were transferred quantitatively in crimp-seal autosampler vials, without capping the vials. A 150 µL aliquot of BSTFA (with 1% TMCS) was added to each sample along with a magnetic stir bar, then the vials were capped using crimpers. The samples were stirred at room temperature for 60 minutes. For the GC-MS analysis, the derivatized samples were injected into the GC-MS (Agilent Technologies 6890N GC coupled with 5973N inert MSD) in electron ionization mode at 70 eV. The temperature ramp used is described as follows: temperature was set at 100°C for 2 min, followed by 100–180°C at 15°C min^{-1}, 180–300°C at 5°C min^{-1}, and a 10 min hold at 300°C. Injector and detector temperatures were set at 250°C and 280°C, respectively, and the flow rate of carrier gas (He) was 1 mL min^{-1}. A split ratio of 1:10 was applied, and the injection volume was 1 µL. The presence of norcraugsodine in the tested samples was determined by comparison with the GC-MS analysis of a norcraugsodine standard derivatized following the same protocol. Tris-derivatized norcraugsodine (473 m/z) was observed at a retention time of 24.79 minutes and showed characteristic fragment ions (458 m/z and 294 m/z) that we respectively attributed to the loss of a methyl radical and to the loss of a 4-((trimethylsilyl)oxy)benzyl radical. The corresponding bis-derivatized aldehyde (282 m/z) was observed at a retention time of 9.28 minutes and showed characteristic fragment ions (267 m/z and 193 m/z) that we respectively attributed to the loss of a methyl radical and to the loss of a (trimethylsilyl)oxy radical.

2.10 *Agrobacterium*-mediated transient expression

The YFP- and LUC-fusion binary vectors were transformed into *A. tumefaciens* strain GV3101 by electroporation and colonies were selected on LB agar plates with rifampicin, kanamycin, and gentamicin at 28°C. The positive colonies were confirmed by colony PCR using PCR parameters: 10 min 95°C 1 cycle, 30 s 95°C, 40 s 55°C, 1 min 68°C for 30 cycles, 5 min 68°C 1 cycle, and a final infinite hold at 4°C. For transient expression, cultures of *A. tumefaciens* were grown overnight in 5 mL LB broth with rifampicin, kanamycin, and gentamicin at 28°C. The cultures were pelleted at 8000 rpm for 5 minutes at room temperature, washed three times with 10 mM $MgCl_2$, resuspended in 5 mL of induction medium (10 mM $MgCl_2$, 10 mM MES [pH 5.6], and 200 µM acetosyringone), and incubated at 28°C with shaking at 200 rpm for 3–4 h. *A. tumefaciens* cultures were diluted in the induction media to OD_{600} = 0.25 and infiltrated into young but fully expanded leaves of five-week-*old N. benthamiana* plants using a 1 mL needleless syringe. After agroinfiltration the plants were incubated in a growth chamber in long day (16 h of light/8 h of dark) conditions at 22°C for 48 h until leaf discs were harvested.

2.11 Split luciferase complementation assay

NpNBS, *NpNR*, *NpTR*, *LaNBS*, *LaNR*, and *LaTR* genes were cloned in frame to firefly luciferase fragments in the binary vector pCAMBIA1300:NLuc or pCAMBIA1300:CLuc. The obtained binary vectors were transformed into *A. tumefaciens*. The desired NLuc- and CLuc-fusion *A. tumefaciens* combinations were mixed at 1:1 ratio (OD_{600} = 0.25) and co-expressed in *N. benthamiana* leaves. Split luciferase complementation assays were performed as described by (Chen et al., 2008) with minor modifications. Three millimeter-diameter leaf discs were harvested 48 h after agroinfiltration and floated abaxial side up in 100 µL of degassed water on a white 96-well plate. Samples were supplemented with 1 mM D-luciferin (Sigma-Aldrich) and incubated in the dark for 2 min with gentle shaking and an additional 8 min at rest to quench fluorescence. Luminescence was measured using a Synergy H1 Microplate reader (BioTek) with integration time set to 2 s and imaged using a Gel Doc XR system (Bio-Rad).

2.12 Yeast two-hybrid analysis

NpNBS, *NpNR*, *NpTR*, *LaNBS*, *LaNR*, and *LaTR* genes were either fused to the GAL4 DNA binding domain (DNA-BD) in the bait vector pGBKT7 or were fused to the GAL4 activation domain (AD) in the prey vector pGADT7 (Clontech Laboratories). The yeast strain Y2H Gold (Clontech Laboratories) was first transformed with the bait vectors (*i.e.*, *NBS*, *NR*, and *TR* in the pGBKT7 vector) and subsequently with prey vectors (*i.e.*, *NBS*, *NR*, and *TR* in the pGADT7 vector). The transformants were selected on synthetically defined (SD) medium lacking leucine and tryptophan (SD-LW). The interactions were verified by testing the activation of the *HIS3*, *ADE2* and *AUR1-C* reporter genes on selective media plates lacking histidine and adenine (SD-LWHA) or containing the antibiotic Aureobasidin A (AbA), respectively.

2.13 Expression of NBS and NR in yeast

NpNBS was amplified and digested with *Bam*HI and *Hin*dIII and ligated into a similarly digested pESC-LEU vector (Stratagene) to produce pESC-LEU : *NpNBS*. Similarly, *NpNR* and *NpTR* were amplified and digested with *Bam*HI/*Hin*dIII and *Bam*HI/*Sal*I and ligated into a similarly digested pESC-LEU vector to produce pESC-LEU : *NpNR* and pESC-LEU : *NpTR*, respectively. To produce pESC-LEU : *NpNBS-NpNR*, the *NpNR* ORF was ligated into pESC-LEU : *NpNBS* plasmid vector digested with *Spe*I/*Bgl*II, with NBS expressed under control of the Gal1 promoter and NR under the Gal10 promoter. Yeast (INVSc1; Invitrogen) was transformed with all the above constructs and selected on SD-LEU plate for 3 d at 28° C. A single colony was used to inoculate 3 mL of SD-LEU glucose medium and incubated with shaking at 28°C for 2 d. A 500-µL aliquot of starter culture was then used to inoculate to 10 mL of SD-LEU galactose medium containing 250 µM tyramine and 250 µM 3,4-DHBA and incubated with shaking at 28°C for 3 d. A culture lacking substrates was used as a control. The cultures were centrifuged, the medium and cell pellet were extracted with 5 mL ethyl acetate, and the extracts were dissolved in mobile phase (100 µL) of (ammonium acetate 10 mM [pH 5.0], and acetonitrile [60:40]). Papaverine (1000 mg/L) was added to all the reaction as an internal standard for the relative quantification. The analysis of the product (norbelladine) was done using a high-performance liquid chromatography (HPLC) system coupled to a tandem mass spectrometer (MS/MS) as described by (Tousignant et al., 2022).

2.14 Protein extraction

For protein extraction from *N. benthamiana* leaves, five leaf discs (1 cm diameter) were frozen in liquid nitrogen, homogenized in 300 µL extraction buffer (100 mM Tris [pH 7.5], 1% [v/v] Triton X-100, 1 mM PMSF, and 0.1x protease inhibitor cocktail), and centrifuged at 17,000 g for 30 min at 4°C. The clear supernatant was collected, and protein concentration was determined using DC protein assay kit (Bio-Rad) according to the manufacturer's instructions.

For protein extraction from yeast, 5 mL overnight-grown cultures were pelleted at 12,000 g for 5 min at 4°C, resuspended in 250 µL ice-cold lysis buffer (4% [v/v] 5 N NaOH and 0.5% [v/v] β-mercaptoethanol), and incubated with 1x SDS sample buffer (30% [v/v] glycerol, 15% [v/v] β-mercaptoethanol, 37.5% [v/v] 500 mM Tris-HCl [pH 6.8], 0.15% [w/v] SDS, and a few grains of Bromophenol Blue) for 10 min at 95°C.

2.15 Western blotting

Equal amounts of protein (100 µg) were fractionated by 10% (v/v) SDS-PAGE. Proteins from gels were transferred onto Polyvinylidene difluoride (PVDF) membrane using Trans-Blot Turbo transfer system (Bio-Rad). The membrane was equilibrated with Tris-buffered saline (TBS) buffer (20 mM Tris, 150 mM NaCl pH 7.6) for 15 min, followed by blocking of membrane for 2 h with TBS buffer containing 0.1% tween 20 (TBST), and 5% skim milk. The PVDF membrane was incubated overnight at 4°C in TBST with 5% milk containing 1:1000 dilution of specific primary antibodies. The primary antibodies used in this study are rabbit anti full-length firefly luciferase antibodies (Sigma-Aldrich), which react with both the N-terminal and C-terminal firefly LUC fragments, mouse anti-GFP/CFP/YFP monoclonal antibody (Cedarlane labs), mouse anti-Myc/c-Myc monoclonal antibody (Santa Cruz Biotechnology), and mouse anti-HA-tag monoclonal antibody (GenScript). After primary antibody incubation, the membrane was washed three times each for 5 min in TBST buffer and incubated for 30 min in TBST containing 5% skim milk and goat anti-rabbit horseradish peroxidase (GAR)-HRP or goat anti-mouse horseradish peroxidase (GAM)-HRP conjugate in 1:10,000 dilutions. The immunoblot was washed three times for 5 min each in TBST buffer and developed using clarity Western ECL substrate (Bio-Rad). Finally, the membrane was washed twice with TBST and stained with Ponceau S stain [0.5% (w/v)

Ponceau S (Sigma-Aldrich) in 1% (v/v) acetic acid] for 1 min and photographed using Gel Doc XR system (Bio-Rad).

2.16 Subcellular localization

To visualize *Np*NBS, *Np*NR, *La*NBS, and *La*NR subcellular localization, the YFP fusion proteins were expressed via *A. tumefaciens* in leaves of 5-week-old *N. benthamiana* plants. Forty-eight hours post infiltration, the abaxial epidermis of leaf discs were placed on a microscopic slide in a water drop, covered by a cover slip, and imaged immediately. Protein localization was visualized by a confocal laser scanning microscope (Leica TCS SP8; Leica Microsystems) with a 40X/1.30 oil immersion objective. Images were first processed with Las AF Lite software (Leica Microsystems). CFP was used as a control for colocalization (Kruse et al., 2010). YFP was excited with an argon laser at 488 nm, while CFP was excited with a diode laser at 405 nm. Emission was detected with a spectral detector set between 500 and 525 nm for YFP and between 420 and 490 nm for CFP. Chlorophyll autofluorescence was observed with an excitation wavelength of 552 nm and the emission of fluorescence signals were detected from 630 to 670 nm. The combined images were generated using the Las X software (Leica Microsystems).

2.17 RNA extraction and Real-time quantitative PCR

Total RNA was isolated from bulbs, roots, stems, leaves, and flowers using the TRIzol reagent (Invitrogen). Briefly, 100 mg of tissues were frozen in liquid nitrogen, fully ground, and homogenized in 1 mL of TRIzol using a mortar and pestle. The liquid was transferred to a microcentrifuge tube, incubated 5 min at room temperature and extracted with 200 µL chloroform. Following centrifugation at 12,000 g for 15 min at 4°C, the upper phase containing RNA was transferred to a fresh tube. The RNA was precipitated with 500 µL of isopropanol for 10 min at room temperature and centrifuged at 12,000 g for 10 min at 4°C. The RNA pellet was washed twice with 1 mL of 75% ethanol (with DEPC water) and centrifuged at 7500g for 5 min at 4°C. Finally, the RNA pellet was air dried and suspended in 40 µL of DEPC-treated water. The quality and quantity of RNA extracted from different tissues were verified on NanoPhotometer (Implen) and 1.5% (w/v) agarose gel electrophoresis. RNA samples (1 µg) were reverse transcribed using SensiFAST cDNA synthesis kit (Bioline) according to manufacturer's protocol and subjected to Real-time quantitative PCR (RT-qPCR) using gene-specific primers (Supplementary Table S2). The experiments were performed in triple technical replicates of each plant sample. A total reaction volume of 20 µL containing 1x SensiFAST SYBR Lo-ROX mix (Bioline), 200 µM of each forward and reverse primer, and 2 µL of template cDNA (50 ng/µL) was used for RT-qPCR analysis. RT-qPCR was performed on CFX Connect Real-Time PCR System (Bio-Rad). Amplification conditions were 95°C for 3 min 1 cycle, 95°C for 10 s, and 60°C for 30 s for 40 cycles followed by dissociation step 95°C for 10 s, 65°C for 5 s and 95°C for 5 s. *LaGAPDH* and *NpHISTONE* were used as internal reference genes for *La* and *Np*, respectively. To verify the specificity of the primers, a melting-curve analysis was also performed. The threshold cycle (C_T) value of each gene was normalized against the C_T value of the reference genes. Mean C_T values calculated from the technical triplicates were used for quantification of relative gene expression involving the comparative C_T method (Pfaffl, 2001). The results were analyzed, and the statistical error was calculated using CFX Maestro software (Bio-Rad).

2.18 Accession numbers

Sequence data from this article can be found in GenBank under the following accession numbers: *N. papyraceus* norbelladine synthase (*NpNBS*; MZ054104), *N. papyraceus* noroxomaritidine/norcraugsodine reductase (*NpNR*; MF979872), *N. papyraceus* histone (*NpHistone*; MF979875), *L. aestivum* norbelladine synthase (*LaNBS*; MW971977), *L. aestivum* noroxomaritidine/norcraugsodine reductase (*LaNR*; MW971981), *L. aestivum* glyceraldehyde-3-phosphate dehydrogenase (*LaGAPDH*; MW971984), *Narcissus pseudonarcissus* 'King Alfred' norbelladine synthase (*NpKANBS*; AYV96792), *N. pseudonarcissus* noroxomaritidine/norcraugsodine reductase (*NpKANR*; KU295569).

3 Results

3.1 Identification and structure analysis of NBS homologs from *N. papyraceus* and *L. aestivum*

The full-length cDNAs of *NpNBS*, *LaNBS*, *NpNR*, and *LaNR* candidate genes were obtained from previously reported transcriptome sequencing of *N. papyraceus* and *L. aestivum* (Hotchandani et al., 2019; Tousignant et al., 2022). The open reading frame (ORF) of both *NpNBS* and *LaNBS* gene is 480 bp and encodes a 159-amino acid protein (Figure S1). *In silico* protein analysis by DNAMAN analysis software indicated that *Np*NBS and *La*NBS candidates had a predicted molecular weight (MW) of 17.4 kDa and a theoretical isoelectric point (pI) of 5.3 and 5.1, respectively. Multiple amino acid sequence alignments of *Np*NBS and *La*NBS candidates with the already characterized protein *NpKA*NBS (Singh et al., 2018) and norcoclaurine synthase from *T. flavum* (*Tf*NCS) (Ilari et al., 2009) showed that *Np*NBS and *La*NBS share over 41% of amino acids sequence identity with the ortholog *Tf*NCS (Figure S1). In addition, *NpKA*NBS, *Np*NBS and *La*NBS share 83% identity between each other, while *Np*NBS and *La*NBS share 85% of identity (Figure S1). Domain search using *NCBI-conserved-domain-search service* revealed the presence of conserved Bet v1 and Pathogenesis-Related (PR-10) protein domains in both *Np*NBS and *La*NBS homologs. Both contained the phosphate-binding loop (P-loop) glycine-rich region (Figure S1), a conserved ligand-binding domain of Bet v1 protein family

(Fernandes et al., 2013). As reported previously, the alignment showed that *Tf*NCS catalytic residues Tyr108, Glu110 and Lys122 are well-conserved in *Np*NBS and *La*NBS, corresponding to Tyr68, Glu71, and Lys83, respectively, in their sequences (Figure S1) (Ilari et al., 2009; Singh et al., 2018). The fourth catalytic residue Asp141 from *Tf*NCS is replaced by hydrophobic Ile102 in both *Np*NBS and *La*NBS, as reported previously for *NpKA*NBS (Singh et al., 2018). Homology modeling of the enzymes from both *N. papyraceus* (*Np*) and *L. aestivum* (*La*) revealed a striking structure similarity with superimposed template crystal of *Tf*NCS, analogous to the overall structure of Bet v1-like proteins family (Figures 2A; S2A; S3A-D). As *Tf*NCS, both NBS homologs are composed by seven-stranded antiparallel β-sheets, two long C- and N-terminal helices and two short ones, enclosing a cleft with polar residues at its entrance and hydrophobic residues in its core (Figures 2A, B; S2A, B).

3.2 Identification and structure analysis of NR homologs from *N. papyraceus* and *L. aestivum*

The ORF of *NpNR* and *LaNR* candidate genes is 810 bp, both encoding a 269-amino acid protein (Figure S4). *Np*NR and *La*NR homologs have a predicted molecular weight (MW) of 29 kDa and theoretical pI of 6.0 and 5.4 respectively. Sequence comparison and domain search confirmed the presence of conserved short-chain dehydrogenases/reductases (SDR) domain in *Np*NR and *La*NR candidates. *NpKA*NR, *Np*NR and *La*NR candidates share over 76% of identity with each other, while *Np*NR and *La*NR share 90% of identity (Figure S4). Like all classical SDRs, *Np*NR and *La*NR contain a TGXXX[AG]XG cofactor binding motif and a YXXXK active site motif, with the Tyr and Lys of the active site serving as critical catalytic residues (Figure S4). Structurally, predicted models of NRs from both species are formed by a seven-stranded parallel β-sheet inserted between a pair of three α-helices (Figures 2C; S2C). A long tunnel is shaped at the C-termini of β-strands partially wrapped by the α-helices and loops that elevate beyond the β-sheets (Figures 2C, D; S2C, D). At the site of ligand interaction, the tunnel expands into a larger pocket where aromatic Phe214 (216 in *NpKa*NR) is conserved, Ala112 replaces Tyr114, both possibly involved in polycyclic substrate orientation and binding. At the extremity, Glu224 (226), Arg265 (267), Cys162 (164), His170 (172) are preserved. A strong similarity in structure of both *Np*NR and *La*NR homologs with *N. pseudonarcissus* noroxomaritidine/norcraugsodine reductase (*NpKA*NR, 5FF9) was noted (Figures S5A-D).

To identify other reductases that could catalyze similar reduction reactions, we searched for homologs of NR in the transcriptome sequences of *N. papyraceus* (Hotchandani et al., 2019) and *L. aestivum* (Tousignant et al., 2022), and identified a candidate tropinone reductase (TR) belonging to the same SDR superfamily in both species. The ORF of the *NpTR* homolog is 825 bp and encodes a 274-amino acid protein while the *LaTR* is 816 bp and encodes a 271-amino acid protein (Figure S4). *Np*TR and *La*TR candidates have a predicted molecular weight (MW) of 30 kDa and 29.5 kDa and theoretical pI of 6.9 and 8.4 respectively. *Np*TR and *La*TR contain the TGXXX[AG]XG cofactor binding motif and the YXXXK catalytic active site motif (Figure S4). Gly206 is replaced by a tryptophan at position 203 and 200 in *Np*TR and *La*TR respectively, although this residue was conserved in active SDR/tropinone reductases (Roth et al., 2018). Multiple sequence alignments showed that *NpKA*NR, *Np*NR, *La*NR, *Np*TR, and *La*TR share over 58% of identity between each other. Predicted TRs structures are similar to NRs with some key differences in the ligand active site, including replacement of Phe216 from *NpKA*NR by Arg213 in *Np*TR and by Leu210 in *La*TR, while Tyr114 is replaced by Asn111 in *Np*TR and Asn108 in *La*TR (Figures 2E, F; S2E, F; S6; Table S1).

3.3 Predicted interactions of ligands with NBS and NR

To shed light on the reactions involved in norbelladine synthesis (Figure 1), we studied the interaction of NBS and NR candidates with their respective proposed ligands through molecular docking analysis *in silico*. Tyramine and 3,4-DHBA were docked with scores of -5.03 and -5.23 kCal/mol inside the NBS pocket respectively (Figures 3; S7; Table S1). Most of the obtained poses displayed the same ligand orientations where 3,4-DHBA and tyramine adopted a stack configuration with their aromatic rings lying on near-to-parallel planes, similarly to dopamine and hydroxybenzaldehyde in crystalized *Tf*NCS (2VQ5) (Figures 3A, B; S7A, B). The carbonyl group of 3,4-DHBA faced the amine group of tyramine. Lys83, whose proposed role is to intercept the carbonyl group of the aldehyde substrate, interacted with 3,4-DHBA carbonyl end through hydrogen bonding (Figure 3B; Table S1). At the other end, the hydroxyl group of C4 was hydrogen-bonded with the possibly base-acting residue Glu71. All predicted poses implied interaction with Glu71 and Lys83 strengthening the probability of their key role in the catalytic mechanism. Tyramine was hold in place by stacking interaction, and hydrogen bonding between its amine and 3,4-DHBA carbonyl group. PLIP software (Adasme et al., 2021) predicted additional hydrophobic interactions between Phe73, Thr85, Phe104 and Ile143, and 3,4-DHBA, as well as two hydrogen bonds between tyramine and Ser31 and Tyr59 (Figures 3B; S7B; Table S1). In general, these predicted interactions and spatial arrangements of the ligands inside NBS are consistent with the reaction proposed by Ilari et al., 2009 that would lead to norcraugsodine biosynthesis.

Following its formation, norcraugsodine would be transferred from NBS to NR active site to be reduced into norbelladine (Figure 1) with NADPH as the electron donor. Upon docking, NADPH positioned into *La*NR and *Np*NR modeled active site following a similar arrangement compared to crystalized reductases such as 5FF9 (*NpKA*NR) with a score of -11.51 kCal/mol (Figures 3C, D; S7C, D; Table S1). It interacted with Gly36, Cys53, Arg55, Val109, Ile35, His170, Thr111, Lys177, Asn108, Thr206. PLIP confirmed these interacting residues and additionally predicted hydrophobic interaction with Ile35, hydrogen bonding with Lys33, Cys79, Gly110, Thr208, Val209

10.3389/fpls.2023.1231809

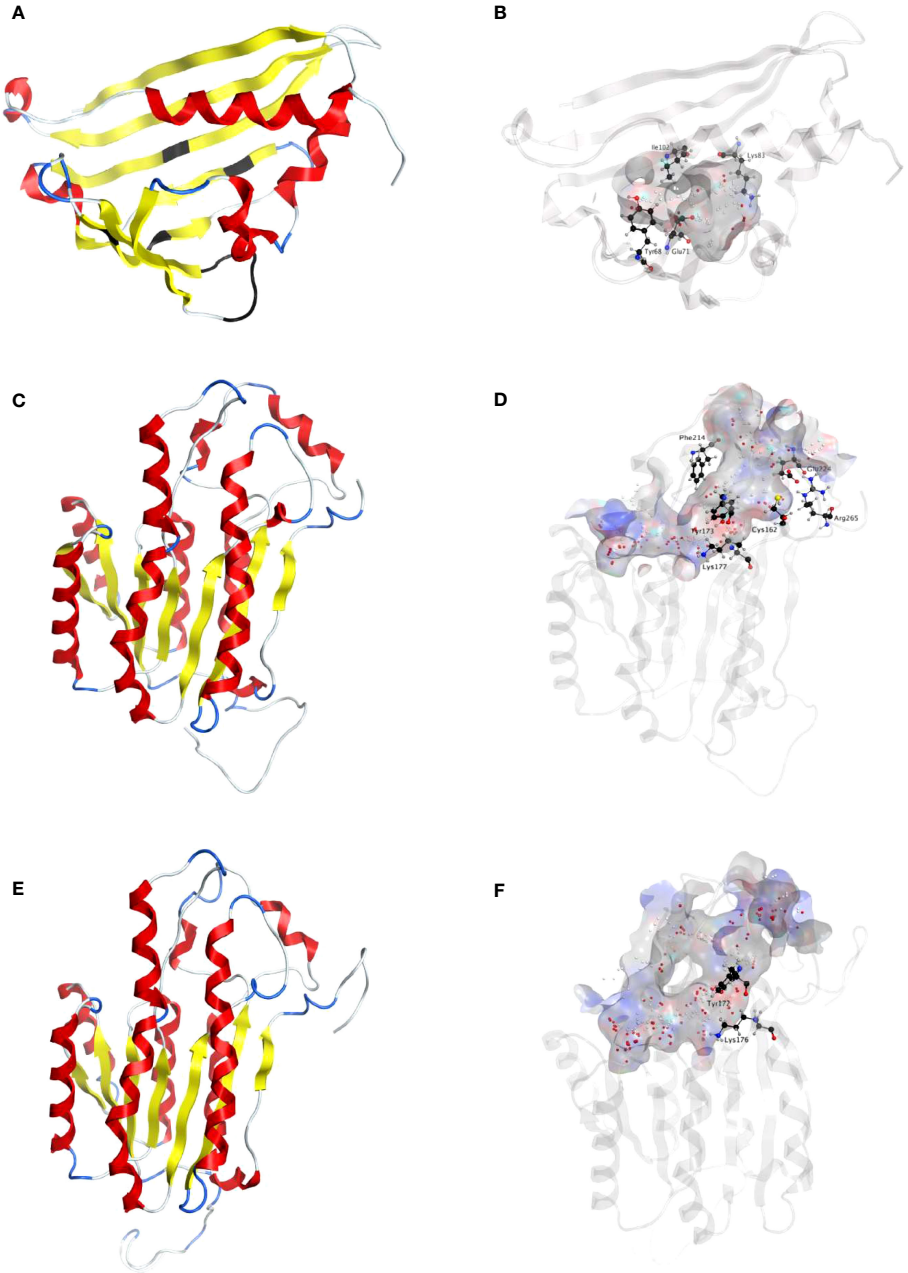

FIGURE 2
Homology modeling of *Np*NBS, NR and TR. **(A)** Ribbon representation of *Np*NBS with colored secondary structures. β-sheets are displayed yellow, α-helices red, and loops blue. Conserved glycine rich P-loop of PR10-/Betv1 enzymes is shown black, as are conserved active site residues of norcoclaurine synthase Tyr68 (Tyr108 from *Tf*NCS), Glu71 (Glu111), Lys83 (Lys123). As *Tf*NCS, NBS are composed by seven-stranded antiparallel β-sheets, two long C- and N-terminal helices and two short ones, enclosing a cleft with polar residues at its entrance and hydrophobic residues in its core. **(B)** Transparent ribbon representation of *Np*NBS with predicted active site pocket in transparent surface. The predicted ligand site computed by the Site Finder tool of MOE software is displayed as white and red alpha sphere centers inside the pocket. *Np*NBS cavities is predicted to contain an active site of 27 residues, surrounded by catalytic Tyr68, Glu71, Lys83 and Ile102 (shown as black sticks), with Tyr68 at its entrance, Lys83 at the other side and the P-loop at the bottom. **(C)** Ribbon representation of *Np*NR with highlighted secondary structures. β-sheets are displayed yellow, α-helices red and loops in blue. **(D)** Cartoon ribbon representation of *Np*NR with transparent surface view of the predicted active site forming a catalytic tunnel that crosses the enzyme. The predicted ligand site is displayed as white and red alpha sphere centers inside the pocket. *Np*NR tunnel active site is predicted to contain 55 residues. Conserved active site residues Cys162, Tyr173, Lys177, Phe214, Glu224, Arg265 surrounding the tunnel are shown as black sticks. In general, amino acids involved in NADPH binding by noroxomaritidine/norcraugsodine reductase (*NpK*ANR, 5FF9) are conserved and similarly oriented, *i.e.*, Val81 (Val83 for *NpK*ANR); Asp80 (82), Arg55 (57), Ser54 (56), Thr32 (34), catalytic residue Tyr173 (175), catalytic residue Lys177 (179), Asn108 (110); Thr208 (210), Pro203 (205), Gly204 (206) and Ala205 (207). **(E)** Ribbon representation of *Np*TR with secondary structures. β-strands are displayed yellow, α-helices red, and loops blue. **(F)** Ribbon representation of *Np*TR with transparent surface view of predicted active site tunnel crossing the enzyme. Predicted ligand site is displayed as white and red alpha sphere centers. Conserved catalytic Tyr172 and Lys176 are shown as black sticks.

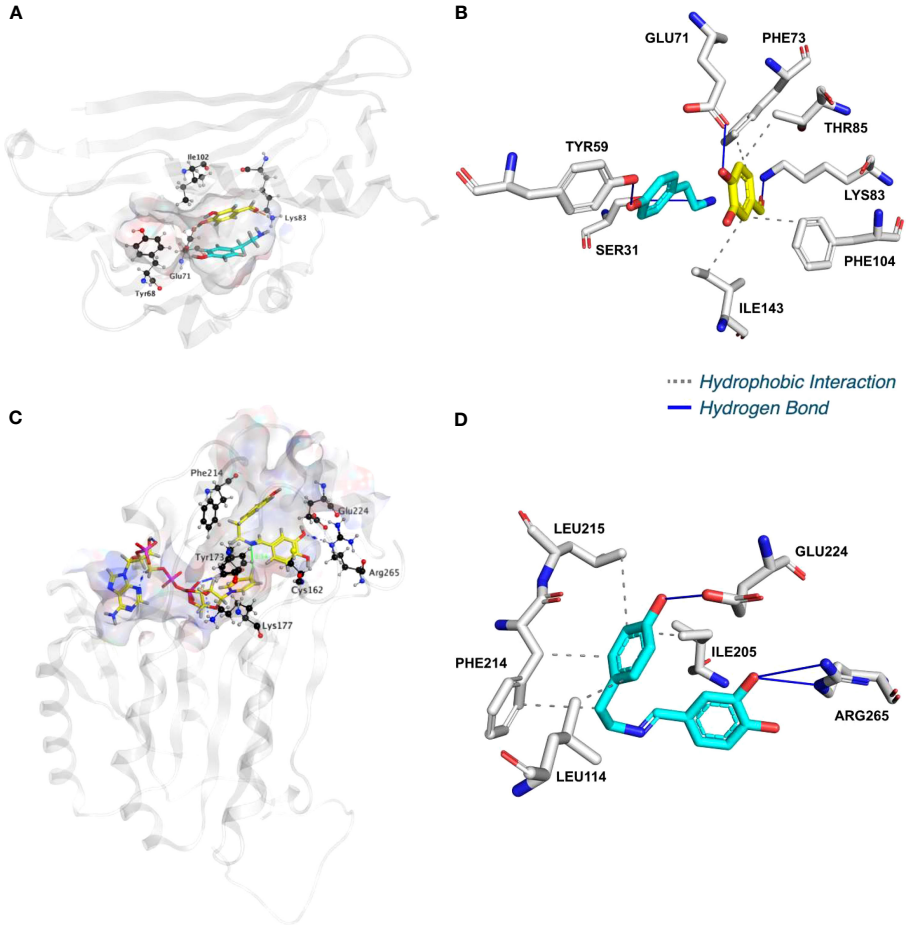

FIGURE 3
*Np*NBS docked with 3,4-dihydroxybenzaldehyde (3,4-DHBA) and tyramine. **(A)** Cartoon representation of *Np*NBS with transparent surface-active site pocket docked with 3,4-DHBA (up) and tyramine (down). Conserved catalytic residues Tyr68 (Tyr108 from *Tf*NCS), Glu71 (Glu110), Lys83 (Lys122) and Ile102 (instead of Asp141) shaping the binding site are shown as black sticks. **(B)** PLIP predicted conformation of interacting residues of *Np*NBS (grey) docked with 3,4-DHBA (turquoise) and tyramine (yellow). **(C)** *Np*NR docked with NADPH and norcraugsodine. Ligands NADPH (left) and norcraugsodine (right) are represented as thick yellow sticks. Conserved active site residues Cys162, Tyr173, Lys177, Phe214, Glu224 and Arg265) shaping the binding site are shown as thin black sticks. **(D)** PLIP predicted interacting residues of docked norcraugsodine (turquoise) with *Np*NR (grey sticks).

and Gln210 along with π-Cation interactions and salt bridges with Arg55 (Table S1). Close to the ligand-binding site, the nicotinamide ring faces Ile158, Pro203, Gly204 on one side, and the substrate-binding pocket on the B-side. As it was the case for docked noroxomaritidine in the active site of noroxomaritidine reductase, docking predicted that norcraugsodine binds to the active site of NR by a combination of polar and non-polar interactions. Docked norcraugsodine displayed two possible conformations in *Np*NR and *La*NR: either bended or diagonal. For both conformations, the amine group of norcraugsodine was positioned close to C4 of NADPH and to Tyr173, obtaining a docking score of -6.36 and -6.15 kCal/mol for *NpNR* and *La*NR respectively (Figures 3C, D; S7C, D; Table S1). In both cases, norcraugsodine phenol cycle was located near Phe214, and its dihydroxybenzene group was positioned close to Glu224, interacting with His170 and Arg265. PLIP predicted additional hydrophobic interactions of norcraugsodine with Leu114, Ile205, Phe214 and Leu215, and hydrogen-bonding with Glu224 (Figures 3C, D; S7C, D; Table S1). These interactions are consistent with the proposed reduction of the imine functional group of norcraugsodine to yield norbelladine by a mechanism involving NADPH and the catalytic residues Tyr173 and Lys177.

3.4 NBS and NR produce higher titers of norbelladine together than separately

To examine the NBS, NR, and TR candidate protein function from both *N. papyraceus* and *L. aestivum*, the full-length ORFs were PCR-amplified from *N. papyraceus* and *L. aestivum* bulb cDNA, cloned, and expressed proteins were purified (Figure S8). We were unable to purify the *La*TR enzyme in our experimental conditions. We first tested the NBS, and NR purified proteins from *N. papyraceus* (*Np*) and *L. aestivum* (*La*) separately in assays containing tyramine, 3,4-DHBA, and NADPH. The resulting assay products were subjected to HPLC-MS/MS analysis using

10.3389/fpls.2023.1231809

positive electrospray ionization mode (ESI+). Before injecting the assays, norbelladine standard was injected at 1 mg/L and predicted parent-ion was observed with a mass-to-charge ratio (m/z) of 260 [M + H]+ at 3.435 min (Figures 4A; S9A-R). Fragmentation of the norbelladine parent-ion yielded to major ion fragments of m/z 121, 123 and 138 using 10 V as collision energy. Multiple reaction monitoring (MRM) transitions of 260 → 138 m/z and 260 → 121 m/z were selected, optimized using MassHunter Optimizer software, and used as quantifier and qualifier ions respectively. We could not observe any parent-ion mass for the norcraugsodine standard, despite repeated trials. We inferred that norcraugsodine was highly unstable in solution and/or thermolabile so the heat used

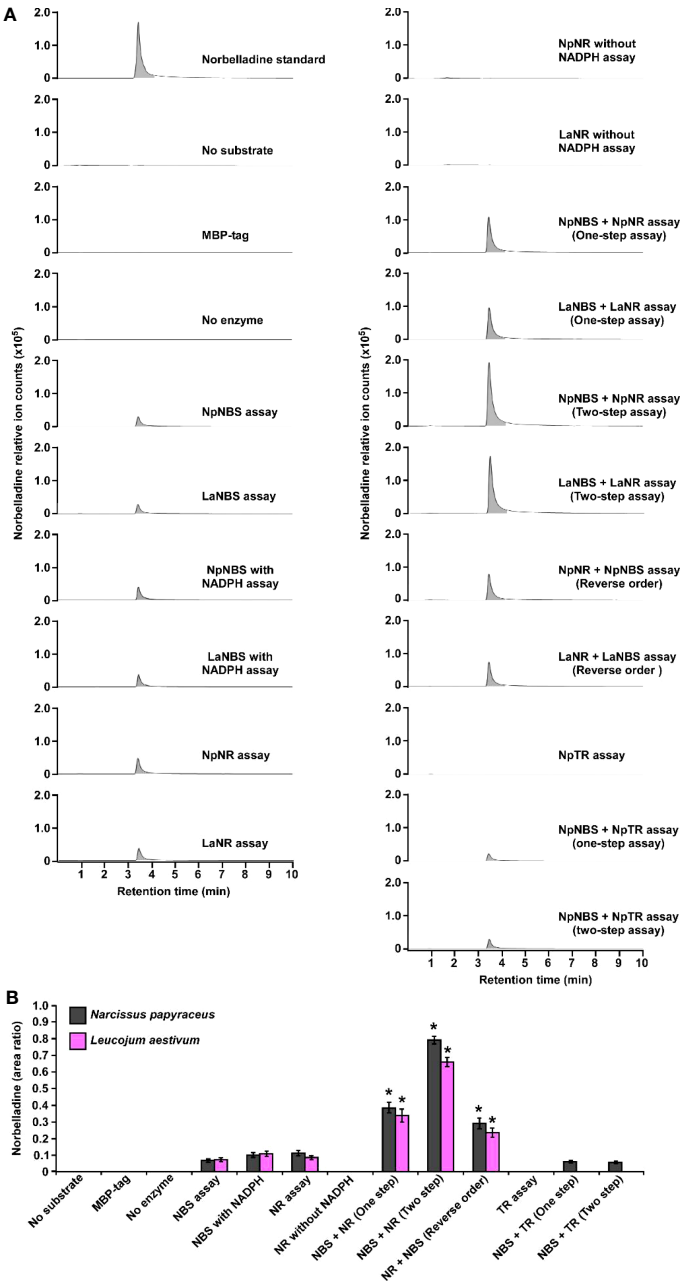

FIGURE 4
Enzymatic activity of NBS, NR and TR. Enzymes were tested separately or together for production of norbelladine, and the reaction product was monitored using HPLC-MS/MS. **(A)** Extracted ion chromatograms of quantifier MRM transition 260 → 138 m/z showing the product norbelladine in different enzymatic assays. The tested substrates used were 3,4-DHBA (300 µM) and tyramine (10 µM), and panels show norbelladine standard; assay without substrates; assay with MBP tag; assay without enzyme; and the complete assay performed with recombinant *Np*NBS, *La*NBS, *Np*NR, *La*NR and NpTR recombinant enzymes as indicated. Parent ion mass-to-charge (m/z) of 260 for norbelladine was subjected to collision-induced dissociation using multiple reaction monitoring (MRM) analysis. **(B)** Comparison and relative quantification of assays shown in Figure 4A in triplicate (mean ± SD, n = 3). The norbelladine product profiles in different assays performed were analyzed by HPLC-MS/MS and the obtained amount were relatively quantified using the area ratio of norbelladine produced in the assay to the papaverine internal standard. Data are means ± *SE* of three biological repeats. Asterisks indicate a significant difference (Student's *t* test, $p < 0.05$) relative to *Np*NBS alone enzymatic assay.

during the ionization process in the HPLC-MS/MS source could lead to its degradation. Enzyme assays containing recombinant NBS candidate protein from *Np* or *La*, 3,4-DHBA, tyramine, and with or without NADPH yielded a peak at 3.435 min in MRM acquisition mode on HPLC-MS/MS which was the same retention time as norbelladine standard (Figures 4A; S9E, F). Similarly, for the assays examining the NR candidates, tyramine and 3,4-DHBA were incubated with NR and NADPH, and the resulting product showed a peak with the same retention time as norbelladine standard in the reaction mixture of *Np* enzyme or *La* enzyme (Figures 4A; S9G, P). Comparison of the mass spectrum obtained after the fragmentation of authentic norbelladine standard using collision-induced-dissociation (CID) with 10V and the mass spectrum of the products obtained from NBS and NR reactions showed fragmentation patterns to be the same for both, thus confirming the identity of the enzymatic product (Figure S10). In assays lacking substrates or enzyme, no norbelladine was detected (Figures 4A; S9B, D). Similarly, MBP tag alone protein purified from *E. coli* transformed with empty pMAL-c2X vector showed no activity (Figures 4A; S9C). The papaverine internal standard (1000 mg/L) was used to normalize each signal obtained by LC-MS/MS to have accurate relative quantification for the produced norbelladine. The relative quantification was made by comparing peak area ratios (i.e., the peak area of norbelladine divided by the peak area of papaverine internal standard) of different samples with each other. As expected, NR assays lacking NADPH resulted in no norbelladine production (Figures 4A; S9C). As reported before (Kilgore et al., 2016b; Singh et al., 2018; Tousignant et al., 2022), our results confirm that both NBS and NR homologs alone from *N. papyraceus* and *L. aestivum* are able to catalyze the reaction of condensation/reduction of tyramine and 3,4-DHBA to produce a low amount (0.07 for NBS and 0.08 for NR relative peak area ratio) of norbelladine (Figure 4A). To examine if NBS and NR work together for the condensation of tyramine and 3,4-DHBA into norcraugsodine followed by its reduction into norbelladine (Figure 1), we tested NBS and NR purified enzymes together in one-step assay and in two-step sequential manner. Our inability to detect the intermediate norcraugsodine through HPLC-MS/MS prompted us to examine the norbelladine production in each assay mixture. We measured the substrates and equal amount of added papaverine (internal standard) in all reaction mixtures for relative quantification of the observed product (Figures S9A-R). Norbelladine production was significantly (six-fold, 0.49 relative peak area ratio) higher when both *Np*NBS and *Np*NR were present in a single reaction, compared to assays with *Np*NBS or *Np*NR separately (Figures 4A, B; S9E-J). Similarly, we observed four-fold higher (0.31 relative peak area ratio) for norbelladine production when *La*NBS and *La*NR were present in a single reaction, compared to assays with *La*NBS or *La*NR individually (Figures 4A, B; S9O-R). When the reactions were performed in a two-step manner: NBS first followed by NR, we observed two-fold higher norbelladine level (0.92 relative peak area ratio) than when enzymes were together in a single-step for both *Np* and *La* enzymes (Figures 4A, B; S9I, J, Q, R), which was 12 fold (*Np*) and 8 fold (*La*) higher in comparison to assays with the enzymes individually (Figures 4A, B). In the reverse order, stepwise reaction for both species consisted of NR first followed by NBS and yielded lower levels (0.3 relative peak area ratio) of norbelladine than observed with the original sequence (*i.e.*, NBS first followed by NR), but still produced higher amounts of norbelladine compared to single enzyme reactions (Figures 4A, B; S9J, K). Our results indicate that NBS and NR function together optimally in a sequential manner (NBS first followed by NR) to produce norbelladine. To further confirm the specificity of NR enzyme in norbelladine production, we tested the *Np*TR purified protein individually and together with *Np*NBS in assays containing 3,4-DHBA, tyramine, and NADPH. We observed no norbelladine formation in assays containing *Np*TR enzyme, and assays with both *Np*NBS and *Np*TR in one-step or two-step yielded similar level (0.07 relative peak area ratio) of norbelladine compared to assays containing only *Np*NBS enzyme (Figures 4A, B; S9L-N). These results confirm the role of NBS and NR together to channel the substrates effectively for the condensation/reduction sequence leading to the formation of norbelladine.

3.5 Derivatized norcraugsodine is detected only in assays with both NBS and NR

Direct analysis of norcraugsodine by HPLC-MS/MS or GC-MS was inconclusive (Figure S11A). Therefore, we derivatized the norcraugsodine using BSTFA reagent (N,O-bis(trimethylsilyl) trifluoroacetamide) (Figure S12). Following derivatization, two signals corresponding to tris-TMS-norcraugsodine (24.79 minutes) and the bis-TMS-3,4-dihydroxybenzaldehyde (9.28 minutes) resulting from the hydrolysis of tris-TMS-norcraugsodine were observed by GC-MS (Figures S11B-D; S12). *La* and *Np* NBS, and NR purified proteins were tested separately in enzymatic assays containing tyramine, 3,4-DHBA, and NADPH. The resulting assay products were dried, reconstituted in acetonitrile, derivatized using BSTFA, and injected into the GC-MS using electron ionization (EI) at 70 eV. As expected, in assays lacking substrates or enzymes, tris-TMS-norcraugsodine was not detected (Figures S13A, C). Similarly, MBP tag alone protein purified from *E. coli* transformed with empty pMAL-c2X vector showed no activity (Figure S13B). Surprisingly, we did not detect any tris-TMS-norcraugsodine in assays with single NBS or NR enzyme with or without NADPH (Figures S13D-K). However, tris-TMS-norcraugsodine was detected in assays containing both enzymes, in a one-step or two-step fashion, from both *Np* and *La* species (Figures S13L-O). In both cases, the detected tris-TMS-norcraugsodine fragmentation pattern matches with the tris-TMS-norcraugsodine standard (Figure S14). In the assays with the reverse order of enzymes, *i.e.*, NR first followed by NBS, a very small signal for tris-TMS-norcraugsodine was detected (Figures S13P, Q), but the fragmentation pattern did not exactly match with the standard due to proximity with the baseline. As expected, the TR enzyme alone or with NBS did not produce any detectable amounts of tris-TMS-norcraugsodine (Figures S13R-T). These results confirm that both NBS and NR are specifically required to harness norcraugsodine and for its efficient reduction into norbelladine.

3.6 NBS and NR form a dimer and NBS physically interacts with NR *in planta* and in yeast

Previous studies suggest that the norcoclaurine synthase (NCS) proteins assemble as dimers to be catalytically active (Samanani and Facchini, 2002; Samanani et al., 2004; Vimolmangkang et al., 2016). Similarly, the NR protein of *N. pseudonarcissus* was shown to exist as a tetramer through crystal structure of the enzyme (Kilgore et al., 2016b). Based on these observations, we hypothesized that NBS and NR form a dimer which impacts their activity. To explore the ability of using split-luciferase-complementation assay (SLCA) in testing the interactions of NBS and NR in *N. benthamiana* leaves, we first examined the physical interactions between *Np*NBS-*Np*NBS, *La*NBS-*La*NBS, *Np*NR-*Np*NR, and *La*NR-*La*NR. *Np*NBS, *La*NBS, *Np*NR, and *La*NR were fused to the N-terminal half of the luciferase protein (NLuc) and co-expressed via *Agrobacterium* in *N. benthamiana* leaves while *Np*NBS, *La*NBS, *Np*NR, and *La*NR were fused to the C-terminal half of luciferase (CLuc) protein. As negative controls, *Np*NBS-NLuc, *La*NBS-NLuc, *Np*NR-NLuc, and *La*NR-NLuc were co-expressed with CLuc empty vector and CLuc-*Np*NBS, CLuc-*La*NBS, CLuc-*Np*NR, and CLuc-*La*NR were co-expressed with NLuc empty vector (Figures 5A-D). Expression of all the fusion proteins was validated by western blot analysis (Figures S15A, B). The homodimeric interactions were monitored by measuring luminescence 48 h after agroinfiltration of the tested protein pairs. Co-expression of *Np*NBS-NLuc with CLuc-*Np*NBS, *La*NBS-NLuc with CLuc-*La*NBS, *Np*NR-NLuc with CLuc-*Np*NR, and *La*NR-NLuc with CLuc-*La*NR resulted in emission of significantly higher luminescence compared to the negative controls indicating a physical interaction *in planta* between NBS-NBS and NR-NR fusion proteins (Figures 5A-D). One explanation for the production of norbelladine in reactions containing NBS and NR is that NR functions as an enzyme that acts on norcraugsodine produced from tyramine and 3,4-DHBA by NBS. Alternatively, NR may alter the catalytic properties of NBS through allosteric regulation, which allows NBS to form norbelladine, or vice versa, but it remains formally possible that NBS and NR are present together in a metabolon, NR playing a regulating role by guiding the substrates to the imine intermediate followed by reduction to norbelladine. To test the importance of physical interactions for norbelladine biosynthesis, the interactions of *Np*NBS and *La*NBS with full-length *Np*NR and *La*NR were examined in *N. benthamiana* leaves by split-luciferase-complementation-assays. *Np*NBS and *La*NBS were fused to the N-terminal half of the luciferase protein (NLuc) and co-expressed via *Agrobacterium* in *N. benthamiana* leaves along with *Np*NR and *La*NR fused to the C-terminal half of luciferase (CLuc). As a control, *Np*NBS-NLuc and *La*NBS-NLuc were co-expressed with CLuc-*Np*TR and CLuc-*La*TR, respectively. As negative controls, *Np*NBS-NLuc and *La*NBS-NLuc were co-expressed with CLuc empty vector and CLuc-*Np*NR and CLuc-*La*NR were co-expressed with NLuc empty vector (Figures 5A-D). Expression of the examined fusion proteins was confirmed by western blot analysis (Figures S15A, B). Protein-protein interactions *in planta* were quantified by measurements of luminescence 48 h after agroinfiltration. In agreement with the enzymatic assays, co-expression of *Np*NBS-NLuc with CLuc-*Np*NR and *La*NBS-NLuc with CLuc-*La*NR resulted in emission of significantly higher luminescence compared to the negative controls and the control protein CLuc-*Np*TR and CLuc-*La*TR (Figures 5A-D), demonstrating a physical interaction *in planta* between NBS and NR fusion proteins.

To validate the interaction detected *in planta* and to check if the observed interactions are direct, the interactions between NBS-NBS, NR-NR, NBS-NR, and NBS-TR were then examined by yeast two-hybrid system. NBS, NR and TR from both plant species were fused to both bait and prey plasmids. Expression in yeast of bait and prey proteins was confirmed by western blot analysis (Figures S15C, D). Similar interactions between NBS-NBS, NR-NR and NBS-NR were observed (Figures 5E, F) when the same protein pairs from both plant species were expressed in yeast as bait and prey proteins in agreement with the observed interaction *in planta*. As observed *in planta*, no interaction was found between NBS-TR in yeast (Figures 5E, F). Taken together, these results obtained in different experimental systems indicated regulatory interactions between NBS and NR and support the possibility that NBS and NR function as heteromultimeric proteins.

3.7 NBS and NR produce norbelladine together *in vivo*

Functional analysis of NBS and NR via RNAi was not possible because Amaryllidaceae transformation has not been achieved. To demonstrate NBS and NR activity *in vivo*, we reconstituted norbelladine biosynthesis in yeast. Yeast cultures expressing *Np*NBS, *Np*NR, and *Np*TR as single enzymes or *Np*NBS together with *Np*NR or *Np*TR were fed with tyramine and 3,4-DHBA, and norbelladine production was monitored in the yeast cell extracts. We measured the equal amount (1000 mg/L) of added papaverine (internal standard) in all reaction mixtures for relative quantification of the observed norbelladine product. Surprisingly, we did not detect norbelladine in any of the yeast cultures expressing single NBS or NR enzyme (Figures 6A, B). However, we detected low levels of norbelladine (0.22 relative peak area ratio) in yeast cultures expressing both NBS and NR (Figures 6A, B). This confirms that both enzymes are required for norbelladine production in an *in vivo* model.

3.8 NBS and NR colocalize in the cell cytoplasm and nucleus

The NBS protein fused with green fluorescent protein (GFP) from both *L. aestivum* and *N. papyraceus* was recently shown to localize to the cell cytoplasm and nucleus (Tousignant et al., 2022). Similarly, we found NR lacked any predicted signal peptides. To investigate NBS and NR subcellular localization, the *NBS* and *NR* coding regions from both *N. papyraceus* and *L. aestivum* plants were fused upstream to the yellow-fluorescent-protein gene (*YFP*).

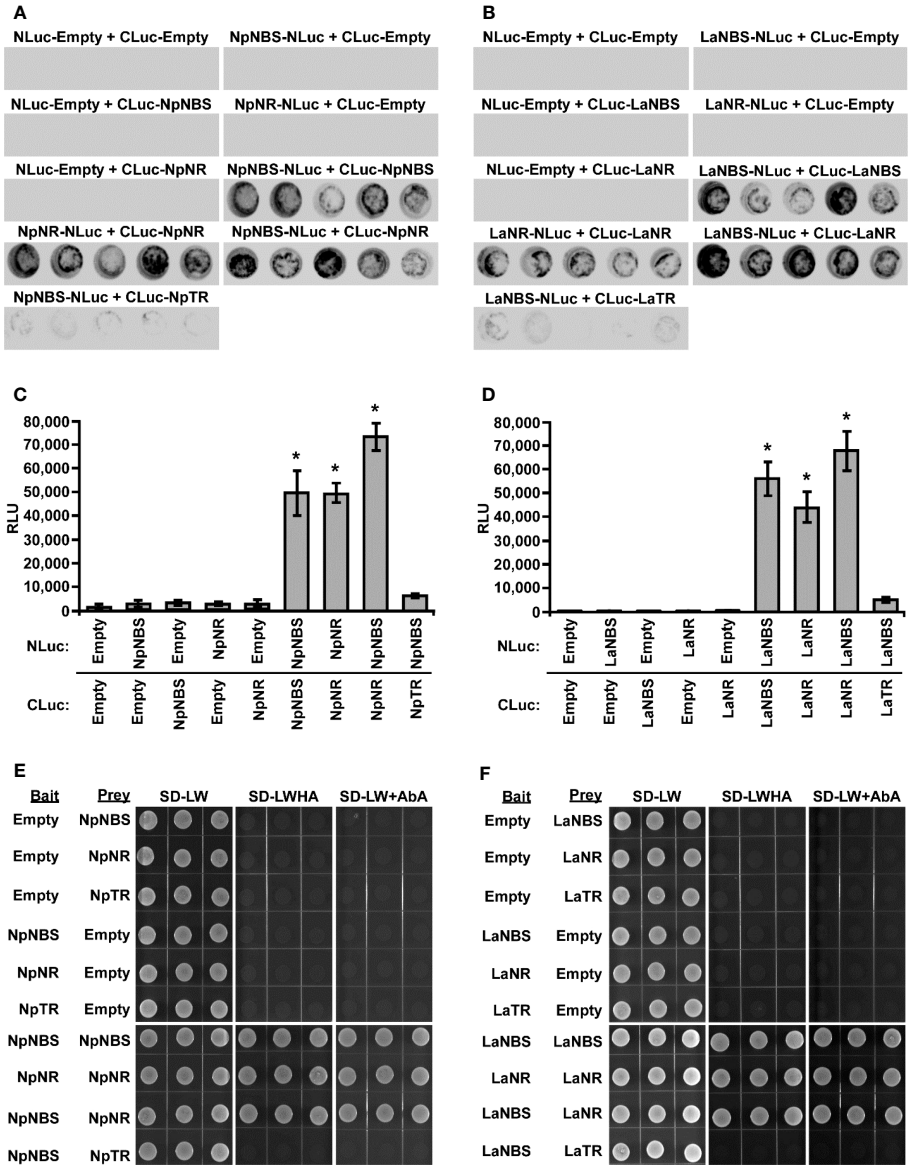

FIGURE 5
Physical interaction of NBS and NR *in planta* and in Yeast. **(A-D)** The indicated proteins fused to NLuc or CLuc were expressed in leaves of *Nicotiana benthamiana* plants via *Agrobacterium tumefaciens* infection. **(A, B)** The images show LUC images of 96-well microtiter plates containing *N. benthamiana* leaf discs expressing the indicated constructs. **(C, D)** Luciferase activity was quantified as relative luciferase units (RLU) 48 hr post-infiltration. Data are means ± *SE* of three biological repeats. Asterisks indicate a significant difference (Student's *t* test, $p < 0.05$) relative to empty vector. **(E, F)** Yeast expressing the indicated proteins fused to the GAL4 DNA-binding domain (Bait) or to the GAL4 DNA activation domain (Prey) were grown on synthetically defined (SD) medium lacking Leu and Trp (SD-LW), SD-LW lacking histidine and adenine (SD-LWHA), or SD-LW supplemented with Aureobasidin A (SD-LW+AbA). Empty vectors (EV) were used as negative controls. * = Asterisks indicate a significant difference (Student's t test, $p < 0.05$).

The *Np*NBS-YFP, *La*NBS-YFP, *Np*NR-YFP, and *La*NR-YFP fusions were transiently expressed in leaves of *N. benthamiana* plants via *A. tumefaciens*, and their localization was monitored by confocal fluorescence microscopy. The cyan fluorescent protein (CFP), which localizes to the cytoplasm and nucleus (Kruse et al., 2010), was used as a control. Expression of all the fusion proteins was validated by western blot (Figure S16). As shown in Figure 7A, the NBS-YFP and NR-YFP fusion proteins from both plant species localized in the cell cytoplasm and nucleus like CFP. These results suggest that both NBS and NR are distributed to the same nucleocytoplasm cellular compartment. To further confirm the colocalization pattern of NBS and NR, the NR coding regions from both *N. papyraceus* and *L. aestivum* plants were fused upstream to the cyan fluorescent protein (CFP) and co-expressed via *Agrobacterium* in *N. benthamiana* leaves while *Np*NBS and *La*NBS were fused to the YFP, and their localization pattern was monitored by confocal microscopy. Expression of all the fusion proteins was validated by western blot (Figure S16). Similar profiles of fluorescence pattern in the cell cytoplasm and nucleus were observed for NBS-YFP and NR-CFP (Figure 7B). These results confirm that NBS and NR which lack predicted signal peptides, colocalized to both the cytoplasm and the nucleus of the cell.

10.3389/fpls.2023.1231809

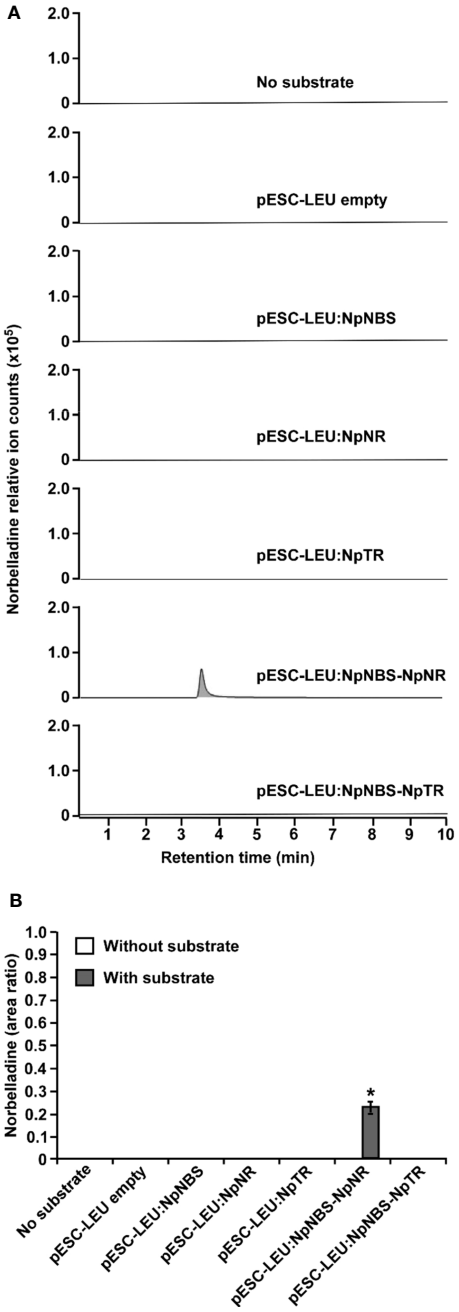

FIGURE 6
In vivo biosynthesis of norbelladine in yeast. HPLC-MS/MS analysis of norbelladine produced in yeast cultures expressing NBS and NR both singly and in combination. **(A)** Extracted ion chromatograms of quantifier MRM transition 260 → 138 m/z showing the product norbelladine in different indicated yeast cultures. **(B)** Comparison and relative quantification of assays shown in Figure 6A in triplicate (mean ± SD, n = 3). The norbelladine product profiles in different assays performed were analyzed by HPLC-MS/MS and the obtained amount were relatively quantified using the area ratio of norbelladine produced in the assay to the papaverine internal standard. Data are means ± *SE* of three biological repeats. Asterisks indicate a significant difference (Student's *t* test, $p < 0.05$) relative to the yeast culture expressing *Np*NBS alone. * = Asterisks indicate a significant difference (Student's t test, $p < 0.05$).

3.9 *NBS* and *NR* are expressed at high levels in the bulbs of *N. papyraceus* and *L. aestivum*

The expression profiles of the *NBS* and *NR* in different tissues including bulb, root, stem, leaf, and flower were evaluated by using quantitative real-time PCR (qRT-PCR) analysis. The results showed that *NBS* was ubiquitously expressed in all tissues detected, with the highest expression levels in bulb and root (Figures 8A, B). The expression patterns of *NpNBS* and *LaNBS* were similar, mRNA accumulated in high amount in bulb and root, and low transcript levels were detected in leaf, stem, and flower (Figures 8A, B). The *NR* expression pattern was different. *LaNR* and *NpNR* mRNA specifically accumulated at high levels in bulbs, and in low amount in other tested tissues (Figures 8C, D). We further checked the expression pattern of *TR* in different tissues to compare tissue expression profiles between *NR* and *TR* and found that *NpTR* and *LaTR* genes were widely expressed in all the examined tissues (Figures S17A, B). These results suggest that the highest transcript levels of *NR* were in bulbs, which parallels with the high expression for *NBS* transcripts in the bulbs. This high expression of *NBS* and *NR* aligns with the higher expression of other AA biosynthetic genes in bulbs of *N. papyraceus* (Hotchandani et al., 2019) and *L. aestivum* (Tousignant et al., 2022).

4 Discussion

To date, PR10/Bet v1-like proteins have been directly implicated in the biosynthesis of two alkaloid classes – the AAs and the benzylisoquinoline alkaloids (BIAs) (Dastmalchi, 2021; Morris et al., 2021). Although end-product alkaloids within these two classes are structurally distinct, the pathways have similar biogenic origins. In the BIAs pathway, NCS catalyzes the condensation between dopamine and 4-HPAA to form (*S*)-norcoclaurine. The initiation of AAs' biosynthesis is proposed to occur via condensation of tyramine and 3,4-DHBA to yield the imine norcraugsodine, which is then reduced to produce norbelladine (Figure 1). Our results confirm that the condensation of tyramine and 3,4-DHBA by *La*NBS and *Np*NBS forms norbelladine at low levels, but not norcraugsodine (Singh et al., 2018; Tousignant et al., 2022), despite the absence of a cofactor for the reduction in the reaction mixture. In our enzymatic assays, even the prepared standard solution of norcraugsodine was highly unstable, indicating that norcraugsodine is difficult to detect because of its instability. Still, the imine reduction of norcraugsodine intermediate into norbelladine by NBS is surprising. NBS is part of the PR10/Bet v 1-like enzymes, which are not known to use cofactors for their activity, with few reported exceptions (Jain et al., 2016). Although unlikely, low but enough bacterial components carrying cofactors could remain in the purified protein and help with the reduction.

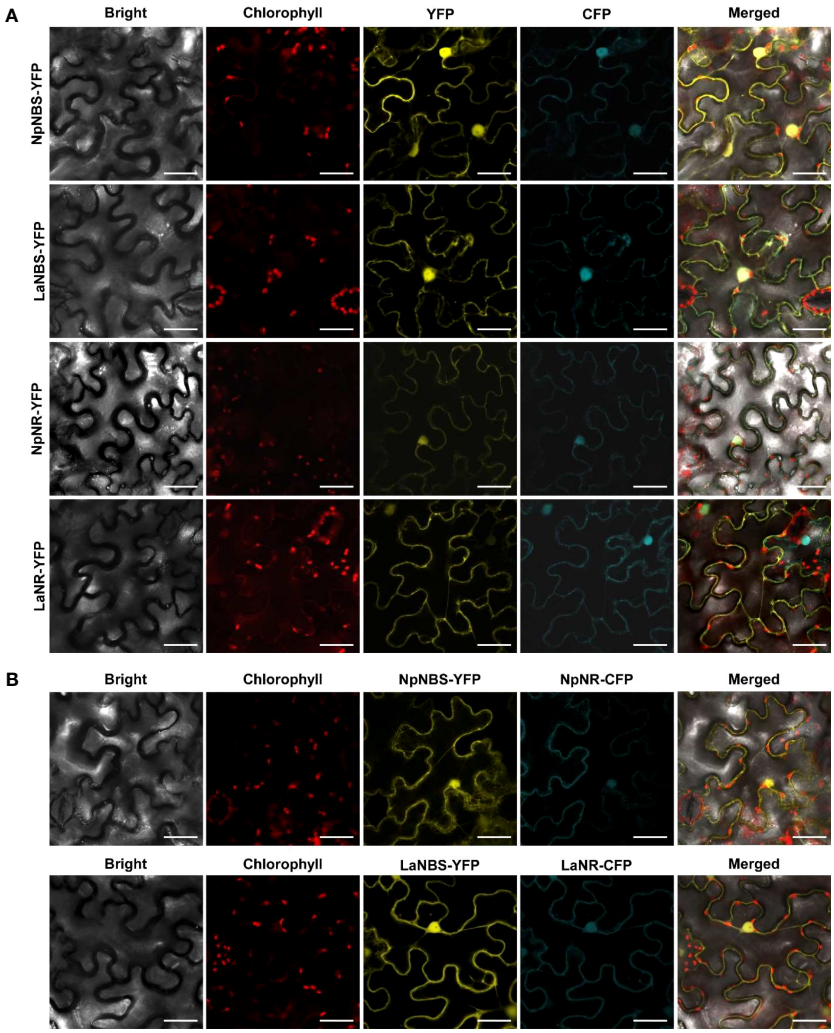

FIGURE 7
NBS and NR colocalize to the cell cytoplasm and nucleus. **(A)** The indicated fusion proteins were co-expressed with the cyan fluorescent protein (CFP) in *Nicotiana benthamiana* leaves via *Agrobacterium tumefaciens*. After 48 hr, fluorescence was monitored in epidermal cells by confocal microscopy. Bright field, chlorophyll, yellow fluorescent protein (YFP), cyan fluorescent protein (CFP), and merged fluorescence images are shown. Scale bars in images represent 50 µM. **(B)** Confocal micrographs of transiently expressed NBS-YFP and NR-CFP in *Nicotiana benthamiana* leaves showing they colocalize to the cytoplasm and nucleus. Bright field, chlorophyll, yellow fluorescent protein (YFP), cyan fluorescent protein (CFP), and merged fluorescence images are shown. Scale bars in images represent 50 µM.

However, in our enzymatic assays, the addition of NADPH to the reaction did not significantly increase the norbelladine production by NBS. Alternatively, *Np*NBS and *La*NBS could possess a reductase activity as found in PR-10 protein *Ca*ARP from chickpea (Jain et al., 2016), but it is improbable as they lack the conserved motifs corresponding to the catalytic signatures of short chain dehydrogenase/reductase (SDR) (Y-X_3-K) and aldo/keto reductase (AKR) (Y-X_{27-30}-K) with the common tyrosine residue (Jain et al., 2016). On the other hand, *NpKA*NR was previously reported to also yield norbelladine following incubation with tyramine, 3,4-DHBA and NADPH, albeit in low yield (Kilgore et al., 2016b). We confirmed that low but detectable amounts of norbelladine can be produced from 3,4-DHBA and tyramine with NR isolated for *N. papyraceus* and *L. aestivum* in enzymatic assays. In theory, other SDR members with imine reduction capability could be able to catalyze this reaction as proposed previously (Roth et al., 2018). In our study, only NR, but not TR, the other identified SDR member, was specifically able to catalyze this reaction. The low yields reported with NBS and NR alone prompted us to hypothesize that they could need to work together to channel the substrates effectively for their condensation into norcraugsodine followed by an immediate reduction into norbelladine. Their interaction could help by improving their catalytic activity, by avoiding degradation of unstable norcraugsodine in decreasing its transit time, and by preventing feedback regulation of norbelladine production.

We used homology modelling and docking studies to model our hypothesis and gain insight of the ligand-enzyme interactions involved in norbelladine synthesis as a two-step reaction. Although performing docking on predicted structures has its limitations, it provides a general scheme on the possible interactions of NBS and NR with their respective ligands that is consistent with the enzymatic reactions they performed. Our

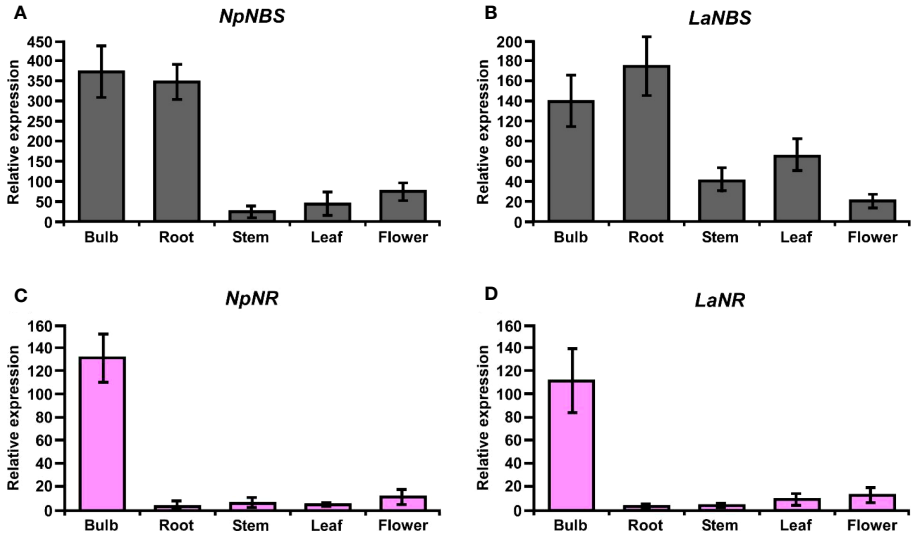

FIGURE 8
Relative expression of *NBS*, and *NR* in different tissues of *N. papyraceus* and *L. aestivum* using reverse transcription quantitative PCR (RT-qPCR) analysis. Different plant tissues as indicated were harvested after flowering, and *NpNBS* **(A)**, *LaNBS* **(B)**, *NpNR* **(C)**, *LaNR* **(D)** mRNA levels were measured by RT-qPCR analysis relative to expression in leaves. *NpHISTONE* and *LaGAPDH* were used as normalizer. Data are means ± *SE* of three biological repeats.

proposed model for norbelladine synthesis involves NBS first where the condensation of 3,4-DHBA and tyramine subunits yields an imine/iminium intermediate (Schiff base) (*i.e.*, norcraugsodine), followed with a reduction by NR leading to norbelladine (Figure 1). Similarly to the NCS catalyzed reaction (Lichman et al., 2017a; Lichman et al., 2017b), homology modeling and docking results suggest that NBS Tyr68, Lys83 and Glu71 surround the active site and interact with 3,4-DHBA and tyramine, probably playing key roles in norcraugsodine synthesis. In this proposed reaction, Lys83 would transfer a proton from the ammonium group of tyramine to the carbonyl oxygen of 3,4-DHBA, stabilizing a partial positive charge on the carbon atom. Lys83-assisted nucleophilic attack of tyramine amine group to the aldehyde carbonyl would lead to the release of a water molecule from the carbinolamine moiety, generating the imine double bond, in a similar reaction to NCS's (Lichman et al., 2017b). Finally, norcraugsodine would be formed following an electrophilic attack and deprotonation assisted by the carboxyl moiety of Glu71, acting as a base. Tyr68 could contribute to the electrostatic properties of the active site and by shaping the cavity entrance. Following its synthesis, norcraugsodine would then be reduced to norbelladine inside NR active site with the assistance of NADPH. In SDR enzymes, the catalytic dyad Tyr175 and Lys179 is conserved and have a double role in the active site, the tyrosine serving as a general acid to protonate the substrate keto-group, while the lysine lowers the tyrosine's pKa to promote proton donation. Noroxomaritidine reduction occurs in a similar structural and chemical arrangement: the substrate ketone is positioned in proximity to Tyr175 and NADPH (Kilgore et al., 2016b). Electrostatic interaction with Lys179 reduces the pKa of Tyr175 to polarize the noroxomaritidine carbonyl group for protonation and hydride transfer, to yield the ketone product with a reduced carbon-carbon double bond (Kilgore et al., 2016b). Similarly, to noroxomaritidine crystal structure in complex with NADPH and tyramine or piperonal, docking results showed that norcraugsodine phenol cycle binds near Phe214, its amine group is positioned close to Tyr173 and NADPH C4, and its dihydroxybenzene binds to Glu224. Lys177 in the proximity of Tyr173 could allow the tyrosine hydroxyl group to serve as a general acid with a hydride transfer from NADPH, leading to norbelladine (*i.e.*, with its reduced imine group). Consistent with reactions catalyzed by the SDR families, docking studies suggest that NADPH, Tyr173 and Lys 177 play key roles in norcraugsodine reduction.

We tested our model pathway of norbelladine biosynthesis using several enzymatic assays. Our results confirmed that when both enzymes are present in the reaction, either in a single-step or in a two-step reaction, significantly higher levels of norbelladine were produced than when using each enzyme separately. The highest yield (12-fold increase) was obtained when the assay was carried out in a two-step manner, with NBS first and NR second. The observation of obtaining more norbelladine in two-step assays than one-step in *in vitro* enzymatic assay is not aligning with our hypothesis that the channelled reactions of the single-step assay would yield highest levels of norbelladine as both the enzymes (NBS and NR) are present together. We propose that the 10 mins boiling step in two-step assays might not have completely inactivated all the NBS protein and the following further 2-hour incubation with NR could have an increased norbelladine production as all the substrates are present in the reactions. Another possibility is that the large MBP tag (42-kDa) present in the fusion protein could be hindering the property of the NBS and NR hetero multimers. Thus, it is possible that NR in inappropriate conformation inhibits NBS or vice versa, but somehow interferes to a lesser extent to that of homo multimers of either or both of NBS and NR. To address this, we

attempted to cleave the MBP-tag with Factor Xa protease. Unfortunately, we observed that upon the tag cleavage, both NBS and NR protein precipitated/aggregated, and we were unable to obtain the NBS or NR protein without a MBP tag fusion. Similarly, we found that these two proteins are prone to be in insoluble fraction with a smaller histidine (HIS)-tag. Lower levels of soluble NBS protein with HIS-tag was also reported by Singh et al., 2018. The MBP tag does not dimerize itself as other larger tags such as glutathione S-transferase (GST) (Reuten et al., 2016), and interaction between the two proteins were confirmed in yeast and colocalization in planta using other tag systems. Hence, the possibility of forced dimerization between NBS and NR, and its false implication on the enzymatic assays is unlikely. However, we cannot completely rule out the possibility that the large fusion tag can interfere with proper conformation of the hetero multimers. Future studies that will mutate important amino acids required for the physical interaction of NBS and NR will shed light on how these hetero multimers are formed, and how they regulate biochemical properties of the enzymes. The initial purpose of the two-step assay was to check if we can detect higher norbelladine as we could not detect the intermediate norcraugsodine in our assays. Overall, our results showed that NBS and NR can co-operate to produce norbelladine *in vitro*.

The inability to detect the intermediate norcraugsodine was a major challenge in our study. With very extensive work we found that norcraugsodine is highly unstable and difficult to detect by LC- or GC-MS analysis. However, we could detect the norcraugsodine by GC-MS upon derivatization with BSTFA. Interestingly, our *in vitro* enzymatic assays showed that to detect the derivatized norcraugsodine both enzymes (NBS and NR) required physically present together. We propose a metabolon with NBS and NR proteins, where NR functions as an enzyme that acts immediately on norcraugsodine produced from tyramine and 3,4-DHBA by NBS and converts it to norbelladine. Alternatively, NR may alter the catalytic properties of NBS through allosteric regulation, which allows NBS to form norbelladine, or vice versa. The other possibility is that NBS and NR are present together in a metabolon, and both play a regulatory role together in guiding the substrates to the imine intermediate and keeping the intermediate norcraugsodine stable, followed by immediate reduction to norbelladine. Hence without both proteins norcragusodine is not stabilized and hence cannot be detected. The formation of norcraugsodine in assays s with NBS or NR alone can not be ruled out but if norcraugsodine was indeed produced, it was below detection levels.

In vivo, enzymes perform their functions in specific subcellular compartments (Huh et al., 2003). We showed that NBS and NR are colocalized to the cell cytoplasm and nucleus. Their colocalization is consistent with their possible cooperation. We propose that the site of their activity is the cytoplasm as previous studies have shown that *La* tyrosine decarboxylase 1 (TYDC1), which catalyzes the conversion of tyrosine to tyramine, was localized to the cytosol (Wang et al., 2019), as were *O*-methyltransferase 1 from *Lycoris aurea* (OMT) and the N4OMT from *Lycoris longituba*, which catalyze the *O*-methylation of norbelladine into 4'-*O*-methylnorbelladine (Sun et al., 2018). In addition, there is some evidence of cytoplasmic localization for tyramine and 3,4-DHBA (Nagahashi et al., 1996). Thus, our results support the hypothesis that the early reactions of AAs are biosynthesized in the cytosol. Our gene expression analysis clearly indicates that both NBS and NR from both species are highly expressed in bulb, but only the former in root. This suggests that root has a reduced catalytic efficiency in norbelladine biosynthesis because of the low level of NR expression and unavailability of catalytically active metabolon containing NBS and NR. These results align with the previous work on *Narcissus papyraceus* (Hotchandani et al., 2019) where transcript levels of other AA biosynthetic genes such as TYDC1, TYDC2, PAL2, C4H, C3H and N4OMT are very high in the bulb, lower in the roots, and lowest in the leaves. By contrast, at the alkaloid level, the opposite was observed: the bulb tissue has the lowest amount of alkaloids and the leaves and roots the highest. A possible explanation is that the biosynthetic enzymes and/or alkaloids produced in the bulb are being transported to other parts of the plant, leading to fewer alkaloids in the bulb and higher amounts in the roots and leaves (Hotchandani et al., 2019). In Amaryllidaceae plants, we observed combined high expression of both NBS and NR in bulbs of *N. papyraceus* and *L. aestivum*, reinforcing their probable cooperation to produce norbelladine *in vivo* in the bulb tissues, later transported to different parts as the plant grows and develops. Future study with a full set of spatio-temporal profiles of NBS and NR expression together with AA accumulation in *Leucojum aestivum* will shed light on the involvement of the proposed AA biosynthetic genes in the production of the AAs at each developmental stage.

Then, we investigated the possibility that NBS and NR interact together in yeast and *in planta*. First, we observed that both NBS and NR proteins physically interact as homodimers in yeast and *in planta*, suggesting that this conformation is important for their function *in vivo*. Then, our results in yeast suggest that the two enzymes directly interact with each other and that additional plant proteins are not required for this interaction. These results support the hypothesis that NBS and NR work together in a metabolon, where NBS as a homodimer synthesizes the intermediate norcraugsodine, which is readily converted into norbelladine by NR, present as a homodimer in the same protein complex. The formation of metabolons allows the intermediate product to be passed directly from one enzyme to the active site of the subsequent enzyme in the metabolic pathway (Zhang et al., 2017). It is also possible that allosteric regulation of NBS by NR (or vice-versa) could explain the enhanced production of norbelladine when both enzymes interact. NBS or NR could play a chaperone-like role in guiding the folding of the norcraugsodine intermediate or of the second enzyme, as has been previously suggested for PR10/Bet V1-like members (Dastmalchi, 2021; Morris et al., 2021). Metabolons are dynamic and transient protein assemblies that facilitate metabolic reactions within the cells (Dahmani et al., 2023). To date, several metabolons in plants have been suggested to mediate channeling of different substrates, including the TCA cycle (Zhang et al., 2017), the glycolytic pathways, and several pathways of specialized metabolism in plants (Laursen et al., 2016; Camagna et al., 2018; Fujino et al., 2018; Gou et al., 2018). All metabolons involve physical association of different enzymes involved in a specific metabolic pathway and plays a crucial role in cellular

metabolism by enhancing reaction rates, protecting unstable intermediates, and minimizing side reactions (Dahmani et al., 2023). In our study we observed all the common features of a metabolon formation like enzyme-enzyme complex, detection of substrate channels, presence of the enzymes in same cellular compartments. Our results clearly showed that NBS and NR are present as homo- and heteromeric complexes, which protect and channel the unstable intermediate norcraugsodine. Furthermore, their interactions are direct, and localization to same nucleocytoplasmic compartments. We propose that, as AAs biosynthesis in Amaryllidaceae plant cells is a very complex process due to the number of subcellular organelles in plant cell, and the number of isoforms of specific enzymes they contain, and the sheer range of metabolites they form, possible formation of different metabolons will be ideal to regulate mechanisms to rapidly and frequently alter metabolic fluxes in response to specific demands or challenges. Future studies involving X-ray crystallography, electron microscopy, and development of artificial intelligence (AI) for accurate prediction of complex structures, will help us to better understand how different sequential enzymes in AAs biosynthesis form structural-functional complexes and how this metabolon is regulated.

Finally, we used a yeast system to express NBS alone, NR alone, or both NBS/NR to show that their interaction is essential to generate higher levels of norbelladine. Our results confirmed that when both NBS and NR are present together, the yeast produces detectable levels of norbelladine, as compared to the absence of detectable norbelladine when each protein was present alone or when the yeast was simply fed with tyramine and 3,4-dihydroxybenzaldehyde. Future studies with metabolic engineering of yeast with the complete elucidated pathway for galanthamine biosynthesis will help us better understand how this pathway is regulated and how to increase the production of norbelladine in heterologous systems.

In conclusion, our study establishes that NBS and NR cooperatively catalyze the biosynthesis of norcraugsodine and its reduction into norbelladine. We show that the two enzymes localize to both the cytoplasm and nucleus, are expressed at high levels in bulbs, and physically interact with each other in yeast and *in planta*. This study unravels the reactions involved in the first key steps of the biosynthesis of all AAs. Deciphering norbelladine synthesis will facilitate the development of the biosynthetic tools required to produce AAs *in vitro* and help fight human diseases, for example via the biosynthesis of galanthamine in heterologous hosts to treat the symptoms of Alzheimer's disease.

Data availability statement

The datasets presented in this study can be found in online repositories. The names of the repository/repositories and accession number(s) can be found in the article/Supplementary Material.

Author contributions

IDP conceived, designed, and supervised the study. BBM designed and performed most of the experiments. SEG performed all the HPLC-MS/MS analysis. NM carried out the protein modelling and docking experiments. SR carried out the derivatization of norcraugsodine and GC-MS analysis. BBM, NM, and IDP wrote the manuscript with input from others. All authors read and approved the final version of the manuscript. All authors contributed to the article.

Funding

This work was funded by the Natural Sciences and Engineering Research Council of Canada (NSERC) award number RGPIN-2021-03218 (Discovery) to ID-P This work was also supported by the Canada Research Chair on plant specialized metabolism Award No 950-232164 to ID-P Thanks are extended to the Canadian taxpayers and to the Canadian government for supporting the Canada Research Chairs Program.

Acknowledgments

We gratefully thank Professor Hugo Germain for helpful discussions, and for providing the *N. benthamiana* seeds and other lab materials used in this study. We also thank Professor Guido Sessa for providing the pBTEX, pCAMBIA1300:CLuc, and NLuc vectors and the *Agrobacterium* GV3101 strain used in this study. We thank Fatma Meddeb for timely help in obtaining the lab materials and helpful discussions, and Melodie B. Plourde for helping with confocal imaging. We thank Professor Patrick Lagüe at the University Laval (Québec, Canada) for sharing his expertise on molecular modeling and docking.

Conflict of interest

The authors declare that the research was conducted in the absence of any commercial or financial relationships that could be construed as a potential conflict of interest.

Publisher's note

Supplementary material

The Supplementary Material for this article can be found online at: https://www.frontiersin.org/articles/10.3389/fpls.2023.1231809/full#supplementary-material

References

Adasme, M. F., Linnemann, K. L., Bolz, S. N., Kaiser, F., Salentin, S., Haupt, V. J., et al. (2021). PLIP 2021: expanding the scope of the protein–ligand interaction profiler to DNA and RNA. *Nucleic Acids Res.* 49 (W1), W530–W534. doi: 10.1093/nar/gkab294

Battersby, A. R., Fales, H. M., and Wildman, W. C. (1961). Biosynthesis in the Amaryllidaceae. Tyrosine and norbelladine as precursors of haemanthamine. *J. Amer. Chem. Soc* 83, 4098–4099. doi: 10.1021/ja01480a037

Camagna, M., Grundmann, A., Bär, C., Koschmieder, J., Beyer, P., and Welsch, R. (2018). Enzyme fusion removes competition for geranylgeranyl diphosphate in carotenogenesis. *Plant Physiol.* 179 (3), 1013–1027. doi: 10.1104/pp.18.01026

Chen, H., Zou, Y., Shang, Y., Lin, H., Wang, Y., Cai, R., et al. (2008). Firefly luciferase complementation imaging assay for protein-protein interactions in plants. *Plant Physiol.* 146 (2), 368–376. doi: 10.1104/pp.107.111740

Dahmani, I., Qin, K., Zhang, Y., and Fernie, A. R. (2023). The formation and function of plant metabolons. *Plant J.* 114 (5), 1080–1092. doi: 10.1111/tpj.16179

Dastmalchi, M. (2021). Elusive partners: a review of the auxiliary proteins guiding metabolic flux in flavonoid biosynthesis. *Plant J.* 108 (2), 314–329. doi: 10.1111/tpj.15446

Desgagné-Penix, I. (2021). Biosynthesis of alkaloids in Amaryllidaceae plants: a review. *Phytochem. Rev.* 20 (2), 409–431. doi: 10.1007/s11101-020-09678-5

Eichhorn, J., Takada, T., Kita, Y., and Zenk, M. H. (1998). Biosynthesis of the Amaryllidaceae alkaloid galanthamine. *Phytochemistry* 49 (4), 1037–1047. doi: 10.1016/S0031-9422(97)01024-8

El Tahchy, A., Boisbrun, M., Ptak, A., Dupire, F., Chretien, F., Henry, M., et al. (2010). New method for the study of Amaryllidaceae alkaloid biosynthesis using biotransformation of deuterium-labeled precursor in tissue cultures. *Acta Biochim. Pol.* 57 (1), 75–82.

El Tahchy, A., Ptak, A., Boisbrun, M., Barre, E., Guillou, C., Dupire, F., et al. (2011). Kinetic study of the rearrangement of deuterium-labeled 4'-O-methylnorbelladine in Leucojum aestivum shoot cultures by mass spectrometry. Influence of precursor feeding on Amaryllidaceae alkaloid accumulation. *J. Nat. Prod* 74 (11), 2356–2361. doi: 10.1021/np200285j

Fernandes, H., Michalska, K., Sikorski, M., and Jaskolski, M. (2013). Structural and functional aspects of PR-10 proteins. *FEBS J.* 280 (5), 1169–1199. doi: 10.1111/febs.12114

Frederick, R. D., Thilmony, R. L., Sessa, G., and Martin, G. B. (1998). Recognition specificity for the bacterial avirulence protein AvrPto is determined by Thr-204 in the activation loop of the tomato Pto kinase. *Mol. Cell* 2 (2), 241–245. doi: 10.1016/s1097-2765(00)80134-3

Fujino, N., Tenma, N., Waki, T., Ito, K., Komatsuzaki, Y., Sugiyama, K., et al. (2018). Physical interactions among flavonoid enzymes in snapdragon and torenia reveal the diversity in the flavonoid metabolon organization of different plant species. *Plant J.* 94 (2), 372–392. doi: 10.1111/tpj.13864

Goodin, M. M., Zaitlin, D., Naidu, R. A., and Lommel, S. A. (2008). Nicotiana benthamiana: its history and future as a model for plant-pathogen interactions. *Mol. Plant-Microbe interactions: MPMI* 21 (8), 1015–1026. doi: 10.1094/MPMI-21-8-1015

Gou, M., Ran, X., Martin, D. W., and Liu, C.-J. (2018). The scaffold proteins of lignin biosynthetic cytochrome P450 enzymes. *Nat. Plants* 4 (5), 299–310. doi: 10.1038/s41477-018-0142-9

Heinrich, M., and Lee Teoh, H. (2004). Galanthamine from snowdrop–the development of a modern drug against Alzheimer's disease from local Caucasian knowledge. *J. Ethnopharmacol* 92 (2-3), 147–162. doi: 10.1016/j.jep.2004.02.012

Holsters, M., Silva, B., Van Vliet, F., Genetello, C., De Block, M., Dhaese, P., et al. (1980). The functional organization of the nopaline A. tumefaciens plasmid pTiC58. *Plasmid* 3 (2), 212–230. doi: 10.1016/0147-619x(80)90110-9

Hotchandani, T., de Villers, J., and Desgagné-Penix, I. (2019). Developmental regulation of the expression of Amaryllidaceae alkaloid biosynthetic genes in. *Narcissus papyraceus. Genes* 10 (8), 594. doi: 10.3390/genes10080594

Huh, W.-K., Falvo, J. V., Gerke, L. C., Carroll, A. S., Howson, R. W., Weissman, J. S., et al. (2003). Global analysis of protein localization in budding yeast. *Nature* 425 (6959), 686–691. doi: 10.1038/nature02026

Ilari, A., Franceschini, S., Bonamore, A., Arenghi, F., Botta, B., Macone, A., et al. (2009). Structural basis of enzymatic (S)-norcoclaurine biosynthesis. *J. Biol. Chem.* 284 (2), 897–904. doi: 10.1074/jbc.M803738200

Jain, D., Khandal, H., Khurana, J. P., and Chattopadhyay, D. (2016). A pathogenesis related-10 protein CaARP functions as aldo/keto reductase to scavenge cytotoxic aldehydes. *Plant Mol. Biol.* 90 (1), 171–187. doi: 10.1007/s11103-015-0405-z

Ka, S., Merindol, N., Sow, A. A., Singh, A., Landelouci, K., Plourde, M. B., et al. (2021). Amaryllidaceae alkaloid cherylline inhibits the replication of dengue and Zika viruses. *Antimicrob. Agents Chemother.* 65 (9), e0039821. doi: 10.1128/aac.00398-21

Kelley, L. A., Mezulis, S., Yates, C. M., Wass, M. N., and Sternberg, M. J. E. (2015). The Phyre2 web portal for protein modeling, prediction and analysis. *Nat. Protoc.* 10 (6), 845–858. doi: 10.1038/nprot.2015.053

Kilgore, M., Augustin, M. M., May, G. D., Crow, J. A., and Kutchan, T. M. (2016a). CYP96T1 of Narcissus sp. aff. pseudonarcissus Catalyzes Formation of the Para-Para' C-C Phenol Couple in the Amaryllidaceae Alkaloids. *Front. Plant Sci.* 7. doi: 10.3389/fpls.2016.00225

Kilgore, M. B., Augustin, M. M., Starks, C. M., O'Neil-Johnson, M., May, G. D., Crow, J. A., et al. (2014). Cloning and Characterization of a Norbelladine 4'-O-Methyltransferase Involved in the Biosynthesis of the Alzheimer's Drug Galanthamine in Narcissus sp. aff. pseudonarcissus. *PloS One* 9 (7), e103223. doi: 10.1371/journal.pone.0103223

Kilgore, M., Holland, C., Jez, J. M., Crow, J. A., and Kutchan, T. M. (2016b). Identification of a noroxomaritidine reductase with Amaryllidaceae alkaloid biosynthesis related activities. *J. Biol. Chem.* 291 (32), 16740–16752. doi: 10.1074/jbc.M116.717827

Kruse, T., Gehl, C., Geisler, M., Lehrke, M., Ringel, P., Hallier, S., et al. (2010). Identification and biochemical characterization of molybdenum cofactor-binding proteins from Arabidopsis thaliana. *J. Biol. Chem.* 285 (9), 6623–6635. doi: 10.1074/jbc.M109.060640

Laursen, T., Borch, J., Knudsen, C., Bavishi, K., Torta, F., Martens, H. J., et al. (2016). Characterization of a dynamic metabolon producing the defense compound dhurrin in sorghum. *Science* 354 (6314), 890–893. doi: 10.1126/science.aag2347

Lichman, B. R., Sula, A., Pesnot, T., Hailes, H. C., Ward, J. M., and Keep, N. H. (2017a). Structural evidence for the dopamine-first mechanism of norcoclaurine synthase. *Biochemistry* 56 (40), 5274–5277. doi: 10.1021/acs.biochem.7b00769

Lichman, B. R., Zhao, J., Hailes, H. C., and Ward, J. M. (2017b). Enzyme catalysed Pictet-Spengler formation of chiral 1,1'-disubstituted- and spiro-tetrahydroisoquinolines. *Nat. Commun.* 8, 14883. doi: 10.1038/ncomms14883

Morris, J. S., Caldo, K. M. P., Liang, S., and Facchini, P. J. (2021). PR10/Bet v1-like proteins as novel contributors to plant biochemical diversity. *ChemBioChem* 22 (2), 264–287. doi: 10.1002/cbic.202000354

Nagahashi, G., Abney, G. D., and Doner, L. W. (1996). A comparative study of phenolic acids associated with cell walls and cytoplasmic extracts of host and non-host roots for AM fungi. *New Phytol.* 133 (2), 281–288. doi: 10.1111/j.1469-8137.1996.tb01895.x

Notredame, C., Higgins, D. G., and Heringa, J. (2000). T-Coffee: A novel method for fast and accurate multiple sequence alignment. *J. Mol. Biol.* 302 (1), 205–217. doi: 10.1006/jmbi.2000.4042

Pfaffl, M. W. (2001). A new mathematical model for relative quantification in real-time RT-PCR. *Nucleic Acids Res.* 29 (9), e45–e45. doi: 10.1093/nar/29.9.e45

Reuten, R., Nikodemus, D., Oliveira, M. B., Patel, T. R., Brachvogel, B., Breloy, I., et al. (2016). Maltose-binding protein (MBP), a secretion-enhancing tag for mamMalian protein expression systems. *PloS One* 11 (3), e0152386. doi: 10.1371/journal.pone.0152386

Roth, S., Kilgore, M. B., Kutchan, T. M., and Muller, M. (2018). Exploiting the catalytic diversity of short-chain dehydrogenases/reductases: versatile enzymes from plants with extended imine substrate scope. *Chembiochem* 19 (17), 1849–1852. doi: 10.1002/cbic.201800291

Saliba, S., Ptak, A., and Laurain-Mattar, D. (2015). 4′-O-methylnorbelladine feeding enhances galanthamine and lycorine production by Leucojum aestivum L. shoot cultures. *Eng. Life Sci.* 15 (6), 640–645. doi: 10.1002/elsc.201500008

Samanani, N., and Facchini, P. J. (2002). Purification and characterization of norcoclaurine synthase. *J. Biol. Chem.* 277 (37), 33878–33883. doi: 10.1074/jbc.M203051200

Samanani, N., Liscombe, D. K., and Facchini, P. J. (2004). Molecular cloning and characterization of norcoclaurine synthase, an enzyme catalyzing the first committed step in benzylisoquinoline alkaloid biosynthesis. *Plant J.* 40 (2), 302–313. doi: 10.1111/j.1365-313X.2004.02210.x

Singh, A., and Desgagné-Penix, I. (2017). Transcriptome and metabolome profiling of Narcissus pseudonarcissus 'King Alfred' reveal components of Amaryllidaceae alkaloid metabolism. *Nat. Sci. Rep.* 7 (1), 17356–17370. doi: 10.1038/s41598-017-17724-0

Singh, A., Massicotte, M.-A., Garand, A., Tousignant, L., Ouellette, V., Bérubé, G., et al. (2018). Cloning and characterization of norbelladine synthase catalyzing the first committed reaction in Amaryllidaceae alkaloid biosynthesis. *BMC Plant Biol.* 18, 338–350. doi: 10.1186/s12870-018-1570-4

Sterling, T., and Irwin, J. J. (2015). ZINC 15–ligand discovery for everyone. *J. Chem. Inf. modeling* 55 (11), 2324–2337. doi: 10.1021/acs.jcim.5b00559

Sun, B., Wang, P., Wang, R., Li, Y., and Xu, S. (2018). Molecular Cloning and Characterization of a meta/para-O-Methyltransferase from Lycoris aurea. *Int. J. Mol. Sci.* 19 (7), 1911–1927. doi: 10.3390/ijms19071911

Tousignant, L., Diaz-Garza, A. M., Majhi, B. B., Gélinas, S.-E., Singh, A., and Desgagne-Penix, I. (2022). Transcriptome analysis of Leucojum aestivum and identification of genes involved in norbelladine biosynthesis. *Planta* 255 (2), 30. doi: 10.1007/s00425-021-03741-x

Vimolmangkang, S., Deng, X., Owiti, A., Meelaph, T., Ogutu, C., and Han, Y. (2016). Evolutionary origin of the NCSI gene subfamily encoding norcoclaurine synthase is associated with the biosynthesis of benzylisoquinoline alkaloids in plants. *Sci. Rep.* 6, 26323. doi: 10.1038/srep26323

Wang, R., Han, X., Xu, S., Xia, B., Jiang, Y., Xue, Y., et al. (2019). Cloning and characterization of a tyrosine decarboxylase involved in the biosynthesis of galanthamine in Lycoris aurea. *PeerJ* 7, e6729. doi: 10.7717/peerj.6729

Wang, P., Li, L.-F., Wang, Q.-Y., Shang, L.-Q., Shi, P.-Y., and Yin, Z. (2014). Anti-dengue-virus activity and structure-activity relationship studies of lycorine derivatives. *ChemMedChem* 9 (7), 1522–1533. doi: 10.1002/cmdc.201300505

Yamashita, A., Kato, H., Wakatsuki, S., Tomizaki, T., Nakatsu, T., Nakajima, K., et al. (1999). Structure of tropinone reductase-II complexed with NADP+ and pseudotropine at 1.9 A resolution: implication for stereospecific substrate binding and catalysis. *Biochemistry* 38 (24), 7630–7637. doi: 10.1021/bi9825044

Yang, J., and Zhang, Y. (2015). I-TASSER server: new development for protein structure and function predictions. *Nucleic Acids Res.* 43 (W1), W174–W181. doi: 10.1093/nar/gkv342

Zhang, Y., Beard, K. F. M., Swart, C., Bergmann, S., Krahnert, I., Nikoloski, Z., et al. (2017). Protein-protein interactions and metabolite channelling in the plant tricarboxylic acid cycle. *Nat. Commun.* 8, 15212–15212. doi: 10.1038/ncomms15212

Zhang, Y.-N., Zhang, Q.-Y., Li, X.-D., Xiong, J., Xiao, S.-Q., Wang, Z., et al. (2020). Gemcitabine, lycorine and oxysophoridine inhibit novel coronavirus (SARS-CoV-2) in cell culture. *Emerging Microbes infections* 9 (1), 1170–1173. doi: 10.1080/22221751.2020.1772676

frontiers | Frontiers in Plant Science

TYPE Original Research
PUBLISHED 13 September 2023
DOI 10.3389/fpls.2023.1205725

OPEN ACCESS

EDITED BY
Zhixing Qing,
Hunan Agricultural University, China

REVIEWED BY
Špela Baebler,
National Institute of Biology (NIB), Slovenia
Qi Jialong,
Chinese Academy of Medical Sciences and Peking Union Medical College, China
Xin Zeng,
Huaibei Normal University, China

*CORRESPONDENCE
Marek Mutwil
mutwil@ntu.edu.sg

RECEIVED 14 April 2023
ACCEPTED 21 August 2023
PUBLISHED 13 September 2023

CITATION
Poh WH, Ruhazat NS, Yang LK, Shivhare D, Lim PK, Kanagasundaram Y, Rice SA and Mutwil M (2023) Transcriptomic and metabolomic characterization of antibacterial activity of *Melastoma dodecandrum*. *Front. Plant Sci.* 14:1205725. doi: 10.3389/fpls.2023.1205725

Transcriptomic and metabolomic characterization of antibacterial activity of *Melastoma dodecandrum*

Wee Han Poh[1,2], Nur Syahirah Ruhazat[2], Lay Kien Yang[3], Devendra Shivhare[2,4], Peng Ken Lim[2], Yoganathan Kanagasundaram[3], Scott A. Rice[1,5] and Marek Mutwil[2*]

[1]Singapore Centre for Environmental Life Sciences Engineering, Nanyang Technological University, Singapore, Singapore, [2]School of Biological Sciences, Nanyang Technological University, Singapore, Singapore, [3]Shared Analytics, Singapore Institute of Food and Biotechnology Innovation (SIFBI), Agency for Science, Technology, and Research (A*STAR), Singapore, Singapore, [4]AAVACC PTE LTD, Singapore, Singapore, [5]Agriculture and Food, Microbiomes for One Systems Health, Commonwealth Scientific and Industrial Research Organisation (CSIRO), Canberra, ACT, Australia

Antibacterial resistance poses a significant global threat, necessitating the discovery of new therapeutic agents. Plants are a valuable source of secondary metabolites with demonstrated anticancer and antibacterial properties. In this study, we reveal that *Melastoma dodecandrum* exhibits both bacteriostatic and bactericidal effects against *Pseudomonas aeruginosa* and *Staphylococcus aureus*. Treatment with plant extracts results in membrane damage and a reduction in *P.aeruginosa* swimming and swarming motility. A comparative analysis of bacterial transcriptomes exposed to M.dodecandrum extracts and four distinct antibiotics indicates that the extracts may trigger similar transcriptomic responses as triclosan, a fatty acid synthesis inhibitor. Activity-guided fractionation suggests that the antibacterial activity is not attributable to hydrolyzable tannins, but to unidentified minor compounds. Additionally, we identified 104 specialized metabolic pathways and demonstrated a high level of transcriptional coordination between these biosynthetic pathways and phytohormones, highlighting potential regulatory mechanisms of antibacterial metabolites in M.dodecandrum.

KEYWORDS

co-expression analysis, antimicrobial, fractionation, Melastoma, Pseudomonas, metabolism, transcriptomics

Introduction

Antimicrobial resistance (AMR) has been identified by the World Health Organization (WHO) as one of the top ten global health threats affecting humanity (Antimicrobial resistance). This problem is exacerbated by the lack of new effective antibacterials within clinical pipelines (Antimicrobial resistance). Breakthroughs in genomics and bioinformatics in the 90s enabled the identification of essential bacterial genes and targets. Consequently, pharmaceutical companies have attempted to generate new leads via target-based rational drug design. However, this strategy had limited success, partly due to an incomplete understanding of resistance mechanisms and factors influencing drug membrane permeability (Payne et al., 2007; Tommasi et al., 2015; Lewis, 2020). Alternatively, bioprospecting, the examination of natural sources for active bioproducts, may be considered in the search for new antibacterial compounds. To this end, the plant kingdom represents a rich source of plant secondary metabolites, many of which are known to have antimicrobial properties and have been used in traditional medicine to treat bacterial infections (Ríos and Recio, 2005; Frey and Meyers, 2010; Kessler and Kalske, 2018; Singh et al., 2018; Lal et al., 2020).

While bioprospecting may enable the discovery of more target-specific and structurally complex active biological compounds, it comes with associated challenges (Cushnie et al., 2020). For example, there may be difficulties in isolating and identifying active compounds from biological extracts which may be further compounded if there are multiple active compounds that contribute synergistically to the therapeutic activity of the extract. Similarly, the subsequent elucidation of the mechanism of action of an active compound may also be a tedious process (Atanasov et al., 2021). Additionally, the further use and industrial production of plant metabolites may be hindered by a limited understanding of their biosynthetic pathways and that the active metabolites may only be produced under specific conditions in specific organs (Kumar et al., 2019; Atanasov et al., 2021). Multi-omics methods, consisting of a combination of transcriptomics, metabolomics, genomics and/or proteomics, have been utilized in the drug discovery process and have been recognized as a useful tool to identify new targets and the mechanisms of lead compounds (Goff et al., 2020). The multi-omics strategy may also be used to discover plant metabolic genes and pathways using co-expression analysis and metabolite-based genome-wide association studies (Zhan et al., 2022; Zhao and Rhee, 2022; Julca et al; Usadel et al., 2009; Lim et al., 2022). Taken together, such multi-omics approaches may represent the means to address challenges associated with bioprospecting and bridge the knowledge gap.

Members of the Melastoma genus, such as *Melastoma malabathricum*, *Melastoma candidum D. Don*, and *Melastoma dodecandrum*, have long been used in areas such as Malaysia, Taiwan, and China as traditional medicine for the treatment of dysentery, wounds, high blood pressure, diabetes, and skin diseases, amongst others (Wang et al., 2008; Joffry et al., 2012). More recently, studies have been carried out to scientifically evaluate *M. malabathricum* and *M. candidum D. Don* for acute toxicity, and antibacterial, antioxidant, and immunomodulatory activities (Alnajar et al., 2012; Wong et al., 2012; Che Omar et al., 2013; Mamat et al., 2013; Zheng et al., 2021). Similarly, efforts have been made to identify the chemical constituents of *M. dodecandrum* and its associated activities (Yang et al., 2014; Wang et al., 2017; Tong et al., 2019; Huang et al., 2021; Xu et al., 2023). However, limited studies have been carried out on evaluating the antimicrobial activity of the plant and identifying associated active compounds or mechanisms, with only a recent paper reporting moderate antibacterial activity of its ethanolic extract against diarrheagenic bacterial pathogens following an activity screen of 32 plants (Kudera et al., 2021).

Through the screenings conducted in this study, we have identified *M. dodecandrum Lour.* as a plant with antimicrobial and bactericidal effects on *Pseudomonas aeruginosa*. Phenotypic studies on *P. aeruginosa* indicate that the plant's active compounds likely result in membrane damage and affect bacteria motility. Additionally, a comparative transcriptomic analysis of *P. aeruginosa* suggests that out of four antibiotics that target various vulnerabilities of bacteria, the plant extract's mode of action overlaps with triclosan. Subsequent evaluation of fractions of the plant extract and activity testing of purified compounds suggests that an unknown compound is responsible for the antibacterial activity. By collecting samples of different organs, and carrying out transcriptomics studies and co-expression analysis, we investigated the biosynthetic potential of M.dodecandrum and showed that the plant likely synthesized many types of phenylpropanoids, with high levels of expression of sulfur-containing compounds, phenylpropanoids, and terpenoids. Finally, we showed co-expression patterns between the specialized metabolic pathways and hormones, suggesting that the pathways in the plant are transcriptionally linked.

Methods

Bacterial strains and culture conditions

P. aeruginosa PAO1 (ATCC BAA-47) was maintained on Luria-Bertani agar containing 10 g/L NaCl (LB10) (644520, Difco). *S. aureus* 25923 was maintained on TSB agar (236920, Difco). Cultures were routinely cultured in 10 mL LB10 media (244620, Difco) at 37°C with 200 rpm shaking overnight.

Plant sampling

The flowers, fruits, leaves, stems, and roots of *M. dodecandrum* were sampled from the NTU Community Herb Garden. Leaves used solely for bioactivity screening were transported in dry ice and lyophilized using a freeze dryer (Labconco). Plant organs used for both bioactivity and transcriptomic studies were transported in liquid nitrogen.

Metabolite extraction

Plant material was ground in liquid nitrogen to a fine powder. One hundred mg of the powder was aliquoted into a screw cap tube. Three 3 mm steel beads and 500 µL of 80% HPLC-MS grade methanol were then added. The sample was subsequently homogenized for two cycles at 2000 rpm (PowerLyzer 24, Qiagen). The steel beads were removed, and the samples were placed on a shaker for 10 mins at 1500 rpm at room temperature in the dark. The samples were centrifuged at 10 min, 12000 × g. The supernatant was transferred into a new 2 mL Eppendorf tube and kept on ice. Five hundred µL of 80% HPLC-MS grade methanol was added to the remaining pellet, and the shaking and centrifuge step was repeated twice until 1.5 mL of supernatant was collected. The supernatant was dried completely using a centrifugal vacuum concentrator (Centrivap, Labconco) and dissolved in 100 – 500 µL of DMSO before use.

Antimicrobial screening and activity testing

Dried methanol extracts derived from 100 mg of plant material or different plant organs were dissolved in 500 µL DMSO to give a stock solution of 200 mg/mL plant material. Overnight bacterial cultures were subcultured 1:10 in 10 mL of LB10 broth until the bacteria reached the exponential phase. Exponential phase bacteria were then diluted in Mueller-Hinton broth (MHB) to a final concentration of 5×10^5 CFU/mL, and 2 µL of the stock DMSO solution was added to 100 µL of MHB to a final concentration of 4 mg/mL starting plant material or 2% v/v DMSO. Evaluation of HPLC fractions was carried out at 2% v/v DMSO, with each fraction corresponding to ~10 mg/mL mass equivalent of the crude methanol extract.

Extraction, bioassay guide fractionation, and chemical characterization

Freeze-dried leaves of *M. dodecandrum* (11 g) were milled and extracted twice with 400 mL of methanol (MeOH). The combined MeOH extract was dried under reduced pressure to afford 3 g of dried MeOH extract. Crude MeOH extract (2 g) dissolved in 5 mL of MeOH was fractionated using a Sephadex LH20 open column (5 x 35 cm). Compounds were eluted sequentially with 1 L of MeOH, 50% aqueous acetone, and acetone to generate 13 fractions. Biological testing results showed activity in only one fraction (58K, 120 mg) which was eluted in the acetone eluent.

50 mg of active fraction 58K was reconstituted in 15% aqueous MeOH, sonicated, and centrifuged. The insoluble pellet was collected (labeled as PPT, 5 mg) while the supernatant was injected into a Waters XTerra Prep MS C18 Column (10 x 300 mm) on an Agilent 1260 Infinity II Preparative HPLC system. The mobile phase consisted of water (A) and acetonitrile (B), both with 0.1% formic acid. The gradient elution started at 15% B for 5 mins, 15-30% B in 20 mins, 30-60% B in 25 mins, held at 60% for 10 mins, then increased from 60-100% B in 2 mins and washed at 100% B for 10 mins. The flow rate was 20 mL/min and the detection UV wavelength was at 254 nm. 8 fractions were generated from the preparative HPLC. All HPLC fractions, PPT and parent fraction 58K were submitted for biological evaluation.

Purified fractions were analyzed on an Agilent UPLC1290 coupled with a Quadrupole Time-of-Flight (Q-TOF) system. Separation was carried out with a reversed-phase C18 column (2.1 x 50 mm) at 0.5 mL/min, using a 10 mins linear gradient with 0.1% formic acid in both solvent A (water) and solvent B (acetonitrile). The typical QTOF operating parameters were as follows: negative ionization mode; sheath gas nitrogen flow, 12 L/min at 275°C; drying gas nitrogen flow, 8 L/min at 250°C; nebulizer pressure, 30 psi; nozzle voltage, 1.5 kV; capillary voltage, 1.5 kV. Lock masses in negative ion mode: TFA anion at m/z 112.9856 and HP-0921 TFA adduct at m/z 1033.9881. 1H NMR spectra were acquired on a Bruker DRX-400 NMR spectrometer with a 5-mm BBI Cryoprobe.

Determination of minimum inhibitory concentrations

Minimum inhibitory concentrations (MIC) were determined using broth microdilution methods as described in (Wiegand et al., 2008). Briefly, plant extracts or equivalent concentrations of DMSO were diluted in MHB to four times the desired final concentration. 50 µL of the samples were added to 50 µL of MHB media on the first column of a 96-well plate, then serially diluted two-fold down the row. Untreated media-only growth control wells were also included. Overnight cultures of PAO1 were subcultured in LB10 medium and further incubated at 37°C with 200 rpm shaking. Exponential phase cells were then diluted in MHB to 1×10^6 CFU/mL. Fifty µL of the bacterial culture was added to each well to a final concentration of 5×10^5 CFU/mL, with the final concentration of plant extract falling between 0 – 50 mg/mL (0 – 5% DMSO). Sterility control wells, consisting of only MHB media, and blank control wells, containing 0 – 50 mg/mL of plant extract and MHB media, were also included. The 96-well plate was incubated for 24 h at 37°C with OD readings taken at 600 nm every 10 mins using a microplate reader (Tecan M200). Readings from blank control wells were subtracted from wells with bacteria added to account for high background readings at high plant extract concentrations. MIC was similarly determined for 0 – 512 µg/mL of the antibiotics and antimicrobial compounds triclosan, rifampicin, ceftazidime, and gentamicin. MIC was defined as the first concentration at which no growth is observed after 24 h incubation.

Antibacterial activities across experiments were compared using the area under the curve (AUC), which represents bacterial growth over a period of 18 h. The AUC is calculated using Graphpad prism (version 9.3.0). The same parameters (t = 0 - 1080 mins) were used for all data. Eighteen hours were used for the AUC calculations even though OD data were collected over 24 h, as cell growth has already plateaued and increased noise was observed at later time points, possibly due to evaporation of the small volume of medium used.

The AUC values were plotted and compared using one-way ANOVA with multiple comparisons in Graphpad prism.

Time-kill kinetics assay

Overnight cultures of PAO1 were subcultured in LB10 medium and further incubated at 37°C with 200 rpm shaking. Exponential phase cells were diluted to 1×10^6 CFU/mL in MHB media and treated with 0 – 2 × MIC of plant extract. Vehicle controls were treated with equivalent volumes of 0 – 5% v/v DMSO. At each timepoint, samples were collected for serial dilution in PBS and CFU enumeration. Five µL of each dilution was spot plated onto LB10 agar plates and incubated at room temperature overnight. The first spots containing between 3 – 30 colonies were counted. The assay was carried out independently twice with two technical replicates each time.

Evaluation of membrane integrity

The effect of plant extract on membrane integrity was evaluated using the LIVE/DEAD stain (L7012, Thermo Fischer) and microtiter plate reader (Tecan) as described in the commercial protocol. Briefly, sub-cultured exponential phase bacterial cells were washed in 1 × PBS (PBS). 5×10^7 CFU/mL of bacterial cells diluted in PBS were subsequently treated with a non-inhibitory concentration of 0 – 4 mg/mL of filtered plant extract or equivolume of DMSO for 10 mins. Samples were then treated for a further 30 mins with LIVE/DEAD stain readings taken with excitation at 485 nm and emission at 535 (red) and 635 nm (green). Dead cells were prepared via incubation of bacteria at 65° C for 30 mins. The percentage of live cells is determined using a standard curve generated through a mixture of live and dead cells and the calculation of the green/red fluorescence ratio as stated in the commercial protocol. When LIVE/DEAD stain is used in microscopy, 2×10^7 cells were seeded into a well of a poly-L lysine pre-treated ibidi 8-well chamber slide (80826, ibidi). The cells were allowed to attach for 10 mins before each well was washed and treated for 10 mins with 0 - 16 mg/mL of plant extract or equivolume of 0 - 1.6% v/v DMSO. Following treatment, each well was washed again and stained with LIVE/DEAD stain as described in the commercial protocol. At least three images per sample were taken using an epifluorescence microscope (Axio Observer Z1, Carl Zeiss) using the FITC filter for imaging SYTO 9 fluorescence and AF 568 filter for imaging propidium iodide (PI) staining. Images of fluorescence staining were analyzed using Image J.

Motility assays

Swimming and swarming assays with *P. aeruginosa* were carried out similarly to (Ha et al., 2014a; Ha et al., 2014b). Briefly, 0.3% w/v or 0.5% w/v of 1X M8 agar (1X M8 solution: 42.3 mM Na_2HPO_4, 22 mM KH_2PO_4, 8.56 mM NaCl) were prepared for use in swimming and swarming assay respectively. Plant extracts or equivalent volumes of DMSO were added to the well with the highest concentration of the extracts, then serially diluted 4-fold down the wells before the agar solidified to a final concentration of 0 – 4 mg/mL plant extract. The agar was dried under laminar flow for 45 mins and used immediately after drying. Overnight cultures of PAO1 were used for inoculation. The agar was inoculated either by dipping an Eppendorf pipette tip into the culture and then stabbing it midway of the depth of the agar (swimming assay) or by spotting 1 µL of the culture on the surface of the agar at the centre of the well (swarming assay). Following inoculation, the plates were incubated at 30°C overnight and the images were taken 16 h after inoculation. Swimming and swarming areas were assessed using Image J by setting an appropriate scale and selecting the region of interest. The resulting values are plotted in Graphpad (9.3.0) and analyzed using one-way ANOVA with multiple comparisons against the control group.

RNA extraction and sequencing

Following *M. dodecandrum* sample collection and grinding into a fine powder (as described in 'Metabolite extraction'), RNA was extracted from 100mg of a sample using Spectrum™ Total Plant RNA Kit (Sigma) Protocol A following manufacturer's instructions. Three biological replicates were collected for each adult organ, while single replicates were collected for the young flowers. To extract RNA from bacteria (PAO1), overnight cultures of PAO1 were first subcultured and grown to mid-log phase. Cells were adjusted to OD=0.4 and then treated with equivolume of 2X antibiotic dissolved in MHB medium to a final concentration of OD=0.2, MIC=1X (or 25 mg/mL plant extract and 128 µg/mL triclosan), and a final volume of 500 µL. The samples were incubated at 37°C statically for 30 mins. Following treatment, 1 mL of RNA protect reagent (76506, Qiagen) was added to 500 µL of the sample. The sample was treated as described in the commercial kit and the dried pellet was stored at -80°C. RNA was extracted using the RNeasy plus mini kit (Qiagen) as per the kit's instructions. For both plant and bacteria, quality control of all extracted RNA was carried out by Novogene (Singapore). Each sample was evaluated for its quantity, integrity, and purity using agarose gel electrophoresis, Nanodrop, and Agilent 2100 Bioanalyzer. Library construction was performed by Novogene where mRNA of plants was enriched from total RNA with oligo(-dT) magnetic beads. No ribosomal RNA depletion was performed for bacteria library construction due to high sequencing depth. The library was quantified with Qubit and real-time PCR, and then sequenced using Illumina NovaSeq 6000, with paired-end sequencing of 150 base pairs (bp) per read and a sequencing depth of approximately 60-70 million reads.

RNA sequencing analysis (*P. aeruginosa*)

Low-quality RNA-seq reads were removed, and the remaining reads were trimmed with fastp (v0.23.2)(Chen et al., 2018). Reads were then aligned to the PAO1 genome (NC_002516.2) and read

counts were obtained using EDGE-pro (Magoc et al., 2013). Due to poor overall read alignment, one DMSO-treated sample (replicate 1) was discarded (data not shown). One-third of the reads from the remaining two DMSO-treated samples were removed and collated to form a new third replicate. To evaluate sample-level variability, read counts were transformed using variance-stabilizing transformation, followed by hierarchical clustering of samples using Euclidean distance as the distance metric (Love et al., 2014). Differentially expressed genes (DEGs) between each antibiotic-treated sample compared to the DMSO control were identified with read counts using DESeq2. Genes with $|log_2$fold change$| \geq 1$ and Benjamini-Hochberg (BH) adjusted p-value< 0.01 were considered significant (Benjamini and Hochberg, 1995) for multiple-testing correction. Gene ontology (GO) enrichment analysis was performed via the GO webtool on each list of significant DEGs against the PAO1 GO biological process data set by applying Fisher's Exact test with BH correction (adjusted p-value< 0.01)(Mi et al., 2019; The Gene Ontology Consortium, 2021).

M.dodecandrum gene expression data preprocessing

Quality control and read trimming of raw RNA-seq data were performed with fastp (v0.23.2). To obtain normalized transcript abundances (transcripts per million; TPM) of the RNA-seq samples, the reads were pseudoaligned against the coding sequences of the *M.dodecandrum* genome (PRJCA005299 from the National Genomics Data Center)(Hao et al., 2022) and quantified using Kallisto (v0.46.1)(Bray et al., 2016). To evaluate sample-level variability, samples were clustered using Spearman's correlation as the distance metric - $d_{x,y} = 1 - |\rho_{x,y}|$, where x and y are vectors comprising TPM expression profiles for all transcripts of a pair of RNA-seq samples respectively and ρ is the Spearman correlation coefficient. The final gene expression matrix was derived after filtering out genes with an average TPM of 0 across all organs. Genes were translated into protein sequences using the transeq module (EMBOSS v6.6.0.0)(Rice et al., 2000).

The following analyses were performed in M.dodecandrum

Enzyme annotation and pathway prediction

Enzyme annotation and pathway prediction were performed following the pipeline described by (Hawkins et al., 2021). Briefly, protein sequences were annotated with E2P2 (v4), pathway membership was predicted using PathoLogic in PathwayTools (v26) with default settings, and semi-automated validation of the final pathways was performed by SAVI (v3.1). All pathways assigned to the manual-to-validate list by SAVI were retained except for PWY0-501 and PWY-5723, following recommended validation steps by SAVI. From SAVI's list of pathways to add, PWY-5173 was discarded as it is a deprecated ID in the current version of MetaCyc used by PathwayTools.

Gene co-expression and pathway subcluster identification

To determine if genes within an SM pathway are more co-expressed than by chance, Pearson's correlation coefficient (PCC) for each gene-pair within a pathway was first calculated. To simulate random pathways, a list of pathway-labeled gene-pairs was generated. The pathway labels were then randomly shuffled amongst the gene-pairs. The PCC for each gene-pair was calculated, and the median PCC of each random pathway was extracted. This was repeated 100 times.

To identify subclusters of a pathway, genes within a pathway were hierarchically clustered based on their pattern of expression across samples using the dendrogram function from scipy with default parameters (where the distance threshold is 70% of the maximum dendrogram distance). A representative subcluster was only identified for a pathway if the subcluster consisted of genes that represented at least 75% of the annotated reactions in the pathway in the plant (degree of completeness). As some pathways have multiple genes catalyzing the same reaction, subclusters of differing sizes can have the same degree of completeness. In these cases, the largest subclusters will be chosen as representative subclusters. For pathways with no representative sub-cluster, the original pathway was the representative 'sub-cluster' in downstream analyses.

Co-expression analysis of connected pathways

To investigate patterns of inter-pathway coexpression within and between SM classes, we generated a pathway coexpression network. First, gene-pairs of all SM genes were calculated using the 'pearsonr' function from the scipy package. Then, p-values were corrected with the BH method (Benjamini and Hochberg, 1995). Gene-pairs with PCC ≥ 0.6 and BH-adjusted p-value (two-tailed)$<$ 0.05 were considered significant. Subsequently, the gene nodes within the gene co-expression network were labeled with their respective SM pathways (as determined by pathway prediction). Multiple pathway labels will be assigned to genes that are predicted to be involved in multiple SM pathways. Labels of "Superpathways", defined as pathways that combine individual pathways, will only be assigned to a gene if the gene is not already labeled with their respective subpathways.

Next, to determine if the intra-pathway coexpression was better than random, the network was then subjected to the following permutation analysis: for each pathway, the number of intra-pathway edges was counted. Pathway labels were then randomly shuffled and the number of intra-pathway edges was counted. The following empirical p-value was calculated for each pathway:

$$p - value = \frac{\sum_{n=1}^{N} I(edge_{observed} \leq edge_{randomized})}{N}$$

where N is the number of permutations, I is an indicator function that takes a value of 0 or 1 if the statement is false or true, respectively. This was repeated 10 000 times. Pathways with BH-adjusted p-values of< 0.05 were considered to be coexpressed (gene members of the particular pathway are coexpressed with each other). Inter-pathway coexpression between pathway-pairs were also determined similarly by counting inter-pathway edges that connect genes across any given two pathways.

To generate a pathway coexpression network, edges were used to connect SM pathways (represented as nodes) that were coexpressed with each other. Nodes were named according to the SM classes each pathway belongs to. Each node has a suffix of "_X" where X represents a single pathway from an SM class. e.g., if a PWY-A belongs to Y number of SM classes, then there will be Y number of PWY-A nodes in the network ("PWY-A_1, "PWY-A_2", …, "PWY-A_Y") while each edge joins 2 significantly coexpressed pathways.

Results

Melastoma dodecandrum Lour. shows antimicrobial activities

To assess the antimicrobial activity of *M. dodecandrum*, we sampled roots, petioles, leaves, vegetative branches, stems, fruits, and flowers from the Nanyang Technological University herb

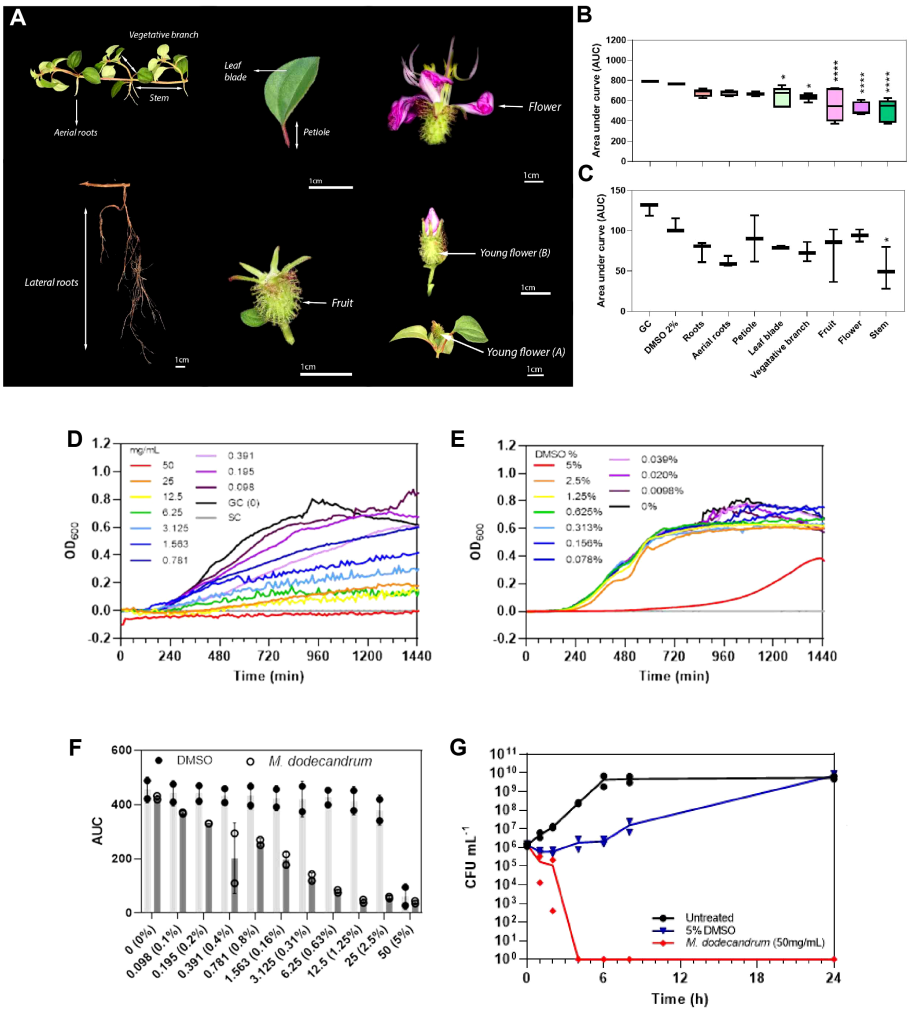

FIGURE 1
Antibacterial activities of *M. dodecandrum*. **(A)** Various organs of *M. dodecandrum Lour* were collected for evaluating antimicrobial activity. The antibacterial activity of each plant organ against **(B)** *P. aeruginosa* PAO1 and **(C)** *S. aureus* 25923 was assessed using 2% v/v of plant methanol extract (~4 mg/mL). The area under the growth curve (AUC) over 18 hours was measured and plotted. GC = Growth control (untreated bacteria in media). Boxplots represent data from at least two biological replicates, with differences in activity evaluated using one-way ANOVA with multiple comparisons against the 2% v/v DMSO control. *, P,< 0.05; ****, P,<0.0001. **(D–G)** Antibacterial activity of methanol plant extract from *M. dodecandrum* leaves was further evaluated in P.aeruginosa at higher concentrations of 0-50 mg/mL **(D)** and equivalent DMSO concentrations of 0-5% v/v **(E)** over 24 hours. The AUC over 18 hours was plotted in **(F)**, the open and closed circles represent data from two biological replicates while error bars represent the standard deviation of the mean. **(G)** The time-kill activity of 50 mg/mL of methanol plant extract from *M. dodecandrum* leaves or equivalent volumes of DMSO was assessed over 24 hours, with data points from each biological replicate plotted.

garden in Singapore (Figure 1A), and tested the antibacterial activity of methanol extracts derived from these organs. Bacterial growth inhibition studies indicated that the plant has antibacterial activity against gram-negative *P. aeruginosa* (Figure 1B; Table S2) and gram-positive *S. aureus* (Figure 1C; Table S2). When tested at 2% v/v (~4 mg/mL extract) against *P. aeruginosa*, the stems showed the highest activity with a 33.13% (ANOVA, $p< 0.0001$) inhibition in growth over 18 h as compared to the DMSO controls, followed by flowers (32.56%), fruits (27.9%), leaves (15.54%), and roots (11.26%) (Figure 1B). Similarly, the stems showed the highest activity against *S. aureus* with 50.21% growth inhibition ($p< 0.05$) (Figure 1C). The vegetative branch, fruit, roots, and leaves showed moderate activity in a descending order ranging from 30.02 – 24.27% growth inhibition. In comparison, the flowers and petiole showed the lowest activity against *S. aureus* at 10.67 and 14.15% growth inhibition, respectively (Figure 1C).

Next, we evaluated the minimum inhibitory concentration (MIC), defined as the concentration at which no growth is observed after overnight incubation. While leaves did not have the strongest activity amongst all organs (Figure 1B), they were the most abundant and easiest to collect. Hence, leaf methanol extract was used to evaluate the MIC of the extract on *P. aeruginosa* via a broth microdilution method. Complete growth inhibition was achieved when the extract was used at 50 mg/mL (Figures 1E, F, Table S4). The inhibitory effect was concentration dependent, with > 50% growth inhibition by 1.563 mg/mL of the extract compared to treatment with equivalent volumes of DMSO (Figures 1E, F, Tables S4, S5). While 5% v/v DMSO treatment resulted in longer lag times, growth resumed by 720 min (Figure 1D).

The leaf methanol extract was bactericidal at 50 mg/mL, with complete cell death within four hours after treatment (Figure 1G, Table S6). In contrast, with the addition of equivalent 5% v/v DMSO, *P. aeruginosa* CFU recovered by 24 h (7.00×10^9 CFU/mL) to levels comparable to that of untreated samples (5.65×10^9 CFU/mL) (Figure 1G). A lower cell count was measured from 0 – 8 h with treatment with 25 mg/mL extract (Figure S1), but the bacterial density reached untreated control levels by 24 h. Finally, *P. aeruginosa* treated with 4 mg/mL of the plant extract or equivalent concentrations of DMSO showed similar growth across all time points (Figure S1), suggesting that a higher concentration of the plant extract is needed to achieve growth inhibition of bacteria.

M.dodecandrum extracts cause membrane damage and reduced swimming and swarming motility

To elucidate how the *M. dodecandrum* extracts affect the bacterial viability, we used LIVE/DEAD staining to assess potential membrane damage. The LIVE/DEAD stain consists of two nucleic acid staining dyes, propidium iodide (PI) and SYTO9. The green fluorescing SYTO9 can enter all cells, while the red fluorescing PI can only enter cells with compromised or damaged cytoplasmic membranes. PI, however, has a stronger affinity to DNA and hence can displace SYTO9 if present (Stiefel et al., 2015). While the kit is more accurately said to distinguish between cells with intact or compromised cell membranes, it is more often used to infer populations of living or dead cells under the assumption that all membrane-compromised cells are likely dead.

DMSO, when used at equivalent volumes of 0 – 0.8% v/v and a treatment time of 10 minutes, did not result in increased uptake of PI (Figure 2A, nearly all cells are green), and the proportion of live cells was calculated to be at ~100% across all concentrations of DMSO (Figure 2B). In contrast, 10-minute treatment with 0 – 8 mg/mL of the plant extract resulted in a concentration-dependent increase in PI uptake and a corresponding reduction in the proportion of live cells from ~100% in untreated samples to 13.6% in 8 mg/mL treated samples (Figures 2A, B, nearly all cells are red, Table S7).

Antibacterial compounds can also negatively affect the motility of bacteria, effectively disrupting their pathogenesis (Erhardt, 2016). Microscopy revealed reduced motility of cells treated with *M. dodecandrum* plant extract compared to the DMSO control groups, even at low concentrations of 1 mg/mL, where most *P. aeruginosa* cells appeared alive following 10 mins of treatment (Video 1 and 2 for DMSO control and extract treatment, respectively). To quantify and evaluate the effect of plant extract treatment on *P. aeruginosa* motility, swarming and swimming motility assays were carried out (Figures 2C–F). Swarming motility was significantly impaired at 0.0625 mg/mL ($p< 0.05$) (Figures 2C, D; Table S7), while swimming motility was impaired at 0.25 mg/mL ($p< 0.0001$) (Figures 2E, F; Table S7). These results indicated that *M. dodecandrum* leaf extracts exhibit a multi-pronged effect on *P. aeruginosa*, inhibiting viability, growth, and motility.

Comparative transcriptomic analysis of antibiotic- and extract-induced gene expression changes in *P. aeruginosa*

Antibiotics can stimulate or depress gene expression in bacteria (Shitikov et al., 2022). Studying gene expression changes in responses to antibiotics can help the understanding of the mode of action of the various drug classes on bacterial adaptive ability, physiology, and metabolism. Since different antibiotics can elicit specific transcriptional responses (Hesketh et al., 2011), we hypothesized that gene expression analysis of *P. aeruginosa*-treated *M. dodecandrum* extracts and several antibiotics would allow us to propose the mode of action of the plant extracts.

To see if transcriptome changes caused by our plant extracts are similar to the changes caused by common antibiotics, we performed a comparative RNA sequencing analysis. We treated *P. aeruginosa* with rifampicin (RNA synthesis inhibitor), triclosan (fatty acid synthesis inhibitor), ceftazidime (cell wall synthesis inhibitor), gentamicin (protein synthesis inhibitor), *M. dodecandrum* extracts and DMSO control (Table S8). Notably, rRNA depletion was not needed to obtain a high number (on average ~20 million) of reads mapping to protein-coding genes when increasing the sequencing depth to ~40 million reads (Table S9), indicating that this expensive step can be skipped if sequencing depth can be adjusted.

10.3389/fpls.2023.1205725

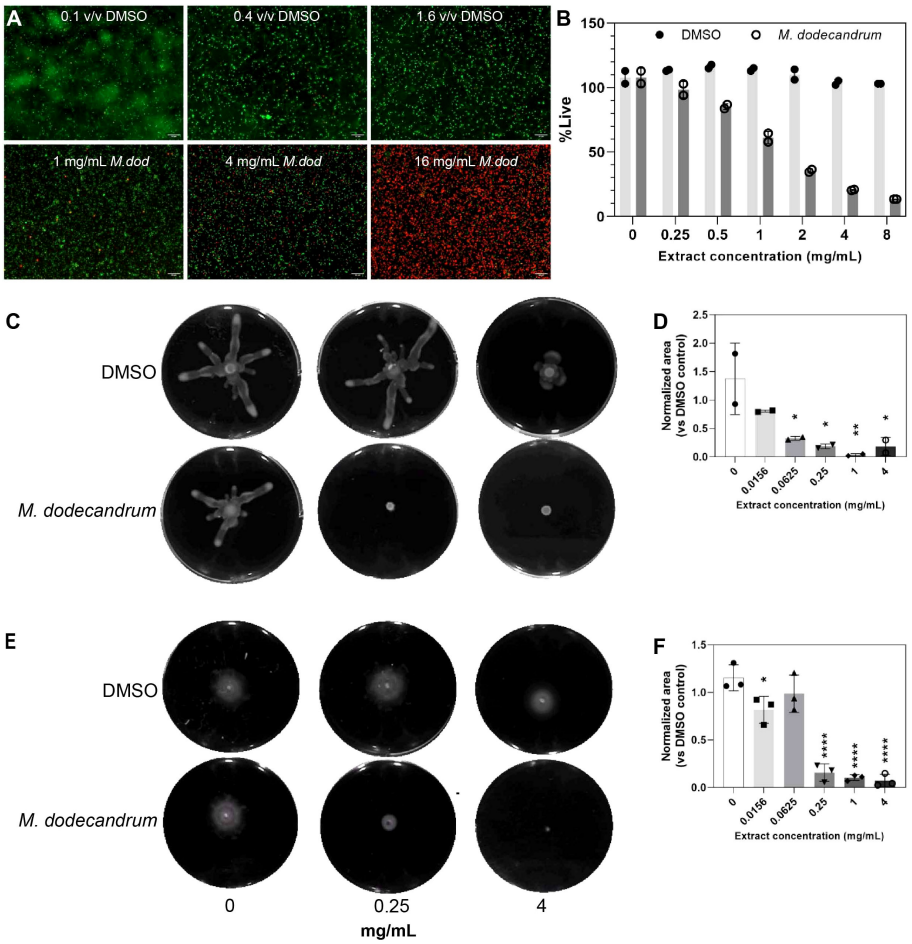

FIGURE 2
Viability, swimming and swarming analysis if P.aeruginosa. **(A)** Confocal microscopy images of P. aeruginosa PAO1 cells treated with equivolume of 0.1% (top left), 0.4% (top middle), or 1.6% v/v (top right) DMSO and 1 mg/mL (bottom left), 4 mg/mL (bottom middle), or 16 mg/mL (bottom right) M. dodecandrum extract and stained with LIVE/DEAD stain. Green and red cells indicate live and dead cells, respectively. **(B)** Percentage of live cells following treatment with 0-8 mg/mL of M. dodecandrum leaf extract or an equal volume of DMSO, as determined using LIVE/DEAD stain and quantified using a microtiter plate reader. Two replicates were performed. **(C)** Swarming area experiment over 0-4 mg/mL M. dodecandrum extract ranges. **(D)** Normalized area values from the swarming area experiments. Two replicates were performed. **(E)** Swimming area experiment over 0-4 mg/mL M. dodecandrum extract ranges. F) Normalized area values from the swimming area experiments. Each data point **(B, D, F)** represents data from at least two independent experiments, with error bars representing the standard deviation of the mean. * = $p \leq 0.05$, ** = $p \leq 0.01$, **** = $p \leq 0.0001$.

Concentrations of extracts and antimicrobial compounds used for RNA-sequencing were selected based on results from microtiter plate growth curves (Figure S2). While 25 mg/mL of the extract did not fully inhibit *P. aeruginosa* growth by 24 h (Figures 1E, H), it was selected over 50 mg/mL as it inhibited growth to a similar extent within 18 h of growth without strong inhibition of growth associated with higher DMSO concentrations at 50 mg/mL (Figure 1F). Rifampicin, ciprofloxacin, and gentamicin were used at 1 × MIC of 32, 0.5, and 2 µg/mL respectively (Figure S2). Lastly, no growth inhibition was observed for triclosan over the range of concentration tested. Higher concentrations of triclosan treatment were not evaluated due to the precipitation of the compound in the media. As such, the highest concentration of 128 µg/mL, where some growth inhibition was observed, was used. DMSO was adjusted to the same concentration of 2.5% v/v for all samples to enable comparison with the control group. The resulting RNA-sequencing data was used to generate the gene expression matrix (Table S10).

Interestingly, the hierarchical clustering analysis of the 18 RNA-seq samples revealed that *M. dodecandrum* extracts show the highest Euclidean distance to all other samples (Figure 3A, *M. dodecandrum* RNA-seq samples form an outgroup). Similarly, rifampicin and triclosan also showed unique transcriptomic responses, while DMSO control, ceftazidime, and gentamicin displayed a similar response (Figure 3A). These responses could be explained by the number of significantly differentially up- (red) and down-regulated genes (Figure 3B, BH-adj. p-value< 0.01). *M.dodecandrum* elicited the highest number of up- (712) and down-regulated (757) genes, followed by rifampicin (331 up, 283 down) and triclosan (250, 135)(Table S11). Conversely, ceftazidime (40, 13) and gentamicin (99, 13) caused the mildest transcriptomic response. Overall, we observed that the M.dodecandrum extracts

10.3389/fpls.2023.1205725

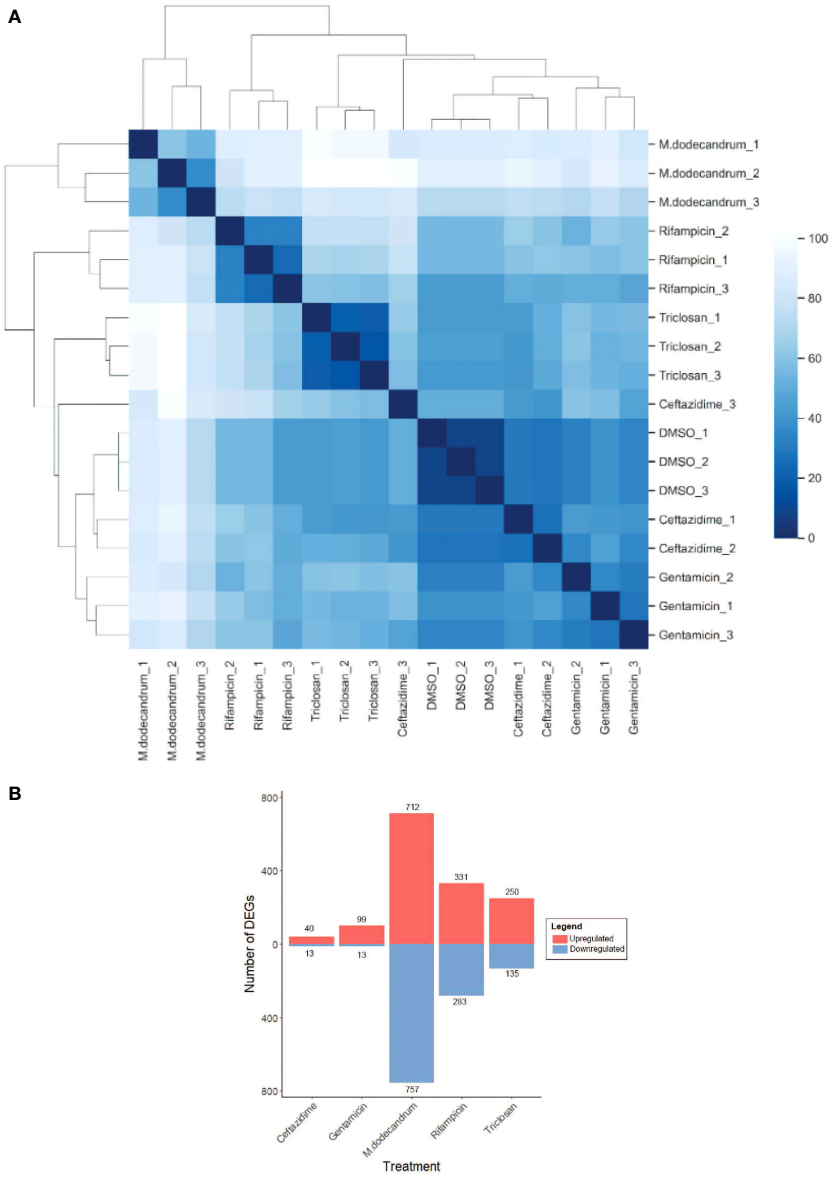

FIGURE 3
Gene expression responses of *P.aeruginosa* to *M. dodecandrum* extracts and four antibiotics. **(A)** Hierarchical clustering of RNA sequencing samples for DMSO, M.dodecandrum extract, and four antibiotics. Each sample type is represented by three replicates, indicated by its suffix. **(B)** The number of significantly differentially expressed genes (BH-adjusted p-value< 0.01), where up- and down-regulated genes are indicated in red and blue bars, respectively.

showed some similarities of the differentially expressed genes with rifampicin and triclosan (Figure S3).

To see which biological processes are differentially expressed, we performed a Gene Ontology enrichment analysis (see methods). We observed that the DEGs caused by triclosan resulted in the highest number of expressed GO terms (Figure S4). These terms comprised many metabolic, biosynthetic, respiration, and macromolecule localization processes. All 8 GO terms enriched in the plant extract-treated samples overlap with triclosan and are mostly metabolic and biosynthetic processes (translation, peptide, amide, protein, and nitrogen compounds). Conversely, rifampicin only induced changes in the type VI secretion system (Figure S4). Interestingly, gentamicin caused changes in terms involved in the high-temperature response (folding, response to heat, and temperature stimulus), while ceftazidime responses were external stimulus and DNA damage (Figure S4). Taken together, these results indicate the M.dodecandrum extracts may have an overlapping mode of action with triclosan (fatty acid synthesis inhibitor).

The antibacterial activity is conferred by unidentified metabolites

To identify the antibacterial compounds in M.dodecandrum, we performed a bioassay-guided purification on the MeOH extract

10.3389/fpls.2023.1205725

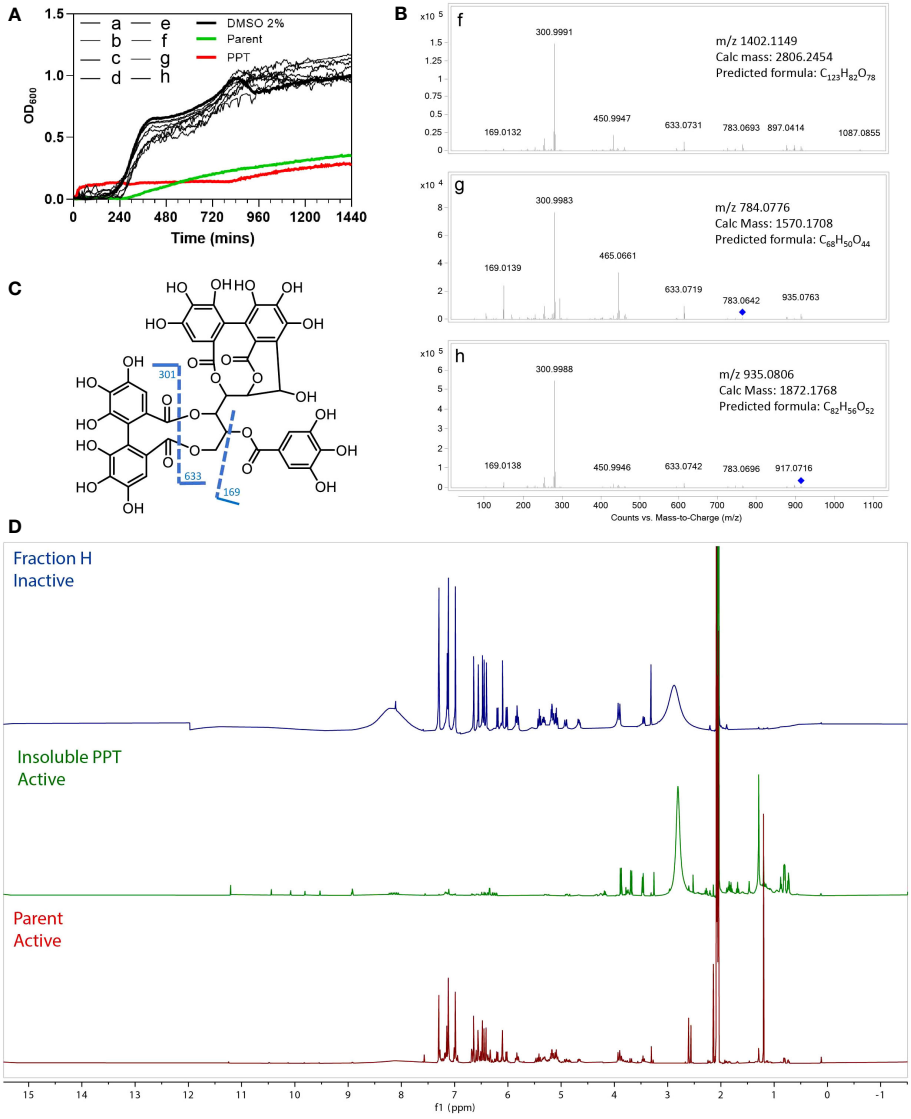

FIGURE 4
Bioassay results for HPLC fractions A-H, Parent fraction, and insoluble pellet (PPT). **(A)** Antibacterial activity of eight HPLC fractions(A–H), Parent, insoluble pellet (PPT) and DMSO control. **(B)** MS/MS profiles of the three fractions (F–H). **(C)** Fragmentation patterns of casuarinin. **(D)** Overlay ^{1}H NMR spectra of fractions H, PPT, and Parent, acquired in acetone-d_6.

from the leaves. The extract was further fractionated by preparative reversed-phase HPLC and yielded 8 subfractions (a-h). Antimicrobial activity was observed in the Parent fraction and PPT, however, no activity was found in the a-h fractions (Figure 4A), indicating that the activity is caused by more than one synergistically-acting metabolites, or that the active metabolite was diluted during the fractionation.

To study which metabolites might be present in the active fractions, we compared the active material (Parent and PPT) to the three inactive fractions f-h, using ^{1}H NMR and LC-HRMS. HR-ESI-MS (High-resolution electrospray ionization mass spectrometry) of fractions f-h showed a major m/z of 1402.1149 [z=2]; 784.0776 [z=2] and 935.0793 [z=2], respectively (Figure 4B). A dominant fragment ion observed at m/z 301 indicated the existence of a hexahydroxydiphenoyl group (HHDP), which was characteristic of ellagitannins (Era et al., 2020). The MS/MS profiles were also in good agreement with that of hydrolyzable tannin casuarinin (m/z 935.0805 [z=1])(Figure 4C)(Chang et al., 2019). Coincidentally, fraction h presented the same m/z 935.0805, but a doubly charged $[M-2H]^{2-}$. Therefore, the mass of h was calculated to be 1872.1738 and the molecular formula was determined as $C_{82}H_{56}O_{52}$. From the predicted formula, fractions h, f ($C_{123}H_{82}O_{78}$), and g ($C_{68}H_{50}O_{44}$) were putatively identified as nobotanin analogs. The ^{1}H NMR spectra (Figure 4D) of the major compound in fraction H also resembles spectra containing nobotanins (Chang et al., 2019). However, as none of the eight fractions a-h is active, it is unlikely that the tannins are significantly conferring antibacterial activity.

The overlay of ^{1}H NMR spectra (Figure 4D) showed that the precipitation of the Parent fraction using 15% MeOH/H_2O removed most of the hydrolysable tannins. ^{1}H NMR of PPT revealed several unidentified signals in the Parent fraction,

10.3389/fpls.2023.1205725

indicating a complex mixture consisting of phenolic compounds (9 - 11 ppm) and other unidentified compounds that could be responsible for the antibacterial activity.

Gene expression analysis of specialized metabolic pathways in M.dodecandrum

To investigate the types of metabolic pathways in M.dodecandrum, we analyzed its 32021 annotated protein-coding genes with PathwayTools (Karp et al., 2016). The analysis revealed that 25.09% (8035) of the genes are enzyme-coding and 12.08% (3867) could be assigned to a pathway (Table S12). Most of these genes were associated with general metabolism (GM, 3097 genes, 80.09% of all enzymes), followed by specialized metabolism (SM, 494 genes, 12.77%) and both GM/SM (276 genes, ~7%, Table S12). From the 463 predicted pathways, 104 (22.4%) were associated with SM (Tables S12, S13).

Next, we investigated the types of metabolites produced by the detected SM pathways. The majority of the compounds belonged to phenylpropanoids, of which flavonoids are most abundant (Figure 5A). Terpenoids, and more specifically diterpenoids biosynthesis comes in a close second. These observations are concurrent with previous studies which report these compounds in the larger M.dodecandrumcae family (Serna and Martínez, 2015).

To propose which specialized metabolites are most abundant in M.dodecandrum, we analyzed the gene expression of the SM pathways. Since SM pathways are thought to be under strong transcriptional control (Mutwil, 2020), we set out to investigate the gene expression patterns in M.dodecandrum. To this end, we isolated RNA from the same samples used to measure antibacterial activity (Figure 1A) and constructed a gene expression atlas for M.dodecandrum (Figure S5, Table S14). We then ranked the SM pathways within each organ based on its average TPM expression. To identify the 20 highest and lowest-ranked pathways, we ordered them according to the sum of their ranks in each organ (Figure 5B). The top 5 pathways included a sulfur-containing compound, two terpenoids, a phenylpropanoid, and a hormone synthesis pathway. There are some pathways that show organ-specific expression (e.g. young-flower-specific nitrogen-containing secondary compound, PWY-6442).

Since SM pathways expand and diversify by gene duplications (Hofberger et al., 2013), the predicted SM pathways might likely represent several separate, related pathways biosynthesizing related metabolites. For example, several enzymes implicated in flavonoid biosynthesis (PWY-7897, Figure 5C) form an aerial root-specific cluster (green clade). This suggests that these genes biosynthesize a flavonoid in aerial roots, which might differ from flavonoids produced in flowers (first five enzymes, pink and brown clade, Figure 5C).

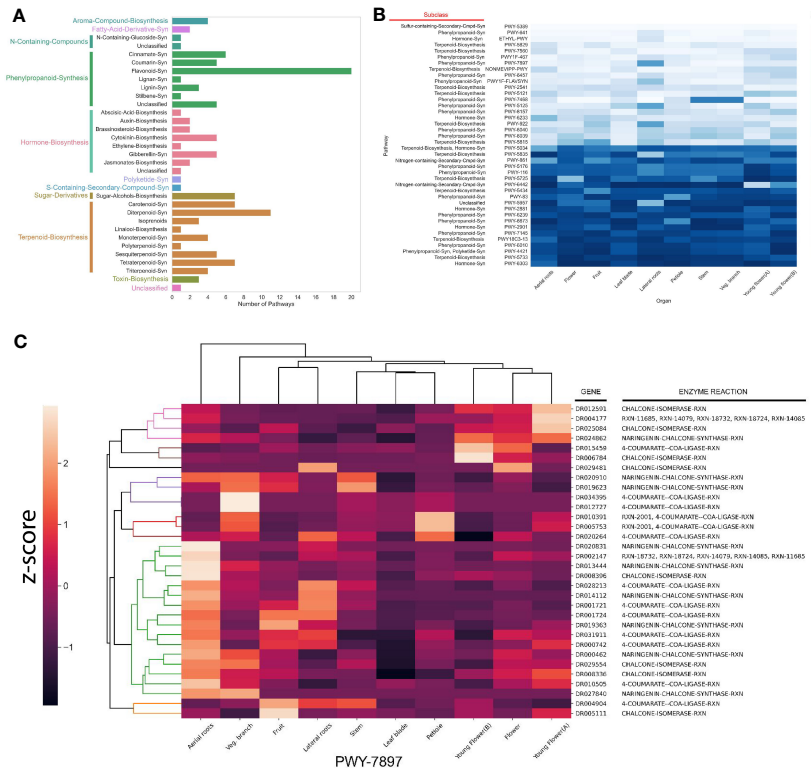

FIGURE 5
Identification of specialized metabolic pathways in *M. dodecandrum*. **(A)** The number and types of putative specialized metabolic pathways identified by PathwayTools. **(B)** Identification of the top 5 most and least expressed pathways from each organ. The scale represents the rank of a pathway (white = lowest rank, dark blue = highest rank). The rows represent pathways, while the columns indicate the sampled organs (as in Figure 1A). The lower rank (lighter color) indicates a higher expression. **(C)** Clustering analysis of flavonoid biosynthesis pathway (PWY-7897).

To investigate whether these functional sub-clusters are frequently found within the predicted pathways, we calculated the gene expression correlation (captured by Pearson Correlation Coefficient, PCC) within a pathway. We assumed that the median PCC should be high if the enzymes within a pathway are involved in the biosynthesis of the same metabolite. Surprisingly, while some of the pathways showed a high average PCC (blue line, Figure S6), many pathways showed average PCC values like randomly chosen gene pairs (orange line, average PCC ~ 0.25). Conversely, using tissue-specific gene expression data to identify the clusters containing >75% of annotated enzymatic reactions within a pathway resulted in a much higher average PCC value for nearly all pathways (green line, Figure S6D). This result shows that sequence similarity-based approaches such as PathwayTools can be supported by gene expression analyses to identify genes from tissue-specific pathways.

Transcriptional wiring of specialized metabolism in M.dodecandrum

M.dodecandrum might express over 100 SM pathways (Table S12) and metabolites (Figure 4A). Since these pathways should have specific functions, we expect the functionally-related pathways to be expressed at the same time and place. To identify such patterns, we investigate which pathways are more connected in the co-expression network than expected by chance. We first set a PCC threshold of ≥0.6, as the PCC values obtained from the randomized pathway assignments were all<0.6 (Figure S5, randomized pathway assignment confidence interval is shown in orange). We then counted the number of co-expression edges connecting any two pathways and calculated which pathways were more connected than expected by chance (see methods). Interestingly, we observed high connectivity between the different pathways, where, e.g., most phenylpropanoid, terpenoid, and hormone biosynthesis pathways were significantly connected, indicating transcriptional coordination between the pathways (Figure 6A). Between 93 pathways, there were 251 significant connections.

To take a closer look at the connections that are found within and across the pathways, we investigated the gene co-expression networks of two connected pathways. The first pathway involves the biosynthesis of the plant hormone ethylene, which has numerous roles in plant development and stress responses (Chang, 2016). Ethylene is synthesized from L-methionine by three enzymatic steps comprising methionine adenosyltransferase, 1-aminocyclopropane-1-carboxylate synthase (synthase), and 1-aminocyclopropane-1-carboxylate oxidase (oxidase) (Chang, 2016) Interestingly, the co-expression network of the ethylene biosynthesis pathway shows several groups of co-expressed synthases and oxidases (Figure 6B, left pathway, blue edges connect co-expressed genes), suggesting that M.dodecandrum contains several ethylene biosynthesis pathways. The other pathway represents the biosynthesis of phytosterol terpenoids, which comprise multiple steps that convert cycloartenol to stigmasterol, crinosterol, and brassicasterol in *Arabidopsis thaliana*. This pathway in M.dodecandrum contains several dehydrogenases, methyltransferases, isomerases, demethylases, and desaturases that modify the cycloartenol (or a related compound) to other sterols (Figure 6B, right pathway). While PWY-2541 has been characterized in Arabidopsis, it is likely that this pathway produces other, related compounds in M.dodecandrum. Within each pathway, we also observed subclusters of genes that are co-expressed with the same gene(s) in the other pathway. While the analysis does not reveal any clear organ-specific clusters like in Figure 4C, this could suggest separate clusters of SM pathway expansion where subclustering occurs not only within a pathway but with other pathways too. The co-expression edges found between the ethylene and phytosterol pathways indicate that the two pathways are transcriptionally positively coordinated. This suggests that an increase in ethylene might result in increased biosynthesis of phytosterols. This is in line with a recent study that showed that exogenous ethylene led to a profound change in the ratio of stigmasterol to sitosterol (Markowski et al., 2022).

Discussion

In this study, we showed that *M. dodecandrum* shows antibacterial activities against gram-positive and -negative bacteria (Figure 1). The plant is known to produce a diverse range of chemical compounds and metabolites, including flavonoids, tannins and ellagitannins, phenylpropanoids, long-chain fatty acids, aromatic acids, terpenoids, steroids, alkaloids, glycosides and monosaccharides (Zheng et al., 2021). Plant specialized metabolites can exert their antibacterial effects through various mechanisms. This includes but is not limited to, inhibition of bacterial nucleic acid and protein synthesis, inhibition of enzymes and respiration or metabolism, disruption of cell wall synthesis or cell membrane permeability or function, influencing the expression of virulence genes or chelation of essential metal ions such as iron (Ríos and Recio, 2005; Payne et al., 2007; Frey and Meyers, 2010; Tommasi et al., 2015; Kessler and Kalske, 2018; Singh et al., 2018; Lewis, 2020).

Results from LIVE/DEAD staining, in conjunction with viable CFU counts, suggest that the *M. dodecandrum* extract results in membrane damage (Figure 2), butviable cell counting suggests that there is no significant difference or drop in CFU compared to the control groups at 25 mg/mL (Figure 1H) or in viable cell counts in time-kill studies involving samples treated with 4 mg/mL w/v of the plant extract within an hour of treatment (Figure 1I). Recent studies suggest intermediate living/dead states in populations of bacteria stained with the LIVE/DEAD kit (Cushnie et al., 2020). Furthermore, there is evidence that, in some cases, PI staining may underestimate the viability of bacterial cells (Rosenberg et al., 2019). Taken together, it is likely that the increased PI staining following extract treatment is partly due to membrane damage and not actual cell death.

In addition to membrane damage, treatment with *M. dodecandrum* extract leads to reduced swimming and swarming motility in *P. aeruginosa* (Figures 2C-F, Video 1). Both forms of motility are flagella-mediated (Kazmierczak et al., 2015). The effects on motility may be related to the extract's effects on the bacterial

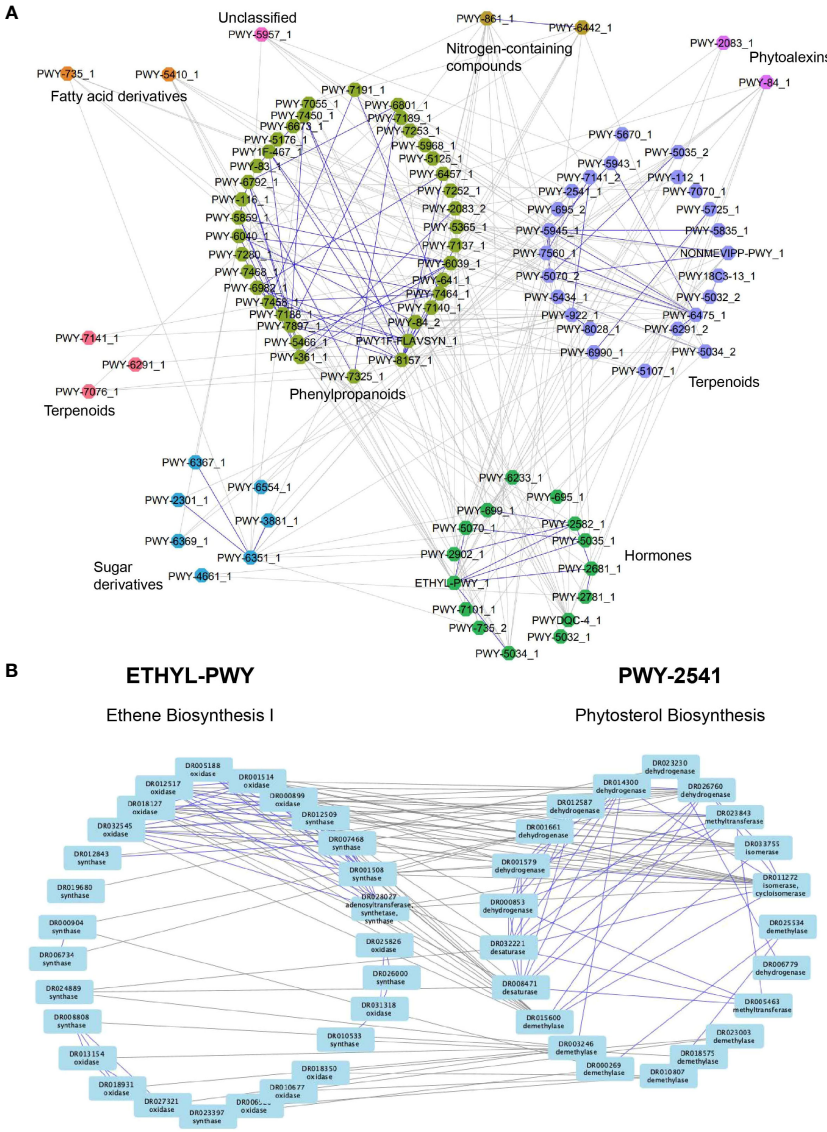

FIGURE 6
Co-expression network analysis reveals a transcriptional association between specialized metabolic pathways and hormones. **(A)** Nodes represent pathways, while edges connect significantly connected pathways. Edges within the same pathway type are colored blue, while edges connecting different pathway types are colored gray. Node colors represent different pathway types. **(B)** Ethylene (left) and phytosterol (right) biosynthesis pathways. Nodes represent enzymes, while edges connect enzymes correlated with r>0.6. Edges within the same pathway are blue, while edges connecting two pathways are gray.

membranes, as flagella rotation is driven by ion flux and membrane-active antibiotics that result in the alteration of membrane and changes in cation permeability have been suggested to reduce flagella activity and in turn, motility in *P. fluorescens* (Faust and Doetsch, 1971; Manson et al., 1980). Similarly, cationic peptides that target cell membranes may also affect flagella integrity, and some cationic peptides can reduce swimming and swarming motility in *E. coli* (Faust and Doetsch, 1971). Unlike swimming motility, swarming motility is a much more complex and tightly regulated adaptation process involving the upregulation of virulence gene expression and antibiotic resistance (Overhage et al., 2008). In addition to functional flagella, swarming is also dependent on quorum sensing and type IV villi (Köhler et al., 2000; Déziel et al., 2003). Several plant metabolites have been reported to inhibit swarming via various mechanisms. For example, ginseng extract reduces swarming by reducing the production of QS signals in *P. aeruginosa*, while some flavonoids act as allosteric inhibitors of QS receptors (Wu et al., 2011; Paczkowski et al., 2017; Rütschlin and Böttcher, 2020). Some phenolic plant compounds or tannins can affect swarming but not swimming motility by affecting surfactant production (O'May and Tufenkji, 2011; Rütschlin and Böttcher, 2020). Beyond plant metabolites, antibiotics such as gentamicin and ciprofloxacin have also been reported to reduce swarming either via disruption of QS or through SOS responses that prevented polar chemosensory array formation (Irazoki et al., 2017; Rütschlin and Böttcher, 2020).

Comparison of gene expression responses of P.aeruginosatreated with M.dodecandrum extracts revealed that the plant extracts elicited

the most unique and highest number of differentially expressed genes compared to four antibiotics (Figures 3A, B). This is not surprising, as the plant extract contains hundreds of different compounds that might synergistically affect different aspects of P.aeruginosabiology. Surprisingly, the observed transcriptomics responses were not aligned with the primary mode of action of the antibiotics (Figure S4). For example, while rifampicin inhibits RNA biosynthesis, the observed transcriptomic changes affect the unrelated type VI secretion system (Figure S4). While these results indicate that transcriptomics might not be suitable to reveal the primary protein target of antibiotics, the downstream secondary effects can still be inferred (O'Rourke et al., 2020). Antibiotics with classical mechanism-of-actions can be clustered using their gene expression profiles (O'Rourke et al., 2020). Thus the overlapping differentially expressed biological processes between M.dodecandrum and triclosan could represent some of the similar downstream transcriptomic effects caused by triclosan (fatty acid biosynthesis inhibitor), which is in line with the observed membrane damage phenotypes (Figure S4). However, more time points and concentrations of the extracts and antibiotics should be compared to differentiate between primary and downstream effects.

To identify the metabolite(s) responsible for the antibacterial activity, we performed activity-guided fractionation. However, none of the purified fractions showed activity (Figure 5A), suggesting that either the activity is caused by multiple metabolites that together cause the activity or that the active metabolite is poorly soluble. The latter is more likely, as the insoluble material showed antibacterial activity (Figure 5A). The ^{1}H NMR analysis of the partially purified Parent fraction indicated the presence of hydrolysable tannins (Figure 5B), which are known to show broad antibacterial activities (Tomiyama et al., 2016), and other health-promoting activities due to their anti-oxidant properties (Abu Zarin et al., 2016). However, a deeper analysis using different fractionation methods showed that the activity was not due to the major hydrolysable tannins, but some other unidentified minor compounds. A larger scale of purification is needed to identify the active compounds.

The genomic and transcriptomic analysis revealed that *M. dodecandrum* contains many phenylpropanoid and terpenoid biosynthetic pathways (Figure 4A), and we were able to identify the most expressed pathways producing a sulfur-containing compound, two terpenoids, a phenylpropanoid (Figure 4B). Interestingly, within the predicted pathways, we observed several groups of highly co-expressed enzymes (Figures 4C, D), suggesting that these groups might represent several related pathways active in the different parts of the plant. Since enzymes biosynthesizing a given metabolite are expected to be expressed in the same cell, tissue and organ (Delli-Ponti et al., 2020), pathway inference approaches should be augmented with gene expression data. With >300,000 RNA-seq samples publicly available for hundreds of species (Julca et al., 2023), and several approaches that can be used to infer the biosynthetic pathways (Delli-Ponti et al., 2020), our and other groups can expect to provide more accurate inventories of specialized metabolism pathways.

Finally, we observed many co-expressed metabolic and hormonal pathways. This indicates that the specialized metabolic pathways are transcriptionally and functionally connected and that they are under hormonal control. This is in line with the existing knowledge linking many hormones to the biosynthesis of specialized metabolites (Chen et al., 2019; Markowski et al., 2022). Since co-expression analysis can identify hormone-pathway pairs (Figure 6A), our analyses can generate testable hypotheses of how plants' hormones and metabolism are wired.

In conclusion, the high connectivity observed between various pathways, such as phenylpropanoid, terpenoid, and hormone biosynthesis pathways in M.dodecandrum, highlights the intricate transcriptional coordination between these pathways, suggesting that they work together to regulate key aspects of plant development, stress responses, and secondary metabolite production, ultimately contributing to the plant's adaptive capabilities and overall survival. Future studies could investigate how modulating plant hormones could affect the production of anti-bacterial metabolites.

Data availability statement

The datasets presented in this study can be found in online repositories. The names of the repository/repositories and accession number(s) can be found in the article/Supplementary Material. The RNA-seq data is available at EBI ENA accessions E-MTAB-12682 and E-MTAB-12652.

Author contributions

WP wrote the manuscript, performed bacterial wet- and dry-lab work with help from NR. NR wrote the manuscript, performed plant wet- and dry-lab work with help from WP. LY did fractionation and structure elucidation of the active compound with help from YK, DS helped identify Melastoma. PL helped with bioinformatics analyses. SR supervised WP. MM conceived the project, supervised WP and NR and helped with writing. All authors contributed to the article and approved the submitted version.

Funding

MM, WP and NR is supported by a NTU Start-Up Grant and Singaporean Ministry of Education grant MOE-T2EP30122-0017. YK and LY is supported by Singapore Institute of Food and Biotechnology Innovation (SIFBI) core fund.

Acknowledgments

We would like to thank NTU herb garden caretakers for providing the herb samples. The authors would like to thank the Mutwil Lab for useful discussions and suggestions during the lab meetings. Finally, we would like to thank Ing Tsyr Beh for help with the initial herb sample collection and screening.

Conflict of interest

Author DS was employed by the company ACM Biolabs Pte Ltd.

The authors declare that the research was conducted in the absence of any commercial or financial relationships that could be construed as a potential conflict of interest.

Publisher's note

Supplementary material

The Supplementary Material for this article can be found online at: https://www.frontiersin.org/articles/10.3389/fpls.2023.1205725/full#supplementary-material

SUPPLEMENTARY FIGURE 1
Time-kill assay of M.dodecandrum extract against PAO1.The time-kill activity of 4 and 25 mg/mL of methanol plant extract respectively from M. dodecandrum leaves or equivalent volumes of DMSO was assessed over 24 hours, with data points from each biological replicate plotted.

SUPPLEMENTARY FIGURE 2
Effects of various antimicrobials on the growth of *P. aeruginosa* PAO1. Effects of the treatment of *P. aeruginosa* with 0 – 128 µg/mL of the antimicrobials triclosan, rifampicin, gentamicin, and ciprofloxacin were evaluated and the area under the curve was plotted. Each data point represents data from one independent biological replicate while error bars represent the standard error of the mean. At least two biological replicates were carried out.

SUPPLEMENTARY FIGURE 3
UpSet plot analysis of differentially expressed genes. The four antibiotics and *M. dodecandrum* plant extract is shown.

SUPPLEMENTARY FIGURE 4
Gene ontology enrichment analysis of the four antibiotics and M.dodecandrum extracts. Antibiotics and the extract are shown in columns, while significantly enriched gene ontology terms are shown in columns. Cell colors indicate the different significance levels of the enrichment.

SUPPLEMENTARY FIGURE 5
Hierarchical clustering analysis of gene expression data from Melastoma. Ward-linkage clustering based on Spearman correlation coefficient distance matrix.

SUPPLEMENTARY FIGURE 6
Correlation analysis of genes in the SM pathways of M.dodecandrum. Pathways without confidence interval bands comprise two genes only.

SUPPLEMENTARY VIDEO 1
Pseudomonas treated with DMSO of equivalent volume to 1 mg/mL of plant extract.

SUPPLEMENTARY VIDEO 2
Pseudomonas treated with 1 mg/mL of plant extract.

References

Abu Zarin, M., Wan, H. Y., Isha, A., and Armania, N. (2016). Antioxidant, antimicrobial and cytotoxic potential of condensed tannins from Leucaena leucocephala hybrid-Rendang. *Food Sci. Hum. Wellness* 5, 65–75. doi: 10.1016/j.fshw.2016.02.001

Alnajar, Z. A. A., Abdulla, M. A., Ali, H. M., Alshawsh, M. A., and Hadi, A. H. A. (2012). Acute toxicity evaluation, antibacterial, antioxidant and immunomodulatory effects of Melastoma malabathricum. *Mol. Basel Switz.* 17, 3547–3559. doi: 10.3390/molecules17033547

Atanasov, A. G., Zotchev, S. B., Dirsch, V. M., and Supuran, C. T. (2021). Natural products in drug discovery: advances and opportunities. *Nat. Rev. Drug Discovery* 20, 200–216. doi: 10.1038/s41573-020-00114-z

Benjamini, Y., and Hochberg, Y. (1995). Controlling the false discovery rate: A practical and powerful approach to multiple testing. *J. R. Stat. Soc Ser. B Methodol.* 57, 289–300. doi: 10.1111/j.2517-6161.1995.tb02031.x

Bray, N. L., Pimentel, H., Melsted, P., and Pachter, L. (2016). Near-optimal probabilistic RNA-seq quantification. *Nat. Biotechnol.* 34, 525–527. doi: 10.1038/nbt.3519

Chang, C. (2016). Q&A: How do plants respond to ethylene and what is its importance? *BMC Biol.* 14, 7. doi: 10.1186/s12915-016-0230-0

Chang, Z., Zhang, Q., Liang, W., Zhou, K., Jian, P., She, G., et al. (2019). A comprehensive review of the structure elucidation of tannins from *terminalia* linn. *Evid. Based Complement. Alternat. Med.* 2019, e8623909. doi: 10.1155/2019/8623909

Chen, X., Wang, D.-D., Fang, X., Chen, X.-Y., and Mao, Y.-B. (2019). Plant specialized metabolism regulated by jasmonate signaling. *Plant Cell Physiol.* 60, 2638–2647. doi: 10.1093/pcp/pcz161

Chen, S., Zhou, Y., Chen, Y., and Gu, J. (2018). fastp: an ultra-fast all-in-one FASTQ preprocessor. *Bioinformatics* 34, i884–i890. doi: 10.1093/bioinformatics/bty560

Che Omar, S. N., Ong Abdullah, J., Khairoji, K. A., Chin Chin, S., and Hamid, M. (2013). Effects of Flower and Fruit Extracts of Melastoma malabathricum Linn. on Growth of Pathogenic Bacteria: Listeria monocytogenes, Staphylococcus aureus, Escherichia coli, and Salmonella typhimurium. *Evid.-Based Complement. Altern. Med. ECAM* 2013, 459089. doi: 10.1155/2013/459089

Cushnie, T. P. T., Cushnie, B., Echeverría, J., Fowsantear, W., Thammawat, S., Dodgson, J. L. A., et al. (2020). Bioprospecting for antibacterial drugs: a multidisciplinary perspective on natural product source material, bioassay selection and avoidable pitfalls. *Pharm. Res.* 37, 125. doi: 10.1007/s11095-020-02849-1

Delli-Ponti, R., Shivhare, D., and Mutwil, M. (2020). Using gene expression to study specialized metabolism-A practical guide. *Front. Plant Sci.* 11, 625035. doi: 10.3389/fpls.2020.625035

Déziel, E., Lépine, F., Milot, S., and Villemur, R. (2003). rhlA is required for the production of a novel biosurfactant promoting swarming motility in Pseudomonas aeruginosa: 3-(3-hydroxyalkanoyloxy)alkanoic acids (HAAs), the precursors of rhamnolipids. *Microbiol. Read. Engl.* 149, 2005–2013. doi: 10.1099/mic.0.26154-0

Era, M., Matsuo, Y., Saito, Y., and Tanaka, T. (2020). Production of ellagitannin hexahydroxydiphenoyl ester by spontaneous reduction of dehydrohexahydroxydiphenoyl ester. *Molecules* 25, 1051. doi: 10.3390/molecules25051051

Erhardt, M. (2016). Strategies to block bacterial pathogenesis by interference with motility and chemotaxis. *Curr. Top. Microbiol. Immunol.* 398, 185–205. doi: 10.1007/82_2016_493

Faust, M. A., and Doetsch, R. N. (1971). Effect of membrane-active antibiotics on motility and 42K permeability of Pseudomonas fluorescens. *Can. J. Microbiol.* 17, 183–189. doi: 10.1139/m71-032

Frey, F. M., and Meyers, R. (2010). Antibacterial activity of traditional medicinal plants used by Haudenosaunee peoples of New York State. *BMC Complement. Altern. Med.* 10, 64. doi: 10.1186/1472-6882-10-64

Goff, A., Cantillon, D., Muraro Wildner, L., and Waddell, S. J. (2020). Multi-omics technologies applied to tuberculosis drug discovery. *Appl. Sci.* 10, 4629. doi: 10.3390/app10134629

Ha, D.-G., Kuchma, S. L., and O'Toole, G. A. (2014a). Plate-based assay for swarming motility in Pseudomonas aeruginosa. *Methods Mol. Biol. Clifton NJ* 1149, 67–72. doi: 10.1007/978-1-4939-0473-0_8

Ha, D.-G., Kuchma, S. L., and O'Toole, G. A. (2014b). Plate-based assay for swimming motility in pseudomonas aeruginosa. *Methods Mol. Biol. Clifton NJ* 1149, 59–65. doi: 10.1007/978-1-4939-0473-0_7

Hao, Y., Zhou, Y. Z., Chen, B., Chen, G. Z., Wen, Z. Y., Zhang, D., et al. (2022). The Melastoma dodecandrum genome and the evolution of Myrtales. *J. Genet. Genomics* 49, 120–131. doi: 10.1016/j.jgg.2021.10.004

Hawkins, C., Ginzburg, D., Zhao, K., Dwyer, W., Xue, B., Xu, A., et al. (2021). Plant Metabolic Network 15: A resource of genome-wide metabolism databases for 126 plants and algae. *J. Integr. Plant Biol.* 63, 1888–1905. doi: 10.1111/jipb.13163

Hesketh, A., Hill, C., Mokhtar, J., Novotna, G., Tran, N., Bibb, M., et al. (2011). Genome-wide dynamics of a bacterial response to antibiotics that target the cell envelope. *BMC Genomics* 12, 226. doi: 10.1186/1471-2164-12-226

Hofberger, J. A., Lyons, E., Edger, P. P., Chris Pires, J., and Eric Schranz, M. (2013). Whole genome and tandem duplicate retention facilitated glucosinolate pathway diversification in the mustard family. *Genome Biol. Evol.* 5, 2155–2173. doi: 10.1093/gbe/evt162

Huang, G., Ge, Y., Gui, Z., Zhu, M., Liu, J., and Wang, H. (2021). Toxicity of Melastoma dodecandrum Lour. and its effects on lipopolysaccharide-induced inflammation and oxidative stress. *Exp. Ther. Med.* 22, 807. doi: 10.3892/etm.2021.10239

Irazoki, O., Campoy, S., and Barbé, J. (2017). The transient multidrug resistance phenotype of salmonella enterica swarming cells is abolished by sub-inhibitory concentrations of antimicrobial compounds. *Front. Microbiol.* 8, 1360. doi: 10.3389/fmicb.2017.01360

Joffry, S. M., Yob, N. J., Rofiee, M. S., Affandi, M.M.R.M.M., Suhaili, Z., Othman, F., et al. (2012). Melastoma malabathricum (L.) smith ethnomedicinal uses, chemical constituents, and pharmacological properties: A review. Evid.-based complement. *Altern. Med. ECAM* 2012, 258434. doi: 10.1155/2012/258434

Julca, I., Mutwil-Anderwald, D., Manoj, V., Khan, Z., Lai, S. K., Yang, L. K., et al. Genomic, transcriptomic, and metabolomic analysis of Oldenlandia corymbosa reveals the biosynthesis and mode of action of anti-cancer metabolites. *J Integr. Plant Biol* 65 (6):1442–1466. doi: 10.1111/jipb.13469

Julca, I., Tan, Q. W., and Mutwil, M. (2023). Toward kingdom-wide analyses of gene expression. *Trends Plant Sci.* 28, 235–249. doi: 10.1016/j.tplants.2022.09.007

Karp, P. D., Latendresse, M., Paley, S. M., Krummenacker, M., Ong, Q. D., Billington, R., et al. (2016). Pathway tools version 19.0 update: Software for pathway/genome informatics and systems biology. *Brief. Bioinform.* 17, 877–890. doi: 10.1093/bib/bbv079

Kazmierczak, B. I., Schniederberend, M., and Jain, R. (2015). Cross-regulation of Pseudomonas motility systems: the intimate relationship between flagella, pili and virulence. *Curr. Opin. Microbiol.* 28, 78–82. doi: 10.1016/j.mib.2015.07.017

Kessler, A., and Kalske, A. (2018). Plant secondary metabolite diversity and species interactions. *Annu. Rev. Ecol. Evol. Syst.* 49, 115–138. doi: 10.1146/annurev-ecolsys-110617-062406

Köhler, T., Curty, L. K., Barja, F., van Delden, C., and Pechère, J.-C. (2000). Swarming of pseudomonas aeruginosa is dependent on cell-to-cell signaling and requires flagella and pili. *J. Bacteriol.* 182, 5990–5996. doi: 10.1128/JB.182.21.5990-5996.2000

Kudera, T., Fiserova, B., Korytakova, M., Doskocil, I., Salmonova, H., Tulin, E. E., et al. (2021). *In vitro* selective antibacterial and antiproliferative effects of ethanolic extracts from Cambodian and Philippine plants used in folk medicine for diarrhea treatment. *Front. Pharmacol.* 12, 746808. doi: 10.3389/fphar.2021.746808

Kumar, P., Sharma, P., Kumar, V., Kumar, A., Singh, R., and Sharma, A. K. (2019). "5. Plant resources: *In vitro* production, challenges and prospects of secondary Metabolites from medicinal plants," Industrial Biotechnology. (Walter de Gruyter GmbH, Berlin/Boston: De Gruyter), 89–104. In 5. Plant resources: *In vitro* production, challenges and prospects of secondary Metabolites from medicinal plants.

Lal, M., Chandraker, S. K., and Shukla, R. (2020). "4 - Antimicrobial properties of selected plants used in traditional Chinese medicine," in *Functional and Preservative Properties of Phytochemicals*. Ed. B. Prakash (Elsevier: Academic Press), 119–143.

Lewis, K. (2020). The science of antibiotic discovery. *Cell* 181, 29–45. doi: 10.1016/j.cell.2020.02.056

Lim, P. K., Zheng, X., Goh, J. C., and Mutwil, M. (2022). Exploiting plant transcriptomic databases: Resources, tools, and approaches. *Plant Commun.* 3, 100323. doi: 10.1016/j.xplc.2022.100323

Love, M. I., Huber, W., and Anders, S. (2014). Moderated estimation of fold change and dispersion for RNA-seq data with DESeq2. *Genome Biol.* 15, 550. doi: 10.1186/s13059-014-0550-8

Magoc, T., Wood, D., and Salzberg, S. L. (2013). EDGE-pro: estimated degree of gene expression in prokaryotic genomes. *Evol. Bioinforma.* 9, 127–136. Online. doi: 10.4137/EBO.S11250

Mamat, S. S., Kamarolzaman, M. F. F., Yahya, F., Mahmood, N. D., Shahril, M. S., Jakius, K. F., et al. (2013). Methanol extract of Melastoma malabathricum leaves exerted antioxidant and liver protective activity in rats. *BMC Complement. Altern. Med.* 13, 326. doi: 10.1186/1472-6882-13-326

Manson, M. D., Tedesco, P. M., and Berg, H. C. (1980). Energetics of flagellar rotation in bacteria. *J. Mol. Biol.* 138, 541–561. doi: 10.1016/S0022-2836(80)80017-9

Markowski, M., Alsoufi, A. S. M., Szakiel, A., and Długosz, M. (2022). Effect of ethylene and abscisic acid on steroid and triterpenoid synthesis in calendula officinalis hairy roots and saponin release to the culture medium. *Plants* 11, 303. doi: 10.3390/plants11030303

Mi, H., Muruganujan, A., Ebert, D., Huang, X., and Thomas, P. D. (2019). PANTHER version 14: more genomes, a new PANTHER GO-slim and improvements in enrichment analysis tools. *Nucleic Acids Res.* 47, D419–D426. doi: 10.1093/nar/gky1038

Mutwil, M. (2020). Computational approaches to unravel the pathways and evolution of specialized metabolism. *Curr Opin Plant Biol.* 55, 38–46. doi: 10.1016/j.pbi.2020.01.007

O'May, C., and Tufenkji, N. (2011). The swarming motility of Pseudomonas aeruginosa is blocked by cranberry proanthocyanidins and other tannin-containing materials. *Appl. Environ. Microbiol.* 77, 3061–3067. doi: 10.1128/AEM.02677-10

O'Rourke, A., Beyhan, S., Choi, Y., Morales, P., Chan, AP., Espinoza, JL., et al. (2020). Mechanism-of-Action classification of antibiotics by global transcriptome profiling. *Antimicrob Agents Chemother (IF: 5.19; Q2)*. 64 (3), e01207–19. doi: 10.1128/AAC.01207-19

Overhage, J., Bains, M., Brazas, M. D., and Hancock, R. E. W. (2008). Swarming of pseudomonas aeruginosa is a complex adaptation leading to increased production of virulence factors and antibiotic resistance. *J. Bacteriol.* 190, 2671–2679. doi: 10.1128/JB.01659-07

Paczkowski, J. E., Mukherjee, S., McCready, A. R., Cong, J.-P., Aquino, C. J., Kim, H., et al. (2017). Flavonoids Suppress Pseudomonas aeruginosa Virulence through Allosteric Inhibition of Quorum-sensing Receptors. *J. Biol. Chem.* 292, 4064–4076. doi: 10.1074/jbc.M116.770552

Payne, D. J., Gwynn, M. N., Holmes, D. J., and Pompliano, D. L. (2007). Drugs for bad bugs: confronting the challenges of antibacterial discovery. *Nat. Rev. Drug Discovery* 6, 29–40. doi: 10.1038/nrd2201

Rice, P., Longden, I., and Bleasby, A. (2000). EMBOSS: the european molecular biology open software suite. *Trends Genet.* 16, 276–277. doi: 10.1016/S0168-9525(00)02024-2

Ríos, J. L., and Recio, M. C. (2005). Medicinal plants and antimicrobial activity. *J. Ethnopharmacol.* 100, 80–84. doi: 10.1016/j.jep.2005.04.025

Rosenberg, M., Azevedo, N. F., and Ivask, A. (2019). Propidium iodide staining underestimates viability of adherent bacterial cells. *Sci. Rep.* 9, 6483. doi: 10.1038/s41598-019-42906-3

Rütschlin, S., and Böttcher, T. (2020). Inhibitors of bacterial swarming behavior. *Chem. – Eur. J.* 26, 964–979. doi: 10.1002/chem.201901961

Serna, D. M. O., and Martínez, J. H. I. (2015). Phenolics and polyphenolics from melastomataceae species. *Mol. Basel Switz.* 20, 17818–17847. doi: 10.3390/molecules201017818

Shitikov, E., Bespiatykh, D., Malakhova, M., Bespyatykh, J., Bodoev, I., Vedekhina, T., et al. (2022). Genome-wide transcriptional response of mycobacterium smegmatis MC2155 to G-quadruplex ligands BRACO-19 and TMPyP4. *Front. Microbiol.* 13. doi: 10.3389/fmicb.2022.817024

Singh, P. A., Desai, S. D., and Singh, J. (2018). A review on plant antimicrobials of past decade. *Curr. Top. Med. Chem.* 18, 812–833. doi: 10.2174/1568026618666180516123229

Stiefel, P., Schmidt-Emrich, S., Maniura-Weber, K., and Ren, Q. (2015). Critical aspects of using bacterial cell viability assays with the fluorophores SYTO9 and propidium iodide. *BMC Microbiol.* 15, 36. doi: 10.1186/s12866-015-0376-x

The Gene Ontology Consortium (2021). The Gene Ontology resource: enriching a GOld mine. *Nucleic Acids Res.* 49, D325–D334. doi: 10.1093/nar/gkaa1113

Tomiyama, K., Mukai, Y., Saito, M., Watanabe, K., Kumada, H., Nihei, T., et al. (2016). Antibacterial action of a condensed tannin extracted from astringent persimmon as a component of food addictive pancil PS-M on oral polymicrobial biofilms. *BioMed. Res. Int.* 2016, 5730748. doi: 10.1155/2016/5730748

Tommasi, R., Brown, D. G., Walkup, G. K., Manchester, J. I., and Miller, A. A. (2015). ESKAPEing the labyrinth of antibacterial discovery. *Nat. Rev. Drug Discovery* 14, 529–542. doi: 10.1038/nrd4572

Tong, Y., Jiang, Y., Chen, X., Li, X., Wang, P., Jin, Y., et al. (2019). Extraction, enrichment, and quantification of main antioxidant aglycones of flavonoids and tannins from *melastoma dodecandrum* lour.: guided by UPLC-ESI-MS/MS. *J. Chem.* 2019, e2793058. doi: 10.1155/2019/2793058

Usadel, B., Obayashi, T., Mutwil, M., Giorgi, F. M., Bassel, G. W., Tanimoto, M., et al. (2009). Co-expression tools for plant biology: Opportunities for hypothesis generation and caveats. *Plant Cell Environ.* 32, 1633–1651. doi: 10.1111/j.1365-3040.2009.02040.x

Wang, Y.-C., Hsu, H.-W., and Liao, W.-L. (2008). "Antibacterial activity of Melastoma candidum D. Don," in *LWT - Food Sci. Technol.* Elsevier, vol. 41. , 1793–1798. doi: 10.1016/j.lwt.2008.02.005

Wang, J., Jia, Z., Zhang, Z., Wang, Y., Liu, X., Wang, L., et al. (2017). Analysis of chemical constituents of melastoma dodecandrum lour. by UPLC-ESI-Q-exactive focus-MS/MS. *Mol. Basel Switz.* 22, 476. doi: 10.3390/molecules22030476

Wiegand, I., Hilpert, K., and Hancock, R. E. W. (2008). Agar and broth dilution methods to determine the minimal inhibitory concentration (MIC) of antimicrobial substances. *Nat. Protoc.* 3, 163–175. doi: 10.1038/nprot.2007.521

Wong, K.-C., Hag Ali, D. M., and Boey, P.-L. (2012). Chemical constituents and antibacterial activity of Melastoma malabathricum L. *Nat. Prod. Res.* 26, 609–618. doi: 10.1080/14786419.2010.538395

Wu, H., Lee, B., Yang, L., Wang, H., Givskov, M., Molin, S., et al. (2011). Effects of ginseng on Pseudomonas aeruginosa motility and biofilm formation. *FEMS Immunol. Med. Microbiol.* 62, 49–56. doi: 10.1111/j.1574-695X.2011.00787.x

Xu, Y., Rashwan, A. K., Ge, Z., Li, Y., Ge, H., Li, J., et al. (2023). Identification of a novel α-glucosidase inhibitor from Melastoma dodecandrum Lour. fruits and its effect on regulating postprandial blood glucose. *Food Chem.* 399, 133999. doi: 10.1016/j.foodchem.2022.133999

Yang, G.-X., Zhang, R.-Z., Lou, B., Cheng, K.-J., Xiong, J., and Hu, J.-F. (2014). Chemical constituents from Melastoma dodecandrum and their inhibitory activity on interleukin-8 production in HT-29 cells. *Nat. Prod. Res.* 28, 1383–1387. doi: 10.1080/14786419.2014.903480

Zhan, C., Shen, S., Yang, C., Liu, Z., Fernie, A. R., Graham, I. A., et al. (2022). Plant metabolic gene clusters in the multi-omics era. *Trends Plant Sci.* 27, 981–1001. doi: 10.1016/j.tplants.2022.03.002

Zhao, K., and Rhee, S. Y. (2022). Omics-guided metabolic pathway discovery in plants: Resources, approaches, and opportunities. *Curr. Opin. Plant Biol.* 67, 102222. doi: 10.1016/j.pbi.2022.102222

Zheng, W.-J., Ren, Y.-S., Wu, M.-L., Yang, Y.-L., Fan, Y., Piao, X.-H., et al. (2021). A review of the traditional uses, phytochemistry and biological activities of the Melastoma genus. *J. Ethnopharmacol.* 264, 113322. doi: 10.1016/j.jep.2020.113322

frontiers | Frontiers in Plant Science

TYPE Review
PUBLISHED 04 October 2023
DOI 10.3389/fpls.2023.1236123

OPEN ACCESS

EDITED BY
Chunpeng (Craig) Wan,
Jiangxi Agricultural University, China

REVIEWED BY
Enrico Doria,
University of Pavia, Italy
Damilohun Samuel Metibemu,
Jackson State University, United States
Maryna De Wit,
University of the Free State, South Africa

*CORRESPONDENCE
Rajeev K. Singla
rajeesingla26@gmail.com
Bhagwati Devi
bhagwatidevi2013@gmail.com
Bairong Shen
bairong.shen@scu.edu.cn

†These authors have contributed equally to this work and share first authorship

RECEIVED 07 June 2023
ACCEPTED 13 September 2023
PUBLISHED 04 October 2023

CITATION
Wang J, Rani N, Jakhar S, Redhu R, Kumar S, Kumar S, Kumar S, Devi B, Simal-Gandara J, Shen B and Singla RK (2023) *Opuntia ficus-indica* (L.) Mill. - anticancer properties and phytochemicals: current trends and future perspectives. *Front. Plant Sci.* 14:1236123. doi: 10.3389/fpls.2023.1236123

Opuntia ficus-indica (L.) Mill. - anticancer properties and phytochemicals: current trends and future perspectives

Jiao Wang[1†], Neeraj Rani[2,3†], Seema Jakhar[4], Rakesh Redhu[4], Sanjiv Kumar[3], Sachin Kumar[3], Sanjeev Kumar[3], Bhagwati Devi[2*], Jesus Simal-Gandara[5], Bairong Shen[1*] and Rajeev K. Singla[1,6*]

[1]Joint Laboratory of Artificial Intelligence for Critical Care Medicine, Department of Critical Care Medicine and Institutes for Systems Genetics, Frontiers Science Center for Disease-related Molecular Network, West China Hospital, Sichuan University, Chengdu, China, [2]Shri Baba Mastnath Institute of Pharmaceutical Science and Research, Baba Mastnath University, Asthal Bohar Rohtak, Haryana, India, [3]Department of Pharmaceutical Sciences, Chaudhary Bansi Lal University, Bhiwani, Haryana, India, [4]Geeta Institute of Pharmacy, Geeta University, Panipat, Haryana, India, [5]Universidade de Vigo, Nutrition and Bromatology Group, Analytical Chemistry and Food Science Department, Faculty of Science, Ourense, Spain, [6]School of Pharmaceutical Sciences, Lovely Professional University, Phagwara, Punjab, India

Cancer is a leading cause of mortality worldwide, and conventional cancer therapies such as chemotherapy and radiotherapy often result in undesirable and adverse effects. Natural products have emerged as a promising alternative for cancer treatment, with comparatively fewer side effects reported. *Opuntia ficus-indica* (L.) Mill., a member of the *Cactaceae* family, contains a diverse array of phytochemicals, including flavonoids, polyphenols, betalains, and tannins, which have been shown to exhibit potent anticancer properties. Various parts of the Opuntia plant, including the fruits, stems/cladodes, and roots, have demonstrated cytotoxic effects against malignant cell lines in numerous studies. This review comprehensively summarizes the anticancer attributes of the phytochemicals found in *Opuntia ficus-indica* (L.) Mill., highlighting their potential as natural cancer prevention and treatment agents. Bibliometric metric analysis of PubMed and Scopus-retrieved data using VOSviewer as well as QDA analysis provide further insights and niche to be explored. Most anticancer studies on *Opuntia ficus-indica* and its purified metabolites are related to colorectal/colon cancer, followed by melanoma and breast cancer. Very little attention has been paid to leukemia, thyroid, endometrial, liver, and prostate cancer, and it could be considered an opportunity for researchers to explore *O. ficus-indica* and its metabolites against these cancers. The most notable mechanisms expressed and validated in those studies are apoptosis, cell cycle arrest (G0/G1 and G2/M), Bcl-2 modulation, antiproliferative, oxidative stress-mediated mechanisms, and cytochrome c. We have also observed that cladodes and fruits of *O. ficus-indica* have been more studied than other plant parts, which again opens the opportunity for the researchers to explore. Further, cell line-

based studies dominated, and very few studies were related to animal-based experiments. The Zebrafish model is another platform to explore. However, it seems like more in-depth studies are required to ascertain clinical utility of this biosustainable resource *O. ficus-indica*.

KEYWORDS

cancer, *Opuntia ficus-indica*, prickly pear, antioxidant, phytochemicals

1 Introduction

Cancer is an uncontrolled division of abnormal cells that can potentially intrude or spread (metastasize) to other body regions (Singla et al., 2022c; Chavda et al., 2023). Cancer is a collection of more than 100 different disorders rather than a single disease. It is an uncontrolled cell division that causes abnormal cell development and spread. These malignant cells may infiltrate other tissues and spread to other body parts (metastasize). Cancer is a collection of over 100 different ailments instead of a single disease. Cancer is the world's second leading cause of death, accounting for 7.6 million deaths in 2005 (Abbas and Rehman, 2018). Globally, an estimated 11 million people have been diagnosed with cancer, which was expected to climb to 16 million by 2020 (Sarfati et al., 2016). According to estimates, one-third of all new cancer cases may be cured if properly diagnosed and treated (Wang et al., 2013; Ricks, 2015). Chemotherapy is a cancer treatment that is widely used. Because cancer cells lack many of the regulatory processes normal cells have, they continue to divide even when normal cells do not. Chemotherapeutic medicines are more sensitive to cancer cells with this characteristic (Zugazagoitia et al., 2016; Prager et al., 2018). A substantial collection of useful chemotherapeutic drugs has been established after almost five decades of systemic medication research and development. Chemotherapeutics, on the other hand, are not without their own set of issues. Chemotherapeutic treatments can result in a wide range of side effects. 5-fluorouracil, for example, is known to produce myelotoxicity (Klein et al., 2022) and cardiotoxicity (Labianca et al., 1982), and has even been demonstrated to serve as a vasospastic agent, in rare but recorded occurrences (Rastogi et al., 1993). Doxorubicin, another commonly used chemotherapeutic, has been linked to cardiac toxicity (Avilés et al., 1993; Desai et al., 2008; Damiani et al., 2016), renal toxicity (Varela-López et al., 2019), and myelotoxicity (Pourtier-Manzanedo et al., 1995). The toxicity of chemotherapeutic drugs can be a severe problem when treating cancer using allopathy or traditional medicine (Zugazagoitia et al., 2016; Gezici and Şekeroğlu, 2019). Like chemotherapy, natural products also play an essential role in preventing cancer (Rani et al., 2022). Plants consist of various phytochemicals which are responsible for anticancer activity. The structure of natural plant chemicals varies greatly; many are aromatic compounds, most of which are phenols or their oxygen-substituted counterparts. It is beneficial to focus on active phytochemicals for herbal therapy to minimize the adverse effects, as well as pathogenic resistance against antibiotics (Kooti et al., 2017). Plants produce a large number of secondary metabolites that are biosynthetically derived from primary metabolites and are a major source of microbicides, insecticides, and a variety of pharmaceutical medications (Garg et al., 2022; Babbar et al., 2023; Kumar et al., 2023). Medicinal plants or their secondary metabolites have played an essential role in human society for a long time in combating diseases, either directly or indirectly (Greenwell and Rahman, 2015; Sharma et al., 2022). Despite the availability of various synthetic antitumor drugs, researchers are still looking for potent naturally occurring anticarcinogens that can prevent, delay, or reverse cancer progression (Singla et al., 2022b). Plants are essential in cancer treatment (Singla et al., 2021a; Singla et al., 2022a). Plant-derived chemicals are thought to account for more than half of all anticancer drugs (Omara et al., 2020). Plant extracts were employed to cure a variety of ailments, and this is the foundation of all Indian medical systems (Singla et al., 2021b). However, compared to modern medicine, this subject is underdeveloped owing to a lack of scientific documentation in this field (Chanchal et al., 2017).

Natural foods and food-derived antioxidants, such as vitamins and phenolic phytochemicals, have recently gotten much attention because they protect against oxidative damage and genotoxicity. During the last 20 years, demand for fresh and ready-to-eat items has increased interest in minimally processed fruits and vegetables, which combine freshness and convenience (Kim et al., 1993). Plant forms have long been known to provide medical benefits (Pandey et al., 2023). This review comprehensively summarizes the anticancer attributes of the phytochemicals found in *Opuntia ficus-indica* (L.) Mill. Several species of cactus pear plants (*Cactaceae* family) evolved in Central America (Mexico). In folk medicine, Opuntia fruits and young stems have long been used to treat diseases such as hypertension, diabetes, allergies and asthma, burns, swelling, and nausea. (Abou-Elella and Ali, 2014). The most significant bioactive substances found in cactus fruit are betaxanthin, betacyanin, and phenolic compounds, which all have potent antioxidant capabilities (Gentile, 2004; Kuti, 2004). Phenolic compounds, especially their effective variants, have an aromatic ring bearing one or more hydroxyl groups. Both chemical compositions and concentrations vary considerably depending on the kind of plant tissue, variety, and ripening phases. *Cactaceae* plants and fruits have been shown to contain glycosylated flavonols, dihydroflavonols, flavonones, and flavonols (Kuti, 2000). Cactus pear fruit is a crucial product for protecting human health against degenerative diseases like cancer, diabetes, hyperglycemia,

hypercholesterolemia, arteriosclerosis, and gastric ailments because of the phenolic compounds' antioxidant qualities (Galati et al., 2003). *O. ficus-indica*'s polyphenolic chemicals have been demonstrated to cause the plasma membrane to become hyperpolarized and to increase the intracellular calcium pool in human Jurkat T-cell strains (Aires et al., 2004).

2 Methodology

An extensive survey of the chemical composition and pharmacological activities of *Opuntia ficus-indica* (L.) Mill. was conducted in scientific databases, including Research Gate, Pubmed, Scopus, Science Direct, Web of Science, and Google Scholar. The search terms "*Opuntia ficus-indica*," "*Opuntia ficus-indica* and biological activity," "*Opuntia ficus-indica* and pharmacological activity," "*Opuntia ficus-indica* and chemical compounds," and "*Opuntia ficus-indica* and chemical profile," were used for data collection. One hundred and ten publications were included, from 1992 to 2022, from the articles focused on phytochemicals obtained from *O. ficus-indica*.

3 *Opuntia ficus-indica* (*O. ficus-indica*)-ethnopharmacological perspectives

O. ficus-indica (L.) Mill., sometimes known as the prickly pear or nopal cactus, pertains to the *Cactaceae* family of dicotyledonous angiosperms, which comprises around 1500 species of cactus (Figure 1A). The plant *O. ficus-indica* is native to the tropics and subtropics (Abou-Elella and Ali, 2014). It can grow in arid and semi-arid environments and can be found in South Africa, Mexico, Latin America, and the Mediterranean region (El-Mostafa et al., 2014). Moroccan inhabitants now recognize three kinds of *O. ficus-indica*. The first is known as "Christians' nopal" and is widely employed as a field barrier. It is made up of thorny cladodes. The second, cladodes of inermis, is known as "Muslims' nopal" and is used as green feed for cattle. The final variation, "Moses' nopal," has huge inermis cladodes and produces a gigantic pear. It grows primarily in the south of Morocco (Madrigal-Santillán et al., 2022). The juice, jam, oil, and tea derived from the prickly pear of the nopal cactus are used in health, nutrition, and cosmetics (El-Mostafa et al., 2014). Indigenous peoples eat large amounts of fresh or dried fruits. Cactus cladodes, fruits, and flowers are highlighted in these populations due to their high antioxidant, pectin polysaccharide, and fiber content (Farag et al., 2020).

In several nations, it is utilized as an natural treatment for various health conditions (Slimen et al., 2017). Fresh or dried fruits are consumed in large quantities by indigenous people. Cactus cladodes, fruits, and flowers are promoted in these populations due to their pectin polysaccharide, high antioxidant, and fiber content (Lu et al., 2019). Recent scientific studies have emphasized the synthesis of many bioactive molecules that promote *O. ficus-indica* (L.) Mill medicinal uses and pharmacological characteristics. These molecules include carbohydrates, minerals, amino acids, fatty acids, vitamins, fibers, and secondary metabolites recognized for their antioxidant and anticancer properties (Trachtenberg and Mayer, 1981). The primary aim of this article is to summarize and emphasize the benefits of *O. ficus-indica* in terms of cancer prevention and treatment (Park and Chun, 2001).

4 *Opuntia ficus-indica* as medicinal and nutritional plant: a bibliometric analysis

We have searched PubMed using the search term "*Opuntia ficus-indica*," and 628 articles were retrieved as of 02.06.2023

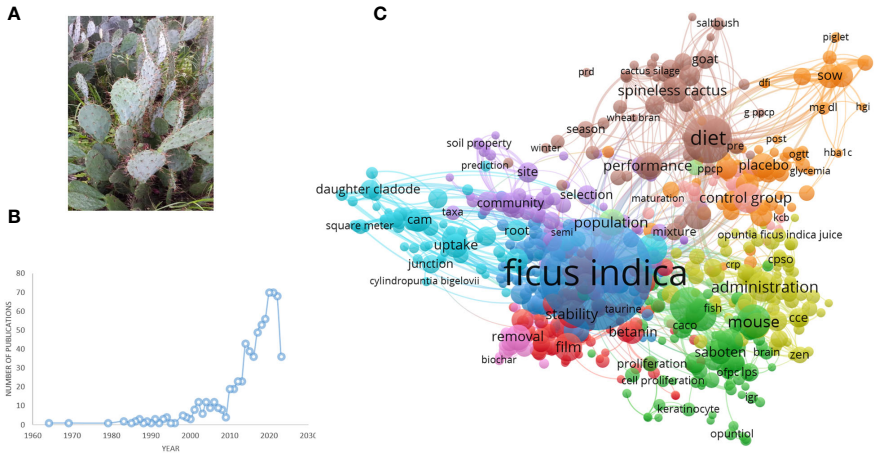

FIGURE 1
(A) *Opuntia ficus-indica*. **(B)** Number of publications related to *Opuntia ficus-indica* over the period until 02.06.2023, as indicated in PubMed. **(C)** Term interaction map based on the literature related to *Opuntia ficus-indica* (the data obtained from PubMed dated 02.06.2023 and processed in VOSviewer).

(Figure 1B), which covered 19 clinical trials articles, three metanalysis articles, 15 randomized controlled trial-based articles, 31 review articles, and four systematic reviews. Some of the countries that researched more on the topics oriented towards *Opuntia ficus-indica* are Italy (98), Brazil (38), Korea (37), Spain (37), France (35), Germany (26), South Africa (17), India (13), China (7), United States (5), Australia (5), and United Kingdom (5). When we processed the title and abstracts of those 628 articles in the VOSviewer, it yielded 16411 keywords. Once we set criteria for a minimum occurrence of a term five times, it resulted in 1229 terms. For each of the 1229 terms, a relevance score will be calculated and based on the score, and with a cutoff of 60% most relevant terms, it finally yielded 737 terms out of 628 articles. The top 10 keywords are given in Table 1, and the overall interactions of all the keywords are illustrated in Figure 1C. The bigger the bubble is, the more it is dominant as keywords in the searched literature.

Nevertheless, we have observed only 1375 MeSH terms and 189 terms that have minimally appeared five times in the selected literature. The top 10 MeSH terms are given in Table 2, and the overall MeSH term map is illustrated in Figure 2. We could see the prevalence of work on *Opuntia ficus-indica* related to apoptosis, cell line tumor, antioxidants, cytoprotection, and reactive oxygen species. It reveals the strong potential of *Opuntia ficus-indica* as a therapeutic reservoir and further encourages us to explore the anticancer potential of *Opuntia ficus-indica.*

5 *Opuntia ficus-indica* with anticancer potential: a bibliometric analysis

When the MeSH terms "*Opuntia ficus-indica*" and "Cancer" were searched on PubMed (dated 01.08.2023), it resulted in 23 articles, including one review article. When the publication data was processed in VOSviewer, it yielded 157 MeSH terms in the title and abstract of these articles. 48 MeSH terms have been repeated in a minimum of 2 publications. Figure 3 is the interactive mapping between these 48 MeSH terms. The most co-occurred MeSH terms were "opuntia," "humans," "antineoplastic agents, phytogenic," "plant extracts," "animals," "apoptosis," "phytotherapy," "cell line, tumor," "cell proliferation," and "mice." We could also observe other vital terms like skin neoplasms, melanoma, colonic neoplasms, HeLa cells, and many others.

TABLE 1 Top 10 keywords as retrieved by VOSviewer from the publications data related to *Opuntia ficus-indica* obtained from PubMed.

Keywords	Occurrences	Relevance
Gardenia seed	5	3.09
Green tea	6	2.93
Sc co	7	2.72
Cactus pear polysaccharide	5	2.71
Ice plant	6	2.68
Nhdf	5	2.57
Metabolic activity	6	2.48
Fibroblast	9	2.16
Susceptibility	5	2.14
M pulegium	5	2.11

TABLE 2 Top 10 MeSH keywords as retrieved by VOSviewer from the publications data related to *Opuntia ficus-indica* obtained from PubMed.

MeSH Keywords	Occurrences	Total Link Strength
Opuntia	352	2255
Plant extracts	182	1364
Animals	154	1184
Male	94	850
Fruit	118	818
Humans	112	817
Antioxidants	94	800
Rats	57	549
Rats, Wistar	41	417
Female	45	360

While exploring Scopus for the articles published with the terms "*Opuntia ficus-indica*" and "cancer," present in Title/Abstract/Keywords, yielded 62 documents. The analyze tool embedded within Scopus was further utilized to do the bibliometric analysis (Figure 4). It has been observed that in the past five years, publications related to "*Opuntia ficus-indica*" and "cancer" have increased significantly (Figure 4A). Four research groups "Antunes-Ricardo, M. et al.," "Attanzio, A. et al.," "Livrea, M.A. et al.," and "Tesoriere, L. et al.," have published four papers each (Figure 4B). Top-most cited article from Antunes-Ricardo, M. et al. was "Induction of Apoptosis in Colon Cancer Cells Treated with Isorhamnetin Glycosides from *Opuntia ficus-indica* Pads" with 71 citations as of date (Antunes-Ricardo et al., 2014). The top-most cited article from Attanzio, A. et al., Livrea, M.A. et al., and Tesoriere, L. et al. was the same. It was entitled "Antiproliferative and pro-apoptotic activity of whole extract and isolated indicaxanthin from *Opuntia ficus-indica* associated with re-activation of the onco-suppressor p16INK4a gene in human colorectal carcinoma (Caco-2) cells" with 50 citations as on date (Naselli et al., 2014). Of 62 documents, 69.4% were articles, followed by 22.6% review articles (Figure 4C), and Italy was recorded as the country with the highest number of documents, followed by Mexico and South Korea (Figure 4D).

When the bibliometric data from these 62 Scopus-retrieved documents were extracted and imported in VOSviewer, there were 1891 indexed keywords. Of these 1891 indexed terms, 59 are visible in at least five publications. Before analysis, some indexed keywords were manually removed like "human," "humans," "nonhuman," "chemistry," "article," "plant extracts," "animal," "animals," "priority journal," "review," "isolation and purification," "human cell," "animal experiment," "animal tissue," "mice," "drug

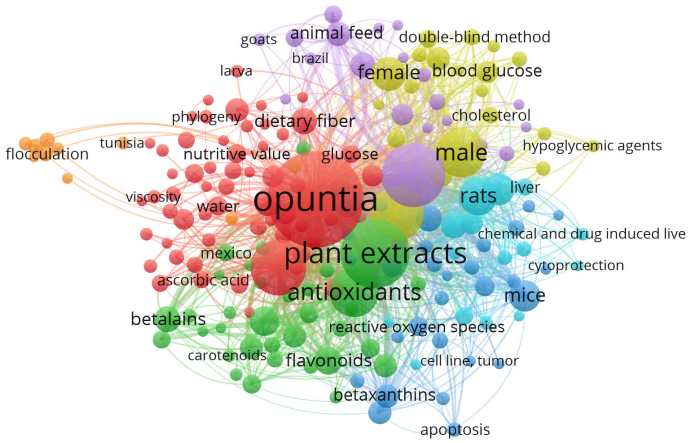

FIGURE 2
MeSH Term interaction map based on the literature related to *Opuntia ficus-indica* (the data obtained from PubMed dated 02.06.2023 and processed in VOSviewer).

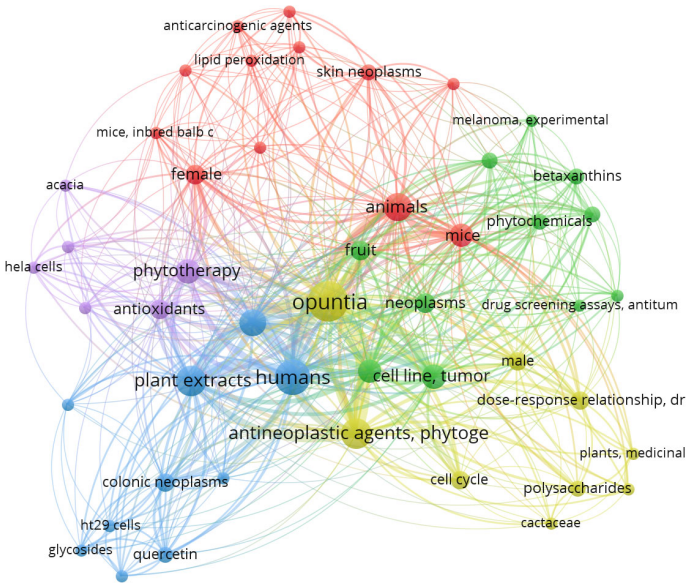

FIGURE 3
MeSH terms interaction map based on the literature on *Opuntia ficus-indica* and cancer (the data obtained from PubMed dated 01.08.2023 and processed in VOSviewer).

mechanism," and "procedures." Figure 5 illustrates the interactive mapping between the selected indexed keywords retrieved from these 62 documents. Along with the *Opuntia ficus-indica* and cancer-specific terms, important co-occurring terms were oxidative stress, antioxidants, anti-inflammatory activity, and diabetes mellitus. Indicaxanthin was strongly connected with cell proliferation and antineoplastic agents. Cell proliferation seems to strongly associate with oxidative stress and lipid peroxidation as a co-occurred term.

6 Role of *Opuntia ficus-indica* in cancer treatment and management

In several studies, abundant Opuntia parts, including prickly pear fruits, seeds, peels, stems, cladodes, and roots, have been shown to have cytotoxic effects on malignant cell lines (Table 3). Antunes-Ricardo et al. (Antunes-Ricardo et al., 2014) investigated the cytotoxic activity of purified isorhamnetin glycosides or cladode flour extracts of *O. ficus-indica* (var. Jalpa) on two types of cancer

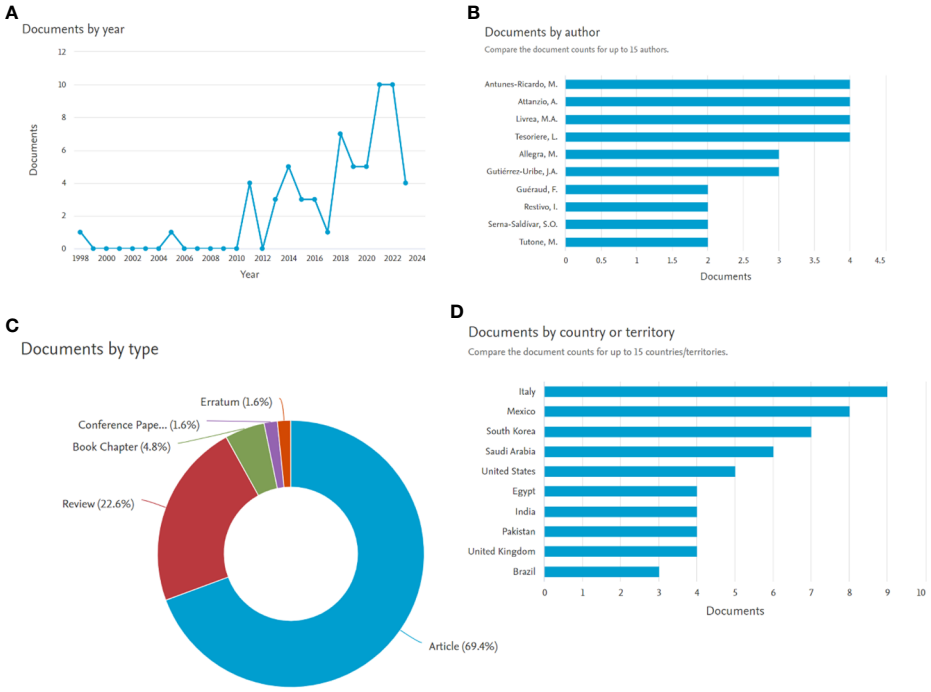

FIGURE 4
Bibliometric analysis of manuscript published with search terms *Opuntia ficus-indica* and cancer (the data obtained from Scopus dated 01.08.2023). **(A)**: Documents by year; **(B)**: Documents by author; **(C)**: Documents by type; **(D)**: Documents by country or territory.

cell lines of the human colon, Caco-2, and HT-29, which represent apoptosis-resistant and apoptosis-susceptible cell lines, successively, with normal fibroblasts (NIH 3T3) were employed as control. According to these authors, the glycosylation pattern of pure isorhamnetin glycosides and extract of cladode flour was more cytotoxic to HT-29 cells than Caco-2 cells. The induction of apoptosis by the caspase cascade, which plays a crucial role in apoptosis pathways, was linked to these effects. Naselli et al. (Naselli et al., 2014) analyzed the results of an aqueous fruit extract of *O. ficus-indica* on the growth of the Caco-2 cancer cell line of the human colon. On proliferating cells, these researchers found no effect on the differentiated cells but a dose-dependent apoptotic effect. This research shows an epigenomic effect on the tumor suppressor gene p16INK4a due to the demethylation of its promoter and stimulation of its expression, indicaxanthin. Betanin, obtained from fruits of *O. ficus-indica*, was found to

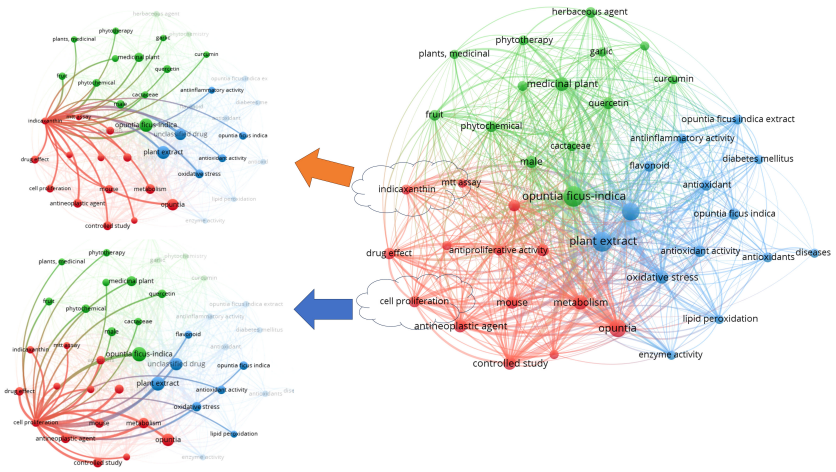

FIGURE 5
Indexed keywords interaction map based on the literature related to *Opuntia ficus-indica* and cancer (the data obtained from Scopus dated 01.08.2023 and processed in VOSviewer).

TABLE 3 Metabolite extracts of *O. ficus-indica* and related species and their anticancer potential.

S. No	The plant part of *O. Ficus-Indica*	Sample Form	Cell lines	Outcome	References
1	Seed	Seed oil	Adeno-carcinoma Cell Lines (Colo-320 and Colo-741)	Reduction in cell viability	(Becer et al., 2018)
2	Stems	Extracts (hexane, ethyl acetate (EtOAc), acetone, methanol (MeOH), and MeOH: water (80:20))	SW480 colon MCF7 breast cancer cells	All except hexane extract exhibited significant cytotoxicity, possibly by COX-2 inhibition and increased Bax/Bcl2 ratio.	(Kim et al., 2015)
3	Fruit	Methanolic extract	U87-MG (glioblastoma multiform; brain cancer) HT-29 (colon cancer) cell lines	Dose-dependent cell death	(Okur et al., 2019)
4	Seed	Seed Oil	Colo-320 Colo-741Colon Carcinoma Cell Lines	Modulates PGE2-mediated and VEGF-dependent angiogenesis	(Becer et al., 2021)
5	Fruit	Aqueous extract	Cancer cell line Caco-2 of the Human colon	Dose-dependent apoptosis	(Naselli et al., 2014)
6	Fruit	Juice	PC3 prostate Caco-2 colon cell lines	The viability of prostate and colon cancer was most affected by juices	(Chavez-Santoscoy et al., 2009)
7	Fruit	Mixture aqueous extract	Ovarian cancer cells (OVCA420, SKOV3)	ROS increase, downregulation of NF-kappaB and p-/SAPK/JNK, and upregulation of p-AKT, the apoptotic effect	(Feugang et al., 2010)
8	Cladode	Powder	Preneoplastic (Apc min/+) immortalized epithelial colon cells	Inhibit LDL oxidation, and increase cytotoxicity	(Keller et al., 2015)
9	Fruit	Alkaline hydrolysis-based extracts	HT-29 and Caco2	More cytotoxic against HT-29 cells than Caco2 cells, increased activity of caspase 3/7	(Antunes-Ricardo et al., 2014)

suppress the development of the human's chronic myeloid leukemia cell line K562 via the apoptotic intrinsic pathway (Sreekanth et al., 2007).

The toxicity impact from prickly pear fruits-filtered juices of several species of *Opuntia* on various cancer cell lines was investigated by Chavez-Santoscoy et al. (Chavez-Santoscoy et al., 2009). The Caco-2 and PC3 prostate cell lines were most impacted, whereas hepatic HepG2 and mammary gland MCF-7 cell lines grew slower. As a control, normal fibroblasts were used. On cancer cells, *O. rastrera* was the most cytotoxic species, with the highest potential and antioxidant content amongst the distinct species exposed to be tested. Kim et al. demonstrated that cladodes extracts from *O. humifusa* may cause apoptosis in human colon SW-480 and MCF-7 cells (Kim et al., 2015). Water-separated fractions of *O. humifusa* stems and fruits suppressed the development of U87MG glioblastoma cells, which was related to cell proliferation and reactive oxygen species (ROS) production (Hahm et al., 2010). The same researchers reported a similar effect on HeLa cancer cells but not on usual fibroblasts (Hahm et al., 2014). Serra et al. (Serra et al., 2013) reported that juice concentrates rich with polyphenols from several Opuntia were found to be cytotoxic to colorectal cancer cell lines HT- 29 but hardly toxic to Caco-2 and that cell-cycle arrest in the same cells was induced more efficiently by the natural juice remnants extracts (peels and seeds) than juice concentrates. Surprisingly, this effect was associated with a rise in ROS in the cells, suggesting that extracts' pro-oxidant effects caused cell death induced by ROS. Feugang et al. (Feugang et al., 2010) observed a similar pro-oxidant effect in ovarian cancer cells when compared to immortalized or normal cells. It is essential to use relevant controls, such as cells of the same type with the same genotype, to make conclusions about compounds' potential benefits. (Phyto)-compounds could be more cytotoxic to cancer cells than their non-cancerous counterparts to be considered as anti-cancer compounds (Keller et al., 2015). Furthermore, various Opuntia cladode flours protect against the cytotoxicity of 4-hydroxynonenal, an oxidation product of dietary lipids that may have a role in promoting red meat for colorectal cancer. Only the usual epithelial cells of the mouse colon showed the protective effect, not on the similar cells that had the Apc type of mutation, whichever is an early phenomenon of colorectal oncogenesis prevalent in humans (Karim and Huso, 2013). Nevertheless, validating the effects seen *in vitro* and *in vivo* studies is essential. Zou et al. observed that aqueous extracts of Opuntia cactus pear inhibited carcinogenesis in nude mice to a similar extent as the synthetic retinamide (4-HPR) retinoid N-(4-hydroxyphenyl) employed as a chemotherapeutic dummy compound (Zou et al., 2005). Hahm et al. demonstrated that *O. humifusa* had a protective effect on HeLa cell xenografts (Hahm et al., 2010). Some researchers

noted that cladode extracts of *O. ficus-indica* reduced genotoxicity and oxidative stress caused by the aflatoxin B1 and mycotoxins zearalenone *in vivo* (Zourgui et al., 2008). Extracts of Opuntia were usually administered into the peritoneal cavity. To determine the protective effects of *Opuntia* spp. additional studies are required, including evaluating the compounds by an oral route or in a more physiological condition that takes into consideration the digestion and bioavailability of compounds alike. In such an approach, in two distinct animal models of skin carcinogenesis, lyophilized powder of *O. humifusa* fruit administered through pelletized food was found to be protecting with a decline in inflammation and skin lipid peroxidation (Lee et al., 2012; Lee et al., 2013). All these findings suggest that *Opuntia* spp., whether in the form of fruits, nopal (Opuntia cladodes or stems), or fruit juice, might be an effective anticancer approach.

7 Phytochemicals present in *O. ficus-indica* and its anticancer attributes

Opuntia ficus-indica is known to have various phytochemicals, which are discussed below.

7.1 Polyphenolic compounds

Phenolics are small plant secondary metabolites with at least one hydroxyl group and an aromatic ring (Singla et al., 2019). More than 8000 phenolic chemicals have been found in the vegetable kingdom, with over 4000 flavonoids now known (El Gharras, 2009). Flavonoids are the most frequent phenolic compounds found in

TABLE 4 Phytochemicals and their contents found in different parts of *O. ficus indica*.

Phytochemicals (unit)	Plant Part	Content	References
Total phenolics (mg/100gm)	Flower	12022–27090	(Fernández-López et al., 2010; Jorge et al., 2013; El-Mostafa et al., 2014; Ammar et al., 2015; Ramírez-Ramos et al., 2018)
	Cladodes	390.90	
	Peels	45.700–425.59	
	Fruits	48.11–218.8	
	Seeds	48–89	
	Fruit Pulp	5.35 mg GAE/g	(Sigwela et al., 2021)
Total flavonoids (mg/100gm)	Flower	6081–6267	(Fernández-López et al., 2010; Jorge et al., 2013; El-Mostafa et al., 2014; Ammar et al., 2015; Ramírez-Ramos et al., 2018)
	Cladodes	73	
	Peels	6.95–23.96	
	Fruits	2.60–15.560	
	Seeds	1.5–2.6	
	Fruit pulp	0.63 mg CE/g	(Sigwela et al., 2021)
Total tannins (mg/100gm)	Flower	768.67	(Figueroa-Pérez et al., 2018; Ramírez-Ramos et al., 2018)
	Cladodes	430–620	
	Peels	23–144	
	Seeds	4.1–205	
Total anthocyanins (mg/100gm)	Cladodes	0.05–0.34	(Alves et al., 2017)
Quinic acid (mg/100gm)	Cladodes	42.983–436.96	(Belhadj Slimen, 2017; Oniszczuk et al., 2020)
	Peels	145.071	

(Continued)

TABLE 4 Continued

Phytochemicals (unit)	Plant Part	Content	References
	Fruits	45.471	
Malic acid (mg/100gm)	Cladodes	3124– 4421.7	(Allai et al., 2016)
trans-Aconitic acid (mg/100gm)	Cladodes	77.15– 88.63	(Allai et al., 2016)
Betalains (mg/Kg)	Cladodes	16.17	(De Wit et al., 2020)
	Peels	13.57	
	Fruits	18.52	
β-Sitosterol(mg/Kg)	Cladodes	16.53	(Ramadan and Mörsel, 2003; Allai et al., 2016)
	Peels	21.1	
	Fruits	11.2	
	Seeds	6.75	
	Seed oil	2.80	
Stigmasterol (mg/Kg)	Cladodes	13.4	
	Peels	0.73	
	Fruits	2.12	
	Seeds	0.30	
Δ7-Avenasterol (mg/Kg)	Cladodes	11.6	
	Seeds	0.05	
Campesterol (mg/Kg)	Cladodes	5.7	
	Peels	8.74	
	Fruits	8.76	
	Seeds	1.66	
	Seed oil	0.51	
Campestanol (mg/Kg)	Cladodes	6.4	
Carotenoids (μg/g)	Peels	12.58–16.83	(Fernández-López et al., 2010)
	Fruits	2.58–6.68	
Saponins (g/Kg)	Cladodes	8.72	(Touré et al., 2015)
	Peels	6.36	
	Seeds	20.4	
Ascorbic acid (mg/100 gm)	Fruit pulp	12.35	(Sigwela et al., 2021)

plants. They feature a diphenylpropane (C_6-C_3-C_6) core structure with two aromatic rings connected by an oxygenated heterocycle (Harborne and Williams, 2000). The fruits and seeds of *O. ficus-indica* had the lowest concentrations of phenolics and flavonoids, whereas peels, flowers, and cladodes had the highest concentrations. The phenolic profile of the whole Opuntia plant includes 40 phenolic acids, 1 gallotannin, 3 flavanones, 8 flavanols, 18 flavonols, 3 flavononols, and 9 flavones (Table 4).

7.1.1 Organic acids

Three organic acids were discovered in *O. ficus-indica* in addition to the phenolic compounds: malic (Figure 6A), quinic (Figure 6B), and aconitic (Figure 6C) acids. Peels and cladodes had the highest concentrations. More research is required to determine the comparable levels in flowers and seeds. Quinic acid ($C_7H_{12}O_6$) is a cyclohexane carboxylic skeleton-containing plant metabolite. Quinic acid is critical in manufacturing aromatic chemicals

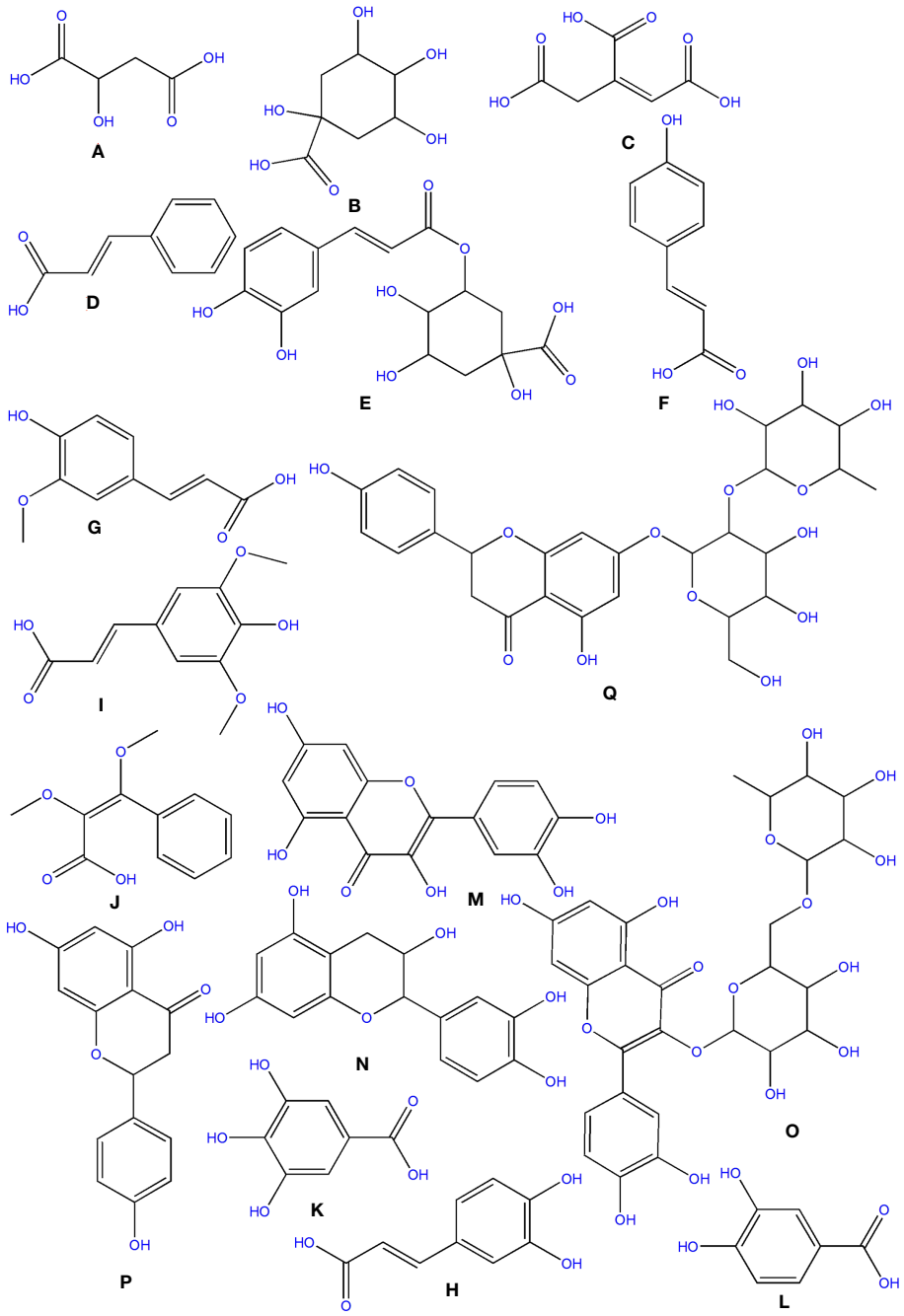

FIGURE 6
Structure of some of the phytochemicals isolated from *O. ficus-indica*. **(A)** Malic acid; **(B)** Quinic acid; **(C)** Aconitic acid; **(D)** Cinnamic acid; **(E)** Chlorogenic Acid; **(F)** p-Coumaric acid; **(G)** Ferulic acid; **(H)** Caffeic Acid; **(I)** Sinapic acid; **(J)** Dimethoxycinnamic acid; **(K)**: Gallic acid; **(L)** Protocatechuic acid; **(M)** Quercetin; **(N)** Catechin; **(O)** Rutin; **(P)** Naringenin; **(Q)** Naringin.

(flavonoids and phenol carboxylic acids) in higher plants, people, and animals (Bai et al., 2018). D-(-)-Quinic acid has been shown to have antioxidant, anti-inflammatory, and antiproliferative characteristics in addition to its antibacterial activity (Belhadj Slimen et al., 2021). This chemical is also linked to neuro- and radioprotective properties (Liu et al., 2020). Antioxidant, anti-inflammatory, and antiproliferative effects have been described for D-(-)-Quinic acid (Alfieri et al., 2021). In experimental mice, cis-aconitic acid prevented carcinogenesis produced by 3, 4-benzopyrene (Belhadj Slimen et al., 2021).

7.1.2 Phenolic acids

Phenolics are secondary metabolites that have recently attracted attention as anti-cancer agents. Phenolics have much potential as anti-cancer medicines since they promote apoptosis, reduce proliferation, and target several elements of cancer (angiogenesis,

growth and differentiation, and metastasis) (Abotaleb et al., 2020). Hydroxybenzoic and hydroxycinnamic acids are different kinds of phenolic acids (Clifford, 1999). Cinnamic acid derivatives include hydroxycinnamic acids. Simple esters containing quinic acid or glucose. Cinnamic (Figure 6D), chlorogenic (Figure 6E), coumaric (Figure 6F), and ferulic (Figure 6G) acids are the most prevalent hydroxycinnamic acids in *O. ficus-indica*. Caffeic (Figure 6H), sinapic (Figure 6I), and dimethoxycinnamic (Figure 6J) acids were found in lower quantities (Bai et al., 2018).

7.1.2.1 Gallic acid

Gallic acid (Figure 6K), chemically known as 3,4,5-trihydroxybenzoic acid, was discovered in the flowers and cladodes of *O. ficus-indica*. It can be found in plants as an ester, free acid, hydrolyzable tannin, or catechin derivatives. Gallic acid, along with its by-products, has been shown to have a broad range of biological activities like bactericide, antiviral, antifungal, inflammatory harmonizer, antidiabetic activities, and antiproliferative (Kahkeshani et al., 2019). Gallic acid and its derivatives have been shown to have an anti-cancer effect *in vivo* and *in vitro* in several investigations (Sun et al., 2002; Bhattacharya et al., 2016). Gallic acid has been shown to have anti-cancer properties in various cancer cells, including human ovarian cancer cells (Dai and Mumper, 2010; De et al., 2013). Gallic acid's anti-cancer properties have been proved to be attributable to its capacity to suppress cell proliferation and promote apoptosis (De Mejia et al., 2009).

7.1.2.2 Protocatechuic acid

Protocatechuic acid (PCA) (Figure 6L), also known as 3,4-dihydroxybenzoic acid, is a dihydroxybenzoic acid in which the hydroxy groups are attached at positions 3 and 4. Recent research suggests that PCA could be a cancer-fighting agent against neoplasms. Its mode of action is related mainly to its radical scavenging activity, which allows it to limit the formation of free radicals while also up-regulating enzymes involved in the neutralization of radicals (Kakkar and Bais, 2014). PCA has also been described as an anticancer agent and found to be a powerful antioxidant (Belhadj Slimen et al., 2021).

7.1.2.3 Cinnamic acid and derivatives

Cinnamic acid ($C_9H_8O_2$) is a plant-derived organic acid. It is less toxic and possesses many biological and antioxidant properties (Sova, 2012). Cinnamic acid derivatives have better antioxidant activity than benzoic acid analogs (Natella et al., 1999). Cinnamic acid and its derivatives (natural and non-natural molecules) have been shown to have anticancer potential in recent decades. Various cinnamoyl compounds and their anticancer effectiveness have gotten much interest in recent decades (De et al., 2011) and promote the proliferation of neural progenitor cells (Otero et al., 2014).

7.1.2.4 Chlorogenic acid

Chlorogenic acid ($C_{16}H_{18}O_9$) (CGA), also termed 3-O-caffeoylquinic acid, is a cinnamate ester produced by conventional condensation of the carboxy group of trans-caffeic acid with the 3-hydroxy group of quinic acid. Chlorogenic acid has long been known to be an antioxidant (Meng et al., 2013; Su et al., 2015; Tajik et al., 2017). Its anticarcinogenic, anti-inflammatory, and antioxidant properties might make it a non-invasive cure or preventative approach for some chronic diseases (Tajik et al., 2017). CGA also works as a potent chemo-sensitizing agent, inhibiting cancer growth by activating and inhibiting critical pathways in cancer metabolism (Slimen et al., 2016). CGA's anticancer molecular processes, on the other hand, are unknown (Abd Elrazik et al., 2019).

7.1.2.5 Coumaric acid and derivatives

P-coumaric acid ($C_9H_8O_3$), also referred to as 4-hydroxycinnamic acid, is a phenyl ring hydroxylated cinnamic acid analog. It is a conjugate of 4-coumarate. The amino acids tyrosine and phenylalanine are used to synthesize p-coumaric acid. Coumaric acid is crucial in phenolic acid production, including rosmarinic, caffeic, chlorogenic, and ferulic acids. Based on the research by Kiliç and Yeşiloğlu, p-coumaric acid is a reasonable scavenger and potent antioxidant of reactive oxygen species and free radicals (Kiliç and Yeşiloğlu, 2013). It was more efficient than vitamin E in reducing oxidative stress in animal models (Guglielmi et al., 2003). This acid has been drawn to suppress cancer cell growth and migration while promoting apoptotic cancer cell death, indicating that it may have antioxidant effects (Roy et al., 2016). It has also been shown in animal models to have chemopreventive effects against colon cancer. The biosynthesis of coumaric acid is shown in Figure 7 (Sharma et al., 2018).

7.1.2.6 Ferulic acid

Ferulic acid (FA) is a trans-cinnamic acid with hydroxy and methoxy aggregates on the phenyl ring at positions 3 and 4. It is an omnipresent phytochemical occurring in the cell walls of the plant. It may be found in both covalently-coupled and free (rarely) forms, one to lignin and others in biopolymers in leaves and seeds. FA readily generates a resonance-stabilized phenoxyl radical, which gives its high antioxidant activity (Graf, 1992; Mancuso et al., 2007). Ferulic acid has been proven to have anti-cancer properties in a range of cancers, including colon and lung cancers and tumors of the central nervous system. However, its possible effect in limiting breast cancer metastasis is still uncertain (Zhang et al., 2016). Trans-ferulic acid inhibited Hsp60-induced cell growth to a significant extent (Fukuoka et al., 2004). FA has been shown to have anticancer properties. Gao et al. (2018) demonstrated that in Hela and Caski cells, FA can substantially reduce cell invasion and

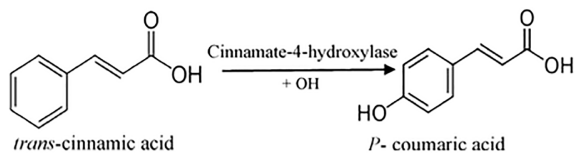

FIGURE 7
Synthesis of coumaric acid.

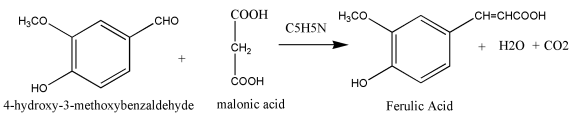

FIGURE 8
Synthesis of ferulic acid.

metastasis. Inhibiting autophagy and triggering cell cycle arrest in human cervical carcinoma cells could make it an anti-cancer therapeutic. The synthesis of Ferulic Acid is shown in Figure 8 (Mancuso and Santangelo, 2014; Gao et al., 2018).

7.1.2.7 Caffeic acid

Caffeic acid (3, 4-dihydroxycinnamic acid) structurally has acrylic and phenolic functional groups (Rocha et al., 2012). It was found in high concentrations in the fruits and flowers of *O. ficus-indica* and was found to have a wide range of biological characteristics. Caffeic acid and its derivatives are effective against oral, colon, and liver cancers and are likely to be cyclooxygenase II inhibitors in malignancies (Slimen et al., 2016). Even though much research has shown caffeic acid's anticancer activity, some researchers have demonstrated carcinogenic effects, even at modest doses (Hirose et al., 1998). The International Agency for Research on Cancerous disease has categorized this acid as a chemical "possibly carcinogenic to humans" in group 2B. As a result, further research is needed before concluding that caffeic acid has a preventive or carcinogenic potential (Slimen et al., 2016).

7.1.3 Flavonoids

Flavonoids are secondary metabolites derived from plants. They are divided into four primary categories: anthocyanidins, flavanols, flavones, and isoflavonoids. They are also classified into subcategories (Duraipandiyan et al., 2017).

7.1.3.1 Flavanols

Flavanols are a structurally complex subclass of phenolic compounds that range from monomers (such as catechin) to oligomers (from dimers to decamers), polymers, and more complex derivatives (such as theaflavins and thearubigins). Quercetin (Figure 6M) and its derivatives, catechin (Figure 6N), and rutin (Figure 6O), a flavan-3-ol, are the vital flavanols found in *O. ficus-indica*. Although flavanols were not found in Opuntia cladodes and peels, they were in high concentrations in flowers and minimal levels in fruits. Flowers have excessive concentrations of flavanols, followed by cladodes, peels, and fruits. More research is required to determine the flavanol concentration in seeds. Because of its high antioxidant action, rutin is a very potent molecule. It was found to have antifungal, anti-allergic, and antibacterial properties, and it is now used to treat many chronic diseases like diabetes, hypertension, hypercholesterolemia, and cancer. Rutin is a non-oxidizable and non-toxic molecule when compared to other flavonoids (Sharma et al., 2013). Flavonoids have been demonstrated to have a wide range of anti-cancer properties, including the ability to modulate ROS, induce apoptosis, autophagy, invasiveness, and reduce cancer cell growth. Flavonoids have a dual role in ROS homeostasis: they are significant pro-oxidants in cancer cells, initiating apoptosis pathways, and they also act as antioxidants in healthy cells, inhibiting pro-inflammatory signaling pathways (Kopustinskiene et al., 2020).

7.1.3.2 Flavanones

Flavanones, commonly called dihydroflavones, are a kind of flavonoid discovered in secondary metabolites of plants. In *O. ficus-indica*, three types of flavanones were found: naringenin (Figure 6P), naringin (Figure 6Q), and hesperidin (Figure 9A) (Zeghad et al., 2019; Hernández García et al., 2020). Hesperidin (16.18–17.46 mg/100 g), which was found mainly in cladodes, had the highest content, followed by naringin, mainly in peels (0.17 mg/100 g) (Belhadj Slimen et al., 2021). In peels, residues of naringenin were detected, while traces of naringenin were identified in fruits. *O. ficus-indica* peels have been verified as a flavanones source, whereas cladodes contain the highest hesperidin amount (Renugadevi and Prabu, 2009). More research is needed to evaluate these compounds in flowers and seeds. The glycosylated derivative of naringenin is naringin ($C_{27}H_{32}O_{14}$), a polymethoxylated flavonoid ($C_{15}H_{12}O_{15}$). The antioxidants naringenin and naringin are both potent (Jung et al., 2003).

7.2 Betalains

Betalains are nitrogen-containing hydro-soluble pigments. They are established in the sap of vacuoles and are mixed as bis-anions there (Brockington et al., 2015). Betalains were discovered in large quantities in the pulp and peel of *O. ficus-indica*. Peels have a higher concentration of betacyanins (19.43 compared to 6.76 mg/kg); however, fruits have a higher concentration of betaxanthins (53.27 compared to 40.72 mg/kg). Peels have more total betalains than fruits. Consequently, the peel's betanin (Figure 9B) concentration is more significant than that of fruits (2473 mg/kg *vs.* 1616 mg/kg). The quantities of betacyanins and betaxanthins were closely related to the fruit coloring (Belhadj Slimen et al., 2021). De Wit et al. had compared seven cultivars of *O. ficus-indica* and one from *O. robusta*. Out of 7 cultivars, seeds of Nepgen (green) contains highest quantities of betacyanins (69.89 mg/Kg) and betaxanthins (48.92 mg/Kg), followed by seeds of Sicilian Indian Fig (pink) with betacyanins (56.50 mg/Kg) and betaxanthins (39.55 mg/Kg). However, seeds of *O. robusta* were having highest betacyanins and betaxanthins (de Wit et al., 2019). Further, in another study, De Wit et al. compared 4 cultivars of *O. ficus-indica* and one cultivar from *O. robusta*. Among various cultivars of *O. ficus-indica*, fresh fruit from Meyers cultivar possesses highest quantity of betacyanins (6.87 mg/kg) and betaxanthins (4.81 mg/Kg). However, again the fresh fruits from *O. robusta* contains betacyanins and betaxanthins, multifolds higher than that of *O. ficus-indica*. Their study also signifies that fresh and dried fruits are containing maximum betacyanins and betaxanthins, and it was significantly reduced in the form of chutney, juice, and preserves

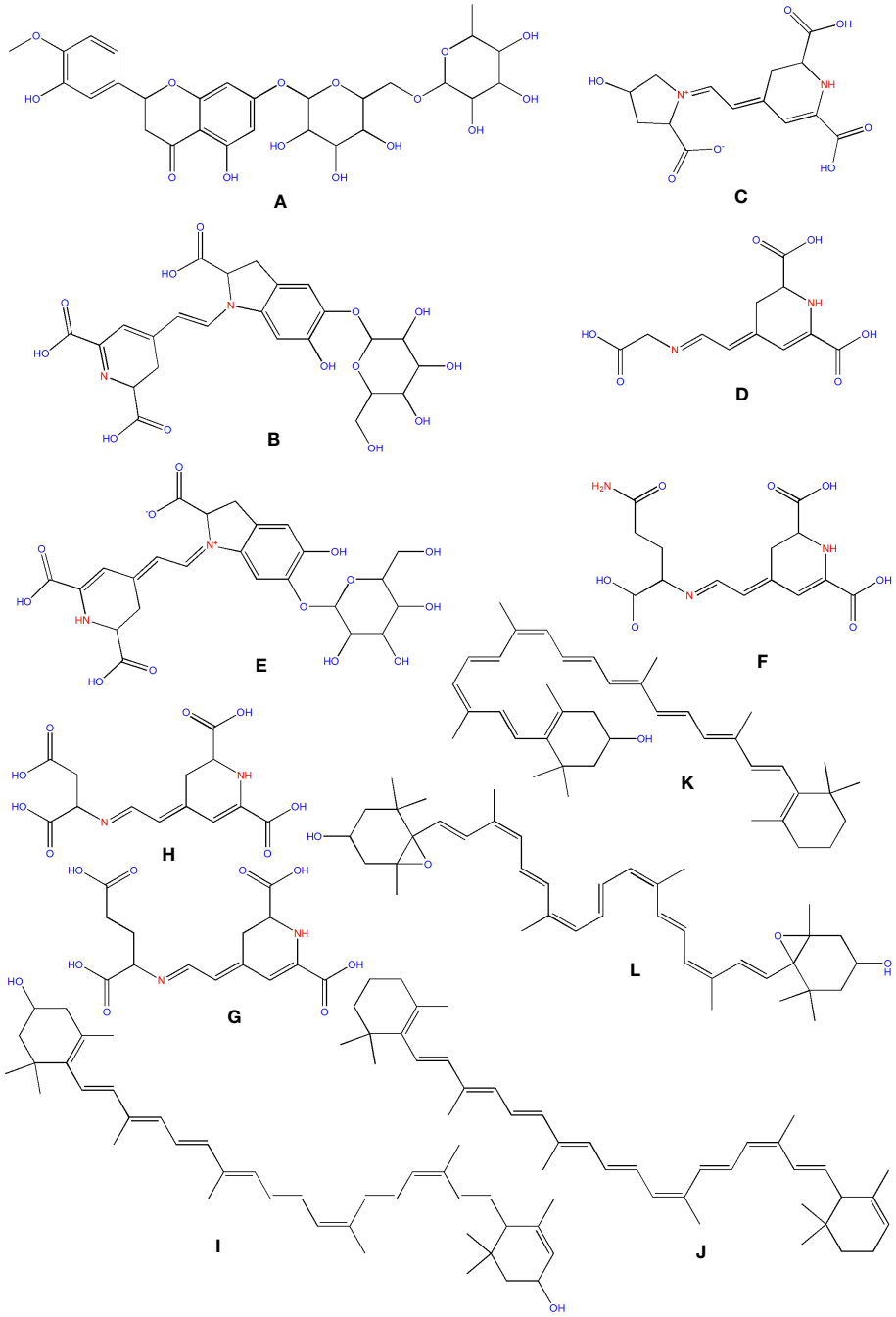

FIGURE 9
Structure of some of the phytochemicals isolated from *O. ficus-indica*. **(A)** Hesperidin; **(B)** Betanin; **(C)** Portulacaxanthin I; **(D)** Portulacaxanthin III; **(E)** Gomphrenin-I; **(F)** Vulgaxanthin I; **(G)** Vulgaxanthin-II; **(H)** Miraxanthin-II; **(I)** Lutein; **(J)** Carotene; **(K)** Cryptoxanthin; **(L)** Violaxanthin.

(De Wit et al., 2020). The peel also consists of muscaaurin, portulacaxanthin I (Figure 9C), portulacaxanthin III (Figure 9D), gomphrenin I (Figure 9E), (S)-valine-betaxanthin, (S)-isoleucine-betaxanthin, (S)-serine-betaxanthin, (S)-phenylalanine-betaxanthin, Vulgaxanthin I (Figure 9F), Vulgaxanthin II (Figure 9G), Vulgaxanthin IV, and miraxanthin II (Figure 9H) (Stintzing et al., 2005; Yeddes et al., 2013). Several investigations have identified betalains as an antioxidant dietary cationized type with a strong radical scavenging capacity (Kanner et al., 2001; de Wit et al., 2019; De Wit et al., 2020; Sigwela et al., 2021).

In vitro research has indicated that betalains elicit the phase II detoxifying enzyme quinone reductase in murine hepatoma cells (Madadi et al., 2020). Betalains actively scavenge free radicals, which may help to prevent cancer and cardiovascular disease. Betalains have been discovered to activate a critical factor of transcription, which causes to activate the endogenous defense of antioxidant systems in cells (Esatbeyoglu et al., 2014). In cancer cells, betalains from *Opuntia ficus-indica* fruits were discovered to have the effect of antiproliferative activity. In nude mice, betalains containing prickly pear fruit extracts inhibited the development of

human ovarian cancer cells compared to a synthetic chemopreventive drug, Fenretinide (4-HPR). In addition, these extracts suppressed 40 to 60 percent of immortal cervical epithelial cells and cervical cancer cells (Zou et al., 2005). Betanin (betalain) was discovered to cause time and dose-dependent apoptosis in the leukemia cell line (K562) of human chronic myeloid, as well as a decrease in the potential of mitochondrial membrane and the presence of cyt C in the cytosolic portions of cells (Sreekanth et al., 2007). Subsequently, treatment with betalains and combining medication, which stops the process at several cell cycle points (G1 and/or S phases), can be a potential scheme for preventing cancerous tumor survival. Although the method by which betalains may prevent cancer is unknown, studies have indicated that they change gene expression and modulates cell development and apoptosis (Zou et al., 2005). Cancer cell lines like K562 and MCF7 enables researchers to investigate possible anticancer chemicals like betalains in a simple, controlled, and repeatable setting. However, because cell cultures cannot mimic tumor behavior and its interaction with the host (HogenEsch and Nikitin, 2012), the efficiency of betalains as an anticancer drug in human clinical trials may differ. Future research, combining cancer cell lines of humans within a model that profoundly resembles the targeted cancer of humans, will have a better chance of determining betalains' anticancer potential (Gengatharan et al., 2015).

7.3 Carotenoids

Carotenoids are abundant in *O. ficus-indica*, and their concentration in the peel is substantially higher than in the pulp. Their maturation stage heavily influences the carotenoid composition of cladodes; the highly rich carotenoids in young cladodes are lutein (Figure 9I), carotene (Figure 9J), and β-cryptoxanthin (Figure 9K). Despite cultivar differences, cladodes carry more carotene than fruit (de Wit et al., 2019). Four carotenes and nine xanthophylls (84–86% of all carotenoids) make up the carotenoid profile of fruits. Lutein and violaxanthin (Figure 9L) were the most abundant xanthophyll compounds (representing 69–72 percent and 5 percent of all amount of carotenoid content in the whole fruit, respectively), whereas carotene was the most abundant pigment of carotene (representing almost 12–14 percent of the total carotenoid content). Lower concentrations of antheraxanthin (Figure 10A), zeaxanthin (Figure 10B), and neoxanthin (Figure 10C) have been found. The highest values were in orange-colored cultivars plants (Cano et al., 2017).

In 2014, Niranjana et al. examined carotenoids' anticancer effectiveness through cell cycle arrest, apoptosis induction, anti-metastasis, and anti-angiogenic activities. One of the main characteristics of cancer cells is that they lose their ability to regulate the cell cycle and limit the proliferation rate. Carotenoids have been demonstrated to limit tumor cell proliferation by interfering with various cell cycle stages. Carotenoids have been shown to have chemopreventive properties in humans, lowering cancer incidence through apoptosis (Niranjana et al., 2015). Creating innovative anti-metastatic medications with minimal toxicity and excellent efficacy is one of the most active fields in contemporary anti-cancer research. Carotenoids have been shown in observational studies to have anti-metastasis properties (Kozuki et al., 2000). Various chemicals from natural sources have been proven to suppress angiogenesis, with carotenoids being particularly effective (Slimen et al., 2016).

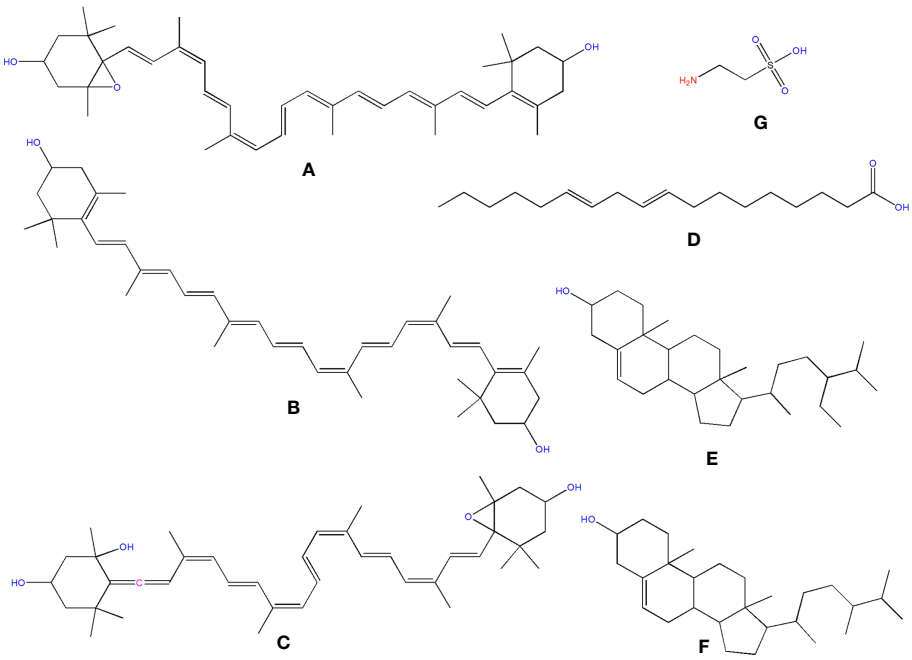

FIGURE 10
Structure of some of the phytochemicals isolated from *O. ficus-indica*. **(A)** Antheraxanthin; **(B)** Zeaxanthin; **(C)** Neoxanthin; **(D)** Linoleic Acid; **(E)** Sitosterol; **(F)** Campesterol; **(G)** Taurine.

Bensadón et al. determined the antioxidant and scavenging properties of polyphenols and carotenoids and other compounds by FRAP and ABTS methods in two varieties of *O. ficus-indica*, the Atlixco (52.22 ± 1.07 and 52.37 ± 2.00, respectively) and Milpa Alta (65.33 ± 2.23 and 57.55 ± 1.83, respectively) (Bensadón et al., 2010).

β-cryptoxanthin has shown its potential in various cancers, including stomach cancer (Sengngam et al., 2022), hepatocellular carcinoma (Lim et al., 2020), lung cancer (Iskandar et al., 2016), and colon cancer (San Millan et al., 2015). Lutein was reportedly having strong anticancer potential against breast cancer (Bulatao et al., 2023), non-small cell lung cancer (Zhang et al., 2023), pancreatic cancer (Han and Song, 2022), and gastric cancer (Eom et al., 2023). Zeaxanthin has anticancer potential against melanoma (Cenariu et al., 2021), colorectal cancer (Kim et al., 2019), dermal fibroblasts (Wu et al., 2010), and gastric cancer (Abnet et al., 2003).

7.4 Fatty acids

Chromatographic techniques were used to determine total lipids in various vegetative sections of *O. ficus-indica*. Linoleic acid (Figure 10D) has been identified as the most abundant cladodes polyunsaturated fatty acid, accounting for about 32.83 percent of the total fatty acid content. Palmitic acid, linolenic acid, oleic acid, and linoleic acid make up about 90% of cladode's total fatty acids (Kolniak-Ostek et al., 2020). The polyunsaturated and mono-unsaturated fatty acid content in fruits ranged from 35.2% to 53.9% and 16.9% to 40.2%, independently, of total fatty acid content. Peels have lower concentrations of mono-unsaturated fatty acids than the concentration of polyunsaturated fatty acids.

Similarly, seed oil has a high proportion of polyunsaturated fatty acids but a low proportion of mono-unsaturated fatty acids. Linoleic acid can be considered the most common fatty acid in seed oil, fruits, and peels, which is interesting. Similarly, the content in peels is higher than that found in fruits (De Wit et al., 2017). Mono-unsaturated and polyunsaturated fatty acid consumption has been suggested for its health-improving qualities. They also help improve various health issues associated with cancer (Simopoulos, 2002).

7.5 Phytosterols

Sitosterol (Figure 10E) was found to be the most abundant sterol in oil fruit, seeds, peel, and pulp of *O. ficus-indica* (Kozuki et al., 2000), with amounts ranging from 6.75 to 21.1 g/kg. Campesterol (Figure 10F) was found in seeds, peels, and fruits in concentrations ranging from 1.66 to 8.76 g/kg. Other phytosterols discovered in trace amounts included stigmasterol, lanosterol, ergosterol, 5-avenasterol, and 7-avenasterol. Ergosterol (ergosta-5,7,22-trien-3-ol) is a sterol present in the cell membranes of fungi and protozoa. In animal cells, it performs the same functions as cholesterol. In human nutrition, ergosterol is a vitamin D_2 provitamin. Remarkably, ergosterol was observed in Opuntia peels in small amounts. Phytosterols have been attributed to a reduced risk of breast, colon, and prostate cancers. Phytosterols, for example, have been found to enhance cancer immune recognition, impact hormonally dependent endocrine cancer growth, cycle arrest, and impede tumor growth and spread (Slimen et al., 2016).

7.6 Taurine

Taurine ($C_2H_7NO_3S$) (Figure 10G) is an organic osmolyte not integrated into proteins. Taurine is an amino acid found in the brain, retina, muscles, and organs all over the body. Taurine is engaged in various processes, from development to cytoprotection, and is regarded as a cell-protective amino acid with antioxidative properties (Devamanoharan et al., 1998). The taurine content in cladodes, peels, and seeds should be examined. Taurine, the most abundant free amino acid, is involved in several biological processes in humans and has been found to have an antitumor effect (He et al., 2016). Kim and Kim examined the protective effects of taurine against anticancer medicines on normal cells, which were recently revealed. However, the anticancer effects of taurine on cancer cells are still unknown. As a result, we looked at the anti-cancer effects of taurine alone as well as taurine combined with cisplatin in human cervical cancer cells. In a time and dosage-dependent way, a single dose of taurine reduced cell growth. Cell proliferation was reduced more when cisplatin was combined with taurine than when cisplatin was used alone. Apoptosis induction resulted in decreased cell growth. Apoptotic cells were studied when cisplatin was treated with taurine. Taurine or cisplatin, in combination, promoted apoptotic cells more than taurine or cisplatin alone. The activation of caspase-3, caspase-6, caspase-7, and caspase-9 was attributed to the induction of apoptosis (Kim and Kim, 2013).

7.7 Saponins

Saponins are glycosides with triterpenoid or spirostane aglycones that have anti-mammalian disease pharmacological properties (Xu et al., 2016). More research on saponins in *O. ficus-indica* is needed. The presence of saponins in the aqueous extract of *O. ficus-indica* cladodes was discovered by Halmi and his associates (Halmi et al., 2018). Figueroa-Pérez and his colleagues found larger quantities in cladodes, averaging 28.13 g equivalents/kg (Figueroa-Pérez et al., 2018). Saponins show strong anti-tumorigenic effects through various anticancer mechanisms due to the considerable heterogeneity of their structures. Unique saponins with potent anticancer properties have also been developed. Ginsenosides, which belong to the dammaranes family, have been proven effective at inhibiting tumor angiogenesis by suppressing its inducer in blood vessel endothelial cells and preventing tumor cell adhesion, invasion, and metastasis. Dioscin, a steroidal saponin, and its aglycone diosgenin have indeed been researched extensively for their anticancer effects *via* cell cycle arrest and apoptosis (Man et al., 2010).

8 Future perspectives

O. ficus-indica contains various phytochemicals ranging from phenolic acids to phytosterols (Figure 11). Many phytochemicals like

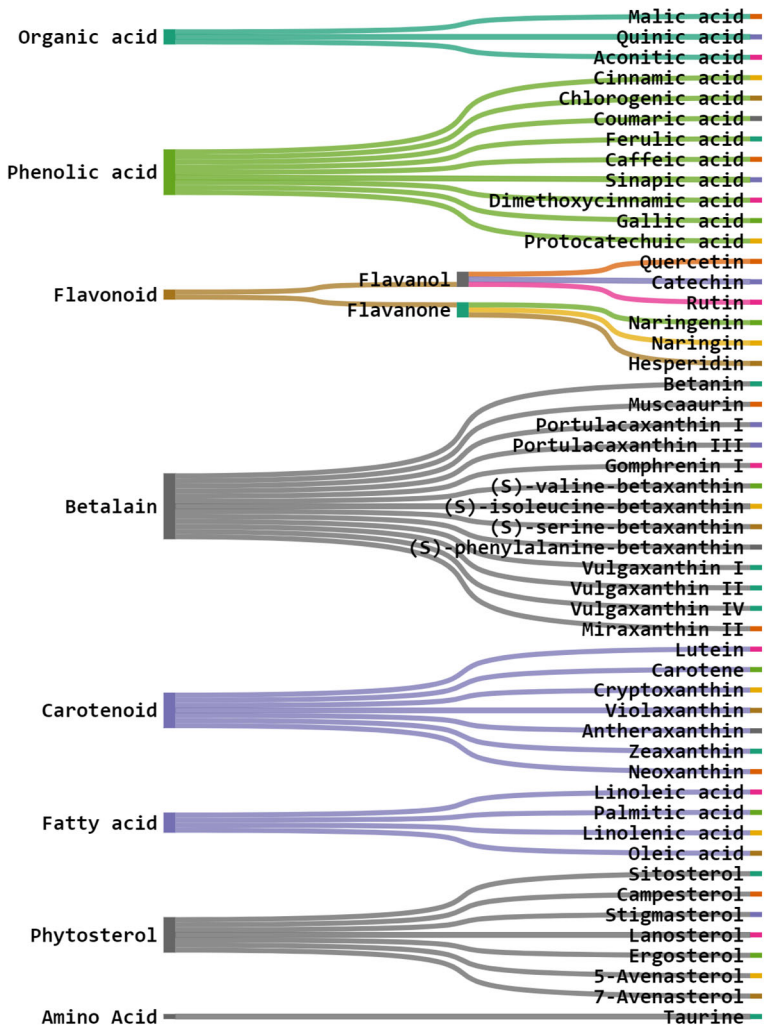

FIGURE 11
Phytochemicals present in *O. ficus-indica* and their phytochemical class.

quercetin, hesperidin, and linolenic acid have already been evaluated and proven to have multifarious therapeutic potentials. However, it seems like more in-depth studies are required to validate the translational potential of *O. ficus-indica* to reach bedside.

Searching on PubMed for *O. ficus-indica* and cancer-related papers yielded 18 results on 02.06.2023 while searching for *O. ficus-indica* and apoptosis-related papers resulted in 9 papers as of 03.06.2023. These studies indicate the increasing interest of researchers to examining anticancer potential of this plant. However, it is still quite low quantitatively and more in-depth research is utmost needed in this direction. Upon removal of duplicates, 21 articles were processed for quantitative data analysis (QDA). Some of the most prominent terminologies found to be "*Opuntia ficus-indica*," "extract," "indicaxanthin," "kaempferol," "glycoside," "Opuntia," "cancer," "colorectal/colon cancer," and "apoptosis." (Figure 12) Indicaxanthin, kaempferol, and isorhamnetin glycosides were most studied as anticancer agents in those studies (Figure 13A). When we looked for the prevalence of the phytochemical class mentioned repeatedly in those 21 articles, we had observed that glycosides dominate, followed by flavonoids and betalains (Figure 13B). Most anticancer studies on *O. ficus-indica* and its purified metabolites are related to colorectal/colon cancer, followed by melanoma and breast cancer (Figure 14). Very little attention has been paid to leukemia, thyroid, endometrial, liver, and prostate cancer, and it should be considered an

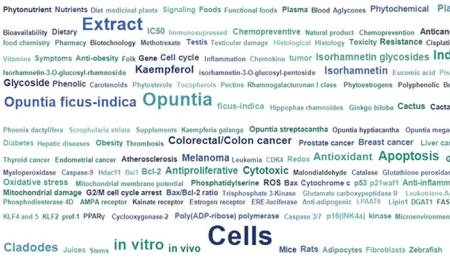

FIGURE 12
Quantitative data analysis-based study to understand the overall prevalence and dominating key terms in papers published with "*Opuntia ficus-indica*" and "Cancer".

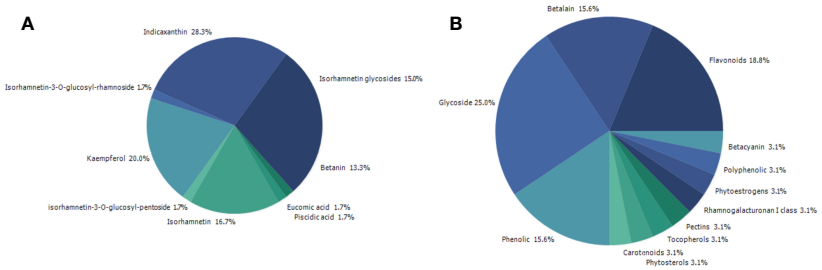

FIGURE 13
Quantitative data analysis-based study to understand the prevalence and dominating key terms in papers published with "*Opuntia ficus-indica*" and "Cancer." **(A)** Prevalence of the studied phytochemicals; **(B)** Prevalence of the study's phytochemical classes.

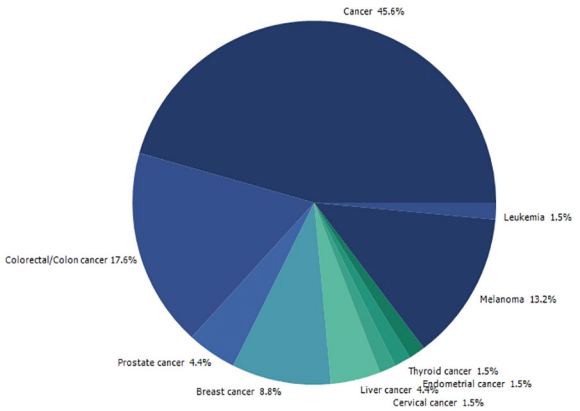

FIGURE 14
Quantitative data analysis-based study to understand the prevalence of the type of cancer being studied in papers published with "*Opuntia ficus-indica*" and "Cancer".

opportunity for the researchers to explore *O. ficus-indica* and its metabolites for these heterogenous cancers. The most notable mechanisms expressed and validated in those studies were apoptosis, cell cycle arrest (G0/G1 and G2/M), Bcl-2 modulation, antiproliferative, oxidative stress-mediated mechanisms, and cytochrome c (Figure 15). We have also observed that cladodes and fruits of *O. ficus-indica* have been more studied than other plant parts, which again opens opportunities for researchers to explore. Further, cell line-based studies dominated, and there were very few studies related to animal-based experiments. The Zebrafish model has also been utilized by one group, and it could open a new platform for others to explore.

FIGURE 15
Quantitative data analysis-based study to understand the most studied and covered anticancer and related mechanisms in papers published with "*Opuntia ficus-indica*" and "Cancer".

9 Conclusion

In this article, we discussed the effectiveness of *O. ficus-indica* against most death-causing diseases, including cancer. Traditional chemo- and radiotherapies can weaken the patient due to their toxic and destructive effects on normal cells. The *O. ficus-indica* plant is a natural means that can be used for the prevention and cure of cancer without any serious side-effects. Various phytochemicals are present in *O. ficus-indica*, which includes flavonoids, polyphenols, betalains, and tannins, which possess various biological activities such as antimicrobial, anti-inflammatory, antioxidant, and most essential, anticancer activity. Based on the available literature we provided in this study, investigations using diverse cancer cell lines have shown compelling evidence of anticancer activity. Only a few investigations employing *in vivo* tumor models have produced comparable results. Currently, very little information is available on whether concentrations demonstrating activity *in vitro* are attainable in the blood or serum of laboratory animals. While this is a restriction in our current knowledge of the anticancer potential of plants in the *Cactaceae* family, future studies are likely to examine this to next level. We believe that the significance of our review lies in drawing the scientific community's attention to this plant family, which is, on the one hand, auspicious in terms of cancer treatment and prevention, but on the other hand, remains mostly unexplored.

Author contributions

JW, NR, SJ, RR, SK, SaK, SvK, BD, JS-G, BS, and RKS wrote different manuscript sections. NR, RKS, and BS laid down the idea and manuscript outline and compiled and finalized the manuscript. BS arranged the funding source. All the authors have reviewed the final version of the manuscript.

Funding

This work was supported by the National Natural Science Foundation of China (32070671, 32270690), the Covid-19 research

projects of West China Hospital Sichuan University (Grant no. HX-2019-nCoV-057).

Conflict of interest

The authors declare that the research was conducted in the absence of any commercial or financial relationships that could be construed as a potential conflict of interest.

Publisher's note

References

Abbas, Z., and Rehman, S. (2018). An overview of cancer treatment modalities. *Neoplasm* 1, 139–157. doi: 10.5772/intechopen.76558

Abd Elrazik, N. A., El-Mesery, M., El-Karef, A., Eissa, L. A., and El Gayar, A. M. (2019). Chlorogenic acid potentiates antitumor effect of doxorubicin through upregulation of death receptors in solid Ehrlich carcinoma model in mice. *Egyptian J. Basic Appl. Sci.* 6 (1), 158–172. doi: 10.1080/2314808X.2019.1682331

Abnet, C. C., Qiao, Y. L., Dawsey, S. M., Buckman, D. W., Yang, C. S., Blot, W. J., et al. (2003). Prospective study of serum retinol, beta-carotene, beta-cryptoxanthin, and lutein/zeaxanthin and esophageal and gastric cancers in China. *Cancer Causes Control* 14 (7), 645–655. doi: 10.1023/a:1025619608851

Abotaleb, M., Liskova, A., Kubatka, P., and Büsselberg, D. (2020). Therapeutic potential of plant phenolic acids in the treatment of cancer. *Biomolecules* 10 (2), 221. doi: 10.3390/biom10020221

Abou-Elella, F. M., and Ali, R. F. M. (2014). Antioxidant and Anticancer Activities of Different Constituents Extracted fromEgyptian Prickly Pear Cactus (Opuntia ficus-indica) Peel. *Biochem. Analytical Biochem.* 3 (2), 1–9. doi: 10.4172/2161-1009.1000158

Aires, V., Adote, S., Hirchami, A., Moutairou, K., Boustani, E.-S. E., and Khan, N. A. (2004). Modulation of intracellular calcium concentrations and T cell activation by prickly par polyphenols. *Mol. Cell. Biochem.* 260 (1), 103–110. doi: 10.1023/b:Mcbi.0000026061.57326.28

Alfieri, M., Leone, A., and Ambrosone, A. (2021). Plant-derived nano and microvesicles for human health and therapeutic potential in nanomedicine. *Pharmaceutics* 13 (4), 498. doi: 10.3390/pharmaceutics13040498

Allai, L., Karym, E. L. M., El Amiri, B., Nasser, B., Essamad, A., Terzioğlu, P., et al. (2016). Evaluation of antioxidant activity and phenolic composition of opuntia ficus-indica cladodes collected from moroccan settat region. *Eurasian J. Analytical Chem.* 12 (1), 105–117. doi: 10.12973/ejac.2017.00148a

Alves, F. A. L., Andrade, A., Bruno, R., Silva, M., Souza, M., and Santos, D. (2017). Seasonal variability of phenolic compounds and antioxidant activity in prickly pear cladodes of Opuntia and Nopalea genres. *Food Sci. Technol.* 37 (4), 536–543. doi: 10.1590/1678-457x.19316

Ammar, I., Ennouri, M., and Attia, H. (2015). Phenolic content and antioxidant activity of cactus (Opuntia ficus-indica L.) flowers are modified according to the extraction method. *Ind. Crops Products* 64, 97–104. doi: 10.1016/j.indcrop.2014.11.030

Antunes-Ricardo, M., Moreno-García, B. E., Gutiérrez-Uribe, J. A., Aráiz-Hernández, D., Alvarez, M. M., and Serna-Saldivar, S. O. (2014). Induction of apoptosis in colon cancer cells treated with isorhamnetin glycosides from opuntia ficus-indica pads. *Plant Foods Hum. Nutr.* 69 (4), 331–336. doi: 10.1007/s11130-014-0438-5

Avilés, A., Arévila, N., Díaz Maqueo, J. C., and Nambo, M. J. (1993). Late cardiac toxicity of doxorubicin, epirubicin, and mitoxantrone therapy for hodgkin's disease in adults. *Leukemia Lymphoma* 11 (3-4), 275–279. doi: 10.3109/10428199309087004

Babbar, R., Kaur, R., Rana, P., Arora, S., Behl, T., Albratty, M., et al. (2023). The current landscape of bioactive molecules against DENV: A systematic review. *Evid Based Complement Alternat Med.* 2023, 2236210. doi: 10.1155/2023/2236210

Bai, J., Wu, Y., Zhong, K., Xiao, K., Liu, L., Huang, Y., et al. (2018). A comparative study on the effects of quinic acid and shikimic acid on cellular functions of staphylococcus aureus. *J. Food Prot.* 81 (7), 1187–1192. doi: 10.4315/0362-028X.JFP-18-014

Becer, E., Kabadayı, H., Meriçli, A. H., Kıvançlı, B., Vatansever, H. S., and Meriçli, F. (2021). Fatty acid composition of opuntia ficus-indica seed oil control angiogenic activity in colon carcinoma cell lines. *Prog. Nutr.* 23 (2), e2021051. doi: 10.23751/pn.v23i2.10042

Becer, E., Kabadayı, H., Meriçli, F., Meriçli, A. H., Kıvançlı, B., and Vatansever, S. (2018). Apoptotic Effects of Opuntia ficus indica L. Seed Oils on Colon Adenocarcinoma Cell Lines. *Proceedings* 2 (25), 1566. doi: 10.3390/proceedings2251566

Belhadj Slimen, I. (2017). LC-MS analysis of phenolic acids, flavonoids and betanin from spineless <i>Opuntia ficus-indica</i> Fruits. *Cell Biol.* 5 (2), 17-28. doi: 10.11648/j.cb.20170502.12

Belhadj Slimen, I., Najar, T., and Abderrabba, M. (2021). "Bioactive Compounds of Prickly Pear [Opuntia Ficus-Indica (L.) Mill.]," in *Bioactive compounds in underutilized vegetables and legumes. Reference series in phytochemistry. Reference series in phytochemistry.* Eds. H. N. Murthy and K. Y. Paek. Cham: Springer. doi: 10.1007/978-3-030-44578-2_12-2

Bensadón, S., Hervert-Hernández, D., Sáyago-Ayerdi, S. G., and Goñi, I. (2010). By-products of opuntia ficus-indica as a source of antioxidant dietary fiber. *Plant Foods Hum. Nutr.* 65 (3), 210–216. doi: 10.1007/s11130-010-0176-2

Bhattacharya, S., Muhammad, N., Steele, R., Peng, G., and Ray, R. B. (2016). Immunomodulatory role of bitter melon extract in inhibition of head and neck squamous cell carcinoma growth. *Oncotarget* 7 (22), 33202–33209. doi: 10.18632/oncotarget.8898

Brockington, S. F., Yang, Y., Gandia-Herrero, F., Covshoff, S., Hibberd, J. M., Sage, R. F., et al. (2015). Lineage-specific gene radiations underlie the evolution of novel betalain pigmentation in Caryophyllales. *New Phytol.* 207 (4), 1170–1180. doi: 10.1111/nph.13441

Bulatao, B. P., Nalinratana, N., Jantaratana, P., Vajragupta, O., Rojsitthisak, P., and Rojsitthisak, P. (2023). Lutein-loaded chitosan/alginate-coated Fe(3)O(4) nanoparticles as effective targeted carriers for breast cancer treatment. *Int. J. Biol. Macromol* 242 (Pt 1), 124673. doi: 10.1016/j.ijbiomac.2023.124673

Cano, M. P., Gómez-Maqueo, A., García-Cayuela, T., and Welti-Chanes, J. (2017). Characterization of carotenoid profile of Spanish Sanguinos and Verdal prickly pear (Opuntia ficus-indica, spp.) tissues. *Food Chem.* 237, 612–622. doi: 10.1016/j.foodchem.2017.05.135

Cenariu, D., Fischer-Fodor, E., Tigu, A. B., Bunea, A., Virag, P., Perde-Schrepler, M., et al. (2021). Zeaxanthin-Rich Extract from Superfood Lycium barbarum Selectively Modulates the Cellular Adhesion and MAPK Signaling in Melanoma versus Normal Skin Cells *In Vitro*. *Molecules* 26 (2), 333. doi: 10.3390/molecules26020333

Chanchal, D. K., Alok, S., Rashi, S., Bijauliya, R. K., Yadav, R. D., and Sabharwal, M. (2017). Various medicinal plants used in the treatment of anticancer activity. *Int. J. Pharm. Sci. Res.* 9 (4), 1424–1429. doi: 10.13040/IJPSR.0975-8232.9(4).1424-29

Chavda, V. P., Nalla, L. V., Balar, P., Bezbaruah, R., Apostolopoulos, V., Singla, R. K., et al. (2023). Advanced phytochemical-based nanocarrier systems for the treatment of breast cancer. *Cancers* 15 (4), 1023. doi: 10.3390/cancers15041023

Chavez-Santoscoy, R. A., Gutierrez-Uribe, J. A., and Serna-Saldívar, S. O. (2009). Phenolic composition, antioxidant capacity and *in vitro* cancer cell cytotoxicity of nine prickly pear (Opuntia spp.) juices. *Plant Foods Hum. Nutr.* 64 (2), 146–152. doi: 10.1007/s11130-009-0117-0

Clifford, M. N. (1999). Chlorogenic acids and other cinnamates – nature, occurrence and dietary burden. *J. Sci. Food Agric.* 79 (3), 362–372. doi: 10.1002/(SICI)1097-0010(19990301)79:3<362::AID-JSFA256>3.0.CO;2-D

Dai, J., and Mumper, R. J. (2010). Plant phenolics: extraction, analysis and their antioxidant and anticancer properties. *Molecules* 15 (10), 7313–7352. doi: 10.3390/molecules15107313

Damiani, R. M., Moura, D. J., Viau, C. M., Caceres, R. A., Henriques, J. A. P., and Saffi, J. (2016). Pathways of cardiac toxicity: comparison between chemotherapeutic drugs doxorubicin and mitoxantrone. *Arch. Toxicol.* 90 (9), 2063–2076. doi: 10.1007/s00204-016-1759-y

De, P., Baltas, M., and Bedos-Belval, F. (2011). Cinnamic acid derivatives as anticancer agents-A review. *Curr. Medicinal Chem.* 18 (11), 1672–1703. doi: 10.2174/092986711795471347

De, A., De, A., Papasian, C., Hentges, S., Banerjee, S., Haque, I., et al. (2013). Emblica officinalis extract induces autophagy and inhibits human ovarian cancer cell proliferation, angiogenesis, growth of mouse xenograft tumors. *PloS One* 8 (8), e72748. doi: 10.1371/journal.pone.0072748

De Mejia, E. G., Ramirez-Mares, M. V., and Puangpraphant, S. (2009). Bioactive components of tea: Cancer, inflammation and behavior. *Brain Behavior Immun.* 23 (6), 721–731. doi: 10.1016/j.bbi.2009.02.013

Desai, G. A., Qazi, N. G., Ganju, K. R., El-Tamer, M., Singh, J., Saxena, K. A., et al. (2008). Medicinal plants and cancer chemoprevention. *Curr. Drug Metab.* 9 (7), 581–591. doi: 10.2174/138920008785821657

Devamanoharan, P. S., Ali, A. H., and Varma, S. D. (1998). Oxidative stress to rat lens in *vitro*: Protection by taurine. *Free Radical Res.* 29 (3), 189–195. doi: 10.1080/10715769800300221

de Wit, M., du Toit, A., Osthoff, G., and Hugo, A. (2019). Cactus pear antioxidants: a comparison between fruit pulp, fruit peel, fruit seeds and cladodes of eight different cactus pear cultivars (Opuntia ficus-indica and Opuntia robusta). *J. Food Measurement Characterization* 13 (3), 2347–2356. doi: 10.1007/s11694-019-00154-z

De Wit, M., Du Toit, A., Osthoff, G., and Hugo, A. (2020). Antioxidant Content, Capacity and Retention in Fresh and Processed Cactus Pear (Opuntia ficus-indica and O. robusta) Fruit Peels From Different Fruit-Colored Cultivars. *Front. Sustain. Food Syst.* 4. doi: 10.3389/fsufs.2020.00133

De Wit, M., Hugo, A., and Shongwe, N. (2017). Quality Assessment of Seed Oil from Selected Cactus Pear Cultivars (Opuntia ficus-indica and Opuntia robusta). *J. Food Process. Preservation* 41 (3), e12898. doi: 10.1111/jfpp.12898

Duraipandiyan, V., William Raja Tharsius, R., Naif Abdullah, A.-D., and Ignacimuthu, S. (2017). Flavonoids: anticancer properties. *Flavonoids* (Rijeka). doi: 10.5772/68095

El Gharras, H. (2009). Polyphenols: food sources, properties and applications – a review. *Int. J. Food Sci. Technol.* 44 (12), 2512–2518. doi: 10.1111/j.1365-2621.2009.02077.x

El-Mostafa, K., El Kharrassi, Y., Badreddine, A., Andreoletti, P., Vamecq, J., El Kebbaj, M., et al. (2014). Nopal cactus (Opuntia ficus-indica) as a source of bioactive compounds for nutrition, health and disease. *Molecules* 19 (9), 14879–14901. doi: 10.3390/molecules190914879

Eom, J. W., Lim, J. W., and Kim, H. (2023). Lutein induces reactive oxygen species-mediated apoptosis in gastric cancer AGS cells *via* NADPH oxidase activation. *Molecules* 28 (3), 1178. doi: 10.3390/molecules28031178

Esatbeyoglu, T., Wagner, A. E., Motafakkerazad, R., Nakajima, Y., Matsugo, S., and Rimbach, G. (2014). Free radical scavenging and antioxidant activity of betanin: Electron spin resonance spectroscopy studies and studies in cultured cells. *Food Chem. Toxicol.* 73, 119–126. doi: 10.1016/j.fct.2014.08.007

Farag, M. A., Sallam, I. E., Fekry, M. I., Zaghloul, S. S., and El-Dine, R. S. (2020). Metabolite profiling of three Opuntia ficus-indica fruit cultivars using UPLC-QTOF-MS in relation to their antioxidant potential. *Food Bioscience* 36, 100673. doi: 10.1016/j.fbio.2020.100673

Fernández-López, J. A., Almela, L., Obón, J. M., and Castellar, R. (2010). Determination of antioxidant constituents in cactus pear fruits. *Plant Foods Hum. Nutr.* 65 (3), 253–259. doi: 10.1007/s11130-010-0189-x

Feugang, J. M., Ye, F., Zhang, D. Y., Yu, Y., Zhong, M., Zhang, S., et al. (2010). Cactus pear extracts induce reactive oxygen species production and apoptosis in ovarian cancer cells. *Nutr. Cancer* 62 (5), 692–699. doi: 10.1080/01635581003605508

Figueroa-Pérez, M. G., Pérez-Ramírez, I. F., Paredes-López, O., Mondragón-Jacobo, C., and Reynoso-Camacho, R. (2018). Phytochemical composition and in vitro analysis of nopal (O. Ficus-indica) cladodes at different stages of maturity. *Int. J. Food Properties* 21 (1), 1728–1742. doi: 10.1080/10942912.2016.1206126

Fukuoka, K., Sawabe, A., Sugimoto, T., Koga, M., Okuda, H., Kitayama, T., et al. (2004). Inhibitory actions of several natural products on proliferation of rat vascular smooth muscle cells induced by Hsp60 from Chlamydia pneumoniae J138. *J. Agric. Food Chem.* 52 (20), 6326–6329. doi: 10.1021/jf0351164

Galati, E. M., Mondello, M. R., Giuffrida, D., Dugo, G., Miceli, N., Pergolizzi, S., et al. (2003). Chemical Characterization and Biological Effects of SicilianOpuntia ficus indica (L.) Mill. Fruit Juice: Antioxidant and Antiulcerogenic Activity. *J. Agric. Food Chem.* 51 (17), 4903–4908. doi: 10.1021/jf030123d

Gao, J., Yu, H., Guo, W., Kong, Y., Gu, L., Li, Q., et al. (2018). The anticancer effects of ferulic acid is associated with induction of cell cycle arrest and autophagy in cervical cancer cells. *Cancer Cell Int.* 18 (1), 102. doi: 10.1186/s12935-018-0595-y

Garg, S., Singla, R. K., Rahman, M. M., Sharma, R., Mittal, V., and Yang, S. (2022). Evaluation of ulcer protective activity of morus alba L. Extract-loaded chitosan microspheres in ethanol-induced ulcer in rat model. *Evidence-Based Complementary Altern. Med.* 2022, 1–17. doi: 10.1155/2022/4907585

Gengatharan, A., Dykes, G. A., and Choo, W. S. (2015). Betalains: Natural plant pigments with potential application in functional foods. *LWT - Food Sci. Technol.* 64 (2), 645–649. doi: 10.1016/j.lwt.2015.06.052

Gentile, C. (2004). Antioxidant betalains from cactus pear (Opuntia ficus-indica) inhibit endothelial ICAM-1 expression. *Ann. New York Acad. Sci.* 1028 (1), 481–486. doi: 10.1196/annals.1322.057

Gezici, S., and Şekeroğlu, N. (2019). Current perspectives in the application of medicinal plants against cancer: novel therapeutic agents. *Anti-Cancer Agents Medicinal Chem.* 19 (1), 101–111. doi: 10.2174/1871520619666181224121004

Graf, E. (1992). Antioxidant potential of ferulic acid. *Free Radical Biol. Med.* 13 (4), 435–448. doi: 10.1016/0891-5849(92)90184-I

Greenwell, M., and Rahman, P. K. (2015). Medicinal plants: their use in anticancer treatment. *Int. J. Pharm. Sci. Res.* 6 (10), 4103–4112. doi: 10.13040/ijpsr.0975-8232.6(10).4103-12

Guglielmi, F., Luceri, C., Giovannelli, L., Dolara, P., and Lodovici, M. (2003). Effect of 4-coumaric and 3,4-dihydroxybenzoic acid on oxidative DNA damage in rat colonic mucosa. *Br. J. Nutr.* 89 (5), 581–587. doi: 10.1079/BJN2003849

Hahm, S.-W., Park, J., Oh, S.-Y., Lee, C.-W., Park, K.-Y., Kim, H., et al. (2014). Anticancer properties of extracts from opuntia humifusa against human cervical carcinoma cells. *J. Medicinal Food* 18 (1), 31–44. doi: 10.1089/jmf.2013.3096

Hahm, S.-W., Park, J., and Son, Y.-S. (2010). Opuntia humifusa partitioned extracts inhibit the growth of U87MG human glioblastoma cells. *Plant Foods Hum. Nutr.* 65 (3), 247–252. doi: 10.1007/s11130-010-0188-y

Halmi, S., Madi, A., Zeghad, N., Berouel, K., and Pacha, Y. H. (2018). Effect of Opuntia ficus indica on Antioxidant Activity and Lipid Profile of Experimental Rats Ingested Thermally Oxidized Oil. *Eur. J. Medicinal Plants* 23 (4), 1–10. doi: 10.9734/EJMP/2018/40946

Han, L., and Song, X. (2022). Lutein induces an inhibitory effect on the Malignant progression of pancreatic adenocarcinoma by targeting BAG3/cholesterol homeostasis. *J. Biochem. Mol. Toxicol.* 36 (2), e22958. doi: 10.1002/jbt.22958

Harborne, J. B., and Williams, C. A. (2000). Advances in flavonoid research since 1992. *Phytochemistry* 55 (6), 481–504. doi: 10.1016/S0031-9422(00)00235-1

He, Y. U., Li, Q. Q., and Guo, S. C. (2016). Taurine attenuates dimethylbenz[a] anthracene-induced breast tumorigenesis in rats: A plasma metabolomic study. *Anticancer Res.* 36 (2), 533–544.

Hernández García, F., Andreu Coll, L., Cano-Lamadrid, M., López Lluch, D., A. Carbonell BarraChina, Á., and Legua Murcia, P. (2020). "Valorization of prickly pear [Opuntia ficus-indica (L.) mill]: Nutritional Composition, Functional Properties and Economic Aspects," in *Invasive Species - Introduction Pathways, Economic Impact, and Possible Management Options*. United Kingdom: IntechOpen Limited.

Hirose, M., Takesada, Y., Tanaka, H., Tamano, S., Kato, T., and Shirai, T. (1998). Carcinogenicity of antioxidants BHA, caffeic acid, sesamol, 4-methoxyphenol and catechol at low doses, either alone or in combination, and modulation of their effects in a rat medium-term multi-organ carcinogenesis model. *Carcinogenesis* 19 (1), 207–212. doi: 10.1093/carcin/19.1.207

HogenEsch, H., and Nikitin, A. Y. (2012). Challenges in pre-clinical testing of anti-cancer drugs in cell culture and in animal models. *J. Controlled Release* 164 (2), 183–186. doi: 10.1016/j.jconrel.2012.02.031

Iskandar, A. R., Miao, B., Li, X., Hu, K. Q., Liu, C., and Wang, X. D. (2016). beta-cryptoxanthin reduced lung tumor multiplicity and inhibited lung cancer cell motility by downregulating nicotinic acetylcholine receptor alpha7 signaling. *Cancer Prev. Res. (Phila)* 9 (11), 875–886. doi: 10.1158/1940-6207.CAPR-16-0161

Jorge, A. J., de la Garza, T. H., Alejandro, Z. C., Ruth, B. C., and Noé, A. C. (2013). The optimization of phenolic compounds extraction from cactus pear (Opuntia ficus-indica) skin in a reflux system using response surface methodology. *Asian Pacific J. Trop. Biomedicine* 3 (6), 436–442. doi: 10.1016/s2221-1691(13)60093-3

Jung, U. J., Kim, H. J., Lee, J. S., Lee, M. K., Kim, H. O., Park, E. J., et al. (2003). Naringin supplementation lowers plasma lipids and enhances erythrocyte antioxidant enzyme activities in hypercholesterolemic subjects. *Clin. Nutr.* 22 (6), 561–568. doi: 10.1016/S0261-5614(03)00059-1

Kahkeshani, N., Farzaei, F., Fotouhi, M., Alavi, S. S., Bahramsoltani, R., Naseri, R., et al. (2019). Pharmacological effects of gallic acid in health and diseases: A mechanistic review. *Iran J. Basic Med. Sci.* 22 (3), 225–237. doi: 10.22038/ijbms.2019.32806.7897

Kakkar, S., and Bais, S. (2014). A review on protocatechuic acid and its pharmacological potential. *ISRN Pharmacol.* 2014, 952943. doi: 10.1155/2014/952943

Kanner, J., Harel, S., and Granit, R. (2001). BetalainsA new class of dietary cationized antioxidants. *J. Agric. Food Chem.* 49 (11), 5178–5185. doi: 10.1021/jf010456f

Karim, B. O., and Huso, D. L. (2013). Mouse models for colorectal cancer. *Am. J. Cancer Res.* 3 (3), 240–250.

Keller, J., Camaré, C., Bernis, C., Astello-García, M., de la Rosa, A.-P. B., Rossignol, M., et al. (2015). Antiatherogenic and antitumoral properties of Opuntia cladodes: inhibition of low density lipoprotein oxidation by vascular cells, and protection against the cytotoxicity of lipid oxidation product 4-hydroxynonenal in a colorectal cancer cellular model. *J. Physiol. Biochem.* 71 (3), 577–587. doi: 10.1007/s13105-015-0408-x

Kiliç, I., and Yeşiloğlu, Y. (2013). Spectroscopic studies on the antioxidant activity of p-coumaric acid. *Spectrochimica Acta Part A: Mol. Biomolecular Spectrosc.* 115, 719–724. doi: 10.1016/j.saa.2013.06.110

Kim, T., and Kim, A. K. (2013). "Taurine enhances anticancer activity of cisplatin in human cervical cancer cells,". *Taurine* 8, 189–198. doi: 10.1007/978-1-4614-6093-0_19

Kim, J., Lee, J., Oh, J. H., Chang, H. J., Sohn, D. K., Kwon, O., et al. (2019). Dietary lutein plus zeaxanthin intake and DICER1 rs3742330 A > G polymorphism relative to colorectal cancer risk. *Sci. Rep.* 9 (1), 3406. doi: 10.1038/s41598-019-39747-5

Kim, D. M., Smith, N. L., and Lee, C. Y. (1993). Apple cultivar variations in response to heat treatment and minimal processing. *J. Food Sci.* 58 (5), 1111–1114. doi: 10.1111/j.1365-2621.1993.tb06126.x

Kim, J., Soh, S. Y., Shin, J., Cho, C.-W., Choi, Y. H., and Nam, S.-Y. (2015). Bioactives in cactus (Opuntia ficus-indica) stems possess potent antioxidant and pro-apoptotic activities through COX-2 involvement. *J. Sci. Food Agric.* 95 (13), 2601–2606. doi: 10.1002/jsfa.6968

Klein, K., Dandulakis, M., and Roque, D. M. (2022). ""Overview of Ovarian Cancer Chemotherapy,"," in *Advances in Diagnosis and Management of Ovarian Cancer,*. Ed. S. A. Farghaly (Cham: Springer International Publishing), 129–169.

Kolniak-Ostek, J., Kita, A., Miedzianka, J., Andreu-Coll, L., Legua, P., and Hernandez, F. (2020). Characterization of Bioactive compounds of opuntia ficus-

indica (L.) mill. Seeds from spanish cultivars. *Molecules* 25 (23), 5734. doi: 10.3390/molecules25235734

Kooti, W., Servatyari, K., Behzadifar, M., Asadi-Samani, M., Sadeghi, F., Nouri, B., et al. (2017). Effective medicinal plant in cancer treatment, part 2: review study. *J. Evidence-Based Complementary Altern. Med.* 22 (4), 982–995. doi: 10.1177/2156587217696927

Kopustinskiene, D. M., Jakstas, V., Savickas, A., and Bernatoniene, J. (2020). Flavonoids as anticancer agents. *Nutrients* 12 (2), 457. doi: 10.3390/nu12020457

Kozuki, Y., Miura, Y., and Yagasaki, K. (2000). Inhibitory effects of carotenoids on the invasion of rat ascites hepatoma cells in culture. *Cancer Lett.* 151 (1), 111–115. doi: 10.1016/S0304-3835(99)00418-8

Kumar, S., Gezici, S., Sekeroglu, N., Atanasov, A. G., and Singla, R. K. (2023). Editorial: Natural products based management of neurological disorders: Mechanistic insight and translational informatics approach. *Front. Pharmacol.* 14. doi: 10.3389/fphar.2023.1170839

Kuti, J. O. (2000). 244 antioxidant activity of opuntia cactus pears. *HortScience* 35 (3), 433B–4433. doi: 10.21273/hortsci.35.3.433b

Kuti, J. O. (2004). Antioxidant compounds from four Opuntia cactus pear fruit varieties. *Food Chem.* 85 (4), 527–533. doi: 10.1016/s0308-8146(03)00184-5

Labianca, R., Beretta, G., Clerici, M., Fraschini, P., and Luporini, G. (1982). Cardiac toxicity of 5-fluorouracil: A study on 1083 patients. *Tumori J.* 68 (6), 505–510. doi: 10.1177/030089168206800609

Lee, J.-A., Jung, B.-G., Kim, T.-H., Lee, S.-G., Park, Y.-S., and Lee, B.-J. (2013). Dietary feeding of opuntia humifusa inhibits UVB radiation-induced carcinogenesis by reducing inflammation and proliferation in hairless mouse model. *Photochem. Photobiol.* 89 (5), 1208–1215. doi: 10.1111/php.12113

Lee, J. A., Jung, B. G., and Lee, B. J. (2012). Inhibitory effects of Opuntia humifusa on 7, 12-dimethyl- benz[a]anthracene and 12-O-tetradecanoylphorbol-13- acetate induced two-stage skin carcinogenesis. *Asian Pac J. Cancer Prev.* 13 (9), 4655–4660. doi: 10.7314/apjcp.2012.13.9.4655

Lim, J. Y., Liu, C., Hu, K. Q., Smith, D. E., Wu, D., Lamon-Fava, S., et al. (2020). Xanthophyll beta-cryptoxanthin inhibits highly refined carbohydrate diet-promoted hepatocellular carcinoma progression in mice. *Mol. Nutr. Food Res.* 64 (3), e1900949. doi: 10.1002/mnfr.201900949

Liu, L., Liu, Y., Zhao, J., Xing, X., Zhang, C., and Meng, H. (2020). Neuroprotective effects of D-(-)-quinic acid on aluminum chloride-induced dementia in rats. *Evidence-Based Complementary Altern. Med.* 2020, 5602597. doi: 10.1155/2020/5602597

Lu, Y.-M., Xie, J.-J., Peng, C.-G., Wang, B.-H., Wang, K.-C., and Li, L.-J. (2019). Enhancing clinical efficacy through the gut microbiota: A new field of traditional chinese medicine. *Engineering* 5 (1), 40–49. doi: 10.1016/j.eng.2018.11.013

Madadi, E., Mazloum-Ravasan, S., Yu, J. S., Ha, J. W., Hamishehkar, H., and Kim, K. H. (2020). Therapeutic application of betalains: A review. *Plants* 9 (9), 1219. doi: 10.3390/plants9091219

Madrigal-Santillán, E., Portillo-Reyes, J., Madrigal-Bujaidar, E., Sánchez-Gutiérrez, M., Mercado-Gonzalez, P. E., Izquierdo-Vega, J. A., et al. (2022). Opuntia genus in human health: A comprehensive summary on its pharmacological, therapeutic and preventive properties. Part 1. *Horticulturae* 8 (2), 88. doi: 10.3390/horticulturae8020088

Man, S., Gao, W., Zhang, Y., Huang, L., and Liu, C. (2010). Chemical study and medical application of saponins as anti-cancer agents. *Fitoterapia* 81 (7), 703–714. doi: 10.1016/j.fitote.2010.06.004

Mancuso, C., and Santangelo, R. (2014). Ferulic acid: pharmacological and toxicological aspects. *Food Chem. Toxicol.* 65, 185–195. doi: 10.1016/j.fct.2013.12.024

Mancuso, C., Scapagini, G., Currò, D., Giuffrida Stella, A. M., De Marco, C., Butterfield, D. A., et al. (2007). Mitochondrial dysfunction, free radical generation and cellular stress response in neurodegenerative disorders. *Front. Biosci.* 12 (3), 1107–1123. doi: 10.2741/2130

Meng, S., Cao, J., Feng, Q., Peng, J., and Hu, Y. (2013). Roles of chlorogenic acid on regulating glucose and lipids metabolism: A review. *Evidence-Based Complementary Altern. Med.* 2013, 801457. doi: 10.1155/2013/801457

Naselli, F., Tesoriere, L., Caradonna, F., Bellavia, D., Attanzio, A., Gentile, C., et al. (2014). Anti-proliferative and pro-apoptotic activity of whole extract and isolated indicaxanthin from Opuntia ficus-indica associated with re-activation of the onco-suppressor p16INK4a gene in human colorectal carcinoma (Caco-2) cells. *Biochem. Biophys. Res. Commun.* 450 (1), 652–658. doi: 10.1016/j.bbrc.2014.06.029

Natella, F., Nardini, M., Di Felice, M., and Scaccini, C. (1999). Benzoic and cinnamic acid derivatives as antioxidants: Structure–activity relation. *J. Agric. Food Chem.* 47 (4), 1453–1459. doi: 10.1021/jf980737w

Niranjana, R., Gayathri, R., Nimish Mol, S., Sugawara, T., Hirata, T., Miyashita, K., et al. (2015). Carotenoids modulate the hallmarks of cancer cells. *J. Funct. Foods* 18, 968–985. doi: 10.1016/j.jff.2014.10.017

Okur, M. E., Karakas, N., Karadag, A. E., Uludag, D., and Polat, D. C. (2019). Investigation of antioxidant and cytotoxic activities of Opuntia ficus-indica (L) Mill. fruit extract. *J. Faculty Pharm. Istanbul Univ.* 49 (3), 154–160. doi: 10.26650/IstanbulJPharm.2019.19035

Omara, T., Kiprop, A. K., Ramkat, R. C., Cherutoi, J., Kagoya, S., Moraa Nyangena, D., et al. (2020). Medicinal plants used in traditional management of cancer in Uganda: A review of ethnobotanical surveys, phytochemistry, and anticancer studies. *Evidence-Based Complementary Altern. Med.* 2020, 3529081. doi: 10.1155/2020/3529081

Oniszczuk, A., Wójtowicz, A., Oniszczuk, T., Matwijczuk, A., Dib, A., and Markut-Miotła, E. (2020). Opuntia fruits as food enriching ingredient, the first step towards new functional food products. *Molecules* 25 (4), 916. doi: 10.3390/molecules25040916

Otero, E., Robledo, S. M., Díaz, S., Carda, M., Muñoz, D., Paños, J., et al. (2014). Synthesis and leishmanicidal activity of cinnamic acid esters: structure–activity relationship. *Medicinal Chem. Res.* 23 (3), 1378–1386. doi: 10.1007/s00044-013-0741-y

Pandey, A. K., Singh, A. K., and Singla, R. K. (2023). Chlorogenic acid: A dietary phenolic acid with promising pharmacotherapeutic potential. *Curr. Medicinal Chem.* 30 (34), 3905–3926. doi: 10.2174/0929867329666220816154634

Park, E. H., and Chun, M. J. (2001). Wound healing activity of Opuntia ficus-indica. *Fitoterapia* 72 (2), 165–167. doi: 10.1016/S0367-326X(00)00265-3

Pourtier-Manzanedo, A., Didier, A., Froidevaux, S., and Loor, F. (1995). Lymphotoxicity and myelotoxicity of doxorubicin and SDZ PSC 833 combined chemotherapies for normal mice. *Toxicology* 99 (3), 207–217. doi: 10.1016/0300-483X(95)03056-L

Prager, G. W., Braga, S., Bystricky, B., Qvortrup, C., Criscitiello, C., Esin, E., et al. (2018). Global cancer control: responding to the growing burden, rising costs and inequalities in access. *ESMO Open* 3 (2), e000285. doi: 10.1136/esmoopen-2017-000285

Ramadan, M. F., and Mörsel, J.-T. (2003). Oil cactus pear (Opuntia ficus-indica L.). *Food Chem.* 82 (3), 339–345. doi: 10.1016/s0308-8146(02)00550-2

Ramírez-Ramos, M., Medina-Dzul, K., García-Mateos, R., Corrales-García, J., Ybarra-Moncada, C., and Castillo-González, A. M. (2018). Nutraceutical components, antioxidant activity and color of eleven varieties of prickly pear (Opuntia sp.). *J. Appl. Bot. Food Qual.* 91, 211–218. doi: 10.5073/10.5073/JABFQ.2018.091.028

Rani, N., Singla, R. K., Redhu, R., Narwal, S., Sonia,, and Bhatt, A. (2022). A Review on Green Synthesis of Silver Nanoparticles and its Role against Cancer. *Curr. Topics Medicinal Chem.* 22 (18), 1460–1471. doi: 10.2174/1568026622666220601165005

Rastogi, N., Chag, M., and Ayyagari, S. (1993). Myocardial ischemia after 5-fluorouracil chemotherapy. *Int. J. Cardiol.* 42 (3), 285–287. doi: 10.1016/0167-5273(93)90061-K

Renugadevi, J., and Prabu, S. M. (2009). Naringenin protects against cadmium-induced oxidative renal dysfunction in rats. *Toxicology* 256 (1-2), 128–134. doi: 10.1016/j.tox.2008.11.012

Ricks, D. (2015). Scientists journey into genomes *via* CRISPR-cas9. *JNCI: J. Natl. Cancer Institute* 107 (11), djv352. doi: 10.1093/jnci/djv352

Rocha, L. D., Monteiro, M. C., and Teodoro, A. J. (2012). Anticancer properties of hydroxycinnamic acids-a review. *Cancer Clin. Oncol.* 1 (2), 109–121. doi: 10.5539/cco.v1n2p109

Roy, N., Narayanankutty, A., Nazeem, P. A., Valsalan, R., Babu, T. D., and Mathew, D. (2016). Plant phenolics ferulic acid and P-coumaric acid inhibit colorectal cancer cell proliferation through EGFR down-regulation. *Asian Pac J. Cancer Prev.* 17 (8), 4019–4023.

San Millan, C., Soldevilla, B., Martin, P., Gil-Calderon, B., Compte, M., Perez-Sacristan, B., et al. (2015). beta-cryptoxanthin synergistically enhances the antitumoral activity of oxaliplatin through deltaNP73 negative regulation in colon cancer. *Clin. Cancer Res.* 21 (19), 4398–4409. doi: 10.1158/1078-0432.CCR-14-2027

Sarfati, D., Koczwara, B., and Jackson, C. (2016). The impact of comorbidity on cancer and its treatment. *CA: A Cancer J. Clin.* 66 (4), 337–350. doi: 10.3322/caac.21342

Sengngam, K., Hoc, T. H., Hang, D. V., and Tran Ngoan, L. (2022). Trans-lycopene and beta-cryptoxanthin intake and stomach cancer in Vietnamese men: A pilot case-control study. *Asian Pac J. Cancer Prev.* 23 (3), 861–865. doi: 10.31557/APJCP.2022.23.3.861

Serra, A. T., Poejo, J., Matias, A. A., Bronze, M. R., and Duarte, C. M. M. (2013). Evaluation of Opuntia spp. derived products as antiproliferative agents in human colon cancer cell line (HT29). *Food Res. Int.* 54 (1), 892–901. doi: 10.1016/j.foodres.2013.08.043

Sharma, S., Ali, A., Ali, J., Sahni, J. K., and Baboota, S. (2013). Rutin: therapeutic potential and recent advances in drug delivery. *Expert Opin. Investigational Drugs* 22 (8), 1063–1079. doi: 10.1517/13543784.2013.805744

Sharma, R., Jadhav, M., Choudhary, N., Kumar, A., Rauf, A., Gundamaraju, R., et al. (2022). Deciphering the impact and mechanism of Trikatu, a spices-based formulation on alcoholic liver disease employing network pharmacology analysis and in *vivo* validation. *Front. Nutr.* 9. doi: 10.3389/fnut.2022.1063118

Sharma, S. H., Rajamanickam, V., and Nagarajan, S. (2018). Antiproliferative effect of p-Coumaric acid targets UPR activation by downregulating Grp78 in colon cancer. *Chem. Biol. Interact.* 291, 16–28. doi: 10.1016/j.cbi.2018.06.001

Sigwela, V., De Wit, M., du Toit, A., Osthoff, G., and Hugo, A. (2021). Bioactive betalain extracts from cactus pear fruit pulp, beetroot tubers, and amaranth leaves. *Molecules* 26 (16), 5012. doi: 10.3390/molecules26165012

Simopoulos, A. P. (2002). The importance of the ratio of omega-6/omega-3 essential fatty acids. *BioMed. Pharmacother.* 56 (8), 365–379. doi: 10.1016/s0753-3322(02)00253-6

Singla, R. K., Behzad, S., Khan, J., Tsagkaris, C., Gautam, R. K., Goyal, R., et al. (2022a). Natural kinase inhibitors for the treatment and management of endometrial/uterine cancer: preclinical to clinical studies. *Front. Pharmacol.* 13. doi: 10.3389/fphar.2022.801733

Singla, R. K., Dubey, A. K., Garg, A., Sharma, R. K., Fiorino, M., Ameen, S. M., et al. (2019). Natural polyphenols: chemical classification, definition of classes, subcategories, and structures. *J. AOAC Int.* 102 (5), 1397–1400. doi: 10.5740/jaoacint.19-0133

Singla, R. K., Sai, C. S., Chopra, H., Behzad, S., Bansal, H., Goyal, R., et al. (2021a). Natural products for the management of castration-resistant prostate cancer: special focus on nanoparticles based studies. *Front. Cell Dev. Biol.* 9. doi: 10.3389/fcell.2021.745177

Singla, R. K., Sharma, P., Dubey, A. K., Gundamaraju, R., Kumar, D., Kumar, S., et al. (2021b). Natural product-based studies for the management of castration-resistant prostate cancer: computational to clinical studies. *Front. Pharmacol.* 12. doi: 10.3389/fphar.2021.732266

Singla, R. K., Sharma, P., Kumar, D., Gautam, R. K., Goyal, R., Tsagkaris, C., et al. (2022b). The role of nanomaterials in enhancing natural product translational potential and modulating endoplasmic reticulum stress in the treatment of ovarian cancer. *Front. Pharmacol.* 13. doi: 10.3389/fphar.2022.987088

Singla, R. K., Wang, X., Gundamaraju, R., Joon, S., Tsagkaris, C., Behzad, S., et al. (2022c). Natural products derived from medicinal plants and microbes might act as a game-changer in breast cancer: a comprehensive review of preclinical and clinical studies. *Crit. Rev. Food Sci. Nutr.*, 1–45. doi: 10.1080/10408398.2022.2097196

Slimen, I., Mabrouk, M., Hanene, C., Najar, T., and Abderrabba, M. (2017). LC-MS analysis of phenolic acids, flavonoids and betanin from spineless opuntia ficus-indica fruits. *Cell Biol.* 5 (2), 17–28. doi: 10.11648/j.cb.20170502.12

Slimen, I., Najar, T., and Abderrabba, M. (2016). Opuntia ficus-indica as a source of bioactive and nutritional phytochemicals. *J. Food Nutr. Sci.* 4 (6), 162–169. doi: 10.11648/j.jfns.20160406.14

Sova, M. (2012). Antioxidant and antimicrobial activities of cinnamic acid derivatives. *Mini-Reviews Medicinal Chem.* 12 (8), 749–767. doi: 10.2174/138955712801264792

Sreekanth, D., Arunasree, M. K., Roy, K. R., Chandramohan Reddy, T., Reddy, G. V., and Reddanna, P. (2007). Betanin a betacyanin pigment purified from fruits of Opuntia ficus-indica induces apoptosis in human chronic myeloid leukemia Cell line-K562. *Phytomedicine* 14 (11), 739–746. doi: 10.1016/j.phymed.2007.03.017

Stintzing, F. C., Herbach, K. M., Mosshammer, M. R., Carle, R., Yi, W., Sellappan, S., et al. (2005). Color, betalain pattern, and antioxidant properties of cactus pear (Opuntia spp.) clones. *J. Agric. Food Chem.* 53 (2), 442–451. doi: 10.1021/jf048751y

Su, P., Shi, Y., Wang, J., Shen, X., and Zhang, J. (2015). Anticancer agents derived from natural cinnamic acids. *Anti-Cancer Agents Medicinal Chem.* 15 (8), 980–987. doi: 10.2174/1871520615666150130111120

Sun, J., Chu, Y.-F., Wu, X., and Liu, R. H. (2002). Antioxidant and antiproliferative activities of common fruits. *J. Agric. Food Chem.* 50 (25), 7449–7454. doi: 10.1021/jf0207530

Tajik, N., Tajik, M., Mack, I., and Enck, P. (2017). The potential effects of chlorogenic acid, the main phenolic components in coffee, on health: a comprehensive review of the literature. *Eur. J. Nutr.* 56 (7), 2215–2244. doi: 10.1007/s00394-017-1379-1

Touré, H., Bouatia, M., Idrissi, M. O. B., and Draoui, M. (2015). Phytochemical screening and antioxidant activity of aqueous-ethanolic extracts of Opuntia ficus indica. *J. Chem. Pharm. Res.* 7 (7), 409–415.

Trachtenberg, S., and Mayer, A. M. (1981). Composition and properties of Opuntia ficus-indica mucilage. *Phytochemistry* 20 (12), 2665–2668. doi: 10.1016/0031-9422(81)85263-6

Varela-López, A., Battino, M., Navarro-Hortal, M. D., Giampieri, F., Forbes-Hernández, T. Y., Romero-Márquez, J. M., et al. (2019). An update on the mechanisms related to cell death and toxicity of doxorubicin and the protective role of nutrients. *Food Chem. Toxicol.* 134, 110834. doi: 10.1016/j.fct.2019.110834

Wang, R., Billone, P. S., and Mullett, W. M. (2013). Nanomedicine in action: an overview of cancer nanomedicine on the market and in clinical trials. *J. Nanomaterials* 2013, 629681. doi: 10.1155/2013/629681

Wu, N. L., Chiang, Y. C., Huang, C. C., Fang, J. Y., Chen, D. F., and Hung, C. F. (2010). Zeaxanthin inhibits PDGF-BB-induced migration in human dermal fibroblasts. *Exp. Dermatol.* 19 (8), e173–e181. doi: 10.1111/j.1600-0625.2009.01036.x

Xu, X.-H., Li, T., Fong, C. M. V., Chen, X., Chen, X.-J., Wang, Y.-T., et al. (2016). Saponins from chinese medicines as anticancer agents. *Molecules* 21 (10), 1326. doi: 10.3390/molecules21101326

Yeddes, N., Chérif, J. K., Guyot, S., Sotin, H., and Ayadi, M. T. (2013). Comparative study of antioxidant power, polyphenols, flavonoids and betacyanins of the peel and pulp of three Tunisian opuntia forms. *Antioxidants* 2 (2), 37–51. doi: 10.3390/antiox2020037

Zeghad, N., Ahmed, E., Belkhiri, A., Heyden, Y. V., and Demeyer, K. (2019). Antioxidant activity of Vitis vinifera, Punica granatum, Citrus aurantium and Opuntia ficus indica fruits cultivated in Algeria. *Heliyon* 5 (4), e01575. doi: 10.1016/j.heliyon.2019.e01575

Zhang, X., Lin, D., Jiang, R., Li, H., Wan, J., and Li, H. (2016). Ferulic acid exerts antitumor activity and inhibits metastasis in breast cancer cells by regulating epithelial to mesenchymal transition. *Oncol. Rep.* 36 (1), 271–278. doi: 10.3892/or.2016.4804

Zhang, S. Y., Lu, Y. Y., He, X. L., Su, Y., Hu, F., Wei, X. S., et al. (2023). Lutein inhibits tumor progression through the ATR/Chk1/p53 signaling pathway in non-small cell lung cancer. *Phytother. Res.* 37 (4), 1260–1273. doi: 10.1002/ptr.7682

Zou, D.-m., Brewer, M., Garcia, F., Feugang, J. M., Wang, J., Zang, R., et al. (2005). Cactus pear: a natural product in cancer chemoprevention. *Nutr. J.* 4 (1), 25. doi: 10.1186/1475-2891-4-25

Zourgui, L., Golli, E. E., Bouaziz, C., Bacha, H., and Hassen, W. (2008). Cactus (Opuntia ficus-indica) cladodes prevent oxidative damage induced by the mycotoxin zearalenone in Balb/C mice. *Food Chem. Toxicol.* 46 (5), 1817–1824. doi: 10.1016/j.fct.2008.01.023

Zugazagoitia, J., Guedes, C., Ponce, S., Ferrer, I., Molina-Pinelo, S., and Paz-Ares, L. (2016). Current challenges in cancer treatment. *Clin. Ther.* 38 (7), 1551–1566. doi: 10.1016/j.clinthera.2016.03.026

frontiers | Frontiers in Plant Science

TYPE Original Research
PUBLISHED 03 January 2024
DOI 10.3389/fpls.2023.1211453

OPEN ACCESS

EDITED BY
Chunpeng (Craig) Wan,
Jiangxi Agricultural University, China

REVIEWED BY
Benjamin Lichman,
University of York, United Kingdom
Qi Tang,
Hunan Agricultural University, China

*CORRESPONDENCE
Neda Aničić
neda.anicic@ibiss.bg.ac.rs
Dragana Matekalo
dragana.bozic@ibiss.bg.ac.rs
Danijela Mišić
dmisic@ibiss.bg.ac.rs

RECEIVED 24 April 2023
ACCEPTED 11 December 2023
PUBLISHED 03 January 2024

CITATION
Aničić N, Matekalo D, Skorić M, Gašić U, Nestorović Živković J, Dmitrović S, Božunović J, Milutinović M, Petrović L, Dimitrijević M, Anđelković B and Mišić D (2024) Functional iridoid synthases from iridoid producing and non-producing *Nepeta* species (subfam. Nepetoidae, fam. Lamiaceae).
Front. Plant Sci. 14:1211453.
doi: 10.3389/fpls.2023.1211453

Functional iridoid synthases from iridoid producing and non-producing *Nepeta* species (subfam. Nepetoidae, fam. Lamiaceae)

Neda Aničić[1]*, Dragana Matekalo[1]*, Marijana Skorić[1], Uroš Gašić[1], Jasmina Nestorović Živković[1], Slavica Dmitrović[1], Jelena Božunović[1], Milica Milutinović[1], Luka Petrović[1], Milena Dimitrijević[2], Boban Anđelković[3] and Danijela Mišić[1]*

[1]Institute for Biological Research "Siniša Stanković" - National Institute of the Republic of Serbia, University of Belgrade, Belgrade, Serbia, [2]Institute for Multidisciplinary Research, University of Belgrade, Belgrade, Serbia, [3]Faculty of Chemistry, University of Belgrade, Belgrade, Serbia

Iridoids, a class of atypical monoterpenes, exhibit exceptional diversity within the *Nepeta* genus (subfam. Nepetoidae, fam. Lamiaceae).The majority of these plants produce iridoids of the unique stereochemistry, with nepetalactones (NLs) predominating; however, a few *Nepeta* species lack these compounds. By comparatively analyzing metabolomics, transcriptomics, gene co-expression, and phylogenetic data of the iridoid-producing *N. rtanjensis* Diklić & Milojević and iridoid-lacking *N. nervosa* Royle & Bentham, we presumed that one of the factors responsible for the absence of these compounds in *N. nervosa* is iridoid synthase (ISY). Two orthologues of ISY were mined from leaves transcriptome of *N. rtanjensis* (*Nr*PRISE1 and *Nr*PRISE2), while in *N. nervosa* only one (*Nn*PRISE) was identified, and it was phylogenetically closer to the representatives of the Family 1 isoforms, designated as P5βRs. Organ-specific and MeJA-elicited profiling of iridoid content and co-expression analysis of IBG candidates, highlighted *NrPRISE2* and *NnPRISE* as promising candidates for ISY orthologues, and their function was confirmed using *in vitro* assays with recombinant proteins, after heterologous expression of recombinant proteins in *E. coli* and their His-tag affinity purification. *Nr*PRISE2 demonstrated ISY activity both *in vitro* and likely *in planta*, which was supported by the 3D modeling and molecular docking analysis, thus reclassification of *Nr*PRISE2 to *Nr*ISY is accordingly recommended. *Nn*PRISE also displays *in vitro* ISY-like activity, while its role under *in vivo* conditions was not here unambiguously

confirmed. Most probably under *in vivo* conditions the *Nn*PRISE lacks substrates to act upon, as a result of the loss of function of some of the upstream enzymes of the iridoid pathway. Our ongoing work is conducted towards re-establishing the biosynthesis of iridoids in *N. nervosa*.

KEYWORDS

iridoid synthase, iridoids, *Nepeta rtanjensis*, *Nepeta nervosa*, functional characterization, metabolomics, transcriptomics

Introduction

Nepetoidae subfamilly of the Lamiaceae family comprises mainly iridoid-lacking taxa. It has been proposed that, during evolution, these plants have lost a key enzyme in the early iridoid pathway, iridoid synthase (ISY) (Boachon et al., 2018), which disabled their iridoid biosynthetic platform. The exception are members of the genus *Nepeta*, which went through the re-establishment of the iridoid biosynthesis by engaging the latent biosynthetic machinery existing in all Nepetoidae, in parallel with convergent evolution of ISY from an alternative ancestor, progesterone 5β-reductase (P5βR) (Lichman et al., 2020). Another evolutionary innovation of the genus *Nepeta* includes NAD-dependent nepetalactol-related short-chain-dehydrogenase/reductase (NEPS) and major latex protein-like (MLPL) enzymes, which, in combination with novel ISYs, gave rise to iridoid aglycones nepetalactones and glycosylated iridoids of unique stereochemistry, exclusively present in this group of plants.

All iridoids in *Nepeta* have a common precursor nepetalactol, which emerges from geranyl pyrophosphate (GPP) originating from the MEP pathway. This central precursor arises in a reaction assisted by the GPP synthase (GPPS), and is further converted into geraniol via geraniol synthase (GES). Nepetalactol arises from geraniol through the series of intermediates and enzymatic reactions catalyzed by geraniol 8-hydroxylase (G8H), 8-hydroxygeraniol oxidoreductase (8HGO), ISY, NEPS(s), and MLPL (Figure 1). In *Nepeta* species, ISYs are mainly responsible for the stereoselective 1,4-reduction of 8-oxogeranial to uncyclized and reactive 8-oxocitronellyl enol, and for determining the stereochemistry of the C7 (Sherden et al., 2017; Lichman et al., 2019b; Lichman et al., 2020; Hernández Lozada et al., 2022). In other iridoid producing plants, including *Catharanthus roseus* L. (Geu-Flores et al., 2012) and *Olea europea* (Alagna et al., 2016) ISYs are responsible for reduction of 8-oxogeranial. The subsequent cyclization step, which gives rise to a core iridoid skeleton characteristic for nepetalactol, is in these plants either mediated by some unknown cyclases, or it occurs spontaneously. Enolate intermediate 8-oxocitronellyl enol in *Nepeta* is cyclized by NEPSs (Lichman et al., 2019a; Lichman et al., 2019b), but can also undergo a spontaneous cyclization to produce predominately *cis,trans*-steroisomer of nepetalactol (Hernández Lozada et al., 2022). NEPS enzymes are also involved in the subsequent enzymatic step, which converts nepetalactol to nepetalactone, and are responsible for setting the stereochemistry of the bridged carbons (C4a and C7a) of nepetalactone (Hernández Lozada et al., 2022). In summary, the family of NEPS enzymes can be divided into 3 subgroups according to their catalytic activity: 1) redox-inactive cyclases (e.g. *N. mussinii Nm*NEPS3); 2) oxidazes (e.g. *Nm*NEPS1 and *Nm*NEPS5); 3) dual-function enzymes catalyzing both stereo selective cyclization and oxidation of various nepetalactols to nepetalactons (e.g. *N. cataria Nc*NEPS3A; *N. mussinii Nm*NEPS4; *N. sibirica Ns*NEPS2) (Lichman et al., 2020; Hernández Lozada et al., 2022). MLPLs are proven to be involved in the biosynthesis of *cis,trans*-nepetalactol stereoisomer (Lichman et al., 2020).

The story of iridoid biosynthesis within the genus *Nepeta* becomes even more fascinating when it comes to taxa lacking iridoids, or producing them in trace amounts. We here hypothesized that a "biochemical reservoir" of enzymes with different catalytic activities related to the iridoid biosynthesis exists in iridoid non-producing *Nepeta* species, but substrates to act upon are missing due to the loss of function/silencing of some of the early biosynthetic genes. In order to test this hypothesis we focused our study towards two chemodiverse *Nepeta* taxa: 1) *N. rtanjensis* Diklić & Milojević, an endemic and critically endangered plant of Serbia, which is characterized by the presence of nepetalactones with *trans,cis*- and *cis,trans*- stereochemistry; and 2) iridoid-lacking *N. nervosa* Royle ex Benth. Following comprehensive metabolomics, we analyzed transcriptomes of *N. rtanjensis* and *N. nervosa* leaves in search for iridoid-related biosynthetic genes, to acquire accurate information on the presence/absence of iridoid biosynthetic gene transcripts and gene nucleotide sequence. Candidates of iridoid biosynthetic genes (*GPPS*, *GES*, *G8H*, *HGO*, *ISY*, *NEPSs*, *and MLPLs*) are identified based on similarity to the previously characterized orthologues from *Nepeta cataria*, *N. mussinii*, *N. rtanjensis*, *N. sibirica*, *C. roseus*, and other iridoid-rich species. As ISYs were identified as genes responsible for the loss of iridoid biosynthesis in the majority of Nepetoidae, and are highlighted as enzymes important for determining the metabolic flux through the pathway, we further aimed to isolate and functionally characterize ISYs from *N. rtanjensis* and *N. nervosa*, and analyze them in a phylogenetic context. Furthermore, it has recently been suggested that the

10.3389/fpls.2023.1211453

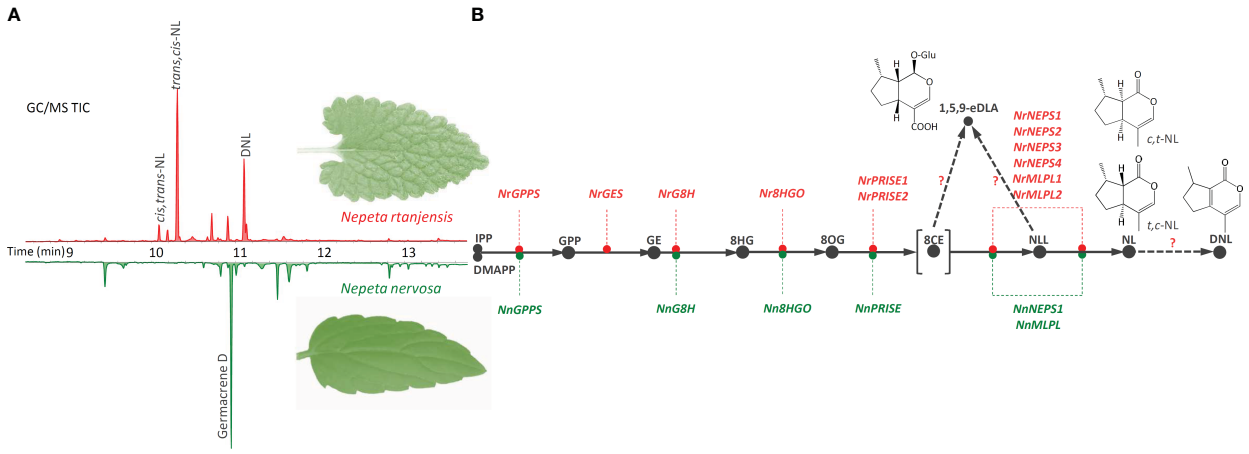

C

	*Nn*GPPS/*Nr*GPPS	*Nn*G8H/*Nr*G8H	*Nn*8HGO/*Nr*8HGO	*Nn*PRISE/*Nr*PRISE1	*Nn*NEPS1/*Nr*NEPS1	*Nn*MLPL/*Nr*MLPL1	*Nn*MLPL/*Nr*MLPL2
Pairwise Sequence Alignment Results	Query cover: 62% Identity: 94.2% Similarity: 97.1%	Query cover: 99% Identity: 93.9% Similarity: 96.6%	Query cover: 87% Identity: 94.9% Similarity: 98.2%	Query cover: 99% Identity: 93.8% Similarity: 96.4%	Query cover: 98% Identity: 84.3% Similarity: 90.7%	Query cover: 87% Identity: 73.5% Similarity: 84.6%	Query cover: 100% Identity: 65.2% Similarity: 75.9%

FIGURE 1
Following GC/MS and UHPLC/QToF MS characterization of methanol extracts of *N. rtanjensis* and *N. nervosa* leaves, iridoid compounds were identifyed only in *N. rtanjensis*, with *t,c*-NL, *c,t*-NL, and DNL predominating on the **(A)** representative GC/MS chromatogram. In parallel, orthologues of iriroid biosynthetic genes were searched in transcriptomes of *N. rtanjensis* (red color) and *N. nervosa* (green color) and the biosynthetic pathway of the two species was reconstructed **(B)**: GPPS- geranyl diphosphate synthase, GES- geraniol synthase, G8H- geraniol 8-hydroxylase, 8HGO- 8-hydroxygeraniol oxidoreductase, PRISE- progesterone-5β-reductase/iridoid synthase activity displaying enzymes, NEPS- nepetalactol-related short-chain dehydrogenase, MLPL- major latex protein-like enzyme. Pairwise sequence alignment results for amino acid sequences of investigated genes belonging to *N. nervosa* with the corresponding *N. rtanjensis* genes **(C)**. IPP, isopentenyl pyrophosphate; DMAPP, dimethylallyl pirophosphate; GPP, geranyl pyrophosphate; GE, geraniol; 8HG, 8-hydroxygeraniol; 8OG, 8-oxogeranial; 8CE – 8-oxocitronellyl enolate; NLL, nepetalactol; NL, nepetalactone; DNL, 5,9-dehydronepetalactone; 1,5,9-eDLA, 1,5,9-*epi*deoxyloganic acid; *t,c*-NL, *trans,cis*-nepetalactone, *c,t*-NL, *cis, trans*-nepetalactone.

presence or absence of ISY-like enzymatic activity controls whether plants accumulate nepetalactones, or whether these molecules are of 7*S* or 7*R* configuration (Hernández Lozada et al., 2022). Iridoids with *7R* stereochemistry predominate outside of *Nepeta* genus, while, up to date, only 7*S* isomers of iridoids are recorded within *Nepeta*, which coincides with the fact that only 7*S*-specific ISYs from *N. cataria* and *N. mussinii* (Sherden et al., 2017), and *N. sibirica* (Hernández Lozada et al., 2022) have been isolated and functionally characterized. As transcripts of only one potential PRISE were recorded in transcriptome of *N. nervosa*, we aimed to investigate whether the loss of function or silencing of this important IBG is, at least partially, responsible for the lack of iridoids in this species.

Materials and methods

Plant material and *in vitro* culture establishment

Seeds of *N. nervosa* were commercially purchased from Grugapark Essen (Germany), while seeds of *N. rtanjensis* were collected in July 2017 in locality Javor (Mt Rtanj, SE Serbia). Seeds were surface sterilized in a 20% solution of commercial bleach for 10 min, rinsed five times with sterile distilled water and germinated in Petri dishes on 20 ml basal medium (BM): solid ½ MS (Murashige and Skoog, 1962) culture medium, supplemented with 20 g l^{-1} sucrose, 7 g l^{-1} agar (Torlak, Serbia) and 100 mg l^{-1} myo-inositol (Merck, Germany). All the cultures were grown in 370 ml glass jars, each containing 100 ml of BM, and kept in a growth chamber under long day conditions (16/8 h light/dark cycle), at 25 ± 2°C. White fluorescent tubes provided a photon flux rate of 32.5 µmol m^2 s^{-1} at the level of plant cultures.

Sufficient plant material for experiments was obtained by micropropagation of one selected genotype of each of the *Nepeta* species, using single-node stem segments as explants, and by subcultivation on fresh BM every 4 weeks. RNA-seq libraries were constructed using leaves of four-week old *in vitro* grown *N. rtanjensis* and *N. nervosa* plants. Leaves, stems, and roots of four month old plants were separately harvested, weighted and immediately frozen in liquid nitrogen, and further stored at −80°C until use. Three individuals (three biological replicates) of one clonally propagated genotype per species, at the same developmental stage, were analyzed separately.

MeJA-elicitation experimental setup

Four weeks-old *N. rtanjensis* and *N. nervosa* plants, propagated on BM under *in vitro* conditions, were used in experiments to

comparatively analyze methyl jasmonate (MeJA)-elicitation effects on iridoid profile and related BG expressions. Plants were transferred on BS supplemented with 250 µM MeJA and leaves were harvested after 24 h and 72 h. Filter-sterilized MeJA (sterile 0.2 µm cellulose filters, Agilent Technologies, Santa Clara, CA, USA) was added to the culture medium after its sterilization by autoclaving at 114°C for 25 min. Control group of plants was simultaneously transferred on BM, and leaves were harvested in parallel with those of MeJA-treated plants. Each of the three biological replicates per treatment consisted of five clonally propagated plants grown in the same jar. After harvesting, leaves belonging to the plants of the same biological replicate were pulled, ground into a fine powder and homogenized in liquid nitrogen, and samples were stored at −80°C until use. The obtained plant material was used for both RNA extraction and quantification of iridoids.

Extraction of plant material for metabolic profiling

Plant material was ground in LN, and extracted with 96% methanol (w:v = 1:10) in an ultrasonic bath for 1 h. After centrifugation for 20 min at 10000 × g, the supernatants were filtered through 0.2µm cellulose filters (Agilent Technologies, Santa Clara, CA, USA) and stored at 4°C until use. All the analyses were performed in triplicates.

GC/MS non-targeted metabolomics of methanol extracts of *N. rtanjensis* and *N. nervosa* leaves

Profiling of volatile compounds in leaves of *N. rtanjensis* and *N. nervosa* grown *in vitro* was performed using Agilent 8890 gas chromatography (GC) System with 5977B GC/MSD (Agilent Technologies, USA) connected to Centri sample extraction and enrichment platform (Markes International Ltd., UK). Chromatographic separations were performed on HP-5MS column (30 m × 0.25 mm, 0.25 µm film thickness) (Agilent Technologies, USA), and using He (99.999%, The Linde Group, Ireland) as a carrier gas at a flow rate of 1.6 ml min^{-1}. Transfer line was heated at 280°C, and detector temperature was set to 270°C. Mass spectra were acquired in positive EI mode (+70 eV), with temperature of the EI source set to 280°C. Column temperature was linearly programmed from 40 to 300°C, at rate of 20°C min^{-1}, and held isothermally at 240°C for the next 10 min. Methanol extract (1 µl) was injected in a split mode (20:1), with split flow 24 ml min^{-1}. Analyses were performed in SCAN mode, tracking the compounds within the range 45 to 500 amu. The constituents of the reaction mixtures were identified by comparison of their mass spectra and retention times with those of the respective standards, and by comparison with the NIST05 library.

UHPLC–QToF–MS non-targeted metabolomics of *N. rtanjensis* and *N. nervosa* methanol extracts

The analyses were carried out on Agilent 1290 Infinity ultra-high-performance liquid chromatography (UHPLC) system coupled with a quadrupole time-of-flight mass spectrometry (6530C Q-ToF-MS) from Agilent Technologies, Inc., CA, USA. The chromatographic separation was performed at 40°C on a Zorbax C18 column (2.1 × 50 mm, 1.8 µm) from Agilent Technologies, Inc., CA, USA. The composition of mobile phases, gradient elution program, and the all chromatography parameters were as previously described by Gašić et al., 2023.

The QToF-MS system was equipped with an Agilent Jet Stream electrospray ionization (ESI) source, operating in both positive (ESI+) and negative (ESI-) ionization modes. The operation parameters for ESI, as well as the other settings of the QToF mass analyzer and data-dependent acquisition (DDA) parameters were the same as in Kostić et al., 2023. Agilent MassHunter software was used for data acquisition. The CAS SciFindern database was used to search for chemical compounds by formulas and structures (https://scifinder-n.cas.org/). For the evaluation of MS data R Studio software (enviPick and xcms R packages) was used (Zengin et al., 2020).

UHPLC/(+)HESI-MS/MS quantification of targeted iridoids

Dionex Ultimate 3000 UHPLC system (ThermoFisher Scientific, Germany) connected to TSQ Quantum Access Max triple-quadrupole mass spectrometer (ThermoFisher Scientific, Switzerland) was used for the determination and quantification of nepetalactone, dehydronepetalactone, and 1,5,9-*epi*deoxyloganic acid in methanol extracts of *N. rtanjensis* and *N. nervosa* leaves, stems and roots, as well as in MeJA-elicited leaves. Elution was performed at 40°C on Hypersil gold C18 column (50 × 2.1 mm) with 1.9 m particle size (ThermoFisher Scientific, USA). The liquid chromatography parameters (mobile phase, gradient elution, and the flow rate) and the mass spectrometry detection settings were set according to Mišić et al., 2015. Mass spectrometry data were acquired in both positive (*trans*,*cis*-nepetalactone, *cis*,*trans*-nepetalactone, and dehydronepetalactone) and negative (1,5,9-*epi*deoxyloganic acid) mode, and collision-induced fragmentations were performed using argon, with collision energy (cE) set to 30 eV. The identification of targeted compounds was additionally confirmed by DAD analysis. Absorption spectrum of nepetalactone isomers was characterized by the λ_{max} at 230 nm, while dehydronepetalactone had a max absorption at λ_{max} = 300 nm. As for 1,5,9-*epi*deoxyloganic acid, its absorption spectra was characterized by λ_{max} = 340 nm.

The amounts of *trans,cis*-nepetalactone, dehydronepetalactone, and 1,5,9-*epi*deoxyloganic acid were evaluated by calculating the

peak areas, based on the calibration curve of pure compounds, as previously described in Aničić et al., 2021. Amounts were expressed as μg per 100 mg of fresh weight (μg 100 mg^{-1} FW). All the analyses were performed in triplicates.

Transcriptome mining and selection of iridoid biosynthesis candidate genes

Transcriptomes of nepetalactone-producing *Nepeta rtanjensis* Diklić & Milojević and nepetalactone-lacking *N. nervosa L.* are searched for the presence/absence of transcripts of iridoid-pathway-related genes (biosynthetic genes and transcription factors), based on the homology with the genes characterised in many iridoids- and alkaloids- producing plants, including those from the *Nepeta* genus (Lichman et al., 2019a; Lichman et al., 2020; Hernández Lozada et al., 2022). Sequences of *N. rtanjensis* iridoid-biosynthetic-pathway-genes coding for *Nr*GPPS.SSU, *Nr*GES, *Nr*G8H, *Nr*8HGO, *Nr*PRISE1, *Nr*PRISE2, *Nr*MLPL1, *Nr*MLPL2, *Nr*NEPS1, *Nr*NEPS2, *Nr*NEPS3, and *Nr*NEPS4 (Aničić et al., 2020) were used for BLAST search of corresponding candidate genes in *N. nervosa* leaf RNA-seq available in our laboratory (data not published). BLAST search derived 6 genes putatively involved in iridoid biosynthesis – *NnGPPS.SSU*, *NnG8H*, *Nn8HGO*, *NnMLPL*, *NnPRISE*, and *NnNEPS1* from *N. nervosa* transcriptomic database. All of the sequences have shown high similarity to the characterized genes from other species present in the NCBI database. For the NCBI accession numbers of all genes from this paper please refer to the Supplementary Table 1.

RNA extraction and qPCR profiling of tissue-specific and MeJA-elicited expression of iridoid-related biosynthetic genes

Once the candidates for the iridoid biosynthesis-related genes were identified in *N. rtanjensis* and *N. nervosa* transcriptomes, highly specific primer pairs for qPCR co-expression analysis were designed using Primer3Plus software (http://www.bioinformatics.nl/cgi-bin/primer3plus/primer3plus.cgi) (Supplementary Table 1). Finally, glyceraldehyde 3-phosphate dehydrogenase (GAPDH) was used as the housekeeping gene, as previously reported by Aničić et al., 2018.

The RNA extraction from leaves, stems, and roots of *N. rtanjensis* and *N. nervosa*, as well as from MeJA-elicited leaves, was performed applying a modified CTAB method (Gasic et al., 2004). RNA was quantified with N60 Nano-Photometer® (Implen GmbH, Munich, Germany) and fluorometrically (Qubit 3.0 Fluorometer, ThermoFisher Scientific, USA), and its integrity was confirmed with gel electrophoresis. Obtained total RNA was treated with DNaze I (ThermoFisher Scientific, USA) for 30 min at 37°C. From 1 μg of total RNA cDNA was constructed using the Revert Aid First Strand cDNA Synthesis Kit (ThermoFisher Scientific, USA) following manufacturers' specifications, with oligo-(dT) primers (Life Technologies, USA). The PCR mixture comprised of cDNA corresponding to 50 ng of total RNA, 1μM primers, 1U of Phusion Hot Start II High-Fidelity polymerase (Thermo Scientific, USA) in a volume of 50 μl. The amplification was carried out in an Eppendorf Mastercycler Nexus (Eppendorf, Germany) thermal cycler with the following amplification profile: initial denaturation (30 s at 98°C), followed by 40 cycles of denaturation (10 s at 98°C), annealing (30 s at 60°C), and extension (45 s at 72°C) with final extension (7 min at 72°C). The obtained amplicons were purified electrophoretically, extracted from gel using GeneJET Gel extraction kit (Thermo Scientific, USA), quantified and serially diluted in a 10^9-10^2 copies μl^{-1} range to be used as standards for the absolute qPCR quantification.

Gene expression analyses were performed by real-time PCR using QuantStudio™ 3 Real-Time PCR System (Life Technologies, USA). Thermocycler conditions were as previously described in Aničić et al., 2018. The reactions were performed using Maxima SYBR Green/ROX Master Mix (2X) (ThermoFisher Scientific, USA), cDNA corresponding to 50 ng RNA and 0.3 μM primers, according to the manufacturer's recommendations. The expression levels of candidate IBGs were calculated according to the $2^{-\Delta\Delta Ct}$ method (Livak and Schmittgen, 2001) using GAPDH as a housekeeping gene, as mentioned above. The data represent means ± SE from three biological replicates.

*Nr*PRISE2 and *Nn*PRISE amplification and cloning

Primers for the full-length amplification of candidate ISYs are presented in Supplementary Table 1. Total *N. rtanjensis* and *N. nervosa* leaf RNAs were isolated with Spectrum™ Plant Total RNA kit (Sigma-Aldrich®, Hamburg, Germany), and cDNA was synthesized using RevertAid First Strand cDNA Synthesis kit (ThermoScientific, Lithuania) following manufacturers' instructions. Full lengths of the selected genes were amplified using AmpliTaq Gold (Thermo Fisher Scientific, USA) and cDNAs as templates. PCR products were gel purified and the products were subsequently cloned into vector PTZ57R/T using InsTAclone PCR Cloning Kit (ThermoScientific, Lithuania). The obtained constructs were used for PCR amplification of candidate PRISEs genes with primers containing restriction enzymes sites (KpnI and SacI) (Supplementary Table 1). After digestion with the appropriate restriction enzymes the digests were ligated to bacterial expression vector pRSETA (N-terminal 6xHis tag). Final constructs were verified by sequencing.

*Nr*PRISE2 and *Nn*PRISE expression in bacteria and protein purification

The pRSETA-NrPRISE2 and pRSETA-NnPRISE constructs were used for heat-shock transformation of *E. coli* strain BL21-CodonPlus (DE3)-RIL (Stratagene, USA). Single colonies were grown in Lauria-Bertani (LB) broth supplemented with 100 μg ml^{-1} ampicillin, 50 μg ml^{-1} kanamycin and 17 μg ml^{-1} chloramphenicol overnight at 37°C. The following day, the

colonies were used to inoculate 20 ml of fresh LB medium and the pre-cultures were grown overnight at 37°C shaking at 220 rpm. The next day, 200 ml of LB medium with antibiotics was inoculated with 20 ml of pre-cultures and bacteria were grown at 37°C shaking at 220 rpm. After reaching an OD_{600} of 0.6, protein expression was induced with 0.1 mM IPGT and bacteria were incubated in a shaker at 18°C for ~ 17h. Subsequently, the cells were harvested, pelleted and re-suspended in 2 ml lysis buffer (50 mM NaH_2PO_4, 300 mM NaCl and 10 mM imidazol, pH 8.0). Following lysozyme (Sigma Aldrich, Germany) (1 mg ml^{-1} final concentration) and protease inhibitor addition, samples were incubated for 30 min on ice. After additional cell disruption by 4 freeze-thaw cycles, RNAse A and DNAse were added to cell suspension following incubation on ice for 15 min. Next, 10 µl of Triton-X (Sigma-Aldrich, Germany), 600 µl of 5M NaCl and 100 µl of glycerol were added. The lysate was centrifuged and His-tagged proteins were purified with Ni-NTA resin (Qiagen, Hilden, Germany) according to manufacturer's instructions. Wash buffer (pH 8.0) contained 50 mM NaH_2PO_4, 300 mM NaCl, and 50 mM imidazole and elution buffer (pH 10.2) contained 50 mM NaH_2PO_4, 300 mM NaCl, and 250 mM imidazole.

Purified protein concentrations were determined fluorometrically using Qubit 3.0 Fluorometer (ThermoFisher Scientific, USA). The recombinant proteins were analyzed on 5%–10% SDS-PAGE using Mini-PROTEAN II Electrophoresis Cell (BioRad, USA) followed by Coomassie blue staining and immuno-blot. His-probe antibody in 1:100 dilution (H-3. sc-8036, Santa Cruz Biotechnology, USA) and goat anti-mouse IgG-HPR (1:5,000, Agrisera Antibodies, Sweden) were used to confirm the presence of 6xHis labeled proteins. The bound antibodies were visualized by enhanced chemiluminescence (ECL). Radiographic film (Kodak X-Omat LS, Sigma-Aldrich, USA) exposure was performed for 10 min for detection.

In vitro enzymatic assays

The activity of the recombinant PRISEs was tested based on the consumption of the putative substrate 8-oxogeranial and the formation of the reaction product *cis,trans*-nepetalactol. The enzyme assay was conducted following the protocol from Sherden et al. (2017), and it contained 50 mM MOPS (pH 7.5), 100 mM NaCl, 1 mM NADPH, tetrahydrofuran (THF) (0.5% v/v), 500 µM 8-oxogeranial (Santa Cruz Biotechnology, USA), and 2.5–5 mg of recombinant ISY. A negative control was conducted without the enzyme. The reactions were incubated overnight at 30°C, followed by extraction with 1:1 (v:v) hexane. Following enzymatic assay for the confirmation of *Nr*PRISE2 and *Nn*PRISE function, reaction products were subjected to GC/MS, UHPLC/(+)MS2, and NMR analyses, for the confirmation of their structure.

GC/MS targeted analysis of 8-oxogeranial and cis,trans-nepetalactol

Pure standards of 8-oxogeranial (Santa Cruz Biotechnology, Dalas, Texas, USA) and *cis,trans*-nepetalactol (SigmaAldrich, St. Louis, MO, SAD) diluted in *n*-hexane (1 mg ml^{-1}), reaction mixtures containing *Nr*PRISE2 and *NnPRISE*, and those lacking recombinant enzymes, were analyzed using GCMS-QP2010 plus instrument (Shimadzu, Japan) equipped with a split-splitless injector. Gas chromatographic separations was achieved adopting a ZB-1 MS column (30 mm × 0.25 mm, 0.25 µm film thickness) (Phenomenex, Austria), and using He (99.999%, The Linde Group, Ireland) as a carrier gas at a flow rate of 1.6 ml min^{-1}. Transfer line and detector temperatures were maintained at 250°C and 270°C, respectively. Mass spectra were acquired in positive EI mode (+70 eV), with temperature of the EI source set to 280°C. The temperature program of the chromatographic oven was set to linearly increase the temperature from 50 to 240°C, at rate of 5°C min^{-1}, and then maintain 240°C for the next 10 min. The splitless mode was applied for injection of samples (2 µl). Analyses were performed in SCAN mode, tracking the compounds within the range 40 to 400 amu, and in Single Ion Monitoring mode (SIM) which was targeted towards masses corresponding to 8-oxogeranial (166) and nepetalactol (168). The constituents of the reaction mixtures were identified by comparison of their mass spectra and retention times with those of the respective standards, and by comparison with the Wiley8, NIST05, and FFNSC3 libraries, using different search engines.

NMR analysis of PRISE reaction products

Detection and structure confirmation of targeted compounds was performed using ^{1}H and 2D H–H *COSY* NMR techniques and comparing the obtained spectral data with in house data of pure compounds. The NMR spectra were recorded on a Bruker AVANCE III 500 MHz NMR spectrometer equipped with a 5 mm inverse broadband (BBI) probe head at 298 K. Samples were dissolved in 500 µL of 99.8% $CDCl_3$ (SigmaAldrich, Germany) with 0.03% (v/v) of internal standard trimethylsilane (TMS).

To generate ^{1}H NMR spectra, 32k data points were collected using standard pulse program *zg30* with 128 scans. Spectral width was set to 20 ppm (10,005.2 Hz), relaxation time to 2 sec (d1), acquisition time 2 sec, and transmitter frequency offset to 8.5 ppm. Spectral referencing was performed used chemical shift of TMS, set to $\delta = 0$ ppm). Total acquisition time was 10 min. For the 2D H–H *COSY* NMR spectra, spectral width was set to 5,502.8 HZ for F1 and F2 frequency axis, relaxation time 2 sec and frequency offset to 5.75 ppm. Spectra were acquired using 32 scans per 256 increments of F1, with FID of 2k data points per F2. Total duration of analyses was 90 min.

Evolutionary analysis of *Nr*PRISEs and *Nn*PRISE by maximum likelihood method

The evolutionary history was inferred by using the Maximum Likelihood method and JTT matrix-based model (Jones et al., 1992). Phylogeny test was conducted by bootstrap method and number of bootstrap replications were 1,000. The tree with the highest log likelihood is shown. The percentage of trees in which the associated taxa clustered together is shown next to the branches. Initial tree(s) for the heuristic search were obtained automatically by applying Neighbor-Join and BioNJ algorithms to a matrix of pairwise distances estimated using the JTT model, and then selecting the topology with superior log likelihood value. The tree is drawn to scale, with branch lengths measured in the number of substitutions per site. This analysis involved 38 amino acid sequences. All positions containing gaps and missing data were eliminated (complete deletion option). There were a total of 344 positions in the final dataset. Evolutionary analyses were conducted in MEGA X (Kumar et al., 2018).

*Nr*PRISE2 and *Nn*PRISE tertiary structure modeling and ligand docking

The tertiary structure of ISY and PRISE proteins was predicted with AlphaFold2.1 (Jumper et al., 2021) via UCSF ChimeraX 1.4 (Pettersen et al., 2021). Assessment of obtained structures was performed via SWISS-MODEL Workspace (Waterhouse et al., 2018) by MolProbity 4.4 (Williams et al., 2018). The obtained PDB structures ware compared to ISY/P5βR enzymes with experimentally resolved 3D structures using the jFATCAT rigid model (Li et al., 2020) and in ChimeraX after superposition using the matchmaker command with default parameters (Pettersen et al., 2021).

Cofactor (NADP) inclusion in the predicted ISY structures was performed by first superposing of *Digitalis lanata* P5βR (PDB:2V6G, Thorn et al., 2008) using the matchmaker command in ChimeraX after which the cofactor atom coordinates were extracted and the predicted ISY protein-cofactor complex energy was minimized using Gromacs 2018.6 (Abraham et al., 2015). For energy minimization the protein topology was prepared using the CHARMM36 all-atom force field (Huang and Mackerell, 2013, jul 2021 version, http://mackerell.umaryland.edu/charmm_ff.shtml#gromacs); ligand topology was generated using CHARMM General Force Field server (Vanommeslaeghe et al., 2009, https://cgenff.umaryland.edu/initguess/). Solvation of the complex was performed using the CHARMM-modified TIP3P water model (*TIP3P*_CHARMM), while energy minimization of the complex was performed using steepest descent algorithm with 50k minimization steps using the following options: emtol = 50.0, emstep = 0.01, nstlist = 1, cutoff-scheme = Verlet, ns_type = grid, rlist = 1.2, coulombtype = PME, rcoulomb = 1.2, vdwtype = cutoff, vdw-modifier = force-switch, rvdw = 1.2, pbc = xyz, DispCorr = no.

The cofactor-protein energy minimized structures were used for ligand docking using AutoDock Vina 1.2.3 (Eberhardt et al., 2021). For docking the following ligands were used: 8-oxogeranial, *trans*- and *cis*- 8-oxocitronellyl enolates, (1R)-*c*,*c*-NLL (PubChem CID: 11194562), (1R)-*c*,*t*-NLL (PubChem CID: 442438), (1S)-*c*,*c*-NLL (PubChem CID: 11298185), (1S)-*c*,*t*-NLL (PubChem CID: 11286692), (1S)-*t*,*c*-NLL and (1R)-*t*,*c*-NL (obtained by reducing *t*, *c*-NL (PubChem CID: 442430) using Avogadro 1.2.0 (Hanwell et al., 2012). 50 conformers of each of the bicyclic ligands was generated via RDKit 2021.09.5 (Landrum et al., 2022) using the ETKDG version 3 method with small ring torsion angle preferences (Wang et al., 2020) and subsequently filtered using an RMSD threshold of 0.5 Å so that only those conformations that are at least 0.5 Å RMSD away from all retained are kept. This resulted in 2–4 conformers per compound. The geometry of the resulting conformers was optimized using Merck molecular force field (MMFF94s) as implemented in RDKit 2021.09.5 (Landrum et al., 2022). 8-Oxogeranial ligand was prepared so that Cα-Cβ bonds were held rigid in the following conformations: 1. C1-C2 s-*cis*, C7-C8 s-*cis*, 2. C1-C2 s-*cis*, C7-C8 s-*trans*, 3. C1-C2 s-*trains*, C7-C8 s-*cis* and 4. C1-C2 s-*trains*, C7-C8 s-*trans*. Two types of ligand dockings were performed: using rigid protein structures and flexible docking where the residues Lys147 and Tyr179 for *Nn*PRISE and Phe153 and Tyr185 for *Nr*ISY were allowed to be flexible. The docking procedures were performed using an exhaustiveness of 64, with autogrid4 precalculated affinity maps (Hanwell et al., 2012). 8-Oxogeranial coordinates from the *C. roseus* ISY (Qin et al., 2016, PDB: 5COB) were used to define the docking box center, after superposition to the AlphaFold models of *Nn*PRISE (grid center: x = 7.484, y = -4.133, z = 3.346) *and Nr*ISY (grid center: x = 6.686, y = -7.040, z = 2.655). The docking box was 40 grid points in each direction, with a grid spacing of 0.375 Å. The highest scoring poses for each ligand were inspected and compared to 8-oxogeranial from the experimental structures of *C. roseus* ISY – PDB: 5COB (Qin et al., 2016) and PDB: 5DBI (Hu et al., 2015).

8-Oxogeranial α,β -conformer energy evaluation and minimization was performed with Avogadro 1.2 (Hanwell et al., 2012) using steepest descent algorithm and the following forcefields: Universal force field (UFF, Rappe et al., 1992), Merck molecular force fields - MMFF94 (Halgren, 1996) and MMFF94s (Halgren, 1999) and the general Amber force field (GAFF, Wang et al., 2004).

Statistical analysis

For the Hierarchical Cluster Analysis (HCA) the input variables were scaled to the [0, 1] range. HCA was based on Pearson method of cluster agglomeration, adopting the Morpheus software (https://software.broadinstitute.org/morpheus). The correlation matrix for the gene expression quantitative data was constructed using Pearson's correlation coefficients, with the Past 4 software (version 4.12; Hammer et al., 2001). Quantitative metabolomics

and gene-expression data were subjected to *post hoc* Tukey's test ($p < 0.05$) of one way ANOVA, or to Student's *t*-tests ($p < 0.05$).

Results and discussion

Untargeted metabolomics of *N. rtanjensis* and *N. nervosa* leaves

The present study describes for the first time the comprehensive profiling of iridoids in *N. rtanj*ensis and *N. nervosa*, by simultaneously acquiring and comparatively analyzing iridoid aglycones and glycosides. Methanol extracts of *N. rtanjensis* and *N. nervosa* leaves, harvested from *in vitro* grown plants, were subjected to non-targeted metabolomics adopting GC/MS for the analysis of iridoid aglycones, and UHPLC/QToF MS^2, in both negative and positive ionization modes, for the analysis of iridoid glycosides and iridoid aglycones. Currently available data on the distribution and diversity of these two subgroups of iridoids across the genus *Nepeta* are fragmentary; only rarely they are simultaneously analyzed. Complementary analytical methodologies and tools, described within the present study, could easily be adopted to other *Nepeta* species, which can facilitate the elucidation of the overall diversity of iridoids at inter- and intra-species level, and further direct the reconstruction of the molecular background of this diversity within the genus.

GC/MS analysis of methanol extracts revealed the presence of a variety of terpenoids in *N. rtanjensis* and *N. nervosa* leaves (Supplementary Table 2). The total number of identified compounds in *N. rtanjensis* and *N. nervosa* leaves was 26 and 10, respectively. In leaves of *N. rtanjensis*, the most abundant were monoterpenoids from the group of iridoid aglycones, 5,9-dehydronepetalactone and *trans*,*cis*-nepetalactone, which were followed by *cis*,*trans*-nepetalactone (Supplementary Table 2; Figure 1). Germacrene D was the major sesquiterpenoid in methanol extracts of *N. rtanjensis*, while monoterpenoids α-thujene and α-copaene were also present in significant amounts. Although iridoids were not identified in methanol extracts of *N. nervosa* leaves, this species contained significant amounts of sesquiterpenoids, among which Germacrene D and Germacrene D-4-ol predominated (Supplementary Table 2). Diterpene phytol was also abundant in leaves of *N. nervosa*.

UHPLC/(+)QToF MS^2 analysis in the positive ionization mode confirmed the presence of the two nepetalactone diasteroisomers and 5,9-dehydronepetalactone in methanol extracts of *N. rtanjensis* leaves, and identified several more iridoid aglycones (Supplementary Table 3). Dihydronepetalactone belongs to the group of iridoid aglycones and is a hydrogenation product of nepetalactone, while nepetaracemoside B aglycone and 7-deoxyloganin aglycone most likely arise through the deglycosilation of nepetaracemoside B and deoxyloganin, two compounds which are a part of the biosynthetic branch leading to iridoid glycosides. Two stereoisomers of nepetalactone, *cis*,*trans*- and *trans*,*cis*-nepetalactone, and 5,9-dehydronepetalactone, were very abundant in *N. rtanjensis* leaves, which is in accordance with previously published data (Mišić et al., 2015; Skorić et al., 2017; Aničić et al., 2021). By studying the exact mass and high-resolution MS^2 fragmentation of iridoid glycosides in the negative ionization mode, 6 compounds (16-21) specific to the *Nepeta* genus were identified in *N. rtanjensis* leaves, as well as 5-deoxylamiol (15), previously found in other Lamiaceae species. A total of 13 iridoid glycosides have previously been found in *N. rtanjensis* cultured *in vitro* (Aničić et al., 2021), including 1,5,9-*epi*deoxyloganic acid, geniposide, 1-*O*-hexosyl-epideoxyloganic acid, and nepetariaside, also identified within the present study (Supplementary Table 2). 1,5,9-*epi*deoxyloganic acid is recognized as the major iridoid glycoside in *N. rtanjensis*, and was previously identified as one of the major compound from this subgroup in other *Nepeta* species, including *N. cataria* (Murai et al., 1984), *N. cadmea* (Takeda et al., 1998), *N. nuda* (Kökdil et al., 1998; Petrova et al., 2022), and *N. argolica* (Ahmed et al., 2006). Interestingly, no iridoids were identified in methanol extracts of leaves of *in vitro* grown *N. nervosa* plants (Supplemetary Tables 1 and 2; Figure 1). Literature search revealed only a few publications dealing with the chemical profiling of *N. nervosa* (Nestorović et al., 2010; Mišić et al., 2015), which pointed to the fact that this species produces no iridoids. However, it should not be ruled out that this species actually produces some of the iridoids in amounts which are below the limits of detection of the adopted analytical instruments. It could also be speculated that *N. nervosa* plants might produce iridoids under more favorable growth conditions.

In addition to iridoids, compounds belonging to the class of phenolics (14 compounds) and other classes (10 compounds) were also identified in analyzed samples (Supplementary Table 3). Hydroxycinnamic acids (10 compounds) were represented by glycosides and esters of caffeic and ferulic acids. Rosmarinic acid, which is structurally a dimer of caffeic acid, was abundant in leaves of both analyzed *Nepeta* species, while 5-*O*-caffeoylquinic acid and 3-O-caffeoylquinic acid were present only in *N. rtanjensis*. Nepetoidin A or B, a derivative of caffeic acid specific for plants from the genus *Nepeta* (Aničić et al., 2021), was identified in leaves of *N. nervosa*. Totally 4 compounds from the group of flavonoids are identified in leaves of *N. nervosa*. Two aglycones (13 and 14), which are methylated flavones according to their structure, are specific for the genus *Nepeta* (Aničić et al., 2021). Luteolin 7-*O*-dihexuronide (11), detected at 5.59 min, showed molecular ion at 637.10464 *m/z* and MS^2 base peak at 285.03234 *m/z* (deprotonated luteolin). MS^2 fragments at 175 and 193 *m/z* originate from hexuronic acid, while the ion found at 351 *m/z* corresponds to the fragment resulting from the neutral loss of the luteolin molecule, which is the proof that 2 molecules of hexuronic acid are interconnected (Dienaitė et al., 2018). For compound 12 at 8.38 min and 577.15518 *m/z*, the proposed molecular formula was $C_{27}H_{29}O_{14}^+$, based on the correct isotopic mass. The MS^2 base peak at 329.10012 *m/z* was formed by the neutral loss of $C_9H_{12}O_8$ (248 Da), which by mass completely corresponds to the malonyl-hexose residue. Such a compound has not been found in the genus *Nepeta* so far, nor in any other plant species. However, a similar compound without malonyl group was detected in *Salvia* species (Qiao et al., 2009), and it is known as salvigenin 5-*O*-glucoside.

Comparative transcriptomics of *N. rtanjensis* and *N. nervosa* leaves

Transcriptomes of *N. rtanjensis* and *N. nervosa* leaves were searched for the presence/absence of transcripts of iridoid pathway-related genes, based on the homology with the genes characterised in iridoids- and alkaloids- producing *C. roseus* (Geu-Flores et al., 2012; Miettinen et al., 2014; Krithika et al., 2015) and those from the genus *Nepeta* (Lichman et al., 2019a; Lichman et al., 2020; Hernández Lozada et al., 2022). This resulted in the list of candidate biosynthetic genes from *N. rtanjensis* and *N. nervosa*. In the transcriptome of *N. rtanjensis* leaves, orthologues of *NrGPPS*, *NrGES*, *NrG8H*, *Nr8HGO*, *NrPRISE1*, *NrPRISE2*, *NrNEPS1*, *NrNEPS2*, *NrNEPS3*, *NrNEPS4*, and *NrMLPL1* and *NrMLPL2* were identified (Aničić et al., 2020) (Figures 1B, C). Due to their affiliation with the "promiscuous" enzyme group – PRISE (Petersen et al., 2016), the potential ISY orthologs were labeled as the PRISE enzymes for the purpose of initial functional characterization and co-expression analyses. The designations include *Nr*PRISE1, *Nr*PRISE2, and *Nn*PRISE. As *N. rtanjensis* is predominately a *trans*, *cis*-nepetalactone producing species, it is not surprising that NEPS4 and NEPS1 homologues were identified in the transcriptome of leaves of this species. It was previously shown that NEPS4 enzymes in *N. cataria* and *N. mussinii* are *trans-cis*-cyclazes, which act with a partner dehydrogenase NEPS1 and ISY to give a rise to *trans,cis*-nepetalactone (Lichman et al., 2020; Hernández Lozada et al., 2022). On the other hand, NEPS1 has also been reported to have *cis,trans*-nepetalactol dehydrogenase activity (Lichman et al., 2019a). *N. rtanjensis* leaves also contain significant amounts of *cis,trans*-nepetalactone, and their transcriptome is shown to possess homologue of NEPS2, which in *N. sibirica* (*Ns*NEPS2) acts as a *cis-trans* cyclase and oxidase (Lichman et al., 2019a; Hernández Lozada et al., 2022). According to the literature data, NEPS3 has specific 7*S-cis, cis*-nepetalactone cyclase activity (Lichman et al., 2019a).

Orthologues of *GPPS*, *G8H*, *8HGO*, *PRISE*, *MLPL*, and *NEPS* were present in the transcriptome of *N. nervosa* leaves, while GES transcripts were lacking. Interestingly, only one orthologue of both PRISE (*NnPRISE*) and NEPS (*NnNEPS1*) were identified in *N. nervosa*. The reaction catalyzed by GES is considered a key gatekeeping step in iridoid biosynthesis, since this enzyme is responsible for diverting metabolic flux away from canonical monoterpenes by converting GPP to geraniol, the precursor of iridoids (Boachon et al., 2018). Silencing of GES in *N. cataria* leaves resulted in significant decrease of the content of all nepetalactoneL isomers and 1,5,9-*epi*deoxyloganic acid (Palmer et al., 2022), while in *C. roseus* the content of iridoid-derived alkaloids was decreased (Kumar et al., 2015). As NEPS and MLPL work in combination with ISY to control the stereochemical mode of 8-oxogeranial cyclization (Lichman et al., 2020), it might be speculated that besides GES, functional ISY and some of the NEPSs are important missing parts to complete the iridoid biosynthesis puzzle in this species. The loss of function of NEPSs, which are directly responsible for nepetalactone formation and stereochemistry at the 4a and 7a carbons (Lichman et al., 2019a; Lichman et al., 2019b), can certainly lead to the absence of nepetalactones in these *Nepeta* species.

We further compared the protein sequences corresponding to iridoid-related biosynthetic genes of the two *Nepeta* species. Pairwise sequence alignment results revealed high level of similarity between the homologues of all identified iridoid-related biosynthetic genes of the two species (Figure 1C). MLPL sequences had shown lowest similarity between the two species, while *Nn*PRISE displayed especially high sequence similarity with *Nr*PRISE1 (96.4%).

Phyllogenetic analysis of *Nr*PRISE2 and *Nn*PRISE

The nucleotide sequences potentially encoding ISYs found in leaf transcriptomes of *N. rtanjensis* – *NrPRISE1* (1164 bp) and *NrPRISE2* (1203 bp), and of *N. nervosa* - *NnPRISE* (1167 bp), have shown to be highly similar to functionally characterized ISYs from other species (Figure 2). The *Nr*PRISE2 is most closely related to the characterized iridoid synthases from *N. cataria* (*Nc*ISY) and *N. mussinii* (*Nm*ISY) (Lichman et al., 2020). Recombinant *Nc*ISY and *Nm*ISY enzymes were shown to be active isoforms, which fully converted 8-oxogeranial to *cis,trans*-nepetalactol in assays *in vitro* (Sherden et al., 2017; Lichman et al., 2020). On the other hand, *Nn*PRISE and *Nr*PRISE1 are more similar to P5βRs isoforms from *N. cataria* (*Nc*P5βR1) and *N. mussinii* (*Nm*P5βR1). P5βR isoforms display very low catalytic activity (Sherden et al., 2017), which is why they are thought not to be physiologically relevant for iridoid biosynthesis (Lichman et al., 2020).

Although phylogenetic relationships of the previously characterized ISYs and PRISE candidates from *N. rtanjensis* and *N. nervosa* indicate a high degree of mutual homology, this information alone cannot predict with absolute certainty the catalytic activity of the enzymes. Furthermore, ISYs belong to the "promiscuous" group of enzymes, together with progesterone-5-β-reductases (PRISE) (Petersen et al., 2016), that are structurally and functionally very close, which additionally makes unreliable the prediction of isolated isoforms activity solely based on the phylogenetic analysis. Therefore, we proceed with the organ-specific and MeJA-induced profiling of iridoids content and expression profiling of corresponding biosynthetic genes to further support the phylogenetic data.

Organ-specific and MeJA-induced patterns of iridoid biosynthesis in *N. rtanjensis* and *N. nervosa*

According to the organ-specific profiling of major iridoids in *N. rtanjensis* shoots grown *in vitro*, leaves displayed the highest content of *trans,cis*-nepetalactone, 5,9-dehydronepetalactone, and 1,5,9-*epi*deoxyloganic acid, and were followed by stems (Figure 3A). Roots contained no targeted iridoids. It has previously been shown that leaves of *N. rtanjensis* are enriched with glandular trichomes, the main site of nepetalactone biosynthesis and accumulation in *Nepeta* species (Aničić et al., 2018; Aničić et al., 2020). In parallel with iridoid profiling, we analyzed co-expression patterns of iridoid biosynthesis-related gene candidates (*NrGPPS*, *NrGES*, *NrG8H*, *Nr8HGO*, *NrPRISE1*, *NrPRISE2*, *NrNEPS1*, *NrNEPS2*, *NrNEPS3*,

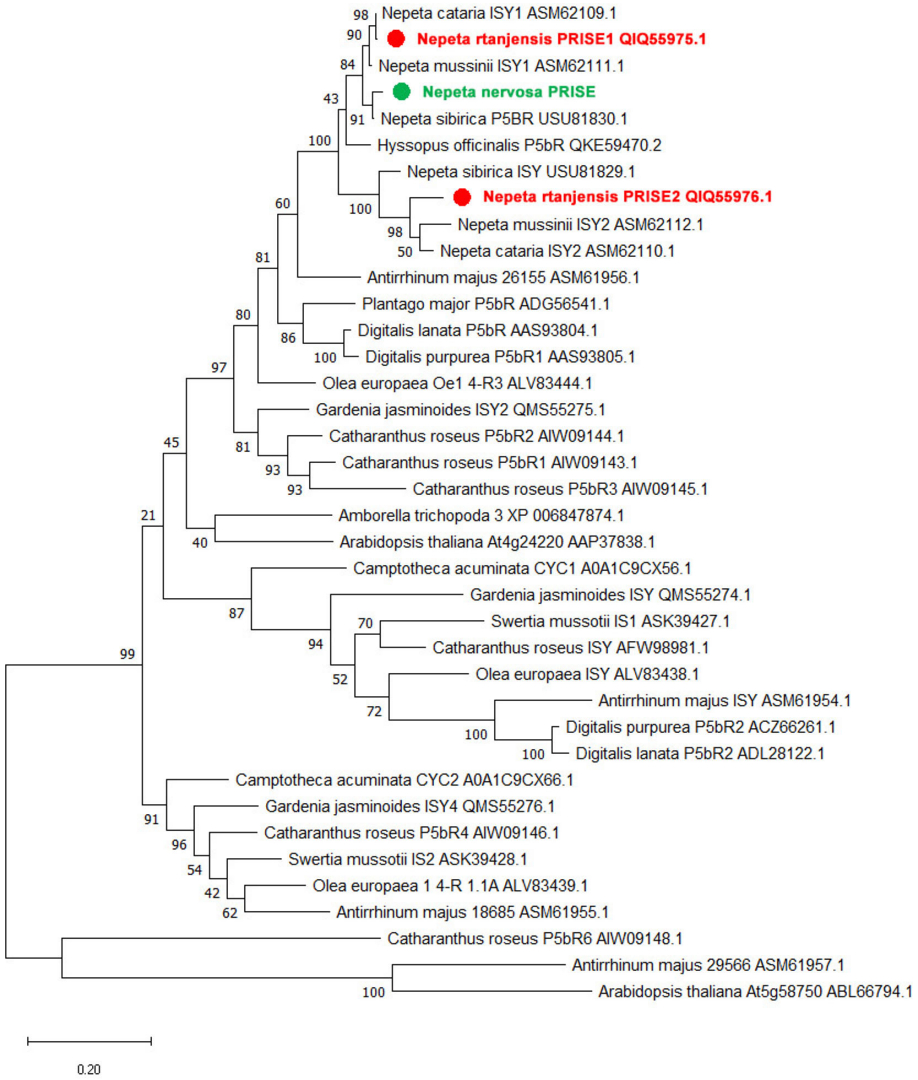

FIGURE 2
The Maximum Likelihood tree generated with MEGA X (version 10.2.6) illustrating the phylogenetic relationship of NrPRISE1, NrPRISE2, and NnPRISE candidates compared to homologous genes from different plant species. The tree with the highest log likelihood is shown. The percentage of trees in which the associated taxa clustered together is indicated next to the branches. Accession numbers of sequences are listed next to species names and protein abbreviations.

NrNEPS4, and *NrMLPL*) in the same organs. Leaves and stems were more enriched with the transcripts of the majority of analyzed biosynthetic genes candidates when compared to roots. The expression of *NrPRISE2* in roots was very low, while in *N. rtanjensis* leaves around 400 fold higher amount of *NrPRISE2* transcripts was recorded (Figure 3B). As for *NrPRISE1*, the highest expression level of this PRISE orthologue was recorded in stems of *N. rtanjensis* (Figure 3B). Expression profiles of selected iridoid-related biosynthetic gene candidates in leaves, stems and roots of *N. rtanjensis* were subjected to the Pearson's correlation analysis. Results indicate that the majority of the analyzed genes are co-expressed while displaying significant positive correlations (Figure 3C). The only exception was *NrPRISE1*, which displayed the lowest level of correlations with other gene candidates. The majority of genes analyzed within the present study (*NrGPPS*, *NrGES*, *NrG8H*, *Nr8HGO*, *NrPRISE1*, *NrPRISE2*, *NrNEPS1*, *NrNEPS2*, *NrNEPS3*, and *NrNEPS4*) were previously analyzed for their expression profiles in detached trichomes and abraded leaves (Aničić et al., 2020), but also in response to PEG-induced dehydration of leaves (Aničić et al., 2020). All these data point to the *NrPRISE2* as a promising candidate for iridoid synthase, an enzyme involved in the reduction of nepetalactol, a critical point determining metabolic flux throughout the iridoid pathway. *N. rtanjensis NrPRISE2* orthologue was further subjected to functional characterization.

Nepetalactone, 5,9-dehydronepetalactone, and 1,5,9-*epi*deoxyloganic acid were not recorded in leaves, stems, and roots of *N. nervosa* grown *in vitro*, as expected (Nestorović et al., 2010; Mišić et al., 2015). No literature data on the organ- or tissue-specific iridoid profiling is available for *N. nervosa*. Organ-specific expression patterns of selected biosynthetic gene candidates (*NnGPPS*, *NnG8H*, *Nn8HGO*, *NnPRISE*, *NrNEPS1*, and *NnMLPL*)

10.3389/fpls.2023.1211453

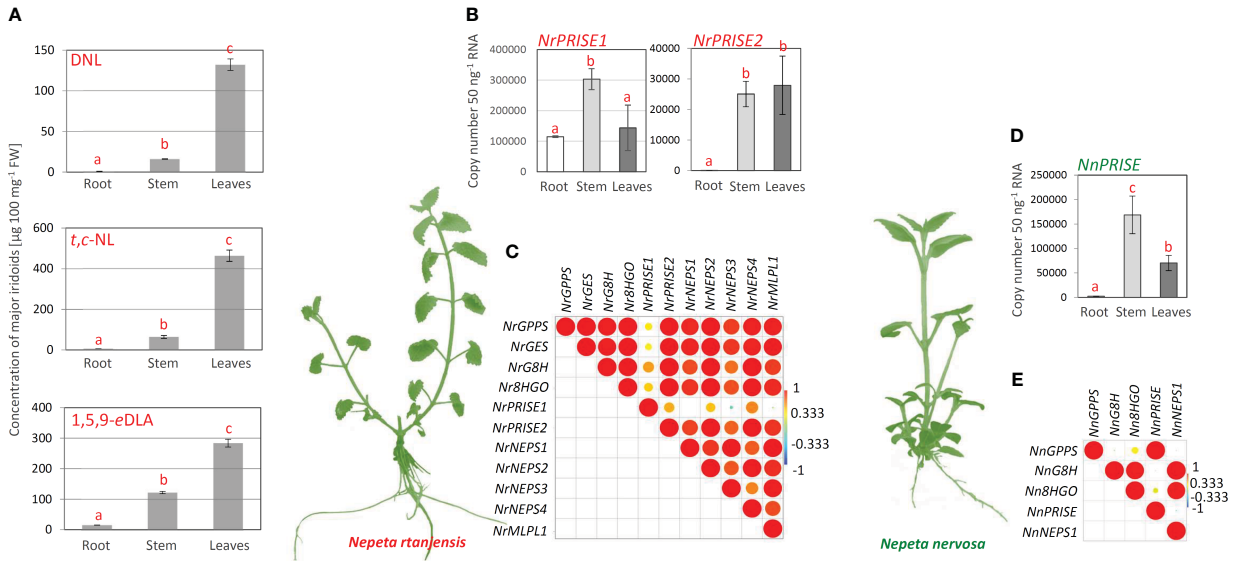

FIGURE 3
(A) Organ-specific profiling of the major iridoid aglycones and iridoid glycosides in *N. rtanjensis* plants grown *in vitro* was performed adopting UHPLC/DAD/(±)HESI–MS^2 analysis. No iridoids were recorded in analyzed *N. nervosa* samples. Error bars represent SE of three biological replicates. In all cases, bars with different letters are significantly different ($p < 0.05$) according to *post hoc* Tukey's test of one way ANOVA. **(B)** Expression profiles of *N. rtanjensis* PRISE candidates (*NrPRISE1* and *NrPRISE2*) and **(D)** *N. nervosa NnPRISE* in roots, stems and leaves of *in vitro* grown plants. Letters above the bars denote significant differences according to Tukey's HSD *post hoc* test at $p < 0.05$. Pearson correlations based on the relative gene expression of iridoid-related biosynthetic genes in **(C)** *N. rtanjensis* and **(E)** *N. nervosa*. Each field in the Pearson's correlation plot indicates the coefficient for a pair of genes, and the value of the correlation coefficient is represented by the intensity of red and yellow (positive correlations) or blue and green (negative correlations), as indicated on the color scales (for the interpretation of the references to color in this Figure legend, the reader is referred to the web version of this article). GPPS, geranyl diphosphate synthase; GES, geraniol synthase; G8H, geraniol 8-hydroxylase; 8HGO, 8-hydroxygeraniol oxidoreductase; PRISE, progesterone-5β-reductase/iridoid synthase activity displaying enzymes; NEPS, nepetalactol-related short-chain dehydrogenase; MLPL, major latex protein-like enzyme; IA, iridoid aglycone; IG, iridoid glycoside; DNL, 5,9-dehydronepetalactone; *t,c*-NL, *trans,cis*-nepetalactone; 1,5,9-eDLA, 1,5,9-*epi*deoxyloganic acid.

were also analyzed in *N. nervosa*. The lowest expression level of the analyzed genes was recorded in roots of *N. nervosa*, while stems and leaves were enriched with transcripts of targeted biosynthetic gene candidates. Of the analyzed genes, *NnPRISE* displayed ~2 fold higher expression in leaves than in roots (Figure 3D), as well as the lowest level of positive correlations with other analyzed genes (Figure 3E). Pearson's correlation analysis showed that the expression of *NnPRISE* is significantly positively correlated with the *NnGPPS*, while no significant correlations were observed with other analyzed genes (Figure 3E). Some of the BG candidates are co-expressed in different tissues (*Nn*GPPS with *Nn*PRISE, as well as *Nn*NEPS1 with *Nn*G8H and *Nn*8HGO), indicating their possible involvement in the iridoid biosynthetic pathway.

To elucidate the interrelation between *N. rtanjensis* and *N. nervosa* metabolome and transcriptome, the effect of methyl jasmonate (MeJA) as a potent elicitor, on iridoid content and relative changes in the expression of biosynthetic gene candidates in leaves of *N. rtanjensis* and *N. nervosa* grown *in vitro*, was investigated. MeJA has previously been used as a potent elicitor of specialized metabolism in plants, including those producing iridoids (e.g. (Wang et al., 2010; Cao et al., 2016; Piątczak et al., 2016; Matekalo et al., 2018; Rubio-Rodríguez et al., 2021; Pu et al., 2022). This elicitor promotes changes in the accumulation of specialized metabolites at the transcriptional level of genes involved in their biosynthesis. Content of major iridoids was significantly increased in MeJA-treated *N. rtanjensis* plants 24 h following the application of the elicitor (Figure 4A). The most significant increase was recorded for 5,9-dehydronepetalactone, which was followed by *trans,cis*-nepetalactone and 1,5,9-*epi*deoxyloganic acid. Significantly higher amounts of 5,9-dehydronepetalactone and *trans,cis*-nepetalactone, and lower amounts of 1,5,9-*epi*deoxyloganic acid were also recorded in MeJA-treated plants than in non-treated plants 72 h after the beginning of the experiment (Figure 4A). The highest increase in the expression of the majority of targeted biosynthetic genes and transcription factors candidates was recorded 24 h after the application of MeJA, and after that the expression decreases (Figure 4B). Still, the expression of the majority of biosynthetic genes and transcription factors is higher in MeJA-treated than in non-treated plants after 72 h of experiment. The changes in the expression levels were the most pronounced for *NrNEPS3* and transcription factors *NrJAZ3* and *NrMYC2*. Similarly, in *Castilleja tenuifora* the increase in the expression of some iridoid biosynthesis-related genes was the most pronounced 24 h after the MeJA treatment (Rubio-Rodríguez et al., 2021). The selection of TF for the co-expression analysis was based on our previous studies, where NrMYC2 and NrYABBY5 are recognized as the potential positive regulators of NL biosynthesis in *N. rtanjensis* (Aničić et al., 2020). *NrPRISE1 and NrPRISE2* clustered close to *NrMLPL2* and *NrCOI1* on Pearson HCA matrix (Figure 4B). All the other analyzed genes formed a separate cluster, which indicates their coordinated changes in the expression levels. To study the interrelation between

10.3389/fpls.2023.1211453

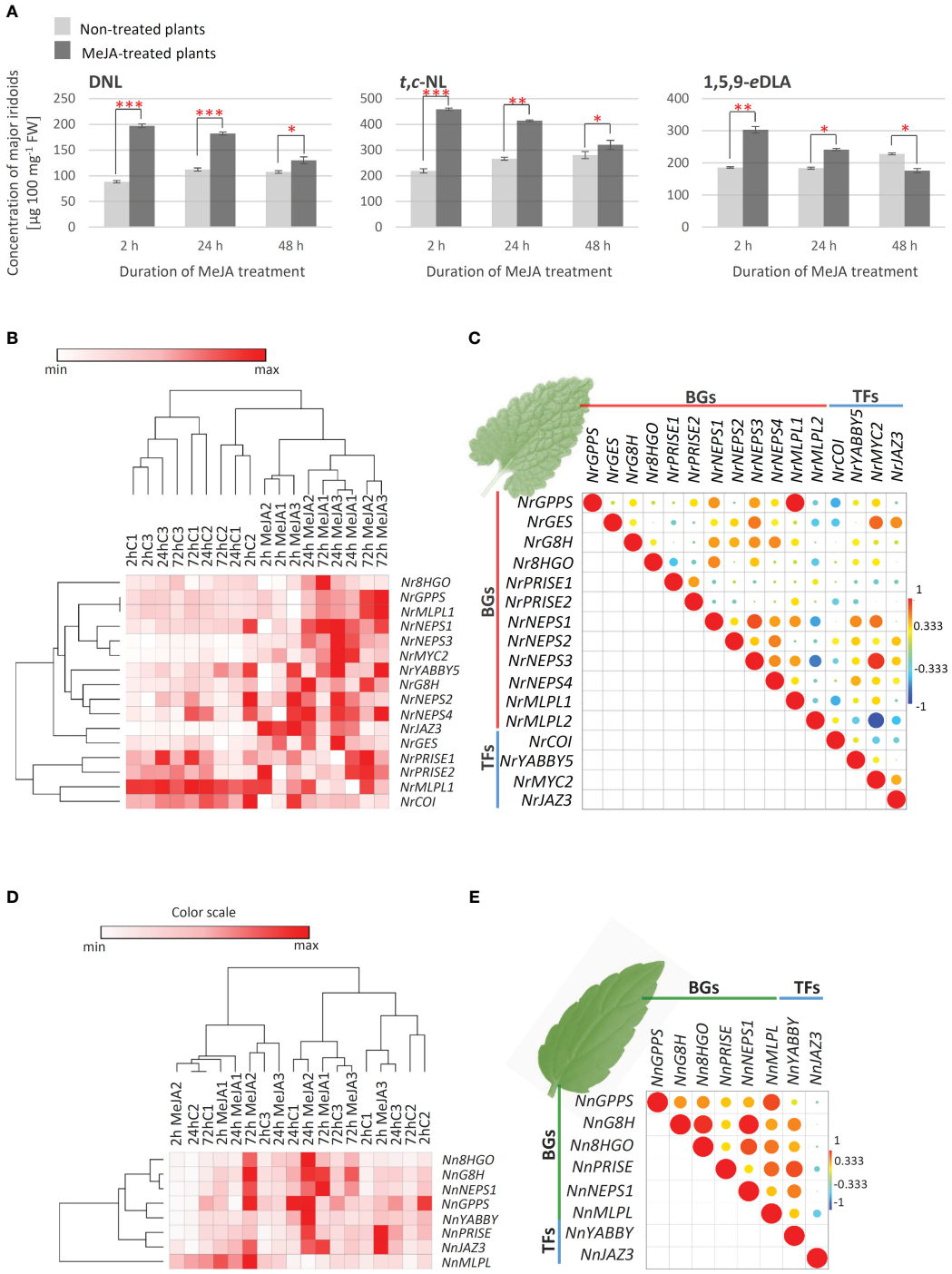

FIGURE 4
(A) MeJA- induced changes in the content of major iridoids in *N. rtanjensis* leaves as quantified using UHPLC/DAD/(+)HESI–MS2 instrument: DNL – 5,9-dehydronepetalactone; *t,c*-NL – *trans,cis*-nepetalactone; 1,5,9-*e*DLA – 1,5,9-*epi*deoxyloganic acid. Error bars represent SE of three biological replicates. In all cases, bars with different letters are significantly different (P < 0.05) according to *post hoc* Tukey's test of one way ANOVA. Red asterisks denote significantly different values according to the *t*-test, *p*-values, *p< 0.05, **p< 0.01, ***p< 0.001. Heatmap of the scaled quantitative data (expression data of iridoid-related biosynthetic genes- BGs and transcription factors- TFs) in *N. rtanjensis* **(B)** and *N. nervosa* leaves (**D**), with the samples (both columns and rows) arranged according to the hierarchical cluster analysis (Pearson method of cluster agglomeration). Intensity of red color indicates the expression levels of targeted genes, with red color representing the max values and white color the min values recorded for individual gene, as indicated in the color scale. Pearson correlation plot based on the gene expression of biosynthetic genes and transcription factors in leaves of **(C)** *N. rtanjensis* and **(E)** *N. nervosa* is presented. Each field in the Pearson's correlation plot indicates the coefficient for a pair of genes, and the value of the correlation coefficient is represented by the intensity of red and yellow (positive correlations) or blue and green (negative correlations), as indicated on the color scales (for the interpretation of the references to color in this Figure legend, the reader is referred to the web version of this article). GPPS, geranyl diphosphate synthase; GES, geraniol synthase; G8H,geraniol 8-hydroxylase; 8HGO, 8-hydroxygeraniol oxidoreductase; PRISE, progesterone-5β-reductase/iridoid synthase activity displaying enzymes; NEPS, nepetalactol-related short-chain dehydrogenase; MLPL, major latex protein-like enzyme; COI, coronatine-insensitive transcription factor; JAZ3, jasmonate ZIM-domain 3; MYC2, transcription factor Mouse-ear cress 2; YABBY5, YABBY5 transcription factor; DNL, 5,9-dehydronepetalactone; *t,c*-NL, *trans,cis*-nepetalactone; 1,5,9-*e*DLA, 1,5,9-epideoxyloganic acid.

the expression profiles of the iridoid-related biosynthetic genes and transcription factors in MeJA-treated leaves, a Pearson's correlation analysis was performed (Figure 4C). The expression levels of the majority of analyzed genes were positively correlated, with the exception of *NrMLPL2, NrCOI1*, *and NrPRISE1* which displayed mainly negative correlations with the rest of analyzed genes (Figure 4C). Although statistically significant positive correlations were observed in several cases (Figure 4C), the results show no clear co-expression patterns of analyzed *N. rtanjensis* genes, but point to the involvement of *Nr*JAZ and *Nr*MYC2 in jasmonate signaling pathway and indicate direct transcriptional regulation of *Nr*GES and *Nr*NEPS1-*Nr*NEPS4 via the above mentioned transcription factors. Thus, our results indicate the involvement of some of the analyzed genes in the same biosynthetic route, and point to the transcriptional regulation of their activity, which is consistent with our previous findings (Aničić et al, 2020). Our research suggested that shoot culture of *N. rtanjensis* in combination with MeJA elicitation has a promising application in biotechnology-assisted iridoid production.

As for iridoid non-producing *N. nervosa*, MeJA treatment did not induce the accumulation of iridoids in leaves. On the other hand, the expression of the majority of analyzed biosynthetic genes was induced 24h and 72h following the application of MeJA (Figure 4D). The most prominent changes were observed for *NnG8H*, *Nn8HGO* and *NnNEPS1*. One of the analyzed transcription factors, *NnYABBY*, clustered close to *NnGPPS* and *NnPRISE* on the Pearson HCA matrix (Figure 4D). *NnJAZ3* was segregated to the other analyzed biosynthetic genes. Pearson correlation analysis revealed positive correlations in the expression of all the analyzed biosynthetic genes and transcription factors, additionally indicating the transcriptional regulation of their activity (Figure 4E).

Based on the organ-specific and MeJA-induced profiling of expression of the PRISE candidates (*NrPRISE1*, *NrPRISE2*, and *NnPRISE*), their co-expression patterns with the rest of IBGs, as well as on the phylogenetic analysis, we further proceeded with functional characterization. As *Nr*PRISE1 showed no activity in enzymatic assays, we presumed that this PRISE candidate was not physiologically relevant for iridoid biosynthesis in *N. rtanjensis*, and we are further presenting the results of *NrPRISE2* and *NnPRISE* functional characterization.

Functional characterization of recombinant NrPRISE2 and NnPRISE expressed in E. coli

SDS-PAGE analyzes and Coomassie Brilliant Blue staining, as well as immunoblot detection of recombinant *Nr*PRISE2 and *Nn*PRISE proteins with anti-His antibodies, confirmed the presence of a single major band of the expected monomer length of 42 kD (Geu-Flores et al., 2012; Sherden et al., 2017), in both *Nr*PRISE2 and *Nn*PRISE lanes (Figure 5). Recombinant *Nr*PRISE2 and *Nn*PRISE were biochemically characterized, adopting *in vitro* enzymatic assay to determine their catalytic activities (Figure 5A). Reaction mixtures with recombinant proteins, 8-oxogeranial as substrate, and a cofactor NADPH, as well as a control assay mixture that did not contain the enzymes, were extracted in hexane. Based on their accurate mass, elemental composition, and fragmentation pattern, the products were characterized as nepetalactol and iridodials using GC/MS and UHPLC/MS^2 analyses (Figures 5B, C). *Cis,trans*-nepetalactol was visible as a peak at Rt = 16.9 min, while 8-oxogeranial was represented by a peak at Rt = 21.5 min on the GC/MS chromatogram (Figure 5B).

By comparing the GC/MS spectra and retention times of compounds from the reaction mixtures with those of pure 8-oxogeranial and *cis,trans*-nepetalactol, as well as with those of the Wiley Mass Spectral Database (Registry of Mass Spectral Data, Palisade Corporation, Newfield, NY, USA), peaks corresponding to the standards were identified (Figure 5C). The mass spectra of the compounds from the reaction mixtures, which correspond to 8-oxogeranial and *cis,trans*-nepetalactol, show fragmentation profiles characteristic for pure standards. GC/MS chromatograms of the control reaction showed only the peak corresponding to 8-oxogeranial. On the other hand, in the assays with *Nr*PRISE2 and *Nn*PRISE, in addition to 8-oxogeranial, peaks corresponding to *cis, trans*-nepetalactol were present (Figures 5B, C). This indicated the enzymatic conversion of 8-oxogeranial into nepetalactol in the presence of *Nr*PRISE and *Nn*PRISE.

An unambiguous assignment of the NMR spectra of *cis,trans*-nepetalactol and 8-oxogeranial was achieved using 1D (^{1}H) and 2D COSY NMR techniques, and the results are shown in Supplementary Figures 1 and 2, respectively. NMR data resembled those reported in the literature (Liblikas et al., 2005). The obtained results of ^{1}H NMR spectra of the reaction products with *Nn*PRISE show a clear appearance of peaks characteristic for *cis,trans*-nepetalactol (H-3, 6.01 and H-1, 4.85 ppm) and 8-oxogeranial (H-6, 6.42 and H-2, 5.91 ppm) which was unequivocal confirmed with crosspeaks in the COSY spectra. In the product of the reaction, which was catalyzed by the *Nr*PRISE2 enzyme, ^{1}H NMR spectra indicate only the presence of *cis,trans*-nepetalactol peaks, while the concentration of 8-oxogeranial is below the detection level of the used spectroscopic technique (Supplementary Figure 1). Despite *Nn*PRISE being phylogenetically closer to P5βR, the NMR COSY spectrum confirmed that this recombinant enzyme converts 8-oxogeranial to *cis,trans*-nepetalactol, although incompletely (Supplementary Figure 2). In other words, *Nn*PRISE probably exhibits a weaker activity than *Nr*PRISE2 under the given reaction conditions, but kinetics studies are needed in order for this to be confirmed. It cannot be ruled out that altered reaction conditions (e.g. buffer pH value, MOPS concentration in the buffer, temperature, etc.) could lead to complete conversion and higher catalytic activity of *Nn*PRISE.

In *Nepeta* species ISYs perform the reduction of 8-oxogeranial and NEPSs are responsible for the subsequent cyclization (Lichman et al., 2019a and Lichman et al., 2019b). As both PRISEss (*Nr*PRISE2 and *Nn*PRISE) resulted in the production of *cis,trans*-nepetalactol in the absence of NEPSs, our results indicate that cyclization occurred spontaneously. This was also confirmed for *Nc*ISY2 and *Nm*ISY2 (Sherden et al., 2017), as well as for ISYs from plants of other genera (Geu-Flores et al., 2012; Alagna et al., 2016; Kries et al., 2017; Xiang et al., 2017; Fellows et al., 2018).

Moreover, in light of *Nr*PRISE2 demonstrated ISY activity both *in vitro* and likely *in planta*, in contrast to *Nn*PRISE which lacks

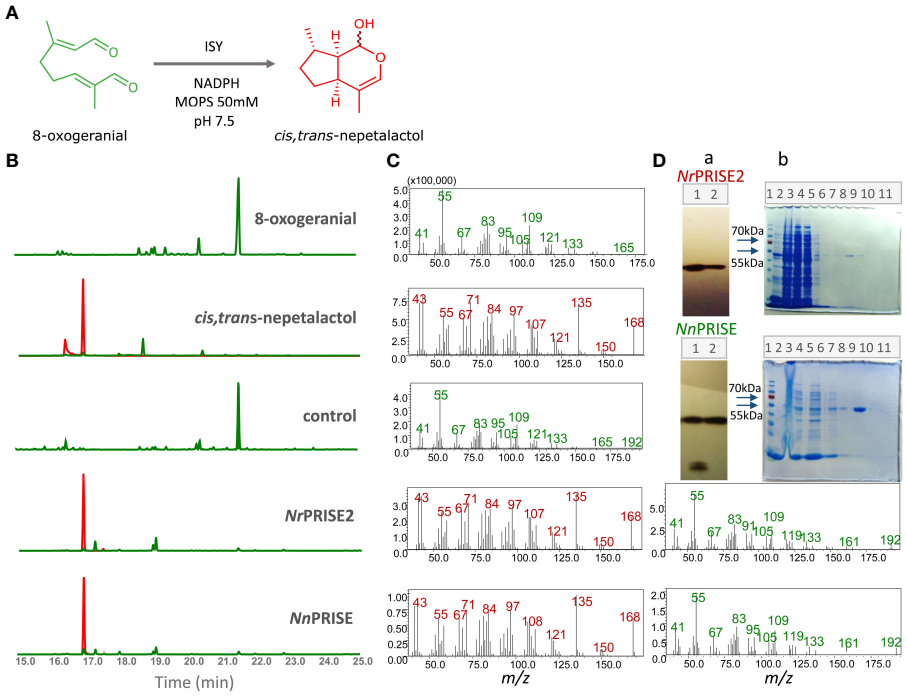

FIGURE 5
GC-MS analysis of *in vitro* assays with recombinant enzymes NrPRISE2 and NnPRISE. An enzymatic reaction is shown, in which iridoid synthase converts 8-oxogeranial to *cis,trans*-nepetalactol in a buffer with 50mM MOPS and pH 7.5 **(A)**. Extracted GC-MS chromatograms for 166 and 168 *m/z*, 8-oxogeranial and *cis,trans*-nepetalactol standards were compared with chromatograms of *in vitro* assays without enzymes (control) and with recombinant enzymes *Nr*PRISE2 and *Nn*PRISE **(B)**. The retention time of the peak corresponding to nepetalactol is Rt= 16.9 min, and 8-oxogeranial is Rt= 21.5 min. The peaks corresponding to the masses of 166 *m/z* are marked green, while the peaks of mass 168 *m/z* are red. The figure also shows the mass spectra **(C)** corresponding to the peaks from the chromatogram on the left with Rt= 16.9 min (red) and 21.5 min (green). Immunoblot **(A)** shows the isolated proteins *Nr*PRISE2 and *Nn*PRISE. 1 – insoluble proteins, 2 – soluble proteins **(D)**. The immunoblot figures have been extracted by cropping from the original images, constituting a part of Supplementary Figure 5. SDS-PAGE **(B)** shows the NI-NTA agarose protein purification process. 1- protein marker; 2 – proteins before IPGT introduction; 3 – insoluble proteins; 4 – soluble proteins; 5 – soluble proteins unbound to the NI-NTA resin; 6,7,8 – wash step 1, 2,3; 9, 10, 11 – elution steps 1,2,3. **(D)**. 8OG, 8-oxogeranial; NLL, *cis,trans*-nepetalactol; PRISE, progesterone-5β-reductase/iridoid synthase activity displaying enzymes.

suitable substrates for enzymatic action and exhibits a closer phylogenetic proximity to progesterone-5-β-reductases (P5BRs), we posit that a nomenclatural adjustment is warranted. Accordingly, we recommend the reclassification of *Nr*PRISE2 to *Nr*ISY, accurately reflecting its functional role as an iridoid synthase.

Overall protein structure of *Nn*PRISE and *Nr*ISY

In order to gain insights into the sequence structure relationships in *Nn*PRISE and *Nr*ISY, multiple sequence alignment with several ISY/5beta-POR enzymes with resolved 3D structures was performed (Figure 6A), and their structure was predicted using AlphaFold (Figures 6B, C). Overall, the structures resemble experimentally determined ISY and P5βR enzyme structures. After superposing with *Digitalis lanata* P5βR (PDB:2V6G, Thorn et al., 2008) the RMSD between aligned pairs of the backbone C-alpha atoms was 1.03 Å for *Nr*ISY and 0.86 Å for *Nn*PRISE. Both predicted structures have a high percent of Ramachandran favored angles (94 – 96%), few Ramachandran outliers, and low clash score (Table 1).

The predicted structures contain a probably disordered N-terminal stretch of amino acids followed by a *β*-strand, which is a part of the parallel 7-stranded sheet sandwiched between alpha helices - the so called Rossmann fold (Figures 6B, C). The C-terminal extension region consists of alpha helices which are located between *β*6 and *β*7 and after *β*7. A short, most likely disordered (low pLDDT), loop is present between *β*5 and *β*6. This loop separates the two active site residues Lys and Tyr (Lys147 and Tyr 179 in *Nn*PRISE) which are located in the helical regions around it. Interestingly the Lys residue is replaced by Phe (Phe153) in *Nr*ISY. In the literature there is conflicting evidence about the role of the mentioned Lys residue; while it is conserved in ISY/P5βR, in *C. roseus* ISY the K146A, K146S, K146M and K146R mutants only suffered a slight loss of catalytic activities (Kries et al., 2015; Qin et al., 2016), while in the *Plantago major* P5βR multisubstrate oxido-reductase K147A and K147M mutations completely abrogated enzymatic activity (Fellows et al., 2018). Considering that *Nr*ISY is active, replacement of the mentioned Lys residue to Phe seems not to disturb the catalytic activity of this enzyme.

The NADP cofactor binding site in ISY/P5βR enzymes (Figure 5A; Supplementary Figure 3) is mostly made up from residues after the *β* strands of the Rossmann fold (Supplementary

10.3389/fpls.2023.1211453

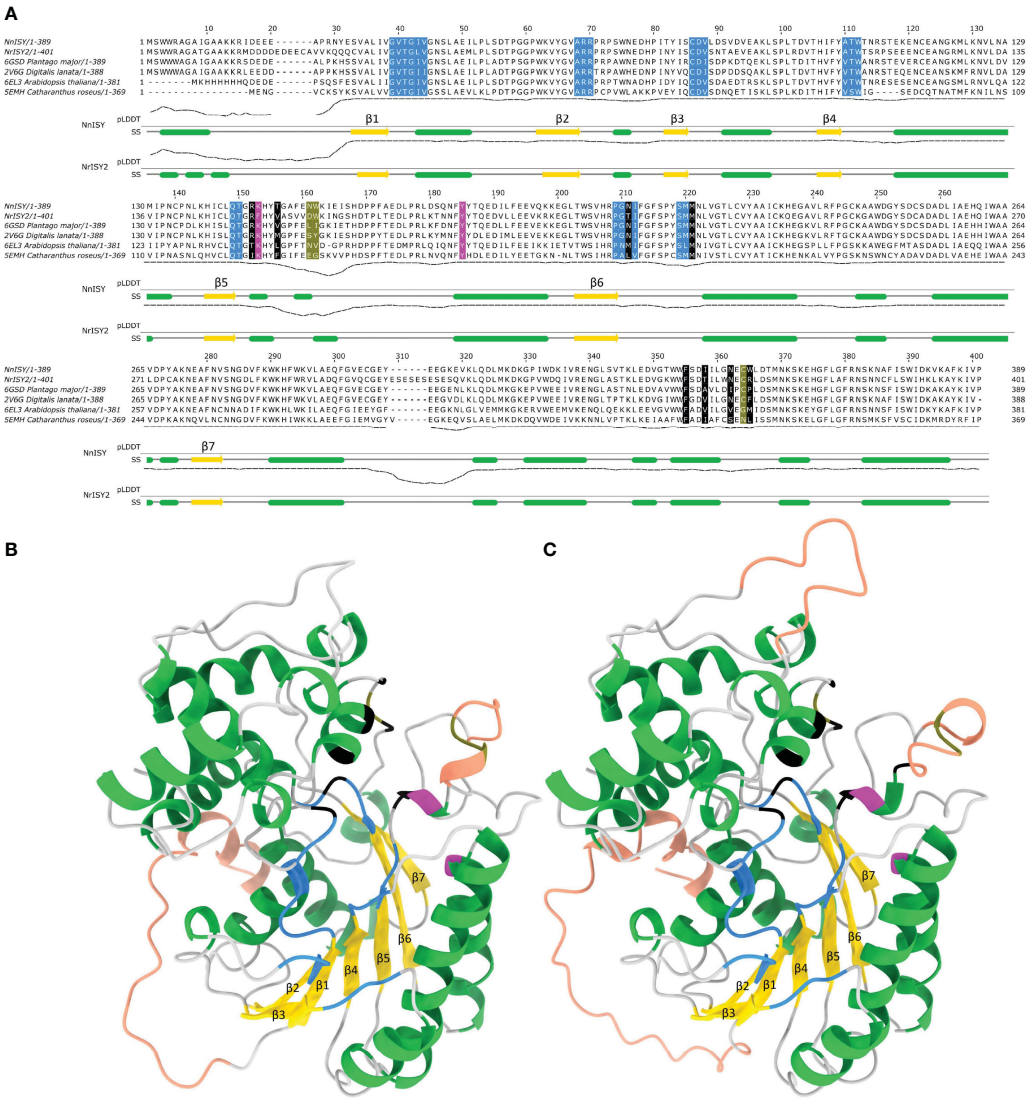

FIGURE 6
Sequence structure relationships in *Nn*PRISE and *Nr*ISY. **(A)** Multiple sequence alignment of *Nn*PRISE, *Nr*ISY and several ISY/P5βR enzymes with resolved 3D structures. Residues involved with NADP binding are colored blue (cdd: cd08948 annotation), catalytic residues are colored magenta (cdd: cd08948 annotation), residues forming the substrate binding cavity are colored black (Qin et al., 2016), while olive-colored residues are crucial loop residues determining substrate specificity (Sandholu et al., 2018). Under the alignment are the pLDDT score (predicted lDDT-Cα) - a per-residue estimate of AlphaFold confidence on a scale from 0 – 100 and the secondary structure (SS) diagram based on the respective AlphaFold models: α-helices are in green, β-strands are in yellow. **(B)** *Nn*PRISE AlphaFold predicted structure, α-helices are colored green, β-strands yellow, coils grey, regions with pLDDT < 80 are shown in tangerine (potential disorder). Specific residues involved in cofactor and substrate binding, important loop residues and catalytic residues are colored as in **(A, C)** NrISY AlphaFold predicted structure: coloring is as in **(A, B)**.

Figure 3). Due to the conservation of residues involved in interaction with NADP the hydrogen bonding network is similar between the *Nn*PRISE (Supplementary Figure 3A) and *Nr*ISY (Supplementary Figure 3B) predicted structures and the experimental *C. roseus* ISY (Supplementary Figure 3C) and *D. lanata* P5βR structures (Supplementary Figure 3D). In order to examine 8-oxogeranial binding to *Nn*PRISE and *Nr*ISY active sites docking was performed with 8-oxogeranial and different configurations of nepetalactol. 8-Oxogeranial is an α,β unsaturated aldehyde from both sides of the molecule

TABLE 1 Evaluation of AlphaFold predicted models of NnPRISE and NrISY.

Structure	MolProbity Score	Clash Score	Ramachandran Favored	Ramachandran Outliers	Rotamer Outliers	RMSD (2V6G)	TM (2V6G)	SI % (2V6G)
***Nn*PRISE**	1.2	1.8	96.12%	0.26%	0.00%	0.86	0.92	82%
***Nr*ISY**	1.32	1.76	94.24%	1.50%	0.00%	1.03	0.89	75%

(Supplementary Figure 3A). Due to conjugative stabilization the rotation around the α,β bond in α,β -unsaturated carbonyl compounds is constrained to s-cis and s-trans forms (Abraham et al., 2006; Supplementary Figure 3A) which exist in an equilibrium dictated by the bulkiness of the groups on the carbonyl, Cα and Cβ atoms. Interestingly 8-oxogeranial is currently present in three enzyme structures deposited to the PDB, two from *C. roseus ISY* - 5COB (Qin et al., 2016) and 5DBI (Hu et al., 2015), as well as one from *P. major* - 5MLH (Fellows et al., 2018). In two of these structures, 5COB and 5MLH, the C1-C2 α,β bond is neither in the s-trans, nor the s-cis form but is rather in between these two forms (Supplementary Figure 3B). It is unclear if this is due to poor goodness of fit of the ligand to experimental data (8 percentile for 5COB, 13% 5MLH and 75% 5DBI) or some other factor. On the other hand, the substrate in the 5DBI structure is in the 1,2 s-trans, 7,8 s-cis conformation, and Hu and associates (2015) provide a mechanistical explanation how this 8-oxogeranialtransoid (1,2 s-trans) is converted to a shunt-reaction product S-10-oxocitronellal (8-oxocitronellal) while the cisoid (1,2 s-cis), as yet experimentally unobserved, is converted to nepetalactol. Some 8-oxogeranial α,β conformations are more stable than others as revealed by examining their energy using several forcefields (Supplemetary Table 4).

In view of all this, docking was performed with the four 8-oxogeranial conformational variants (Supplementary Table 4) so that the rotation of α,β bonds was not permitted. When performing docking to the rigid *Nn*PRISE model active site the highest affinity docked position was of 1,2 s-trans, 7,8 s-cis 8-oxogeranial (same conformer as observed in 5DBI) which assumed an extended conformation where the C1 carbonyl oxygen is at hydrogen bond distance from Tyr179 and the backbone N of Lys147, while the C8 carbonyl oxygen is proximate to the backbone N of Asn205 (Figure 7A). The docked ligand is in a similar position as in 5DBI regarding the hydrogen bonding of C1 carbonyl oxygen as well as the positioning of the C2=C3 double bond on top of the NADP cofactor.

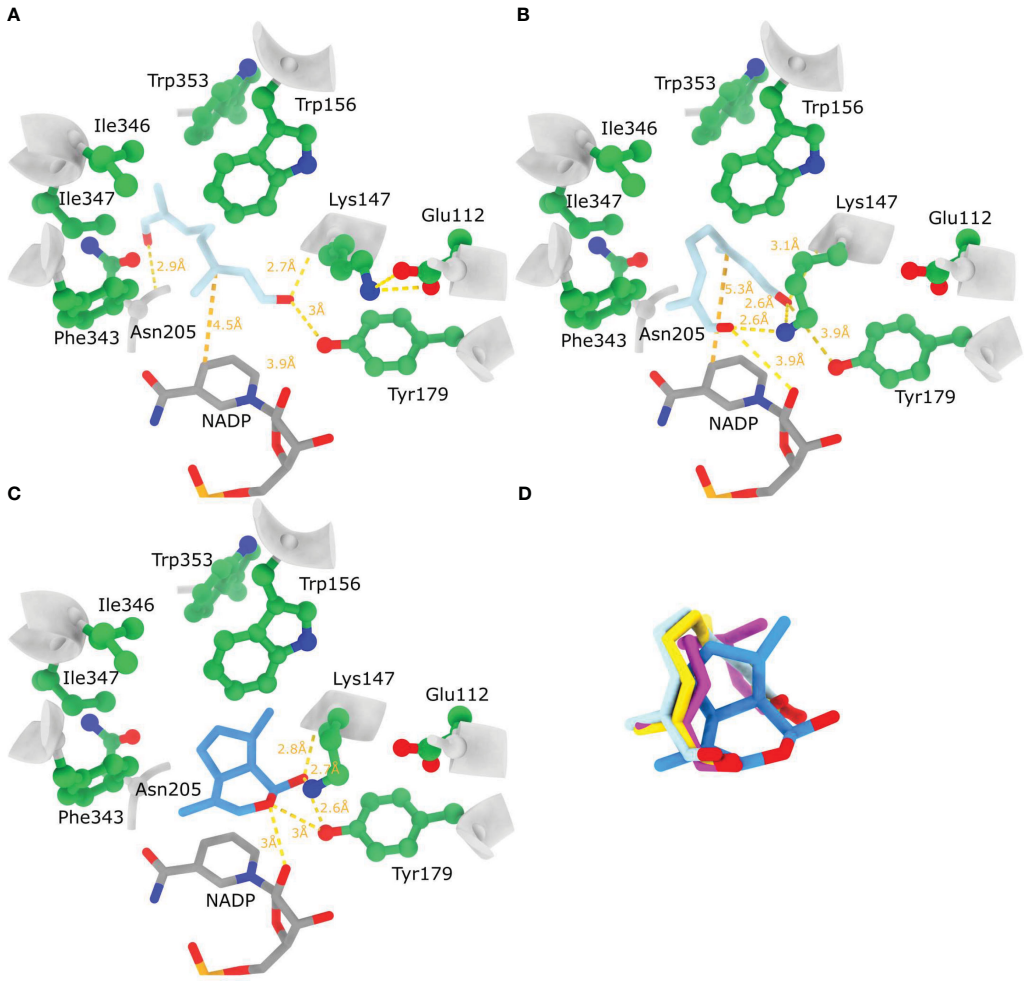

FIGURE 7
Substrate and product binding to the AlphaFold model of *Nn*PRISE. **(A)** Highest affinity docked position of 1,2 s-*trans*, 7,8 s-*cis* 8-oxogeranial to the rigid *Nn*PRISE active site. **(B)** Highest affinity docked position of 1,2 s-*trans*, 7,8 s-*cis* 8-oxogeranial to the *Nn*PRISE active site where the side chains of Lys147 and Tyr179 were allowed to be flexible. **(C)** Highest affinity docked position of 1S- *cis,trans* nepetalactol (PubChem: 11286692) to NnISY active site where the side chains of Lys147 and Tyr179 were allowed to be flexible. **(D)** Superposition of bound substrate, hydride addition products [*trans*- 8-oxocitronellyl enolate (yellow) and *cis*- 8-oxocitronellyl enolate (magenta)] and cyclisation product. Hydrogen bonding between the docked ligands and protein residues is shown with dashed yellow lines (relaxed hydrogen bonding criteria - distance tolerance 1 Å and angle tolerance 20°).

In this structure the ϵ-NH_3 group of Lys147 appears not to have a role in ligand binding because it is facing away from the ligand, and is H-bonded to Glu112 (Figure 7A). Contrary to this when flexible docking was employed (Lys147 and Tyr179 side chains) 1,2 s-trans, 7,8 s-cis 8-oxogeranial assumed a contorted conformation with both carbonyl groups in the direction of the active site residues Lys147 and Tyr179, just above the nicotinamide ring of NADP (Figure 7B). The ϵ-NH_3 group of Lys147 has moved away from Glu112 to contribute to H-bonding with both substrate carbonyl groups (~2.6 Å, Figure 7A). The carbonyl oxygen on C8 is positioned less than 4 Å away from Tyr179 Oζ, while the carbonyl oxygen on C1 is less than 4 Å away from the 2' ribose OH group. This docked position suggests 8-oxogeranial binding to the active site in a conformation that could promote cyclisation. In addition to this the products of the hydride addition reaction trans- and cis- 8-oxocitronellyl enolates assume a very similar highest scoring docked position (Figure 7D) to the before mentioned 1,2 s-trans, 7,8 s-cis 8-oxogeranial. When nepetalactol (1S cis,trans) was docked, Lys147 has pooled towards Tyr179 reducing the distances of nepetalactol oxygens to Tyr179 Oζ, Lys147 ε-NH3 and 2' ribose OH group (Figure 7C). Taken together these *in silico* results suggest that if the Lys147 ε-NH_3 group remains H-bonded to Glu112 during 8-oxogeranial binding then the enzyme most likely catalyzes just the reduction reaction and not the subsequent cyclisation. Lichman et al. (2019a) proposed that ISY in *Nepeta* performs just the reduction of 8-oxogeranial to 8-oxocitronellyl enol/enolate which is converted to nepetalactol either by spontaneous cyclization in solution, or by cyclisation catalyzed by Nepetalactol-related short-chain reductases (NEPS) which subsequently catalyze the reduction of nepetalactol to nepetalactone. In addition, different NEPS isoforms promote formation of different nepetalactone stereochemical configurations (Lichman et al., 2019a).

When docking different conformations of 8-oxogeranial to the rigid active site of the *Nr*ISY model the resulting docked positions were not compatible with the catalysis of the hydride attack because the substrate conformations were bound away from NADP and Tyr185 (not shown). Presumably because the side chain of Phe153 is oriented in such a way that prohibits the 8OG C2=C3 double bound to orient on top of NADP cofactor (Figure 8A). Indeed, with the flexible docking procedure the Phe153 aromatic ring rotated ~90 degrees allowing 8-oxogeranial to bind so that the C1 carbonyl oxygen is at hydrogen bond distance from Tyr185 and the backbone N of Phe153, while the double bond prone to reduction is sandwiched between Phe153 and the nicotinamide ring (Figure 8B). Based on the docked poses it seems *Nr*ISY does not bind 8-oxogeranial in a conformation suitable for cyclization in the enzyme active site. The main difference between *Nn*PRISE and *Nr*ISY is that the active site Lys147 is replaced by Phe (Phe153 in NrISY), and that the *Nn*PRISE substrate binding site is more spatially confined with bulky hydrophobic amino acids such as Trp353 and Trp156. In *Nr*ISY $Trp353_{NnPRISE}$ is replaced by Arg365, while Trp162 which is by position in the sequence equivalent to $Trp156_{NnPRISE}$ is positioned away from the substrate binding cleft. Superposition of NrISY docked 1,2 s-trans, 7,8 s-trans 8-oxogeranial (light blue) and 1,2 s-trans, 7,8 s-cis 8-oxogeranial (purple) is presented in Figure 8C.

Conclusions

Although several ISYs were previously characterized from *Nepeta* species, this is, to the best of our knowledge, the first record of functional ISY (*Nr*ISY) in *trans,cis-nepetalactone* and

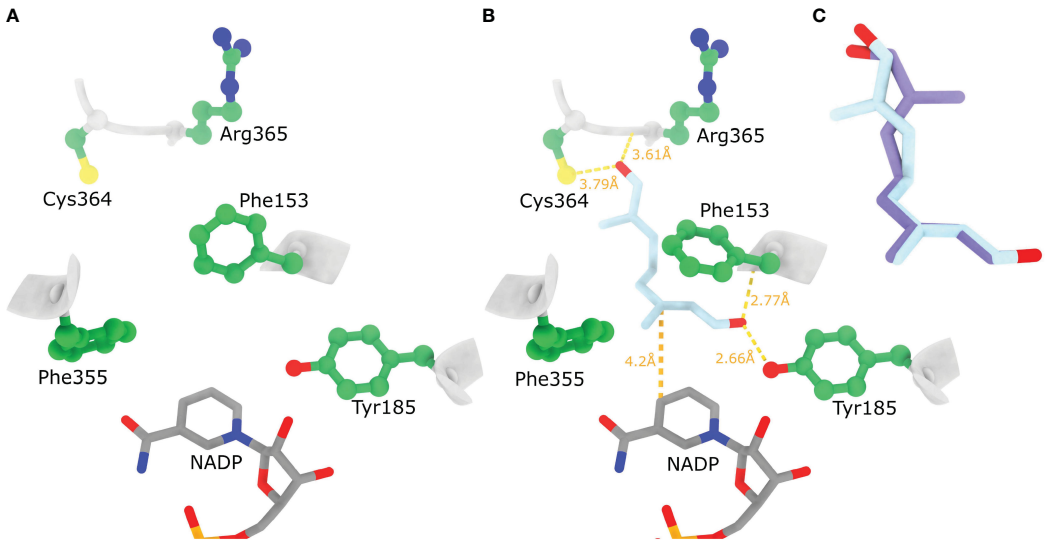

FIGURE 8
Ligand binding to the AlphaFold model of *Nr*ISY. **(A)** AlphaFold model of *Nr*ISY active site. **(B)** Highest affinity docked position of 1,2 s-*trans*, 7,8 s-*trans* 8-oxogeranial to *Nr*ISY active site where the side chains of Phe153 and Tyr185were allowed to be flexible. **(C)** Superposition of *Nr*ISY docked 1,2 s-*trans*, 7,8 s-*trans* 8-oxogeranial (light blue) and 1,2 s-*trans*, 7,8 s-*cis* 8-oxogeranial (purple). Hydrogen bonding between the docked ligands and protein residues is shown with dashed yellow lines (relaxed hydrogen bonding criteria - distance tolerance 1 Å and angle tolerance 20°).

5,9-dehydronepetalactone predominating *N. rtanjensis*. Displaying high catalytic activity under *in vitro* conditions, *Nr*ISY is an enzyme showing organ-specific expression profiles in plants, with leaves being enriched with the enzyme transcripts. On the other hand, PRISE isolated from leaves of *N. nervosa* (*Nn*PRISE) shares high level of similarity with the *Nr*ISY, but is characterized by more spatially confined substrate binding site, which is, most likely, responsible for less efficient conversion of 8-oxogearnial to *cis, trans*-nepetalactol. Future kinetics experiments will be aimed to confirm these statements. Described *Nn*PRISE from *N. nervosa* is actually phylogenetically closer to the representatives of the Family 1 isoforms, designated as P5βRs and displaying very low catalytic activity. However, based on the functional genomics and bioinformatics (3D modeling and molecular docking analyses) data, it could be presumed that this enzyme displays ISY-like function under *in vitro* conditions. Although *Nn*PRISE is expressed in high levels in stems and leaves of *N. nervosa*, more studies are needed to confirm its activity *in vivo*.

MeJA- induced accumulation of iridoids in *N. rtanjensis* leaves was followed by the elevated co-expression of the majority of the iridoid biosynthesis-related genes and transcription factors, which indicated transcriptional regulation of their activity. The same treatment with MeJA slightly increased the expression levels of the candidate biosynthetic genes in *N. nervosa* leaves; however, this induced no appearance of iridoid glycosides and iridoid aglycones (nepetalactone, its precursors, or derivatives). Although *Nepeta nervosa* is lacking detectable amounts of iridoids in leaves, even under MeJA-elicitation conditions, this species most likely possesses iridoid biosynthetic platform, which is silenced. Based on the obtained metabolomics and transcriptomics data, we could presume that there are a few missing points in the iridoid biosynthetic platform of *N. nervosa*, which disables the biosynthesis of iridoids: 1) the absence of GES – like activity, due to the gene silencing, which results in the absence of both iridoid aglycones and iridoid glycosides; 2) the activity of some other NEPSs and MLPLs besides *Nn*NEPS1 and *Nn*MLPL are essential for iridoid aglycones biosynthesis. In the quest for answers, our ongoing work is conducted towards testing these robust hypotheses and re-establishing the biosynthesis of iridoids in this remarkable plant. Interestingly, the majority of putative iridoid biosynthesis-related gens are expressed in leaves of *N. nervosa*, even if there are no substrates to act upon, which is an interesting paradox. The question arises as to how energetically profitable it is for plants to express enzymes that are unable to fulfill their function within specific biosynthetic routes of specialized metabolites. Most likely this is not an isolated example within the plant kingdom, but it certainly deserves our attention.

Data availability statement

The datasets presented in this study can be found in online repositories. The names of the repository/repositories and accession number(s) can be found in the article/Supplementary Material.

Author contributions

DMi, DM, and NA conceived and designed the experiments. NA, DM, UG, JN, SD, JB, MM, MD, BA, LP, and DMi performed the experiments. NA, DM, UG, and DMi organized and wrote the manuscript with editing from all the authors. All authors contributed to the article and approved the submitted version.

Funding

The author(s) declare financial support was received for the research, authorship, and/or publication of this article. The research was financed by the Science Fund of the Republic of Serbia, Grant No. 7749433, project acronym NEPETOME, and is also supported by the Ministry of Science, Technological Development and Innovation of the Republic of Serbia, Grants No. 451-03-47/2023-01/200007, 451-03-47/2023-01/200168, and 451-03-47-/2023-01/200053.

Acknowledgments

The authors would like to acknowledge Dr. Milan Dragićević, for his valuable help with 3D modeling and molecular docking analyses.

Conflict of interest

The authors declare that the research was conducted in the absence of any commercial or financial relationships that could be construed as a potential conflict of interest.

Publisher's note

Supplementary material

The Supplementary Material for this article can be found online at: https://www.frontiersin.org/articles/10.3389/fpls.2023.1211453/full#supplementary-material

References

Abraham, R. J., Mobli, M., Ratti, J., Sancassan, F., and Smith, T. A. D. (2006). Conformational analysis, Part 41. A modelling and LIS/NMR investigation of the conformations of α,β-unsaturated carbonyl compounds. *J. Phys. Org. Chem.* 19, 384–392. doi: 10.1002/poc.1092

Abraham, M. J., Murtola, T., Schulz, R., Páll, S., Smith, J. C., Hess, B., et al. (2015). Gromacs: High performance molecular simulations through multi-level parallelism from laptops to supercomputers. *SoftwareX* 1–2, 19–25. doi: 10.1016/j.softx.2015.06.001

Ahmed, A. A., Hassan, H. E., Hegazy, M. F., Tzakou, O., Couladis, M., Mohamed, A. E.-H. H., et al. (2006). Argolic acid A and argolic methyl ester B, two new cyclopentanomonoterpenes diol from Nepeta argolica. *Nat. Prod. Commun.* 1, 523–526. doi: 10.1177/1934578X0600100701

Alagna, F., Geu-flores, F., Kries, H., Panara, F., Baldoni, L., Connor, S. E. O., et al. (2016). Identification and characterization of the iridoid synthase involved in oleuropein biosynthesis in olive (Olea europaea) fruits. *Am. Soc Biochem. Mol. Biol.* 291, 5542–5554. doi: 10.1074/jbc.M115.701276

Aničić, N., Gašić, U., Lu, F., Ćirić, A., Ivanov, M., Jevtić, B., et al. (2021). Antimicrobial and immunomodulating activities of two endemic nepeta species and their major iridoids isolated from natural sources. *Pharmaceuticals* 14, 414. doi: 10.3390/ph14050414

Aničić, N., Matekalo, D., Skorić, M., Pećinar, I., Brkušanin, M., Živković, J. N., et al. (2018). Trichome-specific and developmentally regulated biosynthesis of nepetalactones in leaves of cultivated Nepeta rtanjensis plants. *Ind. Crops Prod.* 117, 347–358. doi: 10.1016/j.indcrop.2018.03.019

Aničić, N., Matekalo, D., Skorić, M., Živković, J. N., Petrović, L., Dragićević, M., et al. (2020). Alterations in nepetalactone metabolism during polyethylene glycol (PEG)-induced dehydration stress in two Nepeta species. *Phytochemistry* 174, 112340. doi: 10.1016/j.phytochem.2020.112340

Boachon, B., Buell, C. R., Crisovan, E., Dudareva, N., Garcia, N., Godden, G., et al. (2018). Phylogenomic mining of the mints reveals multiple mechanisms contributing to the evolution of chemical diversity in lamiaceae. *Mol. Plant* 11, 1084–1096. doi: 10.1016/j.molp.2018.06.002

Cao, X., Guo, X., Yang, X., Wang, H., Hua, W., He, Y., et al. (2016). Transcriptional responses and gentiopicroside biosynthesis in methyl jasmonate-treated Gentiana macrophylla seedlings. *PloS One* 11, 1–20. doi: 10.1371/journal.pone.0166493

Dienaitė, L., Pukalskienė, M., Matias, A. A., Pereira, C. V., Pukalskas, A., and Venskutonis, P. R. (2018). Valorization of six Nepeta species by assessing the antioxidant potential, phytochemical composition and bioactivity of their extracts in cell cultures. *J. Funct. Foods* 45, 512–522. doi: 10.1016/j.jff.2018.04.004

Eberhardt, J., Santos-martins, D., Tillack, A. F., and Forli, S. (2021). expanded force field, and Python bindings. *J. Chem. Inf. Model.* 61 (8), 1–7. doi: 10.1021/acs.jcim.1c00203

Fellows, R., Russo, C. M., Silva, C. S., Lee, S. G., Jez, J. M., Chisholm, J. D., et al. (2018). A multisubstrate reductase from Plantago major: structure-function in the short chain reductase superfamily. *Sci. Rep.* 8, 1–13. doi: 10.1038/s41598-018-32967-1

Gašić, U., Banjanac, T., Šiler, B., Božunović, J., Milutinović, M., Aničić, N., et al. (2023). Variation in the chemical profiles of three foxglove species in the central Balkans. *Front. Plant Sci.* 14. doi: 10.3389/fpls.2023.1155297

Gasic, K., Hernandez, A., and Korban, S. S. (2004). RNA extraction from different apple tissues rich in polyphenols and polysaccharides for cDNA library construction. *Plant Mol. Biol. Rep.* 22, 437–438. doi: 10.1007/BF02772687

Geu-Flores, F., Sherden, N. H., Courdavault, V., Burlat, V., Glenn, W. S., Wu, C., et al. (2012). An alternative route to cyclic terpenes by reductive cyclization in iridoid biosynthesis. *Nature* 492, 138–142. doi: 10.1038/nature11692

Halgren, T. A. (1996). Merck molecular force field. I. Basis, form, scope, parameterization, and performance of MMFF94. *J. Comput. Chem.* 17, 490–519. doi: 10.1002/(SICI)1096-987X(199604)17:5/6<490::AID-JCC1>3.0.CO;2-P

Halgren, T. A. (1999). MMFF VI. MMFF94s option for energy minimization studies. *J. Comput. Chem.* 20, 720–729. doi: 10.1002/(SICI)1096-987X(199905)20:7<720::AID-JCC7>3.0.CO;2-X

Hammer, Ø., Harper, D. A., and Ryan, P. D. (2001). PAST: Paleontological statistics software package for education and data analysis. *Palaeontologia electronica* 4 (1), 9.

Hanwell, M. D., Curtis, D. E., Lonie, D. C., Vandermeersch, T., Zurek, E., and Hutchison, G. R. (2012). Avogadro: an advanced semantic chemical editor, visualization, and analysis platform. *J. Cheminform.* 4, 17. doi: 10.1186/1758-2946-4-17

Hernández Lozada, N. J., Hong, B., Wood, J. C., Caputi, L., Basquin, J., Chuang, L., et al. (2022). Biocatalytic routes to stereo-divergent iridoids. *Nat. Commun.* 13, 1–13. doi: 10.1038/s41467-022-32414-w

Hu, Y., Liu, W., Malwal, S. R., Zheng, Y., Feng, X., Ko, T. P., et al. (2015). Structures of iridoid synthase from cantharanthus roseus with bound NAD+, NADPH, or NAD +/10-oxogeranial: reaction mechanisms. *Angew. Chemie - Int. Ed.* 54, 15478–15482. doi: 10.1002/anie.201508310

Huang, J., and Mackerell, A. D. (2013). CHARMM36 all-atom additive protein force field: Validation based on comparison to NMR data. *J. Comput. Chem.* 34, 2135–2145. doi: 10.1002/jcc.23354

Jones, D. T., Taylor, W. R., and Thornton, J. M. (1992). The rapid generation of mutation data matrices from protein sequences. *Bioinformatics* 8, 275–282. doi: 10.1093/bioinformatics/8.3.275

Jumper, J., Evans, R., Pritzel, A., Green, T., Figurnov, M., Ronneberger, O., et al. (2021). Highly accurate protein structure prediction with AlphaFold. *Nature* 596, 583–589. doi: 10.1038/s41586-021-03819-2

Kökdil, G., Kurucu, S., and Yildiz, A. (1998). Essential oil composition of Nepeta nuda L. ssp. nuda. *Flavour Fragr. J.* 13, 233–234. doi: 10.1002/(SICI)1099-1026(1998070)13:4<233::AID-FFJ730>3.0.CO;2-7

Kostić, A.Ž., Milinčić, D. D., Špirović Trifunović, B., Nedić, N., Gašić, U. M., Tešić, Ž.Lj., et al. (2023). Monofloral corn poppy bee-collected pollen - A detailed insight into its phytochemical composition and antioxidant properties. *Antioxidants* 12, 1424. doi: 10.3390/antiox12071424

Kries, H., Caputi, L., Stevenson, C. E. M., Kamileen, M. O., Sherden, N. H., Geu-Flores, F., et al. (2015). Structural determinants of reductive terpene cyclization in iridoid biosynthesis. *Nat. Chem. Biol.* 12, 6–8. doi: 10.1038/nchembio.1955

Kries, H., Kellner, F., Kamileen, M. O., and O'Connor, S. E. (2017). Inverted stereocontrol of iridoid synthase in snapdragon. *J. Biol. Chem.* 292, 14659–14667. doi: 10.1074/jbc.M117.800979

Krithika, R., Srivastava, P. L., Rani, B., Kolet, S. P., Chopade, M., Soniya, M., et al. (2015). Characterization of 10-hydroxygeraniol dehydrogenase from Catharanthus roseus reveals cascaded enzymatic activity in iridoid biosynthesis. *Sci. Rep.* 5 (1), 1–6. doi: 10.1038/srep08258

Kumar, K., Kumar, S. R., Dwivedi, V., Rai, A., Shukla, A. K., Shanker, K., et al. (2015). Precursor feeding studies and molecular characterization of geraniol synthase establish the limiting role of geraniol in monoterpene indole alkaloid biosynthesis in Catharanthus roseus leaves. *Plant Sci.* 239, 56–66. doi: 10.1016/j.plantsci.2015.07.007

Kumar, S., Stecher, G., Li, M., Knyaz, C., and Tamura, K. (2018). MEGA X: Molecular evolutionary genetics analysis across computing platforms. *Mol. Biol. Evol.* 35, 1547–1549. doi: 10.1093/molbev/msy096

Landrum, G., Tosco, P., Kelley, B., Vianello, P., Kawashima, E., and Dalke, A. (2022). *Zenodo*, rdkit/rdkit:2022_03_2(Q1 2022).

Li, Z., Jaroszewski, L., Iyer, M., Sedova, M., and Godzik, A. (2020). FATCAT 2.0: Towards a better understanding of the structural diversity of proteins. *Nucleic Acids Res.* 48, W60–W64. doi: 10.1093/NAR/GKAA443

Liblikas, I., Santangelo, E. M., Sandell, J., Baeckstro, P., Svensson, M., Jacobsson, U., et al. (2005). Simplified isolation procedure and interconversion of the diastereomers of nepetalactone and nepetalactol. *J. Nat. Prod.* 68 (6), 886–890. doi: 10.1021/np049647d

Lichman, B. R., Godden, G. T., Hamilton, J. P., Palmer, L., Kamileen, M. O., Zhao, D., et al. (2020). The evolutionary origins of the cat attractant nepetalactone in catnip. *Sci. Adv.* 6. doi: 10.1126/sciadv.aba0721

Lichman, B. R., Kamileen, M. O., Titchiner, G. R., Saalbach, G., Stevenson, C. E. M., Lawson, D. M., et al. (2019a). Uncoupled activation and cyclization in catmint reductive terpenoid biosynthesis. *Nat. Chem. Biol.* 15, 71–79. doi: 10.1038/s41589-018-0185-2

Lichman, B. R., O'Connor, S. E., and Kries, H. (2019b). Biocatalytic strategies towards [4+2] cycloadditions. *Chem. - A Eur. J.* 25, 6864–6877. doi: 10.1002/chem.201805412

Livak, K. J., and Schmittgen, T. D. (2001). Analysis of relative gene expression data using real-time quantitative PCR and the 2-ΔΔCT method. *Methods* 25, 402–408. doi: 10.1006/meth.2001.1262

Matekalo, D., Skorić, M., Nikolić, T., Novaković, L., Lukić, M., Božunović, J., et al. (2018). Organ-specific and genotype-dependent constitutive biosynthesis of secoiridoid glucosides in Centaurium erythraea Rafn, and its elicitation with methyl jasmonate. *Phytochemistry* 155, 69–82. doi: 10.1016/j.phytochem.2018.07.015

Miettinen, K., Dong, L., Navrot, N., Schneider, T., Burlat, V., Ilc, T., et al. (2014). The seco-iridoid pathway from Catharanthus roseus. *Nat. Commun.* 5 (1), 3606. doi: 10.1038/ncomms4606

Mišić, D., Šiler, B., Gašić, U., Avramov, S., Živković, S., Živković, J. N., et al. (2015). Simultaneous UHPLC/DAD/(+/−)HESI-MS/MS analysis of phenolic acids and nepetalactones in methanol extracts of Nepeta species: A possible application in chemotaxonomic studies. *Phytochem. Anal.* 26, 72–85. doi: 10.1002/pca.2538

Murai, F., Tagawa, M., Damtoft, S., Jensen, S. R., and Nielsen, B. J. (1984). doi: 10.1248/cpb.32.2809

Murashige, T., and Skoog, F. (1962). A revised medium for rapid growth and bio assays with tobacco tissue cultures. *Physiol. Plant* 15, 473–497. doi: 10.1111/j.1399-3054.1962.tb08052.x

Nestorović, J., Mišić, D., Šiler, B., Soković, M., Glamočlija, J., Ćirić, A., et al. (2010). Nepetalactone content in shoot cultures of three endemic Nepeta species and the evaluation of their antimicrobial activity. *Fitoterapia* 81, 621–626. doi: 10.1016/j.fitote.2010.03.007

Palmer, L., Chuang, L., Siegmund, M., Kunert, M., Yamamoto, K., Sonawane, P., et al. (2022). *In vivo* characterization of key iridoid biosynthesis pathway genes in catnip (Nepeta cataria). *Planta* 256, 1–11. doi: 10.1007/s00425-022-04012-z

Petersen, J., Lanig, H., Munkert, J., Bauer, P., Müller-uri, F., Petersen, J., et al. (2016). Progesterone 5β-reductases / iridoid synthases (PRISE): gatekeeper role of highly conserved phenylalanines in substrate preference and trapping is supported by molecular dynamics simulations. *J. Biomol. Struct. Dyn.* 34, 1667–1680. doi: 10.1080/07391102.2015.1088797

Petrova, D., Gašić, U., Yocheva, L., Hinkov, A., Yordanova, Z., Chaneva, G., et al. (2022). Catmint (Nepeta nuda L.) phylogenetics and metabolic responses in variable growth conditions. *Front. Plant Sci.* 13. doi: 10.3389/fpls.2022.866777

Pettersen, E. F., Goddard, T. D., Huang, C. C., Meng, E. C., Couch, G. S., Croll, T. I., et al. (2021). UCSF ChimeraX: Structure visualization for researchers, educators, and developers. *Protein Sci.* 30, 70–82. doi: 10.1002/pro.3943

Piątczak, E., Kuźma, Ł., and Wysokińska, H. (2016). The influence of methyl jasmonate and salicylic acid on secondary metabolite production in Rehmannia glutinosa Libosch. Hairy root culture. *Acta Biol. Cracoviensia Ser. Bot.* 58, 57–65. doi: 10.1515/abcsb-2016-0004

Pu, X., Gao, H. C., Wang, M. J., Zhang, J. H., Shan, J. H., Chen, M. H., et al. (2022). Integrative analysis of elicitor-induced camptothecin biosynthesis in camptotheca acuminata plantlets through a combined omics approach. *Front. Plant Sci.* 13. doi: 10.3389/fpls.2022.851077

Qiao, X., Zhang, Y. T., Ye, M., Wang, B. R., Han, J., and Guo, D. A. (2009). Analysis of chemical constituents and taxonomic similarity of Salvia species in China using LC/MS. *Planta Med.* 75, 1613–1617. doi: 10.1055/s-0029-1185866

Qin, L., Zhu, Y., Ding, Z., Zhang, X., Ye, S., and Zhang, R. (2016). Structure of iridoid synthase in complex with NADP+/8-oxogeranial reveals the structural basis of its substrate specificity. *J. Struct. Biol.* 194, 224–230. doi: 10.1016/j.jsb.2016.02.010

Rappe, A. K., Casewit, C. J., Colwell, K. S., Goddard, W. A., and Skiff, W. M. (1992). UFF, a full periodic table force field for molecular mechanics and molecular dynamics simulations. *J. Am. Chem. Soc* 114, 10024–10035. doi: 10.1021/ja00051a040

Rubio-Rodríguez, E., Vera-Reyes, I., Sepúlveda-García, E. B., Ramos-Valdivia, A. C., and Trejo-Tapia, G. (2021). Secondary metabolite production and related biosynthetic genes expression in response to methyl jasmonate in Castilleja tenuiflora Benth. *in vitro* plants. *Plant Cell. Tissue Organ Cult.* 144, 519–532. doi: 10.1007/s11240-020-01975-3

Sherden, N. H., Lichman, B. R., Caputi, L., Zhao, D., Kamileen, M. O., Buell, C. R., et al. (2017). Identification of iridoid synthases from Nepeta species: Iridoid cyclization does not determine nepetalactone stereochemistry. *Manuscr. Submitt.* 145, 1–34. doi: 10.1101/179572

Skorić, M., Gligorijević, N., Čavić, M., Ristić, M., Mišić, D., and Radulović, S. (2017). Cytotoxic activity of Nepeta rtanjensis Diklić and Milojević essential oil and and its mode of action. *Ind. Crops Prod.* 100, 163–170. doi: 10.1016/j.indcrop.2017.02.027

Takeda, Y., Ooiso, Y., Masuda, T., Honda, G., Otsuka, H., Sezik, E., et al. (1998). Iridoid and eugenol glycosides from Nepeta cadmea. *Phytochemistry* 49, 787–791. doi: 10.1016/S0031-9422(98)00125-3

Thorn, A., Egerer-Sieber, C., Jäger, C. M., Herl, V., Müller-Uri, F., Kreis, W., et al. (2008). The crystal structure of progesterone 5β-reductase from Digitalis lanata defines a novel class of short chain dehydrogenases/reductases. *J. Biol. Chem.* 283, 17260–17269. doi: 10.1074/jbc.M706185200

Vanommeslaeghe, K., Hatcher, E., Acharya, C., Kundu, S., Zhong, S., Shim, J., et al. (2009). CHARMM general force field: A force field for drug-like molecules compatible with the CHARMM all-atom additive biological force fields. *J. Comput. Chem.* 20, NA–NA. doi: 10.1002/jcc.21367

Wang, J., Liu, Y., Cai, Y., Zhang, F., Xia, G., and Xiang, F. (2010). Cloning and functional analysis of geraniol 10-hydroxylase, a cytochrome p450 from swertia mussotii Franch. *Biosci. Biotechnol. Biochem.* 74, 1583–1590. doi: 10.1271/bbb.100175

Wang, S., Witek, J., Landrum, G. A., and Riniker, S. (2020). Improving conformer generation for small rings and macrocycles based on distance geometry and experimental torsional-angle preferences. *J. Chem. Inf. Model.* 60, 2044–2058. doi: 10.1021/acs.jcim.0c00025

Wang, J., Wolf, R. M., Caldwell, J. W., Kollman, P. A., and Case, D. A. (2004). Development and testing of a general amber force field. *J. Comput. Chem.* 25, 1157–1174. doi: 10.1002/jcc.20035

Waterhouse, A., Bertoni, M., Bienert, S., Studer, G., Tauriello, G., Gumienny, R., et al. (2018). SWISS-MODEL: Homology modelling of protein structures and complexes. *Nucleic Acids Res.* 46, W296–W303. doi: 10.1093/nar/gky427

Williams, C. J., Headd, J. J., Moriarty, N. W., Prisant, M. G., Videau, L. L., Deis, L. N., et al. (2018). MolProbity: More and better reference data for improved all-atom structure validation. *Protein Sci.* 27, 293–315. doi: 10.1002/pro.3330

Xiang, B., Li, X., Wang, Y., Tian, X., Yang, Z., Ma, L., et al. (2017). Cloning and characterization of two iridoid synthase homologs from swertia mussotii. *Molecules* 22, 1–14. doi: 10.3390/molecules22081387

Zengin, G., Cvetanović, A., Gašić, U., Dragićević, M., Stupar, A., Uysal, A., et al. (2020). UHPLC-LTQ OrbiTrap MS analysis and biological properties of Origanum vulgare subsp. viridulum obtained by different extraction methods. *Ind. Crops Prod.* 154. doi: 10.1016/j.indcrop.2020.112747

frontiers | Frontiers in Plant Science

TYPE Systematic Review
PUBLISHED 21 March 2024
DOI 10.3389/fpls.2024.1268101

OPEN ACCESS

EDITED BY
Chunpeng (craig) Wan,
Jiangxi Agricultural University, China

REVIEWED BY
Annamalai Muthusamy,
Manipal Academy of Higher Education, India
Thomas Brendler,
University of Johannesburg, South Africa

*CORRESPONDENCE
Nokwanda P. Makunga
Makunga@sun.ac.za

RECEIVED 27 July 2023
ACCEPTED 16 February 2024
PUBLISHED 21 March 2024

CITATION
Reddy K, Stafford GI and Makunga NP (2024) Skeletons in the closet? Using a bibliometric lens to visualise phytochemical and pharmacological activities linked to *Sceletium*, a mood enhancer. *Front. Plant Sci.* 15:1268101. doi: 10.3389/fpls.2024.1268101

Skeletons in the closet? Using a bibliometric lens to visualise phytochemical and pharmacological activities linked to *Sceletium*, a mood enhancer

Kaylan Reddy [1], Gary I. Stafford [2] and Nokwanda P. Makunga [1*]

[1]Department of Botany and Zoology, Natural Sciences Faculty, Stellenbosch University, Stellenbosch, South Africa, [2]Department of Plant and Soil Sciences, University of Pretoria, Pretoria, South Africa

Plants from the *Sceletium* genus (Aizoaceae) have been traditionally used for millennia by the Khoe and Khoen people in southern Africa, as an appetite suppressant as well as a mood elevator. In more recent times, this mood-elevating activity has been commercialised in the South African natural products industry for the treatment of anxiety and depression, with several products available both locally and abroad. Research on this species has seen rapid growth with advancements in analytical and pharmacological tools, in an effort to understand the composition and biological activity. The Web of Science (WoS) database was searched for articles related to 'Sceletium' and 'Mesembrine'. These data were additionally analysed by bibliometric software (VOSviewer) to generate term maps and author associations. The thematic areas with the most citations were South African Traditional Medicine for mental health (110) and anxiolytic agents (75). Pioneer studies in the genus focused on chemical structural isolation, purification, and characterisation and techniques such as thin layer chromatography, liquid chromatography (HPLC, UPLC, and more recently, LC-MS), gas chromatography mass spectrometry (GC-MS), and nuclear magnetic resonance (NMR) to study mesembrine alkaloids. Different laboratories have used a diverse range of extraction and preanalytical methods that became routinely favoured in the analysis of the main metabolites (mesembrine, mesembranol, mesembranone, and Sceletium A4) in their respective experimental settings. In contrast with previous reviews, this paper identified gaps in the research field, being a lack of toxicology assays, a deficit of clinical assessments, too few bioavailability studies, and little to no investigation into the minor alkaloid groups found in *Sceletium*. Future studies are likely to see innovations in analytical techniques like leaf spray mass spectrometry and direct analysis in real-time ionisation coupled with high-resolution time-of-flight mass spectrometry (DART-HR-TOF-MS) for rapid alkaloid identification and quality control purposes. While *S. tortuosum* has been the primary focus, studying other *Sceletium* species may aid in establishing chemotaxonomic relationships and addressing challenges with species misidentification. This research can benefit the nutraceutical industry and conservation efforts for the entire genus. At

10.3389/fpls.2024.1268101

present, little to no pharmacological information is available in terms of the molecular physiological effects of mesembrine alkaloids in medical clinical settings. Research in these fields is expected to increase due to the growing interest in *S. tortuosum* as a herbal supplement and the potential development of mesembrine alkaloids into pharmaceutical drugs.

KEYWORDS

alkaloid chemistry, central nervous system activity, Kanna, secondary metabolites, pharmacology, phytochemistry

Introduction

The plant *Mesembryanthemum tortuosum* (syn. *Sceletium tortuosum*) (L.) N.E.Br. has well-documented medicinal activity and ethnopharmacology (Smith et al., 1998; Gericke and Viljoen, 2008) and is thus the most popular from the *Sceletium* genus (Family: Aizoaceae, subfamily: Mesembryanthemoideae). *S. tortuosum* is also referred to as kanna, channa, kougoed, or 'sceletium' (Smith et al., 1998). This species is a climbing or creeping perennial with succulent leaves and stems that become thick and slightly woody with age (Klak et al., 2007). An important diagnostic feature of this genus is the skeletonised veins that are apparent when leaves dry (Figure 1A). The typical growth form exhibits a scandent nature (Figures 1B, C) together with leaves that have idioblasts or 'bladder cells' (Figure 1D). The flower colour of petals ranges from white, yellow to pale pink (Figure 1E). The seeds

FIGURE 1
(A) *Sceletium rigidum*; **(B)** Image of *Sceletium subvelutium* (syn. *Mesembryanthemum varians*); **(C)** climbing or decumbent habit form of growth; **(D)** characteristic idioblasts (bladder-like cells) on *Sceletium* leaves; **(E)** flower structure of *Sceletium* species and **(F)** characteristic kidney-shaped seeds. (All images taken by N Makunga and K Reddy).

of *Sceletium* species are brown to black kidney-shaped, and these are small in diameter ranging from 1 mm to 2 mm (Figure 1F).

The plant is indigenous to southern Africa where it has been traditionally used in folk medicine by the Khoekhoen and Sān (Khoe-Sān/KhoiSan) people as a masticatory agent or as a mood elevator (Gericke and Viljoen, 2008). More recently, *S. tortuosum* has been commercialised as an antidepressant or anxiolytic and it is also recommended for attention-deficit disorders, as it aids in mental alertness (Harvey et al., 2011). The chemical constituents which were recognised for their medicinal activity are a group of mesembrine alkaloids that are uniquely associated with *Sceletium* species; however, they do share some similarities with Amaryllidaceae alkaloids. There has been a particular emphasis on mesembrine (Figure 2A), mesembrenone (Figure 2B), and Δ^7mesembrenone (Figure 2C) as biomarker compounds due to more scientific information being available in terms of chemical characterisation and for commercial quality assurance profiling regimes. Thus far, there have been several comprehensive reviews based on the chemistry of alkaloids found in *Sceletium* (Jeffs et al., 1982; Lewis, 1995; 2001; Jin, 2016; Jin and Yao, 2019). Although this list may not necessarily be comprehensive as it is based on a Scopus database search, other reviews that focus on *Sceletium* and its phytochemistry and pharmacology include the work of Gericke and Viljoen (2008); Stafford et al. (2008); Van Wyk (2011); Van Wyk (2015); Krstenansky (2017); Makolo et al. (2019), and Faro et al. (2020). These reviews discuss 1) the ethnobotanical history and chemical diversity in the genus (Smith et al., 1998); 2) the pharmacological and chemical evidence of ethnobotanical use in *Sceletium* (Gericke and Viljoen, 2008); 3) plants from South Africa with CNS effects used for mental health purposes (Stafford et al., 2008); 4) the commercial potential of medicinal plants in South Africa (Van Wyk, 2011, 2015); 5) the occurrence, chemistry, and pharmacology of mesembrine alkaloids (Krstenansky, 2017); 6) the distribution, structural elucidation, biosynthesis, organic synthesis, chemotaxonomy, and biological activities of (−)-mesembrine from *Sceletium* species (Makolo et al., 2019); and 7) the biomedical activities of new psychoactive substances from natural origins (Faro et al., 2020). Within this current paper, we provide an update on analytical techniques used to study *Sceletium tortuosum* and its relatives, where possible. We also summarise studies that focus on chemical variation as much quantitative and qualitative information is still presently missing with regard to the biochemical components that make up the phytochemical profiles of these plants. This paper also presents findings on the use of VOSviewer to identify gaps and trends in *Sceletium* research, which may be of value for other scientists and industry to decide on areas to research within the available options. Furthermore, there is great interest in the use of *Sceletium* species and *Sceletium* alkaloids against anxiety (Shikanga et al., 2011; Loria et al., 2014) and depression (Gericke and Viljoen, 2008; Krstenansky, 2017) but preclinical and clinical evidence that validates these particular applications, which are grounded in an ethnobotanical context, is still limited. In spite of this, the commercialisation of *S. tortuosum* for various phyto-pharmaceutic markets is on the rise (Patnala and Kanfer, 2013; Krstenansky, 2017).

In order to get an overview of the available literature, a systematic bibliometric analysis was undertaken. Currently, there is a growing body of scientific literature that is based on chemical and pharmaceutical studies that have focused on *S. tortuosum* but recent studies on the taxonomy and geographical occurrence of the other *Sceletium* species are limited. This is of relevance as species misidentifications and biodiversity losses may prevail. The first part of this review thus aimed to collate information linked to the taxonomy and distribution of *Sceletium* species. These data were collected from databases such as SANBI-BODATSA and iNaturalist as an introduction before an update on the pharmacology and chemistry observed within the genus is presented. It is imperative to prioritise the correct collection of species, and as such an understanding of the taxonomy of the genus should be consulted. The current trends within the literature and associated authors on a global scale. The present review summarises the studies conducted on the *Sceletium* genus and its chemical constituents over time in terms of the progress in phytochemistry, ethnobotanical use, and pharmacology. This work intends to expose the current gaps within *Sceletium* research. Here, we report on studies from 1961 to the present and direct attention to recent advancements and future directions that may further develop quality, safety, and toxicological standards for therapeutic and nutraceutical applications concerning *S. tortuosum* and its relatives.

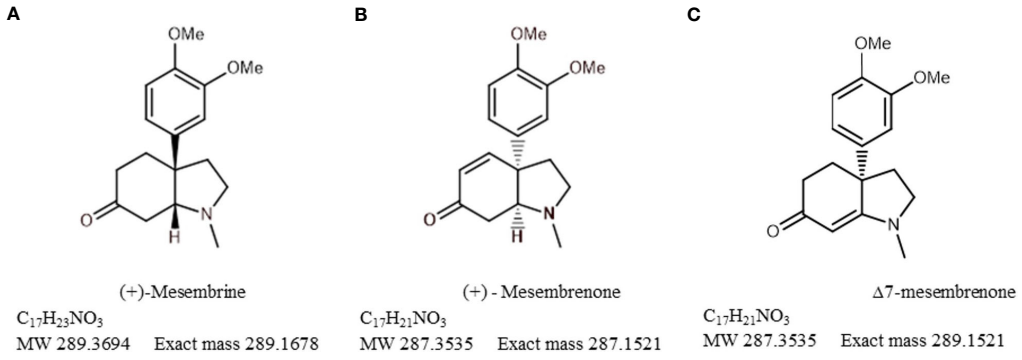

FIGURE 2
Chemical structures of **(A)** mesembrine, **(B)** mesembrenone, and **(C)** Δ^7mesembrenone.

Taxonomy and distribution

The species currently recognised are *S. crassicaule* (Haw.) L. Bolus, *S. emarcidum* (Thunb.) L. Bolus ex H.J. Jacobson, *S. exalatum* Gerbaulet, *S. expansum* (L.) L. Bolus, *S. rigidum* (Figure 1A), L. Bolus, *S. strictum* L. Bolus, *S. tortuosum*, and *S. varians* (Haw.) Gerbaulet (Figure 1B), as revised by Gerbaulet (Gerbaulet, 1996). Several species were reduced to being combined into the same species including *S. joubertii* L. Bol. and *S. namaquense* L. Bol., now considered to be part of the *S. tortuosum* complex. Taxonomically the plant genus was established in 1925 by N.E. Brown, but Klak et al. (2007), in their phylogenetic study of the family, proposed that Mesembryanthemoideae should consist of the single genus *Mesembryanthemum*. Thus, *Sceletium* was reduced to synonymy to *Mesembryanthemum*, and thus, the eight species of *Sceletium* (above) are currently accepted as *Mesembryanthemum crassicaule* Haw., *M. emarcidum* Thunb., *M. exalatum* (Gerbaulet) Klak, *M. expansum* L., *M. archeri* (L. Bolus) Klak (=*S. rigidum*), *M. ladismithiense* Klak (=*S. strictum*), *M. tortuosum* L., and *M. varians* Haw. However, for the purpose of this particular article, *Sceletium* is used as this is still predominantly used in industry, in scientific works on the commercially important *Sceletium tortuosum*, particularly related to its chemistry and pharmacology, and non-scientific settings. The conservation status of species within the *Sceletium* genus is also variable with several members of the genus being evaluated as threatened (*S. expansum*, *S. strictum*, and *S. varians*) by the South African National Biodiversity Institute's Threatened Species Programme (http://redlist.sanbi.org/, Table 1). With *S. strictum*, being categorised as endangered (EN) and *S. expansum* and *S. varians*, both listed as vulnerable (VU). All other species in the genus are considered as being of least concern (LU).

As part of this review, a distribution map of *Sceletium* species was generated from the SANBI-BODATSA (South African National Biodiversity Institute - Botanical Database of Southern Africa); this database contained information sourced from observational data, herbaria, literature, collector information, and species checklists. The majority of the observations were in the Western Cape of South Africa with some in the Northern and Eastern Cape provinces, as illustrated in Figure 3. A particular emphasis has been placed on *S. tortuosum* in the literature for its medicinal properties. The distribution of *S. tortuosum* has been reported in the southwestern areas of South Africa (Gericke and Viljoen, 2008). The plant has an affinity for arid environments and has been reported to grow from Namaqualand through to Aberdeen in South Africa (Chesselet, 2005).

TABLE 1 SANBI Red List conservation status of the species of the *Sceletium* genus.

Species	SANBI Red List conservation status
Sceletium tortuosum (L) N.E.Br	Least concern (LC)
Sceletium varians (Haw.) Gerbaulet	Vulnerable (VU)
Sceletium strictum L. Bolus	Endangered (EN)
Sceletium rigidum L. Bolus	Least concern (LC)
Sceletium crassicaule L. Bolus	Least concern (LC)
Sceletium expansum (L.) L. Bolus	Vulnerable (VU)
Sceletium exaltum L. Bolus Gerbaulet	Least concern (LC)
Sceletium emarcidum (Thunb.) L. Bolus ex H.Jacobsen	Least concern (LC)

Ethnobotany

Simon van der Stel's, the last commander and first Governor of the Dutch Cape Colony, journey to Coperbergh (near present-day Okiep and Carolusberg, in the Northern Cape, South Africa) in 1685 made note of how *kanna* was consumed by the native people, and details of its processing were included in the descriptions related to the species. The journal had the following quotation (translated from Dutch):

"They chew mostly a certain plant which they call Canna and which they bruise, roots as well as the stem, between the stones and store and preserve in sewn-up sheepskins".

Between the date ranges of 1772 and 1774, a Swiss botanist and student of Linnaeus, Carl Peter Thunberg, made journeys to the Eastern Cape and reported on the value of the sedative plants that were found in the locality of present-day Oudtshoorn in the Little Karoo, South Africa (Gordon, 1996). Other reports followed: the plants were used as tinctures (Pappe, 1857), snuffed or smoked or as teas (Jacobson, 1960; Smith et al., 1996; Van Wyk and Wink, 2018), or recreationally (Hartwich and Zwicky, 1914). Watt and Breyer-Brandwijk (1962) indicated that in Namaqualand, both the aerial and underground (root) parts were used to make *kougoed* and how *Sceletium tortuosum* was used as an agent to help with pain, hunger relief, cholic, and restlessness in infants by the Nama people. Since the review paper of Smith et al. (1998), an increasing body of scientific information, associated in particular with *Sceletium tortuosum*, has emerged, leading to continuous progress in the areas of phytochemistry and pharmacology. This review aimed to provide visual networks linked to past research and identified current trends. We provide a historical account of the use of analytical techniques and pharmacological bioassays that have been employed to study *S. tortuosum* and its relatives. Finally, gaps in knowledge, recommendation, and best practice in studying these neurologically acting medicinal plants are presented.

Method—bibliometric analysis

Data sources

The Web of Science Core Collection (Clarivate Analytics, United States) was chosen as the data source. In August 2023, we conducted a search of the topic (phrases appearing in titles, abstracts, and keywords) using the following search terms: 'Sceletium' OR 'mesembrine' NOT 'Gastropoda'. A bibliometric data analysis, for the period 1961–2023, was used to determine trends within previous investigations and how *Sceletium* research

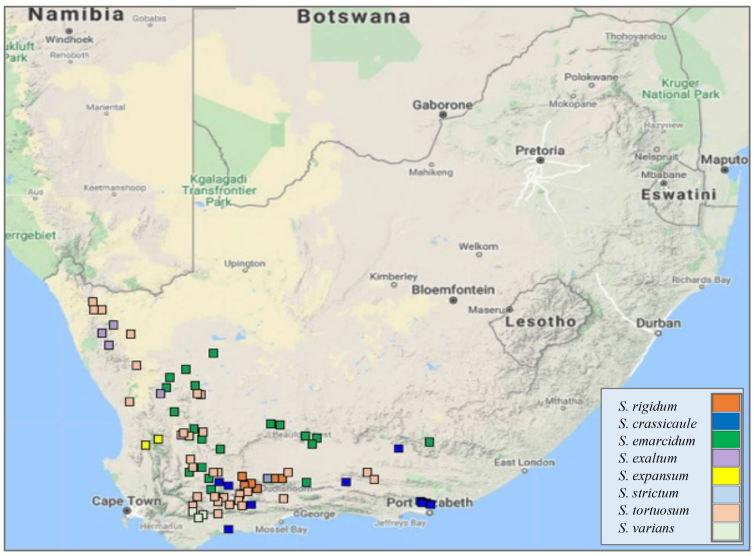

FIGURE 3
A Geographic distribution of wild collections of eight species of *Sceletium* in South Africa (data obtained from SANBI-BODATSA Database).

has evolved, through tracking patterns, trends, relationships, and the development of a discipline over time. Titles and abstracts were screened to exclude false-positives (papers that were not exclusively on *Sceletium* or mesembrine-type compounds found within the *Sceletium* genus). No supplementary restrictions had been placed on document type (review, editorial, letter, etc.) and assay model (*in vivo*, *in silico*, *in vitro*, etc.). The average citation amongst the most popular thematic areas within the body of knowledge associated with *Sceletium* is represented as a bar graph generated in Excel.

The literature search resulted in 348 articles being eligible for the systematic review, and two duplicate studies were removed (Figure 4). After reviewing the abstracts of 346 articles, 27 articles were removed on the basis of 25 being irrelevant due to the study either being focused on a different genus than *Sceletium* or studies investigating the occurrence of mesembrine in other species aside from *Sceletium*. Two additional organic synthesis studies were removed based on their contents not directly linking to mesembrine alkaloid synthesis. Finally, only 319 studies were included for analysis, as indicated in the PRISMA chart (Figure 4).

The data from our WOS searches were read from a bibliographic database file (i.e., the.txt file). Different types of analyses were performed based on our research questions. We were interested in determining the following: 1) the number of contributions in the field and how this changed with time; 2) authorship patterns; 3) geographical location of the producers of the articles, and finally; 4) identification of trends and gaps in the field.

Term maps

Term maps were generated using words in the titles and abstracts whilst authorship and country maps were generated from information associated with the authors and affiliations. Within the bibliographic analysis, 319 articles were analysed and visualised by VOSviewer (Van Eck and Waltman, 2010). VOSviewer is a software that visualises patterns between authors, countries, and terms found in a body of literature. The software creates networks between the data and illustrate them as bubbles

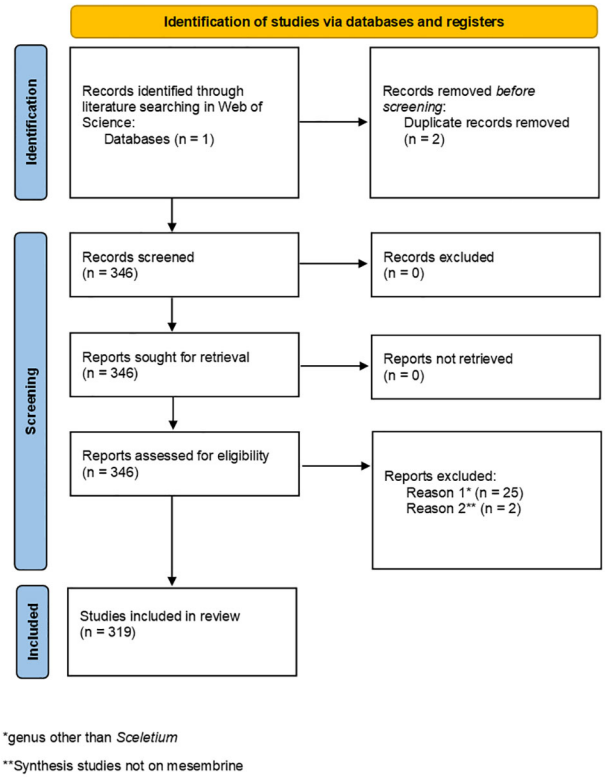

FIGURE 4
PRISMA chart illustrating the process used to screen studies for eligibility in this systematic review.

connected by lines, indicating association. The larger the bubble, the greater its frequency of occurrence. The thicker the lines the greater number of links an item has with others in the network. Irrelevant phrases or repetitions of phrases were excluded.

Discussion

Past and current trends in literature

From the 319 articles that were published on *Sceletium* and Mesembrine-type alkaloids from *Sceletium*, the document types were predominantly articles (n = 264) and reviews (n = 55). The citations received by the 319 articles in this domain ranged from 0 to 230 (mean ± SD = 26.02 ± 28.18). The most cited paper was between two papers, the first an ethnobotanical review by Stafford et al. (2008) investigating traditional South African plants with CNS activity (8.86 citations per year). This was followed by the Gu and You (2011) paper on the organic synthesis of mesembrine isomers (11.27 citations per year). The hundred most cited papers within the field had an average citation of 55, with an average yearly citation of 4.

The thematic areas where the majority of the research is focussed were as follows: Chemistry; Molecular Biology; and Pharmacology. The average citation amongst the most popular thematic areas associated with *Sceletium* research is presented in Figure 5.

For this reason, this review has a stronger emphasis on the work conducted in these fields. A particular focus has been placed on one species, *S. tortuosum* (119 links to other topics), and the membrane-rich extracts (64 links to other topics) of this plant. This has been the trend since the initial scientific interest in the plant in the 1960s. It is also interesting to note a lack of publications between 1980 and 2000. Dominant investigation areas were identified as 'chemistry' and 'pharmacology' especially, those focussing on *Sceletium* alkaloids to further understand the medicinal application of this plant (Figure 5).

Key research themes

Several different research themes appear to be of superior relevance (as indicated by citation trends) in *Sceletium* literature. There were 349 terms that occurred three or more times in the 296 articles (Figure 6 block D); these were separated into 13 thematic clusters identified through the VOSviewer (Figure 6 block C). An analysis of the citations from 1956 to 2023 suggests that research associated with neurological disorders (ageing, depression, and anxiety) received significantly more citations per article (110, 55, and 41 average citations, respectively). This can be seen by the red-coloured bubbles (Figure 6 block D). The neurological topics of ageing, anxiety, and depression had an average of 110, 75, and 40.7 citations each, respectively. Other topics that were relatively highly cited were terms associated with the chemical synthesis of mesembrine alkaloids. These terms, C-H-amination, Claisen rearrangement, cobalt catalysis, and enantiospecific synthesis, had average citation values of 45, 40, 31, and 58, respectively.

Drivers of research

The drivers of research in terms of authors came from 17 authors who had contributed findings associated with *Sceletium* and mesembrine (Figure 6B). These authors were selected on the basis of contributing four or more publications from 1956 to 2023. Amongst the authors, three networks can be observed. The network from South Africa is the greatest contributor in terms of publications, with the leading author contributing 15 papers on the topic. This may be due to their location which allows ease of access to wild-growing plant materials and established working laboratory methods, where plant material is sourced through permits for collection that is not destructive. The network from Egypt contributed 13 documents on the topic. Presently, within South Africa, the Tshwane University of Technology (averaging 11 citations per year) and Stellenbosch

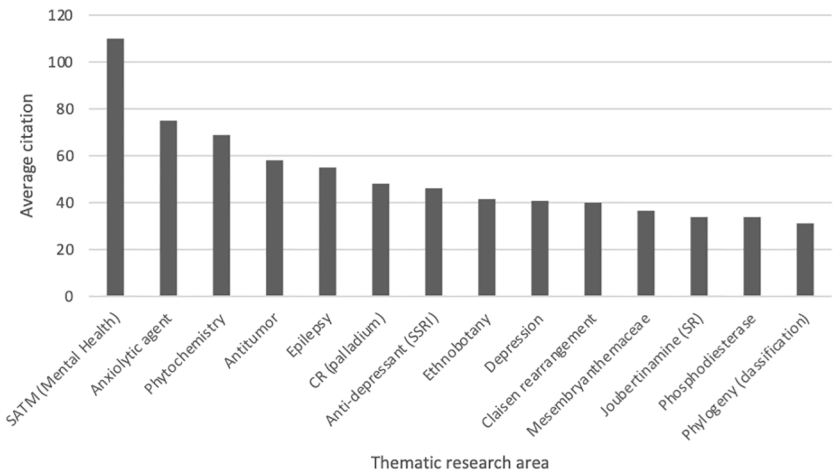

FIGURE 5
Average citation of thematic research areas within *Sceletium* research from Web of Science (n = 296, citation values >30.00). SATM (Mental health), South African Traditional Medicine (Mental Health); CR (palladium), Coupling reactions (palladium); Joubertiamine (SR), Joubertinamine (sigmatropic rearrangements).

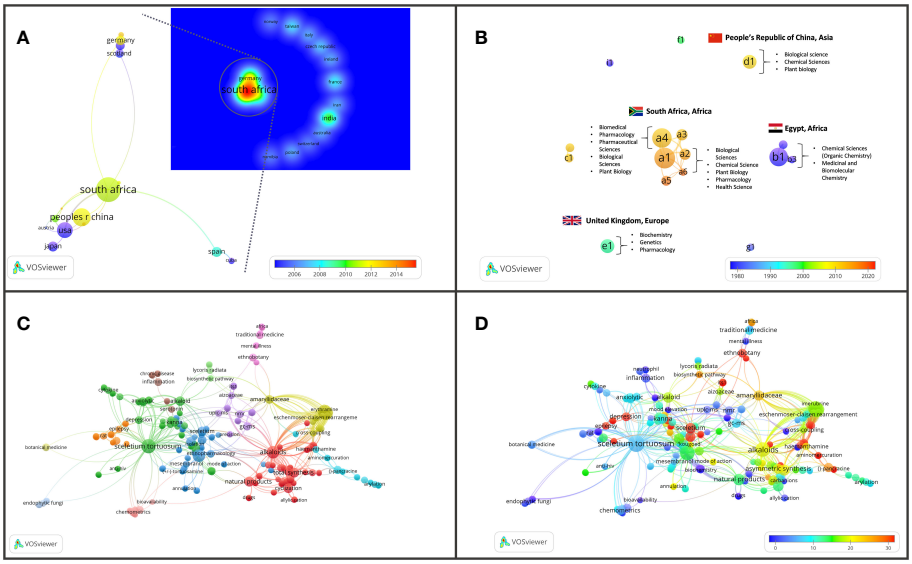

FIGURE 6
Major bibliographic summaries of literature in *Sceletium* research. **(A)** Country network map of the most prolific research network in *Sceletium* research, based on country affiliation. Image additionally illustrating Average publication year. **(B)** Author network map showing linkages and collaboration between various researchers (and institutions) with an overlay of Average publication years weighted by citations. (Map illustrating authors with at least four publications in the area of research), with overlay of associated countries and thematic areas. **(C)** Term map based on co-occurrence of text in both the title and abstract fields using 212 publications based on *Sceletium* research. **(D)** Term map of research related to *Sceletium* with an overlay of the trend in citations over time. Data extracted from Web of Science (n = 212) and visualised with VOSviewer.

University (averaging on 10 citations per year) are the major contributors to research and have contributed the most publications with 18 and 10 publications, respectively.

In terms of highly cited papers, with regard to chemistry from 1967 to 2000, the focus was largely on the isolation and characterisation of alkaloids from *Sceletium* species. Post-2000, the focus shifted to more chemical assays in an effort to develop quality control tools for the medicinally important plant, *S. tortuosum*, that was gaining pharmacological traction in literature as a phytomedicine used for anxiety and depression and as a mental stimulant. VOSviewer maps and an analysis of the literature indicate that the field may be shifting toward a greater focus on the toxicological and pharmacodynamics aspects of these plants (Figure 6C). Gaps in the field of pharmacology in the field were identified as clinical trials and bioavailability studies.

We observed 29 countries/territories with the highest contributing countries being South Africa (50 documents), China (29 documents), and the USA (23 documents) where scientific investigations in *Sceletium* have been conducted. All three are associated in a network and, as such, have exchanged techniques and gained access to analytical tools for more advanced chemical and pharmacological analysis. South Africa is suspected to be the greatest contributor to current research efforts, and this may be due to South African researchers having easier access to plant materials that grow in remote locations in the country and their compliance with Biodiversity laws that govern the issue of collection permits and bioprospecting activities linked to indigenous and endemic plant species in the country. Outside of this collaboration network, India has contributed 14 documents without collaboration with South Africa and these documents mainly cover topics related to the synthesis of mesembrine and joubertiamine alkaloids from *Sceletium* and one paper on the quality control of medicinal plants (Kumar and Sharma, 2018).

Analytical chemistry

The bibliometric analysis, performed in VOSviewer, identified alkaloid chemistry and analytical techniques have been a major area of interest for investigations linked to *Sceletium*. This is seen as the most dominant cluster in terms of publications, indicated by a red cluster. The most commonly used mesembrine alkaloid biomarkers in quality control and analysis are mesembrine (Figure 2A), mesembrenone (Figure 2B), mesembranol (Figure 6, compound 2), and mesembrenol (Figure 6, compound 3). Some alkaloid classes which have been underrepresented in the literature that may hold medicinal activity but have not been tested yet are joubertiamine (Figure 6, compound 5), sceletium alkaloid A_4 (Figure 6, compound 6), and the tortuosamine alkaloid classes of compounds (Figure 6, compound 8), which are also found in *Sceletium* species. The purple cluster represents experimentation related to the isolation and identification of compounds by various analytical means (Figure 6C). The body of work is quite substantial and has had a wide range of analytical techniques applied to the phytochemical characterisation of *Sceletium* species and related commercial products (Table 2). The majority of analytical methods used on *S. tortuosum* have targeted the detection of two alkaloids, mesembrine and mesembrenone (Table 2).

Analytical chemistry in *Sceletium* has been of scientific interest since the 1970s. Many of the studies in the 1970s were mainly

TABLE 2 The analytical techniques used on *Sceletium* species of medicinal importance, with their extraction method, sample preparation, and detectors (LE, liquid extraction).

Species	Plant parts	Biological matrices and plant specimens	Extraction method	Extract	Chemicals detected	Analytical techniques	Detectors	Reference
Sceletium crassicaule (Haw.) L. Bolus (Syn. *Mesembryanthemum crassicaule* L. Bolus)	Aerial	Plant material	LE[1]	Methanol, dichloromethane	Sceletium alkaloid A4	ESI-MS, MS-MS, HPLC-UV	MS, UV	(Patnala and Kanfer, 2015)
	Aerial	Plant material	Acid/ base extraction	Methanol, ammonia (25% w/w), sulphuric acid (98% w/w), and dichloromethane	Mesembrenol Mesembranol Mesembrenone Mesembrine	UPLC-PDA	PDA	(Shikanga et al., 2013)
Sceletium expansum (L.) L. Bolus (Syn. *Mesembryanthemum expansum* L. Bolus)	Aerial	Plant material	LE	Ethanol	Alkaloid hordenine Joubertiamine dihydrojoubertiamine dehydrojoubertiamine	^{1}H-NMR,^{13}C-NMR, UV	UV	(Arndt and Kruger, 1970)
Sceletium strictum L. Bolus (Syn. *Mesembryanthemum strictum*L. Bolus)	Not reported	Not reported	Not reported	Not reported	4′-O-Demethylmesembrenone mesembrenone Channaine	IR, ^{1}H-NMR, MS	MS, IR	(Abou-Donia et al., 1978)
	Root, stem, and leaf	Plant material	Soxhlet extraction	Ethanol	Sceletenone Sceletium alkaloid A4, N-formyltortuosamine, 4′-O-demethylmesembrenone, Δ^{7}-mesembrenone	^{1}H-NMR, 13C-NMR, GLC-MS	MS	(Jeffs et al., 1974b)
	Root, stem, and leaf	Plant material	Soxhlet extraction	Ethanol	4′-O-Demethylmesembranol 4′-O-Demethylmesembrenol Mesembrenol O-Acetylmesembrenol	^{1}H-NMR, ^{13}C-NMR, GLPC-MS	MS	(Jeffs et al., 1970)
Sceletium subvelutium L. Bolus (Syn. *Mesembryanthemum varians*)	Root, stem, and leaf	Plant material	LE	Methanol	(−)-3′-Methoxy-O-methyljoubertiamine (4R)-(−)-O-Methyljoubertiamine Joubertiamine, dihydrojoubertiamine O-Methyldihydrojoubertiamine	PTLC, MS, ^{1}H-NMR, IR, UV	IR, UV, MS	(Nieuwenhuis et al., 1981)
Sceletium tortuosum (L.) N.E. Br. (Syn. *Mesembryanthemum tortuosum* L.; *Kanna*)	Not applicable	Isolated compounds	Not applicable	Methanol	Mesembrenol Mesembrenol Mesembrenone Mesembrine	UHPLC-MS-qToF	MS-qToF	(Maphanga et al., 2022)

(Continued)

1 LE: liquid solvent extraction.

10.3389/fpls.2024.1268101

TABLE 2 Continued

Species	Plant parts	Biological matrices and plant specimens	Extraction method	Extract	Chemicals detected	Analytical techniques	Detectors	Reference
	Aerial and stems	Kanna powder, foliage, stems, and shredded material	LE	Methanol	Hordenine Mesembrenone Mesembrine Mesembrenol Mesembrinol	DART-HRMS	HRMS	(Appley et al., 2022)
	Aerial	Plant material (tissue cultured)	LE	Methanol	N-Demethylmesembrenol 4′-O-Demethylmesembrenol Joubertiamine 4′-O-Demethylmesembrenone Δ^4-Mesembrenone Mesembrenol Mesembrine Mesembrenol Δ^7-Mesembrenone	UHPLC-MS-qToF	QToF-MS	(Makunga et al., 2022)
	Aerial	Zembrin	LE	Water and ethanol	Mesembranol Mesembrenol Mesembrenone Mesembrine	UPLC-MS-PDA	MS, PDA	(Gericke et al., 2022)
	Aerial	Plant material	LE	Methanol	Sceletorine A Sceletorine B	^{1}H-NMR ^{13}C-NMR, UV-vis, IR, QSTAR ToF, HPLC-UV	UV-diode	(Yin et al., 2019)
	Aerial	Plant material	LE	Methanol	Mesembrenol Mesembrenone Mesembranol N-Demethyl-N-formyl Mesembrenone, Mesembrine Sceletium alkaloid A4 Δ^7-Mesembrenone	^{1}H-NMR, UPLC-MS	MS	(Zhao et al., 2018)
	Aerial	Plant material	LE	Methanol	Dihydrojoubertiamine, mesembrenone-M (O-demethyl-) Mesembrenone-M (O-demethyl-dihydro-) Mesembrenone-M (N-demethyl-dihydro-) Mesembrenone Mesembrine Mesembrine-M (dihydro-) Mesembrine-M (N-demethyl-) Mesembrine-M (O-demethyl-)	Leaf spray-MS	MS	(Freund et al., 2018)
	Aerial	Plant material	LE	Acetonitrile	Mesembranol Mesembrenone Mesembrine	UPLC-MS	MS	(Sandasi et al., 2018)

(Continued)

10.3389/fpls.2024.1268101

TABLE 2 Continued

Species	Plant parts	Biological matrices and plant specimens	Extraction method	Extract	Chemicals detected	Analytical techniques	Detectors	Reference
	Aerial	Plant material	Acid/ base extraction	Methanol	Chanaine	HPLC-MS-PDA ^{1}H-NMR	MS, PDA	(Veale et al., 2018)
	Aerial	Plant material	LE	Methanol	Mesembrenone mesembrine	UHPLC-QToF-MS	QToF, MS	(Manda et al., 2017)
	Aerial	Kanna powder	N/A[2]	N/A	4-O-Demetheylmesembranol 4-O-Desmethylmesembrenone, 4-O-desmethylmesembrenol Dihydrojoubertiamine Joubertiamine Mesembrane Mesembranol Mesembrenone Mesembrine O-Methyldehydrojoubertiamine O-Methyljoubertiamine Sceletenone, dehydrojoubertiamine	DART-HRToF-MS	HRToF, MS	(Lesiak et al., 2016)
	Aerial	Plant material	LE	Methanol, dichloromethane	Δ^{7}-Mesembrenone Epimesembranol Mesembranol Mesembrenol Mesembrenone Mesembrine Sceletium alkaloid A4	ESI-MS, MS-MS, HPLC-UV	MS, UV	(Patnala and Kanfer, 2015)
	Aerial	Plant material	Soxhlet extraction	n-Pentane:n-hexane (1:1 v/v)	Bis-Demethyl-dihydromesembrine Mesembranol Mesembrenone Mesembrine N-Demethyl-dihydromesembrine N-Demethylmesembrenone, N-demethyldihydromesembrenone O-Demethyl-dihydromesembrine	^{1}H-NMR, GC-MS, LC-(HR)-MS^{n}	MS, (HR)-MS^{n}	(Meyer et al., 2015)
	Aerial	Plant material	Acid/ base extraction	Methanol, ammonia (25% w/w), sulphuric acid (98% w/w), and dichloromethane	Mesembranol Mesembrenol Mesembrenone Mesembrine	UPLC-PDA	PDA	(Shikanga et al., 2013)

(Continued)

2 N/A: as study directly analysed samples in the inlet source.

10.3389/fpls.2024.1268101

TABLE 2 Continued

Species	Plant parts	Biological matrices and plant specimens	Extraction method	Extract	Chemicals detected	Analytical techniques	Detectors	Reference
	Aerial	Plant material, Kanna powder	LLE	Methanol, dichloromethane, ammonia (25% w/w solution), and sulfuric acid (H_2SO_4; 98.08% w/w)	Mesembranol Mesembrenol Mesembrenone Mesembrine	TLC, HPLC, GC–MS and ^{1}H-NMR ^{13}C-NMR (1 and 2D)	MS	(Shikanga et al., 2013)
	Aerial	Plant material, Kanna powder	Acid/ base extraction	Methanol	Mesembranol Mesembrenol Mesembrenone Mesembrine	TLC, RP-UHPLC-PDA, GC-MS ^{1}H-NMR ^{13}C-NMR (1 and 2D)	PDA, MS	(Shikanga et al., 2012e)
	Aerial	Plant material, Kanna powder	Acid/ base extraction	Methanol	Mesembranol Mesembrenol Mesembrenone Mesembrine	HPTLC, GC-MS	MS	(Shikanga et al., 2012b)
	Aerial	Plant material, Kanna powder	LE	Methanol	Δ^7-4′-O-Demethylmesembranol 4′-O-Demethylmesembrine 4′-O-Demethylmesmbranol Mesembranol Mesembrine	NACE-MS	MS	(Roscher et al., 2012)
	Aerial	Plant material	Acid/ base extraction	Dichloromethane	Mesembranol Mesembrenol Mesembrenone Mesembrine	HSCCC, CC/ PTLC, ^{1}H-NMR GC-MS	MS	(Shikanga et al., 2011)
	Aerial	Plant material	LE	Methanol	Epimesembranol Mesembranol Mesembrenone Mesembrine Δ^7-Mesembrenone	HPLC-UV, HPLC-PDA	PDA, UV	(Patnala and Kanfer, 2010)
	Aerial	Plant material	LE	Methanol	4′-O-Demethylmesembrenol Mesembrine Δ^7-Mesembrenone	LC–UV-MS, HPLC-PDA	MS, UV, PDA	(Patnala and Kanfer, 2009)
	Not reported	*Sceletium* tablets	LE	Methanol	Epimesembranol Mesembranol Mesembrenol Δ^7-Mesembrenone Mesembrenone Mesembrine	CZE-MS	MS	(Patnala and Kanfer, 2008)
	Root, stem, and leaf	Plant material	Soxhlet extraction	Ethanol	4′-O-Demethylmesembrenol Mesembrenone Mesembrine	GC-NPD-MS, TLC	NPD, MS	(Smith et al., 1998)

(Continued)

10.3389/fpls.2024.1268101

TABLE 2 Continued

Species	Plant parts	Biological matrices and plant specimens	Extraction method	Extract	Chemicals detected	Analytical techniques	Detectors	Reference
	Aerial	Plant material	Acid/ base extraction	Chloroform	(+)-N-Acetyltortuosamine (+)-N-Formyltortuosamine 3′-Methoxy-4′-O-methyljoubertiaminol Joubetiamine Mesembrine Sceletium alkaloid A4 Tortuosamine	GLC,^{1}H-NMR,IR	IR	(Jeffs et al., 1982)
	Root, stem, and leaf	Plant material	LE	Methanol	Sceletium A4 Unnamed alkaloid	GC-MS, TLC, ^{1}H-NMR, IR	MS, IR	(Gross et al., 1979)
	Root, stem, and leaf	Plant material	Soxhlet extraction	Ethanol	4′-O-Demethylmesembrenone, sceletium alkaloid A4 Mesembrenone Mesembrine N-Formyltortuosamine Sceletenone Tortuosamine Δ^{7}-Mesembrenone	^{1}H-NMR, ^{13}C-NMR, GLC-MS	MS	(Jeffs et al., 1974b)
	Root, stem, and leaf	Plant material	Soxhlet extraction	Ethanol	Sceletium alkaloid A4	^{1}H-NMR, ^{13}C-NMR, GLC-MS	MS	(Jeffs and Capps, 1979)
	Aerial	Plant material	LE	Ethanol	Dehydrojoubertiamine Dihydrojoubertiamine Hordenine Joubertiamine	^{1}H-NMR, ^{13}C-NMR, UV	UV	(Arndt and Kruger, 1970)

10.3389/fpls.2024.1268101

focused on compound isolation and structural elucidation (Jeffs et al., 1970, 1974b, 1974a; Arndt and Kruger, 1971; Abou-Donia et al., 1978; Nieuwenhuis et al., 1981) with a diversity of alkaloids as seen in Figures 7–10. In terms of *Sceletium*, however, the isolated structures did not necessarily enter into a drug discovery pipeline during the period of 1970 to 1998. The analysis of crude extracts using a variety of techniques, from thin layer chromatography, gas chromatography, and liquid chromatography, is more evident in the literature, and various laboratories have published several papers that focus on analysing mesembrine alkaloids. With changes in research foci in the natural products industry, where the study of complex plant mixtures using metabolomics in the 2000s till present has become an established field, smaller quantities of plant materials are being utilised than large amounts that were needed for isolation in the 1970s. Secondly, the focus has shifted to quality assessment of wild-harvested *Sceletium* species, as a means to compare wild populations to define chemotypes that occur naturally. Also, such application of metabolomics is explored for its potential contribution to the development of quality assurance protocols to ensure that *Sceletium*-based products are scientifically verified to contain the biomarker mesembrine alkaloids, which define their biochemical makeup (Masondo and Makunga, 2019). In a chronological format, using examples we highlight, the different analytical methods that have been used in *Sceletium* phytochemical studies are discussed below.

Jeffs et al. (1970) performed an ethanol extraction on *S. strictum* plant material. The crude alkaloid fraction was then analysed by chromatography. The GLPC allowed for the collection of 7 mg of an unidentified compound, 32 mg of mesembrenone, a 13-mg mixture of mesembrine–mesembrenone, 285 mg mesembrenol, 871 mg mesembrenol–mesembranol (at a ratio of 90:10 (w/w)), and 101 mg mesembrine. All of the structural identifications were possible and were achieved after nuclear magnetic resonance (NMR).

Sceletium A_4 is one of the compounds that is now regarded as one of the biomarker compounds of *S. tortuosum*, and together with mesembrine, mesembrenone mesembranol, and mesembrenol (Figure 2), it can be used to differentiate wild-harvested chemotypes (Masondo and Makunga, 2019). The paper of Jeffs et al. (1971b) identified this particular compound, Sceletium A_4 from *S. namaquense* (syn. *S. tortuosum*), for the first time. However, they did not report on any chromatographic techniques or quantitative data and information on structural characteristics from NMR data was solely presented.

Jeffs et al. (1974b) identified the alkaloids Sceletium alkaloid A_4, tortuosamine, N-formyltortuosamine, and sceletenone isolated

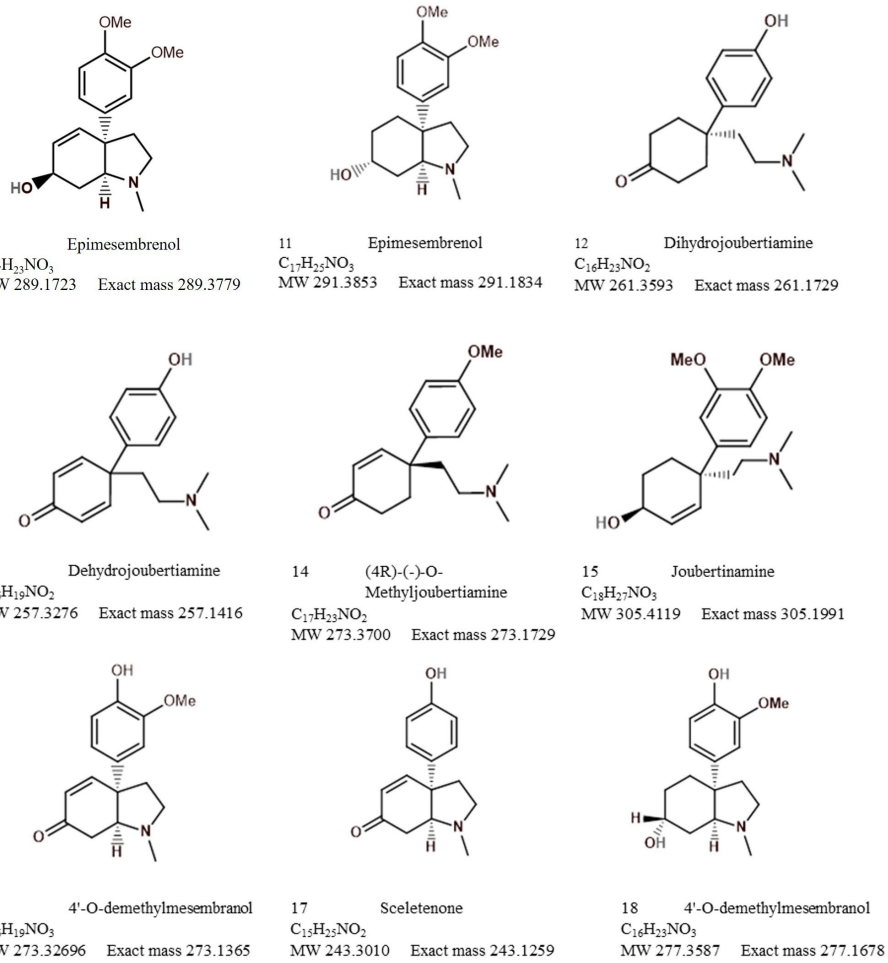

FIGURE 7
Mesembrine alkaloids from *Sceletium* of notable medicinal activity.

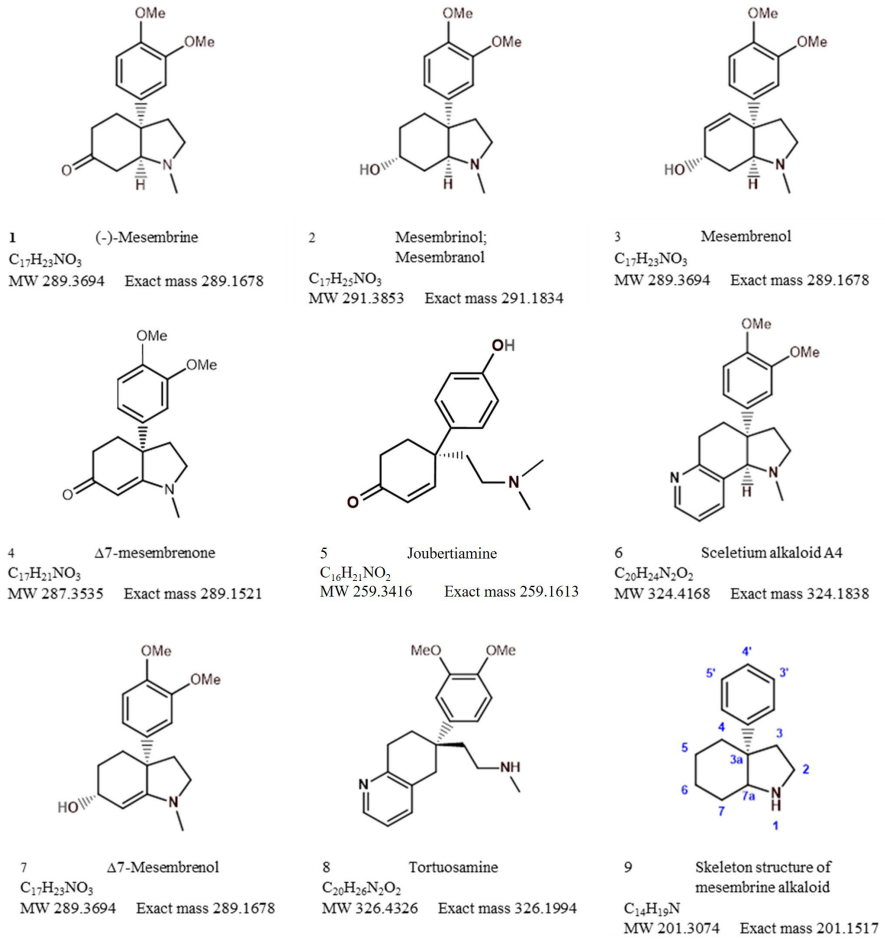

FIGURE 8
Other alkaloids found in *Sceletium* species.

from *S. namaquense* (syn. *S. tortuosum*). Using X-ray crystallography, Abou-Donia et al. (1978) identified the structure channaine from *S. strictum*. However, the authors cautioned and suspected that channaine may have been an artefact from the condensation of two *N*-demethylmesembrenone molecules during the isolation process. With the exception of the recent study by Veale et al. (2018), discussed below in detail, no other reports have shown this unusual alkaloid to occur in *Sceletium* plants since then.

There is a clear lack of analytical isolation methods being used in studying the chemical constituents of *S. tortuosum* and its relatives from the 1980s till 1998. Renewed interest in these species is evident thereafter, with the work of Smith et al. (1998) that tested 21 species from nine genera of the Mesembryanthemaceae, for the distribution of mesembrine alkaloids. As compared with previous studies, significantly less plant material was used per extraction with methods staying relatively the same. The analytical techniques had advanced quite notably with the last research on *Sceletium* and its alkaloids that had been performed 16 years prior. Many investigations after 1998 that use smaller amounts of the plant sample as techniques that are in routine use for metabolite profiling are much more robust. Only semiquantitative data could be generated for this study due to no standards being readily available at that particular time. Out of the species tested, the only species with comparable mesembrine alkaloid levels to that of the *S. tortuosum* was *Aptenia cordifolia*. The relative levels of mesembrine were not reported on nor were *m/z* data for the other species presented.

Methods that allow for high-throughput detection of mesembrine alkaloids are thus sought after for industrial applications. Such methods also need to be less labour intensive and not necessarily require a high level of technical know-how for them to be placed in routine use, more especially to use them as a quality assurance measure and for the standardisation of manufactured products derived from *Sceletium*. As an example, Patnala and Kanfer (2008) investigated the analytical technique of capillary electrophoresis (CE), and this is a technique where electrophoretic mobilities under the influence of an applied electric field enable the separation of charged components. This analytical technique allows for the rapid and efficient separation of compounds leading to rapid analysis (Li, 1992). The technique is favourable due to its high efficacy and efficiency, as well as wide application for both scientific laboratories and industrial manufacturers, plus it requires low running costs during experimentation. Before this study, there was a paucity of reports on commercialised products of *S. tortuosum* despite an industry

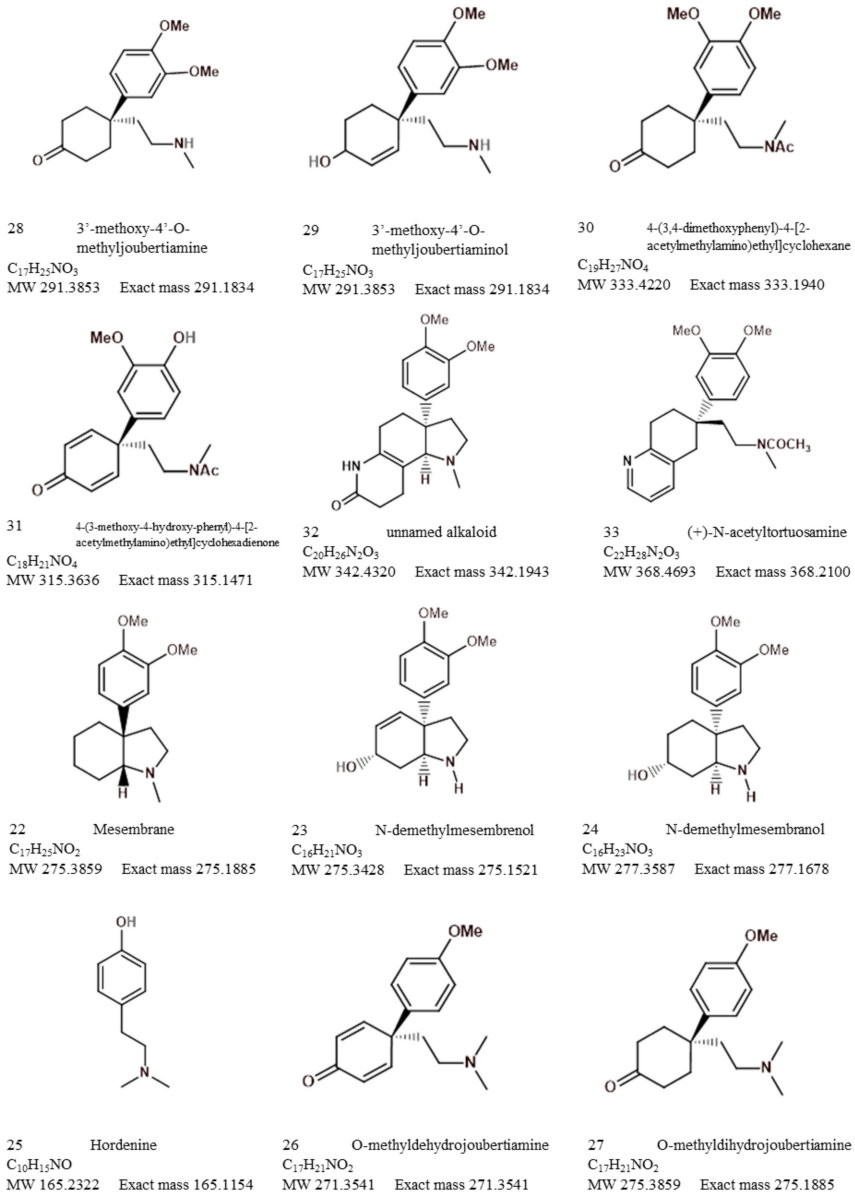

FIGURE 9
Other alkaloids found in *Sceletium* species (cont.).

that had become established in South Africa. The study found the average content of mesembrine per tablet to be 164.30 µg per 12-mg dose of a tablet. Sensitivity and reproducibility were also an important consideration, and the authors confirmed that their protocol was both sensitive and reproducible. However, the exact species of *Sceletium* is not reported on in this study, which hinders the reproducibility of this work as one can merely assume that the focus was on the commercialised plant, *S. tortuosum*. It should be noted that there were some encountered difficulties during experimentation as the method could not conclusively distinguish between compounds with similar *m/z* values (diastereomers at *m/z* 292). Correct taxonomic identities for *Sceletium* species need to be accurate as these plants are difficult to distinguish from their anatomical structures and chemotaxonomic markers have not always played a significant role in delineating sister species from each other (Patnala and Kanfer, 2013).

The analytical tools chosen by Patnala and Kanfer (2009) were HPLC-PDA and LC-MS with a UV detector for qualitative and quantitative analyses of fermented and extracted materials. Fermentation resulted in the transformation of mesembrine. This subsequently led to lower levels being detected, which confounded evidence presented by Smith et al. (1998). Although precision and

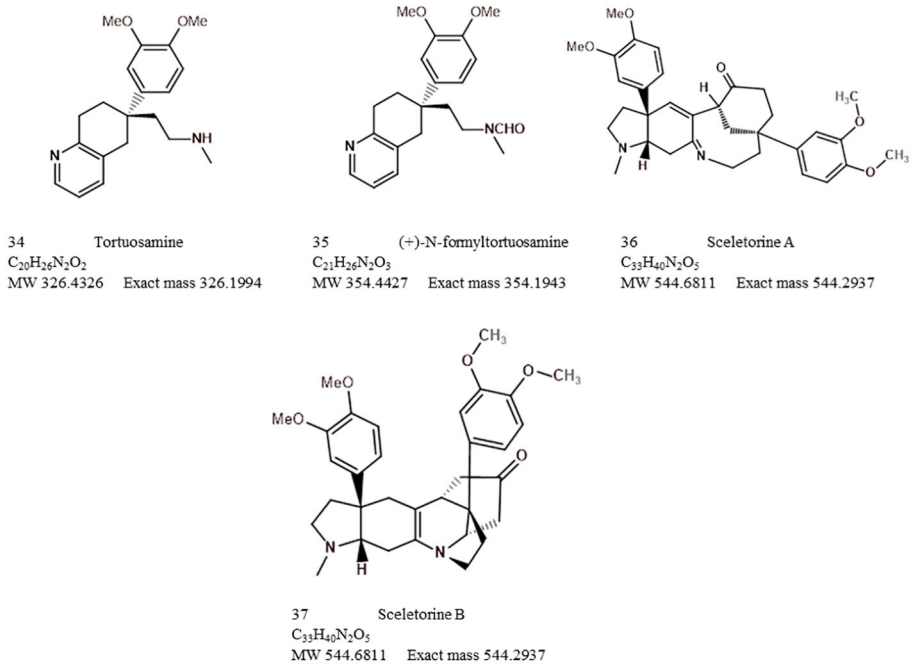

FIGURE 10
Other alkaloids found in *Sceletium* species (cont.).

sensitivity were reported on, the authors did not provide detailed information relating to instrument conditions, making this study rather difficult to reproduce in other laboratory environments. In another study, Patnala and Kanfer (2010) developed and validated an HPLC method for the analysis of *Sceletium* plant material but the exact species used for this investigation was not indicated and one assumes that *S. tortuosum* was the target species. The method showed repeatable, precise, and appropriate resolution of alkaloids for quality control of mesembrine-type alkaloids. Prior to this study, poor validation data had been presented on any analytical techniques described for *Sceletium*. The analytical tools used were an HPLC system connected to a UV and PDA detector. Further structural data were supported by NMR spectra. The lack of standards resulted in several alkaloids assayed *via* chromatography whose identities were unknown to the researchers as no published data on these metabolites was available. Unfortunately, this study did not report on what species of *Sceletium* they had extracted the phytochemicals from, which is an issue in the reproducibility of this study. To iterate, this is highly problematic when some of the *Sceletium* species are difficult to distinguish from each other as they are similar in their appearance and their taxonomy is rather ambiguous (Patnala and Kanfer, 2013). The provenance of the plant samples can alter their phytochemical composition as many different chemotype configurations may exist in wild-collected populations, exhibiting both intra- and inter-specific variability (Shikanga et al., 2012c).

Due to the complex mixture of structurally similar alkaloids, the development of appropriate analytical techniques for chemotaxonomic assessment has proven to be quite a challenge. Further compounding this issue is that, in some species, for example, *S. emarcidum*, the distribution of alkaloids falls below the limit of quantification by the analytical tool (Patnala and Kanfer, 2013). To reduce these challenges, the introduction of reference compounds for all the alkaloids of interest may allow for better specificity during the fingerprinting process, assisting with the assay of plants with stronger precision and accuracy.

Shikanga et al. (2011) employed a high-speed countercurrent chromatography (HSCCC) method to rapidly isolate alkaloids from *S. tortuosum* in high yields. The quantity and purity obtained by HSCCC were higher in all alkaloids as compared with CC/PTLC also performed in this study. The method was efficient and cost effective, requiring relatively smaller amounts of plant material in isolating mesembrine (482.4 mg), mesembrenone (545.2 mg), mesembrenol (300.0 mg), and mesembranol (47.8 mg).

Chemotypic variation observed in *Sceletium* (Roscher et al., 2012; Shikanga et al., 2012c; Zhao et al., 2018) may be due to the ability of plants to exhibit phenotypic plasticity to cope with their environments and climates (Nicotra et al., 2010). Phenotypic plasticity enables plants with a standard genome to adapt their phenotype in response to environmental pressures assisting with survival (Nicotra et al., 2010). This phenotypic plasticity is often correlated with metabolomic differences in the plants in response to their environments; an example of this was observed in *Hippophae rhamnoides* (Kortesniemi et al., 2017). The study of chemical variation linked to plant-environment effects can thus easily be achieved using phytochemical analytical techniques.

The field of plant metabolomics is making major contributions to our understanding of plant biochemistry and metabolism as a metabolomics workflow can facilitate a comprehensive compilation of metabolites within a particular cell, tissue, or organ, but large-scale experiments are notoriously difficult to interpret. In such instances, the complexity of these data sets is enormous and they cannot easily be processed with classical statistics (Van der Kooy

et al., 2008), consequently principal component analysis (PCA), and partial least squares (PLS) analysis have been employed. These types of multivariate statistical applications reduce the dimensionality of the data enabling better pattern recognition that can be correlated with the analysed samples.

Shikanga et al. (2012c) further developed a method for the rapid and simple identification of alkaloids in *S. tortuosum* raw and wild-harvested materials. The intended purpose of this study was to develop an analytical technique for the routine analysis of psychoactive alkaloids in *S. tortuosum* these products. The analytical tool used was a high-performance thin-layer chromatography (HPTLC) densitometric method as this is a superior and more sophisticated form of TLC that is fast and robust for quality testing of botanical materials. One of the advantages of using this method is the automation of the different steps that would mainly be performed by hand with a normal TLC. This makes this method more powerful for metabolite fingerprinting, increasing its resolution and enabling quantitative measurement of phytochemicals.

The first study to use the analytical technique of non-aqueous capillary electrophoresis coupled to mass spectrometry (NACE-MS) was aimed at analysing wild and commercial plant materials extracted from methanol as a solvent from *S. joubertii* (syn. *S. tortuosum*) (Roscher et al., 2012). Another point of interest in this study was to investigate the influence fermentation would have on alkaloid profiles. Wild (calyx, stems, and leaves) and commercial plant material was extracted using methanol as a solvent. Samples were also fermented, and their alkaloid profiles were obtained. The fermentation was performed by crushing the whole wild harvested plant, and this included the calyx, stems, and leaves as plant parts. After homogenisation of the material, it was then stored in an airtight transparent plastic container, left in the sun for 8 days, and vacuum dried later. All analyses were performed on capillary electrophoresis coupled to an Ion Trap 6330. The high selectivity of this method is evident by its ability to distinguish the diastereomers of 4′-O-demethylmesembranol (retention time of 12.3 min); since then, no other analytical techniques have been able to identify it (Smith et al., 1998; Patnala and Kanfer, 2008, 2010). No quantification data were presented in this paper. Furthermore, no comparison is made with a reference technique with the same samples. The technique proved effective in the relative quantification of alkaloids from wild and commercial samples of *Sceletium*. However, the authors do not present any evidence validating the method in terms of linearity, limits of detection, and repeatability. Nevertheless, this technique provided novel opportunities to study samples that potentially have diastereomers and isobaric structures.

Shikanga et al. (2013) performed a study using UPLC and hyperspectral imaging to distinguish between *S. tortuosum* and *S. crassicaule* as these species are difficult to distinguish from each other as they look almost identical, often leading to their misidentification. Hyperspectral imaging is proving a valuable tool in the authentication of herbal products, but it is heavily reliant on good statistical models to make predictions after test materials have been scanned. Its main advantage is that it circumvents an extraction step using organic solvents, making it time efficient, non-destructive, and friendly to the environment and users. This was the first study to investigate the chemical composition of *S. crassicaule*. The purpose of this study was to offer an additional robust tool to reduce the adulteration of *Sceletium* with species that may contain fewer alkaloids of interest and ultimately assist in the authentication of *Sceletium* material. The hyperspectral method combined with chemometrics was thus substantially more efficient in the chemotaxonomic classification of *S. tortuosum* and related species.

Patnala and Kanfer (2013) performed a chemotypic analysis of six species that were selected based on venation patterns as distinguishing morphological characteristics are often used in taxonomy to assign species identities. The plants were grouped into the 'tortuosum' (*S. tortuosum*, *S. expansum*, and *S. strictum*) or 'emarcidum' type (*S. emarcidum*, *S. exaltum*, and *S. rigidum*). The species of *S. varians* and *S. archeri* were not considered in this study; in fact, these species have largely been ignored in terms of their phytochemical profiles. The 'tortuosum'-type plants, *S. tortuosum* and *S. expansum* were predominantly characterised by the presence of mesembrine, mesembrenone, mesembranol, and epimesembranol. *S. strictum* was found to contain measurable amounts of mesembrine, mesembrenone, and one of two epimers, 4′-O-demethyl-mesembrenone or 4′-O-demethyl-mesembrenol, but mesembranol and epimesembranol were in minute relative amounts. Interestingly, the 'émarcidum' types illustrated a complete absence of the mesembrine class of alkaloids traditionally associated with *Sceletium* such as mesembrine, Δ^7mesembrenone, mesembrenone, and mesembranol. Instead, the émarcidum group had O-demethyl-mesembrenone and O-methyl-joubertiamine as the more prominent metabolites and out of the émarcidum' types, *S. exaltum* showed an accumulation of mesembrine. It was concluded that the distribution of mesembrine-type alkaloids is not distributed across the genus and is limited to only a few species, highlighting the importance of quality control testing in the *Sceletium* genus.

It is hypothesised that the *Sceletium* genus may have recently diversified, with minimal time between speciation events (Klak et al., 2007). As a result, these species have had a very brief period of time to accumulate differences in their DNA and subsequently are very similar in morphology. Little information is currently available with respect to the chemical fingerprints of both *S. crassicaule* and *S. emarcidum*. Patnala and Kanfer (2015) analysed wild material of *S. crassicaule* and *S. emarcidum* using electrospray ionisation mass spectrometry (EI-MS) and LCMS to characterise the chemical fingerprints of specific *Sceletium* alkaloids as a tool for the qualitative identification of lesser investigated alkaloids with complex matrices such as Δ^7 mesembrenone, Sceletium A_4, and epimesembranol. Furthermore, the study assessed the potential of the analytical method as a tool in quality control of *Sceletium* commercial products as tablets derived from *S. tortuosum* were included in the analysis. Their technique successfully identified Δ^7mesembrenone, mesembrenol, mesembrenone, Sceletium A_4, mesembranol epimesembranol and mesembrine from several species of *Sceletium*.

The method identified Sceletium A_4 from *S. crassicaule* material. Of interest, *S. emarcidum* did not have any of the reference compounds, which normally occur in *Sceletium* samples. The investigation did not report on any dominant structures that could

be used for the chemotaxonomic classification of this species, as none of the peaks observed corresponded with the standard alkaloids found in *Sceletium* species.

Apart from plant misidentification and the choice of inferior chemotypes that express poor bioactivity, chemical and heavy metal adulterations as well as herbal adulterations of phytomedicines can lead to undesired cytotoxic effects upon human consumption. Metabolite profiling can thus be a complimentary tool to other techniques for the detection of adulterants in herbal medicines. To this end, Lesiak et al. (2016) performed analysis on *S. tortuosum* commercial material using direct analysis in real-time ionisation coupled with high-resolution time-of-flight mass spectrometry (DART-HRTOF-MS). The method was employed as an authentication tool to identify adulterated samples and found that some commercially available samples were indeed spiked with the banned herbal stimulant ephedrine. Commercial powder mixtures were conveniently analysed directly by dipping the closed end of a melting point capillary tube into the powder substance and then between the DART ion source and mass spectrometer inlet. The authors only quantified two of the detectable compounds, mesembranol ranging from 0.3% to 7.0% and mesembrine at 5.1%, but relative amounts are not available for any of the other compounds in the authors' report. The method provided a rapid forensic diagnostic tool of commercial samples sold in the USA, highlighting illicit practices in the manufacture of *Sceletium*-derived products that are of regulatory concern.

Appley et al. (2022) was another analytical study concerned with the authentication of *Sceletium*-based products for the forensic analysis of products containing *Sceletium*, using robust protocol that detected hordenine and mesembrine-type alkaloids from *Sceletium*. Supporting the method used by Lesiak et al. (2016), the use of direct analysis in real time–high-resolution mass spectrometry (DART-HRMS) resulted in effective and rapid detection and quantification of hordenine and mesembrine-type alkaloids. Ephedrine is a concern in natural products as it is lethal when combined with caffeine or other over-the-counter drugs and could potentially be harmful when consumed with *Sceletium* products (Haller and Benowitz, 2000). An advantage of DART-HRTOF-MS is that sample preparation is not needed and thus not prone to solvent bias. Techniques such as LC-MS and GC-MS may not identify adulterants such as ephedrine due to preferential take-up of hordenine due to its polarity over the adulterant ephedrine as these are constitutional isomers of each other, which both occurred at a nominal *m/z* of 166. The authors emphasised that without the use of DART-HRTOF-MS, the compounds would not have been separated and the adulterant would have thus become more difficult to notice and identify.

The study of plant metabolomes has seen an unprecedented rise since the adoption of systems biology approaches in biological sciences and NMR metabolomics can be the preferred choice for this purpose (Verpoorte et al., 2007; Leiss et al., 2011). The advantage of using NMR for generating an overview of the plant metabolome lies in its vast applications, ranging from quality control of foods and botanicals to studies related to investigating the pharmacological activity of phytochemicals. A limitation of NMR spectroscopy is that, without the use of two-dimensional NMR, absolute quantitation is not possible (Verpoorte et al., 2007). The plants collected at different localities studied by Zhao et al. (2018) using NMR were growing under differing biogeographic environments of the Western Cape and Northern Cape. The study found that NMR chemometrics could be an effective tool to distinguish between populations of *Sceletium* and identify notable biomarkers in each population. *N*-Demethyl-*N*-formylmesembrenone, a biomarker that had not been identified in *Sceletium* before, characterised one of the population groups from the Western Cape. Furthermore, the production of alkaloids may be due to genetic composition rather than climatic conditions since plants in close proximity to each other produced variable amounts of alkaloids, suggesting that climate was not a contributing factor to diversity in chemical profiles. Freund et al. (2018) employed an analytical technique that had never been performed on these plants coined leaf spray mass spectrometry (leaf spray MS) (Table 3). Additionally, the setup included tandem mass spectra (MS/MS). This technique circumvents the separation of plant metabolites using chromatography and offers a direct MS injection without the need for sample preparation or extraction, with minimal technical adjustments to the ionisation source being required. An advantage of this tool is the absence of lengthy extraction protocols and solvent bias that may introduce artifacts or prove inefficient in the recovery of phytochemicals as these may not always be extracted. Leaf spray MS can directly analyse plant tissue providing rapid generation of qualitative and quantitative data albeit accurate quantification is more tricky with this approach. The method was successful in analysing intact plant material reducing the amount of processing needed. For leaf spray MS to have wider application for *in planta* analysis of metabolites, optimisations in terms of plant preparation,

TABLE 3 Methods used for fermentation and results obtained from previous research (↑ =increase, ↓ =decrease).

Extraction method	Fermentation procedure	Analytical technique	Conclusion	Reference
Classical acid–base extraction	Plants crushed with soil, placed in a plastic bag, and sealed in an airtight plastic bag.	GC-MS	↓ 4′-O-Demethylmesembrenol ↓mesembrine ↑mesembrenone	(Smith et al., 1998)
Methanol	Aerial plant parts crushed and placed in plastic bag exposed to sun for 10 days.	HPLC-MS (validated)	↓Mesembrine ↑ Δ^7-Mesembrenone	(Patnala and Kanfer, 2009)
Methanol	Plant material stored in airtight plastic container for 8 days.	NACE-MS	Alkaloid profile remained unchanged, no quantitative data reported.	(Roscher et al., 2012)
Methanol	Aerial plant parts gently bruised and placed in an incubator (40°C) for 7 days	UPLC-MS (validated)	↑ Mesembrine ↓Mesembrenone	(Chen and Viljoen, 2019)

presence or absence of solvents, volume of solvents, voltage amplitude, and distance from the ion inlet may be necessary. Some other limitation of this analytical technique is its low dynamic range, resulting in the most abundant metabolites solely being identifiable. Some of the minor alkaloids or structurally similar alkaloids that require stronger resolving power require greater and more sophisticated technical expertise for their detection. Despite this, the analytical method proved to be a powerful tool that eliminated chromatography for the identification of the main phytochemicals from *S. tortuosum*.

Sandasi et al. (2018) performed a study to assess the quality of herbal tea blends using hyperspectral imaging and UPLC-MS in various *Sceletium* tea blends. Five batches of herbal tea that were claimed by the manufacturers to contain a *S. tortuosum* and *Cyclopia genistoides* (commonly known as honeybush) mixture were obtained pulverised and subjected to hyperspectral imaging without any further processing. For UPLC-MS analysis, the tea blends were prepared by adding boiling water (237 ml) to 1.5 g of plant tissue. For the hyperspectral imaging, the same instrument settings were used as in Shikanga et al. (2013) and applied as a rapid and non-destructive method for the quality control of the tea blends. Using a PLS-DA model, the procedure had a 95.8% predictive ability providing high degrees of sensitivity with a stronger metabolite feature selection. Quantitatively, *C. genistoides* was found to be in higher amounts across the samples (>97%), whereas *S. tortuosum* was found in lower quantities (<3%). For this study, the UPLC-MS conditions were optimised for *C. genistoides* but these conditions were not necessarily optimal for *S. tortuosum*. A major limitation of this particular study was that the UPLC-MS procedure alone could thus not conclusively efficiently distinguish the plant components of the herbal mixtures that contained *S. tortuosum* along with another species. Combining hyperspectral imaging with chemometrics proved a more powerful and reproducible tool for the quality control of herbal tea blends containing *Sceletium* and honeybush.

It is not clear why there are so few reports on the isolation and characterisation of channaine; however, it is likely that analytical methods being used by researchers are not necessarily optimised for the detection of this unusual alkaloid channaine. We speculate that this compound may also be produced at minor levels during the lifetime of the plant, making it even more difficult to isolate. Veale et al. (2018) aimed to structurally elucidate the alkaloid, channaine from *S. tortuosum*. This was the second time that channaine was detected since its initial characterisation by Abou-Donia et al. (1978). This was the first full NMR analysis of channaine in the literature. Chemical structures were resolved using ^{1}H, ^{13}C, COSY, HSQC, and HMBC NMR spectroscopy.

The search for novel chemicals from *Sceletium* species has found renewed interest. Recently, Yin et al. (2019) performed an extraction of *S. tortuosum* and isolated sceletorines A and B for the first time with these authors making suggestions on plausible biosynthetic pathways associated with sceletorine production. This kind of information is largely missing in terms of novel alkaloids that become periodically identified in *Sceletium* samples by different research groups. The isolated alkaloids were established to be precursors of the alkaloid channaine identified in previous studies (Abou-Donia et al., 1978; Veale et al., 2018). It was ruled out that these phytochemicals were artefacts as a result of processing due to their presence in fresh material. Sensitivity, reproducibility, and comparison with a reference method of these two new alkaloids were not presented in the paper.

Reddy et al. (2022) investigate the chemotypic variation across populations of *Sceletium* species. This is one of the few studies looking at the chemical composition of other species in the genus and the only one to report on the chemical composition of *S. rigidum* and *S. emarcidum*. The analytical technique of HPLC-MS-MS was employed, and data were processed using Feature-based Molecular Networking to annotate and investigate the chemical space in greater detail to identify minor and coeluting phytochemicals. The study put forward *in silico* results supporting that minor phytochemicals identified in *Sceletium* species may also be responsible for the therapeutic activities observed in the literature (Harvey et al., 2011; Krstenansky, 2017).

The main challenges associated with the purification and identification of *Sceletium* alkaloids are linked to irreversible adsorption to column packing materials, excessive tailing, and poor recovery as well as catalytic changes encountered with solid supports in various analytical systems (Yang and Ito, 2005). This can be overcome to some extent by high-speed counter-current chromatography (HSCCC) (Shikanga et al., 2011) and non-aqueous capillary electrophoresis coupled to mass spectrometry (NACE-MS) (Roscher et al., 2012).

Overall analytical techniques should be performed to assess sensitivity, reproducibility, and comparison with a reference method (i.e., GC-MS) (Shikanga et al., 2012c; Zhao et al., 2018). From the current state of analytical techniques used in the quality control of *Sceletium*, GC-MS, LC-MS, and HPLC-MS will continue to remain popular going forward (Table 2). However, for the effective identification of adulterants and contamination in samples, more advanced tools in tandem with different detectors need to be utilised. Two analytical techniques that stand out for the rapid analysis of samples are direct analysis in real-time ionisation coupled with high-resolution time-of-flight mass spectrometry (DART-HR-TOF-MS) (Lesiak et al., 2016) and leaf spray MS (Freund et al., 2018). These methods do not require the processing of material, and as such there is no solvent bias, loss of phytochemicals during extraction, or artifacts from extraction procedures. Nevertheless, the limitations of these methods are that the machines are not common, are expensive, and require specialised components that may prove to be more laborious to assemble. With these in mind, the application of NMR analysis coupled with chemometrics (Zhao et al., 2018) will also gain more popularity in quality control assurance practices. Non-destructive methods such as hyperspectral imaging may provide additional analytical power for use in commercial settings (Sandasi et al., 2016, 2018). Further advancements in analytical techniques will likely result in novel methods that may be used in the future.

The major and minor alkaloid classes amongst *Sceletium* species have been shown as a pie chart diagram (Figure 11). This diagram represents what past chemical analysis studies have reported to be detected in *Sceletium*. It should be noted that this is just representative of what the respective authors searched for (refer

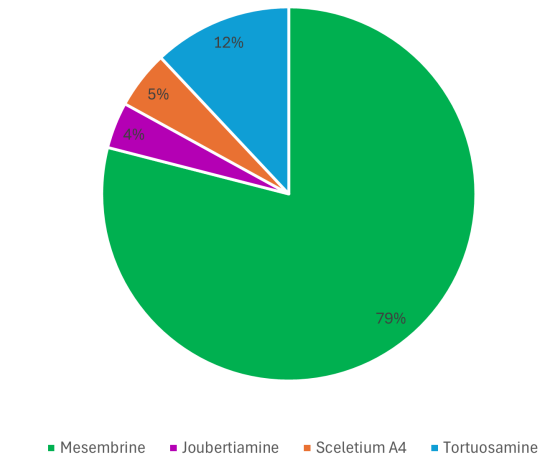

FIGURE 11
Alkaloid diversity reported based on scientific literature across analytical techniques used to study *Sceletium*.

to Table 2) and not of the true alkaloidal distribution *in planta* in *Sceletium*. The distribution of major and minor alkaloid classes in different plants of *Sceletium* has been shown to be highly variable, and at times, plants from the same population may have differing amounts of a particular alkaloid; this has been hypothesised to be resultant from chemical plasticity that may be associated with environmental and genetic responses (Reddy et al., 2022).

Fermentation of *Sceletium*

The fermentation of *Sceletium* and the effect on the medicinally important alkaloids have been of interest due to the traditional preparation and the anecdotal reports of the plant becoming more euphorically potent when fermented (Smith et al., 1996). Although the traditional method of using an animal skin bag is no longer used nowadays, fermentation is thought to enhance the levels of these alkaloids and reduce oxalates, which in turn increases the mood-elevating activity of *Sceletium* (Smith et al., 1996). There seems to be some incongruency in reports related to the effects of fermentation, which further highlights work that needs to be done to better understand the metabolic pathways of these alkaloids and at which steps to manipulate levels.

Many analyses have investigated the effect of fermentation on the alkaloid profile in *S. tortuosum* (Table 3). Smith et al. (1998) used the plastic bag fermentation followed by GC-MS analysis. Their findings indicated that the mesembrine alkaloid composition was comparable with that of the oven-dried (80°C) samples. However, in the fermented sample, there was a significant increase in mesembrenone levels whereas levels of 4′-*O*-demethylmesembrenol and mesembrine decreased. Patnala and Kanfer (2009) further investigated the role of fermentation in alkaloid composition in *Sceletium* using HPLC-MS, where levels of mesembrine decreased [from 1.33% to 0.05% (w/w)], with suspected transformation into Δ^7mesembrenone. Roscher et al. (2012) also investigated the change in alkaloid composition as a result of sample fermentation. No qualitative data were presented in this study; instead, the authors report that no overall change in the alkaloid concentrations as a result of fermentation were detected. The studies conducted up until this point were suggestive that the traditional processing of the plant material through fermentation did not affect the overall potency of the material as there was a decrease or no change in mesembrine levels (Smith et al., 1998; Patnala and Kanfer, 2009; Roscher et al., 2012). However, the most recent study by Chen and Viljoen (2019) reported that the total alkaloid content increased as a result of fermentation. They reported that while mesembrine levels increased (from below 1.6 µg/mL to 7.40 µg/mL–20.8 µg/mL), there was only a marginal increase in mesembrenol and mesembranol content and a significant decrease in mesembrenone content. This study supports the traditional preparation of *Sceletium* plant material to increase the mood-elevating effects of *S. tortuosum*. It may be worthwhile to investigate if phytochemical formation or breakdown is dependent on pH in these analyses and that future analyses should control for this. Previous studies have not indicated the pH of their extracts or used them in their analyses.

Comparing the fermentation studies available in the literature thus far, it is clear that there is no conclusive evidence that fermentation results in a consistent change in the alkaloid profile. More investigation is needed to understand how fermentation affects alkaloids in *Sceletium* and what the best method of fermentation is that most accurately represents traditional ethnobotanical preparation. A better understanding of the biosynthetic pathway(s) could assist in understanding how fermentation influences the metabolite profile. Currently, the biosynthetic pathway of mesembrine-type alkaloids as suggested by Jeffs et al. (1971a) proposed that the perhydroindole portion of mesembrine comes from tyrosine and the aromatic group is derived from phenylalanine. The cinnamic acid derivatives are produced from phenylalanine, but the 3′-aryl oxygen substituent is proposed to be introduced in later steps involving a biosynthetic reaction with sceletenone, mesembrenone, and 4′O-demethylmesembrenone (Jeffs et al., 1978). Since studies in 1971 and 1978, the biosynthetic pathway has not been revised and we thus suggest this become a future avenue of investigation to better understand how fermentation affects the alkaloid profile, pinpointing not only biochemical changes that occur but also the key enzymes and genetic regulatory steps that may control this metabolism.

Present-day ethnobotanical use

Although there is limited current ethnobotanical information on the prevalence of use of the *Sceletium* genus in modern times, the work by Philander (2011) focusing on a group of Rastafarian herbalists clearly points out to the importance of *S. tortuosum* as the main species that is collected as a phytomedicine to reduce depression and anxiety and in some cases, it is consumed together with *Cannabis sativa*, for spiritual purposes (Schell, 2014). With the

increased public interest in biogenic drugs such as *Sceletium*, numerous companies have appeared online selling *Sceletium* in raw powdered form, tablets, teas, and snuffs. This increased popularity may well pose a significant conservation threat to the species if populations are collected from the wild. It appears that some of the present-day uses by indigenous communities of the plant are consistent with the historical uses, i.e., for euphoria and as a mood elevator (Smith et al., 1996; Gericke and Viljoen, 2008).

Biological activities of *Sceletium* extracts and isolated alkaloids

There are limited reports that support the hunger and thirst suppression effects that are claimed of *Sceletium*. There are, however, several reports on the 'mood elevation' activity, particularly focussed on the potential of *Sceletium* to aid with anxiety and depression (Table 4). Recently, there have been more studies that are focused on the pharmacology of *Sceletium*, notably in areas linked to *in vivo* actions and clinical trials of tested extracts (Table 4). The body of pharmacology research on *Sceletium* is quite extensive, with the majority of the reported biological activity being interactions with the central nervous system (CNS) and related neurological pathways (antidepressant, anxiolytic, and psychoactive activity). The scope of the observed CNS activity is broad with observed anxiolytic and antidepressant activity demonstrated for extracts and isolated compounds of *Sceletium* (Table 4). Additionally, there are more *in vivo* behavioural inquiries on rats using a range of pharmaceutical tests (Figure 6D) exhibiting CNS-related activities ranging from suppressant (e.g., anxiolytic and sedative) to excitatory (e.g., antidepressant) activity. Although there is a shift to more *in vivo* studies, there is still much to be tested in terms of different chemotypes and to understand the pharmacokinetics of individual phytochemicals and potential synergism between phytochemicals, aside from mesembrine.

Bennett and Smith (2018) confirmed that a high-mesembrine *Sceletium* extract, Trimesemine™, could hold potential therapeutic activity in cytokine-induced depression, and they propose that the extract modulates the basal inflammatory cytokine profile whilst maintaining that there is no change in the acute response to pathogenic challenge. Furthermore, these findings illustrate a direct benefit to the attenuation of systemic low-grade inflammation in immune cells. This particular study did not test individual alkaloids, and such could not pinpoint the phytochemical constituent(s) responsible for the observed activity. In the future, chemical isolates may prove beneficial if the intention is to correlate bioactivity with specific alkaloid constituents so that our overall understanding of which phytochemicals hold bioactivity can be clarified.

Receptor screening of Zembrin® (a standardised extract of *Sceletium tortuosum*) was conducted against 77 radioligand binding assays (0.75 mg/mL and a panel of phosphodiesterases) to compile a comprehensive list of potential CNS and other pharmacological targets (Harvey et al., 2011). The extract showed binding at the serotonin (5-HT) transporter, δ2- and μ-opioid receptors, the cholecystokinin-1 receptor, >80% inhibition at GABA receptors (non-selective), and PDEs 3 and 4 (Harvey et al., 2011). Some of the therapeutic applications of these targets are emesis, obesity, anxiety, and migraine linked to the serotonin (5-HT) transporter (Pithadia and Jain, 2009). The δ2- and μ-opioid receptors are involved in maintaining epileptic seizure, emotional responses, immune function, obesity, cell proliferation, respiratory and cardiovascular control, and several neurodegenerative disorders (Feng et al., 2012). The cholecystokinin-1 receptor is involved in gastrointestinal and metabolic diseases (Berna and Jensen, 2007), whereas GABA receptors are involved in pathologies ranging from epilepsy, schizophrenia, anxiety disorders, and premenstrual dysphoric disorder (Wong et al., 2003). The PDE3 receptor is responsible for platelet activation/aggregation (Beca et al., 2011) and vascular smooth muscle proliferation (Beca et al., 2011; Begum et al., 2011), whereas the PDE4 receptor is linked to inflammatory conditions including asthma, chronic obstructive pulmonary disease (COPD), psoriasis, atopic dermatitis (AD), inflammatory bowel diseases (IBD), rheumatic arthritis (RA), lupus, and neuroinflammation (Li et al., 2018). This report only presented findings on the affinity of Zembrin® to different receptors. Further studies would need to be investigated for activity against these specific pathologies. Plant extracts have numerous metabolites that work in synergy to affect their biological influence, and it is thus possible that multiple metabolites are potentiating the mood-elevated activity aside from mesembrine alone, as suggested by Lubbe et al. (2010). The Harvey et al. (2011) study supports ethnobotanical use as a mood elevator by the observed serotonin transport activity in response to Zembrin®. The serotonin receptor influences a myriad of biological and neurological processes such as anxiety, appetite, aggression, and depression (Mück-Šeler and Pivac, 2011; Zhang and Stackman, 2015). Evidence of anxiolytic effects of *Sceletium* in humans (Gericke and Viljoen, 2008) has partially been supported in a study using a rat model of restraint induced stress (Smith, 2011). The binding of compounds to various sites on the 5-HT transporter (SERT) is considered evidence of potential serotonin reuptake inhibition, a common target of antidepressant drugs. A selection of alkaloids, mesembrine, mesembrenone, and mesembrenol, from *Sceletium tortuosum*, were tested for their affinity for SERT with *Ki*'s of 1.4 nM, 27 nM, and 63 nM, respectively (Harvey et al., 2011). These values were significantly higher than other alkaloids, such as buphanidrine or distichamine, isolated from Amaryllidaceae, with reported *Ki*'s of 312 μM and 868 μM, respectively (Neergaard et al., 2009). These compounds have been found to already possess well-established antidepressant activity, found in *Boophone disticha* (L.f.) Herb (Amaryllidaceae) (Neergaard et al., 2009). There is some evidence that argues against *Sceletium* purely acting as a selective serotonin reuptake inhibitor (SSRI), as repeated administration of SSRIs has been linked to hyposensitivity to SSRIs, as a result of an upregulation in PDE4 (Ye et al., 2000). However, it has been demonstrated that PDE4 activity decreased after *Sceletium* administration (Harvey et al., 2011). The Harvey et al. (2011) study was the only one testing a *S. tortuosum* extract on a number of receptors. Although the authors' study looked at the pharmacokinetics of individual compounds against each receptor, it may be valuable to examine the extracts with varying concentrations of compounds as a means to assess samples in a context more aligned with ethnobotanical use.

TABLE 4 The CNS-related activity of *Sceletium tortuosum* extracts and compounds (*Note that TRI is an extract of a *S. tortuosum* and *S. expansum* hybrid).

Effect	Compound/ extract	Model/target	Positive control	Formulation/ dosage	Result/mechanism/ method	Reference
Alzheimer's dementia	**Zembrin** extract	Neuropsychological tests: CNS Vital Signs and Hamilton depression rating scale (HAM-D) (targeted at PDE-4)	Placebo capsule, no herbal extract	*In vivo*—clinical trial 25 mg	Zembrin significantly improved cognitive flexibility ($p < 0.022$) and executive function ($p < 0.032$) as compared with placebo	(Chiu et al., 2014)
Analgesic	**Zembrin** extract	Rat pharmaco-EEG (Tele-Stereo-EEG)	0.9% NaCl (1 ml/kg), showed minor effects to delta and alpha2 power in frontal cortex	*In vivo* 1.0, 2.5, 5.0, and 10.0 mg/kg	Zembrin showed second strongest effects were reduction in both the delta and the theta signals	(Dimpfel et al., 2016)
	Full **alkaloid extract**, the **alkaloid enriched fraction**, and **mesembrine**	Hotplate assessment of analgesic activity	Morphine (5 mg/kg), increased hotplate latency response	*In vivo* 100, 20, and 20 mg/kg	Mesembrine showed an increased hotplate latency response.	(Loria et al., 2014)
Antidepressant	**Zembrin** extract	Flinders Sensitive Line (FSL) rat model in Forced swim assessment and open field test (OFT) of antidepressant activity	Escitalopram	*In vivo* 5, 10, 25, 50, or 100 mg/kg	Zembrin at doses of 25 mg/kg and 50 mg/kg significantly reduced immobility compared with saline controls—supporting dose-dependent antidepressant-like activity	(Gericke et al., 2022)
	Chloroform extract of *S. tortuosum*	Chick anxiety-depression model	Imipramine (10 mg/kg), exhibited no effects in anxiety phase but increased $DVoc^3$ in early and late phase depression state.	*In vivo* 10, 20, 30, 50, 75, 100 mg/kg	At concentrations of 10 mg/kg-30 mg/kg extract showed no effect on depressive state. Concentration of 75 mg/kg-100 mg/kg exhibited no effect on depressive state.	(Carpenter et al., 2016)
	Zembrin extract	Rat pharmaco-EEG (Tele-Stereo-EEG)	Citicoline (46 mg/kg), rolipram (0.1 mg/kg	*in vivo* 1.0, 2.5, 5.0 and 10.0 mg/kg	Attenuation of alpha1 waves emerged during the highest dosage in all brain areas.	(Dimpfel et al., 2016)
	Trimesemine extract (TRI*)	Cell culture (SERT and VMAT-2: human astrocytes and murine hypothalamic neurons)	10 µM citalopram, significant downregulation of SERT and no effect on VMAT-2	*In vitro* 1.0, 0.1, 0.01, 0.001, and 0.0001 mg/m	1 mg/ml extract showed comparable activity with positive control (15 min, SERT), 1 mg/ml and 0.1 mg/ml extract showed comparable activity with citalopram (30 min, SERT). Significantly higher VMAT-2 expression noted at extract concentration of 1 ml/ml (15 min, VMAT-2)	(Coetzee et al., 2016)
	Full **alkaloid extract**, the **alkaloid enriched fraction**, and **mesembrine**	Forced swim assessment of antidepressant activity	Imipramine (15 mg/kg), decreased float time	*In vivo* 100, 20, and 20 mg/ kg, respectively	Mean float time for alkaloid enriched fraction was significantly lower than vehicle.	(Loria et al., 2014)
	Zembrin extract, **mesembrine**, **mesembrenone** and **mesembrenol**	5-HT transporter binding assay and PDE4 inhibition (77 radioligand binding assays in broad receptor profiling)	Range of controls for each receptor	*In vitro* 750 µg/ml for Zembrin, 3 M for isolated compounds	Zembrin exhibited potent 5-HT binding (IC_{50} 4.3 g/ml) and PDE4 inhibition (IC_{50} 8.5 g/ml). The isolated alkaloid, mesembrine was the most active alkaloid against the 5-HT transporter (Ki 1.4 nM), whereas mesembrenone was active against the 5-HT transporter and PDE4 (IC50's < 1 M). More than 50%	(Harvey et al., 2011)

(Continued)

3 Distress vocalizations in an avian model.

TABLE 4 Continued

Effect	Compound/ extract	Model/target	Positive control	Formulation/ dosage	Result/mechanism/ method	Reference
					inhibition was observed in the 5-HT transporter, GABA receptors, 2-opioid receptors, and cholecystokinin-1 targets.	
Anti-epileptic	**Zembrin** extract	Glutamate receptor assays (rat hippocampus) NMDA receptor, AMPA receptor, Metabotropic Glutamate Group I/ II receptor, Metabotropic Glutamate Group III receptor	0.05 µM trans ACBD (NMDA agonist) - slight but significant decrease in signal, 0.10 µM (S)-(-)-5-fluorowillardine (AMPA agonist)- not able to exert action, 0.025 µM (±) trans ACPD (metabotropic glutamate receptor I/II agonist)—no change in signal, 0.05 µM O-Phospho-L-Serine (Metabotropic Glutamate Group III receptor agonist)- no change in signal	*ex vivo* 5 and 10 mg/kg Zembrin per day	Repetitive Zembrin administration resulted in mediation of AMPA and NMDA receptor associated with epileptic episodes.	(Dimpfel et al., 2018)
	Mesembrine, **Mesembranol**, **Mesembrenol** and **Mesembrenone**	Glutamate receptor assays - Artificial cerebrospinal fluid (ACSF)	0.10 µM (S)-(-)-5-Fluorowillardine	*In vitro* 8.65 nM Mesembrine, 17 nM for mesembranol, mesembrenol, and mesembrenone	Mesembrenol and mesembranol were able to prevent action of AMPA agonist associated with epileptic seizures.	(Dimpfel et al., 2018)
Anxiolytic	**Ethanolic extract** of **Zembrin (isolated compounds)**	Zebrafish model assay (Thigmotaxis and locomotor activity)	Diazepam (2.5, 5, 10 µM) exhibited best anxiolytic activity at 10 µM.	*In vivo* (extracts at 10, 15, 30, 50 µM)	Mesembrine, mesembranol, mesembrenol, and mesembrenone all demonstrated anxiolytic-like activity (50 µM illustrated highest activity).	(Maphanga et al., 2022)
	Chloroform extract of *S. tortuosum*	Chick anxiety-depression model	Imipramine (10 mg/kg), exhibited no effects in anxiety phase but increased DVoc in early and late phase depression state.	*In vivo* 10, 20, 30, 50, 75, 100 mg/kg	At concentrations of 10-30 mg/kg extract showed no effect on anxiety. Concentration of 75 mg/kg-100 mg/kg exhibited anxiolytic activity.	(Carpenter et al., 2016)
	Full **alkaloid extract**, the **alkaloid enriched fraction**, and **mesembrine**	Elevated plus maze assessment of anxiolytic activity	Chlordiazepoxide (5 mg/kg), spent more time on the open arms than vehicle control	*In vivo* 100, 20, and 20 mg/ kg, respectively	No observed reduction in anxiety. None of the samples altered the time spent on open arms (none statistically significant)	(Loria et al., 2014)
	Zembrin extract	Pharmaco-fMRI (Perceptual-Load and Emotion-Matching Task) human trial (5-HT and PDE4)	Placebo capsule, only inert excipients	*In vivo*—clinical trial 25 mg	Zembrin resulted in a reduction in anxiety through reduction of amygdala reactivity in response to unattended facial fear.	(Terburg et al., 2013)
	Methanol extract of *S. tortuosum*	Elevated plus maze for psychological stress	0.85% sterile saline	*In vivo* 5 or 20 mg/kg/day of *S. tortuosum* extract for 17 days by daily oral gavage	Low doses (5 mg/kg/day) of extract showed marginal positive anxiolytic effects however both doses (5 and 20 mg/kg/day) illustrated negative side effects (inflammation and immune suppression).	(Smith, 2011)

(Continued)

TABLE 4 Continued

Effect	Compound/ extract	Model/target	Positive control	Formulation/ dosage	Result/mechanism/ method	Reference
Ataxia	Full **alkaloid extract**, the **alkaloid enriched fraction**, and **mesembrine**	Rotarod assessment of ataxia	Muscimol (2 mg/kg), fell off the drum significantly faster than vehicle treated group	*In vivo* 100, 20, and 20 mg/ kg, respectively	The alkaloid-enriched fraction showed statistically lower times in assay and higher possibility of ataxia than mesembrine and full alkaloid extract.	(Loria et al., 2014)
Cognitive-enhancement	**Zembrin** extract	Rat pharmaco-EEG (Tele-Stereo-EEG)	0.9% NaCl (1 ml/kg), showed minor effects to delta and alpha-2 power in frontal cortex	*In vivo* 1.0, 2.5, 5.0, and 10.0 mg/kg	Comparable activity observed in Zembrin as seen in controls, Rolipram and Citicoline. Reduction in activity observed in dopaminergic and glutamatergic transmitter systems	(Dimpfel et al., 2018)
Neurodegenerative (Alzheimer's dementia and Parkinson's)	**Trimesemine** extract (TRI*)	Enzyme assays (MAO-A and AChE)	Galanthamine (0.0025 mg/ml, AChE), clorgyline (0.015 mg/ml, MAO-B)	*In vitro* 1.0, 0.1, 0.01, 0.001, and 0.0001 mg/m	TRI showed 30% inhibition against AChE at concentration of 2 mg/ml (IC_{50} AChE: unattainable, IC_{50} Galanthamine: 12.4 µg/ml). TRI showed 40% inhibition against MAO-B at concentration of 2 mg/ml (IC_{50} MAO-B: 408 µg/ml, IC_{50} clorgyline: 0.015 mg/ml)	(Coetzee et al., 2016)
Ergogenic[4]	**Zembrin** extract	Mood questionnaire a visual analog scales (VASs) – to assess fatigue and focus. Additionally, reactive performance assessments: multiple object tracking.	Not applicable	Not applicable	Significant improvement was observed in reactive performance in complex reactive task to improve cognitive load. No improvement in mood for sample group.	(Hoffman et al., 2020)

In vivo testing of *Sceletium* alkaloids has been performed using rat models designed for mental disorders such as neurodegeneration, like Alzheimer's disease (AD), epilepsy, and depression (Loria et al., 2014) (Figure 6C). Loria et al. (2014) found that mesembrine from *S. tortuosum* had analgesic and antidepressant activity. *Sceletium* species have exhibited potential therapeutic activity *in vivo* using rodent models for AD, anxiety, and depression (Gericke and Viljoen, 2008; Krstenansky, 2017). A summary of the CNS-related activity, together with the recent anti-inflammatory activity of *Sceletium*, is presented in Table 4. With the PDE4 activity of *Sceletium* extracts noted by Harvey et al. (2011) and new *in vivo* on the receptor itself, there is evidence suggesting that inhibitors from *Sceletium* can aid to reverse depression, improve cognitive ability, and reduce anxious states. The anxiolytic activity of *Sceletium* may be attributed to other mechanisms in addition to serotonin-reuptake inhibition such as monoamine release (Coetzee et al., 2016). *In vivo* testing of *Sceletium* alkaloids has been performed using rat models designed for mental disorders such as neurodegeneration, like Alzheimer's disease (AD), epilepsy, and depression (Loria et al., 2014) (Figure 6C). Loria et al. (2014) found that mesembrine from *S. tortuosum* had analgesic and antidepressant activity. *Sceletium* species have exhibited potential therapeutic activity *in vivo* using rodent models for AD, anxiety, and depression (Gericke and Viljoen, 2008; Krstenansky, 2017). A new structure–function relationship for *Sceletium* alkaloids was suggested by Timoneda et al. (2019); tests performed on rats using Zembrin® found new evidence of electric excitability of the rat hippocampus supporting this new relationship.

The summarised findings of the proposed molecular mechanisms related to the mood elevation and neuroprotective and anti-inflammatory activity of *Sceletium* is presented in Figure 12. The exact mechanisms of action in the case of *Sceletium* and its alkaloidal metabolites are largely unknown; however, some receptor-based *in vivo* and clinical trials have been performed.

Mesembrenone has shown anti-tumour activity against a murine non-tumoral fibroblast cell line and a human tumoral cell line (Molt4), and Weniger et al. (1995) tested 25 alkaloids from Amaryllidaceae with only mesembrenone showing some specificity for Molt4 cells. Extracts high in mesembrine and Δ^7 mesembrenone were shown to exert anti-inflammatory and

4 Increase in capacity for mental strain and reduction in fatigue.

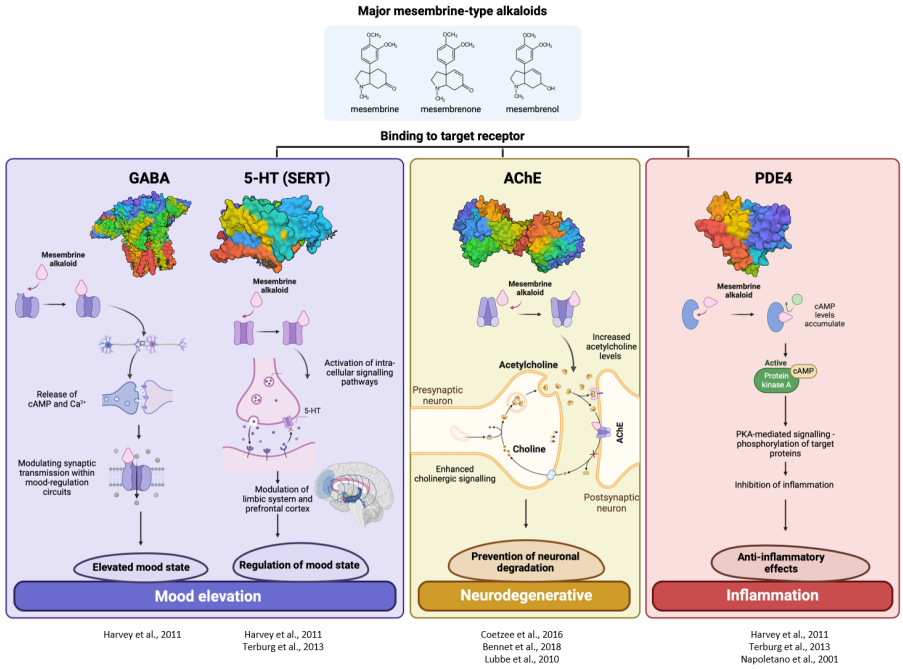

FIGURE 12
Summary of the mechanistic actions reported in literature for *Sceletium* mesembrine metabolites acting on targets regulating mood elevation (GABA and 5-HT), neurodegenerative disease (AChE), and inflammation (PDE4).

antioxidant activities *in vitro*, respectively (Bennett et al., 2018). The mesembrine-rich extract, which was less refined as compared with the Δ^7 mesembrenone extract, exhibited broad dose range efficacy and may serve as a promising therapeutic in the setting for chronic diseases, being safe when administered at low doses. Due to the aetiology of both diabetes and obesity being linked to inflammation and excess glucocorticoid production, these findings may hold value in chronic lifestyle disease management such as diabetes types 1 and 2. For such data to be translated into a pharmaceutical drug discovery chain, endocrine-immune (IL-6 and MCP-1) interactions need to be investigated.

The potential therapeutic activity of mesembrine alkaloids toward inflammatory diseases ranging from asthma, chronic obstructive pulmonary disease, psoriasis, and treating depression has been investigated (Houslay et al., 2005). The anti-inflammatory activity is suspected to be due to the activity of mesembrine-HCl acting as an inhibitor of phosphodiesterase-4 (PDE4), with observed activity at an IC_{50} of 29 µM (Napoletano et al., 2001). The selective inhibition of the PDE4 family of enzymes is predicted to generate great functional effects, as evidenced by PDE4 enzymes being a major therapeutic target for inflammatory diseases (Gericke and Viljoen, 2008). PDE4 has also been identified to play a role in the inflammatory system (Banner and Trevethick, 2004; Dastidar et al., 2007; Li et al., 2018). Harvey et al. (2011) found that the alkaloids mesembrenol, mesembrine, and mesembrenone inhibited PDE4B with IC_{50} values of 16, 7.8, and 0.47 µM, respectively. The positive control, rolipram, had an IC_{50} for PDE4B of 0.13 µM (MacKenzie and Houslay, 2000). Another enquiry illustrated the activity of Zembrin® *in vivo* to correlate this mechanism of action observed *in vitro* in freely moving rats interpreted as an electopharmacogram[5] (Dimpfel et al., 2016).

More recent studies include the work of Reay et al. (2020), where the anxiolytic properties of Zembrin® were assessed in a double-blind, placebo-controlled behavioural study with healthy human volunteers. A dose of 25 mg was administered, and stress was assessed amongst young human adults using multitasking and simulated public speaking frameworks. The study failed to replicate previously reported enhancement of cognitive function, and this was the first evidence of Zembrin® having no impact on non-executive memory processing in healthy participants.

Maphanga et al. (2020) assessed the anxiolytic activity in a zebrafish behavioural assay for a number of medicinal plants, one of which was *S. tortuosum*. Additionally, no toxic effects were observed on the zebrafish in the assay. The model proves to be an appropriate and repeatable assay for assessing the anxiolytic activity of *Sceletium* extracts. Supporting this work is the rising application of the zebrafish animal model as it is claimed to be adequately comparable with humans, sharing approximately 70%–80% genetic homology with humans (Barbazuk et al., 2000; Goldsmith, 2004). The ergogenic effect of a *S. tortuosum* supplement was studied using men and women for 8 days (Hoffman et al., 2020), but no benefits in mood were observed. However, there were significant improvements noted in complex reactive performance tasks that include the stress of cognitive load. Other forms of

5 An analysis recording the field potentials in the frontal cortex, striatum, hippocampus and reticular formation while administered drugs.

assessments linked to measuring cognitive and mood information may yield different results. Furthermore, no pharmacokinetics and absorption data were presented in the study.

Maphanga et al. (2022) assessed isolated alkaloids from the extract described in Shikanga et al. (2011), at concentration ranges of 10 µM, 15 µM, 30 µM, and 50 µM with the greatest activity across alkaloids observed at 50 µM, using a zebrafish assay that focused on toxicity, measured as MTCs (maximum tolerated concentrations), where locomotor activity was above 50 µM. The study of Gericke et al. (2022) reported that Zembrin at doses of 25 mg/kg and 50 mg/kg was effective as an antidepressant in the forced swim test (FST) and performed better than the control (escitalopram). This was the first study to date that compared Zembrin with an SSRI in a rodent model of this kind, supporting the therapeutic use of *S. tortuosum* for mood disorders.

Bioavailability studies on *Sceletium* and its alkaloids are greatly lacking in research. Shikanga et al. (2012a) presented findings on the permeability of mesembrine across the buccal, intestinal, and sublingual mucosal membranes. In that study, mesembrine had a higher permeability across intestinal tissue than the positive control caffeine but the permeability was lower in the buccal and mucosal sublingual membranes. Manda et al. (2017) showed that the oral bioavailability of mesembrine and mesembrenone in mouse plasma (using UHPLC-QToF-MS) was poor and below the detection limit. Bioavailability information regarding other alkaloids and chemotypes from *Sceletium* is still not documented in terms of data on the permeability of these alkaloids across buccal, intestinal, and sublingual mucosal tissues. It is thus imperative that more attention should be placed on such to provide new evidence linked to bioavailability in order to support or refute ethnobotanical claims. It may also be of interest to monitor cultivated and commercially available samples for pesticide residues and toxic alkaloids in other plants that may have mistakenly been gathered during the harvesting of wild populations of *S. tortuosum*, as this species is often found under the canopy of other small shrubs in the wild and in close association with a diverse range of other species. At this present time, there is no information in this respect and the monitoring of plant or chemical contaminants is thus urgently needed.

Biological associations

Recently, a new avenue of investigation was based on investigating the association of endophytic fungal communities on *S. tortuosum* (Manganyi et al., 2018) (Table 5). *Fusarium, Aspergillus*, and *Penicillium* were amongst the fungal endophytes found in the plant. In total, there were 60 endophytic fungal species successfully isolated and identified, belonging to 16 genera. The antibacterial activity of this endophytic fungi was also investigated, where it was found that some fungal isolates could provide sources of novel antimicrobial agents against antibiotic-resistant strains (Manganyi et al., 2019). This is also the first investigation to report on secondary metabolites from endophytic fungi, *F. oxysporum* (GG 008, accession no. KJ774041.1), isolated from *S. tortuosum* (Manganyi et al., 2019).

Plant propagation techniques

Faber et al. (2020) reported on the influence of soilless growth medium (pure silica sand, 50% silica sand with 50% coco peat, 50% silica sand with 50% vermiculite, and 50% silica sand with 50% perlite) and fertigation regimes (nutrient solution administered in intervals from 1 to 5 weeks) on shoot and root growth as well as how these factors influenced alkaloid levels (Δ^7-mesembrenone and mesembrine). Higher mesembrine levels were detected in the shoots whereas roots had higher concentrations of mesembrenone and Δ^7-mesembrenone. The major observation is that the influx of secondary metabolites in *S. tortuosum* seems to possibly respond to biotic and abiotic factors (Bourgaud et al., 2001; Ashraf et al., 2018).

To date, there have only been three studies investigating the micropropagation of the medicinally important, *S. tortuosum* (Sreekissoon et al., 2021a, 2021b; Makunga et al., 2022). The illegal harvesting and exploitation of *S. tortuosum*, due to the demand as a recreational drug linked to its euphoric properties, is a driving factor for the dire need for the development of micropropagation techniques. This approach could offer a direct and standardised source of mesembrine alkaloids. Sreekissoon et al. (2021b) investigated whether *in vitro* regeneration of micropropagules with auxins could be acclimated *ex vitro*. Sreekissoon et al. (2021a) confirm how smoke water influences the germination, seedling vigour and growth of *S. tortuosum* when it is applied at ratio of 1:1,000. A limitation of these studies was that key biomarker compounds were not monitored in the microplant regenerates. Makunga et al. (2022) generated different *in vitro* morphotypes and showed for the first time that Δ4-mesembrenone, mesembrenol, mesembrine, and mesembranol accumulate in micropropagated plants and callus. The utilisation of micropropagation using the dehydrating and rehydration technique outlined in this report resulted in *in vitro* mesembrine accumulation comparable with wild-type material collected (Zhao et al., 2018).

Legislation, toxicology, and safety of *Sceletium* alkaloids

Toxicological assessments on *Sceletium* are limited with the first formal *in vivo* toxicological assay being performed by Murbach et al. (2014) on the mesembrine-rich extract Zembrin® (Table 5). They found that Zembrin®, in male and female Crl:(WI)BR Wistar rats, showed no mortality or treatment-related adverse effects spanning 14 or 90 days with doses of 600 mg/kg bw/day and 5,000 mg/kg bw/day, respectively (Murbach et al., 2014). A greater effort in understanding cytotoxic effects of *Sceletium*-derived extracts and their potential drug–herb interactions is also urgently needed. However, Brendler et al. (2021) indicated that there are no drug–herb interactions that are currently known, although these authors indicate for wise use of serotonin uptake or release medications that may be prescribed for psychiatric conditions.

Clinical administration of *S. tortuosum* has been carried out by Gericke (2001). The clinical case study reported on three individuals who have been prescribed *S. tortuosum* in tablet form. Patients were

TABLE 5 Other notable biological activity of *Sceletium tortuosum* extracts and compounds (*Note that TRI is an extract of a *S. tortuosum* and *S. expansum* hybrid).

Effect	compound/ extract	Model/Target	Positive control	Formulation/ dosage	Result/ mechanism/method	Reference
Anti-bacterial	Secondary metabolites from endophytic fungi on *S. tortuosum* (tested against Gram-positive and Gram-negative bacteria)	Disc diffusion assay	*Enterococcus gallinarum*	*in vitro* 1×10^7 cells/mL of bacteria suspensions for each isolate	*Fusarium oxysporum* displayed antibacterial activity, linked to high levels of 5-hydroxymethylfurfural (HMF) and octadecanoic acid. Narrow spectrum of activity observed in 15% of the fungal extracts.	(Manganyi et al., 2019)
Anti-HIV	*S. tortuosum* extract	Inhibition activity against HIV-1 enzymes; HIV-1 protease assay, HIV-1 reverse transcriptase colorimetric assay and HIV-1 Integrase colorimetric assay	10 µg/mL Acetyl pepstatin (92.6%), 25 µg/mL Doxorubicin (90.1% inhibition), Sodium azide	*in vitro* 25, 50, 100, 150, 200 and 250 µg/mL (Protease assay). 25, 50, 100, 150, 200, 250 µg/mL (reverse transcriptase assay). 0.2, 0.4, 0.8, 1 and 2 mg/mL (integrase assay)	Inhibition of protease (PR) and HIV-1 reverse transcriptase (RT) by ethyl acetate and ethanol extracts, respectively.	(Kapewangolo et al., 2016)
Anti-inflammatory	*S. tortuosum* extract (two extraction method samples)	Human astrocyte viability assay	20 µg/ml *Escherichia coli* lipopolysaccharide (LPS)	*ex vivo* 1 mg/ml extract A and 3.7 mg/ml extract B	Mesembrine-rich extract showed cytoprotetive and anti-inflammatory activity. Extract B showed notable activity in improving the capacity of reductive capacity in basal mitochondria.	(Bennett et al., 2018)
Anti-oxidant	*S. tortuosum* extract (two extraction method samples)	DPPH inhibition	Ascorbic acid	*in vitro* 1 mg/ml extract A and 3.7 mg/ml extract B	Extract B showed good activity in that the total phenolic content was 20 times higher than A and performed comparably with the positive control (ascorbic acid)	(Bennett et al., 2018)
Bioavailability (Mucosal transport)	Plant extract (MeOH, water, Acid extract, pure alkaloids)	Intestinal, buccal and sublingual transport studies	40 µg/mL Caffeine	*in vitro* Mesembrenone: 90 µg/mL, Mesembrenol: 80 µg/mL, Mesembrine: 40 µg/mL, and mesembranol: 40 µg/mL (Pure extracts). Plant extract at 40 µg/mL)	The water extract illustrated best permeability. Overall alkaloids from *S.* tortuosum showed relatively good permeability across sublingual mucosal tissue and poor permeability across buccal tissue.	(Shikanga et al., 2012a)
Immunomodulatory	Trimesemine™ (TRI*)	Primary human monocyte viability	1 mg/ml LPS	*in vitro* 0.01 mg/ml or 1 mg/ml TRI extract	An up-regulation of monocyte IL-10 secretion illustrated anti-inflammatory activity of TRI at a basal level. No cytotoxic effects noted.	(Smith, 2018)
Neuro-protection	*S. tortuosum* extract (two extraction method samples)	Enzyme assays, AChE and tyrosinase	Galantamine and kojic acid	*in vitro* 1 mg/ml extract A and 3.7 mg/ml extract B	Extract A illustrated mild inhibitory effects (IC_{50} – 1.621 ± 0.75) while extract B acted as a potent inhibitor (IC_{50} – 0.5908 ± 0.01).).	(Bennett et al., 2018)
Stress and hypertension	Zembrin extract	Randomised, double-blind, parallel-group, placebo-controlled single centre study	D4-cortisol (15 ng)	*in vivo* Clinical trial. 8mg extract Sceletium tortuosum (Zembrin), 25 mg extract Sceletium tortuosum (Zembrin), and placebo treatment	The apparent difference in vital signs over duration of screening period (3 months). Doses were well tolerated with reported improvements in anxiety in sleep.	(Swart and Smith, 2016)
Safety and tolerance	Trimesemine™ (TRI)	Steroid levels in human adrenocortical	10 µM Forskolin, increased steroid	*in vitro* 1 mg/ml and 1 µg/ml	Inhibition in androstenedione and	(Nell et al., 2013)

(Continued)

TABLE 5 Continued

Effect	compound/ extract	Model/Target	Positive control	Formulation/ dosage	Result/ mechanism/method	Reference
		carcinoma cells (H295R - steroidogenesis).	production significantly (2.3-fold) in all pathways		testosterone production across all doses was observed. The highest dose of TRI (1 mg/ml, 34.5 µM mesembrine) decreased 16-hydroxyprogesterone levels…	
Toxicity and sub-chronic toxicity	Zembrin extract	Repeated dose oral toxicity in rats	Vehicle control	*in vivo* 0 (vehicle-control), 250, 750, 2500 and 5000 mg/kg bw/day by gavage (14-day study) and f 0 (vehicle-control), 100, 300, 450 and 600 mg/kg bw/day by gavage (90-day study)	Within populations of Crl: (WI)BR Wistar rats, irrespective of gender. No adverse effects were noted at a dose of 600 mg/kg bw/day in a 14- and 90-day study.	(Murbach et al., 2014)

being treated for anxiety and depression with one patient having been diagnosed with a personality disorder (dysthymia). In the latter case, the patient described an overall decrease in anxiety and was more able to cope with stress in her life. There were no apparent withdrawal symptoms for all three individuals once they stopped taking the treatment.

The plant is often marketed as a food supplement in the South African natural products sector and not as a scheduled drug. According to Brendler et al. (2021), regulation of herbal medicinal products is highly complex and heterogenous because it is linked to country-specific legislation that governs the use of natural products in different parts of the world. These authors provided a comprehensive and detailed discussion with regard to regulatory legislation that governs the use of *Sceletium* for human consumption. Some of the key points incorporated in that paper are summarised briefly below.

In Europe, at present, *Sceletium*-based products have not been legally approved, but in Russia, specifically, such products fall under the category of scheduled pharmaceutical drugs. Zembrin®, a standardised extract, has had a 'generally recognised as safe' (GRAS) status in the United States of America since 2011, allowing for its inclusion in dietary supplements. On the other hand, in Canada, natural products with *Sceletium* have been approved since 2014 and a wide range of different products are thus available to consumers. Brendler et al. (2021) advocate for an intensive push to research, not only Zembrin® but also other standardised extracts in clinical settings to circumvent regulatory and legislative barriers that may be restricting a wider acceptance and entry of *Sceletium* products into global markets. The United Nations Office on Drugs and Crime flagged *Sceletium* as a plant of concern when reporting on substances of concern in 2013 as part of a report on the obstacles in the identification and regulation of new psychoactive substances (UNODC, 2013). The nature of *Sceletium* being classified as herbal or dietary supplements often exempts it from mandatory testing by the US Food and Drug Administration (FDA). Thus, without adequate quality control and authentication systems in place, herbal product producers can adulterate samples with other stimulants such as ephedrine (which has been banned in herbal products and supplements in Germany) (Lesiak et al., 2016).

Dietary supplementation is popular for those that partake in sports recreationally or as professional athletes, and sports performance-enhancing natural products are thus highly sought after. Legislation around the utilisation of *S. tortuosum* extracts for elite athletes in competitive sports as a dietary supplement hangs in the balance as some regulatory bodies have denoted its status under the categories of 'unauthorised novel food', and it is included also in the European Food Safety Authority Compendium of Botanicals as concerning for human consumption (Jędrejko et al., 2021). Due to its effects on brain function and cognition, it has not necessarily been approved for routine use by the World Anti-Doping Agency (WADA) which regulates permissible dietary supplements for athletes.

Conclusions and future perspectives

The bibliometric analysis showed that South Africa has established a strong network with researchers working on *Sceletium* and its medicinal value, but there is an apparent lack of synergy and coordination between research groups located in the native land of this genus. The reason for this is not obvious but could be linked to historical networks and collaborations being preferred and strong competition for limited funding between research groups. A higher degree of collaboration is thus foreseen to encourage greater progress in transforming latent botanical assets into consumer products.

A portion of the current review has highlighted the development of quality control tools for commercial and wild-harvested *Sceletium* species, with the focus being on *S. tortuosum* due to its rising commercialisation status in global markets. With the popularity of *Sceletium* growing as a recreational natural product, a more diverse range of products emanating from a growing number of manufacturers is an imminent probability. However, the expansion of the industry may bring about an increased frequency of herb–drug adulterations as seen with many other natural products that are popular in commercial settings (Campbell et al., 2013; Seethapathy et al., 2015; Booker

et al., 2016). There is thus a critical urgency that is required in the research and development of analytical techniques and protocols that are rapid, robust, and reproducible, which may be highly efficacious in their detection capacity for adulterants that may occur in products even at minute scales. Such techniques need to be able to have high resolving power and identify adulterants that would otherwise not be identified due to their similarity in polarity with some of the biomarker compounds. From a practical perspective, these instruments are not always common in laboratories and they are expensive, requiring users to have specialised training and highly sophisticated scientific expertise.

The choice of chemo-elite types that can become easily domesticated may assist the production of quality-assured natural products, generating an industry that will gain consumer trust. This is viewed as being of high importance when considering that some *S. tortuosum* wild types may produce mesembrine alkaloids at exceedingly low concentrations and other *Sceletium* spp. show a complete lack of the key biomarker compounds that are routinely examined by the phytopharmaceutical and nutraceutical industries (Patnala and Kanfer, 2013). Because the different species are similar to each other, this makes them highly vulnerable to misidentification and incorrect identification and unregulated collection of these plants may set in motion their overharvesting thereby creating serious conservation concerns of the genus. The number of studies looking into genetic approaches for quality control tools is remarkably absent in *Sceletium* research. DNA fingerprinting and biomarker identification (Klak et al., 2007; Shikanga et al., 2013; Zhao et al., 2018), single-nucleotide polymorphisms (SNPs), and microsatellite loci (nuclear short sequence repeats, SSR) have been commonly used for genetic-based quality control (Laurie et al., 2010). The absence of quality pure chemical standards has greatly hindered the absolute quantification of the mesembrine alkaloids, and more effort is thus required to fill this gap as the lack of reference compounds makes the identification and profiling of both minor and major alkaloids synthesised by *S. tortuosum* and its relatives more challenging.

Historical ethnobotanical records allude to a practice of fermentation of *S. tortuosum* when it is used by local indigenous people, but scientific evidence of the fermentation on phytochemicals of the plants remains in contention as current fermentation studies do not correlate with each other. Studies investigating the manipulation of biosynthetic pathways in combination with fermentation studies may thus prove valuable in deepening the general understanding of the effects of the fermentation treatment(s) and its biological effects in animal systems. Despite this, the pharmacological tests, whether they be in *in vitro* and/or *in vivo* experiments, have increasingly supported the traditional use of *S. tortuosum* as a mood-elevator and anxiolytic agent. However, its anti-inflammatory and immunomodulatory effects have been insufficiently investigated up until recently. At this point, there has been some evidence that highlights the beneficial physiological effects of *S. tortuosum* extracts as a plant medicine, which extend beyond its psychoactive effects, with potential therapeutic activity targeted at diabetes and obesity (Bennett and Smith, 2018). Interest in developing *Sceletium* into an additive for foods, beverages, and supplements aiding in depressive and anxiolytic disorders has been happening for over a decade (Gericke and Viljoen, 2008), with some products finding the market. If this is to be fully realised, a fundamental field of investigation that will need to be looked into is the standardised cultivation of the plants for their phytochemicals. This can be achieved through the manipulation of secondary metabolites using physiological stress such as light, pH, and nutrient stress in *Sceletium* species, which is currently a void in the research scope.

To enable such studies, a reference genome is also urgently needed for *S. tortuosum* as currently the genetic resources that may assist with understanding the genetic and biochemical controls that are involved in the biosynthetic pathways of mesembrine alkaloids are unavailable. Such resources would thus provide additional research efforts into the control of metabolic flux linked to mesembrine biosynthetic pathways and identify regulatory promoters that influence the synthesis of the unique alkaloids of *Sceletium*. Systems biology studies using a multiomics approach may further assist with the full characterisation of pathway interactions that may lead to a better understanding of the metabolic networks that control alkaloid biosynthesis routes of *Sceletium tortuosum* and related sister species.

Ultimately, *Sceletium* and its alkaloids hold great potential in future endeavours and might provide novel insights into the synthesis pathways of *Sceletium*-specific alkaloids and their genetic regulatory controls whilst studies on inflammation activity and its phytomedicinal applications rise in industry.

Data availability statement

The original contributions presented in the study are included in the article/supplementary material. Further inquiries can be directed to the corresponding author.

Author contributions

KR: Data curation, Formal analysis, Investigation, Methodology, Software, Validation, Visualization, Writing – original draft. GS: Conceptualization, Supervision, Writing – review & editing. NM: Conceptualization, Funding acquisition, Project administration, Resources, Supervision, Writing – review & editing.

Funding

The author(s) declare financial support was received for the research, authorship, and/or publication of this article. This study was financed by the National Research Foundation of South Africa (grant number: 129264) awarded to NPM. KR is a recipient of a doctoral fellowship linked to the NRF-Competitive Programme for Rated Researchers (grant number: 145206) for the period of 2022-2023 and the National Research Foundation (NRF) and the

Foundational Biodiversity and Innovation Programme (FBIP) grant (Grant number: 128319) for the period of 2020-2022. GIS is a recipient of a Medical Research Council (South Africa) Self-initiated research (SIR) grant entitled "Validating the anticonvulsant action of African plant extracts".

Conflict of interest

The authors declare that the research was conducted in the absence of any commercial or financial relationships that could be construed as a potential conflict of interest.

The author(s) declared that they were an editorial board member of Frontiers, at the time of submission. This had no impact on the peer review process and the final decision.

Publisher's note

References

Abou-Donia, A., Jeffs, P. W., McPhail, A. T., and Miller, R. W. (1978). X-Ray crystal and molecular structure of channaine, an unusual alkaloid, probably an artefact from *Sceletium strictum*. *J. Chem. Society Chem. Commun.* 23, 1078–1079. doi: 10.1039/c39780001078

Appley, M. G., Chambers, M. I., and Musah, R. A. (2022). Quantification of hordenine in a complex plant matrix by direct analysis in real time–high-resolution mass spectrometry: Application to the "plant of concern" *Sceletium tortuosum*. *Drug Testing Anal.* 14, 604–612. doi: 10.1002/dta.3193

Arndt, R. R., and Kruger, P. E. J. (1970). Alkaloids from *sceletium joubertii* L. Bol. The structure of joubertiamine, dihydrojoubertiamine, and dehydrojoubertiamine. *Tetrahedron Lett.* 11, 3237–3240. doi: 10.1016/S0040-4039(01)98440-0

Arndt, R. R., and Kruger, P. E. J. (1971). Minor alkaloids from *Sceletium strictum* L. Bol. The structure of N-demethylmesembrenol and N-demethylmesembranol. *South Afr. J. Chem.* 24, 235–240. doi: 10.10520/AJA03794350_1908

Ashraf, M. A., Iqbal, M., Rasheed, R., Hussain, I., Riaz, M., and Arif, M. S. (2018). Environmental stress and secondary metabolites in plants: an overview. *Plant metabolites Regul. under Environ. Stress* 153–167. doi: 10.1016/B978-0-12-812689-9.00008-X

Banner, K. H., and Trevethick, M. A. (2004). PDE4 inhibition: A novel approach for the treatment of inflammatory bowel disease. *Trends Pharmacol. Sci.* 25, 430–436. doi: 10.1016/j.tips.2004.06.008

Barbazuk, W. B., Korf, I., Kadavi, C., Heyen, J., Tate, S., Wun, E., et al. (2000). The syntenic relationship of the zebrafish and human genomes. *Genome Res.* 10, 1351–1358. doi: 10.1101/gr.144700

Beca, S., Aschars-Sobbi, R., Panama, B. K., and Backx, P. H. (2011). Regulation of murine cardiac function by phosphodiesterases type 3 and 4. *Curr. Opin. Pharmacol.* 11, 714–719. doi: 10.1016/j.coph.2011.10.017

Begum, N., Hockman, S., and Manganiello, V. C. (2011). Phosphodiesterase 3A (PDE3A) deletion suppresses proliferation of cultured murine vascular smooth muscle cells (VSMCs) via inhibition of mitogen-activated protein kinase (MAPK) signaling and alterations in critical cell cycle regulatory proteins. *J. Biol. Chem.* 286, 26238–26249. doi: 10.1074/jbc.M110.214155

Bennett, A. C., and Smith, C. (2018). Immunomodulatory effects of *Sceletium tortuosum* (Trimesemine^{TM}) elucidated in *vitro*: Implications for chronic disease. *J. Ethnopharmacol.* 214, 134–140. doi: 10.1016/j.jep.2017.12.020

Bennett, A. C., Van Camp, A., López, V., and Smith, C. (2018). *Sceletium tortuosum* may delay chronic disease progression via alkaloid-dependent antioxidant or anti-inflammatory action. *J. Physiol. Biochem.* 74, 539–547. doi: 10.1007/s13105-018-0620-6

Berna, M. J., and Jensen, R. T. (2007). Role of CCK/gastrin receptors in gastrointestinal/metabolic diseases and results of human studies using gastrin/CCK receptor agonists/antagonists in these diseases. *Curr. Topics Med. Chem.* 7, 1211–1231. doi: 10.2174/156802607780960519

Booker, A., Frommenwiler, D., Reich, E., Horsfield, S., and Heinrich, M. (2016). Adulteration and poor quality of *Ginkgo biloba* supplements. *J. Herbal Med.* 6, 79–87. doi: 10.1016/j.hermed.2016.04.003

Bourgaud, F., Gravot, A., Milesi, S., and Gontier, E. (2001). Production of plant secondary metabolites: a historical perspective. *Plant Sci.* 161, 839–851. doi: 10.1016/S0168-9452(01)00490-3

Brendler, T., Brinckmann, J. A., Feiter, U., Gericke, N., Lang, L., Pozharitskaya, O. N., et al. (2021). Sceletium for managing anxiety, depression and cognitive impairment: a traditional herbal medicine in modern-day regulatory systems. *Curr. Neuropharmacol.* 19, 1384. doi: 10.2174/1570159X19666210215124737

Campbell, N., Clark, J. P., Stecher, V. J., Thomas, J. W., Callanan, A. C., Donnelly, B. F., et al. (2013). Adulteration of purported herbal and natural sexual performance enhancement dietary supplements with synthetic phosphodiesterase type 5 inhibitors. *J. Sex. Med.* 10, 1842–1849. doi: 10.1111/jsm.12172

Carpenter, J. M., Jourdan, M. K., Fountain, E. M., Ali, Z., Abe, N., Khan, I. A., et al. (2016). The effects of *Sceletium tortuosum* (L.) NE Br. extract fraction in the chick anxiety-depression model. *J. Ethnopharmacol.* 193, 329–332. doi: 10.1016/j.jep.2016.08.019

Chen, W., and Viljoen, A. M. (2019). To ferment or not to ferment *Sceletium tortuosum* – Do our ancestors hold the answer? *South Afr. J. Bot.* 122, 543–546. doi: 10.1016/j.sajb.2018.10.011

Chesselet, P. (Compton H. 2005). *Sceletium tortuosum*. Compton Herbarium SANBI. Retrieved from https://pza.sanbi.org/sceletium-tortuosum

Chiu, S., Gericke, N., Farina-Woodbury, M., Badmaev, V., Raheb, H., Terpstra, K., et al. (2014). Proof-of-concept randomized controlled study of cognition effects of the proprietary extract *Sceletium tortuosum* (Zembrin) targeting phosphodiesterase-4 in cognitively healthy subjects: implications for Alzheimer's dementia. *Evidence-Based Complementary Altern. Med.* 2014. doi: 10.1155/2014/682014

Coetzee, D. D., López, V., and Smith, C. (2016). High-mesembrine *Sceletium* extract (Trimesemine^{TM}) is a monoamine releasing agent, rather than only a selective serotonin reuptake inhibitor. *J. Ethnopharmacol.* 177, 111–116. doi: 10.1016/j.jep.2015.11.034

Dastidar, S. G., Rajagopal, D., and Ray, A. (2007). Therapeutic benefit of PDE4 inhibitors in inflammatory diseases. *Curr. Opin. Investig. Drugs* 8, 364.

Dimpfel, W., Franklin, R., Gericke, N., and Schombert, L. (2018). Effect of Zembrin® and four of its alkaloid constituents on electric excitability of the rat hippocampus. *J. Ethnopharmacol.* 223, 135–141. doi: 10.1016/j.jep.2018.05.010

Dimpfel, W., Schombert, L., and Gericke, N. (2016). Electropharmacogram of *Sceletium tortuosum* extract based on spectral local field power in conscious freely moving rats. *J. Ethnopharmacol.* 177, 140–147. doi: 10.1016/j.jep.2015.11.036

Faber, R. J., Laubscher, C. P., Rautenbach, F., and Jimoh, M. O. (2020). Variabilities in alkaloid concentration of *Sceletium tortuosum* (L.) N.E. Br in response to different soilless growing media and fertigation regimes in hydroponics. *Heliyon* 6, e05479. doi: 10.1016/j.heliyon.2020.e05479

Faro, A. F. L., Di Trana, A., La Maida, N., Tagliabracci, A., Giorgetti, R., and Busardò, F. P. (2020). Biomedical analysis of New Psychoactive Substances (NPS) of natural origin. *J. Pharm. Biomed. Anal.* 179, 112945. doi: 10.1016/j.jpba.2019.112945

Feng, Y., He, X., Yang, Y., Chao, D., H Lazarus, L., and Xia, Y. (2012). Current research on opioid receptor function. *Curr. Drug Targets* 13, 230–246. doi: 10.2174/138945012799201612

Freund, D. M., Sammons, K. A., Makunga, N. P., Cohen, J. D., and Hegeman, A. D. (2018). Leaf spray mass spectrometry: a rapid ambient ionization technique to directly assess metabolites from plant tissues. *J. Vis. Exp.* 136, e57949. doi: 10.3791/57949

Gerbaulet, M. (1996). Revision of the genus *Sceletium* NE Br.(Aizoaceae). *Botanische Jahrbucher fur Systematik Pflanzengeschichte und Pflanzengeographie* 118, 9–24.

Gericke, J., Lekhooa, M., Steyn, S. F., Viljoen, A. M., and Harvey, B. H. (2022). An acute dose-ranging evaluation of the antidepressant properties of *Sceletium tortuosum* (Zembrin®) versus escitalopram in the Flinders Sensitive Line rat. *J. Ethnopharmacol.* 284, 114550. doi: 10.1016/j.jep.2021.114550

Gericke, N. (2001). Clinical application of selected South African medicinal plants. *Aust. J. Med. Herbalism* 13, 3–7.

Gericke, N., and Viljoen, A. M. (2008). *Sceletium*-A review update. *J. Ethnopharmacol.* 119, 653–663. doi: 10.1016/j.jep.2008.07.043

Goldsmith, P. (2004). Zebrafish as a pharmacological tool: The how, why and when. *Curr. Opin. Pharmacol.* 4, 504–512. doi: 10.1016/j.coph.2004.04.005

Gordon, D. (1996). From rituals of rapture to dependence: the political economy of Khoikhoi narcotic consumption, c. 1487–1870. *South Afr. Historical J.* 35, 62–88. doi: 10.1080/02582479608671247

Gross, P. M., Jeffs, P. W., and Capps, T. M. (1979). Isolation and structure of a new *Sceletium* alkaloid containing a dihydropyridone ring. *Tetrahedron Lett.* 20, 131–132. doi: 10.1016/S0040-4039(01)85902-5

Gu, Q., and You, S. L. (2011). Desymmetrization of cyclohexadienones *via* cinchonine derived thiourea-catalyzed enantioselective aza-michael reaction and total synthesis of (-)-Mesembrine. *Chem. Sci.* 2 (8), 1519–1522. doi: 10.1039/C1SC00083G

Haller, C. A., and Benowitz, N. L. (2000). Adverse cardiovascular and central nervous system events associated with dietary supplements containing ephedra alkaloids. *New Engl. J. Med* 343 (25), 1833-1838. doi: 10.1056/NEJM200012213432502

Hartwich, C., and Zwicky, E. (1914). Channa (*Mesembrianthemum expansum* and *M. tortuosum* L.). *Apotheker-Zeitung* 29, 925–926.

Harvey, A. L., Young, L. C., Viljoen, A. M., and Gericke, N. P. (2011). Pharmacological actions of the South African medicinal and functional food plant *Sceletium tortuosum* and its principal alkaloids. *J. Ethnopharmacol.* 137, 1124–1129. doi: 10.1016/j.jep.2011.07.035

Hoffman, J. R., Markus, I., Dubnov-Raz, G., and Gepner, Y. (2020). Ergogenic effects of 8 Days of *sceletium tortuosum* supplementation on mood, visual tracking, and reaction in recreationally trained men and women. *J. Strength Conditioning Res.* 34, 2476–2481. doi: 10.1519/JSC.0000000000003693

Houslay, M. D., Schafer, P., and Zhang, K. Y. J. (2005). Keynote review: Phosphodiesterase-4 as a therapeutic target. *Drug Discov. Today* 10, 1503–1519. doi: 10.1016/S1359-6446(05)03622-6

Jędrejko, K., Lazur, J., and Muszynska, B. (2021). Risk associated with the use of selected ingredients in food supplements. *Chem. Biodiversity* 343, 1833–1838. doi: 10.1002/cbdv.202000686

Jacobson, H. (1960). *Handbook of succulent plants* (Poole, UK: Blandford Press) 1, 2.

Jeffs, P. W., Ahmann, G., Campbell, H. F., Farrier, D. S., Ganguli, G., and Hawks, R. L. (1970). Alkaloids of *Sceletium* species - Structures of four new alkaloids from *S. strictum*. *J. Organic Chem.* 35, 3512–3518. doi: 10.1021/jo00835a071

Jeffs, P. W., Archie, W. C., Hawks, R. L., and Farrier, D. S. (1971a). Sceletium alkaloids. IV. Biosynthesis of mesembrine and related alkaloids. Amino acid precursors. *J. Am. Chem. Soc.* 93, 3752–3758. doi: 10.1021/ja00744a032

Jeffs, P. W., Campbell, H. F., Farrier, D. S., Ganguli, G., Martin, N. H., and Molina, G. (1974a). Incorporation of phenylalanine and examination of norbelladines as precursors of the mesembrine alkaloids. *Phytochemistry* 13, 933–945. doi: 10.1016/S0031-9422(00)91426-2

Jeffs, P. W., and Capps, T. M. (1979). Isolation and structure of a new *Sceletium* alkaloid containing a dihydropyridone ring. *Tetrahedron Lett.* 20, 131–132. doi: 10.1016/S0040-4039(01)85902-5

Jeffs, P. W., Capps, T., Johnson, D. B., Karle, J. M., Martin, N. H., and Rauckman, B. (1974b). *Sceletium* alkaloids. VI. Minor alkaloids of *S. namaquense* and *S. strictum*. *J. Organic Chem.* 39, 2703–2710. doi: 10.1021/jo00932a008

Jeffs, P. W., Capps, T. M., and Redfearn, R. (1982). *Sceletium* alkaloids. Structures of five new bases from *Sceletium namaquense*. *J. Organic Chem.* 47, 3611–3617. doi: 10.1021/jo00140a003

Jeffs, P. W., Karle, J. M., and Martin, N. H. (1978). Cinnamic acid intermediates as precursors to mesembrine and some observations on the late stages in the biosynthesis of the mesembrine alkaloids. *Phytochemistry* 17, 719–728. doi: 10.1016/S0031-9422(00)94215-8

Jeffs, P. W., Luhan, P. A., McPhail, A. T., and Martin, N. H. (1971b). The structure of sceletium alkaloid A 4, a pyridine alkaloid from *Sceletium namaquense*: direct method X-ray determination. *J. Chem. Soc. D: Chem. Commun.* (22), 1466–1467.

Jin, Z. (2016). Amaryllidaceae and: *Sceletium* alkaloids. *Nat. Prod. Rep.* 33, 1318–1343. doi: 10.1039/C6NP00068A

Jin, Z., and Yao, G. (2019). Amaryllidaceae and: *Sceletium* alkaloids. *Nat. Prod. Rep.* 36, 1462–1488. doi: 10.1039/C8NP00055G

Kapewangolo, P., Tawha, T., Nawinda, T., Knott, M., and Hans, R. (2016). *Sceletium tortuosum* demonstrates in *vitro* anti-HIV and free radical scavenging activity. *South Afr. J. Bot.* 106, 140–143. doi: 10.1016/j.sajb.2016.06.009

Klak, C., Bruyns, P. V., and Hedderson, T. A. J. (2007). A phylogeny and new classification for Mesembryanthemoideae (Aizoaceae). *Taxon* 56, 737–756. doi: 10.2307/25065857

Kortesniemi, M., Sinkkonen, J., Yang, B., and Kallio, H. (2017). NMR metabolomics demonstrates phenotypic plasticity of sea buckthorn (*Hippophaë rhamnoides*) berries with respect to growth conditions in Finland and Canada. *Food Chem.* 219, 139–147. doi: 10.1016/j.foodchem.2016.09.125

Krstenansky, J. L. (2017). Mesembrine alkaloids: Review of their occurrence, chemistry, and pharmacology. *J. Ethnopharmacol.* 195, 10–19. doi: 10.1016/j.jep.2016.12.004

Kumar, D., and Sharma, U. (2018). High-performance thin-layer chromatography: An economical alternative for the quality control of medicinal plants and derived products. *Separation Sci. Plus* 1 (2), 100–134. doi: 10.1002/sscp.201700013

Laurie, C. C., Doheny, K. F., Mirel, D. B., Pugh, E. W., Bierut, L. J., Bhangale, T., et al. (2010). Quality control and quality assurance in genotypic data for genome-wide association studies. *Genet. Epidemiol.* 34, 591–602. doi: 10.1002/gepi.20516

Leiss, K. A., Choi, Y. H., Verpoorte, R., and Klinkhamer, P. G. L. (2011). An overview of NMR-based metabolomics to identify secondary plant compounds involved in host plant resistance. *Phytochem. Rev.* 10, 205–216. doi: 10.1007/s11101-010-9175-z

Lesiak, A. D., Cody, R. B., Ubukata, M., and Musah, R. A. (2016). Direct analysis in real time high resolution mass spectrometry as a tool for rapid characterization of mind-altering plant materials and revelation of supplement adulteration - The case of Kanna. *Forensic Sci. Int.* 260, 66–73. doi: 10.1016/j.forsciint.2015.12.037

Lewis, J. R. (1995). Amaryllidaceae and *sceletium* alkaloids. *Nat. Prod. Rep.* 12, 339–345. doi: 10.1039/np9951200339

Lewis, J. R. (2001). Amaryllidaceae, *Sceletium*, imidazole, oxazole, thiazole, peptide and miscellaneous alkaloids. *Nat. Prod. Rep.* 18, 95–128. doi: 10.1039/a909077k

Li, S. F. Y. (1992). Capillary electrophoresis: principles, practice and applications. *v. 52* (ElsevierAmsterdam: Elsevier (Journal of chromatography library).

Li, H., Zuo, J., and Tang, W. (2018). Phosphodiesterase-4 inhibitors for the treatment of inflammatory diseases. *Front. Pharmacol.* 9, 1048. doi: 10.3389/fphar.2018.01048

Loria, M. J., Ali, Z., Abe, N., Sufka, K. J., and Khan, I. A. (2014). Effects of *Sceletium tortuosum* in rats. *J. Ethnopharmacol.* 155, 731–735. doi: 10.1016/j.jep.2014.06.007

Lubbe, A., Khatib, A., Yuliana, N. D., Jinap, S., and Verpoorte, R. (2010). Cannabinoid CB1 receptor binding and acetylcholinesterase inhibitory activity of *Sceletium tortuosum* L. *Int. Food Res. J.* 17, 349–355.

MacKenzie, S. J., and Houslay, M. D. (2000). Action of rolipram on specific PDE4 cAMP phosphodiesterase isoforms and on the phosphorylation of cAMP-response-element-binding protein (CREB) and p38 mitogen-activated protein (MAP) kinase in U937 monocytic cells. *Biochem. J.* 342, 571–578. doi: 10.1042/bj3470571

Makolo, F., Viljoen, A., and Veale, C. G. L. (2019). Mesembrine: The archetypal psycho-active *Sceletium* alkaloid. *Phytochemistry* 166, 112061. doi: 10.1016/j.phytochem.2019.112061

Makunga, N., Hall, E., and Stander, M. (2022). Mesembrine alkaloid production in *in vitro* culture morphotypes of *Sceletium tortuosum* (L.) N.E. Br. *Ind. Crops Products* 185, 115051. doi: 10.1016/j.indcrop.2022.115051

Manda, V. K., Avula, B., Ashfaq, M. K., Abe, N., Khan, I. A., and Khan, S. I. (2017). Quantification of mesembrine and mesembrenone in mouse plasma using UHPLC-QToF-MS: Application to a pharmacokinetic study. *Biomed. Chromatogr.* 31, 1–7. doi: 10.1002/bmc.3815

Manganyi, M. C., Regnier, T., Kumar, A., Bezuidenhout, C. C., and Ateba, C. N. (2018). Phylogenetic analysis and diversity of novel endophytic fungi isolated from medicinal plant *Sceletium tortuosum*. *Phytochem. Lett.* 27, 36–43. doi: 10.1016/j.phytol.2018.06.004

Manganyi, M. C., Regnier, T., Tchatchouang, C. D. K., Bezuidenhout, C. C., and Ateba, C. N. (2019). Antibacterial activity of endophytic fungi isolated from *Sceletium tortuosum* L. (Kougoed). *Ann. Microbiol.* 69, 659–663. doi: 10.1007/s13213-019-1444-5

Maphanga, V. B., Skalicka-Woźniak, K., Budzynska, B., Enslin, G. M., and Viljoen, A. M. (2020). Screening selected medicinal plants for potential anxiolytic activity using an in *vivo* zebrafish model. *Psychopharmacology* 237, 3641–3652. doi: 10.1007/s00213-020-05642-5

Maphanga, V. B., Skalicka-Wozniak, K., Budzynska, B., Skiba, A., Chen, W., Agoni, C., et al. (2022). *Mesembryanthemum tortuosum* L. alkaloids modify anxiety-like behaviour in a zebrafish model. *J. Ethnopharmacol.* 290, 115068. doi: 10.1016/j.jep.2022.115068

Masondo, N. A., and Makunga, N. P. (2019). Advancement of analytical techniques in some South African commercialized medicinal plants: Current and future perspectives. *South Afr. J. Bot.* 126, 40–57. doi: 10.1016/j.sajb.2019.06.037

Meyer, G. M. J., Wink, C. S. D., Zapp, J., and Maurer, H. H. (2015). GC-MS, LC-MSn, LC-high resolution-MSn, and NMR studies on the metabolism and toxicological detection of mesembrine and mesembrenone, the main alkaloids of the legal high "Kanna" isolated from *Sceletium tortuosum*. *Anal. Bioanal. Chem.* 407, 761–778. doi: 10.1007/s00216-014-8109-9

Mück-Šeler, D., and Pivac, N. (2011). Serotonin. *Periodicum Biologorum* 113, 29–41. doi: 10.1201/b17423-53

Murbach, T. S., Hirka, G., Szakonyiné, I. P., Gericke, N., and Endres, J. R. (2014). A toxicological safety assessment of a standardized extract of *Sceletium tortuosum* (Zembrin®) in rats. *Food Chem. Toxicol.* 74, 190–199. doi: 10.1016/j.fct.2014.09.017

Napoletano, M., Fraire, C., Santangelo, F., and Moriggi, E. (2001). Mesembrine is an inhibitor of PDE4 that follows structure-activity relationship of rolipram. *Chem. preprint Arch.* 2001, 303–308.

Neergaard, J. S., Andersen, J., Pedersen, M. E., Stafford, G. I., Van Staden, J., and Jäger, A. K. (2009). Alkaloids from Boophone disticha with affinity to the serotonin transporter. *South Afr. J. Bot.* 75, 371–374. doi: 10.1016/j.sajb.2009.02.173

Nell, H., Siebert, M., Chellan, P., and Gericke, N. (2013). A randomized, double-blind, parallel-group, placebo-controlled trial of extract *Sceletium tortuosum* (Zembrin) in healthy adults. *J. Altern. Complementary Med.* 19, 898–904. doi: 10.1089/acm.2012.0185

Nicotra, A. B., Atkin, O. K., Bonser, S. P., Davidson, A. M., Finnegan, E. J., Mathesius, U., et al. (2010). Plant phenotypic plasticity in a changing climate. *Trends Plant Sci.* 15, 684–692. doi: 10.1016/j.tplants.2010.09.008

Nieuwenhuis, J., Strelow, F., Strauss, H., and Wiechers, A. (1981). (4 R)-(—)-O-methyljoubertiamine and O-methyldihydrojoubertiamine, two minor alkaloids from

Sceletium subvelutium L. Bolus. *Journal of the Chemical Society, Perkin Transactions* 3, 284–286. doi: 10.1039/P19810000284

Pappe, L. (1857). *Florae capensis medicae prodromus, or, an enumeration of South African plants used as remedies by the colonists of the Cape of Good Hope*. Ed. W Brittain. 2nd ed. Cape Town.

Patnala, S., and Kanfer, I. (2008). A capillary zone electrophoresis method for the assay and quality control of mesembrine in *Sceletium* tablets. *J. Pharm. Biomed. Anal.* 48, 440–446. doi: 10.1016/j.jpba.2008.01.002

Patnala, S., and Kanfer, I. (2009). Investigations of the phytochemical content of *Sceletium tortuosum* following the preparation of "Kougoed" by fermentation of plant material. *J. Ethnopharmacol.* 121, 86–91. doi: 10.1016/j.jep.2008.10.008

Patnala, S., and Kanfer, I. (2010). HPLC analysis of mesembrine-type alkaloids in *Sceletium* plant material used as an African traditional medicine. *J. Pharm. Pharm. Sci.* 13 (4), 558–570. doi: 10.18433/J3DK5F

Patnala, S., and Kanfer, I. (2013). Chemotaxonomic studies of mesembrine-type alkaloids in *Sceletium* plant species. *South Afr. J. Sci.* 109, 5–9. doi: 10.1590/sajs.2013/882

Patnala, S., and Kanfer, I. (2015). Medicinal use of sceletium: Characterization of phytochemical components of *sceletium* plant species using hplc with uv and electrospray ionization – Tandem mass spectroscopy. *J. Pharm. Pharm. Sci.* 18, 414–423. doi: 10.18433/J3330X

Philander, L. A. (2011). An ethnobotany of Western Cape Rasta bush medicine. *J. Ethnopharmacol.* 138, 578–594. doi: 10.1016/j.jep.2011.10.004

Pithadia, A. B., and Jain, S. M. (2009). 5-Hydroxytryptamine receptor subtypes and their modulators with therapeutic potentials. *J. Clin. Med. Res.* 1, 72. doi: 10.4021/jocmr2009.05.1237

Reay, J., Wetherell, M. A., Morton, E., Lillis, J., and Badmaev, V. (2020). *Sceletium tortuosum* (Zembrin®) ameliorates experimentally induced anxiety in healthy volunteers. *Hum. Psychopharmacology: Clin. Exp.* 35, 1–7. doi: 10.1002/hup.2753

Reddy, K., Stander, M. A., Stafford, G. I., and Makunga, N. P. (2022). Mass spectrometry metabolomics and feature-based molecular networking reveals population-specific chemistry in some species of the *Sceletium* genus. *Front. Nutr.* 9. doi: 10.3389/fnut.2022.819753

Roscher, J., Posch, T. N., Pütz, M., and Huhn, C. (2012). Forensic analysis of mesembrine alkaloids in *Sceletium tortuosum* by nonaqueous capillary electrophoresis mass spectrometry. *Electrophoresis* 33, 1567–1570. doi: 10.1002/elps.201100683

Sandasi, M., Chen, W., Vermaak, I., and Viljoen, A. (2018). Non-destructive quality assessment of herbal tea blends using hyperspectral imaging. *Phytochem. Lett.* 24, 94–101. doi: 10.1016/j.phytol.2018.01.016

Sandasi, M., Vermaak, I., Chen, W., and Viljoen, A. (2016). The application of vibrational spectroscopy techniques in the qualitative assessment of material traded as ginseng. *Molecules* 21 (4), 472. doi: 10.3390/molecules21040472

Schell, R. (2014) Sceletium tortuosum *and mesembrine: a potential alternative treatment for depression* (Senior Scripps Theses). Available online at: https://core.ac.uk/download/pdf/148359679.pdf (Accessed 9 February 2024).

Seethapathy, G. S., Ganesh, D., Kumar, J. U. S., Senthilkumar, U., Newmaster, S. G., Ragupathy, S., et al. (2015). Assessing product adulteration in natural health products for laxative yielding plants, *Cassia*, *Senna*, and *Chamaecrista*, in Southern India using DNA barcoding. *Int. J. Legal Med.* 129, 693–700. doi: 10.1007/s00414-014-1120-z

Shikanga, E. A., Hamman, J. H., Chen, W., Combrinck, S., Gericke, N., and Viljoen, A. M. (2012a). In vitro permeation of mesembrine alkaloids from *Sceletium tortuosum* across porcine buccal, sublingual, and intestinal mucosa. *Planta Med.* 78, 260–268. doi: 10.1055/s-0031-1280367

Shikanga, E., Kamatou, G., Chen, W., Combrinck, S., and Viljoen, A. (2012e). Validated RP-UHPLC PDA and GC – MS methods for the analysis of psychoactive alkaloids in *Sceletium tortuosum*. *South Afr. J. Bot.* 82, 99–107. doi: 10.1016/j.sajb.2012.05.004

Shikanga, E. A., Vermaak, I., and Viljoen, A. M. (2012b). An HPTLC – densitometry method for the quantification of pharmacologically active alkaloids in Sceletium tortuosum raw material and products. *JPC-Journal of Planar Chromatography-Modern TLC* 25 (4), 283–289. doi: 10.1556/JPC.25.2012.4.1

Shikanga, E. A., Viljoen, A., Combrinck, S., and Marston, A. (2011). Isolation of *Sceletium* alkaloids by high-speed countercurrent chromatography. *Phytochem. Lett.* 4, 190–193. doi: 10.1016/j.phytol.2011.03.003

Shikanga, E. A., Viljoen, A. M., Combrinck, S., Marston, A., and Gericke, N. (2012c). The chemotypic variation of *Sceletium tortuosum* alkaloids and commercial product formulations. *Biochem. Syst. Ecol.* 44, 364–373. doi: 10.1016/j.bse.2012.06.025

Shikanga, E. A., Viljoen, A. M., Vermaak, I., and Combrinck, S. (2013). A novel approach in herbal quality control using hyperspectral imaging: Discriminating between *sceletium tortuosum* and *sceletium crassicaule*. *Phytochem. Anal.* 24, 550–555. doi: 10.1002/pca.2431

Smith, C. (2011). The effects of *Sceletium tortuosum* in an in *vivo* model of psychological stress. *J. Ethnopharmacol.* 133, 31–36. doi: 10.1016/j.jep.2010.08.058

Smith, C. (2018). Natural antioxidants in prevention of accelerated ageing: a departure from conventional paradigms required. *J. Physiol. Biochem.* 74, 549–558. doi: 10.1007/s13105-018-0621-5

Smith, M. T., Crouch, N. R., Gericke, N., and Hirst, M. (1996). Psychoactive constituents of the genus *Sceletium* N.E.Br. and other Mesembryanthemaceae: A review. *J. Ethnopharmacol.* 50, 119–130. doi: 10.1016/0378-8741(95)01342-3

Smith, M. T., Field, C. R., Crouch, N. R., and Hirst, M. (1998). The distribution of mesembrine alkaloids in selected taxa of the Mesembryanthemaceae and their modification in the *Sceletium* derived "kougoed." *Pharm. Biol.* 36, 173–179. doi: 10.1076/phbi.36.3.173.6350

Sreekissoon, A., Finnie, J. F., and Van Staden, J. (2021a). Effects of smoke water on germination, seedling vigour and growth of *Sceletium tortuosum*. *South Afr. J. Bot.* 139, 427–431. doi: 10.1016/j.sajb.2021.01.025

Sreekissoon, A., Plačková, L., Doležal, K., Finnie, J. F., and Van Staden, J. (2021b). *In vitro* and *ex vivo* vegetative propagation and cytokinin profiles of *Sceletium tortuosum* (L.) N. E. Br.: a South African medicinal plant. *Plant Cell Tiss Organ Cult* 145, 191–202. doi: 10.1007/s11240-020-02001-2

Stafford, G. I., Pedersen, M. E., van Staden, J., and Jäger, A. K. (2008). Review on plants with CNS-effects used in traditional South African medicine against mental diseases. *J. Ethnopharmacol.* 119, 513–537. doi: 10.1016/j.jep.2008.08.010

Swart, A. C., and Smith, C. (2016). Modulation of glucocorticoid, mineralocorticoid and androgen production in H295 cells by Trimesemine™, a mesembrine-rich *Sceletium* extract. *J. Ethnopharmacol.* 177, 35–45. doi: 10.1016/j.jep.2015.11.033

Terburg, D., Syal, S., Rosenberger, L. A., Heany, S., Phillips, N., Gericke, N., et al. (2013). Acute effects of *Sceletium tortuosum* (Zembrin), a dual 5-HT reuptake and PDE4 inhibitor, in the human amygdala and its connection to the hypothalamus. *Neuropsychopharmacology* 38, 2708–2716. doi: 10.1038/npp.2013.183

Timoneda, A., Feng, T., Sheehan, H., Walker-Hale, N., Pucker, B., Lopez-Nieves, S., et al. (2019). The evolution of betalain biosynthesis in Caryophyllales. *New Phytol.* 224, 71–85. doi: 10.1111/nph.15980

United Nations Office on Drugs and Crime. (2013). *The challenge of new psychoactive substances: List of plant-based substances (20 substances)* (Vienna, Austria: United Nations Publication), 101–102.

Van der Kooy, F., Verpoorte, R., and Meyer, J. J. M. (2008). Metabolomic quality control of claimed anti-malarial *Artemisia afra* herbal remedy and *A. afra* and *A. annua* plant extracts. *South Afr. J. Bot.* 74, 186–189. doi: 10.1016/j.sajb.2007.10.004

Van Eck, N., and Waltman, L. (2010). Software survey: VOSviewer, a computer program for bibliometric mapping. *scientometrics* 84, 523–538. doi: 10.1007/s11192-009-0146-3

Van Wyk, B.-E. (2011). The potential of South African plants in the development of new medicinal products. *South Afr. J. Bot.* 77, 812–829. doi: 10.1016/j.sajb.2011.08.011

Van Wyk, B.-E. (2015). A review of commercially important African medicinal plants. *J. Ethnopharmacol.* 176, 118–134. doi: 10.1016/j.jep.2015.10.031

Van Wyk, B.-E., and Wink, M. (2018). *Medicinal plants of the world* (Oxfordshire, UK: CABI).

Veale, C. G. L., Chen, W., Chaudhary, S., Kituyi, S. N., Isaacs, M., Hoppe, H., et al. (2018). NMR structural elucidation of channaine, an unusual alkaloid from *Sceletium tortuosum*. *Phytochem. Lett.* 23, 189–193. doi: 10.1016/j.phytol.2017.11.018

Verpoorte, R., Choi, Y. H., and Kim, H. K. (2007). NMR-based metabolomics at work in phytochemistry. *Phytochem. Rev.* 6, 3–14. doi: 10.1007/s11101-006-9031-3

Watt, J. M., and Breyer-Brandwijk, M. G. (1962). *The medicinal and poisonous plants of Southern and Eastern Africa being an account of their medicinal and other uses, chemical composition, pharmacological effects and toxicology in man and animal* (Edinburgh, UK: E. & S. Livingstone Ltd).

Weniger, B., Italiano, L., Beck, J. P., Bastida, J., Bergonon, S., Codina, C., et al. (1995). Cytotoxic activity of Amaryllidaceae alkaloids. *Planta Med.* 61, 77–79. doi: 10.1055/s-2006-958007

Wong, C., Bottiglieri, T., and Snead, III, O. C. (2003). GABA, γ-hydroxybutyric acid, and neurological disease. *Ann. Neurol.* 6, 225. doi: 10.1002/ana.10696

Yang, F., and Ito, Y. (2005). "Alkaloids: separation by countercurrent chromatography," in *Encyclopedia of Chromatography* (New York: Marcel Dekker New York), 1–5.

Ye, Y., Jackson, K., and O'Donnell, J. M. (2000). Effects of repeated antidepressant treatment on type 4A phosphodiesterase (PDE4A) in rat brain. *J. Neurochem.* 74, 1257–1262. doi: 10.1046/j.1471-4159.2000.741257.x

Yin, H., Ali, Z., Ding, Y., Wang, Y., Cunningham, M. J., Ibrahim, M. A., et al. (2019). Phytochemistry Letters Sceletorines A and B , two minor novel dimeric alkaloids of *Mesembryanthemum tortuosum* (synonym Sceletium tortuosum). *Phytochem. Lett.* 31, 78–84. doi: 10.1016/j.phytol.2019.03.013

Zhang, G., and Stackman, R. W. (2015). The role of serotonin 5-HT2A receptors in memory and cognition. *Front. Pharmacol.* 6. doi: 10.3389/fphar.2015.00225

Zhao, J., Khan, I. A., Combrinck, S., Sandasi, M., Chen, W., and Viljoen, A. M. (2018). 1H-NMR and UPLC-MS metabolomics: Functional tools for exploring chemotypic variation in Sceletium tortuosum from two provinces in South Africa. *Phytochemistry* 152, 191–203. doi: 10.1016/j.phytochem.2018.03.013

Frontiers in
Plant Science

Cultivates the science of plant biology and its applications

The most cited plant science journal, which advances our understanding of plant biology for sustainable food security, functional ecosystems and human health.

Discover the latest Research Topics

See more →

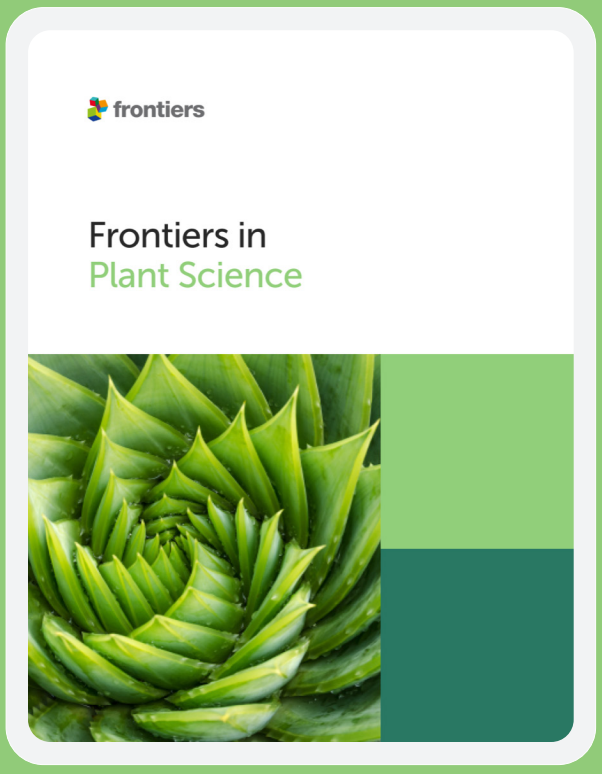

Frontiers

Avenue du Tribunal-Fédéral 34
1005 Lausanne, Switzerland
frontiersin.org

Contact us

+41 (0)21 510 17 00
frontiersin.org/about/contact